Evolution et biodiversité chez les papillons mimétiques néotropicaux

Mael Dore

Muséum National d'Histoire Naturelle

École Doctorale 227

Sciences de la nature et de l'Homme : évolution et écologie

Institut de Systématique, Évolution, Biodiversité (UMR 7205)

Centre d'Écologie et des Sciences de la Conservation (UMR 7204)

Biodiversity and evolution in Neotropical mimetic butterflies

Maël Doré

Thèse de doctorat en Écologie évolutive

Dirigée par **Marianne Elias** & **Colin Fontaine**

Présentée le 01 Juin 2023

Composition du Jury :

Fabien Condamine, CR CNRS, ISEM, Montpellier	Rapporteur
Christine Meynard, DR INRAE, CBGP, Montpellier	Rapportrice
Laurence Després, Professeure, Université de Grenoble	Examinatrice
Wilfried Thuiller, DR CNRS, LECA, Grenoble	Examinateur et Président du Jury
Marianne Elias, DR CNRS, MNHN, Paris	Directrice
Colin Fontaine, CR CNRS, MNHN, Paris	Co-directeur

Biodiversity and evolution in Neotropical mimetic butterflies

Maël Doré

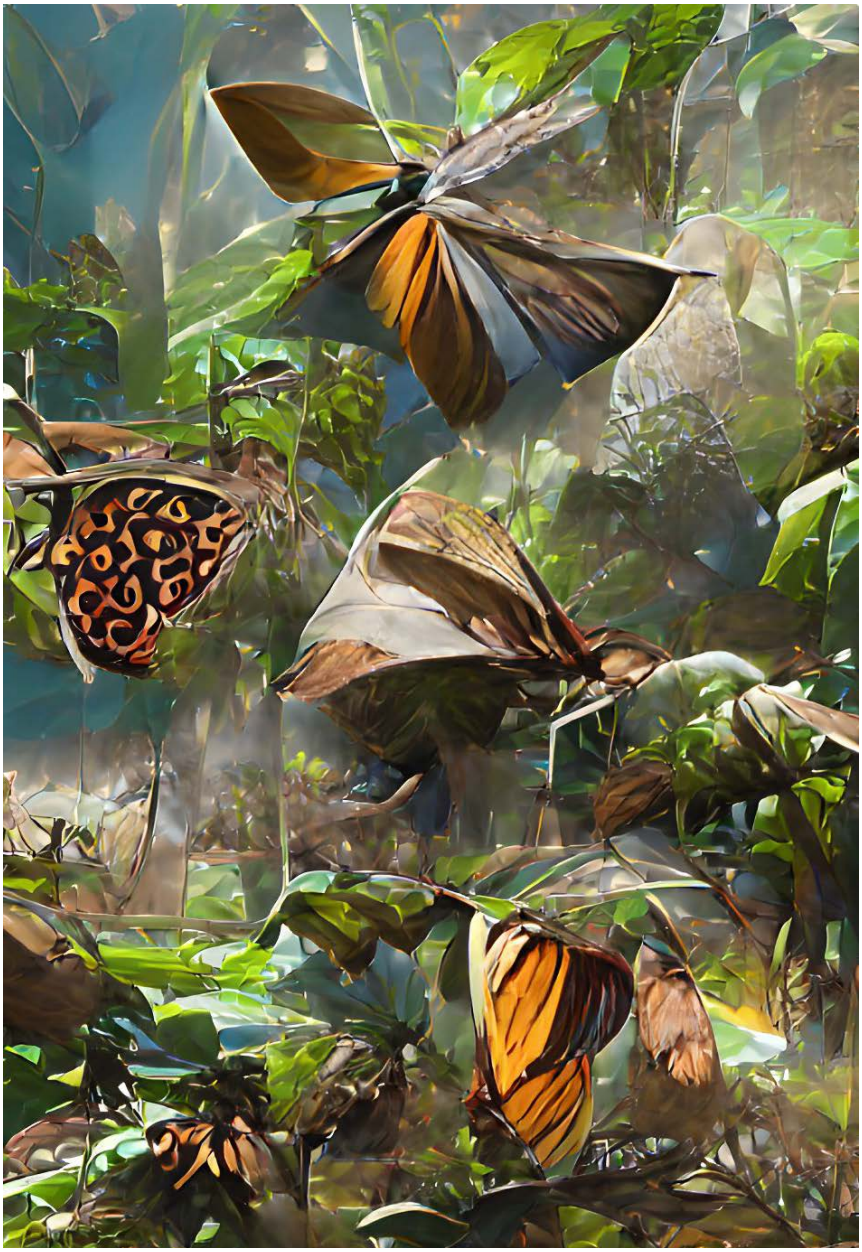

“Very witty quote from some important Scientist”

— *Some important scientist*

Remerciements

Ça y est, c'est donc la fin de cette longue aventure qui annonce le début de beaucoup d'autres. C'est le moment ingrat de remercier tous les gens qui ont, de prêt ou de loin, participé à ce projet scientifique, m'ont soutenu, encouragé et inspiré, et ont occupé une place importante dans ma vie durant ce périple, tout en sachant que j'en oublierais forcément, et que ces quelques mots écrits l'esprit embrumé par un manque évident de sommeil ne rendront pas justice à leur implication et leur apport à ses travaux de thèse et bien au-delà. Néanmoins, voici ma tentative.

Tout d'abord, je tiens à remercier très chaleureusement ma directrice de Thèse Marianne Elias qui m'a accompagné de mes premiers pas hésitants dans son bureau pour solliciter un stage de Master il y a cinq ans de ça, jusqu'à aujourd'hui. Merci beaucoup pour m'avoir fait confiance et m'avoir guidé toutes ces années, en étant à la fois une mentor scientifique et un modèle d'humanité. Merci pour ta disponibilité, ta générosité, ton expertise et ton dynamisme à tout épreuve. Merci pour la liberté que tu m'as laissée dans mes choix pour mener cette thèse dans les directions que je souhaitais et pour le soutien et les brillants conseils que tu m'as toujours apportés, quelles que soient ces directions. J'espère pouvoir m'inspirer de cette expérience à tes côtés pour guider moi-même des étudiants dans la voie de la recherche dans le futur. Je remercie également mon co-directeur de thèse Colin Fontaine pour avoir toujours répondu présent depuis les prémices de ce projet en Master, et pour avoir su trouver les mots justes pour m'accompagner et m'encourager toutes ces années. Promis, un jour je les ferai vraiment ces fameux réseaux d'interactions dont on parle depuis plus de trois ans ! Merci à eux deux pour m'avoir laissé l'opportunité de mener à bien ce super projet de recherche et d'avoir été à la fois exigeants, compréhensifs, et encourageants, pendant ces années. Ça a été un réel plaisir de travailler et d'apprendre à vos côtés.

Plus largement, je profite de cet instant pour remercier toutes celles et ceux qui m'ont aidé, encadré et soutenu lors de mon parcours universitaire, de mes premiers stages au côté de Priscilla Decottignies, puis Bruno Jesus à l'Université de Nantes à base de courses de nudibranches, en passant par les nombreuses personnes exceptionnelles en charge du Master Tropimundo qui m'ont tant apporté, et Elisa Thébault à l'IEES qui m'a guidé dans la publication de mon premier article. Je suis aussi reconnaissant à tous les membres de mon comité de thèse et de mon jury pour avoir accepté de consacrer une partie de leur précieux temps à se plonger dans mon travail scientifique, et pour les riches discussions passées et à venir qui en naîtront.

Les travaux de cette thèse sont le centre de gravité des multiples collaborations qui l'ont rendu possible. Un grand merci à toutes les personnes qui ont fourni des spécimens, des séquences, des conseils sur le terrain, de l'assistance au labo et dans les analyses, et qui ont

participé de près ou de loin à ce projet. Je suis particulièrement reconnaissant envers Keith Willmott pour m'avoir fait confiance et avoir accepté de partager ces précieuses données d'occurrences qui auront été la base de ces travaux, ainsi que pour sa Science infinie des ithomiines, et sa patience pour répondre à mes nombreuses sollicitations. Je remercie aussi Boris Leroy pour ses nombreux conseils et sa pédagogie qui m'ont ouvert les portes de l'univers foisonnant des modèles de niches. Merci à Rémi Mauxion, Violaine Ossola, et Erika Páez Vargas pour ces courtes mais si riches semaines passées dans la jungle équatorienne à chasser les papillons et tester les cocktails locaux sur fond de mauvais Reggaeton. Merci encore Erika pour m'avoir si chaleureusement accueilli dans ta famille sur place, et permis de rendre ce séjour encore plus mémorable. Et merci à mes collègues de bureau pour avoir animé ces trois années et participé à cette aventure.

Un remerciement particulier pour mes parents, pour m'avoir transmis leur intérêt pour la Nature, leur curiosité, et leur créativité, qui font une grande partie de qui je suis, et qui m'ont toujours encouragé dans mes aventures quelles qu'elles soient.

Merci à la saga Pokémon pour m'avoir donné envie de les attraper tous (et les relâcher) pour les mettre dans mon Pokedex de la connaissance, et pour avoir contribué à forger ma fascination inassouvissable (si, si, ça se dit !) pour les anecdotes sur les petites bébêtes qui m'auront amené des années plus tard à toquer à la porte du Muséum.

Enfin, un grand merci à tous mes amis du Muséum, de Paris, de Nantes, et d'ailleurs pour faire partie de ma vie et être une source inépuisable de joie, d'énergie, et d'inspiration qui m'anime chaque jour. En vrac, et de manière totalement arbitraire et non-exhaustive : merci aux collègues du badminton pour les suées hebdomadaires ; merci aux potos du Master pour les soirées clandestines (y a prescription !) à enchaîner plus de bières que de courses sur Mario Kart ; merci aux potes grimpeurs pour les humiliations régulières sur les voies d'Arkose ou les gros cailloux de Fontainebleau ; merci aux potes du BDEM pour les meilleures Sangria du quartier ; merci aux quais de Seine pour avoir été une valeur sûre de tant de soirées printanières et estivales, et au Reset pour avoir pris la relève l'hiver ; merci aux amis de la Denéenne pour être simplement les meilleurs ; merci à Alice et Arthur pour les si nombreuses soirées à rire à ne plus pouvoir en respirer (rien à voir avec l'asthme !) ; merci à Teddy, Lou, Sabrina, Guillaume, Paul, Léa et tant d'autres pour les moments partagés autour d'un périphérique de cantine ou d'un café au miel ; bref merci à toutes celles et ceux qui partagent un bout de ma vie et qui ont été et seront encore là pour moi pendant et après cette Thèse.

Abstract

In the face of global change, understanding the mechanisms underlying species distributions and coexistence is both a priority and a challenge, especially for biodiversity hotspots such as the Neotropics. This research work focuses on the emblematic case of Müllerian mimicry in two tribes of Neotropical butterflies, the Ithomiini (Nymphalidae: Danainae) and Heliconiini (Nymphalidae: Heliconiinae), in which multiple species share a similar wing pattern, thereby forming mimicry rings. This evolution is driven by selective pressures from predators, which learn to avoid toxic prey more quickly when they encounter more frequently individuals with similar warning signals. My PhD thesis aims to unravel effects of mimicry on large-scale spatial and evolutionary patterns of biodiversity, employing an integrative approach across biogeography, phylogenomics, and community ecology.

In **Chapter 1**, I employ species distribution models in order to map the taxonomic, phylogenetic and mimetic facets of Ithomiini biodiversity. I identify areas of evolutionary and ecological importance for conservation, and evaluate their overlap with current anthropogenic threats. I show that tropical montane forests that host high species and mimetic diversity as well as rare species and mimicry rings appear particularly under threat. These results support the role of ithomiine butterflies as a suitable flagship indicator group for Neotropical butterfly diversity, and reinforce the position of the tropical Andes as a flagship region for butterfly biodiversity conservation.

In **Chapter 2**, I present a new phylogenetic hypothesis for the Ithomiini tribe, building upon phylogenomic methods to resolve and support deep evolutionary relationships in the group. This phylogeny reinforces the monophyly of the core-group, a clade associated with a recent adaptive radiation linked to multiple colonizations of new areas following the demise of the Pebas aquatic system in Western Amazonia. It comforts the basal position of the Melinaeina subtribe and suggests the Mechanitina subtribe as the sister-group of the core-group. Altogether, this new phylogeny provides a stable tool for macroevolutionary analyses in ithomiine butterflies.

In **Chapter 3**, I describe a new method to quantify similarity in wing patterns in the context of mimicry. I build an interactive website to carry out a Citizen Science collection of the perception of wing pattern similarity, and adapt the t-STE machine learning algorithm to generate 3D perceptual maps of the variation of heliconiine butterfly wing patterns at the continental scale. I map the local phenotypic diversity as the degree of clustering in the

perceptual space, and use Gaussian mixture models to cluster wing patterns in mimicry rings reflecting mutualistic interactions. Altogether, the perceptual map approach offers a new tool to investigate and quantify similarity in ecological signals in general.

In **Chapter 4**, I link all previously explored geographic, evolutionary, and phenotypic dimensions of biodiversity, to study the effects of mutualistic interactions on large-scale spatial distributions and niche evolution of ithomiine butterflies. I use phylogenetic comparative methods to test for spatial congruence and climatic niche convergence among comimetic species. I show that mimicry drives large scale spatial association among phenotypically similar species, providing new empirical evidence for the validity of Müller's model at a macroecological scale. Additionally, I show that mimetic interactions drive the evolutionary convergence of species climatic niche, thereby strengthening the co-occurrence of co-mimetic species.

Overall, my research work provides new insights into the importance of mutualistic interactions in shaping both niche evolution and species assemblages at large spatial scales. Critically, in the context of global change, it highlights the vulnerability to extinction cascades of mimetic communities tied by positive interactions.

Résumé

Face au changement global, la compréhension des mécanismes qui sous-tendent la distribution et la coexistence des espèces est essentielle, en particulier dans les points chauds de biodiversité. Ce travail de recherche se concentre sur le cas du mimétisme Müllérien dans deux tribus de papillons néotropicaux, les Ithomiini (Nymphalidae: Danainae) et les Heliconiini (Nymphalidae: Heliconiinae), au sein desquelles plusieurs espèces partagent un motif alaire, formant ainsi des cercles mimétiques. Ma thèse vise à étudier les effets du mimétisme sur les motifs spatiaux et évolutifs de la biodiversité à grande échelle, en utilisant une approche intégrative mêlant biogéographie, phylogénomique et écologie des communautés.

Dans le **Chapitre 1**, j'utilise des modèles de distribution d'espèces afin de cartographier la diversité taxonomique, phylogénétique et mimétique des Ithomiini. Je montre que les forêts tropicales de montagne qui abritent la plus grande diversité d'espèces et de motifs mimétiques, ainsi que la plupart des espèces et motifs rares, sont particulièrement menacées. Ces résultats confirment le rôle des papillons ithomiines en tant que groupe indicateur pour la diversité des papillons néotropicaux, et renforcent la position des Andes tropicales en tant que région cruciale pour la conservation de la biodiversité.

Dans le **Chapitre 2**, je présente une nouvelle phylogénie pour la tribu des Ithomiini s'appuyant sur des méthodes phylogénomiques pour résoudre des relations évolutives profondes au sein du groupe. Cette phylogénie renforce la monophylie du 'core-groupe', un clade associé à une radiation adaptative récente concomitante au retrait du système aquatique du Pebas en Amazonie occidentale. Elle conforte la position basale de la sous-tribu Melinaeina et suggère la sous-tribu Mechanitina comme groupe frère du 'core-group'. Dans l'ensemble, cette nouvelle phylogénie fournit un outil stable pour les analyses macroévolutives chez les papillons ithomiines.

Dans le **Chapitre 3**, je décris une nouvelle méthode pour quantifier la similarité des motifs alaires dans le contexte du mimétisme. J'utilise des données de perception collectées dans le cadre d'un projet de Sciences Participatives et j'adapte l'algorithme d'apprentissage automatique t-STE pour générer des cartes perceptuelles en 3D de la variation des motifs alaires des papillons heliconiines à l'échelle continentale. Je cartographie la diversité phénotypique locale tel le degré de regroupement dans l'espace perceptuel, et j'utilise des modèles de mélange gaussien pour regrouper les motifs alaires dans des cercles mimétiques reflétant les interactions

mutualistes. Dans l'ensemble, l'approche de la carte perceptuelle offre un nouvel outil versatile pour étudier et quantifier la similarité des signaux écologiques.

Dans le **Chapitre 4**, je lie toutes les dimensions géographiques, évolutives et phénotypiques de la biodiversité précédemment explorées, afin d'étudier les effets des interactions mutualistes sur les distributions spatiales et l'évolution des niches des papillons ithomiines. J'utilise des méthodes comparatives phylogénétiques pour tester la congruence spatiale et la convergence des niches climatiques entre les espèces co-mimétiques. Je montre que le mimétisme entraîne une association spatiale à grande échelle entre des espèces phénotypiquement similaires, fournissant ainsi une nouvelle preuve empirique de la validité du modèle de Müller à une échelle macroécologique. En outre, je montre que les interactions mimétiques mènent à la convergence évolutive de la niche climatique des espèces, renforçant ainsi la co-occurrence d'espèces co-mimétiques.

Dans l'ensemble, mon travail de recherche met en lumière l'importance des interactions mutualistes dans l'évolution des niches et des assemblages d'espèces à large échelle spatiale. Dans le contexte du changement global, il souligne la vulnérabilité aux cascades d'extinction des communautés mimétiques liées par des interactions positives.

Table of Contents

GENERAL INTRODUCTION

1 On the study of biodiversity

Biodiversity is the variety of living organisms on Earth represented by nearly 2 million documented species to-date (Costello *et al.* 2022), each with a specific combination of morphological, physiological, behavioral and ecological traits. One of the major objectives of natural sciences is the inventory, description, quantification and mapping of this biodiversity, as well as the understanding of the mechanisms generating and shaping it. This pursuit of knowledge about the natural world surrounding us is worthy *per se*. In the face of the ongoing biodiversity crisis, it become crucial. A large portion of current studies are now dedicated to monitor and alert on the global decline of biodiversity, and unravel its causes to promote conservation of ecosystems, species, and evolutionary trajectories, ideally before they disappear due to anthropogenic threats (Barnosky *et al.* 2011; IPBES 2019a).

The study of biodiversity has a long and complex history that can be traced back to the work of Aristotle (4th century BC), far before the idea of biodiversity itself emerged as a significant concept in the scientific community during the 20th century (Díaz & Malhi 2022). Aristotle laid the foundations for the systematic study of biodiversity. In his work *Historia Animalium*, he provided detailed observations of the anatomy, habitat and behavior of living organisms and proposed a classification into different groups based on their shared characteristics (Fürst von Lieven & Alexander Humar 2008). He established the concept of taxonomic hierarchy through its core ideas of *eidos*, the form of natural beings, and the *genos*, the class of forms reflecting Earth's natural order (Wilson 2010).

Following this seminal antique work, a long line of naturalists and taxonomists have come to complement this endless task of the description of biodiversity, typically embellishing their work with naturalistic illustrations reflecting the complexity of life. Among the most significant to my personal aesthetic taste comes the work of Ernst Haeckel (1834-1919), a German biologist who, besides proposing some of the most influential early models for the 'Tree of Life', and a definitely less inspiring racial theory of human evolution, created a hundred of scientific and artistic prints of biological organisms organized in systematic groups and summarized in his *Kunstformen der Natur* (**Fig. 1**). His illustrations fulfilled educative, artistic, and scientific goals at the same time. They displayed organisms poorly known outside of the scientific community, providing a more complete depiction of the diversity of Life than commonly thought. They harbored vivid colors and were arranged in visually stunning composition for maximum aesthetic impacts. Finally, they also accounted for the diversity of

traits and functions, and highlighted the morphological symmetries found in different levels of organization, illustrating the strength of comparative qualitative descriptions to carry meanings to describe biodiversity.

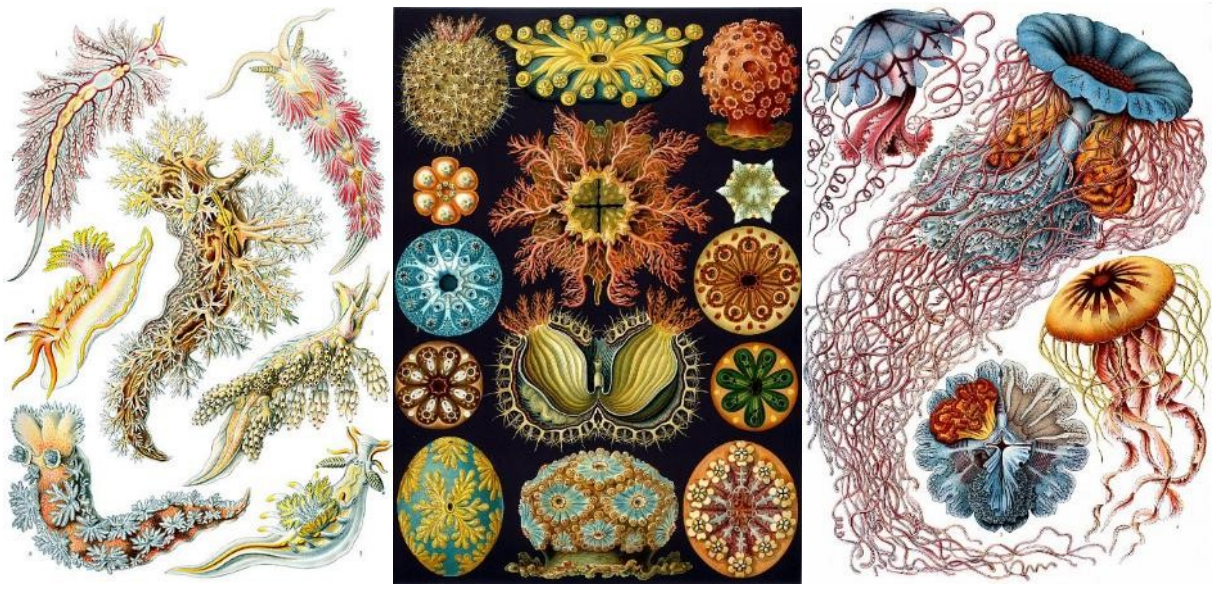

Figure 1: Lithographic prints from *Kunstformen der Natur* by Ernst Haeckel illustrating the beauty and diversity of the natural world. From left to right: N°43, Nudibranchia ; N°85, Ascidiaceae ; N°8, Discomedusae.

Nowadays, the work of taxonomists still revolves around the description of morphological and ecological characters, their informative visual representation with scientific sketches, and the production of a diagnosis to describe species. However, the taxonomist toolkit has grown exponentially with the addition of diverse data sources and associated analytic methods such as phylogeography, comparative geometric morphometrics, population genetics, and phylogenetic reconstruction, used to design hypotheses for the delimitations of species in an integrative framework (Dayrat 2005). Most of these approaches illustrate the shift from a qualitative perspective to describing phenotypic species traits to integrated quantitative approaches based on numerical quantifications. The same evolution affects the work of the modern ecologists and evolutionary biologists who rely now heavily on statistics, programming and computational methods to design their analyses and carry out their daily work (Legendre & Legendre 2012; Revell & Harmon 2022). This ‘quiet revolution’ (Bisby 2000) supported by the emergence of powerful computer architectures and algorithms, and massive online biodiversity-related information systems has led to the characterization of an entire ‘new’ field of study: ‘Biodiversity informatics’. (On a personal note, I realize writing those lines that, despite not having received any education in informatics, this is probably my scientific field of

research, while I have always considered myself a bit of a quantitative ecologist, a (macro-) evolutionary biologist, and a biogeographer, and not entirely any of them at the same time)

Biodiversity informatics thrives in the age of Big Data, a term describing the massive increase in the volume of (biodiversity) data available, from all sort of sources (geographic, genetic, phenotypic, demographic, phylogenetic, etc.), generated at an increasing rate. Accompanying this transformation of the scientific landscape, we have witnessed the emergence of numerous online open databases, sometimes coupled with Citizen Science projects, aiming to collect, aggregate, organize, harmonize, curate and share publicly this heterogeneous and chaotic amount of data, with forefront examples being the Global Biodiversity Information Facility (GBIF; https://www.gbif.org) for occurrence data and the Gene Bank of the National Center for Biotechnology Information (NCBI; https://www.ncbi.nlm.nih.gov/genbank/) for molecular data. This speed up of the acquisition and sharing of data has surely accelerated the exploration of biodiversity, but it has also caused a new issue with the rate of data accumulation overwhelming our ability to carry out analyses and produce sense out of raw information (Johnston *et al.* 2023). More recent developments in data analyses are now lurking toward Data Science to find efficient solutions to handle this massive amount of data, with machine learning algorithms emerging as a potential solution (Wüest *et al.* 2020; Lürig *et al.* 2021).

My research work builds upon this global revolution of Biodiversity Informatics and Big Data in Science to explore three important dimensions of biodiversity patterns (**Fig. 1**). In **Chapter 1**, I investigate patterns of biodiversity in **space** applying species distribution models in a biogeographic framework to produce large-scale maps of several biodiversity facets. In **Chapter 2**, I explore patterns of diversity in **time** using state-of-the-art phylogenomics approaches to unravel deep evolutionary relationships. In **Chapter 3**, I propose a new method to explore patterns of diversity through **phenotypic variation** building upon the quantification of the perception of ecological signals. Finally, in **Chapter 4**, I offer to link **all three dimensions** in an integrative perspective investigating the mechanisms behind the effect of ecological interactions, mediated by phenotypes, on large scale spatial and evolutionary patterns of biodiversity.

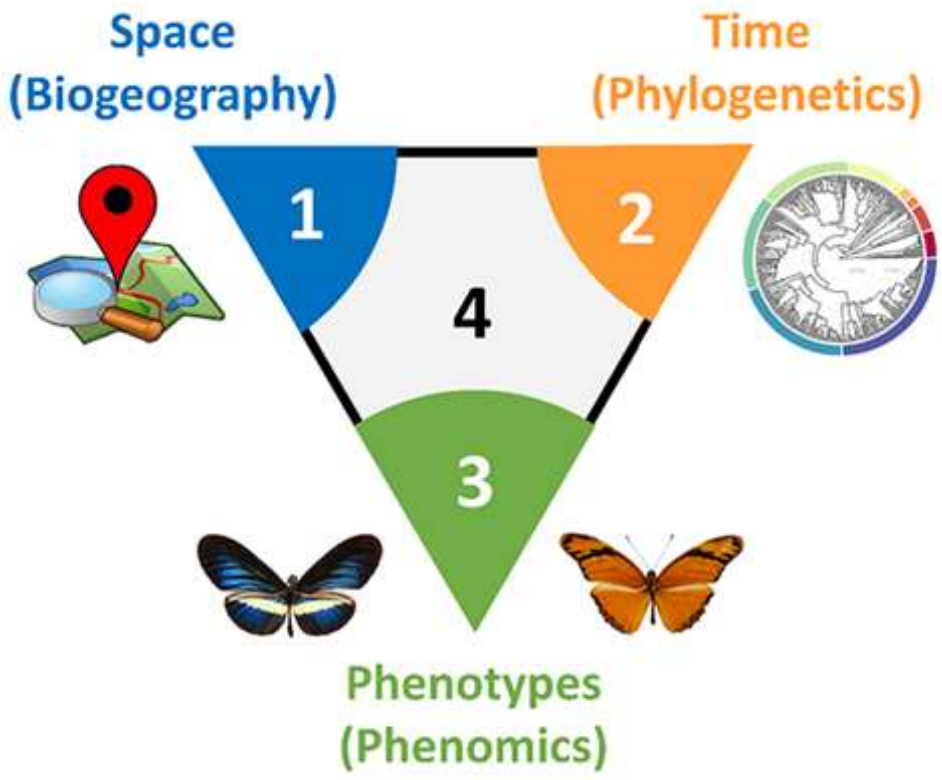

Figure 1: The biodiversity triangle with three important dimensions of the study of biodiversity explored throughout this research work. **Chapter 1** studies patterns of biodiversity in **space**. **Chapter 2** studies patterns of diversity in **time**. **Chapter 3** studies patterns of diversity through **phenotypic variation**. **Chapter 4** links **all three dimensions** in an integrative perspective.

2 Biodiversity in space (Chapter 1)

To my opinion, one of the most synthetic and impactful representation of biodiversity patterns are maps. There is a diversity of maps that enable describing the patterns of variation of biodiversity in space, each conveying specific information about the spatial organization of biologic entities: maps of species distributions, maps of species diversity, maps of bioregions delimiting areas of regional endemism, etc. Biogeography, the field of science that produces such wonderful maps has a long scientific history that has also been transformed by conceptual, technological and methodological revolutions (Lomolino, 2016).

Early biogeographic studies were largely descriptive in nature, with researchers documenting the distribution of organisms and identifying patterns of similarity and differences across regions. Alexander von Humboldt (1769-1859) was an inspirational figure of this early developments, and is considered as one of the father of Biogeography (Schrodt *et al.* 2019). In

particular, his expeditions in South America led to the recognition of the importance of altitude and climate in determining the distribution of organisms. He was the first to propose comparisons of the distribution of regional flora along environmental gradients, illustrating the strength of maps to connect spatial patterns and the processes generating them (**Fig. 2**). In particular, his work was seminal in highlighting the relationship between climate and large-scale species distributions, leading to the emergence of the concepts of biomes and latitudinal and elevational gradients (Schrodt *et al.* 2019).

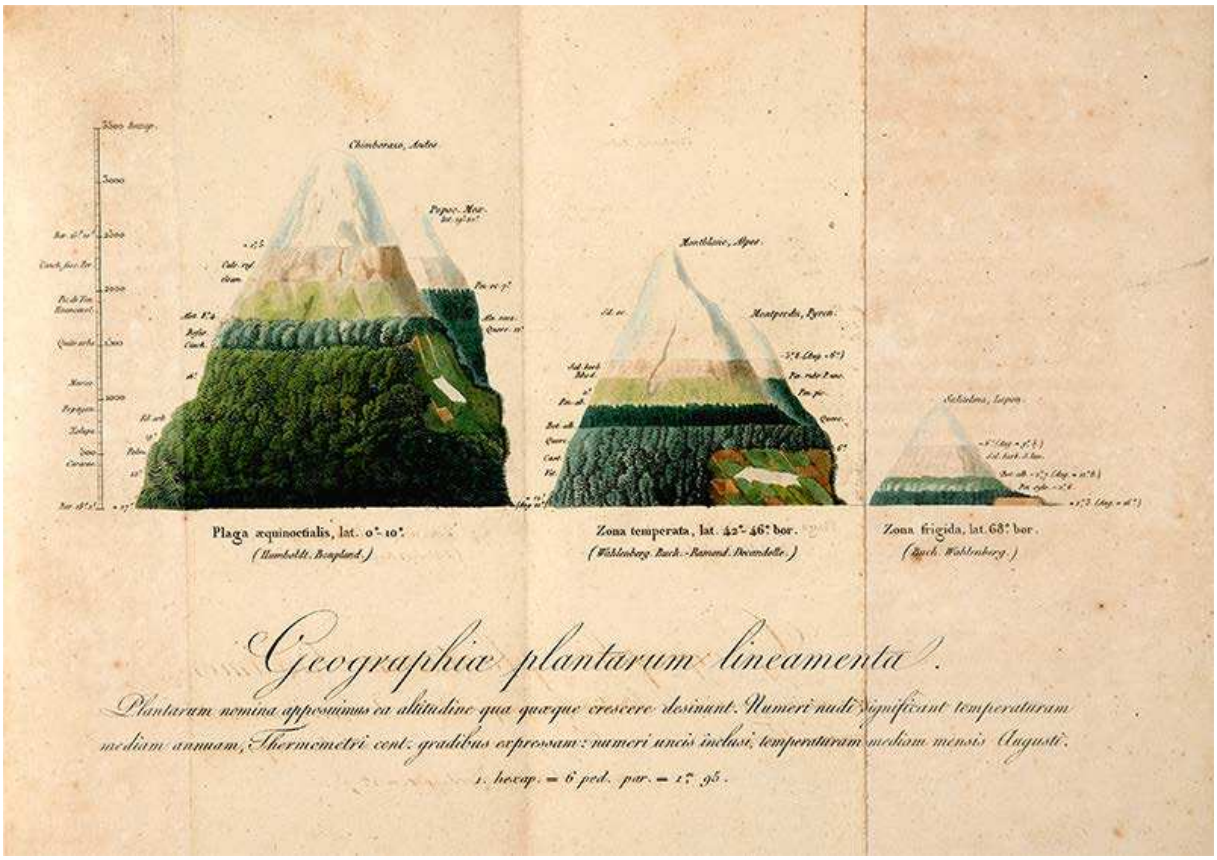

Figure 2: Illustration from Alexander von Humboldt in *De distributione plantarum* (1817) on which he reported and compared the biotope stratification along the slopes of three mountains in different climatic zones: Mont Chimborazo (Ecuador) in the tropical zone, Mont Blanc (France) in the temperate zone, and Sulitelma massif (Laponia) in the arctic zone. A famous prototypic example for Biogeography with a synthetic and comparative map of regional variation of plant distributions in space related to environmental conditions.

Fascinated by Humboldt's tales of naturalistic and scientific adventures, Alfred Russel Wallace (1823-1913) dedicated its life to the exploration of the Tropical lands and their extraordinary biodiversity. As a pioneer of biogeography, he proposed one of the first map of regional divisions of Earth in six zoogeographic kingdoms based on lists of regional fauna encompassing major vertebrate groups, insects and mollusks (**Fig. 3**). He also offered mechanistic explanations to the spatial distribution of biodiversity by suggesting the effects of

factors such as the formation of mountains, the depth of oceans, and the historical effects of ice ages on the specific characteristics of local fauna (Wallace 1855, 1876). He identified the Wallace Line, a sharp turnover of fauna that separates the Indonesian archipelago into two distinct parts: a western portion in which the animals are largely of Asian origin, and an eastern portion where the fauna reflects the Australasian zooregion. This biogeographic boundary is still a relevant feature in modern Biogeography (Rueda *et al.* 2013).

Figure 3: Zoogeographic regions according to Alfred R. Wallace in *The Geographical Distribution of Animals* (1876). It described the divisions of Earth in regions based on lists of regional fauna encompassing major vertebrate groups, insects and mollusks, and defined by the regional occurrence of endemic genera and families of animals.

In the 20th century, scientists became more focused on understanding the ecological, historical and evolutionary factors that shaped the distribution of organisms. For instance, Joseph Grinnell (1877-1939) devised the concept of 'ecological niche' as the physiological and ecological requirements conditioning the presence of a species in a given area such as climate, pedology, habitat structure, etc. (Grinnell 1917). Charles Elton (1900-1991) soon refined this vision by describing species ecological niches as determined by the interactions with other species and resources representing the species' function in an ecosystem (Elton 1927). Finally, George Evelyn Hutchinson (1903-1991) offered a formal mathematical abstraction merging both qualitative concepts of Grinnellian and Eltonian niches. He described the niche an hypervolume found in a multidimensional continuous ecological space defined by all biotic and biotic factors acting on the distribution of species. The species niche was then characterized by

its position along multiple environmental and ecological gradients (Hutchinson 1957). Armed with this new mathematical description, biogeography became more quantitative, with researchers using statistical methods to analyze biogeographic data. One of the most influential approaches in evolutionary biogeography was the use of parsimony analysis, which involves inferring the minimum number of historical events required to explain the observed distribution of species, to propose hypotheses for ancestral range reconstructions (Wiley 1988). The emergence of probabilistic methods of phylogenetic inferences later complemented the picture, providing more and more complex models to explore the historical dispersal events shaping current spatial distribution of biodiversity (Ree & Smith 2008; Albert & Antonelli 2017).

With the advent of Geographic Information Systems (GIS) and remote sensing in the 21th century, biogeographers have been able to produce and access large amount of data to create detailed maps of habitat types and environmental variables, as well as to track changes in vegetation cover and land use over time (Hansen *et al.* 2013). Taking advantage of the access to this new information, scientists developed algorithms defined as "species distribution models" that relate environmental data with georeferenced occurrences to offer refine continuous predictions of the distribution of species (Guisan & Thuiller 2005). Such developments allowed to investigate and map more finely the long-known latitudinal biodiversity gradient and its evolution through geological time (**Fig. 4**; Mannion et al., 2014), but also to question atypical patterns that do not follow this rule (Kindlmann *et al.* 2012).

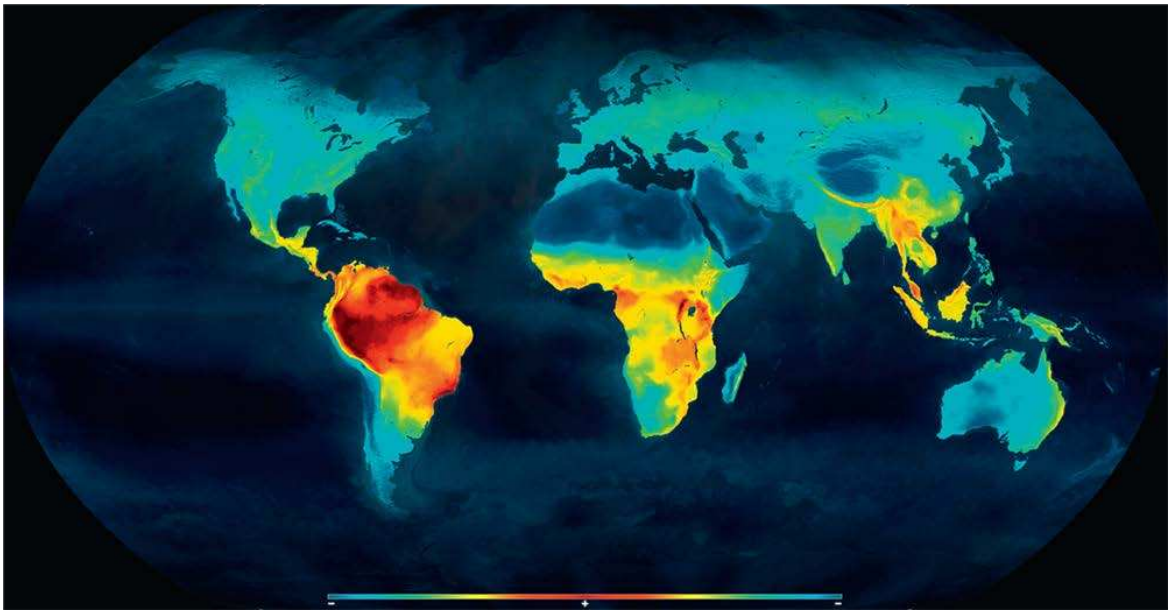

Figure 4: Distribution of extant terrestrial vertebrate species richness on Earth. Global pattern shows a latitudinal biodiversity gradient with species richness concentrated in the equatorial regions (red end of color spectrum) and decreasing toward the poles (blue end of color spectrum). Figure from Mannion et al. (2014).

More recently, the increasing availability of open-access biodiversity databases and data sharing platforms has made it easier for researchers to access and analyze large comprehensive datasets, facilitating collaboration and enabling researchers to ask new and more complex questions about biodiversity (Antonelli 2017). Online platforms and mobile apps have made it easier for non-scientists to contribute data to such open-access biodiversity databases, allowing researchers to tap into a vast pool of observations from all over the world. As a prime example, the Global Biodiversity Information Facility (GBIF; https://www.gbif.org) is an international network and data infrastructure that centralizes numerous occurrence databases in a unique open access source aiming to encompass the whole taxonomic diversity of Life. Complementarily, Map of Life (MoL; https://mol.org) provides an online platform to access to species distribution data and species range maps for a wide range of taxa.

Overall, the evolution of methods and data sources in biogeography has enabled researchers to ask increasingly complex questions about the distribution of life on Earth (Jetz et al., 2012; Lomolino et al., 2016). For instance, recent studies have aimed to investigate the role of niche-based vs. neutral mechanisms in the assembly of species along a latitudinal biodiversity gradient (Bosch *et al.* 2021) as well as to separate the biotic and abiotic factors controlling species distributions at multiple spatial scales (König *et al.* 2021). Meanwhile, international collaborations have allowed researchers to unravel the patterns and drivers of global distributions of species richness in ants (Kass *et al.* 2022) and bees (Orr *et al.* 2021), two important steps into helping to address the Wallacean shortfall (i.e., relative paucity of geographic information) affecting insects in general, a gap this research work also aims to contribute to fill.

Crucially in the context of global changes and the ongoing biodiversity crisis, biogeography can provide new insights into the impacts of human activities on biodiversity (Ellis 2019). It becomes now possible to quantify biodiversity responses to land use worldwide (Newbold *et al.* 2015) and to conduct large scale comprehensive assessment of extinction risk status for thousands of species at once based on predictions of future distributions under scenarios of climate changes (Gomes *et al.* 2019). Such ambitious researches provide the primary resources to produce international assessment of biodiversity trends aiming to support the political conservation agenda worldwide (IPBES 2019b).

3 Biodiversity in time (Chapter 2)

"Nothing in Biology Makes Sense Except in the Light of Evolution". This is the title of a famous essay published by the evolutionary biologist Theodosius Dobzhansky in 1973. To a modern biologist, this goes without saying. But this vision has not always being shared by naturalists who for centuries promoted fixism: the idea that life forms are fixed in time following a natural and typically divine order.

One of first major revolution in Systematics, the field of science that (very roughly) focused on making sense in this 'natural' order of living beings, was the work of the Swedish botanist Carl Linnæus (1707-1778). He developed in his books *Species Plantarum* and *Systema Naturae* a system for naming and classifying hierarchically organisms according to their similarities and differences that is still in use today. Since he offered to employ a two-part naming system for species, with the first part representing the genus and the second part defining the species, followed by a diagnostic description, this system has remained known as the binomial nomenclature (Linnæus 1753, 1758). The different levels in this 'Linnæan hierarchy' such as kingdoms, phyla, classes, orders, families, genera, and species are supposed to reflect the natural and harmonious order of the products of Creation in Linnæus's mind (Farber 2000). His system of classification allowed scientists to communicate more effectively and provided a foundation for the development of modern taxonomy, yet no genealogy between its well-ordered species was considered during his time.

The change of paradigm came a century later with the Theory of Evolution. In his milestone book *On the Origin of Species by Means of Natural Selection, or the Preservation of Favoured Races in the Struggle for Life* (Darwin 1859), Charles Darwin (1809-1882) provided massive and compelling evidence for the ongoing process of evolution and one of its major mechanism: natural selection. Its core idea is that all organisms shared a common ancestor and that diversity emerged though the principle of "descent with modification", when organisms evolve over time through the accumulation of random heritable changes at each generation that may provide a survival advantage in a given environment and be passed to the next generations. As such, he provided at the same time a mechanism to explain how species change over time (i.e., 'evolve'), how new species arise from existing ones, and how most of them go extinct at some point. Critically, he offered a new perspective to understand the 'natural order' of living beings described by his predecessors, that in this view reflects the evolutionary relationships across species, and can be summarized by the mean of an evolutionary tree (**Fig. 5**).

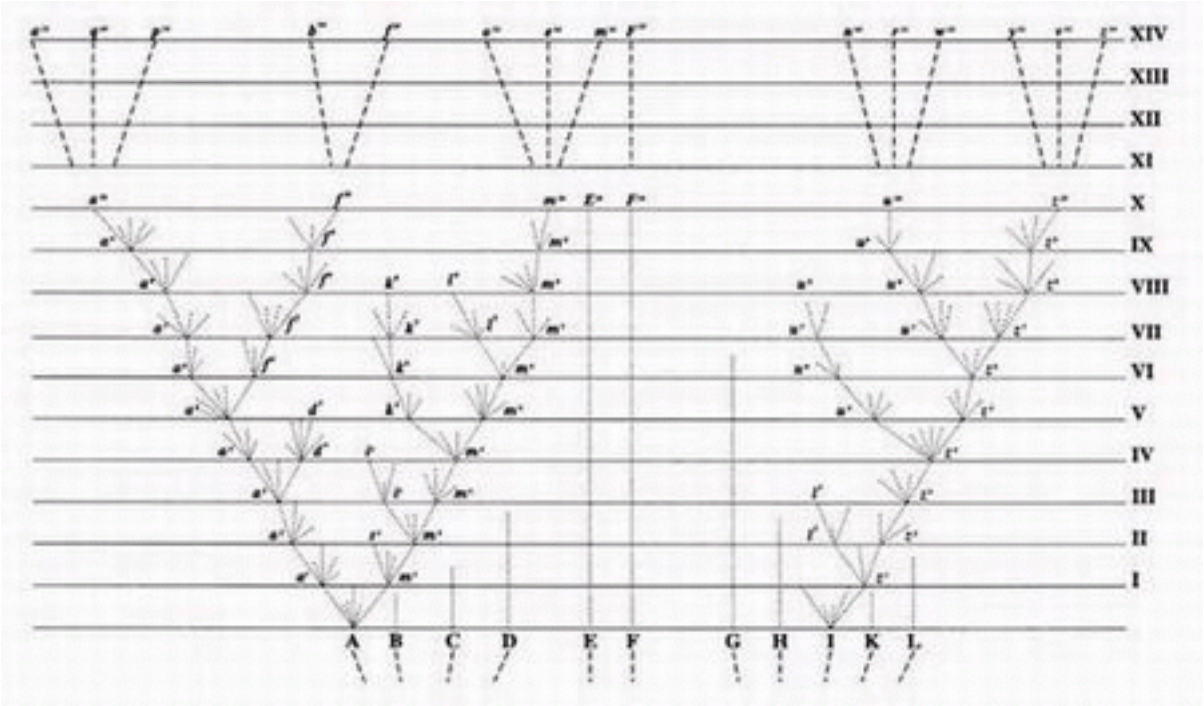

Figure 5: Darwin's sketch of evolutionary relationships among lineages from a hypothetical genus (labeled A–L on the horizontal axis) across numerous generations and time steps (labeled I-XIV on the vertical axis). This is the only illustration in the first Edition of *On the Origin of Species by Means of Natural Selection, or the Preservation of Favoured Races in the Struggle for Life* in 1859. It is particularly remarkable how it encapsulates at the same time the idea of descent with modification, but also the random appearance of variants, the extinction of many, and the selection of a few, typically the variants presenting the most divergent phenotype, thus limiting potential interspecific competition, between each evolutionary step.

In the wake of the Darwinian revolution, the figure of the phylogenetic tree has become the major representation of the evolutionary order of life. Nevertheless, it was not until the 1950's and the brilliant intuition of a German entomologist that a formal analytical framework was made available to construct and support the evolutionary hypotheses depicted by these phylogenetic trees. Willi Hennig (1913 - 1976) proposed that the hierarchical groups represented in phylogenetic trees were not build based on overall similarity among their components, but on the increasing number of shared derived states of traits among species, founding the cladistic method (Hennig 1950, 1965). In this perspective, the only valid supra-specific evolutionary units are the monophyletic groups formed by grouping of synapomorphies (i.e., shared derived states of traits), which are the only units that must be given a name (**Fig. 6**). As such, the long-established fishes, reptiles or protists were not to be considered as valid evolutionary groups. With this method, systematists were now able to clearly expose their hypotheses and test them in an objective and reproducible statistical framework using a

parsimony criterion (i.e., the most likely evolutionary tree is the one that involves the least number of state changes across all traits and species). Initially, Hennig's cladistic method was largely employed on morphological and anatomical data, but with the emergence and improvement of DNA sequencing, molecular data quickly stepped into the game.

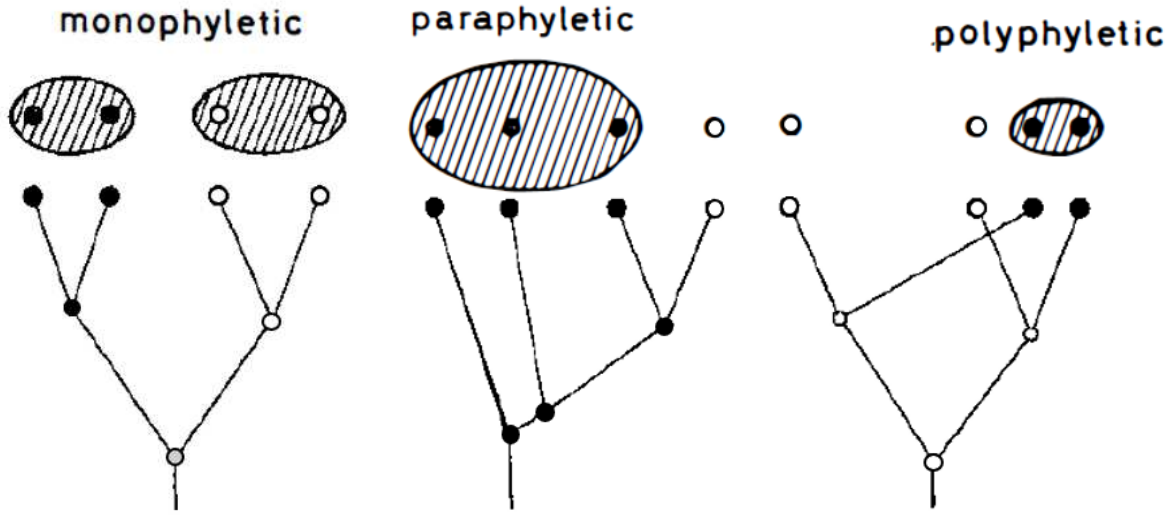

Figure 6: Schematic representation of the different groups formed by similarity of trait states (black or white) illustrating the core concept of cladistics. Contrary to previous hierarchical biologic classification, the only recognized evolutionary groups in cladistics are monophyletic groups regrouped on the basis of synapomorphies (i.e., shared derived states). Polymorphic groups are formed when grouping organisms that are similar by convergence (i.e., non-homologous states, not inherited from a common ancestor). Paraphyletic groups are formed when grouping organisms by synplesiomorphies (i.e., shared ancestral states). Modified from Hennig (1965).

The discovery of the structure of DNA in 1953 by Rosalind Franklin, and its publication by James Watson and Francis Crick (Watson & Crick 1953), revolutionized evolutionary biology, providing a foundation for the study of genetics and the mechanisms of inheritance. The development of increasingly efficient DNA sequencing techniques such as the Sanger sequencing (Sanger *et al.* 1977) later coupled with the Polymerase Chain Reaction (Mullis *et al.* 1992) opened doors for the use of molecular data in phylogenetics. The main asset of molecular data is that DNA and derivatives (RNA, proteins, …) are universal in the living world. Thus, molecular data enabled the investigation of evolutionary relationship at much greater taxonomic scales that morphological data, using routinely thousands of characters (i.e., the nucleotide sites). Meanwhile, the American biologist and statistician Joseph Felsenstein developed a probabilistic approach to the description of phylogenetic trees and their relation to molecular data based on substitution models describing rates of nucleotide changes along the tree branches. He proposed the maximum likelihood approach for constructing phylogenetic

trees (Felsenstein 1981), later completed with Bayesian inferences employing Monte Carlo Markos Chain algorithms (Yang & Rannala 1997; Larget & Simon 1999) that allowed to incorporate uncertainty and hypothesis testing in the framework of phylogenetic analyses (Felsenstein 1985; Huelsenbeck & Rannala 2004; Posada & Buckley 2004).

A major limit of molecular phylogenetics resides in the nature of DNA. There are only four types of nucleotides, thus four states possible for each position in the sequences. When nucleotide substitutions accumulate at a much faster rate than the rate of divergence between lineages, a phenomenon known as saturation, it becomes difficult to determine the true ancestral states, and differentiate homoplasy (i.e., similarity via convergence) from homology (i.e., similarity via inheritance), and thus to reconstruct the deep evolutionary relationships. Fortunately, the progress in DNA sequencing never stopped and a new generation of incredibly powerful high-throughput sequencing methods (Illumina (Bentley *et al.* 2008), Oxford Nanopore (Jain *et al.* 2016) , Ion Torrent (Rothberg *et al.* 2011), etc.) paved the way to the current era of phylogenomics (Delsuc *et al.* 2005).

Phylogenomics aims to reconstruct the evolutionary history of organisms based on the analysis of large-scale molecular dataset encompassing many genes, sometimes entire genomes, building upon the opportunities offered by high-throughput sequencing (Young & Gillung 2020). In parallel, the deployment of high-performance computing technologies has made it possible to process and analyze large amounts of genomic data in a relatively short period of time. Similarly to the last developments in the field of Biogeography, such breakthroughs have only been made possible because of the development and multiplication of open-access databases and data sharing platforms to store, manage and share this stupendous amount of molecular data generated on a daily basis by high-throughput sequencers around the world (Katz *et al.* 2022). The most massive one is the NCBI's GenBank (Benson et al., 2013; https://www.ncbi.nlm.nih.gov/) that centralizes and provides public access to annotated collection of DNA sequences from any organisms. Complementarily, the Barcode of Life Data System (BOLD; https://boldsystems.org/) is an online database that provides a comprehensive and centralized repository for DNA barcodes (i.e., genes used to identify taxa).

Altogether, phylogenomics has made it easier for researchers to access and analyze large comprehensive datasets, and provide more accurate and robust phylogenetic reconstructions to larger taxonomic scales, opening new opportunities to investigate patterns of diversification, divergence times and ancestral state reconstruction across the Tree of Life (Young & Gillung 2020). Evolutionary biologists can now use the statistical power of thousands of genes and

millions of nucleotide sites to resolve long-standing debates about the relationships among major groups of organisms, such as the origins of animals (Dunn *et al.* 2008), plants (Wickett *et al.* 2014), and even eukaryotes as a whole (Burki *et al.* 2020).

4 Biodiversity through the phenotypes (Chapter 3)

As previously discussed in this Introduction, the field of taxonomy has witnessed a formidable shift from the qualitative approach to describing phenotypic traits to integrated quantitative approaches mixing multiple data sources and methods to capture the complex multidimensional nature of phenotypic traits (Dayrat 2005). The new challenge for biologists is to find efficient ways to integrate these multiple sources of information. A crucial step resides in the automation of data acquisition processes in order to increase the rate of data generation and provide standardized outputs. Such outputs can be exploited in analytic pipelines to provide comprehensive and reproducible analyses, mimicking the strategies at play for geographic and molecular data. The field of phenomics has emerged from this realization, aiming to study organisms as collections of multidimensional phenotypes acquired with a wide range of quantitative and high-throughput methods in order to empower the exploration of relationships between genotypes, phenotypes and the environment (Bilder *et al.* 2009).

For instance, such large scale collections of phenotypic information allowed researchers to identify the combinations of plant functional traits proved evolutionary viable in today's terrestrial biosphere highlighting the strong trade-off driving plant evolution (Díaz *et al.* 2016), or to unravel the relationships between morphological and trophic diversity across virtually all species of birds (Pigot *et al.* 2020) Moreover, phenomics unlock the possibility to test the unfolding at large spatial scale of long-established hypothesis such as the thermal melanism hypothesis. This hypothesis claims that darker colors, produced by the accumulation of melanic pigments, should be positively selected in cold environments, particularly in ectothermic organisms whose internal temperature is varying according to external conditions (Clusella Trullas *et al.* 2007). Indeed, darker individuals are expected to heat up faster under similar light conditions because they absorb more radiation than lighter individuals, thereby benefiting from higher metabolic and physiological activities. This pattern has been supported historically in *Colias* pierid butterflies in North America (Watt 1968). Recently, phenomic approach have permitted its detection at large spatial and taxonomic scales for Eurasian vipers (Martínez-Freiría *et al.* 2020) and North American and European butterflies as a whole (Stelbrink *et al.* 2019; Kang *et al.* 2021).

In latest developments, phenomics have been applied to museum collection as a way to rediscover and value this immense biological patrimony thanks to high-throughput characterization of phenotypes, mostly based on computer-based image analyses (Lürig *et al.* 2021). As such, researchers have been able to obtain not only high-throughput multispectral data from specimen collections (**Fig. 7**; Chan *et al.*, 2022), but also automatized geometric morphometrics measurements (Porto & Voje 2020). The extension of such promising phenomic pipelines relies on our ability to build comprehensive open-access databases to store, manage and share phenomic data, similar to what has been undertaken for geographic and molecular data.

To date, no publicly available online database aims to aggregate and standardized data generated from high-throughput phenomic pipelines. Efforts have been mostly concentrated on building platforms aggregating information produced from collections of a specific institution such as the Data Portal of the Natural History Museum of the United Kingdom (https://data.nhm.ac.uk/) or the Museum National d'Histoire Naturelle de Paris (https://science.mnhn.fr/). Alternatively, initiatives from international scientific communities have focused on providing access to phenomic data on a restricted taxonomic group such as the Global Ant Database for ants (Parr *et al.*, 2017) or the LepTraits database for butterflies (Shirey *et al.* 2022). Next avenue for biodiversity research likely lies in the aggregation of all biodiversity data source in a single platform facilitating the collection, curation, organization, harmonization and sharing of this fundamental knowledge of life on Earth as envisioned by the Encyclopedia of Life project (Parr *et al.*, 2014; https://eol.org/).

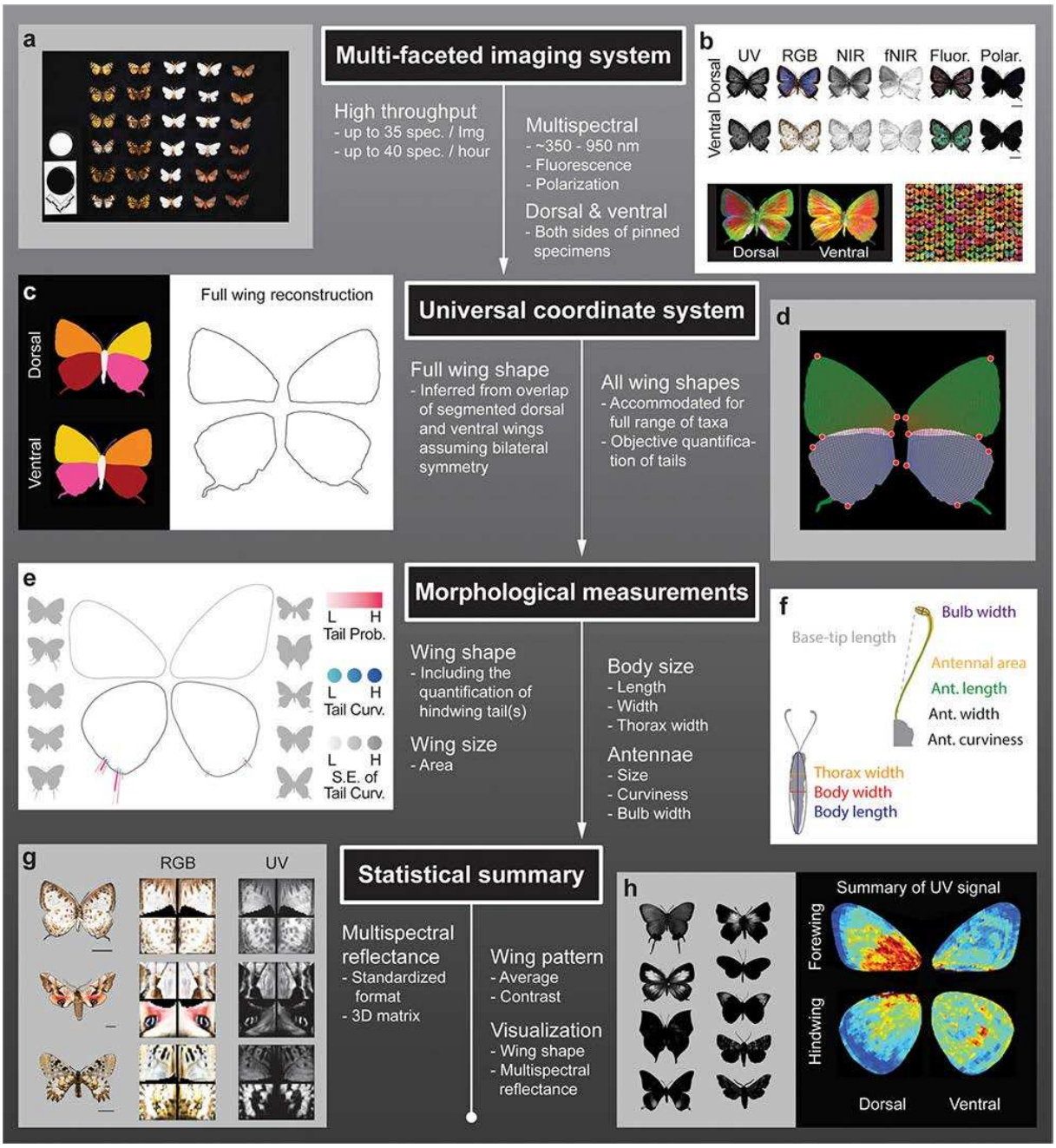

Figure 7: Summary of a high-throughput phenomic pipeline based on multi-faceted imaging methods applied on specimen collections. The workflow runs from top to bottom, starting with multispectral photos of specimens, and ending with the generation of multiple complex multivariate traits data encompassing the chromatic and morphologic aspects of the phenome. Figure from Chan *et al.*, 2022.

5 Ecological interactions: the fourth dimension

5.1 Crossing frontiers: towards an integrative study of biodiversity

The Big Data Science revolution have greatly contributed to the extension of our knowledge and understanding of biodiversity patterns throughout the Tree of Life. I presented in the previous sections a few examples of recent advances in the fields of Biogeography, Phylogenomics and Phenomics. Yet, such advances are not restricted to their own field of studies and many researchers now conduct ambitious studies at the interface of disciplines, integrating geographic, molecular and phenotypic data in the same analytic framework to answer complex questions about biodiversity on Earth.

Bridging phylogenetic reconstructions and biogeographic data, it becomes possible to address the mechanisms governing the generation of large scale biogeographic patterns such as the latitudinal biodiversity gradient in an evolutionary perspective. For instance, Rolland *et al.* (2014) built upon a comprehensive collection of distribution ranges of mammals species (Jones *et al.* 2009), a newly assembled supertree of the group (Fritz *et al.* 2009), and recently developed models to infer speciation and extinction rates across lineages and associated bioregions (Goldberg *et al.* 2011) to investigate variations in speciation and extinction rates across biomes. They showed that the latitudinal biodiversity gradient found in mammals can be explained by higher speciation and lower extinction rates in the Tropics, associated with dispersal into higher latitudes. Alternatively, Chazot *et al.* (2021) found that a similar latitudinal diversity gradient in brush-footed butterflies (Family Nymphalidae) cannot consistently be explained by differences in diversification rates across regions, but is mostly due to niche conservatism among tropical lineages. Moreover, improvement of computer performances now allows researchers to map phylogenetic diversity in space while encompassing numerous taxa and testing for significant patterns against randomization-based hypotheses (Mishler 2023). For instance, Murali *et al.* 2021 carried out a global analysis of phylogenetic endemism patterns of land vertebrates and their climatic drivers, allowing to identify crucial areas for the conservation of key elements of evolutionary history.

High throughput phenomic approaches combined with georeferenced specimens or remote sensing data now allow to efficiently map functional diversity at large spatial scale. Durán *et al.* (2019) used a combination of field measurements and remote sensing airborne images to infer functional canopy traits of tree communities alongside a broad temperature and elevation gradient across the Amazon and the Andes. Thereby, they were able to map variation

in functional diversity along this environmental gradient but also investigate the climatic drivers of such variation. For instance, they detected a signal of scale-dependent trait convergence consistent with environmental filtering acting on the phenotypes represented locally and corresponding to local adaptations to environmental conditions (Durán *et al.* 2019). This type of workflow combining phenomics and biogeographic data can also be applied to value museum collections. Zeuss *et al.* (2017) estimated body volume of European butterflies, damselflies and dragonflies species from images of digitalized and georeferenced specimens. They tested for the extension of the Bergmann's rule, which claim body size should increase in cold environments as a thermoregulatory advantage explained by a lower surface-to-volume ratio (Bergmann 1848), to ectothermic species. As such, they showed that the average body volumes of these communities of ectothermic insect species decreased significantly with latitude following temperature gradients contrasting with the predictions from the Bergmann's rule (Zeuss *et al.* 2017).

Finally, the increased availability of both molecular and phenotypic data allowed scientists to investigate evolution of traits in newly explored taxonomic and evolutionary scales. Building upon a crowd-sourced collection of 3D-scanned bill morphology and a species-level comprehensive phylogeny of birds, Cooney *et al.* (2017) explored the evolutionary trajectories of bird lineages in the bill morphospace. They found that rates of bill evolution vary among lineages while being globally stable through time. In particular, they highlighted the fact that bill evolution is characterized by few important rapid transitions followed by morphological packing (Cooney *et al.* 2017). Such macroevolutionary pattern underlies global scale adaptive radiations supporting the Darwinian (Reznick & Ricklefs 2009) and Simpsonian (Simpson 1944) ideas of microevolution within adaptive zones and accelerated evolution between distinct adaptive peaks. Beyond the investigation of tempo and mode of evolution, large-scale molecular and phenotypic data allow to reconstruct ancestral traits back to previously unexplored evolutionary times. For instance, thanks to international collaborative efforts aiming to gather plant phenotypic traits to an unprecedent taxonomic scale, we now dispose of a 3D model of the predicted ancestral flower of all Angiosperm plants (Sauquet *et al.* 2017).

5.2 Disentangling the Network of Life

Despite the exponential growth of data accessibility that allows the completion of ambitious studies merging large taxonomic, phenotypic and geographic scopes, there are still many aspects of biodiversity that remain poorly known and understood. In particular, the role

of ecological interactions in shaping large-scale biodiversity patterns is often overlooked in macroecological studies (Gaüzère *et al.* 2022; Windsor *et al.* 2023). Indeed, assessing global patterns of ecological interactions is challenging. The sampling of ecological interactions typically involved substantial costs in time and resources associated with the detection and characterization of the interactions such as in gut content analyses for trophic networks, records of flower visitation for pollination networks, curation of camera trap videos to identify plant-seed dispersers networks, etc. Although we witnessed recent international efforts to aggregate and standardize ecological interactions datasets in openly accessible databases (GloBI: Poelen *et al.* (2014); Interaction Web DataBase: www.ecologia.ib.usp.br/iwdb/; Web of Life: www.web-of-life.es), there are still many gaps in our global knowledge of the biogeography of ecological interactions (Poisot *et al.* 2021).

Yet, understanding the organization of ecological interactions at large spatial scales, and their effects on the patterns of biodiversity is essential. Ecological interactions affect directly the survival and reproductive success of species (Elton 1927), their dispersal abilities (Svenning *et al.* 2014), and organize the flux of nutrients across biological entities (Tilman *et al.* 2014), which in turn determine the structure, resilience and functioning of ecosystems as a whole (Grime 1997; Bascompte 2009; Schneider *et al.* 2016). Crucially in the context of climate changes, implementing ecological interactions in the big picture of biodiversity helps to improve our understanding of community dynamics to provide reliable predictions to inform conservation actions (Tylianakis *et al.* 2010; McDonald-Madden *et al.* 2016; Pollock *et al.* 2020). For instance, predictions of future species distributions are likely to be overestimated when biotic interactions are not implemented in the modeling framework (e.g., Flores-Tolentino *et al.* 2020).

Recent studies have tackled the challenge of integrating ecological interactions in biogeographic and macroecological studies. For instance, Gaüzère *et al.* (2022) built upon a recently gathered metaweb of European terrestrial vertebrates (Tetra-UE; Maiorano *et al.* 2020) to explore the diversity of trophic interactions at the continental scale. They highlighted how interaction diversity (i.e., the number of local trophic interactions) provides a complementary information to the functional and phylogenetic facets of biodiversity (Gaüzère *et al.* 2022). From an evolutionary perspective, Drury *et al.* (2020) explored the drivers of evolution of interspecific competition in birds. They showed that interspecific territoriality is widespread among birds and that its maintenance is strongly associated with hybridization and resource overlap during breeding season rather that habitat structure. They found that the modality of

territorial signals depended on the evolutionary age of the interacting species, with plumage phenotypes being mostly selected for interactions within-families, while songs appeared prominent in between-families interactions (Drury *et al.* 2020). Such studies highlight the importance of ecological interactions as both a unique component of biodiversity and a driver of trait evolution at large spatial and phylogenetic scales.

These two examples focus on mapping and investing the evolutionary consequences of antagonistic interactions (i.e., with a negative outcome for at least one of the interacting members) falling into the historical tradition of community and evolutionary ecology to focus on the interplay between antagonistic interactions (e.g., competition, predation) and common ancestry, and how this interplay drives both the assembly of communities and species trait evolution (MacArthur & Levins 1964; Pianka 1981; Brown & Maurer 1989; Webb *et al.* 2002; Kraft *et al.* 2007). However, many studies have recently extended this vision by documenting the importance of positive interactions in determining species coexistence and the stability of communities (Okuyama & Holland 2008; Elias *et al.* 2009a; Thébault & Fontaine 2010; Alexandrou *et al.* 2011; Mougi & Kondoh 2012; Hale *et al.* 2020), the coevolution of functional traits (Guimarães *et al.* 2011, 2017; Nuismer *et al.* 2013; Newman *et al.* 2014; O'Brien *et al.* 2021), the support of ecosystem functions such as pollination or seed dispersal (Millennium Ecosystem Assessment 2005), and the origins and maintenance of biodiversity (Bascompte & Jordano 2007; Gross 2008; Bastolla *et al.* 2009; Pascual-García & Bastolla 2017).

Therefore, my research work aims to contribute to resolve this imbalance (Elias *et al.* 2009a) by investigating the effect of mutualistic interactions on the spatial, phenotypic and evolutionary dimensions of biodiversity. To this end, I employ Müllerian mimicry, an emblematic case of mutualism, where co-occurring non-profitable prey species have evolved similar warning color patterns (i.e., aposematic patterns; Poulton 1890), thereby sharing the cost of educating local predators to their noxiousness (Müller 1879; Sherratt 2008), as a well-characterized and charismatic case study of mutualistic interactions shaping the spatial distributions of species, driving the evolution of the phenotypes, and affecting the assembly of species (Jiggins & Lamas 2016).

6 Müllerian mimicry as a case study

6.1 Color patterns under selection

Among the multiple facets of phenotypes, one of the most striking to the human eye is coloration (Sherratt *et al.* 2015). The evolution of colors, and their associated patterns (i.e., the organization of color patches) are under multiple selective pressures associated with abiotic environmental conditions, but mostly linked to the functions carried by the visual signal they transmit.

Coloration can be constrained by the abiotic environment, with certain colors providing a better fitness under local climatic conditions as described previously with the thermal melanism hypothesis in ectotherms linked to thermoregulation and immune defense abilities (Clusella-Trullas & Nielsen 2020). Color patterns also evolve under selective pressures applied by other organisms as long as they are involved in the transmission of an ecological signal. Those pressures can be intra-specific, meaning they are applied by conspecifics, typically the reproductive partners, or inter-specific, implying ecological interactions across species such as prey-predatory interactions.

Sexual selection is the most prominent example of intra-specific selection applied on coloration. Indeed, exuberant coloration can be positively selected as an honest signal of overall good health for an individual following the handicap principle (Zahavi 1975): color pigments are costly to produce, thus an individual (typically male) able to harbor greater displays of those costly conspicuous signals would be positively selected by its conspecific of the opposite sex (typically female). The famously conspicuous colors of the male Paradise birds are a textbook example of coloration driven by sexual selection (**Fig 8.B**; Owens & Short, 1995). Coloration can also be under diverging selection between closely-related sympatric species as it favors the recognition of conspecifics, thus limit reproductive interferences with other species (Le Roy *et al.* 2021).

Prey-predatory interactions notoriously affect the trait evolution of species as in the academic example of evolutionary arm-race between the gazelles and the cheetahs used to explain their running and evasive abilities (Hilborn *et al.* 2012). Such interactions can also strongly affect the evolution of coloration in prey classified under different ecological concepts according to the function fulfilled by their color pattern. Deimatic patterns refers to pattern involved in the scaring of predators, enabling inoffensive prey to escape predation attempts,

such as the colorful head frills displayed by fill-necked lizards facing predators (**Fig. 8.A**; Shine, 1990). Cryptic patterns refers to a type of camouflage were the prey is easily confounded with the background, reducing the ability of predators to detect them. A classic example in evolutionary biology described the increasing frequency of black forms of peppered moths (*Biston betularia*) during the industrial revolution in England in response to the darkening of tree bark due to industrial soot (Cook *et al.* 2012). Another type of camouflage is the case of masquerade, where undefended prey resemble inanimate models with no value for predators. For instance, some caterpillars of moths are known to closely resemble bird droppings which, combined with adaptive bending behaviors increasing the similarity, provides them with an efficient protection against predators (**Fig. 8.C**; Suzuki & Sakurai, 2015). Conversely, color patterns can be associated with true predatory-defense abilities as in the case of aposematic patterns (Poulton 1890). For instance, toxic dendrobatid frogs harbor highly conspicuous colors (**Fig. 8.D**) that act as warning signals for predators, which learned the hard way to associate their color patterns with toxicity (Symula *et al.* 2001).

Interestingly, crypsis and aposematism are based on opposite principles inducing contrasting modes of selection. Indeed, cryptic species rely on their ability to avoid being detected and individuals of those species benefit from the rarity of their phenotype in the community because predators are poorly trained to detect them. Therefore, the lowest the frequency of the phenotype in the community, the higher the fitness of the individual (Mappes *et al.* 2005), a process known as negative frequency-dependent selection. By contrast, aposematism relies on the conspicuousness of the color pattern, and the ability of predators to detect, recognize and associate such pattern with a negative experience due to the defense ability of the prey (e.g., toxicity, unpalability, evasiveness, etc.), leading them to avoid such prey. In this case, the process of predator learning is favored when encounters are common, thus when the frequency of the phenotype is high in the prey community. From the prey perspective, the more individuals share an aposematic pattern, the smaller the individual cost of educating predators. As such, aposematic patterns are under positive frequency-dependent selection favoring color pattern similarity not only within, but also across species (Müller 1879; Sherratt 2008), eventually leading to distant evolutionary convergence (Vences *et al.* 2003).

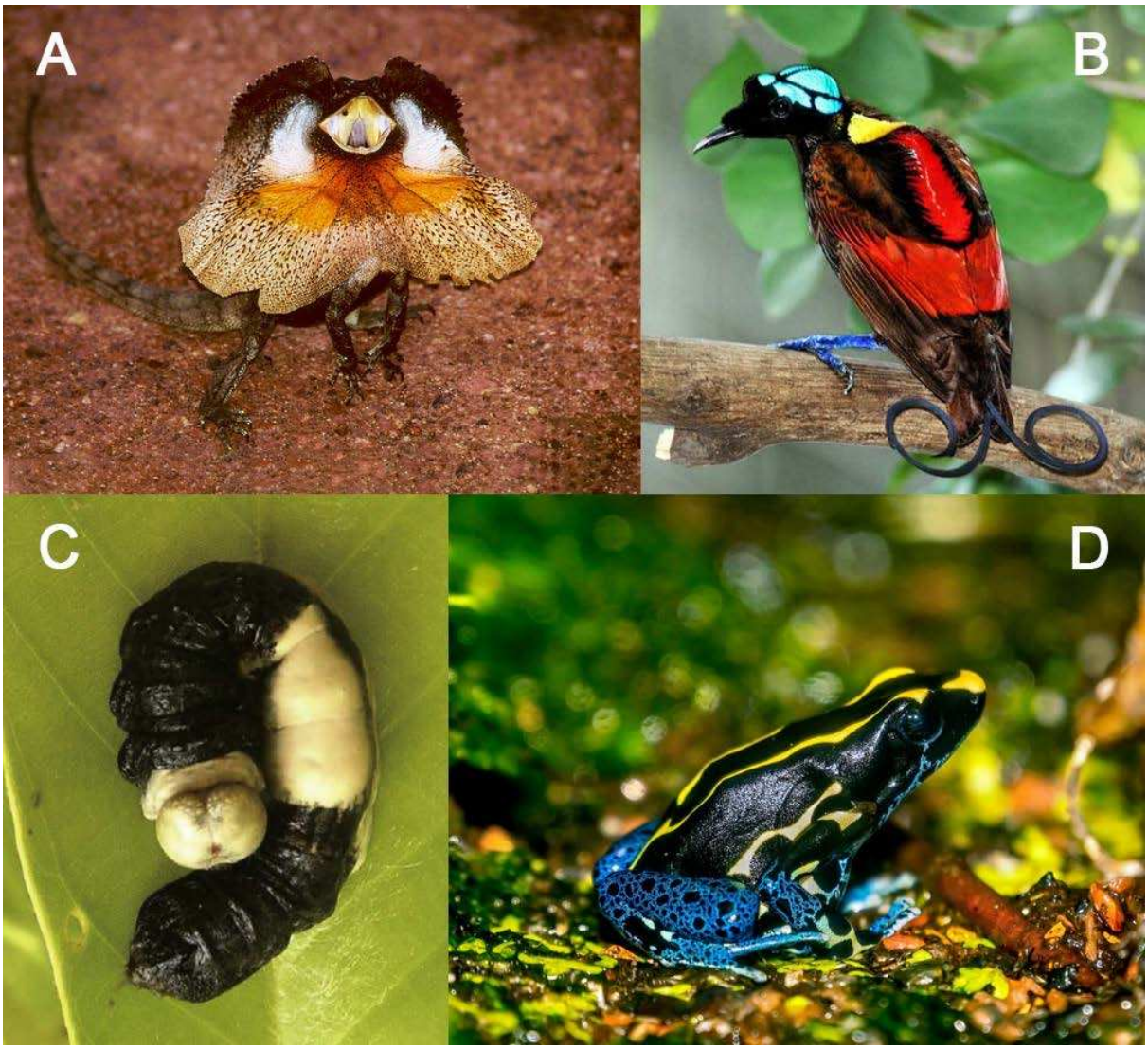

Figure 8: Diversity of color patterns under selection. (A) Frill-necked lizard *Chlamydosaurus kingii* in deimatic display showing off its colored head frills to deter predators. Credits: Miklos Schiberna. **(B)** Male specimen of Wilson's Bird of Paradise (*Cicinnurus respublica*) harboring extravagant colors shaped by sexual selection. Credits: Serhanoksay. **(C)** Caterpillar of the Asian moth *Macrauzata maxima* resembling a bird dropping as example of masquerade. Credits: T. Yamamoto. **(D)** Dyeing poison dart frog (*Dendrobates tinctorius*) displaying colorful examples of aposematic patterns associated with toxicity. Credits: Aquàrium de Barcelona.

6.2 Batesian and Müllerian mimicry in the light of evolution

Mimicry is the inter-specific consequence of aposematism. It describes similarity in phenotypes between organisms favored by natural selection and mediated by biotic interactions. Such group of phenotypically similar species are called ‘mimicry rings’ (Weismann 1904; Papageorgis 1975). When mimicry evolves in the context of defenses, it does so because at least one of the interacting organisms possesses efficient predatory-defense mechanisms. As such, it harbors aposematic patterns that predators learn to avoid through experience (Sherratt 2008).

Mimicry and one of its evolutionary mechanism was first formally described by Henri Walter Bates (1825 - 1892) during his nine-year expedition in the rainforests of Amazonia. He noticed that some unprotected palatable pierid butterflies (Dismorphiinae) were locally resembling the chemically protected unpalatable nymphalid butterflies (Ithomiini), and seems to benefit from fewer predation attempts from local birds, dragonflies and lizards (Bates 1862). These butterflies not only looked similar, but they also changed patterns across regions while preserving the local resemblance. Thus, he concluded that this phenomenon should be adaptive and he offered an explanation that conveniently supported the recently advertised Theory of Evolution (Darwin 1859). He argued that natural selection favored the local advergence (i.e., directional selection of one pattern towards a stable model) of wing patterns in mimetic pierids towards their local nymphalid models as it leads to higher survival due to lower attack rates. This form of mimicry where the mimic is unprotected is now called Batesian mimicry.

Although Bates noticed that protected heliconiine butterflies could be considered mimics of the protected ithomiines, he could not explain yet why such unpalatable species would converge to a similar warning signal. About twenty years later, Fritz Müller (1822 - 1897) provided an explanation supported by what is considered as the first mathematical model in evolutionary biology (Mallet 2001). Müller argued that pairs of unpalatable species gained mutualistic benefits from resemblance since both species would share the burden of losing individuals during predator learning. As such, aposematic patterns conveying the warning signals must be considered under positive frequency-dependence since the more frequent they are, the lower the cost per individual, and the most efficient the learning process of predators (Sherratt 2008). This form of mimicry where both interacting species are protected is now called Müllerian mimicry.

Batesian mimicry and Müllerian mimicry represent different types of ecological interactions with different evolutionary expectations. In Batesian mimicry, the unprotected mimics benefit from cooccurrence with the protected models, while the latter see their protection diminished since the presence of palatable prey harboring the same warning signal interferes with predator learning. This mimetic interaction is considered parasitic as it is positive for the Batesian mimic and negative for the model (Mallet 2001). In Müllerian mimicry, both interacting species are protected. Thus, cooccurrence increasing the frequency of their warning signal in the community is mutually beneficial for the species. As such Müllerian mimetic interactions are mutualistic. These differences in the nature of ecological interactions lead to antagonist coevolutionary scenarios. In the case of a pair of protected species, natural selection

is expected to favor the local convergence of patterns, increasing the efficiency of the warning signal, and the protection of the species involved in mutualistic Müllerian mimicry (Müller 1879). On the other hand, Batesian mimics and their models are predicted to be stuck in an eternal chase-away race with undefended mimics being selected for the advergence of their pattern towards the defended model, and the latter being selected to evolve away from their parasitic chasers (Huheey 1976). While theoretical models support the chase-away selection in Batesian systems (Franks *et al.* 2009), empirical supports are scarce (Akcali *et al.* 2018). My personal intuition is that chase-away selection rarely occurs because in natural communities models of Batesian mimics are typically involved in Müllerian interactions with other defended species (Joshi *et al.* 2017). As such, contradictory selective pressures imped phenotype divergence because Müllerian mimicry conversely selects for convergence and stability of the phenotype once convergence is achieved. Interestingly, parasitic Batesian and mutualistic Müllerian mimicry are now seen as the two extremes of a continuous spectrum with the extent of gains and losses from interactions depending on the relative noxiousness of interacting prey (Turner 1984; Balogh *et al.* 2008).

6.3 Mimicry in space

We exposed previously how Müllerian mimicry is predicted to drive color pattern convergence among defended species in local communities (Müller 1879). However, mimetic communities are typically composed of a variety of mimicry rings defined as sets of individuals sharing the same (honest or not) warning signals (Weismann 1904; Papageorgis 1975). This paradox is mostly explained by the fine-scale structuration of mimicry patterns along different ecological dimensions (Joron & Mallet 1998). Theoretical models have showed that heterogeneous communities of habitat-specialist predators that select locally for different optimal warning signals can induce a segregation of mimicry rings across microhabitats (Gompert *et al.* 2011; Birskis-Barros *et al.* 2021). In the field, mimetic neotropical butterflies demonstrate significant degree of segregation of mimicry rings across nocturnal roosting habitat height (Mallet & Gilbert 1995), flight height (Beccaloni 1997b; DeVries *et al.* 1997), and forest structures (Elias *et al.* 2008; Willmott *et al.* 2017) explaining the maintenance of local diversity of mimicry patterns.

At the regional scale, the distribution of mimetic species, as for any species, results from the interplay of neutral and selective processes such as stochastic dispersion, and adaptation to local environmental conditions. However, specific processes applies to Müllerian mimicry

systems. Indeed, the availability of interaction partners in potential areas of dispersion can affect the probability of success. Translocation experiments showed new patterns are counter-selected by local naïve predators as expected from frequency-dependent selection (Mallet & Barton 1989; Langham 2004), thus limiting the dispersal of mimetic species in areas where their pattern in still unknown. A result of such mechanism is the formation of a spatial mosaic of mimicry patterns bordered by suture zones where foreign patterns are counter-selected by predation from naïve predators (Thompson 2005; Sherratt 2006). On the field, such regional segregation of mimicry patterns has been detected along an altitudinal gradient, again for neotropical butterflies (Chazot *et al.* 2014). The geographic association of the different forms of *Heliconius erato* and *Heliconius melpomene* has been described and studied intensively (Brown Jr *et al.* 1974; Mallet 1993; Hines *et al.* 2011). However, how mimicry can affect the spatial distribution of entire clades of species at continental scales remains to be investigated, and will be one of the focus of this research work (see **Chapter 4**).

6.4 Müllerian mimicry as a case study for mutualistic interactions

Historically, community and evolutionary ecology have focused on the interplay between antagonistic interactions, such as competition and predation, and species relatedness to explain both the assembly of communities and species trait evolution (Pianka 1981; Brown & Maurer 1989; Webb *et al.* 2002; Kraft *et al.* 2007). However, more recently, many studies have extended this vision by documenting the importance of positive mutualistic interactions in determining species coexistence and the stability of communities (Thébault & Fontaine 2010; Mougi & Kondoh 2012; Hale *et al.* 2020), the coevolution of functional traits (Guimarães *et al.* 2011; O'Brien *et al.* 2021), and the origins and maintenance of biodiversity (Gross 2008; Pascual-García & Bastolla 2017).

Müllerian mimicry offers an ideal case study to pursue this rehabilitation and further investigate the effects of mutualistic interaction on the patterns of biodiversity. Contrary to many ecological interactions, Müllerian mimicry is believed to be relatively easy to document and straightforward to define: species that share a color pattern and coexist interact mutualistically, while those that harbor different color patterns do not. However, this view may be a little simplistic and this research work will seek to offer a new reproducible method to define these interactions when similarity is questionable (see **Chapter 3**).

Moreover, even if most of the empirical work on Müllerian mimicry has been focused on neotropical butterflies, instances of Müllerian mimicry can actually be found in many animal

lineages around the World. For instance, bees and stinging wasps all over the World are engaged in Müllerian mimicry (**Fig. 9.1.A-B**) with over a hundred described mimicry rings, involving a thousand species that belong to 19 aculeate Hymenoptera families (Chatelain *et al.* 2023). Similarly, lycid beetles have been suggested to form the largest Müllerian mimicry rings known up-to-date with more than 4000 species involved worldwide (Motyka *et al.* 2021). Outside of the insect world, one of the most emblematic example concerns dendrobatid frogs in the neotropical forests (**Fig. 9.1.C-H**; Symula *et al.* 2001). Müllerian mimicry also occurs in catfishes in South American rivers (Alexandrou *et al.* 2011), in Asian pit vipers (**Fig. 9.2.I-J**; Sanders *et al.* 2006), and between endemic toxic birds from New Guinea (**Fig. 9.2.K-L**; Dumbacher & Fleischer 2001).

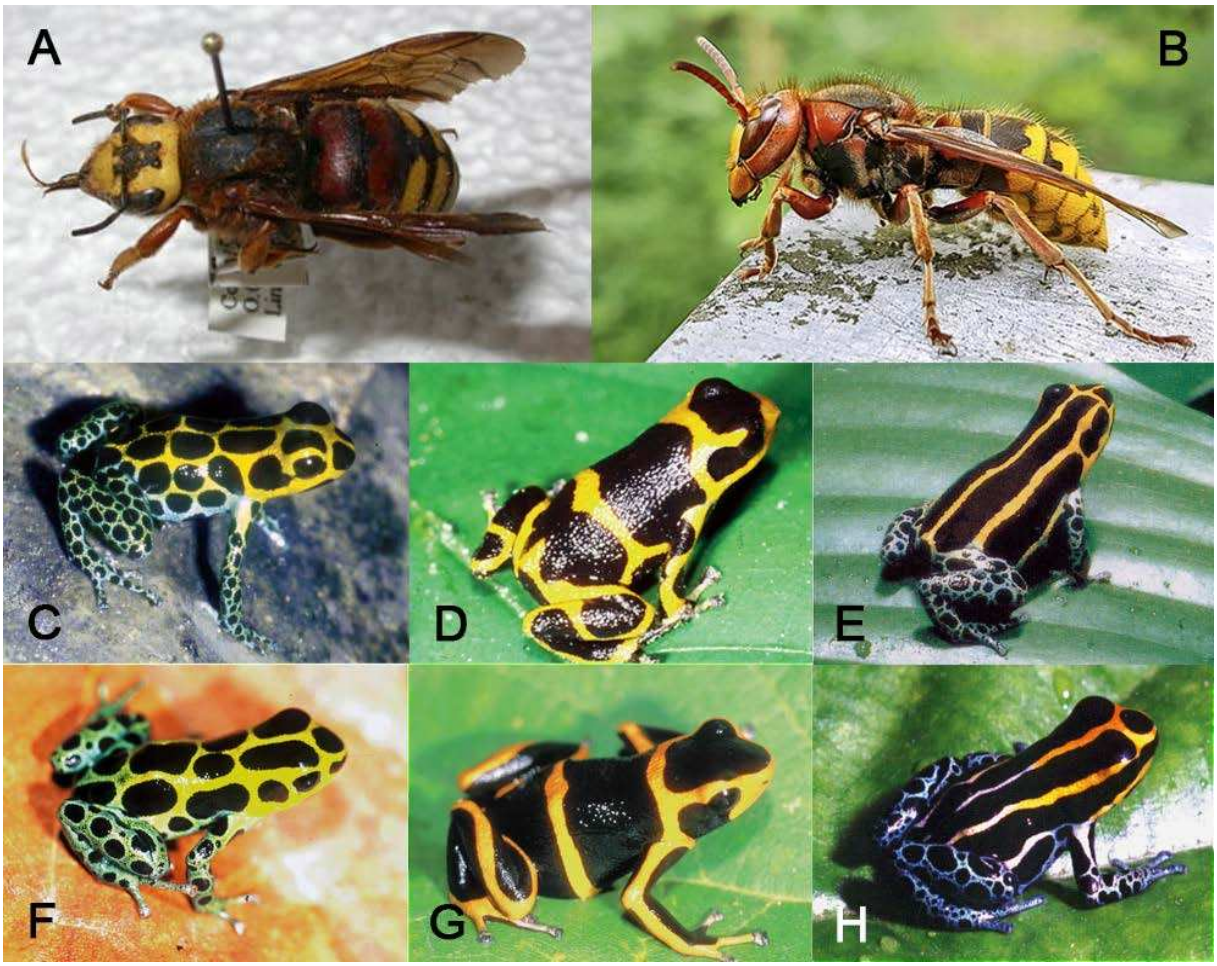

Figure 9.1: Müllerian mimicry across animal lineages. (A-B) Müllerian mimicry across families of Hymenoptera: **(A)** *Rhodanthidium sticticum*, a megachilid bee found in Turkey and close mimic to **(B)** the common European hornet (*Vespa crabro)* found all around Europe and beyond. Credits: Jelle Devalez, Bernard Sabatier. **(C-H)** Müllerian mimicry in dendrobatid frogs in Peru: C to E are all geographic morphs of *Dendrobates imitator* mimicking their local equivalent in others species such as **(F)** *Dendrobates variabilis* in Tarapoto, **(G)** *Dendrobates fantasticus* in Huallaga Canyon, and **(H)** *Dendrobates ventrimaculatus* in Yurimaguas. Credits: Symula et al. (2001).

Figure 9.2: Müllerian mimicry across animal lineages. (I-J) Müllerian mimicry in Asian pit vipers: **(I)** *Trimeresurus popeiorum* found in Kaeng Krachan National Park, Thailand, presenting the characteristic red band of **(J)** *Viridovipera gumprechti* found in a large portion of continental South-East Asia. Credits: Rushen, Andy Ana. **(K-L)** Müllerian mimicry in toxic pitohui birds of New Guinea: **(K)** Northern variable pitohui (*Pitohui kirhocephalus*) in its orange-brown morph matching patterns of **(L)** the hooded pitohui (*Pitohui dichrous*) in Varirata National Park, Papua New Guinea. Credits: Katerina Sam, John C. Mittermeier.

7 Ithomiine and heliconiine butterflies as model groups

Most studies that have so far attempted to describe and understand the mechanisms behind large-scale spatial patterns of neotropical diversity have focused on vertebrate and plant groups (Ter Steege *et al.* 2006; Weir 2006; Sedano & Burns 2010; Wesselingh *et al.* 2010; Hughes *et al.* 2013; Hutter *et al.* 2013; Bogoni *et al.* 2021). In comparison, macroecological studies about arthropods are scarcer because high-quality and high-density primary geographic information is typically lacking, especially in the Tropics. This realization is particularly striking given that arthropods may represent 70% of Earth species (Stork 2018), which had led geneticist J.B.S. Haldane to declare: "If He exists the creator has an inordinate fondness for beetles.". The relative lack of biodiversity data regarding arthropods in the Tropics illustrates the strong taxonomical and geographic biases still existing in the Wallacean shortfall described as the paucity of geographic information compare to the vastness of existing biodiversity (Lomolino 2004). Yet, Neotropical mimetic butterflies might be a counter-example.

We described earlier how neotropical butterflies, and particularly Ithomiini and Heliconiini have been instrumental in the emergence of the theory of mimicry in the late nineteenth century, thanks to the work of Henry Walter Bates (Bates 1862) and Fritz Müller (Müller 1879). The history of those two tribes of mimetic butterflies are entangled despite being separated by more than 80 My of evolution (Chazot *et al.* 2021). Indeed, as reported by Bates, those two tribes of toxic butterflies share mimicry patterns. As such, they are engaged in mutualistic Müllerian mimetic interactions, within tribes, but also between tribes (**Fig. 10**). They are even at the center of much larger mimetic interaction networks as species belonging to Pieridae, Papilionidae or even moth species share wing patterns identical to those harbored by Ithomiini and Heliconiini species (Beccaloni 1997a).

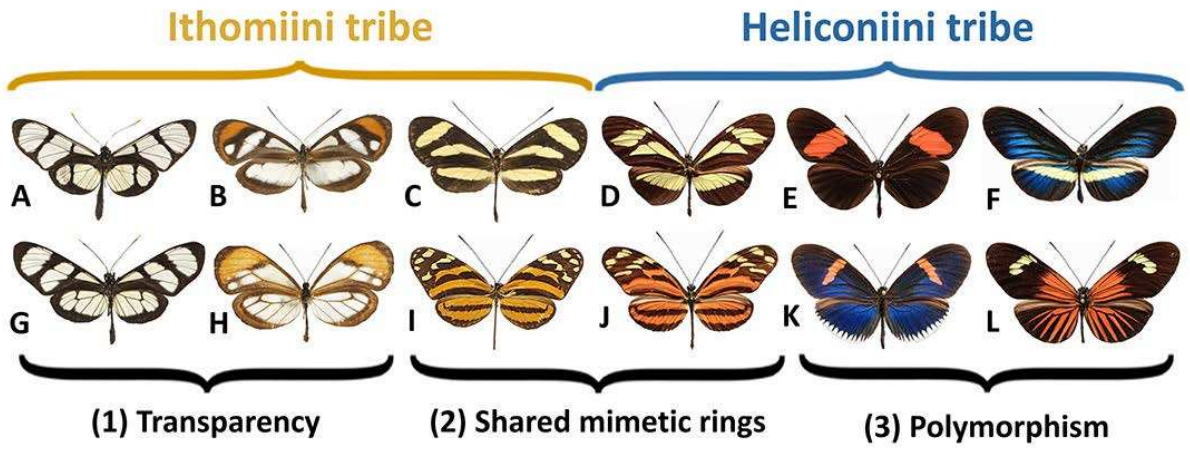

Figure 10: Diversity and convergence of wing patterns within and between ithomiine and heliconiine butterflies. Ithomiine butterflies display different degrees of transparency in several mimicry rings **(1)**, but also share mimicry patterns with Heliconiini **(2)**. Heliconiini, similarly to Ithomiini, demonstrate high degree of polymorphism, even within species as shown with examples from *Heliconius erato* **(3)**. From left to right and top to bottom: **(A)** *Methona confusa psamathe* **(B)** *Oleria gunilla lerdina* **(C)** *Aeria eurimedia pacifica* **(D)** *Heliconius nattereri* **(E)** *Heliconius erato adana* **(F)** *Heliconius erato chesteronii* **(G)** *Methona themisto* **(H)** *Pseudoscada florula aureola* **(I)** *Melinaea lilis imitate* **(J)** *Heliconius ismenius telchinia* **(K)** *Heliconius erato cyrbia* **(L)** *Heliconius erato emma*.

Ithomiines and heliconiines are both brush-footed butterflies (Nymphalidae), whose evolutionary history diverged when the Danainae sub-family, comprising the Ithomiini, split around 85 My ago from a group that would later gave birth to the Heliconiini (Chazot *et al.* 2021). Both tribes have a relatively similar stem age, estimated around 26 My, and are described as adaptive radiations considering their rapid diversification across the Neotropics (Ithomiini: Chazot *et al.* 2019; Heliconiini: Kozak *et al.* 2015). Nevertheless, they present important differences in their evolutionary history. While the Heliconiini tribe encompasses 8 genera, 77 species and around 457 subspecies (Kozak *et al.* 2015; Jiggins & Lamas 2016) spreading all

across America from Canada to Argentina (Rosser *et al.* 2015), Ithomiini comprises more than five times more taxonomic diversity with 396 documented species for around 1476 subspecies distributed among 42 genera and 10 subtribes mostly limited to the Neotropics, from Mexico to the Brazilian Atlantic forest (Chazot *et al.* 2019b). Both tribes occupy a diversity of habitats, but are mostly found in forests from sea levels up to 3500m in the Andes for some ithomiine species (Chazot *et al.* 2014). They are considered as the numerically dominant component of mimetic butterfly communities throughout their spatial range (Beccaloni 1997a).

All ithomiine and heliconiine butterflies are toxic to predators to some degree. However, how they gain their defenses at different life stages differs between the two tribes. Ithomiine caterpillars are highly specialized on Solanaceae plant species with a few of exceptions feeding on members of the Gesneriaceae and Apocynaceae (Willmott & Mallet 2004). However, contrary to most toxic butterflies that sequester toxic compounds from their hostplants, ithomiine species acquire most of the pyrrolizidine alkaloids (PAs) that provide them with chemical protection during the adult stage while feeding on fresh or rotten flowers and stems of Asteraceae and Boraginaceae. Surprisingly, almost only the male ithomiines gather the precious chemical compounds during foraging (Trigo & Brown Jr 1990). They use PAs as precursors for male pheromones as well as for toxin production (Brown Jr 1984; Schulz *et al.* 2004). Females mostly obtain their PAs during fecundation as the spermatophore transmitted by males is highly concentrated in PAs (Brown Jr 1984). On the other hand, heliconiine butterflies more classically obtain their toxic chemical compounds, mostly cyanogenic glucosides, from their hostplants (Castro & Zurano 2019). They are also highly specialized, but on passion vine species (Passifloraceae family) with which they are suspected to have coevolved in an adaptive mirror radiation (Jiggins & Lamas 2016, p.37). Additionally, heliconiines are able to synthetize their own toxins from digested amino-acids (Nahrstedt & Davis 1983).

As a final touch to their portrait, it is worth mentioning that an important portion of ithomiine species display different degrees of transparency on their wing (**Fig. 10.1**). As Lepidoptera (*lepis* = scale + *pteron* = wing), ithomiines achieve transparency though erection, or reduction of size and number of the scales that typically cover the membrane of their wing (Binetti *et al.* 2009), and the addition of nanostructures reducing light reflection (Siddique *et al.* 2015; Pinna *et al.* 2021; Pomerantz *et al.* 2021). Transparency can appear quite paradoxical for aposematic species whose survival strategy relies on conspicuousness rather than cryptic abilities. However, a recent study showed that these transparent sections are also involved in

the convergence of wing patterns across mimetic species, and thus can be part of the warning signal (Pinna *et al.* 2021), while also offering a primary cryptic defense against predation (Arias *et al.* 2019; McClure *et al.* 2019).

Ever since the initial expeditions of Bates and Müller, ithomiine and heliconiine butterflies have fascinated scientists who have continued to collect them on the field, and accumulate extensive phenotypic and genetic information. As such we now dispose of the high-quality data needed to carry out large-scale analyses with comprehensive occurrence databases, specimen collections to extract genetic sequences, and databases of wing pattern images. Therefore, they appear as ideal models to explore variation in biodiversity patterns from the phenotypic, geographic and phylogenetic perspectives in the context of mutualistic interactions, illustrated here by Müllerian mimicry.

8 Main questions and objectives

During the course of this research work, I employ Müllerian mimicry in ithomiine and heliconiine butterflies as a case study to explore the effect of mutualistic interactions on biodiversity patterns. I focus mostly on recent methods and approaches developed in the framework of Biodiversity informatics to handle large datasets and accommodate multivariate quantitative information.

In the **first Chapter**, I explore biodiversity patterns in **space**. I build upon a comprehensive database of ca. 30,000 georeferenced occurrences of ithomiine butterflies at continental scale gathered from multiple expert-curated sources and employ species distribution models to map the different facets of current Ithomiini biodiversity. As such, I intend to test for the correlation of the multiple facets of ithomiine diversity, as well as to identify areas of evolutionary and ecological importance for conservation, and evaluate their overlap with current anthropogenic threats.

In the **second Chapter**, I explore biodiversity patterns in **time.** I employ state-of-the-art phylogenomics approaches on a large molecular dataset of ca. 11,000 genes across 368 species out of the 396 documented (i.e., 92.3%) in order to resolve and support deep evolutionary relationships in ithomiine butterflies. As such, I aim to generate a phylogeny that will be employed as a stable tool for future macroevolutionary analyses of Ithomiini evolution.

In the **third Chapter**, I propose a new method to explore patterns of diversity through **phenotypic variation** based on the quantification of the perception of wing pattern variation in

heliconiine butterflies. I develop a Citizen Science project in order to gather perception information from a diversity of sources, and introduce a machine learning algorithm that converts triplets of relative perceptual distances into a perceptual space. I illustrate the versatility of such approach to explore the structure of phenotypic diversity at multiple spatial scale. First, I investigate the global structure of variation in heliconiine wing patterns and map phenotypic diversity at the continental scale. Second, I address the delimitations of mimicry rings in local communities to unravel ecological interactions among mimetic species. Overall, I intend to provide a new generic tool for the exploration of biodiversity that could be included in phenomic pipelines to quantify phenotypic variation in any visual signals through perception.

Finally, in the **fourth Chapter**, I offer to link **all three dimensions** in an integrative perspective investigating the effect of ecological interactions acting through **phenotype similarity** (i.e., Müllerian mimicry) on large scale **spatial** and **evolutionary** patterns. I aim to test for the unfolding at large spatial scale of the predictions of Müller's model regarding convergence of species harboring aposematic patterns. Specifically, I use phylogenetic comparative analyses to test for spatial congruence and climatic niche convergence among comimetic species of ithomiine butterflies as a way to illustrate the importance of mutualistic interactions into shaping macroecological and evolutionary patterns.

CHAPTER 1

Anthropogenic pressures coincide with Neotropical biodiversity hotspots in a flagship butterfly group

Maël Doré[1,2], Keith Willmott[3], Boris Leroy[4], Nicolas Chazot[5], James Mallet[6], André V. L. Freitas[7], Jason P. W. Hall[8], Gerardo Lamas[9], Kanchon K. Dasmahapatra[10], Colin Fontaine[2], and Marianne Elias[1]

[1]*Institut de Systématique, Evolution, Biodiversité, MNHN-CNRS-Sorbonne Université-EPHE-Université des Antilles, Muséum national d'Histoire naturelle de Paris, 45 Rue Buffon, 75005, Paris, France*

[2]*Centre d'Ecologie et des Sciences de la Conservation, UMR 7204 MNHN-CNRS-Sorbonne Université, Muséum national d'Histoire naturelle de Paris, 45 rue Buffon, 75005, Paris, France*

[3]*McGuire Center for Lepidoptera and Biodiversity, Florida Museum of Natural History, University of Florida, Gainesville, FL, United States of America*

[4]*Unité Biologie des Organismes et Ecosystèmes Aquatiques (BOREA UMR 7208), Muséum National d'Histoire Naturelle, Sorbonne Universités, Université de Caen Normandie, Université des Antilles, CNRS, IRD, Paris, France*

[5]*Swedish University of Agricultural Sciences, Uppsala, Sweden*

[6]*Dept of Organismic and Evolutionary Biology, Harvard University, Cambridge, MA, United States of America*

[7]*Departamento de Biologia Animal and Museu da Biodiversidade, Instituto de Biologia, Universidade Estadual de Campinas, 13083-862 Campinas, São Paulo, Brazil*

[8]*Department of Entomology, National Museum of Natural History, Smithsonian Institution, Washington, DC 20560-0127, United States of America*

[9]*Museo de Historia Natural, Universidad Nacional Mayor de San Marcos, Lima, Peru*

[10]*Dept of Biology, University of York, Wentworth Way, Heslington, UK*

Reference:

Doré, M., Willmott, K., Leroy, B., Chazot, N., Mallet, J., Freitas, A. V. L., Hall, J. P. W., Lamas, G., Dasmahapatra, K. K., Fontaine, C., & Elias, M. (2022). Anthropogenic pressures coincide with Neotropical biodiversity hotspots in a flagship butterfly group. Diversity and Distributions, 28(12), 2912–2930. https://doi.org/10.1111/ddi.13455

Author contributions:

This paper is the result of over 30 years of collaborative efforts to collect, describe and classify Ithomiini butterflies. MD and ME conceived the study and designed the analyses. ME, KW, AVLF, JM, KK, & JH provided occurrence data. MD aggregated and curated the database, wrote the R scripts, carried out the analyses, produced all maps, results and figures, and led the manuscript writing. All authors critically contributed to the article and gave final approval for publication.

Abstract

The biodiversity crisis has highlighted the need to assess and map biodiversity in order to prioritize conservation efforts. Clearwing butterflies (tribe Ithomiini) have been proposed as biological indicators for habitat quality in Neotropical forests, which contain the world's richest biological communities. Here, we provide maps of different facets of Ithomiini diversity across the Neotropics to identify areas of evolutionary and ecological importance for conservation, and evaluate their overlap with current anthropogenic threats.

We ran species distribution models on a dataset based on 28,986 georeferenced occurrences representing 388 ithomiine species to generate maps of geographic rarity, taxonomic, phylogenetic, and Müllerian mimetic wing pattern diversity. We quantified and mapped the overlap of diversity hotspots with areas threatened by or providing refuge from current anthropogenic pressures.

The eastern slopes of the Andes formed the primary hotspot of taxonomic, phylogenetic and mimetic diversity, with secondary hotspots in Central America and the Atlantic Forest. Most diversity indices were strongly spatially correlated. Nevertheless, species-poor communities on the Pacific slopes of the Andes also sheltered some of the geographically rarest species. Overall, tropical montane forests that host high species and mimetic diversity as well as rare species and mimicry rings appeared particularly under threat.

Remote parts of the Upper Amazon may act as refuges against current anthropogenic pressures for a limited portion of Ithomiini diversity. Furthermore, it is likely that the current threat status may worsen with ongoing climate change and deforestation. In this context, the tropical Andes occupy a crucial position as the primary hotspot for multiple facets of biodiversity for ithomiine butterflies, as they do for angiosperms, tetrapods, and other insect taxa. Our results support the role of ithomiine butterflies as a suitable flagship indicator group for Neotropical butterfly diversity, and reinforce the position of the tropical Andes as a flagship region for biodiversity conservation in general, and insect and butterfly conservation in particular.

Keywords

anthropogenic pressures, biodiversity hotspots, geographic rarity, Human Footprint, human impacts, Ithomiini butterflies, Müllerian mimicry, phylogenetic diversity, species richness.

1 Introduction

The global biodiversity crisis is a critical environmental issue (IPBES 2019a) with unprecedented rates of species loss across multiple taxonomic groups, now referred to as the sixth mass extinction (Barnosky *et al.* 2011; Ceballos *et al.* 2015). Such species loss significantly alters biodiversity patterns and affects ecosystem functions worldwide. In particular, there is growing evidence for recent massive declines in insects (Cardoso *et al.* 2020; Eggleton 2020; Montgomery *et al.* 2020), which represent the bulk of current biodiversity (Mora *et al.* 2011; Stork 2018). This loss is concomitant with the global increase in human pressures on ecosystems, with currently 75% of the planet's non-frozen land surface impacted (Venter *et al.* 2016b). These alarming trends are compelling scientists to better assess and map biodiversity in order to prioritize conservation efforts given limited time and resources (Brooks *et al.* 2006).

One early approach towards identifying global priority areas for conservation was the delimitation of biodiversity hotspots (Myers *et al.* 2000): areas with high levels of vascular plant species richness and endemism, and significant loss of primary natural habitats. The Neotropics encompass seven of these biodiversity hotspots, including the richest of them: the Tropical Andes (Myers *et al.* 2000). However, it is not known how well such hotspots, identified on the basis of vascular plant diversity and confirmed for vertebrates, provide adequate surrogates for the diversity of other taxa, especially insects (Stork & Habel 2014). Indeed, georeferenced primary biodiversity data for insects, particularly in the Neotropics, are very scarce due to the challenges of collecting, digitalizing and verifying taxonomic identifications for records covering often inaccessible, remote regions (Short *et al.* 2018; Stork 2018). Moreover, whether species richness and endemism adequately reflect other facets of biodiversity such as phylogenetic and functional diversity may depend on the group considered (Prendergast *et al.* 1993; Williams *et al.* 1996; Allouche *et al.* 2006; Devictor *et al.* 2010; Mazel *et al.* 2014; Zupan *et al.* 2014; Albouy *et al.* 2017). There is therefore an urgent need to explore to what extent existing hotspots identified for well-studied taxa coincide with those of other less well-known groups, and how well those hotspots represent facets of biodiversity beyond species richness and endemism. Here, we tackle this issue by investigating the spatial distribution of different metrics of biodiversity in an integrative assessment that covers its multifaceted nature (Pollock *et al.* 2017, 2020). We focus our assessment on a diverse insect

group, the butterfly tribe Ithomiini Godman & Salvin, 1879 (Nymphalidae: Danainae), in the world's biologically richest region, the Neotropics.

The tribe Ithomiini comprises 396 described species distributed among 42 genera and 10 subtribes (Chazot *et al.* 2019b). These butterflies form diverse communities in humid forests from sea level to 3000 m, throughout the Neotropics. Their habitats are threatened by high rates of deforestation associated with cattle ranches, soybean and oil palm plantations, as well as industrial logging, mining, and road building (Armenteras *et al.* 2017; Fearnside 2017; Sonter *et al.* 2017; Rajão *et al.* 2020). In this context, ithomiine butterflies have been proposed as indicator species for habitat quality and local butterfly diversity (Beccaloni & Gaston 1995; Brown Jr 1997; Uehara-Prado & Freitas 2009 but see Brown & Freitas 2000). Ithomiini also represent the most diverse radiation of aposematic and Müllerian mimetic butterflies, whereby co-occurring unpalatable species display similar wing color patterns that advertise their distastefulness to predators. Müllerian co-mimetic species interact mutualistically, because they share the cost incurred during the learning process of predators (Müller 1879; Joron & Mallet 1998; Sherratt 2008). All Ithomiini species engage in Müllerian mimicry, and drive mimicry in other distantly related groups of Lepidoptera (Beccaloni, 1997; Brown Jr. & Benson, 1974). Remarkably, many ithomiines have partly transparent wings (Papageorgis 1975; McClure *et al.* 2019; **Fig. 1a**), which has inspired their common name of 'clearwing' butterflies. Overall, ithomiine butterflies combine their potential role as biological indicators with positive public image (e.g., Barua *et al.* 2012; Sumner *et al.* 2018), making them candidate flagship species for conservation in the Neotropics. Previous studies have already investigated the historical biogeography of the tribe. Ithomiini likely originated in the eastern Andean foothills and a major clade, composed of the five most species-rich subtribes and comprising 80% of species, diversified in Central Andes 20 to 10 My ago (Chazot *et al.* 2019b). Those areas, which harbor heterogeneous landscapes favoring speciation, also coincide with known hotspots of species richness for three diverse ithomiine genera (*Ithomia*, *Napeogenes*, and *Oleria*; Chazot *et al.* 2016b). However, patterns of species diversity remain to be documented at the level of the entire tribe, across the Neotropics. Similarly, patterns of phylogenetic diversity, geographic rarity, and mimicry richness remain largely uncharacterized at such scales.

Phylogenetic diversity has become a fundamental component of biodiversity assessments that addresses the evolutionary distinctiveness of species assemblages (Faith 1992). It is recognized by the Intergovernmental Science-Policy Platform on Biodiversity and Ecosystem Services (IPBES) as a key indicator for the maintenance of options in nature's

contribution for people (IPBES 2019a), and is included in conservation tools such as the EDGE index for Evolutionarily Distinct and Globally Endangered species (Isaac *et al.* 2007). High phylogenetic diversity reflects the presence of species with distinctive evolutionary pathways, which provide a proxy for evolutionary novelties of high value for conservation (Faith 2018).

Geographic rarity is another component of biodiversity that relates to the spatial dimension of rarity, with species with restricted distributions being considered rare compared to species with wider ranges (Rabinowitz 1981). Species with small geographic ranges can support original functions in ecosystems (Mouillot *et al.* 2013), while they often face higher risks of extinction (Purvis *et al.* 2000; Cardillo *et al.* 2008; Böhm *et al.* 2016). Species range size is therefore commonly incorporated into diversity indices (Jetz *et al.* 2014; Maritz *et al.* 2016; Gumbs *et al.* 2020). Mapping species geographic rarity provides an additional tool for conservation prioritization (Cadotte & Davies 2010), as another complementary facet of diversity patterns linked to species vulnerability and areas of endemism.

Biotic interactions, although rarely integrated in biodiversity assessments, represent the architecture of life that reflects the interdependence of all units of biodiversity (Bascompte 2009). For example, mutualistic interactions can shape species distributions and community composition (Sherratt 2006; Duffy & Johnson 2017), affecting ecosystem stability (Pascual-García & Bastolla 2017; Hale *et al.* 2020), and supporting ecosystem services such as pollination function or seed dispersal (Millennium Ecosystem Assessment 2005). Müllerian mimicry systems, such as ithomiine butterflies, provide an excellent opportunity to study mutualistic interactions, because interacting species can be identified through their similarity in warning patterns. Müllerian mimicry is known to affect individual fitness and constrain species distribution (Mallet & Barton 1989; Kapan 2001; Langham 2004; Sherratt 2006; Chazot *et al.* 2014; Aubier *et al.* 2017). Additionally, mimetic species form adaptively-assembled mutualistic communities that are predicted to suffer more from community disassembly due to the loss of those mutualistic interactions (Toby Kiers *et al.* 2010), and to be more sensitive to co-extinction cascades (Dunn *et al.* 2009). Therefore, Müllerian mimicry systems provide opportunities to map patterns of mimicry richness and geographic rarity, which reflect the distribution of mutualistic interactions in space, a component of functional diversity that is particularly relevant for conservation.

In this study, (1) we provide modeled distribution maps of taxonomic, phylogenetic and mimetic diversity as well as geographic rarity, for the entire tribe Ithomiini across the

Neotropics, in order to identify biodiversity hotspots as areas of both evolutionary and ecological importance for conservation; (2) we evaluate the spatial relationships among those facets of Ithomiini diversity; (3) we assess current anthropogenic threats to Ithomiini biodiversity hotspots, highlighting risk areas with high anthropogenic pressures, and potential refuges with currently low levels of human influence.

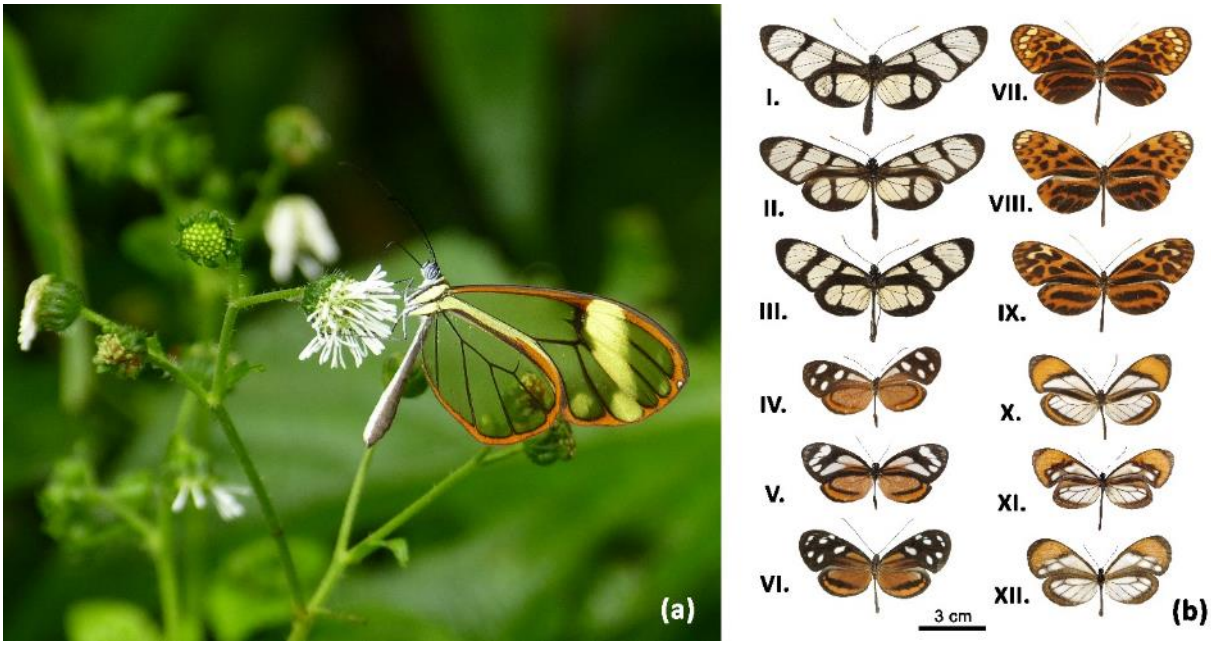

Figure 1: Wing patterns in ithomiine butterflies. (a) Specimen of *Hypomenitis libethris* harboring the wing pattern LIBETHRIS with transparent areas. Photo credits: Andrew Neild, 2016. (b) Illustration of the convergence of wing patterns across Ithomiini. Mimicry ring CONFUSA: *Methona confusa psamathe* (I), *Thyridia psidii ino* (II), *Methona themisto* (III). Mimicry ring ILLINISSA: *Oleria ilerdina priscilla* (IV), *Napeogenes sylphis ercilla* (V), *Hyposcada illinissa illinissa* (VI). Mimicry ring MAELUS: *Melinaea satevis cydon* (VII), *Hypothyris anastasia anastasina* (VIII), *Hypothyris fluonia pardalina* (IX). Mimicry ring AURELIANA: *Napeogenes sylphis corena* (X), *Hypoleria aureliana* (XI), *Pseudoscada florula aureola* (XII). Photo credits: Nicolas Chazot, 2015.

2 Methods

2.1 Data sources

We compiled from multiple sources an initial dataset of 28,986 georeferenced occurrences for 388 ithomiine butterfly species in their natural habitats, out of the 396 known species, spanning 25 countries across the Neotropics (see maps of occurrences, sampling effort, sampling completeness and bioregions in **Fig. S1.1, S1.2, S1.3 & S1.4**). This dataset provided 19,271 species-grid-cell records for distribution modeling at a 0.25° x 0.25° spatial resolution

after removing duplicate records from single grid cells, which are available from Zenodo at 10.5281/zenodo.4696055. The data come from fieldwork by the authors over the past five decades, and records from over 60 museums and private collections detailed in the online archive metadata. Each record is associated with its location, its taxonomic identity, and its mimicry ring membership (i.e., a wing color pattern shared by individuals reflecting mutualistic interactions). The current classification of wing patterns presents 44 mimicry rings (**Fig. S2.5**) updated from previous works (Beccaloni, 1997; Chazot *et al.,* 2014, 2019; Elias *et al.,* 2008; Jiggins *et al.,* 2006; Willmott & Mallet, 2004).

Sets of co-mimetic species (i.e., sharing a wing pattern) form mimicry rings (**Fig. 1b**). Most Ithomiini species comprise several to many subspecies that may belong to distinct Müllerian mimicry rings. Additionally, some subspecies show a sexual dimorphism with males and females belonging to different mimicry rings. Since we intended to map mimicry ring distribution as well as species distribution, we defined Operational Mimicry Units (OMUs) as the set of individuals within the same species that shared the same mimicry pattern. An OMU may either be equivalent to an entire species, if all individuals of all subspecies of that species share the same pattern, or it may represent individuals from a smaller group of subspecies that share a common mimicry pattern, in which case a single species may be represented by multiple OMUs. A total of 783 OMUs were used as modeling units for distribution models (complete list in ***SI Appendix 4***). The mimicry classification of all 1,511 subspecies is available from Zenodo at 10.5281/zenodo.5497876.

To compute indices of phylogenetic diversity, we used a recently published time-calibrated phylogeny of the Ithomiini (Chazot *et al.* 2019; **Fig. S3.6**) which represents 339 out of the 388 species with georeferenced records.

2.2 Data analyses

2.2.1 Species Distribution Modeling (SDM)

In order to map the current distributions of ithomiines, we developed species distribution models (SDMs) relating occurrence data with a set of environmental variables. We describe our SDM methods following the ODMAP (Overview, Data, Model, Assessment, Prediction) protocol for species distribution models (Zurell *et al.* 2020). Here, we provide the Overview of the distribution models while the remaining ODMAP sections, providing details in modeling

steps, justifications for modeling choices and a more in-depth discussion about potential caveats and limits, are detailed in ***SI Appendix 5***.

We aimed to model the current distribution of species and mimicry rings, as well as to infer the current patterns of geographic rarity and taxonomic, phylogenetic, and mimicry ring diversity (as described further below) for the whole Ithomiini tribe. We proceeded as follows: (1) we retrieved environmental predictors of Ithomiini distribution, (2) we obtained multiple environmental suitability maps for each OMU employing a set of SDM algorithms, (3) we derived for each OMU a median ensemble model depicting its modeled distribution, (4) we stacked these modeled distribution maps in order to obtain in each pixel the predicted occurrence of OMUs, while observed binary maps of OMU with less than six occurrences were included directly at this step, then we (5) derived species and mimicry ring distribution maps and compute various taxonomic, phylogenetic and mimicry diversity and geographic rarity indices (**Fig. 2**).

Our models encompassed the entire distribution of the tribe in the Neotropics (Longitude 120° E - 30° E, Latitude 37° S – 28° N) at a 0.25° x 0.25° spatial resolution. Thus, each quarter-degree grid cell (hereafter, pixel) represents a virtual community of ca. 27.8 km × 27.8 km. This resolution is appropriate for niche models based on large scale predictors such as climate (McGill, 2010), limits commission errors (Di Marco *et al.* 2017), and appears sufficient to identify broad geographic patterns of diversity at a scale relevant to biodiversity conservation (e.g., Roll *et al.* 2017; Gumbs *et al.* 2020; Abreu-Jardim *et al.* 2021; Robuchon *et al.* 2021). We selected climate, represented by annual temperature and humidity levels and seasonality (MERRAclim v.2.0; Vega *et al.,* 2017), elevation (SRTM Dataset v.4.1; Farr *et al.,* 2007) and vegetation cover (GLCF; Sexton *et al.,* 2013), as environmental predictor variables for distribution modeling. Indeed, these environmental dimensions have been regarded as important in determining large-scale distribution patterns and structuring ithomiine communities (Beccaloni, 1997; Chazot *et al.,* 2014).

We fitted SDMs for 563 OMUs for which we had at least six occurrences available (71.9% of OMUs, encompassing 335 species, i.e. 86.3% of species with known occurrences). We included the remaining 220 OMUs (28.1%) in stacks as binary rasters of presences-absences. We fitted SDMs in *biomod2* v.3.4.6 (Thuiller *et al.* 2020) using three machine learning algorithms to cope with small sample sizes: Random Forest, Generalized Boosted Models, and Artificial Neural Networks. We drew pseudo-absences from those occurrences in

a target group strategy (Mateo *et al.* 2010), a procedure to increase the likelihood that sampled pseudo-absences were effectively located in sites where OMUs were absent. We evaluated model performance with maximized Jaccard indices. For 361 OMUs with small sample sizes ($N < 30$; 46.1%), models were evaluated upon the calibration dataset. For 202 OMUs with large sample sizes ($N \geq 30$; 25.8%), we ran an additional 3-fold spatial block cross-validation step (Roberts *et al.* 2017; Valavi *et al.* 2019) to improve model evaluation. We discarded models with a poor performance (Jaccard index < 0.95 without cross-validation; Jaccard index < 0.6 with cross-validation), and produced an ensemble model based on the median of predictions. We clipped final outputs with OMU-specific buffered alpha-hulls and, where relevant, we constrained outputs to the east or west of the Andean continental divide, to limit the extent of possible distributions to reasonable areas.

We derived species and mimicry ring distribution maps from the modeled distribution maps of OMUs as the likelihood of finding at least one of the OMUs belonging to the species/mimicry ring in the community (i.e., in the pixel). In the final post-processing step we computed six diversity and geographic rarity indices based directly on the stack of species and mimicry ring maps. Additionally, we present in ***SI Appendix 9*** four additional indices evaluating similar facets of diversity with alternative methods to explore the robustness of our analyses to index selection.

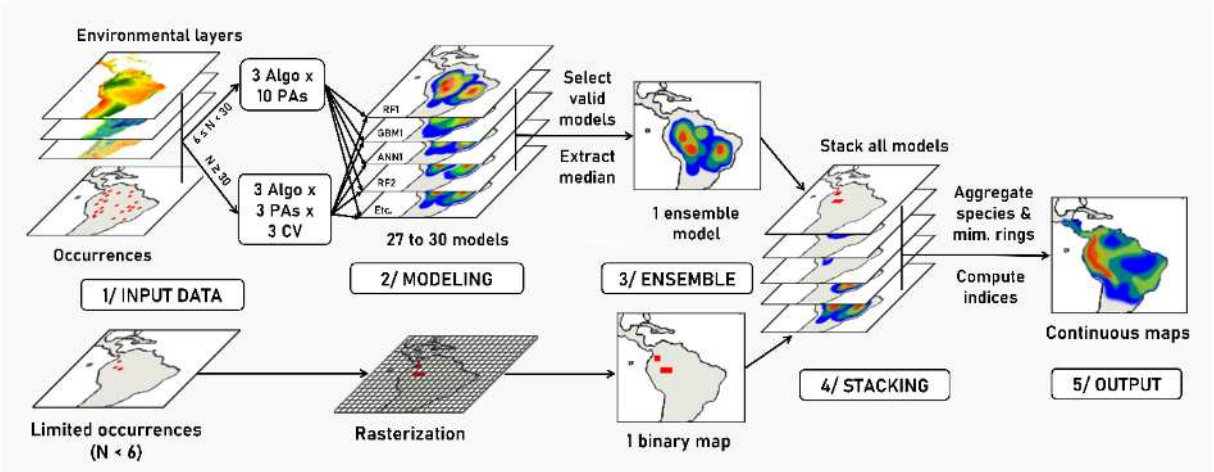

Figure 2: Species Distribution Model (SDM) workflow depicting the different analytical steps performed. Distribution models are computed for each OMU. Depending on sample size, modeling steps and settings differed. Clipping step to constrain SDM projections to plausible distribution ranges is not shown on the chart. Algo = algorithms used in the study, namely random forest (RF), gradient boosting models (GBM), and artificial neural networks (ANN); PAs = sets of pseudo-absences; CV = cross-validation folds; mim. rings = mimicry rings.

2.2.2 Diversity and geographic rarity indices

We computed species and mimicry richness as the expected number of species and mimicry rings found in our communities (i.e., in each pixel), by summing the continuous outputs from models as recommended by Calabrese *et al.* (2014). To estimate phylogenetic diversity, we computed Faith's Phylogenetic Diversity index (Faith, 1992) based on the phylogeny of the Ithomiini tribe (Chazot *et al.* 2019b) encompassing 339 species and 719 OMUs. This index estimates the total length of branches connecting all the species within a community, capturing the quantity of evolutionary history they represent.

We assigned geographic rarity weights for each species and mimicry ring based on their relative geographic ranges following the threshold-dependent exponentially decaying weighting scheme of Leroy *et al.* (2013). This method assigns weights that exponentially increase below the chosen rarity threshold, and rapidly decay to zero above the threshold, thereby limiting the impact of common species on community indices. We chose the rarity threshold at which the average proportion of rare species in communities was 25%, as detailed in Leroy *et al.* (2012). Next, we used these rarity weights to calculate an index of rarity for each community, which was the average rarity weight for all species or mimicry rings. These indices can be seen as proxies for relative levels of endemism since they quantify the relative importance of species or mimicry ring with small ranges in communities.

To quantify the importance of mutualistic interactions, we estimated the mean size (i.e., number of species) for mimicry rings within each community. Communities with high mean mimicry ring size correspond to greater frequencies of mutualistic interactions, while communities with low mean mimicry ring size host in average species engaged in fewer mutualistic interactions. Assuming that the richest mimicry rings also tend to be the most abundant, species belonging to smaller mimicry rings, thus harboring locally rare patterns, are likely more vulnerable to predation by naïve predators, and thereby to local extinctions (Müller 1879). As such, a low mean mimicry ring size may relate to higher vulnerability on average in the mimicry community.

Additionally, we computed indices of effective richness based on Shannon's diversity indices and an index of evolutionary distinctiveness based on Fair-Proportions (Redding, 2003), and we mapped the size of the main mimicry ring in each community (see **Fig. S9.22**). A flowchart and additional details on index computation based on our modeled distribution maps are provided in ***SI Appendix 8***. The robustness of indices was tested with several sensitivity

analyses as described in the ODMAP protocol. Results showed no qualitative difference with the results presented in the main text (see **Fig. S5.12 to S5.16**).

2.2.3 Estimation of index correlation

We computed pairwise Spearman's rho coefficients (ρ) to estimate the spatial congruence among our indices. We tested for the significance of these relationships with corrected degrees of freedom accounting for the positive spatial autocorrelation among observations (Clifford *et al.* 1989; Haining 1991). Then, we built a heatmap of spatial congruence among indices based on the absolute Spearman's rho coefficients. Additionally, we ran a hierarchical clustering analysis based on those same absolute coefficients as distances from perfect correlation (i.e., $d = 1 - |\rho|$) with a complete linkage method to produce a dendrogram revealing classes of indices showing highly similar patterns. We distinguished four classes of indices that represented the main facets of biodiversity while grouping indices that were highly correlated and revealed virtually similar hotspots. This resulted in applying a threshold of $|\rho|$ equal to 0.94 (see details in Results). Then, we selected one index per class for subsequent analyses of anthropogenic threats on diversity hotspots.

2.2.4 Spatial overlap between biodiversity hotspots and anthropogenic threats

We used the 2009 Human Footprint index (Venter *et al.,* 2016a) as a measure of anthropogenic threats to our communities of ithomiine butterflies. Despite representing anthropogenic pressures from a decade ago, Human Footprint remains the most comprehensive and recent map available for worldwide cumulative human pressures on terrestrial ecosystems (see **Fig. S6.17**). It is still widely used in similar large-scale conservation assessments, which allows for standardization and comparative analyses (e.g., Di Marco *et al.* 2018; Tucker *et al.* 2018; Allan *et al.* 2019; Elsen *et al.* 2020; Maron *et al.* 2020). The index combines eight variables that measure direct human impacts on the environment, namely, (1) human population density, (2) night-time light pollution, (3) extent of built environments, (4) crop landcover, (5) pasture landcover, (6) proximity to railways, (7) to major roadways, and (8) to navigable waterways.

We defined two levels of hotspots as the top 5% and 25% of communities showing the highest values for each of our indices. Similarly, we defined areas of very high (top 5%), high (top 25%), low (bottom 25%) and very low (bottom 5%) threats based on the Human Footprint scores of communities. Then, we characterized as risk areas communities showing the highest values in a facet of Ithomiini diversity (i.e., hotspots), and the highest levels of anthropogenic

pressures. Risk areas should be considered as priorities for reactive conservation with the goal of reducing high anthropogenic impact on threatened biodiversity (Brooks *et al.* 2006). Conversely, we characterized refuge areas as communities within hotspots with the lowest levels of pressures. Refuges should be prioritized for proactive conservation, with the goal of preserving these diverse areas from future anthropogenic threats (Brooks *et al.* 2006), providing shelter for a portion of ithomiine biodiversity. Finally, we mapped risk areas and refuge areas for four indices selected to represent our classes of highly correlated indices, namely, (1) species richness, (2) mean species geographic rarity, (3) mimicry richness, and (4) mean mimicry geographic rarity.

2.3 Reproducibility and data availability

We conducted all analyses using R 3.6.2 (R Core Team 2019) with packages 'raster' 3.0-12 (Hijmans 2020), 'biomod2' 3.4.6 (Thuiller *et al.* 2020), 'sf' 0.9-0 (Pebesma 2018), 'blockCV' 2.1.1 (Valavi *et al.* 2019), 'alphahull' 2.2 (Pateiro-Lopez & Rodriguez-Casal 2019), 'ape' 5.3 (Paradis & Schliep 2019), 'geiger' 2.0.6.1 (Harmon *et al.* 2008), 'Rarity' 1.6.3 (Leroy 2016) and others. All R scripts are available on GitHub at https://github.com/MaelDore/ithomiini_diversity. Species-grid-cell records and the mimicry classification used for modeling are available from Zenodo at 10.5281/zenodo.4696055 and 10.5281/zenodo.5497876.

3 Results

We inferred the distribution for each of the 388 species and 44 mimicry rings based on the 783 OMUs. All OMU/species/mimicry ring modeled distribution maps can be found at 10.5281/zenodo.4673446. Examples are provided in ***SI Appendix 7***.

3.1 Index maps

The Eastern slopes of the Andes appeared as the primary hotspot of Ithomiini taxonomic, phylogenetic and mimetic diversity, especially between 500 and 2500 m (**Fig. 3a, 3c, 3d, 3g**). We estimated that some quarter-degree grid cells (hereafter referred to as communities) may harbor as many as 120 species, representing up to 28 mimicry rings, especially in Ecuador and Peru. These species totals partly represent alpha-diversity and partly different habitats contained within single quarter-degree grid cells. The Atlantic Forest and the highlands of Central America appeared as secondary hotspots but fall far behind in terms of

numbers of species, mimicry richness, and phylogenetic diversity. Conversely, we estimated species and mimicry richness, and phylogenetic diversity, to be relatively low in regions with low forest cover such as in the Llanos, in the semi-arid Caatinga, in the seasonal Cerrado savannas, and the Pantanal wetlands (see map of bioregions in **Fig. S1.4**). Regions around the outer margin of the Ithomiini distribution such as the north of Central America, the Chaco region and the Pampas grasslands from Northwest Argentina to Uruguay (see map of bioregions in **Fig. S1.4**), also show relatively low levels of richness and phylogenetic diversity.

Mean geographic rarity of species and mimicry peaked on the western slopes of the Andes facing the Pacific coast and appeared generally high in the Andes (**Fig. 3b, 3e, 3h**). Mean species geographic rarity was also estimated to reach high levels in Central America. Conversely, few species and mimicry rings with restricted ranges occurred in the species-poor Cerrado savannas, in the Chaco region, and in the semi-arid Caatinga (**Fig. 3b, 3e**). The Amazon basin also hosted few rare species and mimicry rings, with the notable exception of the regions around the course of the Amazon river in the Upper Amazon (**Fig. 3b, 3e, 3h**).

Communities with the largest mimicry rings on average, that host the highest proportion of mutualistic interactions, were estimated to occur in Central America in Panama and Costa Rica, on the eastern slopes of the Andes in Ecuador and Peru, along the Amazon river, and in the Atlantic Forest (**Fig. 3f, 3i**). Conversely, communities in the species-poor Llanos, Caatinga, Cerrado, and Chaco regions contained the most vulnerable mimicry rings with the fewest species on average (**Fig. 3f**).

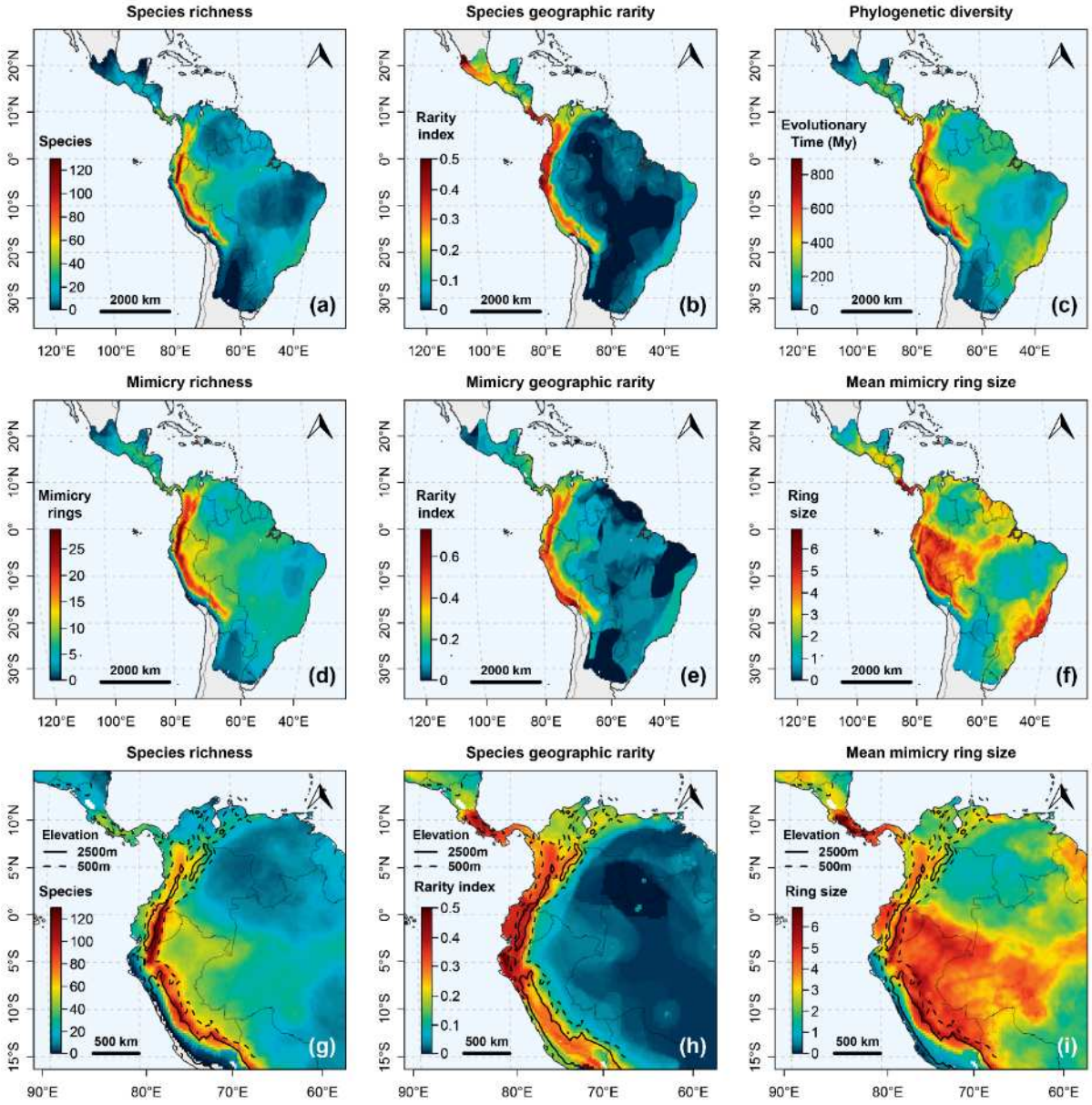

Figure 3: Heatmaps of the different facets of Ithomiini diversity in the Neotropics for quarter-degree grid cells. (a) Species richness. **(b)** Mean species geographic rarity based on species range. **(c)** Faith's Phylogenetic Diversity (Faith 1992). **(d)** Mimicry richness (i.e., number of mimicry rings). **(e)** Mean mimicry geographic rarity based on mimicry ring range. **(f)** Mean mimicry ring size as mean number of species per mimicry ring. **Maps g, h & i**: Zoom on the northwestern Andes region for species richness **(g)**, species geographic rarity **(h)**, and mean mimicry ring size **(i)**. Contour lines represent elevation for 500 m (dashed lines) and 2500 m (solid lines). Political boundaries are displayed in light grey. All maps are projected under Mollweide's projection, centered on the meridian 75°E.

3.2 Correlation among indices

All indices were significantly positively correlated (**Table S10.26**: Clifford's correction for Spearman's rank test, all pairwise p-values < 0.001). We distinguished four classes of indices based on their levels of correlation (**Fig. 4**). The dendrogram and correlation heatmap for the full set of ten indices are presented in **Fig. S9.23**.

The first class represented a set of indices strongly correlated with species richness (**Fig. 4**; **Table S10.27).** Species richness appeared to be a very strong predictor of Faith's phylogenetic diversity (**Tables S10.26 & S10.27**: $\rho = 0.996$, $t = 84.0$, Clifford's $df = 56.7$, $p < 0.001$), and mean mimicry ring size (**Tables S10.26 & S10.27**: $\rho = 0.941$, $t = 21.2$, Clifford's $df = 57.9$, $p < 0.001$).

Mimicry richness also correlated strongly with species richness (**Tables S10.26 & S10.27**: $\rho = 0.934$, $t = 19.7$, Clifford's $df = 56.6$, $p < 0.001$) but it was less strongly correlated with the other indices of the first group (**Table S10.26**: $\rho = 0.854$ in average). Moreover, the relationship between species richness and mimicry richness was not strictly linear: some communities with the highest number of mimicry rings are not the most speciose (**Fig. S10.24c**). Since this pattern can lead to differences in hotspot identification, we attributed mimicry richness to a second class of indices on its own (**Fig. 4**).

Geographic rarity indices (species and mimicry) were more closely correlated with each other (**Tables S10.26 & S10.27**: $\rho = 0.657$, $t = 7.05$, Clifford's $df = 65.5$, $p < 0.001$) than with any other indices. However, they were less correlated with each other than the first group of indices. As such, they formed a third and fourth class of indices (**Fig. 4**). They were nonetheless moderately correlated with species richness (**Tables S10.26 & S10.27**: $\rho = 0.473$, $t = 4.34$, Clifford's $df = 65.4$, $p < 0.001$ for mean species geographic rarity; $\rho = 0.606$, $t = 5.98$, Clifford's $df = 61.5$, $p < 0.001$ for mean mimicry ring geographic rarity). Indeed, species-rich communities tended to present high mean geographic rarity values, while species-poor communities exhibited the entire range of relative levels of species endemism (**Fig. S10.24a & S10.24b**). Similarly, communities with high mimicry richness showed high mean mimicry geographic rarity, while communities with few mimicry rings could exhibit the entire range of relative levels of mimicry endemism (**Fig. S10.24d**).

Correlations including the four additional indices computed (namely, species Shannon's diversity, mimicry Shannon's diversity, Evolutionary Distinctiveness, and the maximum

mimicry ring size) supported the classification in four classes of indices, and can be found in **Appendices 9 & 10**.

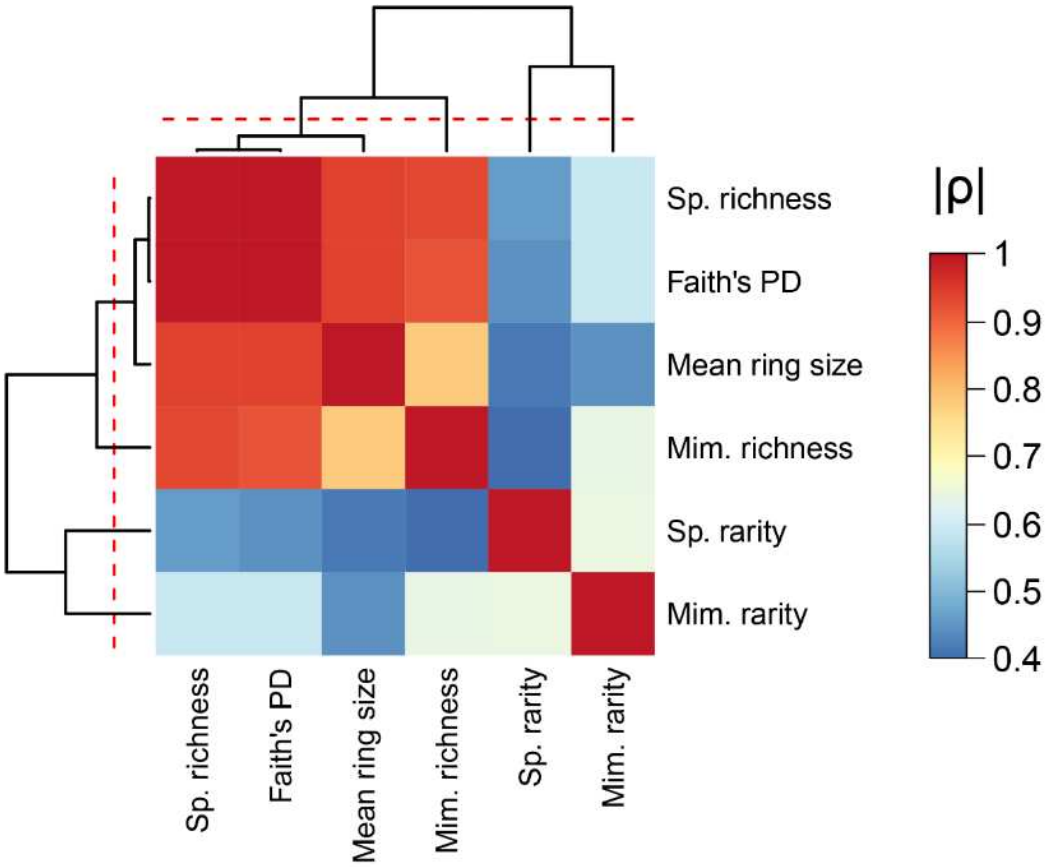

Figure 4: Heatmap of spatial correlations across Ithomiini biodiversity indices with associated dendrogram depicting the hierarchical clustering of the indices. Correlations are estimated as the absolute values of Spearman's rho statistics (ρ). Dendrogram built with a complete link method. Red dashed lines represent the threshold used to regroup indices with strong correlation (|ρ| = 0.94). Sp. = Species. Mim. = Mimicry. PD = Phylogenetic Diversity. Rarity as mean geographic rarity.

3.3 Threat and refuge maps

Our assessment of current anthropogenic threats on Ithomiini diversity hotspots showed that the northern Andean cordilleras combine high taxonomic and mimetic diversity with high levels of human impact, making them a region of focus for conservation. Meanwhile, remote portions of the Upper Amazon rainforest may act to some extent as refuges for the different facets of Ithomiini diversity (**Fig. 5**). However, the top 5% hotspots consistently demonstrated very limited to no overlap with potential refuge areas for all indices (**Fig. 5b,d,f,h & Fig. 6b**).

We estimated hotspots of species richness to be under relatively high anthropogenic pressures in the Andes, with most of the mountainous areas below 2500 m coinciding with

species-rich communities and high human impact levels (**Fig. 5a**). The Atlantic Forest, as the secondary hotspot for Ithomiini species richness, appeared to be the most threatened with a large portion of its range falling under high levels of threats, including the top 5% of the most threatened communities (**Fig. 5a**). The Upper Amazon encompassed a significant part of potential refuge areas with low levels of threats (**Fig. 5a & 6a**; 33.3% of hotspots compared to the expected 25% overlap) but these areas showed limited overlap with the top 5% of the richest communities (**Fig. 5b & 6b;** 13% of hotspots compared to the expected 25% overlap).

We estimated mean species geographic rarity hotspots to be relatively more threatened than the other facets of Ithomiini diversity, and also to deviate positively from that expected from a random distribution of anthropogenic threats (**Fig. 5c-d & 6**). This trend remained detectable when exploring other thresholds to define the hotspots (**Fig. S11.28**). Hotspots in the Andes, the coastal part of the Atlantic Forest, and the mountainous spine of Central America showed high to very high levels of threats (**Fig. 5e;** 42.9% of overlap compared to the expected 25%, and 10.3% compared to the expected 5% for the highest levels of threats). Meanwhile, only a small portion of the Upper Amazon was estimated as a potential refuge area for communities with high levels of endemism (**Fig. 5c & 6a;** 4.5% compared to the expected 25% overlap), and virtually none encompassed the top 5% of the communities with the rarest species on average (**Fig. 5d & 6b**).

Hotspots of mimicry richness showed similar patterns to species richness due to the relatively high spatial congruence between the two indices (**Fig. 4 & 5**). The main difference was that the Atlantic Forest did not rank as a hotspot for mimicry diversity, and therefore reduced perceived threat levels on mimicry richness hotspots compared to species richness hotspots (**Fig. 5a, 5e & 6a**; 15.8% for mimicry richness and 23.9% for species richness vs. 25% expected overlap).

Likewise, we estimated hotspots for mean mimicry ring geographic rarity to face high levels of threats in the Andes, Central America, and the coastal part of the Atlantic Forest. They also extend moderately to the relatively less threatened part of the Upper Amazon, along the course of the Amazon river (**Fig. 5g-h)**. However, the top 5% hotspots found in the Andes and on the Pacific coast coincided with very few potential refuge areas (**Fig. 5h & 6b**; 1.5% and 0% vs. 25% and 5% expected overlaps respectively for the low and very low levels of threats) while being more threatened than expected from a random distribution of anthropogenic threats (**Fig. 6b**; 34.4% and 6.7% vs. 25% and 5% expected overlaps).

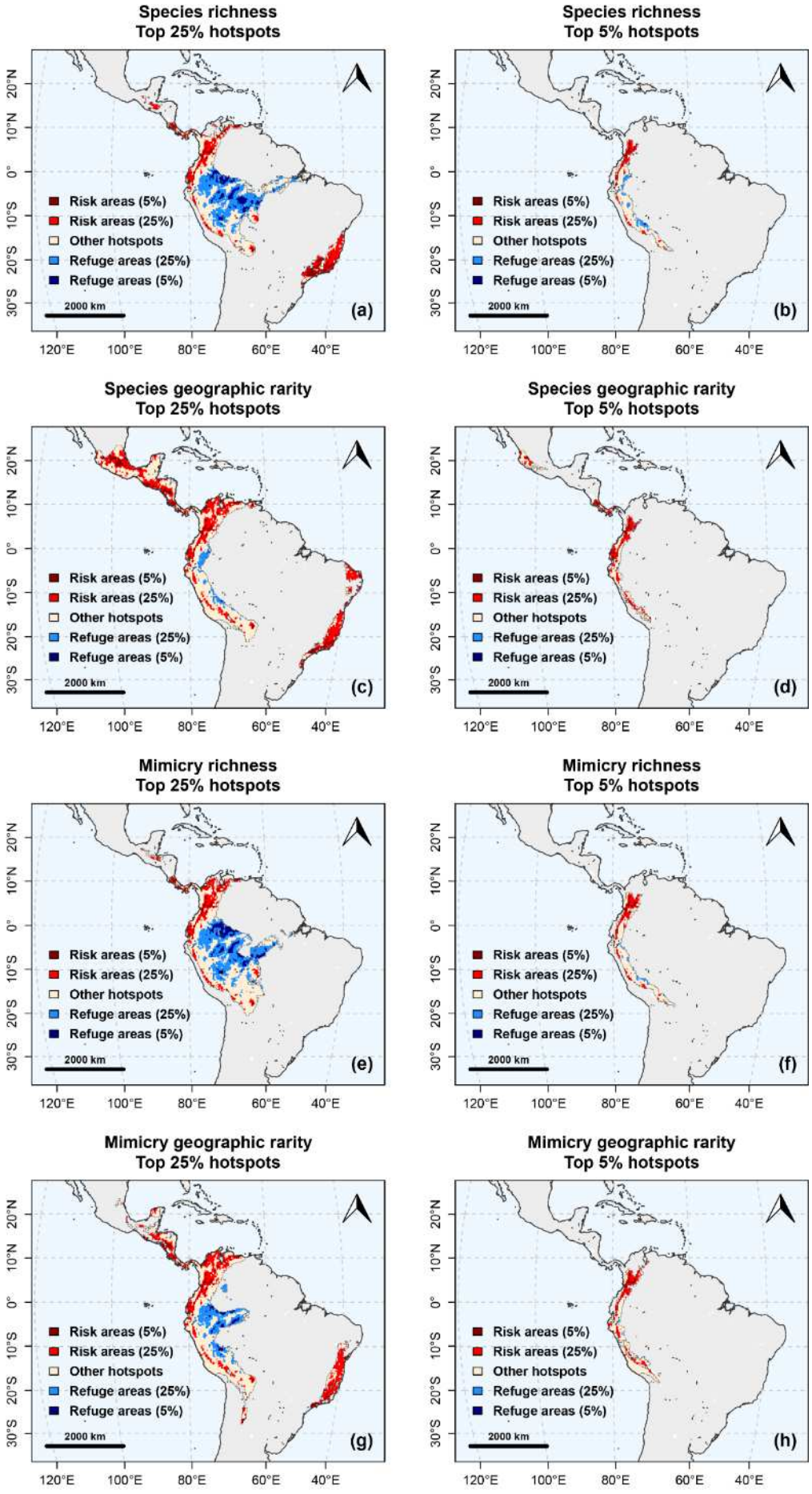
Species richness
Top 25% hotspots
Species richness
Top 5% hotspots
Species geographic rarity
Top 25% hotspots
Species geographic rarity
Top 5% hotspots
Mimicry richness
Top 25% hotspots
Mimicry richness
Top 5% hotspots
Mimicry geographic rarity
Top 25% hotspots
Mimicry geographic rarity
Top 5% hotspots
Risk areas (5%)
Risk areas (25%)
Other hotspots
Refuge areas (25%)
Refuge areas (5%)
2000 km
(a)
(b)
(c)
(d)
(e)
(f)
(g)
(h)
120°E
100°E
80°E
60°E
40°E
20°N
10°N
0°
10°S
20°S
30°S

Figure 5: Maps of risk and refuge areas for four predicted Ithomiini diversity hotspots. Only hotspots are displayed, defined as the top 25% (**Panels a, c, e, g, on the left**) or top 5% (**Panels b, d, f, h, on the right**) of highest-ranking communities for each index. Anthropogenic threat levels are based on the Human Footprint index, classified within quantiles 5% and 25% for lower and upper end of the distribution. Risk areas (in red) represent areas of overlap between high threat zones and hotspots. Refuge areas (in blue) represent areas of overlap between low threat zones and hotspots. Hotspots not falling into areas of high or low threat levels are displayed in light color. **(a) & (b)**: Species richness. **(c) & (d)**: Mean species geographic rarity based on species range. **(e) & (f)**: Mimicry richness (i.e., number of mimicry rings). **(g) & (h)**: Mean mimicry geographic rarity based on mimicry ring range.

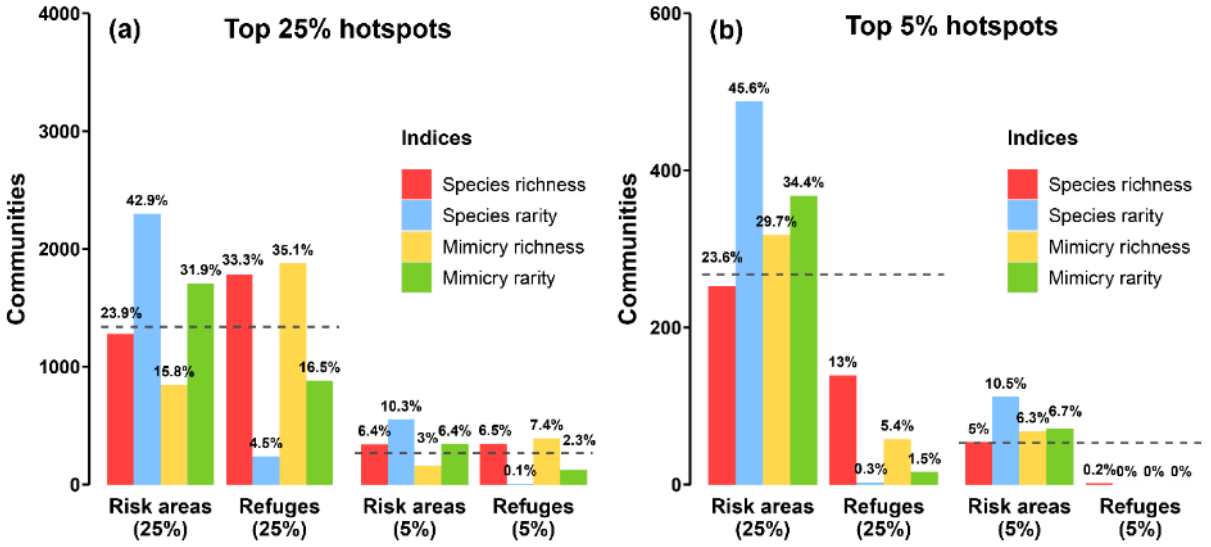

Figure 6: Comparison of extent of risk and refuge areas between indices. Risk areas represent areas of overlap between high anthropogenic pressures and biodiversity hotspots. Refuge areas represent areas of overlap between low anthropogenic levels and biodiversity hotspots. Y-axis represents the number of communities (i.e., grid cells) within risk and refuge areas for each biodiversity hotpots. Species rarity describes mean geographic rarity based on species range. Horizontal dashed lines represent the expected size of the overlap for a random distribution of anthropogenic threats. Percentages displayed on bars represent the proportion of the hotspot overlapping with the threat area. **(a)** For the top 25% hotspots. **(b)** For the top 5% hotspots.

4 Discussion

4.1 Spatial congruence of the facets of Ithomiini diversity

In our integrative approach to mapping Ithomiini diversity, we found that estimated species, mimicry and phylogenetic diversity indices are strongly correlated across the Neotropics. All indices peaked on the eastern slopes of the Peruvian and Ecuadorian Andes, and in the Upper Amazon region, while the Atlantic Forest and Central American mountains

appeared as secondary richness hotspots (**Fig. 3a, 3c, 3d**). We also uncovered relatively low levels of biodiversity in the Llanos, the Guyana Shield and the Cerrado savannas. As is common in stack-SDM procedures, these predictions likely overestimate richness and diversity within individual grid cells because species are likely absent in at least some environmentally suitable grid cells where they are predicted to occur (see **ODMAP** in ***SI Appendix 5***). However, this potential bias affects all cells evenly and therefore does not prevent the generation of meaningful insights into the relative patterns of biodiversity and the identification of hotspots.

Spatial patterns of ithomiine biodiversity likely result from the combined effects of historical, ecological and topographical factors. The tribe likely originated in the eastern Andean foothills, about 26 My ago and diversified in the Andes throughout the Miocene (Chazot *et al.* 2019b). The demise of the Pebas, a large wetland system that occupied the lowlands on the eastern side of the Andes, led to the expansion of the modern Amazonian forest (Hoorn & Wesselingh 2010), allowing multiple colonizations and diversification in the Upper Amazon during the last 10 My (Chazot *et al.,* 2016, 2018, 2019; De-Silva *et al.,* 2016, 2017; Elias *et al.,* 2009). Ithomiini are strongly specialized on their larval hostplants, and hostplants are likely a limiting resource (Drummond III & Brown Jr, 1987; Willmott & Mallet, 2004). The diversity of Solanaceae, on which most Ithomiini feed as larvae, also peaks in the Andes and the Upper Amazon (Knapp 2002; Ulloa Ulloa *et al.* 2017), thereby potentially enabling greater local Ithomiini diversity. This apparent spatial correlation between species diversity in ithomiines and their hostplants is consistent with a hostplant-mediated adaptive radiation scenario (Willmott & Freitas 2006). Finally, the topological complexity of the Andes and adjacent foothills creates high variability in abiotic conditions, habitat and vegetation types (Osborne, 2012), which generates species turn-over, mimicry shifts and fosters vicariant speciation (Chazot *et al.,* 2014; Elias *et al.,* 2009; Jiggins *et al.,* 2006). Therefore, the tropical Andes represent the primary hotspot of alpha-diversity (**Fig. 3a**), but also beta-diversity with high local endemicity (**Fig. 3b & 3h**) and turn-over across communities, both of high interest for conservation. The Upper Amazon, because of its proximity and historical exchanges with the Andes, its soil enriched with orogenic sediments, as well as a more variable climate and heterogeneous forest structure hosting numerous microhabitats, tends to host more diverse communities than the more stable forests found in the Lower Amazon (**Fig. 3a** ; Sombroek 2000; Brown Jr. & Freitas 2002; Brown Jr. 2005).

Conservation efforts focused on hotspots of taxonomic diversity alone may not necessarily be effective for conserving a large fraction of species, or other aspects of

biodiversity (Devictor *et al.,* 2010; Godoy-Bürki *et al.,* 2014; P. Williams *et al.,* 1996; Williams & Humphries, 1994; Zupan *et al.,* 2014). As such, areas that host rare and endangered biological features should also be considered (Prendergast *et al.,* 1993; Lawler *et al.,* 2003; e.g., Alliance for Zero Extinction: Parr *et al.,* 2009; Key Biodiversity Areas: KBA Standards and Appeals Committee 2020). Our mean geographic rarity indices provide a useful tool to predict areas of high endemicity that may differ from diversity hotspots. Still, geographic rarity indices appeared positively correlated with species and mimicry richness at the continental scale (**Fig. S10.24a & S10.24d)**. Species-rich communities that host mostly species with small ranges were found in the Andean and Central American mountains (**Fig. 3b**). These regions harbor steep environmental gradients (Osborne 2012) enabling strong hostplant turn-over (Knapp 2002), which may limit ithomiine species ranges. Yet, some species-poor communities also coincide with high levels of species and mimicry rarity. Such communities are found in the outer edges of the global distribution of Ithomiini, especially on the Pacific slopes of the Andes (**Fig. 3b, 3e, 3h**). There, a strong environmental gradient and geographic barriers such as the Pacific Ocean, the Peruvian coastal desert and the Central Andes could explain the restricted ranges of the few resident species and mimicry rings. Moreover, unusual environmental conditions found at the outer edges of the Ithomiini range may select for specific lineages and mimicry patterns due to environmental filtering.

Overall, Ithomiini biodiversity hotspots appear fairly congruent with biodiversity hotspots based on vascular plant species richness and endemism (Myers *et al.* 2000). As such, the tropical Andes stand out as the primary hotspot for the multiple facets of Ithomiini biodiversity. Secondary hotspots of Ithomiini diversity, namely the Atlantic Forest, Central American mountains and the Pacific slopes of the Andes, also coincide with areas previously recognized as biodiversity hotspots (Myers *et al.* 2000). Moreover, our inferred patterns of diversity and endemism are in line with the trends observed for other taxa in the Neotropics. Angiosperms and tetrapods show a peak of diversity and endemism in the western part of Amazonia and in the Andean foothills (Ter Steege *et al.* 2003; Morawetz & Raedig 2007; Kier *et al.* 2009; Jenkins *et al.* 2013; Roll *et al.* 2017; Gumbs *et al.* 2020). Among insect taxa, the overall biodiversity patterns of Ithomiini are consistent with those of Cicindelinae beetles (Pearson & Carroll 2001), *Adelpha* butterflies (Mullen *et al.* 2011), Nymphidiina butterflies (Hall 2018) and Heliconiini butterflies (Rosser *et al.* 2012). Conversely, the distribution of bees in the Neotropics presents an opposite trend, with higher richness per area reached in the Chaco regions, Caatinga, dry Southern Andes, and Atlantic forest, reflecting the great success of this

group in xeric and seasonal habitats (Orr *et al.* 2021). Overall, these results support the role of ithomiine butterflies as suitable flagship indicator group for Neotropical butterfly diversity, and reinforce the position of the tropical Andes as the flagship region for biodiversity conservation in general and insect and butterfly conservation in particular.

4.2 Distribution patterns of mimetic interactions

Mimicry rings displayed strong distinctive geographic patterns, suggesting different underlying biogeographical trajectories (see examples in **Fig. S7.20**; names are provided in capital letters hereafter). Central America and the Atlantic Forest are secondary hotspots for Ithomiini species richness and host relatively large mimicry rings (**Fig. 3a, 3f & 3i**), but few of those rings are endemic to these regions (**Fig. 3e**). Only two mimicry rings are endemic to the Atlantic Forest (HEMIXANTHE and LYSIMNIA), while in Central America, some mimicry rings extend south to the northern Cordilleras of the Andes (DILUCIDA, EXCELSA, PARALLELIS), and others span a large part of the entire distribution of Ithomiini (e.g., AGNOSIA, EURIMEDIA, MAMERCUS). By contrast, the Amazon forest harbors about ten endemic mimicry rings, whose centers of species richness are located in the Upper Amazon (e.g., AURELIANA, MAELUS, SINILIA) close to the predicted center of origin of the tribe, and along the Amazon river (i.e., DOTO, EGRA). Most narrow-ranging and species-poor mimicry rings are found in the Andes (**Fig. 3e**), where mimicry rings are strongly segregated along the altitudinal gradients (Chazot *et al.* 2014). Lowland communities shelter mostly wide-ranging rings (e.g., CONFUSA, HERMIAS, LERIDA) while highland communities host rare, narrow-ranging rings (e.g., DERCYLLIDAS, HEWITSONI, THEUDELINDA) comprising species adapted to higher altitudes. Paradoxically, mimicry rings with transparent patterns tend to be found in higher proportions at high elevations (e.g., THABENA-F, PANTHYALE, OZIA), in contrast to predictions of the thermal melanism hypothesis that opaque patterns should be under positive selection under colder climates (Clusella Trullas *et al.* 2007; Dufour *et al.* 2018). As such, further research is still needed to better understand the selective advantages of these transparent wings that shape the biogeography of mimicry patterns in ithomiines.

Altogether, mimicry richness is expected to follow species richness since more species provide greater opportunities to harbor different wing patterns. In parallel, mimicry fuels species richness by limiting the exclusion effect of competition among co-occurring co-mimetic species (Gross 2008). However, aposematic signals are predicted to converge locally due to

positive frequency-dependent selection incurred by predators (Müller 1879). Therefore, mimicry richness should increase more slowly than species richness and plateau when all ecological niches are occupied and a (set of) wing pattern(s) already dominates each niche (Joron & Mallet 1998). The relationship between Ithomiini mimicry and species richness was positive (**Fig. 4**) but it appeared only slightly saturated (**S10.24c**). This suggests that even in species-rich communities there is some free ecological space, or that the effect of selection for wing pattern convergence is weaker than thought in Müllerian mimetic communities. For instance, the high numbers of mimicry rings found in the most speciose communities in the Ecuadorian and Peruvian tropical Andes may arise because the steep environmental and altitudinal gradients in these regions create a small scale mosaic of zones within each grid cell, hosting locally adapted species and mimicry rings with fuzzy limits (Sherratt 2006; e.g., altitudinal bands; Chazot *et al.* 2014). This dense spatial structuring facilitates the recurrent permeation of species and mimicry rings from adjacent zones that may not represent local adaptive peaks of the available niches. Yet, such species could persist, rescued by recurrent immigration (Brown Jr. & Freitas 2002; Joron & Iwasa 2005), thereby fueling local mimicry richness. From a conservation point of view, preserving high species richness should also ensure the preservation of mimicry richness. We estimated that rich communities may not only harbor the highest number of species, but also the highest proportion of mutualistic interactions in the ithomiine butterfly communities, with the largest mimicry rings on average (**Fig 3a & 3f, Fig. 4**). Thus, species in those communities might be better protected against secondary extinctions that would result from the loss of mutualistic interactions associated with the extirpation of their co-mimetic species.

4.3 Threats and refuges for Ithomiini diversity hotspots

In this study, we highlighted areas of high risks for biodiversity loss, of priority interest for reactive conservation to reduce high anthropogenic pressures on biodiversity. In parallel, we defined refuge areas, of priority interest for proactive conservation to provide shelters for biodiversity from human pressures (Brooks *et al.* 2006). As such, hotspots for species and mimicry richness, and phylogenetic diversity, located in the Andes and the Upper Amazon, face contrasting situations. While the Upper Amazon has some of the most intact ecosystems in remote areas, the Andes, particularly the rich communities in the western foothills in Ecuador and the three Andean cordilleras in Colombia, are facing high levels of human impacts (**Fig. 5a-b, 5e-f & 6**). The second diversity hotspot, the Atlantic Forest, is also of great concern,

demonstrating the highest level of human pressures and relentless fragmentation of its forested habitats (Ribeiro *et al.* 2009). Communities with geographically rare species and mimicry rings are found mostly in Andean and Central American mountain ranges, coinciding with areas of high human impacts (**Fig. 5c-d**). Their situation is of particular concern since species with small distribution ranges are known to face higher risks of extinction (Purvis *et al.* 2000; Cardillo *et al.* 2008; Böhm *et al.* 2016), thereby also impacting the narrowly distributed mimicry rings they represent.

The spatial location of threats and refuges for Ithomiini biodiversity uncovered here appear consistent with trends observed for vertebrates in general. The slopes of the northern and central Andes and the Atlantic Forest are the regions with the highest number of threatened and near-threatened vertebrates (along with South East Asia), while the Amazon rainforest has been suggested as the major refuge for vertebrate richness (Allan *et al.* 2019). Our study complements this picture by casting light on the specific situation of tropical highlands in the Neotropics. Mountains provide heterogeneous landscapes that host a high diversity of ithomiine species and mimicry rings, especially geographically rare and vulnerable ones. They act as a refuge for lowland species that become increasingly restricted to higher altitudes by climate warming (Chen *et al.* 2009), while species already adapted to high elevations, with narrow physiological specializations, are threatened by the extirpation of their climatic niche (Ohlemüller *et al.* 2008). Yet, many tropical species, with typically narrow niches and slow niche evolutionary rate, are suspected to lag behind the shift of their climatic envelope (Jezkova & Wiens 2016). In the case of Ithomiini, which rely on local mutualistic interactions with co-mimics and host plants, the threat of community disassembly due to climate change is even more profound (Toby Kiers *et al.* 2010; Sheldon *et al.* 2011). Mountain habitats are particularly under threat from human activities, with high deforestation rates due mostly to the competition for arable lands (Armenteras *et al.* 2017). Even where human population density is low in remote mountain regions, natural habitats may come under threat from road-building and mining operations (Sonter *et al.* 2017; Bax *et al.* 2019).

Remote portions of the Upper Amazon forest may currently act as refuges for a fraction of Ithomiini diversity. Yet, even within protected areas, landscape level changes can impact insect faunas (Hallmann *et al.* 2017, 2020; Salcido *et al.* 2020). The Upper Amazon remains largely exposed to climate change, notably increases in temperature and drought intensity (Malhi *et al.* 2008; Nobre *et al.* 2016), and to deforestation threats (Carvalho *et al.* 2019; Escobar 2020). Thus, the potential refuge areas we have mapped represent only the currently

less threatened areas of Ithomiini diversity hotspots, but do not guarantee the conservation of all the biodiversity facets they currently host, especially in the face of global changes. The next avenue for research is therefore to model the effects of climate change and future land use changes on the patterns of Ithomiini diversity to refine conservation perspectives in a changing world.

Data Accessibility Statement

All R scripts are available on GitHub at https://github.com/MaelDore/ithomiini_diversity. Species-grid-cell records and mimicry classification used for modeling are available from Zenodo at 10.5281/zenodo.4696055 and 10.5281/zenodo.5497876. All OMU/species/mimicry ring modeled distribution maps are available from Zenodo at 10.5281/zenodo.4673446.

Supplementary Information

Supplementary Information for CHAPTER 1: "Anthropogenic pressures coincide with Neotropical biodiversity hotspots in a flagship butterfly group" can be found in **ANNEXE 1** and **ANNEXE 2**.

Acknowledgements

The authors certify that they have no affiliations with or involvement in any organization or entity with any financial interest, or non-financial interest in the subject matter or materials discussed in this manuscript. MD is financed by the French Ministry of Research (MENSR).

We thank the museum curators who allowed us to examine the Ithomiini collections under their care, and individuals who provided access to or shared information from their private collections or field work, including Keith S. Brown Jr., Eric Quinter, Allan & Lesley Wolhuter, Steven Heydon, Jeff & Cathy Smith, Lynn Kimsey, John Rawlins, Olaf Mielke, Mirna Casagrande, Chris Jiggins, Fabio Vitale, Jackie Miller, Andy Warren, Andrei Sourakov, Francisco Piñas, Gerrit ten Broek, Santiago Villamarín, Jamie Radford, Jean-François Le Crom, Jean-Claude Petit, Wolfram Mey, Miguel Monné, Tomasz Pyrcz, Phil Ackery, Blanca Huertas, George McGavin, Pierre Boyer, Fernanda Checa, Sebastián Padrón, Heinz Schröder, Christoph Häuser, Bob Robbins, Don Harvey, Brian Harris, Axel Hausmann, Lisa de Silva, Melanie McClure and Paola Santacruz. We thank S. Villamarín, S. Nogales, the INABIO and Ecuadorian Ministerio del Ambiente for arranging the necessary permits for research in

Ecuador, most recently under the project 'Diversity and Biology of Lepidoptera in Ecuador' (No. 006-19 IC-FLO-FAU-DNB/MA). Museum and field work in Ecuador were funded in part by the Leverhulme Trust, the Darwin Initiative, the FLMNH Museum Associates, the National Geographic Society (Research and Exploration Grant # 5751-96) and NSF (# 0103746, #0639977, #0639861, #0847582, #1256742). We thank the INRENA/SERFOR for arranging the necessary permits for research in Peru. We thank the Instituto Chico Mendes de Conservação da Biodiversidade (ICMBio) for providing a research permit in Brazil (SISBIO no. 10802-5). Brazilian species are registered at the Sistema Nacional de Gestão do Patrimônio Genético e do Conhecimento Tradicional Associado (SisGen – AD7B279, AD23304, ACCDE4A, A33D8D7, ADF1F75, A37A48D). ME acknowledges funding by the ANR grant CLEARWING (ANR-16-CE02-0012) and a Human Frontier Science Program grant (RGP0014/2016). AVLF acknowledges the FAPESP (Biota-FAPESP grants 2011/50225-3, 2012/50260-6 and 2013/50297-0), the Brazilian CNPq (563332/2010-7 and 303834/2015-3) and United States Agency for International Development (USAID) and the U.S. National Academy of Sciences (NAS) under the PEER program (Mapping and Conserving Butterfly Biodiversity in the Brazilian Amazon – Sponsor Grant Award Number: AID-OAA-A-11-00012).

For their companionship and assistance in the field, we thank Julia and Jamie Robinson Willmott, Alexandre Toporov, Raúl Aldaz, and Ismael Aldas. We thank the numerous people who contributed to databasing museum specimens, particularly Fraser Simpson.

Models were run with the support of the computer cluster 'Plateforme Calcul Intensif Algorithmique' (UMS2700-PCIA) of the Muséum national d'Histoire naturelle MNHN.

CHAPTER 2

Phylogenomics resolve deep evolutionary relationships in clearwing butterflies

Maël Doré[1,2], Jérémy Gauthier[3], Rémi Allio[4], Nick Grishin[5], Joana Meier[6,7], Nicolas Chazot[8], Keith Willmott[9], and Marianne Elias[1,10]

[1]*Institut de Systématique, Evolution, Biodiversité, MNHN-CNRS-Sorbonne Université-EPHE-Université des Antilles, Muséum national d'Histoire naturelle de Paris, 45 Rue Buffon, 75005, Paris, France*

[2]*Centre d'Ecologie et des Sciences de la Conservation, UMR 7204 MNHN-CNRS-Sorbonne Université, Muséum national d'Histoire naturelle de Paris, 45 rue Buffon, 75005, Paris, France*

[3]*Natural History Museum of Geneva, Geneva, Switzerland*

[4]*Centre de Biologie pour la Gestion des Populations, INRAE, CIRAD, IRD, Montpellier SupAgro, Université de Montpellier, Montpellier, France*

[5]*Department of Biochemistry, University of Texas Southwestern Medical Center, Dallas, TX, United States of America*

[6]*Department of Zoology, University of Cambridge, Cambridge, CB2 3EJ, United Kingdom*

[7]*Tree of Life Programme, Wellcome Sanger Institute, United Kingdom*

[8]*Swedish University of Agricultural Sciences, Uppsala, Sweden*

[9]*McGuire Center for Lepidoptera and Biodiversity, Florida Museum of Natural History, University of Florida, Gainesville, FL, United States of America*

[10]*Smithsonian Tropical Research Institute, Panamá, Panamá*

Reference:

Doré, M., Gauthier, J., Allio, R., Grishin, N., Meier, J., Chazot, N., Willmott, K., & Elias, M. (2023). Phylogenomics resolve deep evolutionary relationships in clearwing butterflies. *In prep.*

Author contributions:

KW, NG, JM, NC & ME provided sequence data. MD, NC, KW & ME collected specimens from the field. MD, JG & RA conceived the phylogenomic pipeline. MD performed DNA extractions, wrote the BASH and R scripts, carried out the analyses, produced results and figures, and led the manuscript writing. All authors critically contributed to the manuscript draft.

Abstract

The most up-to-date knowledge about evolutionary relationships among ithomiine butterflies (Nymphalidae family: Danainae sub-family: Ithomiini tribe) has previously been inferred from molecular sequences extracted from nine genes. While the existing phylogeny offers a relevant tool for comparative phylogenic analyses, uncertainties remain regarding the branching of subtribes as the latest topology partly disagrees with the most parsimonious evolutionary scenarios regarding important morphological and ecological characters, such as hostplant use and caterpillar morphology.

In order to clarify and provide greater support to the deep evolutionary relationships in the Ithomiini tribe, we built a large dataset of ca. 7.8 million nucleotide sites representing over 11,000 orthologous genes from 155 taxa obtained from whole genome shotgun sequencing. We implemented state-of-the-art phylogenomic methods to infer a strongly supported backbone phylogeny that we employed to fix the deep topology of a final species-level phylogeny encompassing 356 out of the 396 documented species (i.e., 89.9%).

This final phylogeny confirmed the monophyly of the core-group, a clade comprising the five most recent and species-rich subtribes. Our new phylogenetic hypothesis established the Mechanitina subtribe as the sister-group of the core-group, a position in agreement with its hostplant use and caterpillar morphology. However, it placed the Melinaeina subtribe in a basal position within the Ithomiini tribe, while an extensive higher-level phylogeny based on morphological characters suggested a clade composed of the subtribes Tithoreina and Methonina as sister to all other Ithomiini lineages, a topology more parsimonious with regard to hostplant use. Such basal position of Melinaeina, supported by all molecular inferences so far, suggests that ithomiine butterflies may have switched at least twice during their evolution between Apocynaceae and Solanaceae hostplants, or retained the ability to feed on both plant lineages, at least in early evolutionary steps.

Overall, this new phylogenetic hypothesis provides better agreement with the putative evolution of morphological and ecological traits, highlighting the power of phylogenomic approaches to resolve previously conflicting deep evolutionary relationships. Altogether, it provides a stable tool for further macroevolutionary analyses in ithomiine butterflies.

Keywords

ancestral trait reconstruction, backbone phylogeny, clearwing butterflies, Neotropics, niche evolution, phylogenomics, Whole-Genome Sequencing.

Preamble

The work presented in this Chapter is still ongoing. All the phylogenomic part of the thesis project had to be delayed due to the COVID health crisis in 2020/2021. The fieldwork initially planned for March 2020 to collect samples was finally carried out in November 2021. Thus, the results presented here are still in development. In particular, we are finalizing a method to better evaluate and select the best topologies obtained through the multiple inference methods and molecular datasets. This should allow us to improve the support for the selection of the final phylogenies to include in the consensus forming the backbone phylogeny. Additionally, we are planning to illustrate the potential of our new species-level phylogeny to explore macroevolutionary questions in ithomiine butterflies by mapping ancestral climatic niche reconstruction in relation to inferred historical colonization routes of the group (Chazot *et al.* 2019b).

1 Introduction

High-throughput sequencing technologies, also called Next-generation sequencing (NGS), relies on massively parallel DNA sequencing to produce vast amount of molecular sequences in a relatively short time and at a reduced cost (Slatko *et al.* 2018). Coupled with whole-genome shotgun (WGS) sequencing techniques that involve the random break up of DNA extracts into small fragments, efficiently sequenced as reads through NGS, then assembled into potentially chromosome-size contiguous sequences (Pareek *et al.* 2011; Putnam *et al.* 2016), it allows researchers to produce genome-scale molecular datasets for virtually any group of organisms, beyond the historical models for genetic exploration (Ellegren 2014). In parallel, the deployment of high-performance computing infrastructures (Lampa *et al.* 2013; Ekblom & Wolf 2014), complemented by dedicated powerful genome assembly and phylogenetic inference algorithms (Bankevich *et al.* 2012; Sohn & Nam 2016; Kozlov *et al.* 2019; Minh *et al.* 2020b), has made it possible to process and analyze large amounts of genomic data in a relatively short period of time, giving birth to the field of phylogenomics (Delsuc *et al.* 2005).

Phylogenomics pursues the goal to infer phylogenetic relationships between taxa based on large molecular datasets covering significant portion of genomes (Young & Gillung 2020). Indeed, researchers can now use the statistical power of thousands of genes and millions of nucleotide or amino-acid sites to provide robust phylogenetic hypotheses that resolve long-standing debates about the relationships among major groups of organisms throughout the Tree of Life such as the origins of animals (Dunn *et al.* 2008), plants (Wickett *et al.* 2014), and even eukaryotes as a whole (Burki *et al.* 2020). Building upon the opportunities opened by WGS technologies and phylogenomics, we aimed here to clarify deep evolutionary relationships in clearwing butterflies (Nymphalidae Family: Danainae Sub-family: Ithomiini tribe), a group recently emerging as a model for mimicry comparative genetic studies (Gauthier *et al.* 2023).

Long-before the advent of comparative genomics, ithomiine butterflies, also coined as clearwing butterflies for the remarkable transparent wing sections harbored by many species in the group (**Fig. 1 & 2.B**), have been renowned among naturalists. With few other Neotropical butterfly groups, ithomiines have been instrumental in the design of the first theories of mimicry by Henri Walter Bates (Bates 1862) and Fritz Müller (Müller 1879) inspired by their respective journey in the Amazonian forest in the 19th century. Indeed, adult ithomiine butterflies are unpalatable and share warning color patterns throughout the Neotropics (**Fig. 1**). Their

unpalability results from the accumulation of pyrrolizidine alkaloids that are collected by adult males feeding on Asteraceae flowers (**Fig 2.B**) and withered and decaying Boraginaceae plants (Brown Jr 1984; Trigo & Brown Jr 1990). Such unpalability is associated with aposematic patterns acting as warning for predators (Poulton 1890). Since similarity in warning signals facilitates learning from shared local predators and divides the cost of predation among comimetic species, Müller predicted the convergence of wing patterns across unpalatable species which then form 'mimicry rings' (**Fig. 1**), a phenomenon labeled as Müllerian mimicry (Müller 1879). Ithomiine butterflies are found in humid forests from sea level to 3000 m altitude, from Mexico to Northern Argentina and across some Caribbean islands, where they dominate numerically the mimetic communities (Poole 1970; Beccaloni 1997a). As such, they likely act as models for palatable (Batesian mimicry) and unpalatable (Müllerian mimicry) species of other butterflies and moths taxa including Heliconiini (Müller 1879), Dismorphiinae (Bates 1862; Poulton 1898), Dioptinae (DeVries 1994), Pericopina (Brown Jr 1979), and even damselflies (Outomuro *et al.* 2013; Corral-lopez *et al.* 2021).

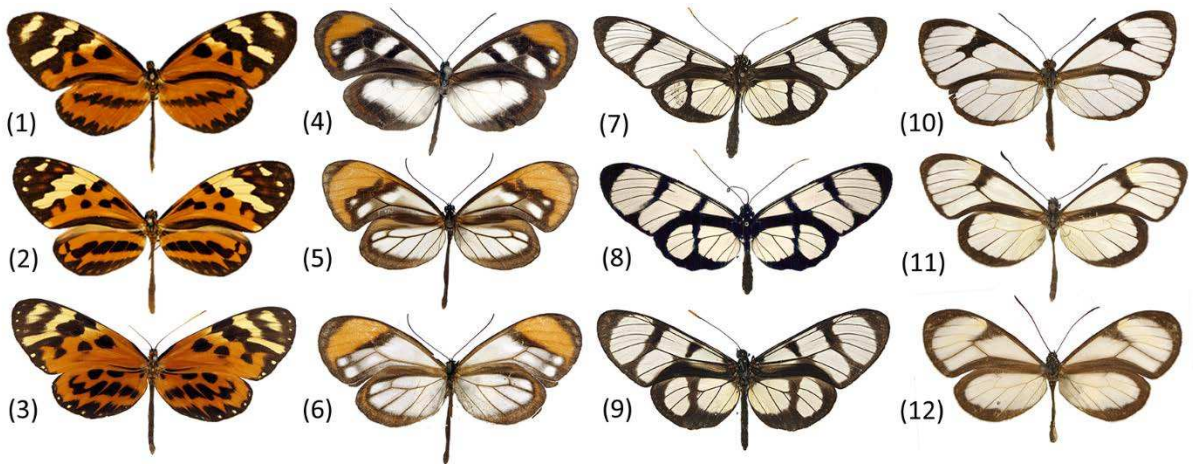

Figure 1: Dorsal view of ithomiine wing patterns illustrating the convergence of patterns across four mimicry rings with increasing degree of transparency. HERMIAS ring: (1) *Mechanitis polymnia veritabilis*, (2) *Melinaea mneme*, (3) *Forbestra equicola equicoloides*. AURELIANA ring: (4) *Oleria ilerdina ilerdina*, (5) *Hypoleria aureliana*, (6) *Pseudoscada florula aureola*. CONFUSA ring: (7) *Methona confusa psamathe*, (8) *Paititia neglecta*, (9) *Thyridia psiidi*. AGNOSIA ring: (10) *Ithomia agnosia pellucida*, (11) *Episcada philoclea* (12) *Pteronymia vestilla sparsa*. Credit photos: N. Chazot.

Thanks to their abundance, their conspicuousness, and the relatively important knowledge of their taxonomy, biology, and distribution, ithomiines have been the topics of a large body of studies encompassing historical biogeography (Brown Jr 1977, 1982; Chazot *et al.* 2019b), diversification patterns (Elias *et al.* 2009b; Chazot *et al.* 2016b, 2018), community ecology (Beccaloni 1997b; DeVries *et al.* 1997; Elias *et al.* 2008; Willmott *et al.* 2017), chemical ecology (Brown Jr 1984; Trigo *et al.* 1996; Schulz *et al.* 2004), cytogenetics (Brown Jr *et al.*

2004; McClure *et al.* 2018), speciation processes (Whinnett *et al.* 2005; Jiggins *et al.* 2006), insect-plant coevolution (Drummond 1986; Brown & Henriques 1991), and conservation (Brown Jr 1977; Uehara-Prado & Freitas 2009; Doré *et al.* 2022, see **Chapter 1**). Despite, this important corpus of research, there are still uncertainties regarding the evolutionary relationships within the group.

The Ithomiini tribe currently encompasses 396 documented species (Doré *et al.*, 2022; See check list in **ANNEXE 1, *SI Appendix 4***) that stands as the largest known radiation of Müllerian mimetic butterflies. One of the earliest systematic arrangement attempting to portray the evolutionary relationships within the group was the work of Doubleday, who used characters of the wing venation and male foreleg to group genera, and sort them from basal to derived (Doubleday 1847; Willmott & Freitas 2006). He also identified the presence of patches of elongated hair-like androconial scent scales on the costal margin of the dorsal hindwing of adult males (**Fig. 2.A**) as the diagnostic synapomorphy of the group. Following this seminal work, D'Almeida (1941) and Fox (1940, 1956) established eight of the ten currently recognized subtribes (initially described as tribes within the former Ithomiinae subfamily). The Methonini tribe was proposed initially by Mielke and Brown, 1979, and later requalified as subtribe Methonina (Brower *et al.* 2006). Finally, the Athesitina subtribe was jointly identified by Willmott & Freitas (2006) from on a phylogeny of 105 species encompassing 45 genera (i.e., 26% of extant species and 100% of then described genera) based on 306 informative morphological and ecological characters, and Brower *et al.* (2006) from a phylogeny of 81 species and 41 genera (i.e., 20% of extant species and 91.1% of genera) based on four genes (i.e., COI, COII, *wingless*, EFα). Later, Brower *et al.* (2014) offered to aggregate the previous morphological and molecular datasets to produce a new phylogenetic hypothesis for 87 species encompassing all 45 documented genera at that time. Garzón-Orduña *et al.* (2015) suggested an alternative time frame for divergence ages relying on independent secondary calibrations from a newly estimated time-calibrated phylogeny of Solanaceae (Särkinen *et al.* 2013). Finally, the most recent attempt into offering a phylogenetic hypothesis for the evolutionary relationships among ithomiines employed molecular data obtained from Sanger sequencing methods to infer a phylogeny from nine genes encompassing 340 species (i.e., 87% of extant species) representing all 48 currently accepted genera (Chazot *et al.* 2019b).

Despite this intense systematic activity and recurrent updates building upon the availability of new methods and data sources, there are still uncertainties and conflicts between parsimonious evolution of morphological and ecological traits, and molecular-based

relationships. The monophyly of the different subtribes has become stable across recent phylogenetic hypotheses (Brower *et al.* 2006, 2014; Chazot *et al.* 2019b), with strong support for the monophyly of the most species-rich subtribes (i.e., Ithomiina, Napeogenina, Oleriina, Dircennina and Godyridina), which form a strongly supported clade characterized by higher diversification rates and labeled as the 'core-group' (Chazot *et al.* 2019b). Yet, branching patterns among the five remaining relatively species-poor and most basal subtribes (i.e., Tithoreina, Methonina, Melinaeina, Mechanitina, and Athesitina) remain unstable and sometimes poorly supported (Brower *et al.* 2014). In particular, the most up-to-date hypothesis based on Sanger sequencing proposed a topology that disagrees with the existence of a clade formed by Mechanitina and the core-group, placing Athesitina as the sister-group of the core-group (**Fig. 5**; Chazot *et al.* 2019). Such putative clade, present in the former morphological and ecological-based approaches (Willmott & Freitas 2006), regroups all subtribes with members feeding on the diverse *Solanum* genus and also conveniently limit the number of inferred independent loss of subdorsal filaments in the last instar caterpillar, a conspicuous plesiomorphic feature shared by most basal ithomiines and other danaines, but not found in the core-group and Mechanitina species (**Fig. 2.C & 2.D; Fig. 5**). Moreover, all molecular-based phylogenetic hypotheses discard the clade formed by Tithoreina and Methonina as the sister-group of all ithomiines, favoring Melinaeina for this position (**Fig. 5**; Brower *et al.* 2006, 2014; Chazot *et al.* 2019), despite Tithoreina being the only subtribe to share its hostplant family Apocynaceae with the Tellervini tribe, the closest relative of ithomiines (Willmott & Freitas 2006).

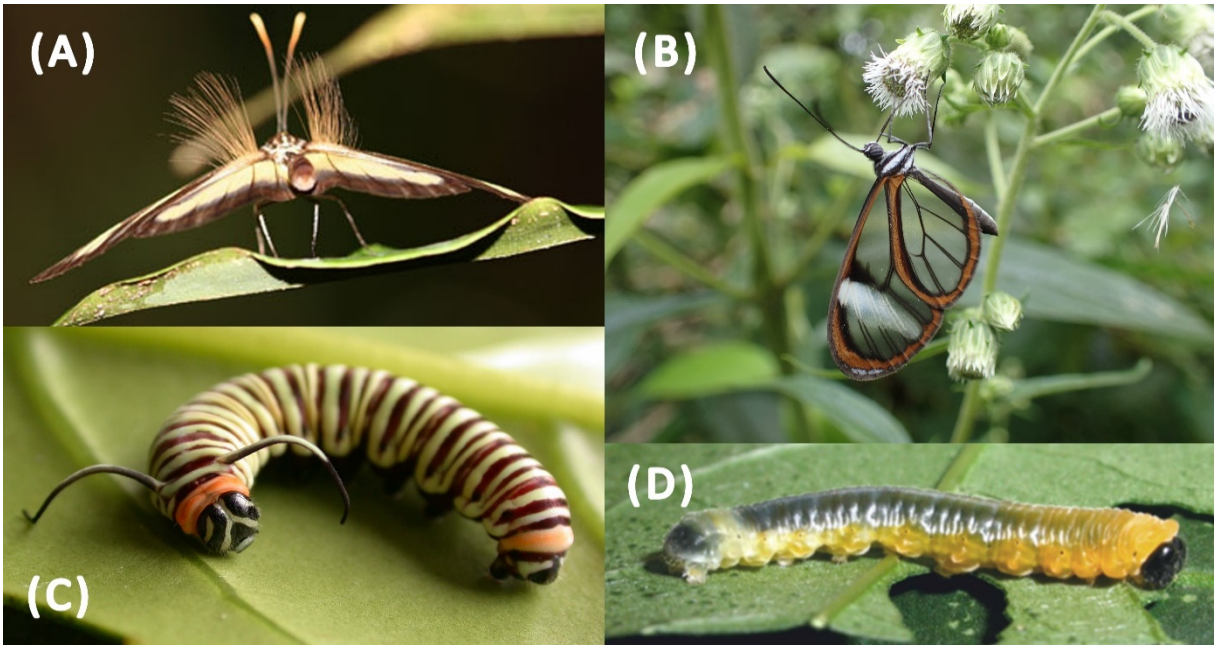

Figure 2: Key morphological traits of ithomiine butterflies. (A) Male *Napeogenes inachia* disseminating pheromones through its elongated hair-like androconial scent scales. **(B)** Male *Pseudoscada timna* feeding on an Asteraceae flower providing it with pyrrolizidine alkaloids. **(C)** Fifth and last instar caterpillar of *Melinaea menophilus* (Melinaeina subtribe) displaying conspicuous subdorsal filaments **(D)** Fourth and last instar caterpillar of *Scada karschina delicata* (Mechanitina subtribe) harboring no subdorsal filaments. Credit photos: K. Willmott and AVL Freitas.

Therefore, while the most up-to-date phylogeny offers a relevant tool for comparative phylogenic analyses (See **Chapter 4**), uncertainties remain regarding the branching of subtribes and the evolution of hostplant use and key morphological features. In this study we aimed to address such conflicts and provide greater support to the deep evolutionary relationships in the Ithomiini tribe. As such, we built the largest molecular dataset ever assembled for clearwing butterflies with ca. 7.8 million nucleotide sites representing over 11,000 genes from 155 taxa obtained from whole genome shotgun sequencing. Then, we implemented phylogenomic methods to infer a strongly supported backbone phylogeny which we employed to fix the deep topology of a final species-level phylogeny encompassing 356 out of the 396 documented species (i.e., 89.9%). Finally, we discuss how this new phylogenetic hypothesis may shed new lights on our understanding of the evolution of ithomiine butterflies.

2 Materials & Methods

The full analytical pipeline to produce the time-calibrated phylogeny from butterfly sampled caught in the Neotropical forest is summarized and illustrated in **Figure 3**. All steps are detailed below.

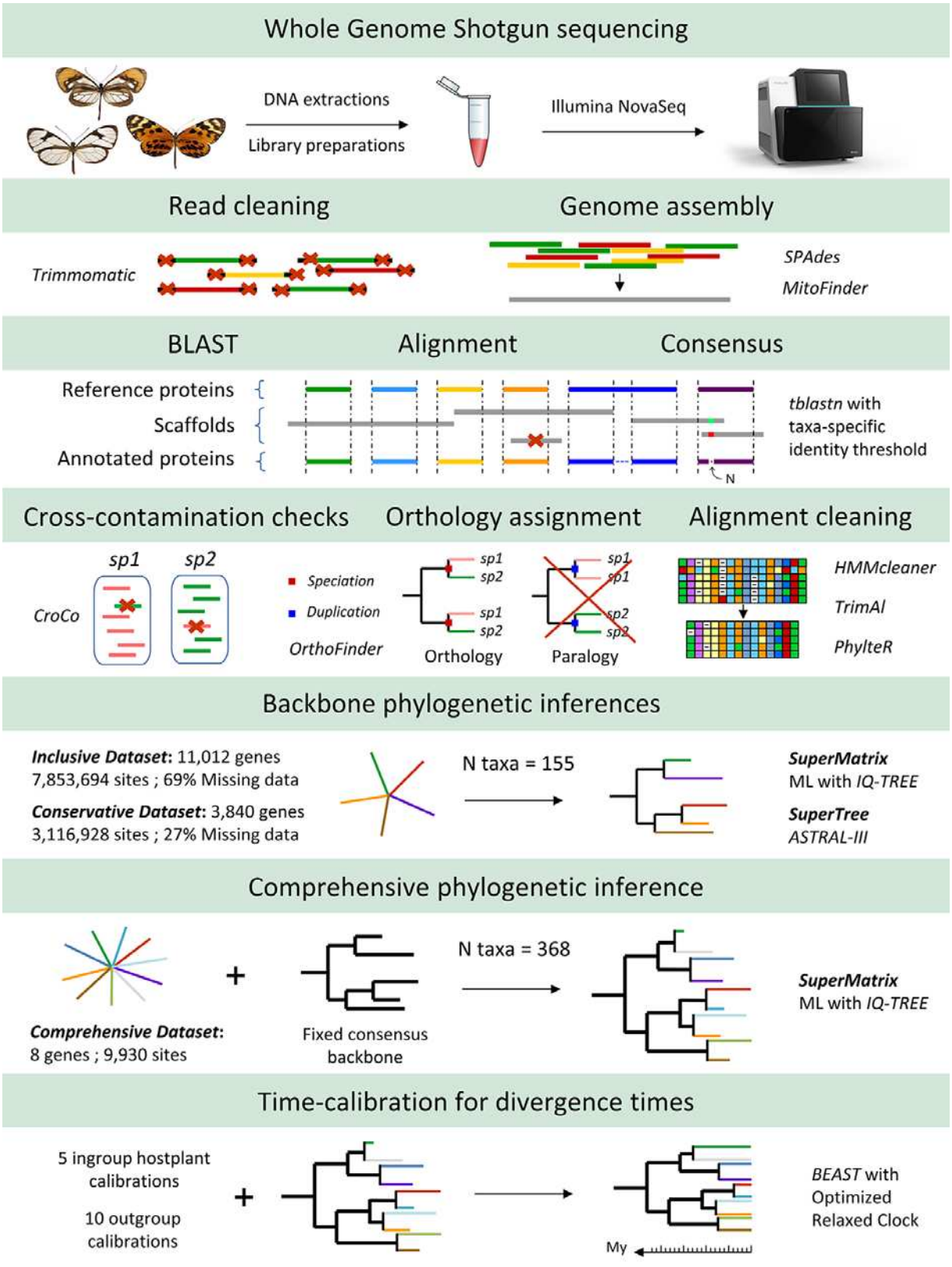

Figure 3: Analytic phylogenomic pipeline from wild specimens to a time-calibrated phylogeny as carried out in this study. Adapted from Allio *et al.* (2020b).

2.1 Taxon sampling, DNA extraction, and Illumina sequencing

Ithomiine samples were collected in tropical forests during the course of several field trips including Ecuador, Peru, Panama and Brazil over the last twenty years and preserved in DMSO at -20°C. The field specimen collection was complemented with specimens from museum collections from the Florida National Museum of Natural History in order to cover evenly the diversity of species. Final sample collection for WGS analyses encompassed 151 species across all 48 currently accepted genera (Doré *et al.* 2022; See complete check list in **ANNEXE 1, *SI Appendix 4*)**. We added to this collection 12 already assembled high-quality genomes of outgroup species spreading across Lepidoptera lineages including two moth species to root the tree. Complete metadata associated with specimens used for sequencing and phylogenomic inferences can be found in the ***SI Appendix 1*, Table S1**.

We extracted DNA from thorax or legs. Total genomic DNA extraction was performed with DNeasy Blood and Tissue Kits (Qiagen®) on previously ground tissues, digested overnight with 20 µL of proteinase K per sample. Extractions yielded DNA with a concentration ranging from 2 to 100 ng/µL (mean = 26.9 ng/µL ± 20.4 sd). We used the Illumina® Nextera DNA Sample Preparation Kit for library preparation to tag each sample with unique adapter sequences. We sequenced DNA through multiple multiplexed runs of Illumina® NovaSeq 6000 S2 V1.5 (300 cycles on 150 bp paired reads) for an expected coverage depth of 25x. We employed Trimmomatic 0.39 (Bolger *et al.* 2014) to clean reads by removing sections with low quality bases within a sliding window (window width = 4bp, minimum mean quality Q-score = 15) and reads with short length (below 50 bp). We provide sequencing summary statistics for each sample in ***SI Appendix 1*, Table S1**.

2.2 *De novo* assembly of genomes

We assembled reads from all 151 ithomiine species independently using the genome assembler SPAdes 3.15.4 employing de Bruijn graph heuristics to reconstruct long DNA sequences as scaffolds (Bankevich *et al.* 2012). We ran SPAdes with default parameters exploring best assemblies across several k-mer sizes (k = 21, 33, 55, and 77). We favored *de novo* assembly (i.e., without reference) over mapping on a reference genome since our samples covered a large taxonomic diversity with different degree of divergence to any ithomiine reference genome that would have imped read matches for the most distant sampled, and lead to bias across samples. Moreover, *de novo* assembly allows to recover potentially any section of the genome, not only the annotated genes found in a given reference genomes, thus yielding

a larger molecular dataset suitable for further genomic exploration. We produced generic summary statistic (e.g., N50, number of scaffolds, genome size, GC content, etc.) to evaluate the quality of each genome assembly with QUAST 5.0.2 (Mikheenko *et al.* 2018) and employed BUSCO 5.2.2 (Manni *et al.* 2021b) to quantify the proportion of orthologous genes retrieved from a set of 5,286 single-copy orthologous Lepidopteran references genes identified from 16 reference genomes (Manni *et al.* 2021; Lepidoptera ODB10 dataset). We provide genome assembly statistics for each sample in ***SI Appendix 1*, Table S1**.

2.3 Building and curating alignments of single-copy orthologous coding DNA sequences (CDS)

To build a set of orthologous sequences across our 151 WGS-based genome assemblies and the additional 12 outgroups genome assemblies retrieved directly from NCBI GeneBank, we performed a BLAST search using the *tblastn* tool (Gerts *et al.* 2006) for all genomes against all 54,431 available proteins in a recently published annotated high-quality reference genome of *Melinaea menophilus* encompassing ca. 500 Mbp (Gauthier *et al.* 2023). We removed *a priori* the mitochondrial proteins to avoid mismatch due to the difference in genetic code between invertebrate nuclear and mitochondrial genes. We favored the use of a unique reference genome to build a unique set of homologous annotated coding sequences while applying a sample-specific identify threshold to detect or discard matching scaffolds accounting for the variable degree of divergence of samples with respect to the reference genome (See ***SI Appendix 3*** for details on the rationale for choosing sample-specific thresholds). We matched only scaffolds with more than 50 AA and built strict consensus sequences from all retained hits for a given assembly and reference protein. However, prior to create CDS consensus sequences, we discarded all scaffolds whose same region matched on several reference proteins to prevent risk of paralogs, and removed all hits that were embedded into other scaffolds to limit polymorphism leading to uninformative consensus. As such, we obtained pre-aligned sets of annotated CDS for each sample that putatively reflected orthologous sequences.

As we used multiplexed runs to sequence our samples, we were exposed to the risk of cross-contamination (i.e., sequenced identified to the wrong sample (Ballenghien *et al.* 2017)). Thus, we used CroCo 1.1 (Simion *et al.* 2018) to investigate potential cross-contamination in our CDS dataset and filter out all dubious sequences that displayed a higher match with raw reads from other samples that from its original read pool (See ***SI Appendix 4***). Next, we used OrthoFinder 2.5.4 (Emms & Kelly 2019) to assign all CDS sequences to orthogroups that

tentatively represent sets of genes descending from a single gene found in a common ancestor. Among those genes, orthologs refers to the genes that evolved through cladogenesis, in contrast with paralogs that may arise from duplication events within a lineage. Thus, in theory the evolutionary history of orthologous genes should depict the evolutionary relationships among lineages (Kuzniar *et al.* 2008). Here, we selected only orthogroups with one gene per species to limit gene duplication issues. Additionally, we removed orthogroups with annotated sequences associated with multiple reference proteins in the reference genome, and sets of orthogroups with sequences matching the same reference protein. In the end, we kept only unique orthogroups that encompassed one sequence per species matching a unique reference protein corresponding to sets of single-copy orthologous sequences.

Each set of single-copy orthologs were mapped onto a unique reference protein during the BLAST search step so they are already forming alignments. Yet, to ensure the quality of such alignments, we ran HMMCleaner 1.8 to detect and remove poorly aligned sections of sequences based on hidden Markov models profiles (Di Franco *et al.* 2019). Additionally, we removed sites with few aligned nucleotides due to sequence gaps using trimA1 1.2rev59 (Capella-Gutiérrez *et al.* 2009) with the *gappyout* parameter to detect bimodal distributions of gaps across sites and remove the ones falling into the poorly represented portion. Once those cleaning steps were achieved, we kept only sample sequences that had 30% of sites overlapping with at least 50% of sequences in order to minimize missing data in the final alignments. Finally, we used the R package *phylter* 0.9.3 (de Vienne *et al.* 2023) to detect overall outlier sequences based on gene distance matrices with an adjusted k parameter (k = 4.0) to balance the gain in matrix concordance gain with limited data loss. We removed all individual outlier sequences from alignments and we got rid of entire alignments with more than 20% of outliers detected to be conservative.

We provide BLAST search, cross-contamination cleaning, orthology assignment, and outlier detection statistics for each sample in ***SI Appendix 1*, Table S1**.

2.4 Generating molecular datasets

2.4.1 WGS datasets

After all the curation steps, we were left with 16,859 alignments of single-copy orthologous genes including from 2 to 153 taxa distributed across 163 species (151 ithomiines + 12 outgroups). We used AMAS (Borowiec 2016) to concatenate genes into datasets with a

combination of gene and taxa representativeness thresholds, and compute the number of remaining genes, taxa, and informative sites for each threshold combination. Histograms and heatmaps summarizing the exploration of dataset features according to threshold choices are available in ***SI Appendix 5***. As a result of this exploration, we chose to design two datasets to account for the effect of missing data on downstream analyses: (i) an *Inclusive dataset* aiming to maximize the number of genes and taxa involved, even if some gene alignments encompass few taxa, and some species record few genes; (ii) a *Conservative dataset* aiming to limit missing data and remove genes with low representativeness. As such, we set a minimum of 4 taxa per alignments (the minimum to build quartet trees) in the *Inclusive dataset*, while we retained only genes encompassing at least half of taxa (i.e., 82 species) for the *Conservative dataset*. In both datasets, we removed taxa present in less than 0.5% of the alignments (i.e., with sequences recovered for less than 84 genes) to limit missing data while keeping a maximum of taxa.

2.4.2 A new comprehensive molecular dataset

Our WGS datasets were designed to produce phylogenetic hypotheses for the backbone phylogeny in order to resolve and support deep evolutionary relationships within ithomiine lineages. Yet, even the most inclusive dataset covered 'only' 143 ithomiines species (i.e., 36.1% of extant species). In order to expand the taxonomic scope of our final phylogeny, we extracted from our WGS datasets the sequences for the eight protein-coding genes covering 340 species in Chazot *et al.* (2019) and merged both datasets. Since nine former species used in Chazot *et al.* (2019) had been split in two separated taxa since, we retrieved individual sequences for each pair of taxa from NCBI GeneBank to replace the former chimeric consensus sequences used by Chazot *et al.* (2019). Additionally, we assembled mitochondrial sequences (mtDNA) from our pools of WGS reads using MitoFinder 1.4.1 (Allio *et al.* 2020a) for all sequenced taxa, and also added newly sequenced barcode data for 3 new species (*Hypoleria asellia*, *Hypomenitis nsp4*, *Oleria bifurcata*). Then, we used MUSCLE 5.1 (Edgar 2022) to align each newly complemented set of gene sequences and used HMMCleaner 1.8 and trimA1 1.2rev59 to curate final alignments.

Complete metadata associated with specimens and sequences used in the *Comprehensive dataset* forming taxa-rich alignments used in final phylogenetic inferences, including taxonomic updates for species names and chimera split can be found in the ***SI Appendix 2*, Table S2**.

2.5 Phylogenetic inferences

For each of the two WGS datasets, we performed SuperTree inferences assembled from individual gene trees and SuperMatrix inferences based on concatenated alignments.

2.5.1 Phylogenetic inferences with SuperTree

We first estimated the best fitted gene tree for each gene alignment with IQ-TREE 2.2.0.3 (Minh *et al.* 2020b) using maximum likelihood optimization and full model selection across all available nucleotide substitution models including free rate categories (Parameter settings: -m MFP -mrate R) with ModelFinder (Kalyaanamoorthy *et al.* 2017) to visualize the complexity heterogeneity in gene evolution. Free rates categories are a more flexible and generalized alternative to discretized Gamma distributions to model heterogeneity in substitution rates across sites that allowed to assigned any substitution rate values to each category of sites (Soubrier *et al.* 2012). Since gene trees inferred with GTR models (Tavaré 1986) showed a similar global behavior to trees inferred with models selected via ModelFinder, we used the best fitted GTR + R models for downstream analyses (See ***SI Appendix 6*** for visualization of gene evolution complexity and comparison of substitution models for ML gene tree inferences). To avoid poorly supported relationships to have an impact on the SuperTree inferences, we collapsed all branches with a length inferior to 0.5 divided by the number of sites in the alignment or an Ultrafast Bootstrap support (UFBS) below 10% (Minh *et al.* 2013).

Next, we used ASTRAL-III 5.7.8 (Zhang *et al.* 2018) to infer a SuperTree from both *Inclusive* and *Conservative* sets of previously inferred gene trees. ASTRAL is a summary method : it finds the species tree that maximizes the number of induced quartet trees in unrooted gene trees that are shared by the species tree. We estimated normalized quartet scores as support values for each node computed as the proportion of induced quartet gene trees satisfied by the topology of a given branch (Mirarab *et al.* 2014). Additionally, we computed local posterior probabilities as the probability that the branch were present in the true species tree which generated the input gene trees assuming a multispecies coalescence model (Sayyari & Mirarab 2016). Finally, we assessed the congruence between individual gene trees and the final species SuperTrees obtained for each dataset (See ***SI Appendix 7)***.

2.5.2 Phylogenetic inference with SuperMatrix

We conducted maximum likelihood estimates of best species trees based on concatenated alignments in SuperMatrices with IQ-TREE 2.2.0.3 (Minh *et al.* 2020b). First, we ran a partition

merging run without inferring the species tree (Parameter settings: -m MF+MERGE), only to obtain the partitioning of genes, with a limited set of GTR models with free rates categories ranging from 2 to 6 (Parameter settings: -mset GTR -mrate R -cmin 2 -cmax 6) to cover most of best model options selected from gene tree inferences (See ***SI Appendix 6***). We obtained 332 partitions for the 11,012 genes in the *Inclusive dataset* and 178 partitions for 3,518 genes in the *Conservative dataset*. Second, we ran the final species tree inferences with ModelFinder selecting among all available substitution models for nucleotides, using the gene partition scheme inferred in the previous step (Parameter settings: -m MFP). We estimated node support values with 1000 UFBS and SH-aLRT tests (Guindon *et al.* 2010). We did not run Bayesian inferences to obtain backbone topologies since the size of our datasets made it unrealistic to achieve MCMC convergence in reasonable time frames (e.g., Allio *et al.* 2020b).

2.5.3 Supporting backbone topologies and building a consensus

In complement to normalized quartet scores and local posterior probabilities for SuperTrees and UFBS and SH-aLRT tests for SuperMatrix-based species trees, we computed gene and site concordance factors (gCF and sCF; Minh *et al.* 2020a) in IQ-TREE to evaluate the percentage of gene trees and sites that support a particular branch topology. We also tested if gCF and sCF scores for the current local quartet topology were higher than the support provided for the two local NNI alternative quartet topologies, known as discordance factors (i.e., whether gCF > max(gDF_1, gDF_2) and sCF > max(sDF_1, sDF_2); Minh *et al.* 2020a). Then, we compared node support values across all WGS-based phylogenetic hypotheses, for different taxonomic levels (i.e., inter-subtribes, subtribes, intra-subtribes).

Beyond the comparison of node supports values across the four final backbone phylogenies (i.e., two datasets × two inference methods), we are planning to compare the support values for global topologies using gene-wise phylogenetic signal (ΔGLS) in the framework described in Shen *et al.* (2021). Such index allows us to visualize and compare the support provided by each gene alignment to a set of alternative global topology to evaluate. Our goal is to compare the mean support for each global topology from the sets of gene alignments and associated gene trees based on maximum likelihood and normalized quartet scores. We suspect that such framework will provide even stronger support for the selection of the suitable backbone topologies than the comparison of node support values already does.

Based on the previous support metrics, we selected the two topologies inferred from the concatenated SuperMatrices as the most supported topologies. Thus, we build the final backbone topology as the strict consensus between these two selected topologies.

2.5.4 Inferring species tree with all taxa

We estimated the final comprehensive phylogeny that encompasses all ithomiine species with available molecular data via maximum likelihood optimization in IQ-TREE based on the *Comprehensive dataset* encompassing 368 taxa and 9,930 sites across 8 genes. We ran a GTR model with gene partition scheme selecting best number of free rate categories for each gene model (Parameter settings: -m MFP -mset GTR -mrate R). Crucially, we constrained the tree topology exploration to satisfy the backbone consensus topology estimated from WGS data for the 155 species included in the backbone, while all other branches could be swapped around during optimization (Parameter settings: -g backbone_phylogeny.tree).

2.6 Estimation of divergence times

Finally, we performed Bayesian inferences of the node ages using BEAST 2.5.0 (Bouckaert *et al.* 2019). Time-calibration of the consensus backbone phylogeny based on the top 1% of genes (ca. 150,000 sites across 110 genes) with highest taxa representativeness from the WGS dataset is still ongoing due to the important computation time needed (10 million of iterations reached in ca. two weeks of CPU-time). The final goal is to use the 95% HPD intervals obtained for internal node ages of the in-group of the time-calibrated backbone phylogeny as secondary calibrations for the final comprehensive phylogeny. Meanwhile, we ran time calibration for the final comprehensive phylogeny using directly the alignments of the *Comprehensive dataset* (9,930 sites across 8 genes).

For all analyses, we fitted an Optimized Relaxed Clock model (Douglas *et al.* 2021) with uncorrelated substitution rates of branches drawn from a unique log-normal distribution (UCLN model) based on a birth-death tree prior for speciation/extinction events. Since no fossil are available for ithomiine butterflies, we applied five secondary calibrations on ingroup (Ithomiini) internal nodes as uniform priors with upper bounds based on the maximum estimated age of the Solanaceae hostplant lineage associated with each ithomiine clade, as retrieved from (De-Silva *et al.* 2017). We applied ten additional secondary calibrations on outgroup nodes based on larger phylogenies of Nymphalidae (Chazot *et al.* 2021), Papilionoidea (Chazot *et al.* 2019a), and Lepidoptera as a whole (Kawahara *et al.* 2019). These

calibrations consisted in normal priors adjusted such as their 95% confidence interval matched with the 95% Height Posterior Density (HPD) of node age posterior distributions reported in these higher phylogenies (See ***SI Appendix 8*, Table S3** for details on secondary calibrations). All Bayesian exploration of parameter space were performed using the ML-inferred comprehensive phylogeny as fixed topology: only the branch lengths were allowed to vary. We ran two independent MCMC chains with 10^8 iterations and merged both run after checking for convergence and removal of the first 10^7 iterations as a conservative burn-in. Credible ranges of node ages were assessed as the 95% Height Posterior Density (95% HPD) from the posterior distributions of nod ages in the remaining trees.

3 Results

3.1 WGS sequencing and Genome assembly

Illumina® NovaSeq WGS sequencing provided an average of 2 × 62.4 million paired-reads per sample. Once filtered with Trimmomatic 0.39 (Bolger *et al.* 2014) for high-quality reads, we recorded 2 × 50.7 million paired-reads per sample, yielding an average coverage depth of 34.4x. We obtained 151 genome assemblies from SPAdes 3.15.4 (Bankevich *et al.* 2012) with a mean size of 237.7 Mbp that scales to ca. 47.6% of total genome size in comparison to high-quality chromosome-scale genome assemblies from two *Melinaea* species (Gauthier *et al.* 2023). These assemblies were highly fragmented with 4,922 scaffolds and a N50 of 4,908 bp in average that yielded a 52.9% recovery rate for complete genes in the BUSCO set. Yet, we were able to reconstruct long sequences with the maximum scaffold size being 133.5 Kbp in average. Besides, we obtained a high recovery rates for the mitochondrial genome with 13.6 genes out of 15 (90.7%) recovered per samples representing 11,786 bp in average. We provide WGS sequencing and genome assembly statistics for each WGS sample in ***SI Appendix 1*, Table S1**.

3.2 Curation of the molecular datasets for phylogenetics

Using custom BLAST search procedures, we reconstructed 20,534 proteins per sample in average, representing 37.7% of the 54,431 suspected genes available in the reference genome (Gauthier et al. 2023). We detected 8.8% of dubious sequences via cross-contamination checks conducted with CroCo 1.1 (Simion *et al.* 2018). Contrary to expectations (see Allio *et al.* 2021), this cross-contamination step did not allow us to identify a higher number of orthogroups, but it efficiently cleaned sequences initially forming dubious small putative orthogroups with very

few sequences/taxa involved (See ***SI Appendix 4*, Figure S2**). We retrieved 16,859 alignments of single-copy orthologous genes including from 2 to 153 taxa distributed across 163 species (151 ithomiines + 12 outgroups). Each taxon was represented in 5,341 alignments in average. We further removed 8.7% of sequences detected as outliers on the basis of abnormal distances within and between alignments. We removed 8 taxa that were present in less than 0.5% of the alignments (i.e., with sequences recovered for less than 84 genes) and we applied two minimum taxa representativeness thresholds (i.e., $N_{Inclusive} \leq 4$ taxa and $N_{Conservative} \leq 82$ taxa) to design our *Inclusive* and *Conservative datasets* representing varying degree of missing information. As a result, the *Inclusive dataset* comprised 155 taxa and 11,012 genes for 7,853,694 nucleotide sites including 69.1% of missing data, 40.2% of variable sites, and 30.4% of parsimony-informative sites. In average, each sample was represented by 3,116,928 sites across 3,840 genes including 26,7% of missing data among available genes with only 0,3% of undefined nucleotides. Meanwhile, the *Conservative dataset* encompassed the same 155 taxa, and 3,518 genes for 3,327,087 sites including 50.8% of missing data, 50.2% of variable sites, and 40.9% of parsimony-informative sites. On average, each sample featured 2,093,747 sites across 2,165 genes including 27,4% of missing data among available genes with only 0,2% of undefined nucleotides. We provide BLAST search, cross-contamination cleaning, orthology assignment, and outlier detection statistics for each WGS sample in ***SI Appendix 1*, Table S1**.

Building upon a previously assembled dataset of eight genes encompassing initially 340 ithomiine species (Chazot *et al.* 2019b), we assembled a new *Comprehensive dataset* aggregating the previous data, our WGS data, new barcode information, and additional sequences from NCBI GeneBank to generate taxon-rich alignments used to produce the final comprehensive phylogeny. This *Comprehensive dataset* comprised 9,930 sites across 8 genes for 368 taxa (356 ithomiines + 12 outgroups) covering 89.9% of the 396 documented ithomiine species (Doré *et al.* 2022). It included 59.7% of missing data, 47.4% of variable sites, and 37.8% of parsimony-informative sites. On average, each sample featured 5,648 sites across 4.6 genes including 25.8% of missing data among available genes with only 0.2% of undefined nucleotides. We provide metadata and summary statistics for each taxon found in the *Comprehensive dataset* in ***SI Appendix 2*, Table S2**.

3.3 Support and selection of backbone topologies

We obtained four different phylogenetic hypotheses based on WGS data for the backbone topology crossing our two datasets (*Inclusive vs. Conservative*) vs. two phylogenetic inference

methods (SuperMatrix with IQ-TREE vs. SuperTree with ASTRAL), provided in ***SI Appendix 9* (Fig. S9, S10, S11 & S12)**. The deep relationships between subtribes were similar for the two SuperMatrix-based phylogenies, while the two datasets led to different deep topologies for the SuperTrees. All four topologies suggested the existence of a clade formed by Mechanitina and the core-group, which encompasses all subtribes with members feeding on the diverse *Solanum* genus, and having lost their subdorsal filaments in the last instar caterpillar (Willmott & Freitas 2006). However, the branching of the remaining four subtribes (i.e., Melinaeina, Athesitina, Tithoreina, and Methonina) varies across topologies. The two SuperTree topologies suggested an unusual (i.e., never suspected in previous systematic explorations) unique clade for these four tribes, sister to the 'Solanum-feeders' clade, while the SuperMatrix topologies both featured the Melinaeina tribe as sister to all other ithomiines. Additionally, the SuperTree topology based on the *Inclusive* dataset did not retrieve the well-established Tithoreina/Methonina clade found in all modern propositions (Brower *et al.* 2006, 2014; Willmott & Freitas 2006; Chazot *et al.* 2019b). At a more recent scale, the relationships between genera within the subtribes were almost all identical across the four phylogenies. Most genera were established as monophyletic, and the few ones that were not (i.e., *Hypothyris-Hyalyris* complex, paraphyletic *Hypoleria* and *Hyalenna*, *Episcada-Ceratinia* complex) were similarly problematic across all four phylogenetic hypotheses, hinting for the need of taxonomic revisions.

Altogether, nodes showed high support values across all topologies with mean UFBS scores ranging from 98.2% to 98.6% for SuperMatrix-based trees, and mean local posterior probabilities ranging from 97.4% and 98.1% for SuperTrees. The nodes suggesting the monophyly of the subtribes obtained the highest support, while the conflicting nodes reflecting deep evolutionary relationships across subtribes received the lowest support across all four phylogenies (**Table 1**). In particular, SuperTree topologies provided low supports for the relationships between subtribes with 4 inter-subtribes nodes out of 10 failing to demonstrate higher site supports for their current local topology compare to NNI alternatives, while also showing relatively low gCF scores in average (i.e., 20.7 % and 21.7 %; **Table 1**).

Table 1: Node support values across all four WGS-based phylogenetic hypotheses. gCF = gene concordance factors as the percentage of decisive gene trees supporting the local branch topology from the species tree. sCF = site concordance factors as the percentage of decisive sites supporting the local branch topology from the species tree. gDF and sDF relate to support to the two alternative NNI topologies of local branches known as discordance factors. We tested whether concordance factors scored higher than any discordance factors. UFBS = Ultra-Fast Bootstraps. SH-aLRT = alternative likelihood ratio tests. Scores in bold represent the highest support across phylogenetic hypotheses for a given set of nodes and support index. Scores in red highlight relatively low support values.

	SuperMatrix (ML with IQ-TREE)		**SuperTree (Summary with ASTRAL)**	
	Inclusive dataset (N = 11,012)	**Conservative dataset (N = 3,518)**	**Inclusive dataset (N = 11,012)**	**Conservative dataset (N = 3,518)**
gCF	**Mean ± sd**	**Mean ± sd**	**Mean ± sd**	**Mean ± sd**
All nodes	46.6 ± 25.8	47.3 ± 26.8	45.7 ± 26.2	**47.9 ± 26.9**
Ingroup nodes	47.0 ± 25.9	48.1 ± 27.2	46.8 ± 26.1	**49.0 ± 26.9**
Inter-subtribe nodes	40.6 ± 22.8	43.0 ± 23.5	20.7 ± 15.0	21.7 ± 15.4
Subtribe crown nodes	59.5 ± 30.1	**59.9 ± 18.8**	56.4 ± 20.8	59.2 ± 20.6
Intra-subtribe nodes	46.5 ± 25.7	47.1 ± 27.1	47.9 ± 26.1	**50.2 ± 26.2**
sCF	**Mean ± sd**	**Mean ± sd**	**Mean ± sd**	**Mean ± sd**
All nodes	51.3 ± 16.8	51.2 ± 17.0	**51.6 ± 16.9**	51.3 ± 16.8
Ingroup nodes	**52.4 ± 17.1**	51.7 ± 17.2	52.3 ± 17.2	52.1 ± 17.1
Inter-subtribe nodes	46.3 ± 13.5	46.0 ± 13.2	39.7 ± 8.3	39.7 ± 8.4
Subtribe crown nodes	61.2 ± 21.3	**64.2 ± 19.9**	53.0 ± 15.2	52.6 ± 15.2
Intra-subtribe nodes	51.7 ± 16.7	51.1 ± 16.9	**53.2 ± 17.5**	53.0 ± 17.4
gCF > max(gDF_1, gDF_2)	**# support (%)**	**# support (%)**	**# support (%)**	**# support (%)**
All nodes	**147 (96.7 %)**	144 (94.1 %)	143 (92.9 %)	145 (94.8 %)
Ingroup nodes	**139 (97.9 %)**	134 (94.4 %)	134 (94.4 %)	136 (95.8 %)
Inter-subtribe nodes	**9 (100%)**	**9 (100%)**	7 (77.8%)	**9 (100%)**
Subtribe crown nodes	**10 (100%)**	**10 (100%)**	**10 (100%)**	**10 (100%)**
Intra-subtribe nodes	**120 (97.6 %)**	116 (94.3 %)	117 (95.1 %)	117 (95.1 %)
sCF > max(sDF_1, sDF_2)	**# support (%)**	**# support (%)**	**# support (%)**	**# support (%)**
All nodes	136 (89.5 %)	135 (88.2 %)	**138 (90.8 %)**	137 (90.2 %)
Ingroup nodes	128 (90.1 %)	125 (88.0 %)	**130 (91.5 %)**	128 (90.1 %)
Inter-subtribe nodes	**8 (88.9%)**	**8 (88.9%)**	6 (66.7%)	6 (66.7%)
Subtribe crown nodes	**10 (100%)**	**10 (100%)**	**10 (100%)**	**10 (100%)**
Intra-subtribe nodes	110 (89.4 %)	107 (87.0 %)	**114 (92.7 %)**	112 (91.1 %)
UFBS	**Mean ± sd**	**Mean ± sd**	**Mean ± sd**	**Mean ± sd**
All nodes	**98.6 ± 5.8**	98.2 ± 8.8	NA	NA
Ingroup nodes	**98.5 ± 6.0**	98.1 ± 9.2	NA	NA

Inter-subtribe nodes	**99.3 ± 1.0**	97.3 ± 4.0	NA	NA
Subtribe crown nodes	**100 ± 0.0**	**100 ± 0.0**	NA	NA
Intra-subtribe nodes	**98.3 ± 6.4**	98.0 ± 9.8	NA	NA

SH-aLRT	**Mean ± sd**	**Mean ± sd**	**Mean ± sd**	**Mean ± sd**
All nodes	**99.2 ± 7.1**	98.6 ± 6.7	NA	NA
Ingroup nodes	**99.1 ± 7.4**	98.5 ± 6.9	NA	NA
Inter-subtribe nodes	**100 ± 0.0**	**100 ± 0.0**	NA	NA
Subtribe crown nodes	**100 ± 0.0**	**100 ± 0.0**	NA	NA
Intra-subtribe nodes	**99.0 ± 8.0**	98.3 ± 7.4	NA	NA

Normalized Quartet scores	**Mean ± sd**	**Mean ± sd**	**Mean ± sd**	**Mean ± sd**
All nodes	NA	NA	65.1 ± 20.8	**66.4 ± 21.1**
Ingroup nodes	NA	NA	65.9 ± 20.9	**67.4 ± 21.2**
Inter-subtribe nodes	NA	NA	55.6 ± 19.6	**57.8 ± 21.5**
Subtribe crown nodes	NA	NA	80.3 ± 16.8	**82.8 ± 16.7**
Intra-subtribe nodes	NA	NA	65.5 ± 20.8	**66.9 ± 21.0**

Local posterior probabilities	**Mean ± sd**	**Mean ± sd**	**Mean ± sd**	**Mean ± sd**
All nodes	NA	NA	**98.1 ± 9.9**	97.4 ± 11.5
Ingroup nodes	NA	NA	**98.0 ± 10.3**	97.3 ± 11.9
Inter-subtribe nodes	NA	NA	**99.0 ± 3.0**	90.3 ± 29.0
Subtribe crown nodes	NA	NA	**100 ± 0.0**	**100 ± 0.0**
Intra-subtribe nodes	NA	NA	**97.8 ± 11.0**	97.6 ± 10.2

As a result, we selected the two topologies based on the *Inclusive* and *Conservative datasets* inferred with IQ-TREE from the concatenated SuperMatrices as the best supported topologies. Thus, we built the final backbone topology as the strict consensus between these two selected topologies. We elaborate further on the rationale behind this selection in the *Discussion* section.

The consensus backbone topology encompassed 143 ithomiine species and 12 outgroups and comprised four polytomies reflecting minor disagreements between the two selected topologies for the consensus (**Fig. 3**). Such polytomies reflected uncertainties in the branching of *Mechanitis* species, *Pteronymia* species, the *Ceratinia-Episcada* complex, and the *Hypothyris-Hypoleria* complex. We aimed to address them with the taxa-rich alignments providing higher taxonomic sampling in these groups for the inference of the final comprehensive phylogeny (**Fig. 4**).

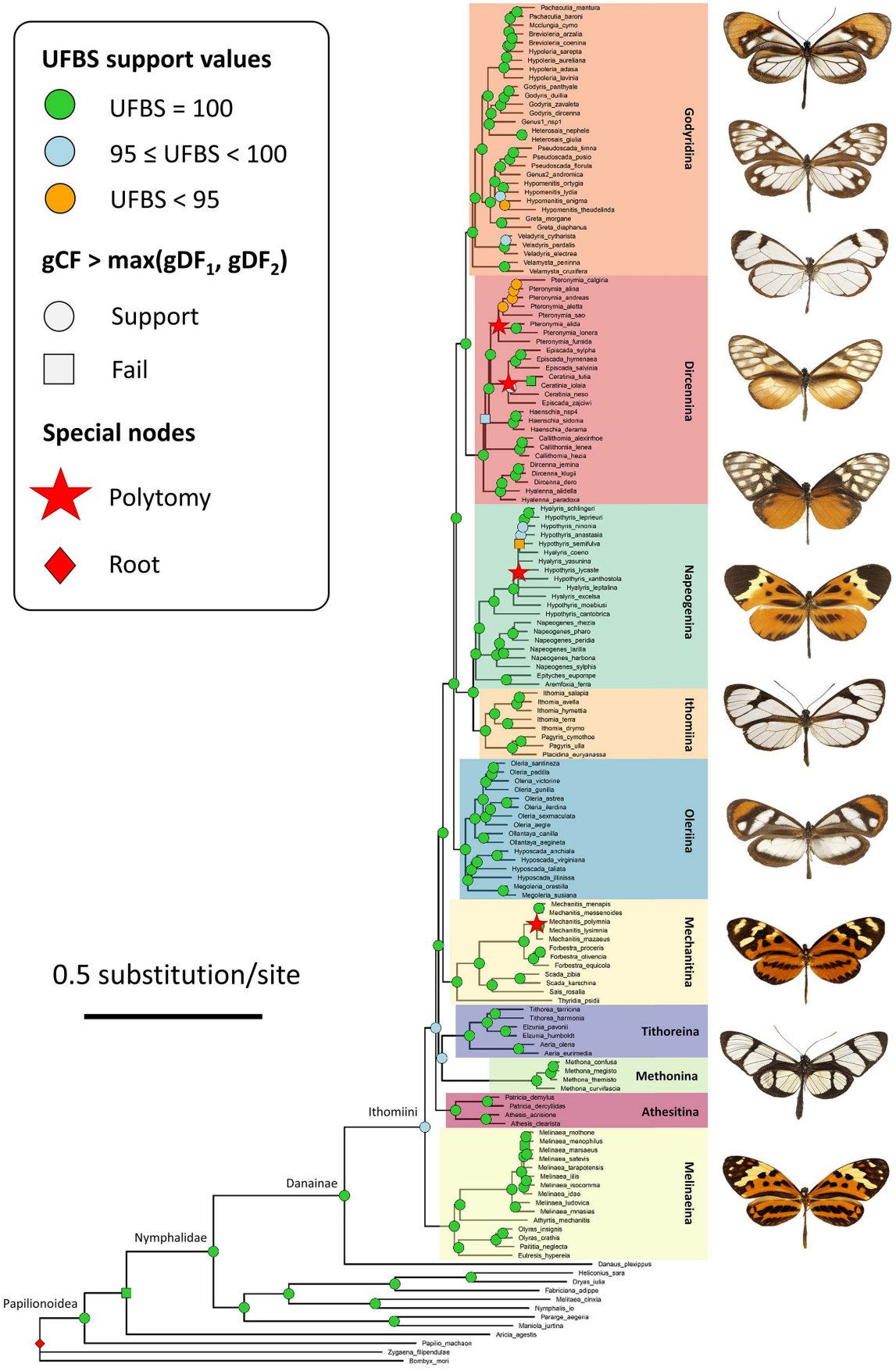
UFBS support values
UFBS = 100
95 ≤ UFBS < 100
UFBS < 95
gCF > max(gDF1, gDF2)
Support
Fail
Special nodes
Polytomy
Root
0.5 substitution/site
Godyridina
Dircennina
Napeogenina
Ithomiina
Oleriina
Mechanitina
Tithoreina
Methonina
Athesitina
Melinaeina
Ithomiini
Danainae
Nymphalidae
Papilionoidea
Danaus_plexippus
Heliconius_sara
Dryas_iulia
Fabriciana_adippe
Melitaea_cinxia
Nymphalis_io
Pararge_aegeria
Maniola_jurtina
Aricia_agestis
Papilio_machaon
Zygaena_filipendulae
Bombyx_mori

Figure 3: Consensus topology for the backbone phylogeny inferred from WGS data encompassing 143 ithomiine species and 12 outgroups. The strict consensus was obtained by merging final topology inferred with IQ-TREE from two SuperMatrices encompassing respectively 11,012 genes and 3,518 genes. It includes four polytomies, symbolized with red stars, reflecting minor disagreements between the two topologies used for the consensus. Branch lengths relates to the inferred mean number of substitutions per site along each branch. Colored clades correspond to the ten known subtribes. Node support values are illustrated with colored symbols according to mean UFBS scores and gene concordance factors (gCF) tests against support for alternative local topologies (i.e., gDF = discordance factors).

3.4 Time-calibrated comprehensive phylogeny

The final comprehensive species-level phylogeny inferred from the *Comprehensive dataset* using the fixed backbone topology established from WGS data encompassed 368 taxa (356 ithomiines + 12 outgroups) covering 89.9% of the 396 documented ithomiine species (Doré *et al.* 2022). Its topology was generally well supported with 86.0 % supports from UFBS in average, even for nodes establishing deep evolutionary relationships across subtribes (mean UFBS = 92.7%).

We performed Bayesian inferences of the node ages of the final comprehensive phylogeny using secondary calibrations based on the ages of hostplant lineages for ingroup calibrations and reference Lepidopteran phylogenies for the outgroup calibrations. We obtained a crown age of 29.8 My for the Ithomiini tribe (95% HDP: 27.3-32.0 My) despite a prior set around 24.8 My following the most up-to-date calibration for Nymphalidae butterflies (Chazot *et al.* 2021). All subtribes diverged relatively early (within the first 8 My), but the current extent diversity within each subtribe emerged mostly in the late Miocene (ca. 12-8 My) likely following the demise of the Pebas aquatic system in Western Amazonia (**Fig. 4**; Chazot *et al.* 2019b).

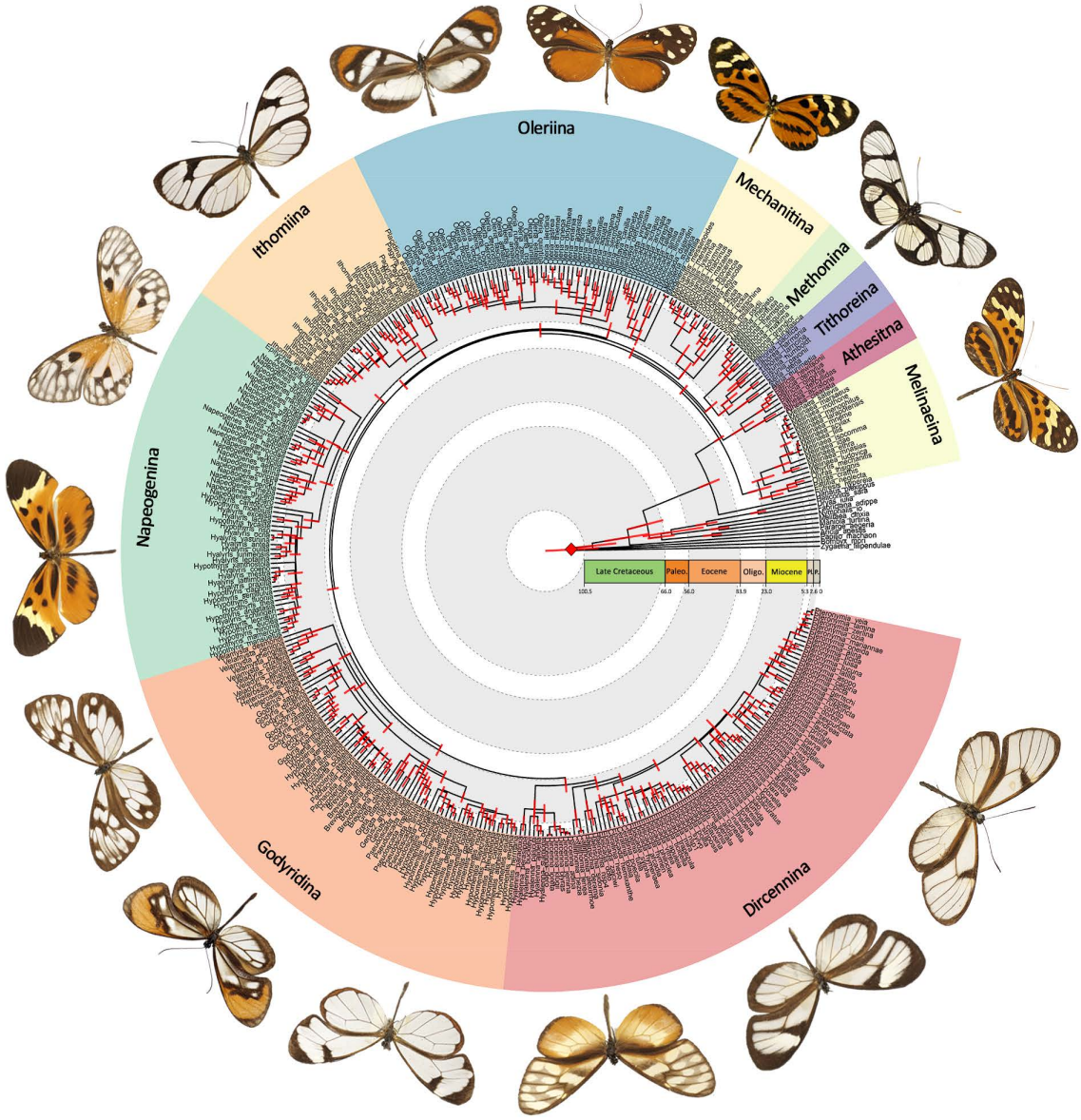

Figure 4: Comprehensive time-calibrated species-level phylogeny encompassing 356 ithomiine species and 12 outgroups. The topology was inferred with IQ-TREE from the SuperMatrix of the *Comprehensive dataset* encompassing 9,930 sites across 8 genes, using the WGS-based backbone phylogeny as constraints for the topology exploration. Node ages were estimated from Bayesian inference with BEAST using secondary calibrations from hostplant and higher-level phylogenies. Median node ages are shown inside their 95% Height Posterior Density intervals obtained through Bayesian inference (red bars). Colored clades correspond to the ten known subtribes. Detailed time-calibrated phylogenies zooming on specific clades are available in ***SI Appendix 10***.

Overall, node ages in our phylogeny were generally slightly older but still compatible with those inferred in Chazot *et al.* (2019b). However, they generally proved significantly older than in Garzón-Orduña *et al.* (2015), a study that relied on secondary calibration from unlikely

young ages for Solanaceae (Särkinen *et al.* 2013), the main hostplants of ithomiines (**Table 2;** see Lisa De-Silva *et al.* (2017) for further discussion of such differences).

Table 2: Crown age estimates for major ithomiine clades obtained from secondary calibrations in this study, compared to previous inferences and initial priors. Calibrations were performed on the *Comprehensive dataset* covering 9,930 sites across 8 genes using an Optimized Relaxed Clock model with an uncorrelated log-normal model for substitution rates and based on a birth-death tree prior for speciation/extinction events. Ages are shown in My as median estimates with 95% HPD intervals. Priors relates to uniform distribution bounded with the maximum age estimates of associated hostplant lineages, except for the Ithomiini tribe were a normal distribution based on previous reference estimates was used and for which bounds represent the 95% confidence interval (*).

	This study			Chazot *et al.*, 2019b			Garzón-Orduña *et al.*, 2015			Set priors	
Node	**Median**	**-**	**+**	**Median**	**-**	**+**	**Median**	**-**	**+**	**-**	**+**
Ithomiini	29.8	27.3	32.0	26.4	22.0	31.5	31.04	23.0	39.0	21.8*	27.8*
Melinaeina	19.8	17.1	27.7	18.4	15.7	21.7	12.5	10.0	14.0	0.0	37.2
Methonina	11.6	7.2	16.1	6.1	4.6	8.0	10.6	7.0	13.0	0.0	41.3
Tithoreina	20.8	17.0	24.9	16.8	13.6	20.0	11.1	8.0	14.0	NA	NA
Athesitina	18.8	13.0	24.8	12.9	10.0	16.6	11.6	9.0	13.0	0.0	24.8
Mechanitina	22.1	17.8	26.3	21.6	16.3	26.3	13.1	11.0	15.1	NA	NA
Core-group	25.9	23.4	28.5	19.1	16.6	22.3	13.7	11.9	15.0	NA	NA

4 Discussion

4.1 Selection of WGS-based backbone topologies

The uncertainty accompanying the evolutionary relationships across ithomiine subtribes is a known phenomenon (Brower *et al.* 2014) and a primary impulse for this study. Such instability observed across the successive phylogenetic hypotheses (Willmott & Freitas 2006; Garzón-Orduña *et al.* 2015; Chazot *et al.* 2019b) is apparent in the conflicts showed in the results of our four different phylogenetic hypotheses for the backbone topology (***SI Appendix 9***), and the relatively low support provided to these relationships (See Inter-subtribe nods in **Table 1**). The difficulty to settle on a robust topology for the relationships among ithomiine subtribes likely arise from the historical biogeography of the group. Ithomiini are suspected to have started diversifying along the early Andean foothills at the transition with Western Amazonia, coinciding with the uplift of the eastern cordillera of Central Andes during the late Oligocene (Eude *et al.* 2015; Chazot *et al.* 2019b). These early lineages underwent a rapid early diversification that is reflected in the short branches featured in both the uncalibrated ML optimized trees illustrating few substitutions inferred along branches (***SI Appendix 9*, Fig. S9**

& S10), and the final time-calibrated tree depicting rapid diversification (**Fig. 4**). Such rapid radiation may have induced high degree of incomplete lineage sorting (ILS) across the subtribes that is notably problematic for deep evolutionary inferences (Suh *et al.* 2015; Esquerré *et al.* 2022; Feng *et al.* 2022).

Summary methods based on congruency in gene-level phylogenetic signal such as ASTRAL (Mirarab *et al.* 2014) are quick and efficient solutions to deal with large molecular dataset. In our case, they provided a final topology in three days against more than 45 days for maximum likelihood optimizations, while Bayesian inferences were considered virtually infeasible in reasonable time. However, despite being designed to handle ILS by considering a consensus among the potentially divergent evolutionary histories produced by independent genes, thus being statistically consistent with the multi-species coalescent model (Zhang *et al.* 2018), we struggled to come up with robust phylogenetic hypotheses based on a summary approach (see gCF, sCF and associated tests for SuperTree phylogenies in **Table 1**). Such issue may hint for large incongruency in phylogenetic signal at gene-level due to high ILS associated with the rapid early radiation of subtribes. Indeed, ILS can affect large portion of the genome (e.g., 50% of marsupial genomes in Feng *et al.* (2022); 35% of the analyzed loci of neoavian birds in Suh *et al.* (2015), even if incongruency seems reasonable in our dataset (See ***SI Appendix 7,* Fig. S7 & S8)**. Moreover, the incorporation of alignments encompassing few species may have increased the risk of gene tree estimation errors due to fewer available information to guarantee homology in the alignment, which could limit the performance of summary methods (Molloy & Warnow 2018).

Altogether, we obtained four different phylogenetic hypotheses for the backbone topology based on phylogenomic datasets. While globally well-supported, SuperTrees showed inconsistency regarding the branching of subtribes with different hypotheses depending on the degree of missing data and the completeness of the gene dataset used (i.e., *Inclusive* vs. *Conservative*; see ***SI Appendix 9*, Fig. S9 & S10**). Both hypotheses yielded relatively poor supports with low gCF and sCF associated to relationships among subtribes that were not always evaluated as the best alternative for local topologies (see gCF, sCF and associated tests in **Table 1**). They offered unusual topologies involving the grouping of four subtribes (i.e., Melinaeina, Athesitina, Tithoreina, and Methonina) in a unique clade never suspected in previous systematic studies (Brower *et al.* 2006, 2014; Willmott & Freitas 2006; Chazot *et al.* 2019b). Meanwhile, the SuperMatrix-based trees led to consistent scenarios for the deep evolutionary relationships across subtribes, showing robustness to gene sampling with no

difference between the *Inclusive dataset* (ca. 11,000 genes) and the *Conservative dataset* (ca. 3,500 genes). As such, the type of inference methods had more effects on our final phylogenetic hypotheses than genetic sampling, likely because the scope of the *Conservative dataset* was sufficient to provide relevant and representative phylogenetic signal for site-based inferences (e.g., SuperMatrices). In the end, we favored the selection of the two SuperMatrix-based phylogenetic hypotheses to build the backbone phylogeny used in downstream analyses.

4.2 Subtribal classification

Our final time-calibrated phylogeny offers a new phylogenetic hypothesis that contrasts with previous results based on morphological and ecological traits (Willmott & Freitas 2006) and the most up-to-date hypothesis based on molecular data obtained from Sanger sequencing (Chazot *et al.* 2019b).

Our results confirmed the monophyly of the well-established ten ithomiine subtribes providing high supports value for all subtribes (**Table 1**). It also supported the monophyly of the core-group, a clade of five subtribes (i.e., Oleriina, Ithomiina, Napeogenina, Dircennina, and Godyridina) associated with a shift in diversification dynamics leading to a recent radiation associated with multiple colonizations of new areas following the demise of the Pebas aquatic system in Western Amazonia during the late Miocene (Elias *et al.* 2009b; De-Silva *et al.* 2017; Chazot *et al.* 2019b). Within the core-group, our time-calibrated phylogeny suggested the Oleriina subtribe as the sister-group of all others, a topology proposed by Garzón-Orduña *et al.* (2015) based on the recalibration of a previous molecular-based phylogeny (Brower *et al.* 2006) following new inferences of the ages of hostplant lineages (Särkinen *et al.* 2013).

Contrary to Chazot *et al.* (2019b) who suggested Athesitina as the sister-group of the core-group, we found that the Mechanitina tribe received the most support for this position. From an ecological and morphological perspective, such topology allows to regroup in a clade (i.e., Mechanitina and the core-group) all lineages with members feeding on the vast nightshade plant genus Solanum (Solanaceae family), which also all share the presence of fused tibia and tarsus on the male forelegs (Willmott & Freitas 2006). Conveniently, it also provides a more parsimonious evolutionary history for caterpillar morphology by grouping Mechanitina with the core-group (**Fig. 5**), two clades that share (alongside the Methonina subtribe) the loss of the conspicuous subdorsal filaments visible on the last instar of many other danaine butterflies (albeit sometimes on different segments; Kitching 1985). From the biogeographic perspective, the members of the Athesitina subtribe are found in the Central Andes in contrast to

Mechanitina species that are mostly Amazonian (See **Chapter 1**; Doré *et al.* 2022). While the latest reconstruction of ancestral ranges have left undecided the origin of ithomiines between the Central Andes and the Western Amazonia (Chazot *et al.* 2019b), a more basal position of Athesitina than previously estimated would provide additional weight for an Andean origin of the Ithomiini tribe.

The evolution of hostplant use in ithomiine butterflies is complex and intimately link to their dynamic of diversification. Ithomiine species are highly specialized on their hostplant species, whit distinct clades mostly specialized on distinct unique hostplant clades belonging mainly to the Solanaceae family (Drummond & Brown Jr 1987), in a pattern known as host-plant conservatism (Winkler & Mitter 2008). However, evidence for coevolution associated with simultaneous cladogenesis are lacking (Drummond 1986; Brown Jr 1987) and tend to favor an Escape and Radiate hypothesis (Ehrlich & Raven 1964; Thompson 1989) where the early shift to Solanaceae hostplants enabled ecological speciation on newly available niches (i.e., already existing Solanaceae lineages; Dupin *et al.* 2017), thus powering diversification of ithomiine butterflies (Brown & Henriques 1991; Peña & Espeland 2015). Indeed, ithomiine species feed almost exclusively on Solanaceae plants with the exception of the clade *Megoleria-Hyposcada* in Oleriina that feeds on Gesneriaceae (Drummond & Brown Jr 1987), and the Tithoreina subtribe members that feed on *Prestonia* and other Apocynaceae (Brown Jr 1987; Brown Jr. & Freitas 1994), a hostplant group shared with the other two tribes of Danainae (Ackery & Vane-Wright 1984; Ackery 1987). As such, a basal position of the Tithoreina subtribe would suggest a single host shift from Apocynaceae to Solanaceae after the divergence of the Tithoreina lineage. Yet, all recent phylogenies found Tithoreina to form a clade with Methonina (Willmott & Freitas 2006; Brower *et al.* 2014; Garzón-Orduña *et al.* 2015; Chazot *et al.* 2019b), a highly autapomorphic group that feed on *Brunfelsia* and the only ithomiines to feed on any member of the subfamily Petunioideae within the Solanaceae family.

In our phylogenetic hypothesis, as in all modern molecular-based phylogenies (Brower *et al.* 2006, 2014; Garzón-Orduña *et al.* 2015; Chazot *et al.* 2019b), the Melinaeina subtribe appears as the most basal lineage, while the Tithoreina/Methonina clade occupies diverse positions within the Ithomiini tribe, leaving open the scenario of a single early shift to Solanaceae followed by a recolonization of Apocynaceae hostplants by Tithoreina (**Fig. 5**). Alternatively, instead of complete shift(s) to a new plant group, early evolutionary steps of ithomiine butterflies could have followed the Oscillation hypothesis (Janz & Nylin 2008). In the case of Ithomiini, such scenario would involve the primary expansion of the niche breath

with the acquisition of the ability to feed on a new plant group (i.e., Solanaceae) associated with the retention of the ability to feed on the ancestral group (i.e., Apocynaceae), followed by multiple ecological speciation illustrated by cladogenesis associated with host breath reduction among lineages forming the early subtribes, including Melinaeina, Athesitina, Tithoreina, and Methonina. Moreover, specialization in the realized niche (i.e., hostplant use) may mask the retention of polyphagous abilities as found in host shift experiments (Freitas 1999; McClure & Elias 2016). Furthermore, this scenario of ephemeral generalist feeding diet powering diversification is compatible with the rapid early diversification of subtribes we observed on our time-calibrated phylogeny (**Fig. 4**), but dedicated investigations involving niche breadth evolution are still needed to support either scenario (Jousselin & Elias 2019).

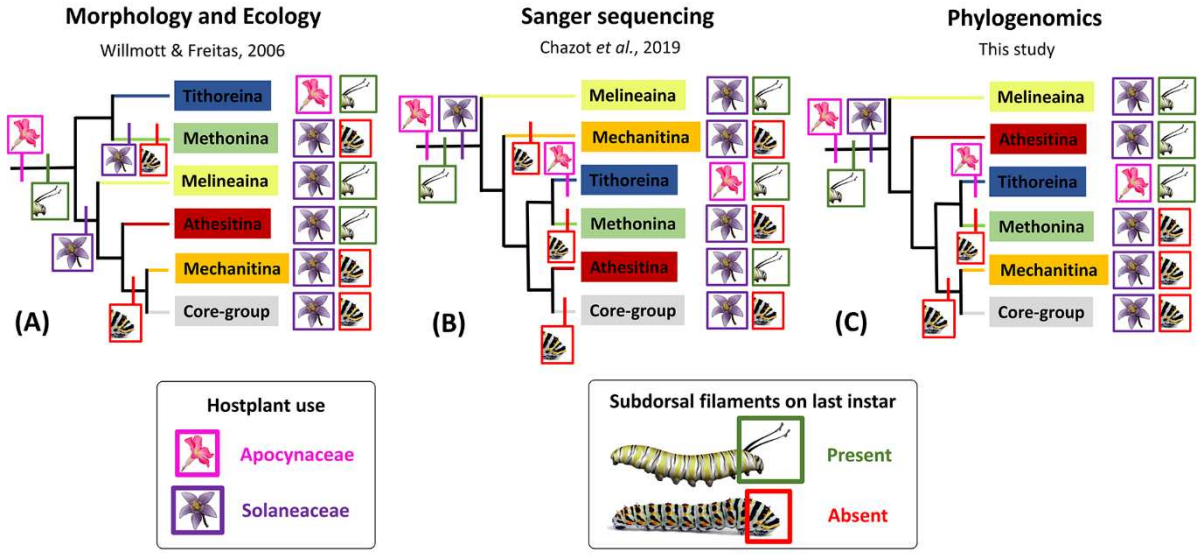

Figure 5: Comparison of cladograms built from (A) 306 morphological and ecological characters (Willmott & Freitas 2006), (B) Sanger sequencing of 7,083 sites across 8 genes (Chazot *et al.* 2019b)**, (C) phylogenomic pipeline on ca. 7.8 million nucleotide sites representing 11,012 genes (this study)**. Cladograms depict evolutionary relationships inferred across subtribes. The core-group (labeled in grey) represents a strongly supported monophyletic group of five subtribes: Oleriina, Ithomiina, Napeogenina, Dircennina, Godyridina. Colored marks and framed symbols illustrate parsimonious hypotheses for shifts in hostplant use (Apocynaceae or Solanaceae) and presence or absence of subdorsal filaments on the last instar caterpillars. Note that a single switch to Solanaceae at the root of Ithomiini associated with the recolonization of Apocynaceae by Tithoreina is as parsimonious in the morphology and ecology-based tree (A) as the two independent switches to Solanaceae presented here. Similarly, independent evolution of subdorsal filaments in polyphyletic groups is as parsimonious as loss in their respective sister-group on the Sanger-based tree (B).

4.3 Generic classification

Besides new hypotheses for deep evolutionary relationships, our time-calibrated phylogeny shed light on potential issues in the current taxonomy of ithomiine butterflies. As we recovered monophyletic groups for most of the 48 currently accepted genera in ithomiines, we also found at least four cases, already identified as problematic in previous studies, were the current taxonomy is in conflict with the evolutionary relationships inferred from our analyses. All cases are found in the most recent taxa-rich subtribes of the core-group, which underwent a recent rapid diversification that may impede our ability to retrieve clear evolutionary relationships.

The relationship between the genera *Hypothyris* and *Hyalyris* in Napeogenina were left with an important polytomy in our backbone phylogeny (**Fig. 3**) and formed a polyphyletic complex in our final time-calibrated phylogeny illustrating the difficulty to classify these species. They presented a similar conundrum in previous phylogenetic hypotheses (Brower *et al.* 2014; Chazot *et al.* 2019b), while Willmott & Freitas (2006) found *Hyalyris* as monophyletic but yet considered "there are no clear synapomorphies" to support it. Overall, the most conservative solution may be to lump the two genera in a single genus for which at least monophyly is established.

The genus *Hypoleria* in the Godyridina subtribe has already been identified as paraphyletic with respect to *Mcclungia* and *Brevioleria* genera by Brower *et al.* (2014) employing a non-exhaustive sampling. Chazot *et al.* (2019b) revealed a similar pattern for *Hypoleria* when including the missing taxa, but additionally found *Brevioleria* as being paraphyletic with respect to *Pachacutia*, despite *Brevioleria*'s monophyly being convincingly supported by shared morphological derived characters (Willmott & Freitas 2006). Our own hypothesis found *Hypoleria* as paraphyletic with respect to *Mcclungia*, *Brevioleria*, and *Pachacutia* but reestablished the monophyly of *Brevioleria*. Altogether, *Hypoleria* genus deserves more attention to define generic subdivisions that will reflects evolutionary relationships as initiated by Willmott & Lamas (2007) with the newly described genus *Pachacutia*.

We detected the genus *Hyalenna* as paraphyletic in relation to *Dircenna* in the Dircennina subtribe. In particular, we predicted the clade formed by *Hyalenna paradoxa* and *Hyalenna perasippa* to have diverged before the split of *Dircenna* and other *Hyalenna* species. Such relationship was left unresolved in Brower *et al.* (2014), but was not found in Chazot *et al.*

(2019b), where both genera appeared monophyletic. Besides, the monophyly of *Hyalenna* is well supported by numerous morphological synapomorphies in recent a cladistic revision (Willmott & Lamas 2006), casting doubt on our hypothesis.

Finally, the *Ceratinia* genus did not show monophyly in the Dircennina subtribe where it was polyphyletic with respect to several *Episcada* species, such as *Episcada hemixanthe* (also found within Ceratinia in Brower *et al.* (2014)), *E. zajciwi* and *E. doto*. Association of those species with the genus *Ceratinia* was also detected on the basis of morphological characters, but also involved *Episcada hymenaea* (Willmott & Freitas 2006), which appeared within the clade sister to *Ceratinia* with the remaining *Episcada* species in our phylogeny. Undoubtedly, further investigations are needed to obtain a stable list of *Episcada* species that should be incorporated into the *Ceratinia* genus.

4.4 Perspectives for studies on the macroevolution of ithomiines

During the course of this project, we have built a large molecular dataset of ca. 11,000 orthologous genes to carry out phylogenomic inferences of evolutionary relationships among ithomiine butterflies. Such comprehensive dataset offers new opportunities to explore macroevolutionary questions that involve genome-wide macroevolutionary signatures of selection associated for example with hostplant shift (Allio *et al.* 2021) or adaptation to elevation (Nevado *et al.* 2016). Additionally, we generated a new robust time-calibrated species-level phylogeny encompassing 356 out of the 396 extant species (i.e., 89.9%) that resolved previous uncertainties regarding deep evolutionary relationships across the different subtribes. Overall, our phylogenetic hypothesis provides better agreement with the putative evolution of morphological and ecological traits, highlighting the power of phylogenomic approaches to resolve previously conflicting deep evolutionary relationships.

This comprehensive time-calibrated phylogeny provides a stable tool to empower future macroevolutionary analyses in ithomiine butterflies that may help to unravel and test for relationships between diversification dynamics and key traits such as wing transparency (Pinna *et al.* 2021), mimetic patterns (Jiggins *et al.* 2006), climatic niche (See **Chapter 1**; Doré *et al.* 2022) or hostplant shift (Jousselin & Elias 2019).

Data Accessibility Statement

All BASH and R scripts forming the assembly and annotation pipeline and used to carry out all downstream analyses are available in the GitHub repository https://github.com/MaelDore/Ithomiini_phylogenomics. All raw sequences from Illumina runs, curated sequences and alignments can be found in NCBI under BioProjects (reference **TBA**).

Supplementary Information

Supplementary Information for CHAPTER 2: "Phylogenomics resolve deep evolutionary relationships in clearwing butterflies" can be found in **ANNEXE 3.**

Acknowledgments

We thank Fabien Condamine, Romain Nattier, and Elise Gay for advises on phylogenomic analyses and encouragements to impulse this project. We thank Rémi Mauxion, Erika Páez Vargas, Patricio Salazar, Raul Aldaz, Ismael Aldas, and Caroline Bacquet, for their companionship and assistance during fieldworks. We thank the numerous, sometimes anonymous, people who contributed to make this project possible and provided assistance on the field. We thank the BOEM laboratory, and particularly Violaine Llaurens and Manuela Lopez Villavicencio to have provided equipment, advices and access to facilities during the DNA extractions. We warmly thank Pierre Boyer for providing specimens from his personal collection. We thank Jing Zhang for facilitating our access to DNA sequences, and Eduardo de Proença Barbosa for sharing access its own sequences. We acknowledge the GenOuest bioinformatics core facility (https://www.genouest.org) for providing the computing infrastructure to carry out the bioinformatic pipeline.

We are thankful to the Peruvian and Ecuadorian governmental authorities for collection permits (373‑2017-SERFOR-DGGSPFFS, MAMAE-DNB-CM-2016-0045, MAATE-DBI-CM-2021-0176). In particular, we thank S. Villamarín, S. Nogales, the INABIO and Ecuadorian Ministerio del Ambiente for arranging the necessary permits for research in Ecuador, most recently under the project 'Diversity and Biology of Lepidoptera in Ecuador'. This work was funded by Clearwing ANR project (ANR-16-CE02-0012) and HFSP project (RGP0014/2016). MD is financed by the French Ministry of Research (MENSR).

CHAPTER 3

Perceptual maps: a new tool to investigate mimicry patterns from Citizen Science to individual perception

Maël Doré[1,2], Eddie Pérochon[1,3], Thomas G. Aubier[4], Mathieu Joron[5*], and Marianne Elias[1,6*]

[1]*Institut de Systématique, Evolution, Biodiversité, MNHN-CNRS-Sorbonne Université-EPHE-Université des Antilles, Muséum national d'Histoire naturelle de Paris, 45 Rue Buffon, 75005, Paris, France*

[2]*Centre d'Ecologie et des Sciences de la Conservation, UMR 7204 MNHN-CNRS-Sorbonne Université, Muséum national d'Histoire naturelle de Paris, 45 rue Buffon, 75005, Paris, France*

[3]*Department of Ecology and Evolution, University of Lausanne, Lausanne, Switzerland.*

[4]*Laboratoire Évolution & Diversité Biologique, Université Paul Sabatier Toulouse III, UMR 5174, CNRS/IRD, 31077 Toulouse, France*

[5]*Centre d'Ecologie Fonctionnelle et Evolutive, Université de Montpellier, CNRS, EPHE, IRD, Montpellier, France*

[6]*Smithsonian Tropical Research Institute, Panamá, Panamá*

**Co-last authors*

Reference:

Doré, M., Pérochon, E., Aubier, T.G., Joron, M. & Elias, M. (2023). Perceptual maps: a new tool to investigate mimicry patterns from Citizen Science to individual perception. *In prep.*

Author contributions:

All authors contributed to the emergence of the concept of perceptual map and the conception of the study. EP & MD gathered the image database. TA built the first version of the website. EP and MD successively built on this work to reach the current version. MD adapted the MATLAB scripts for the t-STE algorithm, wrote all the R scripts for downstream analyses, produced all results and figures, and led the manuscript writing. All authors critically contributed to the manuscript draft.

Abstract

One of the major objectives of natural sciences is the inventory and description of biodiversity. In this study, we present a new approach to quantify variation in ecological traits that carry visual signals based on perceived similarity. We built upon a Citizen Science project to describe phenotypic variation in mimicry patterns of heliconiine butterflies at continental scale. Our results support the unfolding to large spatial scales of Müller's prediction for trait convergence between sympatric species in a context of mimicry. We also illustrate the versality of our approach by showing its suitability to build individual perceptual maps at local scale as well. Altogether, this work opens new perspectives to the study of ecological trait variation at multiple geographic and phylogenetic scales, integrating altogether the morphological, chromatic, and cognitive dimensions of trait variation. As a new tool for ecologists and evolutionary biologists, it may stimulate further studies on the evolution of ecological traits whose complexity has so far prevented large scale comparison.

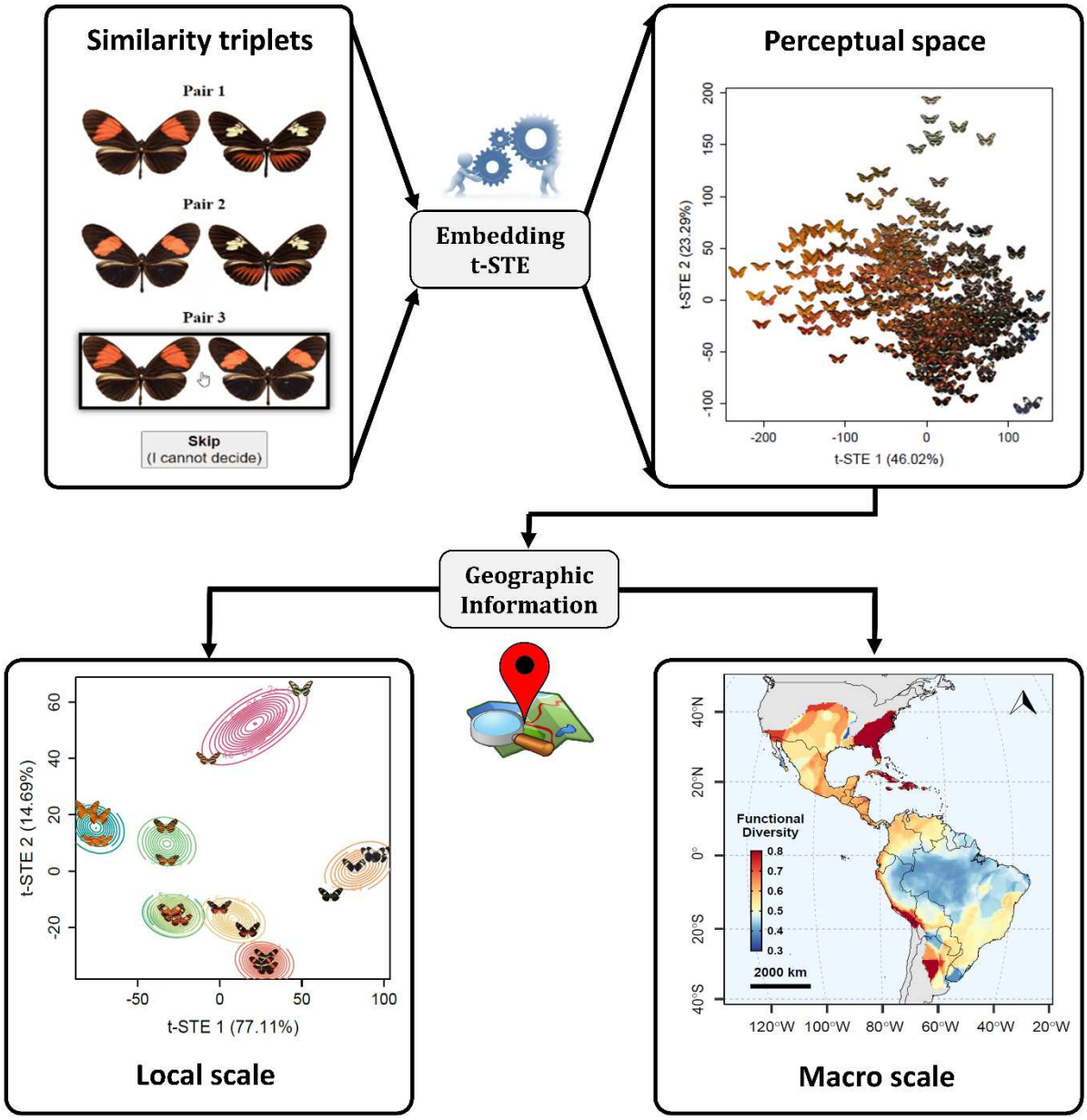

Graphical Abstract: Perceptual maps: a new tool to investigate phenotypic variation in visual signals from local maps of individual perception to Citizen Science projects aiming to map macroecological patterns of functional diversity at continental scale.

Keywords

Citizen Science, evolutionary convergence, functional diversity, heliconiine butterflies, machine learning, Müllerian mimicry, Neotropics, perceptual map, phenomics, visual signals.

1 Introduction

There are about 2 million documented species on Earth (Costello *et al.* 2022), each with a specific niche and set of traits reflecting this incredible biodiversity. One of the major objectives of natural sciences is the inventory and description of this diversity. In the last century, the evolution of data acquisition methods has been characterized by a shift from a qualitative approach to describing phenotypic traits to integrated quantitative approaches leading for instance to recent developments in image analysis using convolutional neural networks (Schuettpelz *et al.* 2017; Weinstein 2018; Mäyrä *et al.* 2021; Irisson *et al.* 2022). Compared to a qualitative description of diversity providing nominal variables (e.g., red *vs.* yellow, ovoid *vs.* spherical, etc.), a quantitative description of multidimensional complex traits such as shape, behavior or color patterns allows to account for intra-group variation, as well as providing a quantification of trends and relative positions of groups in a multidimensional space (e.g., morphospace, RGB space, phenotypic space, etc.). Numerical quantification also enables the use of a vast diversity of methods developed in numerical ecology and evolution (Legendre & Legendre 2012; Revell & Harmon 2022). Computers are decisive tools in this numerical revolution, yet they may be limited to grasp the specificity of traits involved in ecological signals (i.e., traits perceived by other individuals).

The evolution of traits is driven by multiple integrated selective pressures incurred by the abiotic environment and ecological interactions. When ecological interactions involve the exchange of information between two individuals, conspecific or not, those interactions are typically mediated by a signal involving visual, acoustic, or olfactory modalities (Endler 1992). In the case of visual signals, what affects the outcome of the selective pressure is not only the photonics of the biological feature underlying the signal, but also the cognitive process of perception involving several levels of abstraction between the capture of the physical input, through the conception of the mental image of the signal, to the trigger of a behavioral response (Farina *et al.* 2005).

Müllerian mimicry (hereafter, mimicry) is an iconic example of ecological interactions involving a visual signal. Mimicry is predicted to drive the convergence of aposematic signals (i.e., conspicuous traits associated with anti-predator defenses in prey, typically toxicity) because of positive frequency-dependent selection on those signals: the most common signals are favored because the mortality risk entailed by predator learning is shared among a larger number of individual prey (Müller 1879; Sherratt 2008). The sets of phenotypically similar

species resulting from such evolution are named mimicry rings (Weismann 1904; Papageorgis 1975). Convergence of aposematic signals is mediated by the perception of predators, which may vary in their levels of generalization depending on species-specific visual and cognitive abilities, individual experience, condition (e.g. , degree of satiety), as well as the diversity of signals they encounter (Bosque *et al.* 2018). As such, species with moderately similar patterns could still be under selection for convergence from picky predators, while they could be considered as the same type of prey by another predator and therefore not under selection for convergence, potentially explaining instances of imperfect mimicry (Dittrich *et al.* 1993; Kikuchi & Pfennig 2013).

Based on the knowledge that perception is an essential component of the quantification of traits underlying ecological signals, especially in an evolutionary perspective (Endler 1992), we propose a new method to quantify similarity in traits that integrate directly perception in its framework. We offer to produce multidimensional perceptual spaces in which proximity of object/specimen/species coordinates reflect the perceived similarity between their ecological signals. Beyond the critical involvement of perception in the process, this type of approach also allows to directly integrate the multimodal nature of signal, for instance embracing the perception of similarity in shapes and patterns in a single framework, which is technically difficult to achieve with computer-based signal processing methods relying on pattern alignment (e.g., Le Poul et al., 2014; Van Belleghem et al., 2018).

To illustrate the potential of this new approach to quantify similarity in phenotypes involved in ecological signals, we focused on the emblematic and historical case of Müllerian mimicry in heliconiine butterflies (tribe Heliconiini, subfamily Heliconiinae, family Nymphalidae). We aimed to study variation in wing patterns reflecting potential mutualistic interactions between species for the entire spatial range and taxonomic diversity of heliconiine butterflies. The Heliconiini tribe encompasses 8 genera, 77 species and 457 subspecies (Kozak *et al.* 2015; Jiggins & Lamas 2016) with a large diversity of wing patterns. In order to collect enough data to cover such diversity of patterns, as well as integrating a diversity of perception needed to avoid sampling bias and reflecting the diversity of perceptions of natural predators, we designed a Citizen Science project linked to an online survey hosted on a dedicated website (http://memometic.cleverapps.io/).

Building upon this large collection of perceptual information, we aimed to investigate how phenotypical variation of wing patterns in heliconiine butterflies is structured in the perceptual and geographical space. Specifically, we:

(1) Mapped wing pattern similarity in the perceptual space for 432 subspecies.

(2) Mapped the spatial distribution of local phenotypic diversity measured as the degree of clustering in the perceptual space.

(3) Mapped the spatial variation of mean phenotype across communities.

(4) Tested for the convergence of perceived patterns between spatially congruent taxa.

This description of the structure of phenotypic patterns at large macroecological scale can only provide hypotheses on mutualistic interactions acting at local scale. Indeed, subspecies with patterns perceived as similar may not co-occur, thus do not interact mutualistically, at least not directly. Thus, we also investigated the suitability of our Citizen Science approach to address questions for local communities:

(5) Is the Citizen Science map suitable to describe local phenotypic variation?

(6) Is the Citizen Science map suitable to define local mimicry rings?

2 Materials and Methods

2.1 Materials

2.1.1 Study group

We focused our study on the textbook case of Müllerian mimicry in heliconiine butterflies (Nymphalidae: Heliconiini). This group is well-known for the important variation of its aposematic patterns (Jiggins & Lamas 2016) and for the existence of local geographic forms reflecting parallel adaptive radiations between species (Brower 1996). Heliconiines are widely distributed across the American continent, from Canada to the North of Argentina with peaks of diversity in the Andes, in Central America, and in the Amazon basin (Rosser *et al.* 2015; Pérochon *et al.* 2023). The study of wing patterns of heliconiines, among other groups of mimetic neotropical butterflies, has been instrumental in the emergence of the theory of mimicry in the late nineteenth century, notably by Henry Walter Bates (Bates 1862) and Fritz Müller (Müller 1879) who gave their names to the two major types of mimicry: Batesian mimicry and Müllerian mimicry. All species of heliconiine butterflies are engaged in Müllerian mimicry which implies some degree of toxicity associated with conspicuous warning signals

displayed by wing patterns. Some species share mimicry patterns with other groups of Neotropical mimetic butterflies, mostly ithomiine butterflies (Poole 1970; Brown Jr. & Benson 1974; see **ANNEXE 6**, Pérochon et al., 2023).

2.1.2 Image collection

We retrieved standardized images of dorsal view of specimens in mounting position from museum and private collections for 432 subspecies (94.5%) of heliconiines butterflies among the 457 described subspecies. The most important contributors were the McGuire Center for Lepidoptera and Biodiversity (Gainesville, FL, USA), the Natural History Museum London (UK), and the Muséum National d'Histoire Naturelle (Paris, France). Due to the diversity of sources needed to retrieve such a collection of images, we included whenever possible a color reference chart on images. We standardize all images to achieve similarity in brightness, hue and saturation when comparing the color reference charts between images.

Polymorphism within subspecies is rare since subspecies are typically described on the basis of phenotypic variation in wing patterns. However, in the rare cases of polymorphism we encountered, we tried to select a specimen for which we considered the pattern to be the most representative (the closest to a "mean" phenotype). Heliconiine butterflies notably lack sexual dimorphism in wing patterns (Jiggins & Lamas, 2016, p. 73), thus we selected indifferently male or female specimens according to availability. A complete list of taxa used for this study, with associated metadata is available in **Table S1** in **SI Appendix 1**.

2.1.3 Online Citizen Science survey

We designed a website interface presented as a game and linked to an SQL database dedicated to the collection of information regarding the perception of similarity in wing patterns by thousands of players. The website is accessible in four languages (i.e., English, French, Spanish, Brazilian/Portuguese) to encourage people from all around the world, and especially in regions were heliconiine butterflies are native, to participate: http://memometic.cleverapps.io/.

This website is presented as a Citizen Science project with three goals: (1) introducing a wide public to the basis of ecological and evolutionary concepts involved in Müllerian mimicry by offering a short introduction to those concepts; (2) collecting an important and diverse amount of data regarding the global perception of similarity in the wing patterns of heliconiine butterflies; (3) involving citizens around the world into the collective building of

scientific knowledge, and allowing them to access preview of new research development by providing feedback on the results acquired thanks to their contribution.

A typical game session involved 30 random sets of triplets of images drawn from the set of 432 subspecies. For each triplet, we asked the player to select the pair of images which it perceived as the most similar (see **Fig. S2** in **SI Appendix 2** for an illustration of the website). Therefore, for each vote the player provided a set of relative distances such as if it selected the pair A-B, we recorded the following relative distances: $d_{A\text{-}B} < d_{A\text{-}C}$ and $d_{B\text{-}A} < d_{B\text{-}C}$ where distances are symmetrical ($d_{A\text{-}B} = d_{B\text{-}A}$). In case of doubt, we allowed the player to skip the triplet and request a new one to evaluate, avoiding accumulation of noise in the data due to forced random choices. Each game session included two triplets drawn from a set of controlled trials for which the perceived relative similarity was striking (see **Fig. S2** in **SI Appendix 3** for visual illustration of the controlled trials used). Thus, we were able to filter game sessions that provided suspicious results by removing those that failed at least one controlled trial.

Before each game, we recorded demographic information (age, scientific background, colorblindness, experience with the game, language, and location), and game statistics (time taken per triplets, number of skips, score as a deviation to the mean). All this information is summarized and analyzed in the **SI Appendix 4**.

Altogether, we recorded 1,422 game sessions from 1,242 distinct players across 53 countries providing 85,320 triplets of relative distances. We kept 75,240 for downstream analyses after filtering of improper game sessions having failed controlled trials, or declared colorblindness.

2.1.4 Spatial distributions

We retrieved predictions of spatial distributions for 439 subspecies from a soon-to-be-published research project which built upon a dataset of 77,577 georeferenced occurrences and employed species distributions models to map subspecies distributions (See Pérochon et al., 2023 in **ANNEXE 6**) at the continental scale for a resolution of 0.25° arc (ca. 30 km). Maps of functional mimetic diversity (**Fig. 1b**) and community mean phenotype (**Fig. 2b**) encompass the 422 (92.3%) subspecies for which we had both distribution patterns and reference image available.

2.1.5 Local communities

In order to investigate the power of the Citizen Science dataset to inform on local patterns of phenotypic diversity, we produced analyses for a set of local communities based on the individual perception of five butterfly experts. We selected five local communities among the 23,661 available communities defined as a unique grid-cell in the 30 km × 30 km raster maps of subspecies distributions, namely Cayenne (French Guyana), Gamboa (Panama), Jatun Sacha (Napo, Ecuador), Manaus (Amazonas, Brazil), and Santa Teresa (Espírito Santo, Brazil). Thus, we extracted for each one a list of taxa whose presence was predicted by the spatial distributions extracted from Pérochon et al., 2023 (See **ANNEXE 6**). This selection was made in order to (1) present a diversity of geographic location across the heliconiine range, (2) display a diversity of phenotypes, (3) display a diversity of level of richness for local species and mimicry patterns. The geographic location of each local communities is featured on the maps of functional phenotypic diversity (**Fig. 1**) and local mean phenotype (**Fig. 2**). A visual list of subspecies for each local community can be found in **Fig. S13-S17** in **SI Appendix 5**.

We generated sets of 600 triplets of relative distances across images of local taxa for each expert, for each local community. These sets were used to generate the local individual perceptual maps described in the next section. For each community, individual triplet datasets were aggregated among all five experts to produce the 'triplet-aggregated' local maps described in subsequent analyses.

2.2 Methods

2.2.1 t-STE

In order to convert the lists of triplets of relative distances in maps of wing pattern (dis)similarity based on perception (i.e., perceptual maps), we adapted the t-distributed Stochastic Triplet Embedding method (t-STE; van der Maaten & Weinberger, 2012). t-STE is a supervised contrastive machine learning algorithm based on similarity triplets under the form "A is more similar to B than to C" that produces an embedding of data whose coordinates in the new reduced space agree with the relative distances described in the similarity triplets. In the context of the perceptual map, triplets of perceived relative distances among images are converted into coordinates in a perceptual space where distances depict perception of (dis)similarity among the images.

In contrast to a Generalized Non-Metric Multidimensional Scaling (Agarwal *et al.* 2007) which also converts triplets of relative distances into coordinates in a reduced space, t-STE does not only favor triplet satisfaction (i.e., A is closer to B than to C in the embedded space), but favor triplet optimization by including a stochastic description of how well a triplet is modeled in the embedded space (i.e., the probability that the triplet is satisfied under a stochastic selection rule; van der Maaten & Weinberger, 2012). As a result, the algorithm tends to keep pushing for the clustering of objects for which triplets provide no evidence of dissimilarity and to keep pulling apart objects for which triplets provide no evidence that they are similar, even once triplet satisfaction is achieved. However, the use of a Student's t-distribution with heavy tails to model triplet probabilities allows to smooth the increase of reward/penalization for triplet satisfaction/violation until it becomes infinitesimal for large differences (van der Maaten & Weinberger 2012). As a result, the influence of outlier triplets (i.e., conveying an unusual information relative to the whole dataset) on the optimization gradient is reduced, which is a desirable feature to avoid individuals with uncommon perceptions to drive the final topology of our perceptual maps aiming to represent the general consensus of perceptions.

The algorithm starts with a random set of coordinates for each object in a reduced space of user-defined number of dimensions (three dimensions in our case, see below). At each step, it computes the likelihood for each triplet (the data) to be satisfied given the current coordinates of the images (the model). The cost function is the log-likelihood of the current embedded space defined as the sum of the log-likelihood of each triplet computed as follows:

$$L_{abc} = \frac{\left(1 + \frac{\|X_a - X_b\|^2}{\alpha}\right)^{-\frac{\alpha+1}{2}}}{\left(1 + \frac{\|X_a - X_b\|^2}{\alpha}\right)^{-\frac{\alpha+1}{2}} + \left(1 + \frac{\|X_a - X_c\|^2}{\alpha}\right)^{-\frac{\alpha+1}{2}}} \qquad \text{(Eqn. 1)}$$

where L_{abc} is the likelihood of the triplet of images A, B, and C, following X, their respective coordinates in the embedded space, and adjusted by α, the degree of freedom of the Student-t kernel equal to the requested final number of dimensions minus one (van der Maaten & Weinberger 2012). As such, the larger is the Euclidean distance between A and C, compare to A and B, the higher will be the likelihood of the triplet, and conversely. Following a gradient-descent optimization, the coordinates of images in the embedded space are modified in order to maximize the cost function at each step. Therefore, the algorithm learns iteratively the best embedding to optimize the distances of images in the reduced space satisfying the initial triplets.

In this study, we stopped all runs after 30,000 iterations as a conservative threshold since we detected that stability was reached fairly quickly, typically after a couple of hundreds of iterations (see **Fig. S24** in **SI Appendix 7**).

t-STE allows the user to define a priori the final number of dimensions of the embedding. A higher number of dimensions offers more possibilities to satisfy triplet similarities, but it also prevents easy visualization of the output, and limits performance of clustering algorithms in high dimensionality (Wang *et al.* 2008). With the objective of quantifying and visualizing the variation in wing patterns while obtaining hypotheses for phenotypic-based mimicry rings issued from clustering, we favored the use of three-dimensional perceptual spaces as our targeted number of dimensions. Independently to the choice of the number of dimensions, it is important to keep in mind that contrary to a PCA, the axes of a t-STE are not organized so that they represent successively orthogonal decreasing axes of variation. The order of the axes is arbitrary, and they can be correlated such as patterns mostly lie on the diagonal of two axes, hinting that less dimensions could be enough to represent adequately the information embedded from the similarity triplets.

The t-STE algorithm has the advantage to allow to retrieve coordinates in space for all images despite having information only on a subset of all possible relative distances among the images. For instance, for our 432 images, there are 13,343,760 unique combinations of triplets of images that could be evaluated, yet we managed to find a stable embedding with less than 30,000 triplets (see **Fig. S18** in **SI Appendix 6)**. Similarly, we studied the stability of individual perceptual maps for local community and showed 600 triplets were enough to reach a stable embedding for local maps (see **Fig. S19** in **SI Appendix 6**) displaying a fairly reduced diversity of phenotypes compared to the macro-scale analyses, with 18 to 44 local patterns *vs.* 432 patterns in total.

Additionally, we carried out complementary analyses exploring the ability for t-STE to provide stable topologies and satisfy a maximum proportion of similarity triplets for different size of image sets, across ranges of sampling effort as the number of triplets, and learning effort as the number of iterations (see **SI Appendix 7**).

2.2.2 Gaussian Mixture Models and putative mimicry rings

To propose hypotheses for local mimicry rings, we ran Gaussian mixture-models (GMM; Reynolds, 2015) to cluster wing patterns within groups of phenotypically similar patterns. Any clustering method could potentially be applied on the perceptual space to define

such hypotheses for mimicry rings, however Gaussian mixture-models offer a couple of advantages. Clusters represent Gaussian distributions that can have different size (i.e., number of objects), ellipsoidal shapes, and orientations. It allows to detect outliers by forming singletons (i.e., group of a single object). In the context of mimicry, the underlying Gaussian distributions can be seen as selective values in an adaptive landscape describing an adaptive peak for phenotypes (i.e., learned by local predators as associated with toxicity, thus favored by selection) as a high probability density. If known, the local abundances of taxa can be used to provide weights influencing the clustering outcome. Finally, it allows to fit a model with any given number of groups/mimicry rings and to compare them with criteria for goodness-of-fit (e.g., likelihood, BIC, AICc). This versatility allows the researcher to define a priori its final number of groups according to a required degree of generalization/refinement for the phenotypic groups, or to compare results and select the appropriate value according to a chosen criterion.

2.2.3 Map variation of phenotypic patterns at large-scale

Employing the t-STE algorithm on the similarity triplets gathered from our Citizen Science collection of perception data, we obtained a 3D perceptual space with coordinates of images representing the aggregated perception of wing pattern similarity in heliconiine butterflies for patterns found on the entire range of the group. We decomposed this 3D perceptual space into 2D perceptual maps and displayed the images used during the survey on their given coordinates (**Fig. 1a, 1c, 1d**). Combining this information with predicted distribution data of each subspecies, we computed within each community (i.e., pixel in the grid-cell) the local functional mimetic diversity as the mean pairwise Euclidean distance in the perceptual space, reflecting the degree of clustering of local phenotypes in the perceptual space (**Fig. 1b**).

By converting each axis on a 0-255 scale, we assigned an RGB color to each image based on its coordinates in the perceptual space. We computed the mean local phenotype within each community and displayed its associated color on the RGB space decomposed in 2D maps (**Fig.2a, 2c, 2d**), and in the geographic space (**Fig.2b**).

2.3 Statistical Analyses

2.3.1 Tests for similarity and convergence in the perceptual space

Müller's theory of mimicry (Müller 1879) predicted the convergence of local toxic prey towards a similar aposematic pattern. To evaluate if this prediction could influence large-scale

patterns of phenotypic distributions, we tested if the perceptual distances between subspecies were correlated with the geographic distances between their spatial distributions. We defined pairwise perceptual distances as the Euclidean distances in the perceptual space between pairs of subspecies. We computed pairwise geographic distances as 1 - Schoener's D (Schoener 1970) in the geographic space as follows:

$$1 - D_{12} = \frac{1}{2}\sum_{ij}\left|z_{1ij} - z_{2ij}\right| \quad \text{(Eqn. 2)}$$

where D_{12} is Schoener's D, *ij* is a cell in the geographic raster grid, z_{1ij} the occupancy of taxa 1 in cell *ij*, and z_{2ij} the occupancy of taxa 1 in cell *ij* with the sum of occupancy data for each entity summing to 1. As such a distance of 0 relates to a pair of taxa with the exact same geographic distribution, a distance of 0.8 relates to a moderate spatial overlap, and a distance of 1 relates to no overlap.

We used Multiple Regression on Distance Matrices (MRM) to test for a relationship between pairwise perceptual distances and pairwise geographic distances. Significance of the test was based on random permutations of distances in the matrices such as the null hypothesis described a random association between perceptual and geographic distances across heliconiine subspecies (**Fig. 3a & 3b**).

Furthermore, to test for a pattern of wing similarity among spatially co-occurring subspecies that goes beyond the expectation from evolutionary relationship across the taxa, hinting for a case of evolutionary convergence as described in Müller's model, we used MRM to test for a relationship between pairwise perceptual distances and pairwise geographic distances accounting for phylogenetic distances as an additional predictor (**Fig 3c & 3d**). To compute phylogenetic distances, we used pairwise patristic distances on the phylogeny of Heliconiini (Kozak *et al.* 2015) with terminal branches of null length to describe the relative position of subspecies in their associated species.

Because Schoener's D tend to be sensitive to a threshold effect since any distance between two subspecies with no overlap would equals zero independently from their spatial adjacency or farness, we also ran complementary analyses describing geographic distances as two categories: sympatric *vs.* allopatric using a threshold of 1 – Schoener's D = 0.8 to discriminate between categories (See **Fig. S25** in **SI Appendix 8**).

2.3.2 Compare local perceptions vs. Citizen Science

We investigated the ability of our macro-scale Citizen Science-based approach of mimicry pattern similarity to inform about local patterns of wing similarity within communities. We compared perceptual maps obtained from the aggregation of similarity triplets provided by a panel of experts evaluating only the patterns of local taxa (labeled as 'triplet-aggregated' map) *vs.* coordinates of those same local patterns in the macro-scale Citizen Science perceptual map involving all 432 subspecies patterns (labeled as 'CS' map). We also compared local maps with the individual perceptual maps obtain from the 600 triplets provided by each expert individually for each community. In a complementary analysis, we showed that compiling five individual perceptions was enough to obtain stable local perceptual maps and mimetic classifications (See **Fig. S26** & **S27** in **SI Appendix 8**). As a visual comparison, we plotted the perceptual maps extracted from CS map *vs.* the triplet-aggregated map for each local community, displaying probability densities associated to GMM clustering applied on those same perceptual maps (**Fig. 4**).

We compared the topology of the CS map, the triplet-aggregated map, and each individual map using the Procrustes correlation statistics obtained from pairwise Procrustes Analyses (Gower 1975) minimizing distances across homologous points in two topologies by applying scaling, translation and rotation actions on the initial coordinates. Similarly to a Pearson coefficient, the Procrustes correlation is computed as follows:

$$Procrustes'\ r = \sqrt{1 - SS} \qquad \text{(Eqn. 3)}$$

where *SS* is the sum of squared distances between Procrustes adjusted coordinates of two maps scaled so that the maximum value is 1. We set the triplet-aggregated map as reference, and computed such index for each map across all five local communities (**Fig. 5a**).

Furthermore, we compared the putative mimicry rings obtained from GMM clustering applied on each local map using the Cohen's Kappa index (Cohen 1960). This index is a measurement of agreement between multinomial classifications. It allows to quantify the degree of similarity between two classifications were groups are not necessarily paired across classifications (i.e., mimicry rings do not have to be equivalent between the two classifications). In our case, it was computed from a co-membership confusion matrix summarizing the number of pairs of objects found in a similar/different group in one or the two classifications. The more the two classifications agreed on whether a pair of objects (e.g., butterfly wing patterns) should belong to the same or to a different group, the higher the Cohen's Kappa was. A Cohen's Kappa

close to zero reflected a random agreement between the classifications. A Kappa higher than 0.5 reflected relatively important agreement. A Kappa close to 1 reflected an agreement close to perfection. Thus, we computed the Cohen's Kappa of each map relative to the classification obtained for the triplet-aggregated map, for each local community. We ran similar analyses based on GMM with a reasonable number of mimetic groups (k) ranging from 5 to 10, and aggregated results as the mean across all k (**Fig. 5b**).

2.4 Data availability

All MATLAB and R scripts to carry out analyses are available on GitHub at https://github.com/MaelDore/Perceptual_map_Heliconiini. All 2D perceptual maps, 3D animated perceptual spaces, mimicry ring lists and subspecies images used in the online survey are available in online archives in Zenodo (**TBA**).

3 Results

3.1 Patterns of mimetic diversity at large spatial scale

We built a 3D perceptual space with coordinates of images representing the aggregated perception of wing pattern similarity in heliconiine butterflies from our Citizen Science data. We decomposed this 3D perceptual space into 2D perceptual maps (**Fig. 1a, 1c, 1d**). These maps showed that the main axes of variation in perceived mimicry patterns was mostly colors. Patterns along the first axis ranged from plain orange patterns such as those of *Dryas* and *Dione* butterflies, also presenting characteristics elongated and slightly curved forewing tips, to almost plain dark patterns of *Heliconius melpomene plesseni* or *Heliconius wallacei wallacei*. The second axis presented a similar color trend, but also demonstrated a pattern trend from large (red or white) bands of *Heliconius erato hydara* and *Heliconius cydno cydno*, through stripes of tiger heliconiines like *Heliconius ethilla ethilla* or *Eueides isabella eva,* to plain patterns of *Dryas* and *Dione*. The third axes mostly discriminated the *Philaethria* genus with its distinctive light green tone, elongated shape and black stripes.

We mapped on the geographic space the local functional mimetic diversity as the mean pairwise Euclidean distance in the perceptual space reflecting the degree of clustering of local phenotypes in the perceptual space (**Fig. 1b**). Results showed the local clustering of phenotype is relatively more important (i.e., functional diversity is low) in Amazonia than in the Andes, Central America or Brazilian Atlantic forest. Higher values were found in the USA and in the

Peruvian coastal desert, mostly reflecting the predicted presence of very few taxa that display different patterns (thus, showing a low clustering and high functional diversity).

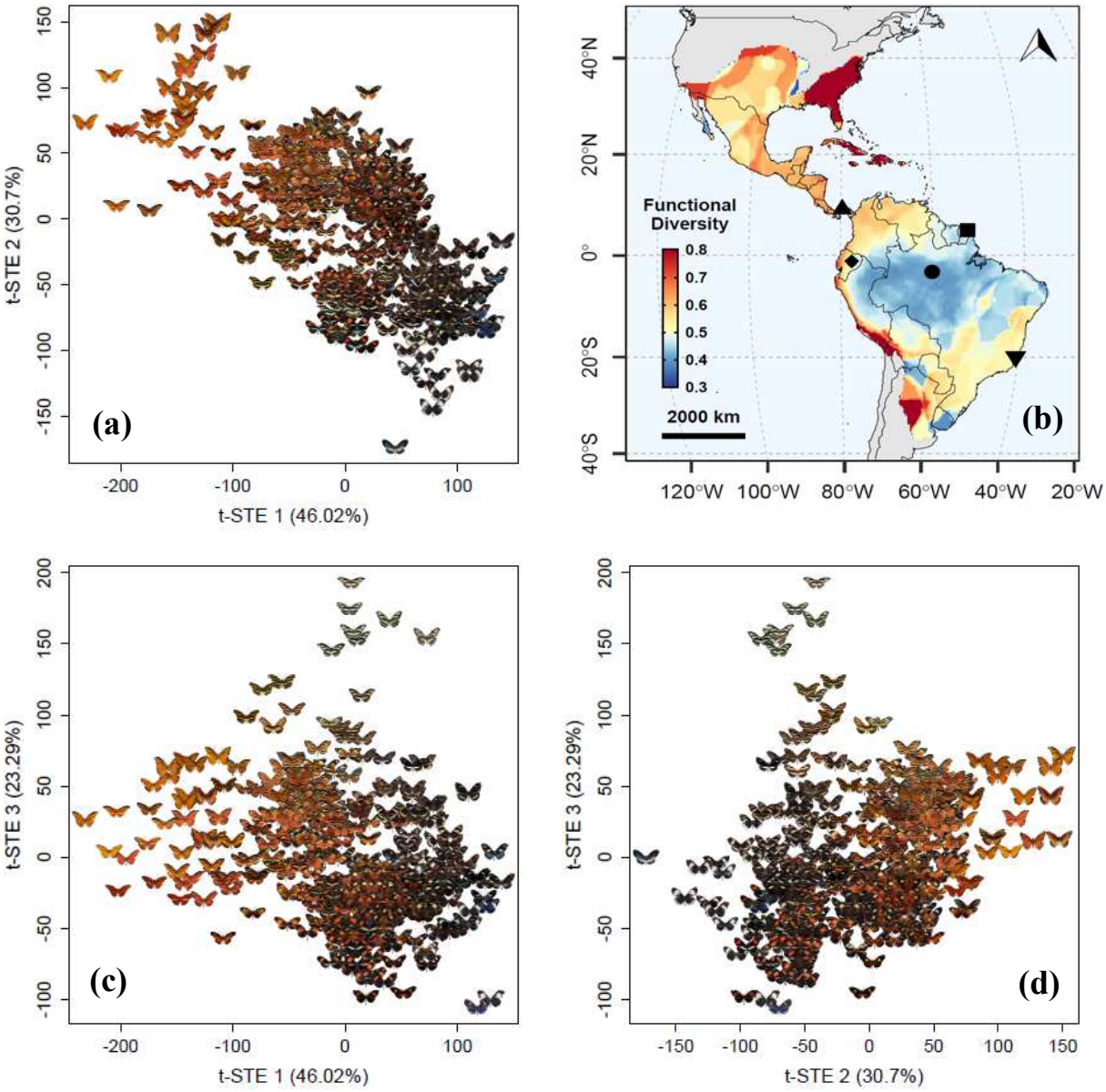

Figure 1: Perceptual maps at macro-scale built from Citizen Science data. (a-c-d) 2D perceptual maps displaying 432 images of subspecies used during the perception survey to their t-STE coordinates in the embedded space. Distances between patterns reflect global perception of dissimilarity. **(b)** Map of functional mimetic diversity computed as the mean pairwise Euclidean distance in the perceptual space, reflecting the degree of clustering of local phenotypes. Perceptual map of the local communities symbolized with shapes are presented in **Figure 4**: square = Cayenne, up-triangle = Gamboa, diamond = Jatun Sacha, circle = Manaus, down-triangle = Santa Teresa.

By converting the perceptual space in an RGB color space, we assigned a color to each community based on the coordinates of its mean phenotype. The distribution of communities

in the perceptual space showed that no community displayed a mean phenotype falling in the region of dark patterns with high t-STE 1 and low t-STE 2 and t-STE 3 (**Fig. 2a, 2c, 2d**). In the geographic space, the most species-rich regions of the Andes and Amazonia presented, by construction, a mean phenotype close to the centroid of the perceptual space symbolized by a brownish tone (**Fig. 2b**). The Cerrado and Brazilian Atlantic forest demonstrated a trend towards a majority of orange and tiger patterns symbolized by the reddish tone (**Fig. 2b**), and illustrated by the relatively marginal position of local community of Santa Teresa in the RGB space (down-triangle symbol in **Fig. 2**). North America was clearly an outlier with its orange tone, having a mean phenotype falling among the plain orange patterns since the few heliconiine species found in this area are from the *Agraulis*, *Dione*, *Dryas* and *Dryadula* genera all displaying an orange-based pattern, with the notable exception of the stripped *Heliconius charithonia* (**Fig. 2b**).

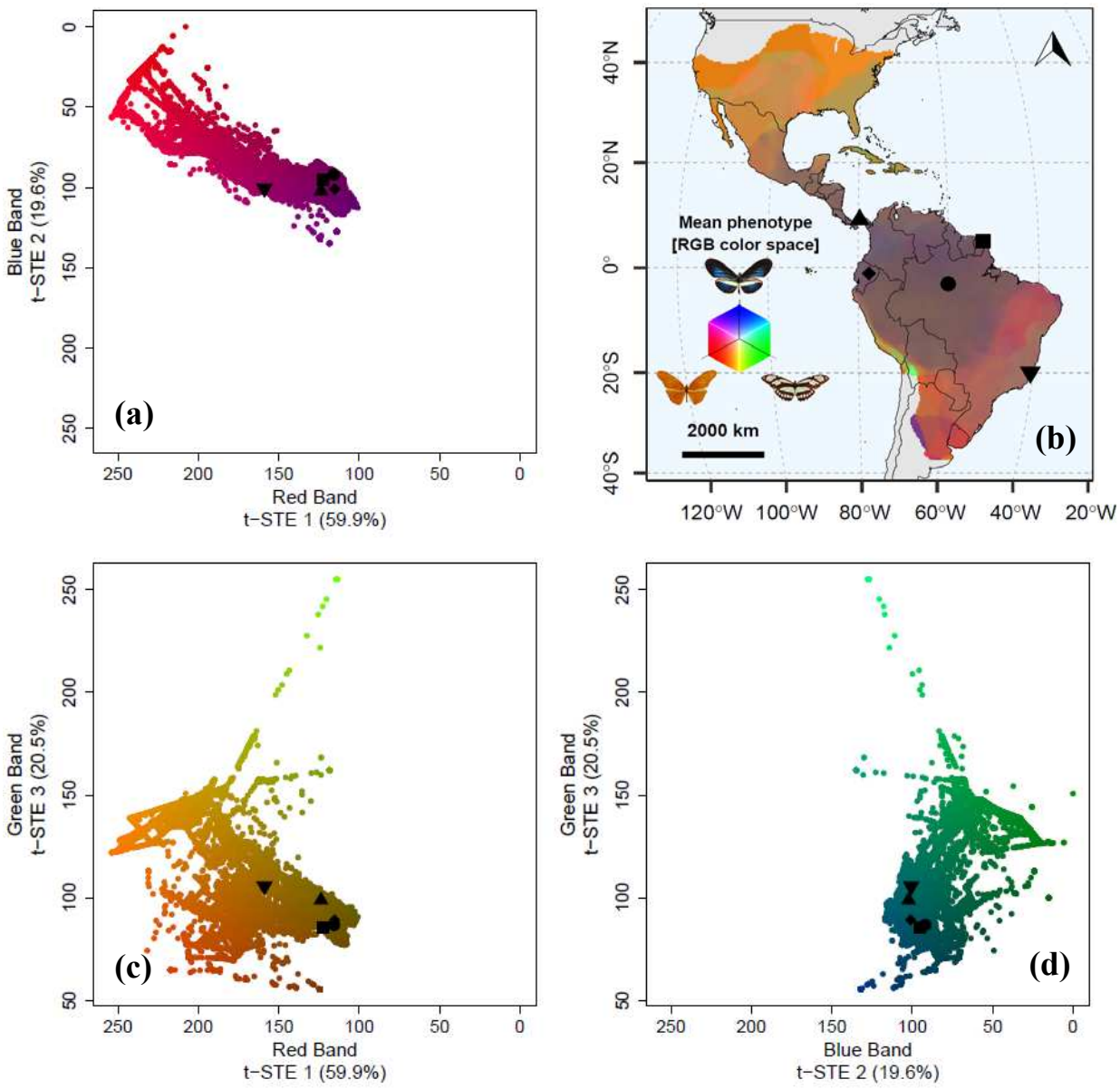

Figure 2: RGB maps of local mean phenotype built from Citizen Science data. (a-c-d) 2D RGB maps displaying the mean phenotype found in the 23,661 communities defined as 30 km x 30 km grid cells within the range of heliconiine butterflies. Axes range from 0 to 255 scaled on the range of the coordinates of the subspecies in the initial perceptual space (**Fig. 1b**). Distances between communities reflect global perception of dissimilarity in the mean local phenotype. **(b)** Map of mean local phenotype whose color corresponds to its coordinates in the RGB space. Differences in color relates to dissimilarity in mean local phenotypes. Symbols represents local communities highlighted in **Figure 4**: square = Cayenne, up-triangle = Gamboa, diamond = Jatun Sacha, circle = Manaus, down-triangle = Santa Teresa.

3.2 Convergence of sympatric taxa in the perceptual space

We tested if the perceptual distances between subspecies were correlated with the geographic distances between their spatial distributions. First, we tested for such a relationship without accounting for the effects of phylogenetic relatedness as a test of phenotypic similarity,

regardless of its origin (convergence or common ancestry). We showed perceptual distances between pairs of taxa were significantly correlated with geographic distances when considering spatial distributions at the continental scale (**Fig. 3a & 3b**; MRM: $\beta_{obs} = 0.078$, Q95% = 0.040, $p = 0.003$).

Second, we tested for a correlation between perceptual distances and geographic distances accounting for the effects of phylogenetic relatedness as a test of evolutionary convergence. We showed residual perceptual distances between pairs of taxa were significantly correlated with geographic distances even when the effect of phylogenetic relatedness was accounted for (**Fig. 3c & 3d**; MRM: $\beta_{obs} = 0.085$, Q95% = 0.039, $p \leq 0.001$).

Complementary analyses using categorical groups of spatial distances defined as sympatry and allopatry led to similar results (See **Fig. S25** in **SI Appendix 8**).

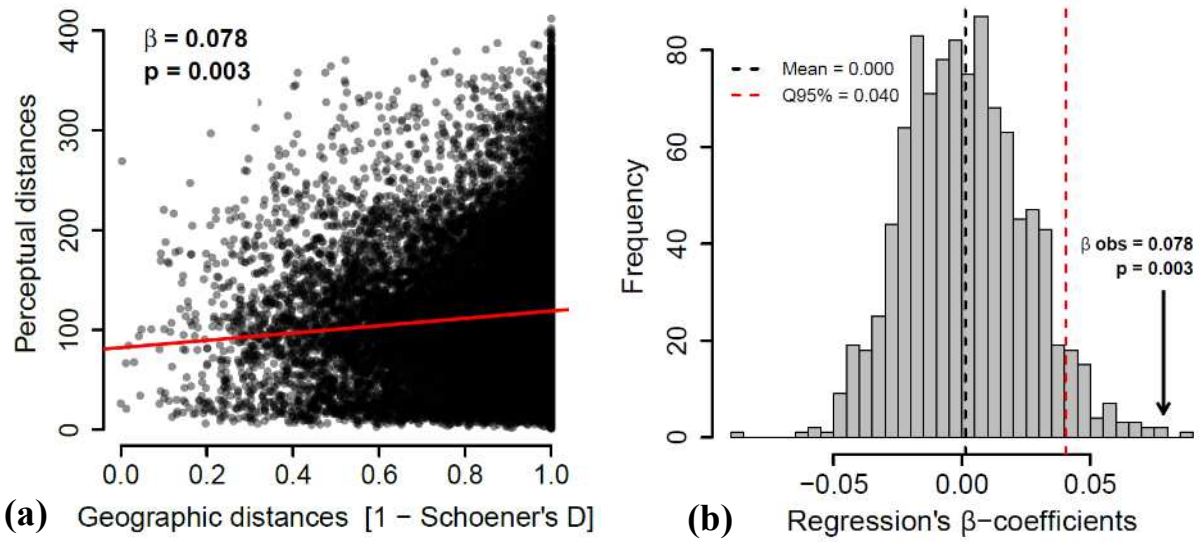

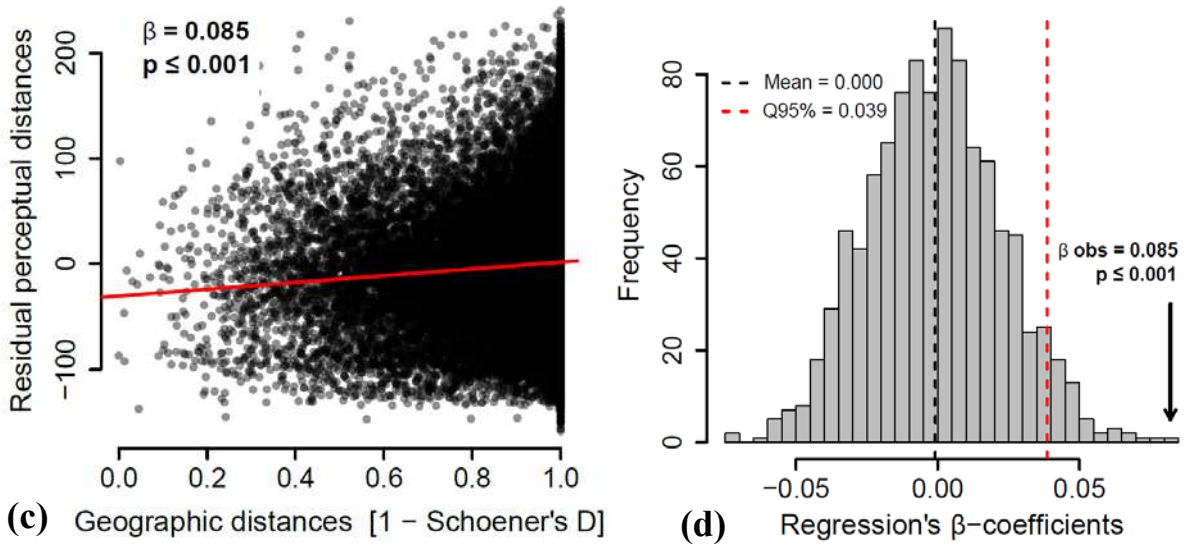

Figure 3: Pairwise perceptual distances between heliconiine subspecies correlate with geographic distances. (a) Scatter plot for the similarity test showing the positive correlation between perceptual distances (Euclidean distances in the perceptual space) and geographic distances (1 – Schoener's D of predicted spatial distributions). **(b)** Null distribution of the MRM statistics (β-coefficient of standardized regression) showing a significant positive relationship for the similarity test. **(c)** Scatter plot for the convergence test showing the positive correlation between residual perceptual distances (once accounted for the effect of phylogenetic distances) and geographic distances (1 – Schoener's D of predicted spatial distributions). **(d)** Null distribution of the MRM statistics (β-coefficient of standardized regression) showing a significant positive relationship for the convergence test.

3.3 Mimicry rings in local communities

We compared perceptual maps obtained from the aggregation of similarity triplets provided by a panel of experts evaluating only patterns of local taxa (labeled as 'triplet-aggregated' map) *vs.* maps of those same local patterns in the macro-scale perceptual map involving all 432 subspecies patterns (labeled as 'CS' map). We added the probability densities associated to GMM clustering applied on those same perceptual maps for a number of groups specific to each local community (**Fig. 4**). Even if the relative position of mimicry groups, and sometimes the composition of the groups can vary between the two approaches (cf. lists of mimetic groups in **Fig. S28-S32** in **SI Appendix 10**), perceptual maps appeared relatively consistent across methods for all local communities with main axes of variation reflecting similar perception of local wing pattern similarity. The local community of Manaus displayed visibly less mimetic diversity (i.e., higher clustering in the perceptual space) than others, as expected from our global map of mimetic diversity (**Fig. 1b**).

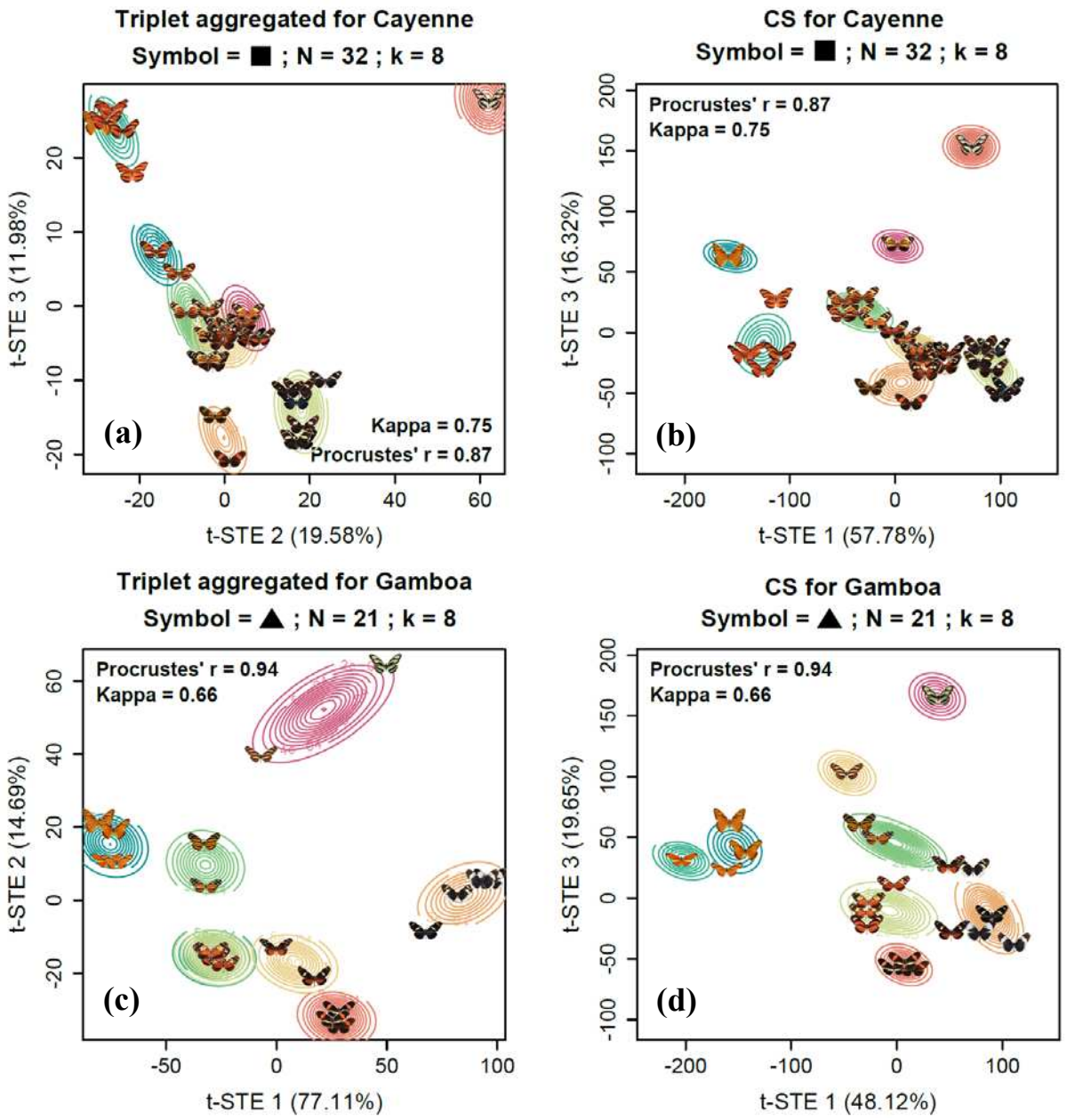
Triplet aggregated for Cayenne
Symbol = ■ ; N = 32 ; k = 8
t-STE 3 (11.98%)
t-STE 2 (19.58%)
(a)
Kappa = 0.75
Procrustes' r = 0.87
CS for Cayenne
Symbol = ■ ; N = 32 ; k = 8
Procrustes' r = 0.87
Kappa = 0.75
t-STE 3 (16.32%)
t-STE 1 (57.78%)
(b)
Triplet aggregated for Gamboa
Symbol = ▲ ; N = 21 ; k = 8
Procrustes' r = 0.94
Kappa = 0.66
t-STE 2 (14.69%)
t-STE 1 (77.11%)
(c)
CS for Gamboa
Symbol = ▲ ; N = 21 ; k = 8
Procrustes' r = 0.94
Kappa = 0.66
t-STE 3 (19.65%)
t-STE 1 (48.12%)
(d)

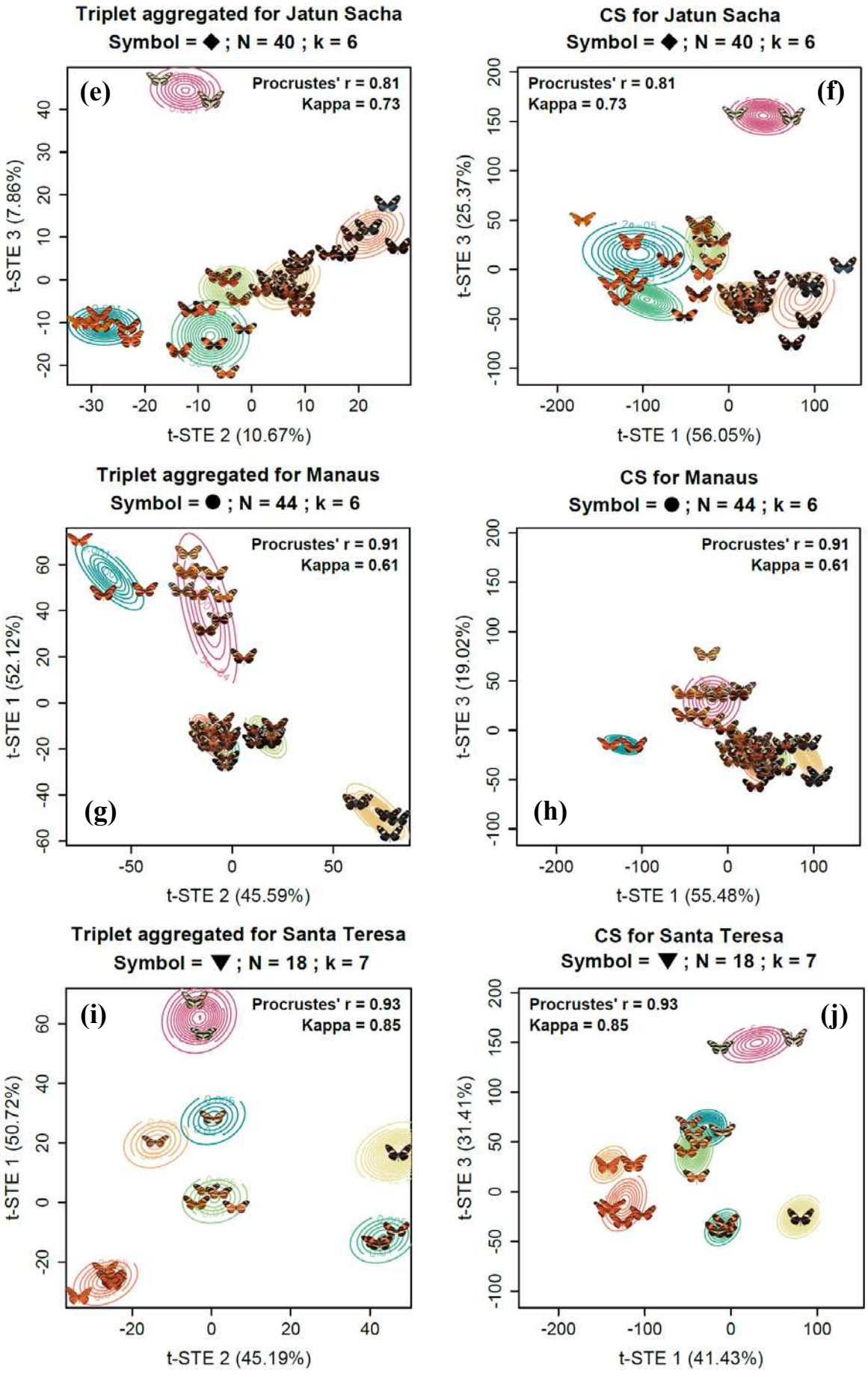
Triplet aggregated for Jatun Sacha
Symbol = ◆ ; N = 40 ; k = 6
(e)
Procrustes' r = 0.81
Kappa = 0.73
t-STE 3 (7.86%)
t-STE 2 (10.67%)
CS for Jatun Sacha
Symbol = ◆ ; N = 40 ; k = 6
(f)
Procrustes' r = 0.81
Kappa = 0.73
t-STE 3 (25.37%)
t-STE 1 (56.05%)
Triplet aggregated for Manaus
Symbol = ● ; N = 44 ; k = 6
(g)
Procrustes' r = 0.91
Kappa = 0.61
t-STE 1 (52.12%)
t-STE 2 (45.59%)
CS for Manaus
Symbol = ● ; N = 44 ; k = 6
(h)
Procrustes' r = 0.91
Kappa = 0.61
t-STE 3 (19.02%)
t-STE 1 (55.48%)
Triplet aggregated for Santa Teresa
Symbol = ▼ ; N = 18 ; k = 7
(i)
Procrustes' r = 0.93
Kappa = 0.85
t-STE 1 (50.72%)
t-STE 2 (45.19%)
CS for Santa Teresa
Symbol = ▼ ; N = 18 ; k = 7
(j)
Procrustes' r = 0.93
Kappa = 0.85
t-STE 3 (31.41%)
t-STE 1 (41.43%)

Figure 4: Perceptual maps of local communities with GMM probability densities for 'triplet-aggregated' and 'CS' maps. Only two axes among the three are displayed. 'Triplet-aggregated' maps were built from similarity triplets based only on local patterns and provided by five experts. 'CS' maps were extracted from the macro-scale (**Fig.1**) built from Citizen Science data. Axes t-STE 1 and t-STE 3 for the 'CS' maps correspond to the axes showed in **Fig. 1**. Axes shown in 'triplet-aggregated' maps were selected to represent similar pattern trends relative to the axes shown in 'CS' maps. Procrustes correlation measures similarity in map topology. Cohen's Kappa measures agreement in GMM classifications. Both metrics are symmetric, thus they were identical between the two maps for a given community. N = number of local patterns. k = chosen number of mimicry groups.

3.4 From large-scale Citizen Science data to local perceptions

We investigated the ability of our macro-scale Citizen Science approach of mimicry pattern similarity to inform about local patterns of wing similarity within local communities. First, we used Procrutes correlations indices to evaluate the similarity in perceptual map topologies across triplet datasets, using as reference for each community the 'triplet-aggregated' maps based only on local patterns and provided by five experts. We showed that the global topologies of the perceptual spaces built from Citizen Science data based on the whole 432 subspecies patterns are within the range of similarity of the individual perceptual maps built from 600 similarity triplets provided by experts (**Fig. 5a**). As such, the Citizen Science approach provided as much information regarding the quantification of local pattern similarity than the perception of an individual expert.

Second, we used Cohen's Kappa to evaluate the similarity in GMM classifications obtained from the different maps across triplet datasets, also employing the 'triplet-aggregated' maps as reference for each community. We showed again that the mimetic classification obtained from CS maps were within the range of agreement of the classification obtained from individual perceptual maps (**Fig. 5b**). As such, the Citizen Science approach provided as much information regarding the classification of patterns within mimicry rings than the perception of an individual expert.

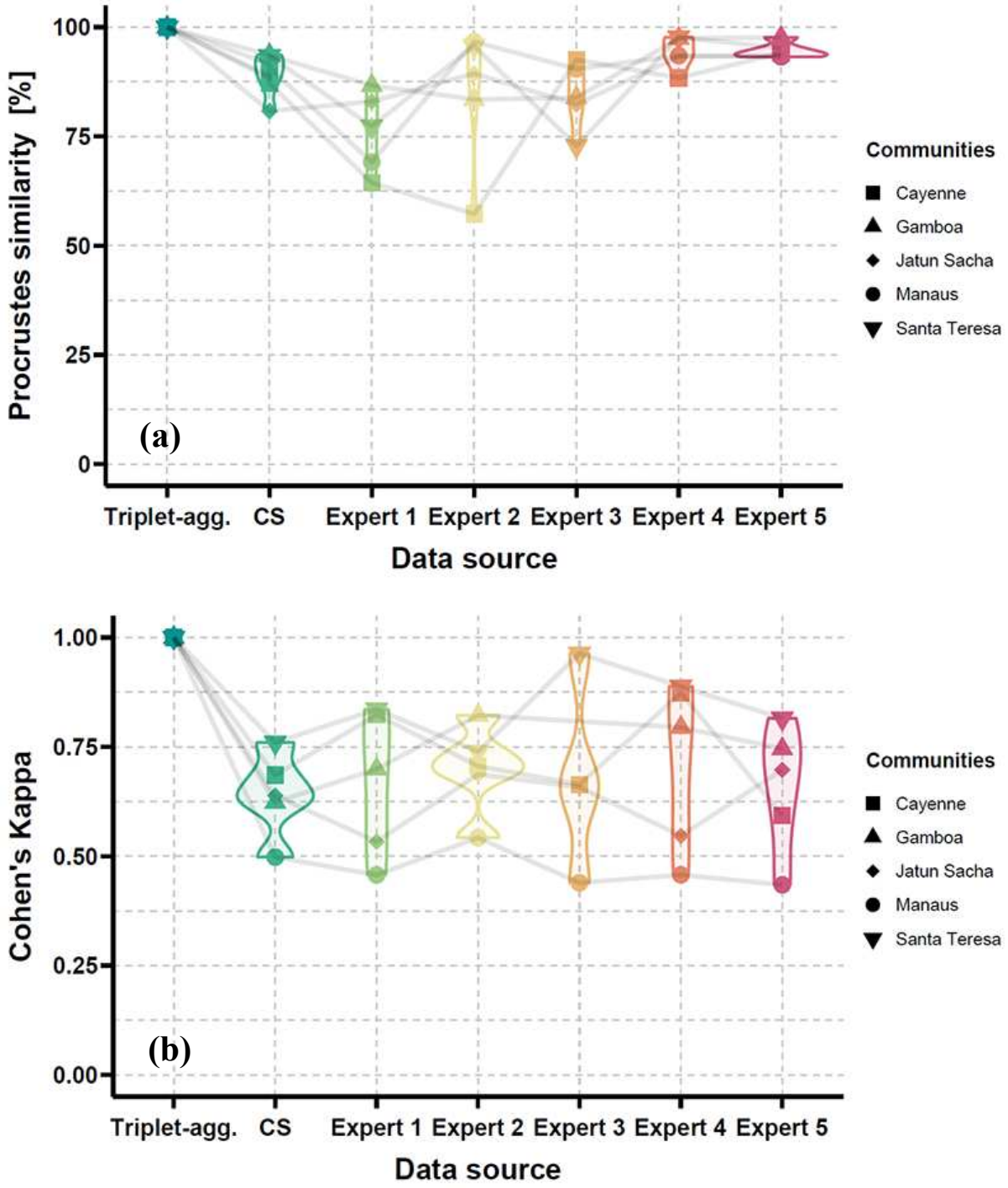

Figure 5: Comparison of topologies of local perceptual maps (a) and mimetic classifications (b) between triplet datasets/data source using triplet-aggregated (Triplet-agg.) maps as reference. CS maps were extracted from the Citizen Science-based maps built from 75,240 triplets collected for 432 images. Expert maps were built from 600 triplets of local patterns representing the perception of a single expert. Triplet-aggregated maps were built from databases aggregating all expert triplets. **(a)** Procrustes similarity reflects similarity in the global topology of perceptual spaces. **(b)** Cohen's Kappa measures agreement in mimetic classifications. Values presented for Cohen's Kappa were averaged across a credible range of number of groups (k from 5 to 10). Symbols represents the five local communities investigated with values for a unique community linked by grey lines across triplet datasets.

4 Discussion

In this study, we present a new method based on perceived similarity to quantify phenotype variation in ecological traits that carry visual signals. We illustrate the potential of this method by describing phenotypic variation in mimicry patterns of heliconiine butterflies at continental scale. Our results comfort and extend the long-time theorized pattern of trait convergence between sympatric species in a context of mimicry to large-scale spatial distributions. As such, we show how this method can be applied successfully in a context of high pattern diversity, integrating altogether the morphological, chromatic and cognitive dimensions of trait variation. Moreover, we demonstrate the versality of this new method by carrying out in parallel a Citizen Science project as a proof of concept for its relevant use in macroecological analyses involving the collection of a large amount of data, as well as its suitability for smaller scale analyses aiming to build local perceptual maps. Altogether, this work opens new perspectives to the investigation of ecological trait variation at multiple geographic and phylogenetic scales and may stimulate further studies of the evolution of ecological traits whose complexity prevented large scale comparison until now.

4.1 Mimicry: a discrete utopia in a continuous reality?

The representation of perceived phenotypic variation in wing patterns of heliconiine butterflies showed a continuum of patterns spread along the three axes of the perceptual space (**Fig. 1a, 1c, 1d**). This continuum is consistent with results from a previous study addressing large-scale pattern variation in mimetic bumblebees (Ezray *et al.* 2019) and also revealing a continuum of patterns in its phenospace. Yet, in the context of mimicry leading to the local convergence of patterns, it may seem surprising to obtain a global continuum rather than relatively defined clusters of patterns representing mimicry rings. This apparent paradox between a theory arguing for a discrete distribution of patterns and the continuous reality we quantified can be explained at multiple level.

At local-scale, within communities, Müller's model predicts the convergence of aposematic patterns mediated by predator perception and learning of pattern similarity and their association to toxicity. However, mimicry does not need to be perfect to ensure optimal protection (Kikuchi & Pfennig 2013). Small variations could be ignored or even not perceived by predators (Dittrich *et al.* 1993). The diversity of the perceptions of local predators could lead to a fuzzy plateau of optimality in the perceptual space where slightly different patterns provide

equal protection against attacks from multiple predators. Selection could be relaxed for patterns that are relatively rare locally and for which protection and selective pressure are therefore weak (Sherratt 2002). Developmental and genetic constraints could also limit the possibility to evolve better mimetic signals, even if imperfect signals are sub-optimal (Smith *et al.* 1985). Local imperfect mimicry is illustrated in our perceptual maps of local communities which despite demonstrating relatively significant degree of pattern clustering into mimetic groups, also show the existence of small pattern variation within mimetic groups (**Fig 4**).

Even if local mimicry were perfect (which it is not), the suite of predators applying selective pressures varies at regional scale. Consequently, peaks of optimality in the perceptual space vary smoothly due to variation in predator assemblages and spatial stochasticity. This variation leads to the existence of phenotypic clines at regional scales even within mimicry rings (Hill *et al.* 2013). This variation becomes steeper in suture zones (Mallet & Barton 1989) delineating the mosaic of geographical forms arising through a combination of selective and neutral processes such as dispersal, genetic drift and local frequency-dependence selection (Sherratt 2006). Altogether, local imperfection in mimicry, combined with the geographic drift of selected patterns lead to a continuum of patterns in the perceptual space when all communities are pooled in a macroecological perspective.

4.2 From large-scale Citizen Science aggregation to individual local perceptions

We deployed a Citizen Science online platform to collect a diversity of perception data from thousands of people in order to address macroecological questions regarding wing pattern variation. Our resulting perceptual space combining color, shape, internal patterns, and their cognitive integration showed the main feature structuring the perceived wing pattern variation is color, with at least two axes organized along a color gradient (**Fig. 1**). These results consolidate previous experimental findings showing that color is a highly salient feature that is primarily used by bird predators (Aronsson & Gamberale-Stille 2012) and humans (Sherratt *et al.* 2015) to assess global similarity, over similarity in patterns and shape.

Moreover, the Citizen Science data collection allowed us to quantify local mimetic diversity as the degree of clustering of local patterns in the perceptual space. We showed that functional diversity is relatively low in the Amazon basin compared to other species-rich regions such as Central America and the Brazilian Atlantic forest (**Fig. 2b**), similarly to what has been highlighted for mimetic richness measured as counts of mimetic groups defined on

expert knowledge (Pérochon et al., 2023; see **ANNEXE 6**). As a consequence, local mimetic groups in Amazonia are composed of more (sub)species (see lists of local mimicry rings in **Fig. S31** in **SI Appendix 10**). This lower phenotypic diversity could be explained by a more homogenous climate in the area coupled with the relative absence of strong geographic barriers to dispersal of butterflies and their predators in the Amazonian forest (Melo et al., 2009, but see Rosser et al., 2021) leading to relatively homogeneous selective predation pressures across the entire region.

The Citizen Science approach opens major opportunities for biogeographic studies of trait variation at large spatial scales. However, in the context of mimicry, the relevant scale to define the mutualistic ecological interactions supported by similarity in aposematic patterns is the local scale, where individuals can co-occur and ecological interactions are realized (Joron & Mallet 1998). Thus, we explored the ability for the Citizen Science dataset to inform on local variation of wing patterns and to provide relevant data to define mimetic groups. This ability could be impaired by the limited number of similarity triplets in the Citizen Science dataset encompassing each independent set of local patterns in local communities. Moreover, differences in the pool of patterns evaluated at the global and local scale could influence the perception of similarity (Bai *et al.* 2020). Nonetheless, we showed that perceptual space topologies and derived mimetic classifications from Citizen Science data were as much similar to those obtained from aggregated expert data on local patterns than the ones from individual experts (**Fig. 5**). As such, large-scale Citizen Science data collection seems a relevant approach to describe phenotypic variation, and in this case mimetic interactions, in potentially any local community, as long as distribution data are available.

Altogether, the perceptual approach is a new versatile tool to the ecologist and evolutionist's toolbox that may allow them to study ecological trait variation from the global scale integrating a diversity of perceptions, to the local scale focusing on individual perceptions, according to the study design and objectives.

4.3 Uses and advantages of the perceptual approach

The perceptual approach has been designed to incorporate altogether the morphological, chromatic and cognitive dimensions of trait variation. It is particularly suitable to study ecological signals mediated through perception such as aposematic patterns in the context of mimicry. In addition, it can provide a practical solution to quantify highly complex patterns for which image analyses is suboptimal due to difficulties to handle conjointly variations in shapes,

colors and patterns. Indeed, a current solution to such issues is to simplify color patterns in standardized templates (Ezray *et al.* 2019; Wilson *et al.* 2022) or to decompose the complex trait in independent features studied in parallel (Ortiz-Acevedo *et al.* 2020). The perceptual approach is not limited by the multidimensional complexity of traits, and allows to quantify any trait variation as long as relative similarity between triplets of objects can be informed, opening opportunities to study complex trait variation at large phylogenetic scales.

A classic limitation of convolutional neural networks aiming to summarize variation in visual information is that the output has high numbers of dimensions, limiting opportunities for clear visualization, and preventing efficient clustering analyses (Wang *et al.* 2008) and macroevolutionary analyses (Adams & Collyer 2018). A typical solution is to apply additional downstream dimension reduction techniques to obtain a suitable output in low dimensions. Yet, the proportion of the original variance retained in the final selected dimensions may be limited (e.g., Hoyal Cuthill *et al.* 2019), restricting the significance of subsequent analyses. The perceptual approach allows to circumvent this issue by letting the user define a priori the final number of dimensions of the embedding according to its objectives and needs. Additionally, the perceptual approach can be applied in complementarity with convolutional neural networks in order to provide a human classifier that can be used to evaluate and train the neural networks.

In this article, we illustrate how clustering can be applied in the perceptual space to generate hypotheses for local mimicry rings based on perceived pattern similarity. We recommend the use of Gaussian Mixture-Models (GMM) to achieve clustering (see details in dedicated Methods section), but alternative clustering algorithms can be employed such as HDBSCAN (Hahsler *et al.* 2019) or Spectral clustering (Karatzoglou *et al.* 2004). However, the mere use of clustering need to be considered carefully. The perceptual approach produces quantitative continuous space or maps of chosen dimensionality, which provides the most accurate description of pattern variations as coordinates and distances that are directly suitable for downstream biogeographic and macroevolutionary analyses (Revell & Harmon 2022). Applying a clustering algorithm leads to discrepancy of information and must be limited to questions that require a classification in perceived groups such as defining local mutualistic interactions based on mimicry.

4.4 Limits and perspectives for the study of phenotypic diversity at multiple scales

One of the main limits when addressing perception is the variation of perception between individuals, but also between species. The mimicry patterns of heliconiine butterflies are under selective pressures from their natural predators, mostly birds specialized in flying-insect predation such as jacamars (Chai 1986). Since we could not easily ask jacamars directly about their perceived relative distances among triplet of heliconiine butterflies, we did so with human subjects as surrogate predators. One could argue that a perceptual space built on human perception is not a valid description of perceived similarities by the suite of natural predators. Indeed, most birds possess four to five classes of cones receiving photonic wavelengths emitted by butterfly wings, including a class of cones specialized in ultraviolet wavelengths invisible to the human eye (Cuthill & Bennett 1993). Meanwhile some heliconiine butterflies are known to harbor UV-reflecting pigments that could be perceived by birds and not by humans (Bybee *et al.* 2012). Thus, the question to ask is whether human visual perception and associated cognitive processing of visual signals are sufficiently close to bird vision to inform us on the selective pressures at play in nature.

A first answer to this interrogation relies on a very pragmatic observation: "our ability to detect and describe mimicry shows that our perceptual systems must be fairly similar to those of the predators causing such mimicry" (Joron & Mallet 1998). Several experimental findings support the idea that human vision and bird vision is sharply similar when it comes to the perception of mimicry patterns. For instances, pigeons broadly rank hoverfly mimics similarly to humans (Dittrich *et al.* 1993). Color appears to be a particularly salient feature for both birds and humans that can overshadow other discriminative cues such as shape and patterns (Sherratt *et al.* 2015). Finally, humans and great tits demonstrated strikingly quantitatively similar abilities to learn and generalized aposematic signals of unpalability (Beatty *et al.* 2005). As such, it seems reasonable to consider human-based quantification of mimetic traits as informative and ecologically relevant (Penney *et al.* 2012).

Our study aims to describe variation in mimicry patterns of heliconiine butterflies at the global and local scales relying on perception of similarity. The distribution and clustering of mimicry patterns in the perceptual space way be influenced locally and globally by the pool of patterns included in the analysis (Bai *et al.* 2020). While we focused this study on heliconiine butterflies, it is worth considering the existence of other taxonomic groups in communities of

Neotropical mimetic butterflies. For instance, ithomiine butterflies (tribe Ithomiini, subfamily Danainae, family Nymphalidae) are preponderant members of these mimetic communities, sharing mimicry rings with Heliconiini (Bates 1862). Their spatial distributions can influence the spatial distributions of heliconiines (Brown Jr 1979; Pérochon *et al.* 2023; see **ANNEXE 6**) but also the perception of pattern similarity. For instance, two species of heliconiine which may be considered non-mimetic because they are sufficiently apart in the perceptual space, could be reconsidered with the inclusion of an ithomiine species with an intermediate pattern. To overcome this limit, we call for future studies involving all members of the mimetic communities, independently of taxonomic boundaries.

Altogether, the perceptual approach opens new perspectives to the investigation of ecological trait variation at multiple geographic and phylogenetic scales, especially traits whose complexity prevented large scale comparison until now. It will be possible to compare the quantification of trait variation between a perceptual and an analytical approach, investigating the influence of cognitive processes. Thanks to its versatility the perceptual approach makes it also accessible to compare trait perception between individuals and/or social groups (see **Fig. S10** & **S11** in **SI Appendix 4** for an example with age and cultural and educational background). The fine characterization of the occupation of the perceptual space at multiple scales could inform us on constraints and processes acting on the evolution of traits. Finally, by integrating the cognitive processes behind the transmission of information through ecological signals, the perceptual approach offers an innovative point of view inaccessible to analytical approaches, and potentially opens the way to the study of any kind of ecological signal (e.g., colors, shapes, songs, smells, behaviors, etc.) for the field of phenomics.

Data Accessibility Statement

All MATLAB and R scripts to carry out analyses are available on GitHub at https://github.com/MaelDore/Perceptual_map_Heliconiini. All 2D perceptual maps, 3D animated perceptual spaces, mimicry ring lists and subspecies images used in the online survey are available in online archives in Zenodo (**TBA**). The online survey for the Citizen Science data collection is available on http://memometic.cleverapps.io/.

Supplementary Information

Supplementary Information for CHAPTER 3: “Perceptual maps: a new tool to investigate mimicry patterns from Citizen Science to individual perception” can be found in **ANNEXE 4.**

Acknowledgements

We warmly thank Chris Jiggins for agreeing to share with us his highly valuable collection of Heliconiini pictures gathered throughout the years during visits to several institutions, and that forms the basis of our image collection. We thank museum curators who allowed us to examine the Heliconiini collections under their care, and to take pictures of specimens for our image database, or send us directly the desired pictures, including Keith Willmott (FMNH), Augusto H.B. Rosa (UniCamp), André V.L. Freitas (UniCamp), Rodolphe Rougerie and Jérôme Barbut (MNHN). Some images were gratefully provided by the Natural History Museum London (NHMUK), with the assistance of staff members Blanca Huertas and Robyn Crowther. We also deeply thank the people who agreed to share images from their private collections to complete our image database: Pierre Boyer, Michel Cast, Gerardo Lamas, Andrew D. Warren, Daniel H. Janzen, Jim P. Brock, Kim Garwood, Luis Miguel Constantino, and Christian Brévignon. Finally, we thank the expert lepidopterists who helped us to curate our taxonomic lists of local communities including Rémi Mauxion, Ombeline Sculfort, Olivier Claessens, Leila Teruko Shirai, and Kelve Franklimara de Sousa Cézar.

CHAPTER 4

Mutualistic interactions shape global spatial congruence and climatic niche evolution in Neotropical mimetic butterflies

Maël Doré[1,2], Keith Willmott[3], Sebastien Lavergne[4], Nicolas Chazot[5], André V. L. Freitas[6], Colin Fontaine[2], and Marianne Elias[1,7]

[1]*Institut de Systématique, Evolution, Biodiversité, MNHN-CNRS-Sorbonne Université-EPHE-Université des Antilles, Muséum national d'Histoire naturelle, 45 Rue Buffon, 75005, Paris, France*

[2]*Centre d'Ecologie et des Sciences de la Conservation, UMR 7204 MNHN-CNRS-Sorbonne Université, Muséum national d'Histoire naturelle, 45 rue Buffon, 75005, Paris, France*

[3]*McGuire Center for Lepidoptera and Biodiversity, Florida Museum of Natural History, University of Florida, Gainesville, FL, United States of America*

[4]*Laboratoire d'Ecologie Alpine, Université Grenoble Alpes, Université Savoie Mont Blanc, CNRS, FR-38000 Grenoble, France*

[5]*Swedish University of Agricultural Sciences, Uppsala, Sweden*

[6]*Departamento de Biologia Animal and Museu de Diversidade Biológica, Instituto de Biologia, Universidade Estadual de Campinas, 13083-862 Campinas, São Paulo, Brazil*

[7]*Smithsonian Tropical Research Institute, Panamá, Panamá*

Reference:

Doré, M., Willmott, K., Lavergne, S., Chazot, N., Freitas, A. V. L., Fontaine, C. & Elias, M. (2023). Mutualistic interactions shape global spatial congruence and climatic niche evolution in Neotropical mimetic butterflies. *Ecology Letters*, In production. https://doi.org/10.1111/ele.14198

Author contributions:

MD and ME conceived the study and designed the analyses. ME, KW & AVLF provided occurrence data. MD wrote the R scripts, carried out the analyses, produced all results and figures, and led the manuscript writing. All authors critically contributed to the article and gave final approval for publication.

Abstract

Understanding the mechanisms underlying species distributions and coexistence is both a priority and a challenge for biodiversity hotspots such as the Neotropics. Here, we highlight that Müllerian mimicry, where defended prey species display similar warning signals, is key to the maintenance of biodiversity in the c. 400 species of the Neotropical butterfly tribe Ithomiini (Nymphalidae: Danainae). We show that mimicry drives large scale spatial association among phenotypically similar species, providing new empirical evidence for the validity of Müller's model at a macroecological scale. Additionally, we show that mimetic interactions drive the evolutionary convergence of species climatic niche, thereby strengthening the co-occurrence of co-mimetic species.

This study provides new insights into the importance of mutualistic interactions in shaping both niche evolution and species assemblages at large spatial scales. Critically, in the context of climate change, our results highlight the vulnerability to extinction cascades of such adaptively-assembled communities tied by positive interactions.

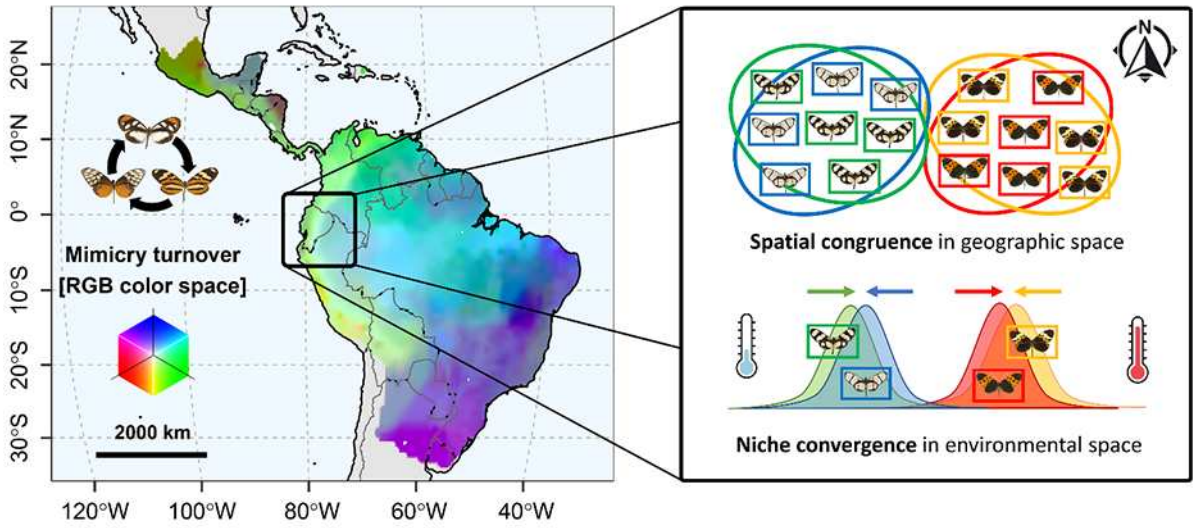

Graphical Abstract: Mutualistic interactions shape global spatial patterns and climatic niche evolution in Neotropical mimetic butterflies. Mimicry turnover at continental scale demonstrates large scale spatial congruence of phenotypically similar ithomiine butterflies (Nymphalidae: Danainae) associated with the climatic niche convergence of mimetic species.

Keywords

Müllerian mimicry, Neotropical butterflies, evolutionary convergence, climatic niche, spatial co-occurrence, community composition, species assemblages, mutualistic interactions, biodiversity hotspot, extinction cascade.

1 Introduction

Traditionally, community and evolutionary ecology have focused on the interplay between antagonistic interactions (i.e., competition, predation) and common ancestry, and how this interplay drives both the assembly of communities and species niche evolution (Pianka 1981; Brown & Maurer 1989; Webb *et al.* 2002; Kraft *et al.* 2007). However, more recently, many studies have extended this vision by documenting the importance of positive interactions in determining species coexistence and the stability of communities (Okuyama & Holland 2008; Elias *et al.* 2009a; Thébault & Fontaine 2010; Alexandrou *et al.* 2011; Mougi & Kondoh 2012; Hale *et al.* 2020), the coevolution of functional traits (Guimarães *et al.* 2011, 2017; Nuismer *et al.* 2013; Newman *et al.* 2014; O'Brien *et al.* 2021), the support of ecosystem functions such as pollination or seed dispersal (Millennium Ecosystem Assessment 2005), and the origins and maintenance of biodiversity (Bascompte & Jordano 2007; Gross 2008; Bastolla *et al.* 2009; Pascual-García & Bastolla 2017).

Positive and negative interactions are expected to have opposite consequences on the evolution of species traits and on the assembly of communities. Competitive interactions may drive character displacement (e.g., divergence in traits involved in resource use) and local competitive exclusion, leading to a decrease in ecological niche similarity among species within communities (Brown & Wilson 1956; Webb *et al.* 2002; Dayan & Simberloff 2005). By contrast, positive interactions are predicted to drive the convergence of traits that enhance the local co-occurrence of interacting species, leading to an increase in ecological niche similarity within communities (Bruno *et al.* 2003; Thompson 2005; Elias *et al.* 2009a; Nuismer *et al.* 2013; Aubier & Elias 2020). However, the consequences of this interplay on community composition at large spatial scales and on the evolution of species climatic niche, which drive species distributions at such scales, remain poorly explored, outside of plant facilitation (Valiente-Banuet & Verdú 2007; Brooker *et al.* 2008).

Species within ecological guilds are linked by the use of a common resource (e.g., trophic resources or microhabitat space), thereby interacting negatively through exploitative competition. Yet, many species also engage in positive interactions (Crowley & Cox 2011). For instance, birds commonly form multispecies flocks, which increases foraging efficiency (Wiley 1971) and reduces predation risk (Beauchamp 2004). Mixed-species groups of mammals often cooperate through beneficial joint hunting or shared vigilance (Stensland *et al.* 2003). Beyond ubiquitous facilitative interactions (Brooker *et al.* 2008), co-occurring plants can also benefit

from jointly attracting shared pollinators (Moeller 2004), driving convergence in flowering phenology (Sakai 2002) as well as in their chemical and visual floral traits acting as cues for pollinators (Thomson & Wilson 2008; Kantsa *et al.* 2017). Because intraguild systems may be simultaneously subject to the effects of both mutualistic interactions and competition, they appear particularly suited to investigate the outcome of positive and negative interactions in shaping community composition and species niche evolution.

Müllerian mimicry is an emblematic case of intraguild mutualism, where non-profitable prey species have evolved similar warning color patterns (i.e., aposematic patterns) under positive frequency-dependent selection imposed by predators, which learn more efficiently to recognize and avoid patterns that are more common (Müller 1879; Sherratt 2008). Resulting sets of co-mimetic species, which share the same warning pattern, are called mimicry rings (Joron & Mallet, 1998; Mallet & Gilbert, 1995; Papageorgis, 1975; Weismann, 1904). As such, identifying sets of species locally engaged in mutualistic interactions (i.e., co-mimics) is relatively straightforward. Those species may often compete for resources (e.g., micro-habitat space or trophic resources), despite interacting mutualistically by sharing the cost of educating their naïve predators. Thus, Müllerian mimicry offers an excellent case-study to explore the interplay between positive and negative interactions on natural communities. While Müllerian mimicry (hereafter, mimicry) has been observed independently in numerous taxa around the world, such as Hymenoptera (Williams 2007; Wilson *et al.* 2015), Coleoptera (Muñoz-Ramírez *et al.* 2016; Motyka *et al.* 2021), frogs (Symula *et al.* 2001), fishes (Alexandrou *et al.* 2011), snakes (Sanders *et al.* 2006), and even birds (Dumbacher & Fleischer 2001), it was historically described and formalized in the 19th century by Fritz Müller based on observations of Neotropical ithomiine and danaine butterflies (Müller 1879).

The butterflies of the Neotropical tribe Ithomiini Godman & Salvin, 1879 (Nymphalidae: Danainae), commonly called clearwing butterflies because of the transparent wing areas seen in most species (Papageorgis 1975; McClure *et al.* 2019; **Fig. 1**), represent the most diverse radiation of mimetic butterflies, with 396 species documented to date. All species are engaged in Müllerian mimicry (Brown Jr. & Benson 1974; Beccaloni 1997a; Chazot *et al.* 2019b), but at the same time may compete for various kinds of resources. Ithomiine larvae are almost all confined to the plant family Solanaceae, in some cases sharing the same host plant species, which are often understory herbs or vines with limited foliage (Drummond & Brown Jr 1987; Willmott & Mallet 2004; Beccaloni *et al.* 2008). Furthermore, adult males of most species may compete for access to composite flowers (Asteraceae) and wilted borages

(Boraginaceae) which provide them with the pyrrolizidine alkaloids needed for chemical protection against predators (Brown Jr 1984; Trigo & Brown Jr 1990), as well as sex pheromone precursors (Schulz *et al.* 2004).

Previous works on Ithomiini provided the first evidence that mutualistic interactions can partially outweigh competition and drive ecological convergence along multiple ecological axes that enhance local co-occurrence, such as microhabitat (DeVries *et al.* 1999; Elias *et al.* 2008; Hill 2010; Gompert *et al.* 2011; Willmott *et al.* 2017), flight height (Beccaloni 1997b; Elias *et al.* 2008), and hostplant preferences (Willmott & Mallet 2004), and at broader scales across altitudinal gradients (Chazot *et al.* 2014). However, the extent to which ecological niche convergence driven by positive interactions applies at larger spatial scales remains largely unknown. Notably, the effects of mimicry on the evolution of species climatic niches, which contribute to determining global geographic distribution patterns, is of particular interest in the context of current and future climate changes.

This study aims to examine the impact of intraguild mutualistic interactions on community composition and climatic niche evolution of interacting species at a macroecological scale, using the butterfly tribe Ithomiini as a study system. Specifically, we investigated three questions:

(1) Does mimicry structure Ithomiini community composition by promoting the spatial congruence of phenotypically similar species at the scale of their geographic range?

(2) Is the climatic niche of species more similar within than between mimicry rings, enhancing the spatial congruence of phenotypically similar species?

(3) If so, does such similarity of climatic niche among phenotypically similar species arise from shared ancestry or from evolutionary convergence across distinct lineages?

Figure 1: Mimicry ring classification for Ithomiini butterflies. Wing patterns are classified into 44 groups defined as mimicry rings. Dorsal view is shown on the left side against a dark background to highlight transparency when present. Ventral view is shown on the right side. The number of species in each mimicry ring is provided in parenthesis aside the name of each ring. 'Co' symbolizes the presence (in green) or absence (strikethrough in grey) of a significant pattern of species spatial congruence within each mimicry ring. The green solid line frames all mimicry rings with significant species spatial congruence. 'Cv' symbolizes the presence (in

blue) or absence (strikethrough in grey) of a lower variance in species climatic niche within each mimicry ring than expected from the phylogeny. When significant, this suggests an adaptive convergence of species climatic niche within the mimicry ring. The blue solid line frames all mimicry rings with significant signal for climatic niche convergence. The grey dashed lines frame all mimicry rings without significant signal for either spatial congruence or niche convergence, or both (double frame). Mimicry rings for which the tests could not be performed because they encompass only one ithomiine species each are displayed on the last line, without associated 'Co' and 'Cv' symbols associated. Photo credits: K. Willmott. Adapted from Doré *et al.* (2021).

2 Materials and Methods

2.1 Data sources

2.1.1 Study system: the tribe Ithomiini

Ithomiini (Nymphalidae: Danainae) represents the most diverse radiation of mimetic butterflies, with 1542 subspecies distributed among 396 species, 42 genera, and 10 subtribes (Chazot *et al.* 2019; see phylogeny in ***SI Appendix 1*, Fig. S1**). All species are engaged in Müllerian mimetic interactions. Ithomiini often numerically dominate butterfly communities in Neotropical forests from Mexico to northern Argentina (Chazot *et al.* 2019b) and act as mimetic models for other Lepidoptera species (Brown Jr. & Benson 1974; Brown Jr 1988; Beccaloni 1997b; Joron & Mallet 1998). The classification of wing patterns defined on the basis of pattern similarity follows the most recent update (Doré *et al.* 2022), and comprises 44 mimicry rings (**Fig. 1**; https://doi.org/10.5281/zenodo.5497876). This phenotypic-based classification outlines "putative" mimicry rings (e.g., Symula *et al.* 2001; Sanders *et al.* 2006) in the sense that it delineates groups of biological entities with patterns assumed to be perceived as similar by predators (e.g., Symula *et al.* 2001; Wilson *et al.* 2015; Hoyal Cuthill *et al.* 2019).

Most Ithomiini species contain several subspecies, which often belong to distinct mimicry rings (***SI Appendix 13*, Fig. S12**). In order to study the interplay between Müllerian mimicry and the distribution and climatic niche of ithomiine butterflies, we defined Operational Mimicry Units (OMUs; Doré *et al.* 2021) as the set of conspecific individuals that share the same mimicry pattern (***SI Appendix 2*, Fig. S2**). As such, a mimicry ring typically comprises multiple OMUs representing different species. The 783 currently known OMUs in the Ithomiini tribe were the ecological units used for our analyses (Doré *et al.* 2022). For the sake of simplicity, we use "co-mimetic species" and "phenotypically similar species" in the text to refer to the OMUs sharing the same mimicry pattern.

2.1.2 Estimating community composition

In order to investigate the effect of mimicry on the composition of Ithomiini communities, we retrieved maps of the estimated distribution of all 783 OMUs obtained from species distribution models based on a dataset of ca. 29,000 georeferenced occurrences (Doré *et al.* 2021; https://doi.org/10.5281/zenodo.4696055; https://doi.org/10.5281/zenodo.4673446). These models predicted the distribution of ithomiine butterflies based on the relationship between occurrences and associated climatic variables, forest cover and elevation. They provided scores interpreted as the likelihood of presence of each OMU within each community represented as a quarter-degree grid-cell of ca. 30 km x 30 km. This approach allowed us to build a complete list of likelihood of presences of species and associated putative mimicry rings for each of the 21,415 communities (i.e., quarter-degree grid-cells) considered within the entire Ithomiini range. We used those scores as predictions of OMUs assemblages in each community. A map of Ithomiini species richness based on those distribution is provided in ***SI Appendix 3*, Fig. S3**.

2.1.3 Describing the climatic niche of species

For each OMU, we extracted the set of climatic conditions found at its associated georeferenced records in the occurrence database. We defined the climatic niche of each OMU as the centroid of these occurrence points within the climatic space expressed in four dimensions: mean annual temperature, mean annual specific humidity, temperature seasonality, and specific humidity seasonality (Vega *et al.* 2017; MERRAclim v.2.0, https://doi.org/10.5061/dryad.s2v81, accessed on 04/02/2020). As such, each OMU was associated with a set of climatic data describing its mean climate, or its bioclimatic optimum (e.g., Hof *et al.* 2010; Barnagaud *et al.* 2012), strictly reflecting the centroid of its realized niche (Hutchinson 1957; Soberón & Nakamura 2009). Despite being a subset of the fundamental niche, measurements of the position of the realized niche in the environmental space based on occurrences can provide relevant insights on the evolution of the species fundamental niche (Gouveia *et al.* 2014), and are commonly used to investigate climatic niche evolution (Broennimann *et al.* 2012; e.g., Kozak & Wiens 2010a; Castro-Insua *et al.* 2018; Rolland *et al.* 2018).

2.2 Data analyses

R scripts to carry out all analyses are available on GitHub at https://github.com/MaelDore/ithomiini_convergence.

2.2.1 Community structure analyses

To examine whether phenotypically similar species co-occur more often than expected at random in communities, we employed a modified version of a community differentiation index: the I_{ST} (Hardy & Senterre 2007). I_{ST} is analogous to the F_{ST} index used in population genetics. It quantifies differences in species composition across communities by partitioning additively the diversity between its alpha (within communities) and beta (between communities) components. In our framework, we apply I_{ST} to mimicry rings instead of species, using the number of species in each ring as the measure of abundance. As such, I_{ST} represents the mimicry turnover among our predicted communities, and a high I_{ST} reflects the spatial clustering of co-mimetic species within communities. This index conveniently allows us to quantify mimicry turnover at both global level and between pairs of communities. As such, we tested whether observed I_{ST} was significantly higher than expectations if mimicry patterns were distributed randomly among OMUs (as in Chazot *et al.* 2014).

We also developed a complementary approach to investigate if the dissimilarity between spatial distributions of species was lower for phenotypically similar species. We computed pairwise Bray-Curtis distances (Bray & Curtis 1957) across the predicted distributions, obtained from species distribution models, of all pairs of OMUs with the R package *vegan* 2.5-4 (Oksanen *et al.* 2019; see ***SI Appendix 6***). A high Bray-Curtis value corresponds to a large dissimilarity in species spatial distributions, while a low value relates to an important spatial overlap (**Fig. 2**). We evaluated the significance of the mean value obtained for pairs of phenotypically similar species (i.e., putative co-mimics) by random permutation of mimicry patterns among the OMUs. We carried out this analysis for 39 putative mimicry rings for which the analysis could be performed since they hosted more than one species/OMU (**Fig. 1**: mimicry rings showing significant spatial congruence are associated with a 'Co' symbol in green). In this framework, a significant spatial congruence between similar-looking OMUs provides evidence that this hypothesized "putative" mimicry ring based on wing pattern similarity likely correspond to an "effective" mimicry ring reflecting current positive ecological interactions in local communities supported by mimicry (Sanders *et al.* 2006; Alexandrou *et al.* 2011; Wilson *et al.* 2022).

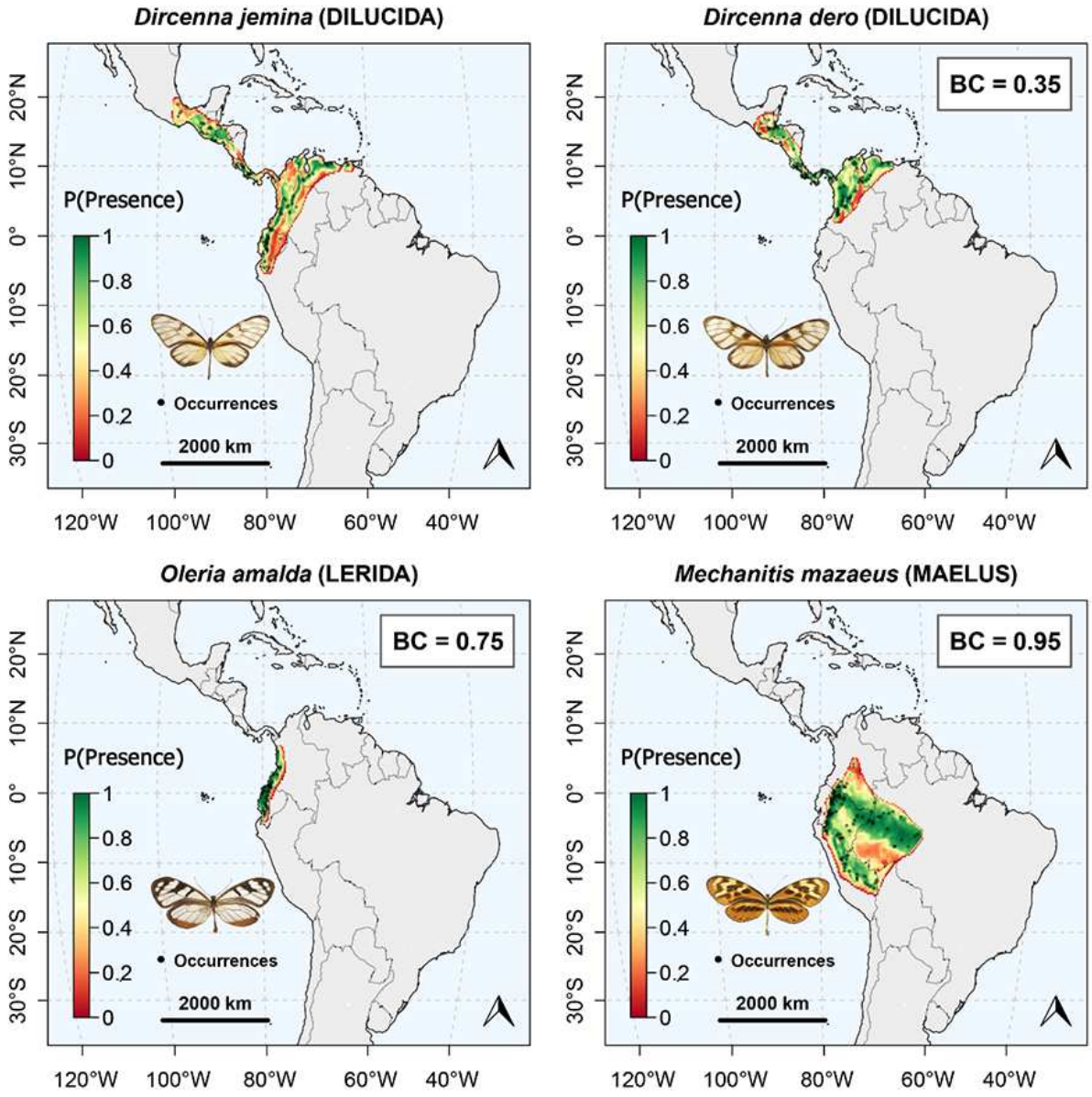

Figure 2: Illustration of spatial dissimilarity in distribution range between pairs of species. Spatial dissimilarity is quantified with Bray-Curtis distances (BC) based on the comparison of species likelihood of presence across each grid-cell. *Dircenna jemina* within mimicry ring DILUCIDA is used as the reference (upper left). The three other species show an increasing BC distance (decreasing spatial congruence) with the reference. A co-mimetic species, *Dircenna dero* within mimicry ring DILUCIDA (upper right), shows the highest spatial congruence (BC = 0.35). Non co-mimetic *Oleria amalda* within mimicry ring LERIDA (bottom left) and *Mechanitis mazaeus* within mimicry ring MAELUS (bottom right) display lower spatial congruence with the reference (BC = 0.75 and 0.95, respectively). Maps adapted from Doré *et al.* (2021). Photo credits: Nicolas Chazot, 2015.

2.2.2 Climatic niche similarity

Spatial congruence between phenotypically similar species may only be partially due to non-climatic dispersal limits (Soberon & Peterson 2005), but a similar climatic niche would indicate a potential for future increase in the spatial congruence of such species associated with enhanced mutualistic interactions in the context of Müllerian mimicry. Thus, to examine whether mimetic interactions have led to the similarity of realized climatic niches between phenotypically similar species, thereby reinforcing their pattern of spatial congruence, we explored the relationship between mimetic turnover (i.e., pairwise I_{ST}) and climatic distances (i.e., Euclidian distances in a standardized multivariate climatic space formed by our four bioclimatic variables) between pairs of communities. First, we represented mimicry turnover and climatic diversity across all communities by projecting community pairwise distances (i.e., pairwise I_{ST} and Euclidean climatic distances) into three-dimensional RGB color spaces employing Nonmetric Multidimensional Scaling (NMDS; **Fig. 3**). Second, we tested whether such mimicry turnover between communities correlated with their climatic distances, hinting at an association between mimicry rings and specific climatic niches. We randomly subsampled 1000 communities in order to limit spatial autocorrelation and limit computation time. We applied partial Mantel tests and Multiple Regressions on distance Matrices (MRM; Legendre *et al.* 1994) between pairwise I_{ST} and climatic distances taking into account a possible confounding effect of geographic distances (as in Chazot *et al.* 2014; **Fig. 4.A-C**). A significant positive correlation/effect means that communities undergoing similar climatic conditions display similar mimicry patterns, and *vice versa*. We performed these analyses a hundred times to ensure random subsampling of communities had no effect on the results (**see *SI Appendix 7*, Tables S2 & S3**).

To further investigate the similarity of realized climatic niches of species within each putative mimicry ring, we performed a perMANOVA on species climatic niche optimum observed from occurrences (i.e., mean bioclimatic conditions at centroids), with the climatic space reduced to two dimensions after applying a phylogenetic PCA (pPCA; Revell 2009) on the four initial climatic variables (**Fig. 4.D**). This analysis aimed to detect whether co-mimetic OMUs shared their climatic niche optimum more than expected at random. Small mimicry rings with less than 10 OMUs were discarded because of their small sample size, which limits statistical power. As a result, 23 mimicry rings out of 44 (52.3%) were retained for the analysis, encompassing 619 OMUs among the 719 represented on the phylogeny (86.1%; see ***SI Appendix 4*, Fig. S4**). We also conducted post hoc pairwise comparisons between pairs of

mimicry rings. Finally, complementarily to these analyses of niche dissimilarity based on distances between niche centroids, we explored differences in climatic niche overlap between co-mimetic OMUs (***SI Appendix 9*, Fig. S9, Table S4**).

2.2.3 Climatic niche evolution

Spatial congruence and niche similarity within mimicry rings can be caused by adaptive convergence (selection favors increased overlap in range, and therefore increased similarity in climatic niche, more than predicted by phylogenetic relatedness), but also phylogenetic inertia (species inherit color pattern and climatic niche associated with spatial range from their common ancestors). Thus, we further took into account the phylogeny in subsequent phylogenetic comparative analyses. First, we tested for the presence of phylogenetic signal in the evolution of both climatic niche and mimicry patterns (Losos 2008; see ***SI Appendix 10*, Fig. S10, Table S5**) on a phylogeny of the Ithomiini tribe (Chazot *et al.* 2019; ***SI Appendix 1*, Fig. S1**) that includes 339 species (85.6%) out of the 396 found in the clade. Then, we simulated the stochastic evolution of species mean bioclimatic conditions observed from occurrences (i.e., climatic niches optimum) under the best fitting neutral macroevolutionary model: a Brownian Motion with an additional Pagel's λ parameter (λ = 0.408) to account for the intensity of the phylogenetic signal (**see *SI Appendix 11*, Table S6, Fig. S11**).

Next, we performed a phylogenetic MANOVA to test whether any pattern observed with the perMANOVA was due to shared ancestry or whether it was caused by evolutionary convergence of the niche associated with mimicry. This test compares Wilk's λ statistics of MANOVAs, which quantify the proportion of variance in the climatic niche optimum that is not explained by mimicry rings, obtained from the observed climatic niche optimum extracted from occurrences, with the null distribution of this statistic obtained from simulated climatic niche optimum under the chosen neutral model of macroevolution. The p-value for this test corresponded to the probability of obtaining by chance a lower Wilk's λ statistic than the simulated values in the null distribution. As for the perMANOVA, small mimicry rings with less than 10 OMUs were discarded from the analysis because of their small sample size, which limits statistical power (see ***SI Appendix 4*, Fig. S4**).

Complementarily, we compared the observed pairwise mean climatic distance (i.e., Euclidean distances between niche centroids) between the niche optimum of co-mimetic OMUs standardized by the overall mean pairwise climatic distance across the entire tribe with the null distribution of that same statistic in our simulations. A lower value than the simulated values in

the null distribution would indicate that co-mimetic OMUs display more similar climatic niche optimum than expected under the sole effect of the phylogenetic signal. We conducted this test for all co-mimics, and per putative mimicry ring (**see *SI Appendix 12*, Table S7**).

3 Results

3.1 Müllerian mimicry shapes community composition

We tested whether species sharing similar wing patterns (i.e., putative co-mimetic species) present significantly congruent distribution patterns at large spatial scales in two ways. First, we found a significantly high global mimicry turnover, as assessed by I_{ST} based on number of species in mimicry rings (Hardy & Senterre 2007), compared to values obtained from random permutations of mimicry patterns among OMUs (***SI Appendix 5*, Fig. S5.A**; I_{ST} obs = 0.164, mean I_{ST} null = 0.090, CI 95% = 0.103, $p \leq 0.001$). This result is consistent with a global spatial clustering of phenotypically similar species within communities.

Second, we investigated whether phenotypically similar species tend to have similar spatial distributions, by examining whether the dissimilarity between the spatial distributions of OMUs was lower for co-mimetic OMUs as in **Fig. 2**. Overall, we found that phenotypically similar species exhibited significantly lower mean Bray-Curtis distances (i.e., spatial dissimilarity) than expected at random (***SI Appendix 5*, Fig. S5.B**; Mean BC obs = 0.896 across all pairs of co-mimics, mean BC null = 0.950, CI 5% = 0.946, $p \leq 0.001$). Likewise, when the analysis was repeated for each putative mimicry ring comprising at least two species, 33 mimicry rings out of the 39 for which the analysis could be performed showed a significant pattern of spatial clustering (**Fig. 1**: mimicry rings associated with 'Co' symbol in green). The remaining six non-significant mimicry rings all had low species richness (i.e., $N < 10$, except for DOTO) which constrains the statistical power of the permutation tests. As such, the pattern of large-scale spatial congruence of phenotypically similar species appeared largely ubiquitous in all regions of the Neotropics, and most putative mimicry rings qualify as effective mimicry rings depicting current mutualistic interactions (***SI Appendix 6*, Table S1**).

3.2 Mimicry patterns correlate with species climatic niche

3.2.1 Mimicry turnover correlates with climatic distances across communities

To investigate whether species belonging to the same mimicry ring tend to have similar realized climatic niche, thereby enhancing their potential for spatial congruence, we examined whether communities experiencing similar climatic conditions tend to harbor a similar

predicted composition in mimicry patterns. The maps of mimicry turnover (**Fig. 3.A**) and climate diversity (**Fig. 3.B**) tend to show qualitatively similar patterns, with broad regional distinctions between the Atlantic Forest, the Pampas, the Cerrado and Caatinga, the Amazon Basin, the Andes, and Central America. Yet, the Andes appear as an important geographic barrier to dispersal, drawing sharp contrasts in term of mimicry composition between the two sides of Cordilleras (**Fig. 3.A**), while climate appears relatively similar between sides (**Fig. 3.B**). Furthermore, we tested whether mimicry turnover between predicted communities correlated with the climatic distances between these communities (see ***SI Appendix 7*, Tables S2 & S3**). In all tests, pairwise I_{ST} (i.e., mimicry turnover between communities) was correlated with the pairwise climatic distance between communities (**Fig. 4.A**: MRM: $\beta_{obs} = 0.367$, Q95% = 0.023, p-value ≤ 0.001). Although pairwise I_{ST} was also correlated with geographic distance between communities (**Fig. 4.B:** MRM: $\beta_{obs} = 0.598$, Q95% = 0.024, p-value ≤ 0.001), the correlation between pairwise I_{ST} and pairwise climatic distance between communities persisted even when accounting for spatial distance (**Fig. 4.C & *SI Appendix 5*, Fig. S6.A:** MRM: $\beta_{obs} = 0.216$, Q95% = 0.027, p-value ≤ 0.001). All Mantel tests yielded results consistent with MRM (see ***SI Appendix 7*, Tables S2 & S3**). Therefore, the significant mimicry turnover across communities was partially explained by differences in local climatic conditions linked to a dissimilarity between the climatic niches of species across mimicry rings.

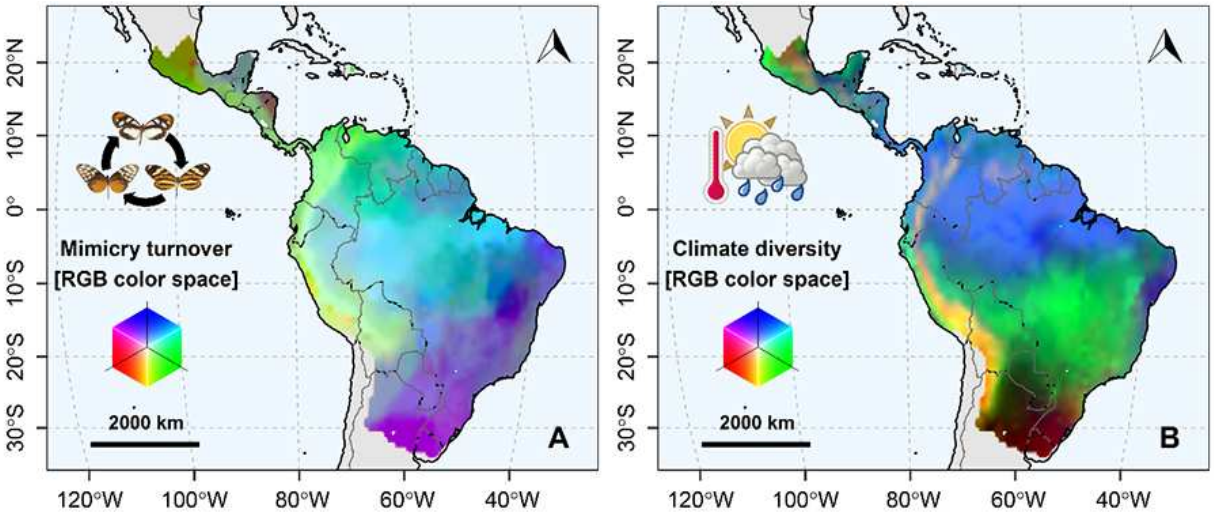

Figure 3: Mimicry turnover (A) and climate diversity (B) across communities. Colors represent coordinates in the RGB color space. They relate to dissimilarity in the predicted mimicry composition (A) or climatic conditions (B) across all communities obtained from NMDS applied on pairwise mimicry turnover (A) and Euclidean climatic distances (B). Colors are not comparable between maps, but they reflect patterns of dissimilarity.

3.2.2 Species climatic niches are more similar within than between mimicry rings

We tested whether species' realized niches are more similar within than between mimicry rings, regardless of the origin of the similarity/difference (i.e., convergent evolution or shared ancestry). We found a significant association between species climatic niches and their mimicry patterns (**Fig. 4.D**; perMANOVA: $R^2 = 0.416$, Pseudo-F = 19.35, $p \leq 0.001$; ***SI Appendix 5*, Fig. S6.B**). Moreover, perMANOVA post hoc pairwise comparisons of mimicry rings revealed that the vast majority of mimicry ring pairs exhibited significantly different climatic niches (***SI Appendix 8*, Fig. S8:** 186 out of 253 pairs (73.5%) with a p-value ≤ 0.001; 226 (89.3%) with a p-value lower than 0.05). Complementary analyses based on climatic niche overlap rather than niche centroids led to similar results (***SI Appendix 9*, Fig. S9, Table S4**).

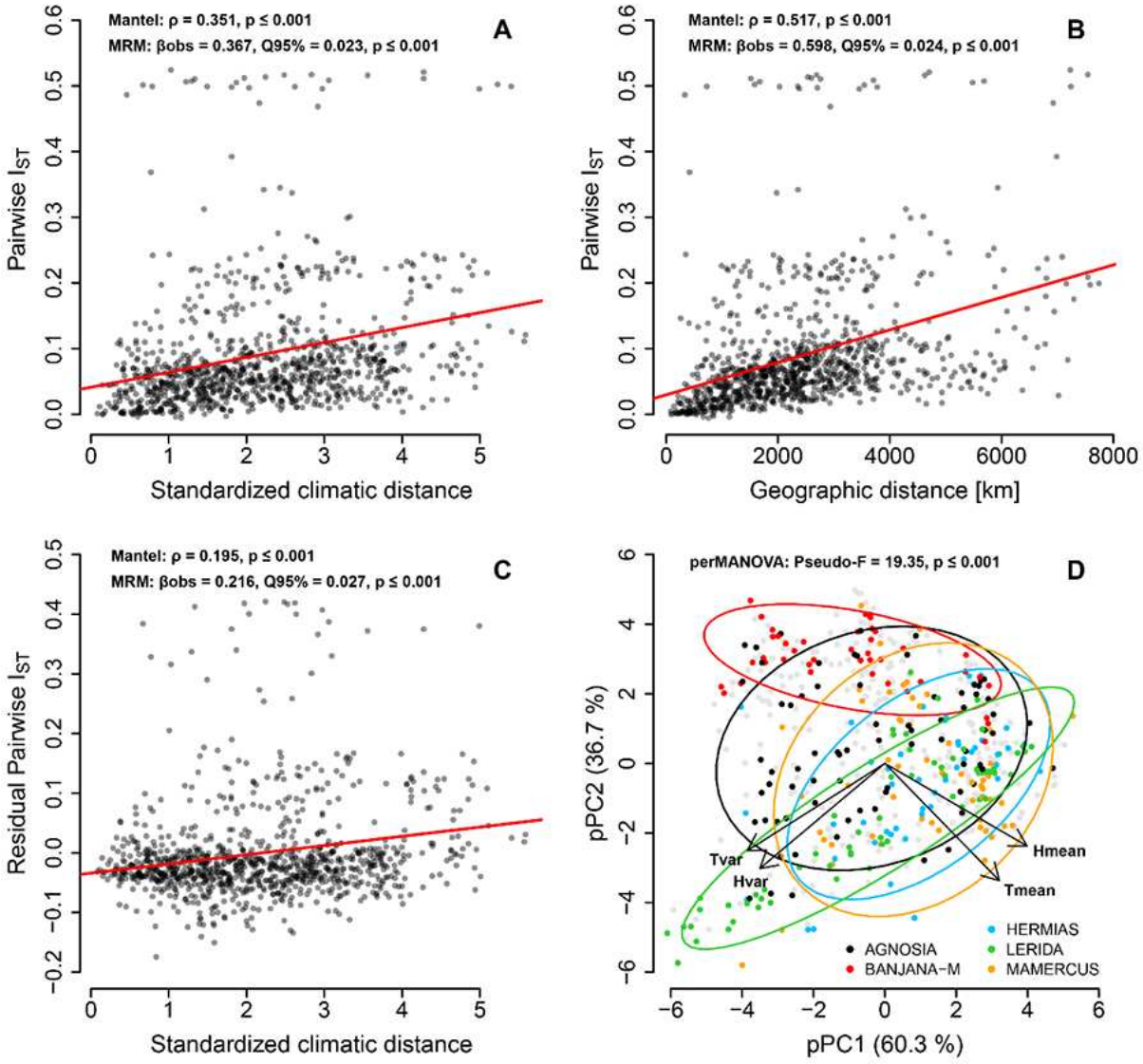

Figure 4: Association between climate and mimicry patterns: mimicry turnover explained by climatic and geographic distances across pairs of communities (A, B, C) relates to the segregation of species climatic niche between mimicry rings (D). Scatter plots display relationship between mimicry turnover and climatic and geographical distances across pairs of communities for a random sample of 1000 distances among the 499 500 distances computed for clarity. ρ = Spearman's rho coefficient for non-parametric correlation associated with p-value from Mantel tests with 999 permutations. βobs = β-coefficient from Multiple Regression on distance Matrices (MRM) with 999 permutations; Q95% = quantile used as threshold for right-tailed significance tests. (A) Mimicry turnover (pairwise I_{ST}) correlates with climatic distances. (B) Mimicry turnover (pairwise I_{ST}) correlates with geographic distances. (C) Mimicry turnover (pairwise I_{ST}) correlates with climatic distances after accounting for the effect of geographic distance. (D) Ordination of species bioclimatic optimum for the five richest mimicry rings in the reduced climatic space resulting from a pPCA (Revell 2009). AGNOSIA = 74 species (in black). LERIDA = 63 species (in green). MAMERCUS = 56 species (in orange). HERMIAS = 47 species (in blue). BANJANA-M = 43 species (in red). Grey dots represent species belonging to other mimicry rings. Tvar = Temperature seasonality. Hvar = Specific humidity seasonality. Hmean = Mean specific humidity. Tmean = Mean temperature. Ellipses represent normal-probability contours (quantile = 0.8) for each mimicry ring.

3.3 Müllerian mimicry drives climatic niche convergence

In subsequent analyses, we built upon the phylogeny of the group (Chazot *et al.* 2019b) to disentangle the effects of shared ancestry and evolutionary convergence in niche similarity among co-mimetic species. We found a significant phylogenetic signal in the evolution of mimicry patterns: phenotypically similar species were significantly closer than expected by chance in the phylogeny (MPD obs = 34.43 My, mean MPD null = 37.16 My, CI 5% = 36.73 My, $p \leq 0.001$; see ***SI Appendix 10*, Fig. S10.A, Table S5** and ***SI Appendix 13*, Fig. S12**). In parallel, we observed a weak but significant phylogenetic signal in the evolution of species climatic niche (K_{mult} obs = 0.120, mean K_{mult} null = 0.083, CI 95% = 0.110, p = 0.013; see ***SI Appendix 10*, Fig. S10.B).** Therefore, the association we revealed between mimicry rings and climatic niche could be at least partly explained by common ancestry (Losos 2008). However, we found that the association between climatic niche and mimicry patterns was significantly stronger than expected given species evolutionary relationships (***SI Appendix 5,* Fig. S7.A**; phylogenetic MANOVA, Wilks' λ obs = 0.271, mean Wilks' λ null = 0.899, CI 5% = 0.844, $p \leq 0.001$).

To further assess if climatic niches of co-mimetic species are more similar than expected from a process of neutral niche evolution, we computed the standardized mean climatic distance (MCD) among co-mimetic species. The observed value was lower than expected under neutral evolution where climatic niche was allowed to evolve on the phylogeny in any direction of the

climatic space (***SI Appendix 5*, Fig. S7.B**; MCD obs = 0.782, mean MCD null = 0.984, CI 5% = 0.959, $p \leq 0.001$), again suggesting an evolutionary association between mimicry and climatic niche that goes beyond the pattern of niche similarity among co-mimetic species. Additionally, 32 out of 39 putative mimicry rings for which the analysis could be performed showed a significant signal for convergence of the climatic niche (**Fig. 1**: mimicry rings associated with 'Cv' symbol in blue; see ***SI Appendix 12*, Table S7** for a detailed statistical summary). No mimicry ring showed a signal of divergence (i.e., MCD higher than expected under neutral climatic niche evolution). Altogether, most mimicry rings (29 out of 44 = 65.9%) exhibited both species spatial congruence and climatic niche convergence all across the Neotropics (**Fig. 1**).

4 Discussion

In this study, we investigated the impact of positive interactions on the composition of species assemblages and the evolution of species climatic niche in a diverse clade of Neotropical butterflies. We showed that intraguild mutualistic interactions, specifically Müllerian mimicry, drive the large-scale spatial association of interacting species and channel the convergence of species climatic niche across lineages. As such, we showed that the effects of mimicry can outweigh both common ancestry, which promotes similarity among related species, and potential competition within ecological guilds, which would promote divergence, thereby affecting the global distribution of a highly diverse group at large spatial scales.

4.1 From large-scale spatial congruence to fine-scale ecological dimensions

Traditionally, community ecology and biogeography have focused on the interplay between antagonistic interactions such as competition and predation, and common ancestry, to explain community structure and macroecological patterns of biodiversity (Pianka 1981; Brown & Maurer 1989; Webb *et al.* 2002; Cardillo 2011). Under this paradigm, the importance of positive interactions for shaping large-scale species distribution patterns has remained largely overlooked, despite a growing literature calling attention to their significance for structuring species assemblages and maintaining stability and diversity at the community-level (Bastolla *et al.* 2009; Pascual-García & Bastolla 2017; Hale *et al.* 2020). As a case-study of the effects of intraguild mutualism, we showed here that phenotypically similar ithomiine species co-occur at large spatial-scales more often than expected by chance. This result comforts the idea that similarity of aposematic patterns in ithomiine butterflies largely arose through adaptive

convergence induced by Müllerian mimicry. As such, positive interactions, in this case Müllerian mimicry, could outweigh potential effects of competition, notably the geographical overdispersion of phylogenetically close and ecologically similar species (Pianka 1981; Webb *et al.* 2002; Kunte 2008). Co-occurrence among phenotypically similar species of Ithomiini has already been documented at smaller scales, across microhabitats (Beccaloni 1997b; DeVries *et al.* 1999; Elias *et al.* 2008; Hill 2010; Willmott *et al.* 2017) and altitudinal gradients (Chazot *et al.* 2014). Here, we showed that this pattern extends to the entire Ithomiini clade, over its global distribution across the Neotropics, supporting the idea that positive interactions can strongly affect the global spatial distribution patterns of entire diverse groups. Our study provides new empirical evidence at a macroecological scale for the validity of the oldest mathematical model of evolution, namely Müller's prediction of local convergence in warning patterns among toxic aposematic species (Müller 1879).

Our findings further revealed that mutualistic interactions can lead to the convergence of climatic niches among co-mimetic species, thereby enhancing co-occurrence, and potentially supporting high community diversity (Gross 2008). In turn, enhanced co-occurrence among phenotypically similar species also potentially increases competition for local resources. Theoretical models showed that while co-mimetic species are expected to use the same trophic resources when these resources are highly segregated across microhabitats, they are instead expected to partition their diet when multiple types of resources are available in their shared microhabitat, thereby lessening the negative effects of competition for resources (Aubier & Elias 2020). These predictions are partly confirmed in the field, where co-mimetic species sometimes use the same larval host plants, but in other cases do not (Willmott & Mallet 2004). At these finer scales, mutualistic interactions can therefore still drive convergence, especially in ecological dimensions that favor co-occurrence in the eyes of predators. For example, communities of habitat-specialist predators that select locally for different optimal warning signals can induce the segregation of mimicry rings across microhabitats (Birskis-Barros et al., 2021; Willmott et al., 2017). This fine-scale structuring helps explain the apparent paradox of high local mimicry richness (Joron & Mallet 1998), with eight or more ithomiine mimicry rings co-occurring in west Amazonian communities (Doré *et al.* 2022), in the context of Müllerian mimicry predictions of local convergence in color patterns (Gompert *et al.* 2011).

Beyond the emblematic case of ithomiine butterflies and Müllerian mimicry, the opposite effects of intraguild positive and negative interactions are found in other biological systems, at multiple spatial scales. For instance, co-mimetic catfish species tend to co-occur at

the scale of large river basins, while at local scales diet partitioning, coupled with morphological dissimilarity, appear to be the main factors structuring species assemblages (Alexandrou *et al.* 2011). Likewise, plants that attract similar pollinators benefit from co-occurrence and facilitative interactions (Moeller 2004), and may demonstrate convergence for attractive scents and floral morphology (Thomson & Wilson 2008; Kantsa *et al.* 2017), while they can also present different mechanisms for pollen deposition (Huang & Shi 2013) and contrasted phenologies (Armbruster & Herzig 1984) that limit reproductive interference.

Altogether, the interplay between positive and negative intraguild interactions on community structure and trait evolution may have different outcomes at different spatial scales. At large-scales, we found that convergence in climatic niche, strengthening the spatial congruence of the distributions of mutualistic species, seems favored. At fine-scales, the similarity of species ecological niches may depend on whether the benefits of mutualistic interactions outweigh the effects of competition that otherwise promote niche partitioning.

4.2 A scenario for niche convergence in mutualistic communities

Our results hint for an adaptive association between climatic niche and mimicry patterns in Ithomiini species, thereby reinforcing the local co-occurrence of mutualistic species. Indeed, species harboring the same mimicry pattern benefit from evolving towards similar climatic niches, since this often results in increased spatial overlap and exposure to the same suite of predators within communities (Sherratt 2006). However, a pattern of niche similarity within mimicry rings could actually arise from the opposite mechanism: species with a similar climatic niche and living at least partly in sympatry are expected to undergo convergence in their aposematic patterns (Müller 1879). Both adaptive mechanisms likely act together, as suggested by modeling approaches (Gompert *et al.* 2011).

A plausible scenario involves an initial partial climatic and spatial overlap of species niches, perhaps guided by the spatial congruence of their respective host plants (**Fig. 5**; Step 1: Initial partial overlap). Thus, in the context of Müllerian mimicry, one may expect those species to converge towards one mimicry pattern, at least in the area of distribution overlap (**Fig. 5**; Step 2: Pattern convergence). Next, the expansion of the range of each species towards areas occupied by co-mimetic species (potentially harboring different climatic conditions) will be facilitated, since these new areas offer an increased protection against predators, compared to areas where co-mimics are absent (Kapan 2001; **Fig. 5**; Step 3: Niche expansion). Meanwhile, populations retaining the ancestral pattern, where the co-mimetic partner is absent, experience

weaker protection from predators and may sometimes go extinct (Mallet & Barton 1989; Langham 2004; **Fig. 5**; Step 4a: Niche thinning). Alternatively, these populations may persist to result in the generation of a polymorphic species with two independent sets of mimetic individuals (i.e., Operational Mimicry Units (OMUs) as in Doré *et al.* 2021; **Fig. 5**; Step 4b: Niche partitioning). This coexistence generates a spatial mosaic of aposematic patterns bordered by suture zones where hybrids are counter-selected by predation from naïve predators (Mallet & Barton 1989; Thompson 2005; Sherratt 2006). Conveniently, this scenario offers an explanation for the relatively high prevalence of polymorphism in mutualistic systems, with several OMUs per species. In the long run, these OMUs may diverge enough to be considered as separated species (**Fig. 5**; Step 5b: Speciation) and fuel the high diversity typically observed in mutualistic clades (Joron & Mallet 1998; Aubier *et al.* 2017; Motyka *et al.* 2021). Either way, the distributions of the mimetic populations of the species will gradually increase in overlap, leading to the convergence of climatic niches (**Fig. 5**; Step 5a & 5b: Final overlap). Therefore, both mechanisms of color pattern and niche convergence likely act jointly to generate the adaptive association of species climatic niche and mimicry patterns we detected for ithomiine butterflies.

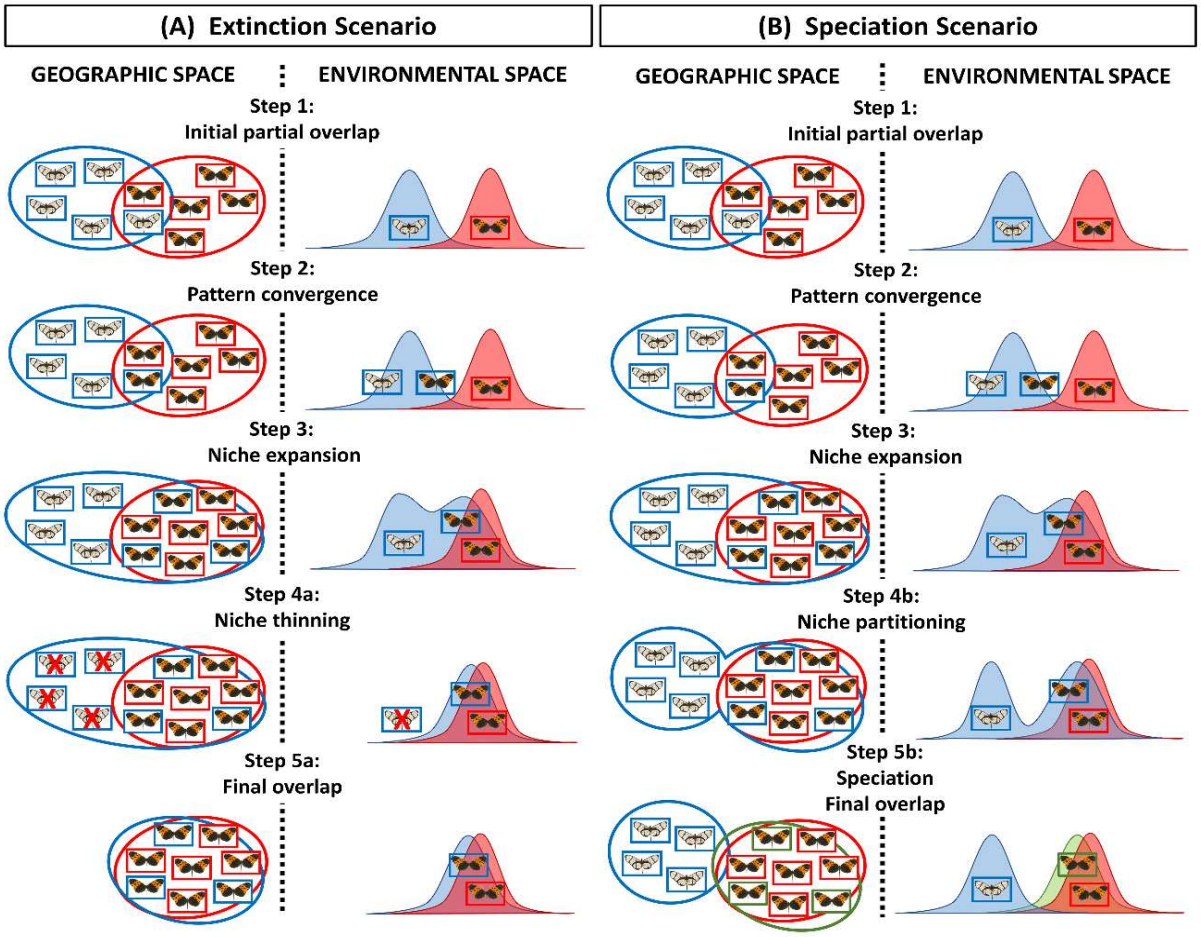

Figure 5: Scenarios for niche convergence between co-mimetic species. Five steps to reach spatial and environmental overlap between co-mimetic species leading to the predator-driven adaptive association of environmental niche and mimicry pattern. Scenario A involves the extinction of non-mimetic populations and the convergence of two monomorphic species. Scenario B involves the generation of a polymorphic species leading to speciation. Strictly, instead of convergence these scenarios describe the likely more frequent case of advergence (Mallet 1999) since the lineage in blue, then green, starts with CONFUSA pattern and adverges to MOTHONE pattern, while the species in red starts with MOTHONE pattern and maintains it over time.

4.3 Consequences for mutualistic systems in the context of global change

The power of mimicry to shape large-scale community composition and drive species climatic niche convergence illustrates the importance of intraguild mutualistic interactions in shaping both the ecology and evolution of interacting species. In the context of global changes, the fate of those mutualistic communities is even more uncertain due to the positive nature of their interactions. Indeed, climate change and habitat loss force species to migrate at unprecedented rates to follow their climatic niches (Pearson 2006; Boeye *et al.* 2013). Mutualistic partners may adapt differently, at different rates, or even impede their respective migration rates (Brooker *et al.* 2007; Svenning *et al.* 2014). Such effects may quickly lead to community disassembly and the loss of the positive mimetic interactions, especially in tropical mountainous regions (Uehara-Prado & Freitas 2009; Sheldon *et al.* 2011), where distribution ranges are often narrow and most Ithomiini diversity is found (***SI Appendix 3*, Fig. S3**).

Mutualistic communities are particularly sensitive to community disassembly because of the long-standing history of co-evolution and interdependency between co-occurring species (Toby Kiers *et al.* 2010). They are more prone to extinction cascades, since the local disappearance of a species can weaken the network of mutualistic interactions supporting their robustness and resilience to perturbations (Dunn *et al.* 2009; Vidal *et al.* 2019). Even if climatic niche similarity between interacting partners, such as co-mimetic species, may limit community disassembly to a certain extent by allowing congruent dispersal trajectories in the face of climate change, climatic niche overlap is hardly ever complete (***SI Appendix 9*, Fig. S9, Table S4**). Moreover, despite relatively similar climatic niche optima, tolerance to climate change and extremes, as well as species dispersal abilities, may still differ among species, limiting opportunities for co-dispersal trajectories. Finally, the effects of climate change on biotic factors that affect local abundance, such as hostplants (Willmott & Mallet 2004) and parasitoids (Gentry 1998) in the case of Ithomiini butterflies, may also differ among interacting species.

Altogether, mutualistic communities form tightly coevolved assemblages tied by positive interactions, making them particularly vulnerable to global environmental changes (Tylianakis *et al.* 2008). Our results stress the need to include species interactions, illustrated here by Müllerian mimicry, in the framework of macroecological and global change studies, as well as in species distribution modeling and conservation assessments (Brooker *et al.* 2007; Toby Kiers *et al.* 2010; Tylianakis *et al.* 2010; Staniczenko *et al.* 2017; Windsor *et al.* 2023).

Data accessibility statement

All R scripts used to conduct the analyses and generate the figures are available on GitHub (https://github.com/MaelDore/ithomiini_convergence) and Zenodo (https://doi.org/10.5281/zenodo.6277769).

Occurrences data, maps of the distribution of Operational Mimicry Units (OMUs) and species, and mimicry classification used in this study are available from Zenodo :

- Occurrences data: https://doi.org/10.5281/zenodo.4696055;
- Distribution maps: https://doi.org/10.5281/zenodo.4673446;
- Mimicry classification: https://doi.org/10.5281/zenodo.5497876.

All results reported in this manuscript can be reproduced with the scripts and data provided.

Supplementary Information

Supplementary Information for CHAPTER 4: “Mutualistic interactions shape global spatial congruence and climatic niche evolution in Neotropical mimetic butterflies” can be found in **ANNEXE 5.**

Acknowledgments

We gratefully thank all the researchers, field assistants, technicians and students that were involved in the collection of the occurrence data from which we predicted our community composition. The authors certify that they have no affiliations with or involvement in any organization or entity with any financial interest, or non-financial interest in the subject matter or materials discussed in this manuscript. MD is financed by the French Ministry of Research (MESRI). ME acknowledges funding by the ANR grant CLEARWING (ANR-16-CE02-0012), a Human Frontier Science Program grant (RGP0014/2016), a Leverhulme Trust grant and an ATIP grant. KRW thanks S. Nogales, the INABIO and Ecuadorian Ministerio del Ambiente for

arranging permits for research in Ecuador, most recently under the project 'Diversity and Biology of Lepidoptera in Ecuador' (No. 006-19 IC-FLO-FAU-DNB/MA), and the Leverhulme Trust, the Darwin Initiative, the FLMNH Museum Associates, the National Geographic Society (Research and Exploration Grant # 5751-96) and NSF (# 0103746, #0639977, #0639861, #0847582, #1256742). AVLF thanks FAPESP (2012/50260-6, 2013/50297-0 and 2021/03868-8), the Conselho Nacional de Desenvolvimento Científico e Tecnológico Pq-1A grant (CNPq 304291/2020-0), RedeLep-SISBIOTA-Brasil/CNPq (563332/2010-7), and NSF (DEB 1256742). Brazilian butterfly species are registered under SISGEN (ADF1F75).

DISCUSSION AND PERSPECTIVES

In the face of global change, understanding the mechanisms underlying species distributions and coexistence is both a priority and a challenge, especially for biodiversity hotspots such as the Neotropics. In this research work, I explored several dimensions of biodiversity patterns in Neotropical mimetic butterflies employing an integrative approach across biogeography, phylogenomics, and community ecology. Specifically, I focused on two tribes engaged in Müllerian mimicry, the Ithomiini (Nymphalidae: Danainae) and Heliconiini (Nymphalidae: Heliconiinae), in order to illustrate the importance of mutualistic interactions for shaping large-scale spatial and evolutionary patterns of biodiversity.

In **Chapter 1**, I employed species distribution models to map the taxonomic, phylogenetic and mimetic facets of Ithomiini biodiversity. I identified areas of evolutionary and ecological importance for conservation, and evaluate their overlap with current anthropogenic threats. I showed that tropical montane forests that host high species and mimetic diversity as well as rare species and mimicry rings appear particularly under threat. These results support the role of ithomiine butterflies as a suitable flagship indicator group for Neotropical butterfly diversity, and reinforce the position of the tropical Andes as a flagship region for butterfly biodiversity conservation.

In **Chapter 2**, I presented a new phylogeny for the Ithomiini tribe, building upon phylogenomic methods to resolve and support deep evolutionary relationships in the group. This phylogeny reinforces the monophyly of the core-group, a clade associated with a recent adaptive radiation linked to multiple colonizations of new areas following the demise of the Pebas aquatic system in Western Amazonia. It comforts the basal position of the Melinaea subtribe and suggests the Mechanitina subtribe as the sister-group of the core-group. Altogether, this new phylogeny provides a stable tool for macroevolutionary analyses in ithomiine butterflies.

In **Chapter 3**, I described a new method to quantify similarity in wing patterns in the context of mimicry. I built an interactive website to carry out a Citizen Science collection of the perception of wing pattern similarity, and adapted the t-STE machine learning algorithm to generate 3D perceptual maps of the variation of heliconiine butterfly wing patterns at the continental scale. I mapped the local phenotypic diversity as the degree of clustering in the perceptual space, and used Gaussian mixture models to cluster wing patterns in putative mimicry rings reflecting mutualistic interactions. I illustrated the versatility of the perceptual approach showing its suitability to carry out both macroecological analyses and local

community-level studies. Altogether, I believe the perceptual approach can become a new flexible tool to the ecologist and evolutionist's toolbox that will allow them to investigate and quantify similarity in any ecological signals transmitted through perception.

Finally, in **Chapter 4**, I linked all previously explored geographic, evolutionary, and phenotypic dimensions of biodiversity, to study the effects of mutualistic interactions on large-scale spatial distributions and niche evolution of ithomiine butterflies. I used phylogenetic comparative methods to test for spatial congruence and climatic niche convergence among comimetic species. I showed that mimicry drives large scale spatial association among phenotypically similar species, providing new empirical evidence for the validity of Müller's model at a macroecological scale. Additionally, I showed that mimetic interactions drive the evolutionary convergence of species climatic niche, thereby strengthening the co-occurrence of co-mimetic species.

Overall, my research work provides new insights into the importance of mutualistic interactions in shaping both niche evolution and species assemblages at large spatial scales. Here, I offer to shed light on potential limits of this research work that could also affect future studies beyond the scope of my case study, discuss ways to overcome them, and outline future directions for research:

(1) I discuss the concept of 'mimicry ring', both fundamental and transversal to all my research work, in order to clarify its use, and offer a theoretical framework to build upon for future studies on mimicry.

(2) I highlight the importance of multi-taxa approaches in the context of mimicry and I illustrate what such integrated comparison can bring to the picture.

(3) I open a window on the importance of mimetic interactions to understand the assembly of ecological communities at large spatial scales.

(4) Finally, I outline possible consequences of global changes on the biodiversity patterns described in this research work and describe opportunities to predict if not prevent them.

In the face of global change, understanding the mechanisms underlying species distributions and coexistence is both a priority and a challenge, especially for biodiversity hotspots such as the Neotropics. In this research work, I explored several dimensions of biodiversity patterns in Neotropical mimetic butterflies employing an integrative approach across biogeography, phylogenomics, and community ecology. Specifically, I focused on two tribes engaged in Müllerian mimicry, the Ithomiini (Nymphalidae: Danainae) and Heliconiini (Nymphalidae: Heliconiinae), in order to illustrate the importance of mutualistic interactions for shaping large-scale spatial and evolutionary patterns of biodiversity.

In **Chapter 1**, I employed species distribution models to map the taxonomic, phylogenetic and mimetic facets of Ithomiini biodiversity. I identified areas of evolutionary and ecological importance for conservation, and evaluate their overlap with current anthropogenic threats. I showed that tropical montane forests that host high species and mimetic diversity as well as rare species and mimicry rings appear particularly under threat. These results support the role of ithomiine butterflies as a suitable flagship indicator group for Neotropical butterfly diversity, and reinforce the position of the tropical Andes as a flagship region for butterfly biodiversity conservation.

In **Chapter 2**, I presented a new phylogeny for the Ithomiini tribe, building upon phylogenomic methods to resolve and support deep evolutionary relationships in the group. This phylogeny reinforces the monophyly of the core-group, a clade associated with a recent adaptive radiation linked to multiple colonizations of new areas following the demise of the Pebas aquatic system in Western Amazonia. It comforts the basal position of the Melinaea subtribe and suggests the Mechanitina subtribe as the sister-group of the core-group. This new topology provides better agreement with the putative evolution of morphological traits, highlighting the power of phylogenomic approaches to resolve previously conflicting deep evolutionary relationships. Altogether, this new phylogeny provides a stable tool for macroevolutionary analyses in ithomiine butterflies.

In **Chapter 3**, I described a new method to quantify similarity in wing patterns in the context of mimicry. I built an interactive website to carry out a Citizen Science collection of the perception of wing pattern similarity, and adapted the t-STE machine learning algorithm to generate 3D perceptual maps of the variation of heliconiine butterfly wing patterns at the continental scale. I mapped the local phenotypic diversity as the degree of clustering in the perceptual space, and used Gaussian mixture models to cluster wing patterns in putative

mimicry rings reflecting mutualistic interactions. I illustrated the versatility of the perceptual approach showing its suitability to carry out both macroecological analyses and local community-level studies. Altogether, I believe the perceptual approach can become a new flexible tool to the ecologist and evolutionist's toolbox that will allow them to investigate and quantify similarity in any ecological signals transmitted through perception.

Finally, in **Chapter 4**, I linked all previously explored geographic, evolutionary, and phenotypic dimensions of biodiversity, to study the effects of mutualistic interactions on large-scale spatial distributions and niche evolution of ithomiine butterflies. I used phylogenetic comparative methods to test for spatial congruence and climatic niche convergence among comimetic species. I showed that mimicry drives large scale spatial association among phenotypically similar species, providing new empirical evidence for the validity of Müller's model at a macroecological scale. Additionally, I showed that mimetic interactions drive the evolutionary convergence of species climatic niche, thereby strengthening the co-occurrence of co-mimetic species.

Overall, my research work provides new insights into the importance of mutualistic interactions in shaping both niche evolution and species assemblages at large spatial scales. Here, I offer to shed light on potential limits of this research work that could also affect future studies beyond the scope of my case study, discuss ways to overcome them, and outline future directions for research:

(1) I discuss the concept of 'mimicry ring', both fundamental and transversal to all my research work. The classic definition I used throughout my work implies a hard classification of aposematic patterns into independent groups with strict boundaries, while in nature ecological interactions are typically fuzzier and lie on continuums. Here, I discuss the rationale for a fuzzy classification of mimicry rings, and offer a theoretical hierarchical framework to build upon for future studies on mimicry.

(2) I highlight the limit of using a unique group model in a context of mimicry involving convergence across distant lineages. I illustrate how the omission of members of the mimetic communities can affect outcomes of analyses, therefore emphasizing the importance of multi-taxon approaches in the context of mimicry.

(3) I discuss the potential of the joint exploration of mimetic and taxonomic diversity patterns to open a window on mechanisms driving the assembly of ecological communities at large spatial scales.

(4) Finally, I consider the potential consequences of global changes on the biodiversity patterns described in this research work. In particular, I discuss the limits of identifying refuge areas for conservation based on current anthropogenic threats, and I outline opportunities to predict future risks, if not prevent them.

1 Redefining the concept of 'mimicry ring'

1.1 Mimetic classifications: going hard or stay fuzzy?

Throughout all my research work, I employed the concept of 'mimicry ring' which I defined as "a set of individuals sharing the same (honest or not) warning signals" (Papageorgis, 1975; Weismann, 1904). This definition underlies a strict classification of warning signals, and the biologic entities that display them (individuals, Operational Mimicry Units, species, etc.), into bounded groups that in the end reflect ecological interactions. Indeed, the implied consequence here is that in a local community, individuals from the same mimicry ring are engaged in mimetic interactions with each other, while individuals from two different mimicry rings do not interact, at least through mimicry (Joron & Mallet 1998).

However, in **Chapter 3**, I showed that local patterns of mimetic species were not perfectly clustered, and that some degrees of uncertainty remained with patterns being inconsistently classified in different putative mimicry rings according to the source of the dataset used. From the methodological point of view, I designed those hard classifications (i.e., with a strict membership defined for each object) applying Gaussian Mixture Models that provide as initial outputs the likelihood for each pattern to belong to each group. Therefore, they directly quantify the uncertainty inherent to such classifications. Yet, I attributed each subspecies to its most likely group in order to define the desired putative mimicry rings.

In practice, ecologists may not be satisfied with a fuzzy classification that provides probabilities of membership to a group instead of a strict membership for each species. Yet, it is worth taking the time to think about the biological nature of the ecological interactions these mimetic groups aim to represent. When they involve two species, Müllerian mimetic interactions represent the fitness gains obtained by the individuals of those species when they happen to co-occur such that the species share the cost of educating predators to their noxiousness. Such gains (or losses for models in case of Batesian mimicry) are not binary. In theoretical modeling they are typically represented by a continuous (possibly bounded) quantity

depending on many factors, including the relative frequencies of species, their palatability, their degree of phenotypic similarity, the composition, visual abilities, experience and behavior of the predator community, the availability of alternative prey and the structuration among microhabitat of prey and predators (Kokko *et al.* 2003; Lindström *et al.* 2004; Gompert *et al.* 2011; Aubier & Elias 2020; Birskis-Barros *et al.* 2021). For instance, even though predators are expected to show a sharp boundary between what they like or always reject according to the degree of palatability (Joron & Mallet 1998), thus reflecting a binary interaction (i.e., present if always rejected, absent if always eaten), the diversity of predator preferences can be sufficient to blur this sharp individual distinction. Beyond the spectrum of palatability (Turner 1984), this is also true regarding imperfect mimicry (i.e., the fact some mimics are not perfectly similar to models but can still be considered as the same type of prey by predators who tend to generalize their aposematic signals; Kikuchi & Pfennig 2013) and the diversity of predator visual abilities and foraging choices. Indeed, in a community with a diversity of predators, the protection gains of Müllerian mimetic species unknown to the predators is expected to vary in a non-linear and non-binary fashion according to their degree of similarity with the local model, if ignoring other factors (**Fig. 1**).

At large spatial scale, the idea of imposing a hard classification of mimicry rings with strong boundaries is even more delicate. Indeed, in **Chapter 3** I showed that the perceptual space of heliconiine butterflies is filled with a continuum of wing patterns rather than clearly defined clusters of mimicry patterns. This continuum can be explained by both the local imperfect mimicry, and the geographical drift of patterns selected by the different local communities of predators. If zooming out sufficiently in the geographic space, we can encounter cases where pairs of species that show high pattern dissimilarity are actually linked through a chain of partly overlapping pairs of species showing locally high similarity of patterns (**Fig. 2**). This geographic structure reflects what can be observed for 'ring species' where subspecies at the extremum of the 'ring' cannot reproduce, but are not strictly genetically isolated due to gene flow occurring through a chain of partly overlapping intermediate subspecies (Stebbins 1949). Such ring structure is also observed in bird songs that may be highly similar from short geographic distances, but show a gradual divergence following a spatial gradient such as the conspecifics at two extremums of the chain do not recognize each other's songs (Irwin *et al.* 2001). In our case, mimicry rings not only encompass local ecological interactions acting at local scale, but also distant connections relying on intermediate forms in partial spatial overlap in what can be seen as a network of mimetic interactions.

Altogether, it seems reasonable to consider the idea that local mimicry rings and the ecological interactions they represent are not always strictly bounded/binary, especially at large spatial scales. As such, the use of fuzzy classifications may offer new perspectives to account for uncertainty, but also to reflect the true fuzzy nature of the interactions. At local scale, they would allow to account for complex variable gains and losses associated with co-occurrence of interacting species that may not be simply binary. At regional scale, they would allow to account for spatially mediated distant interactions that blur the boundaries between mimicry rings. Beyond the case of mimetic interactions, fuzzy classifications appear as a useful tool to describe ecological interactions often reduced to their discrete binary expression for operational reasons, while their underlying nature is complex and continuous (Bronstein 1994; Drew *et al.* 2021; Dracxler & Kissling 2022).

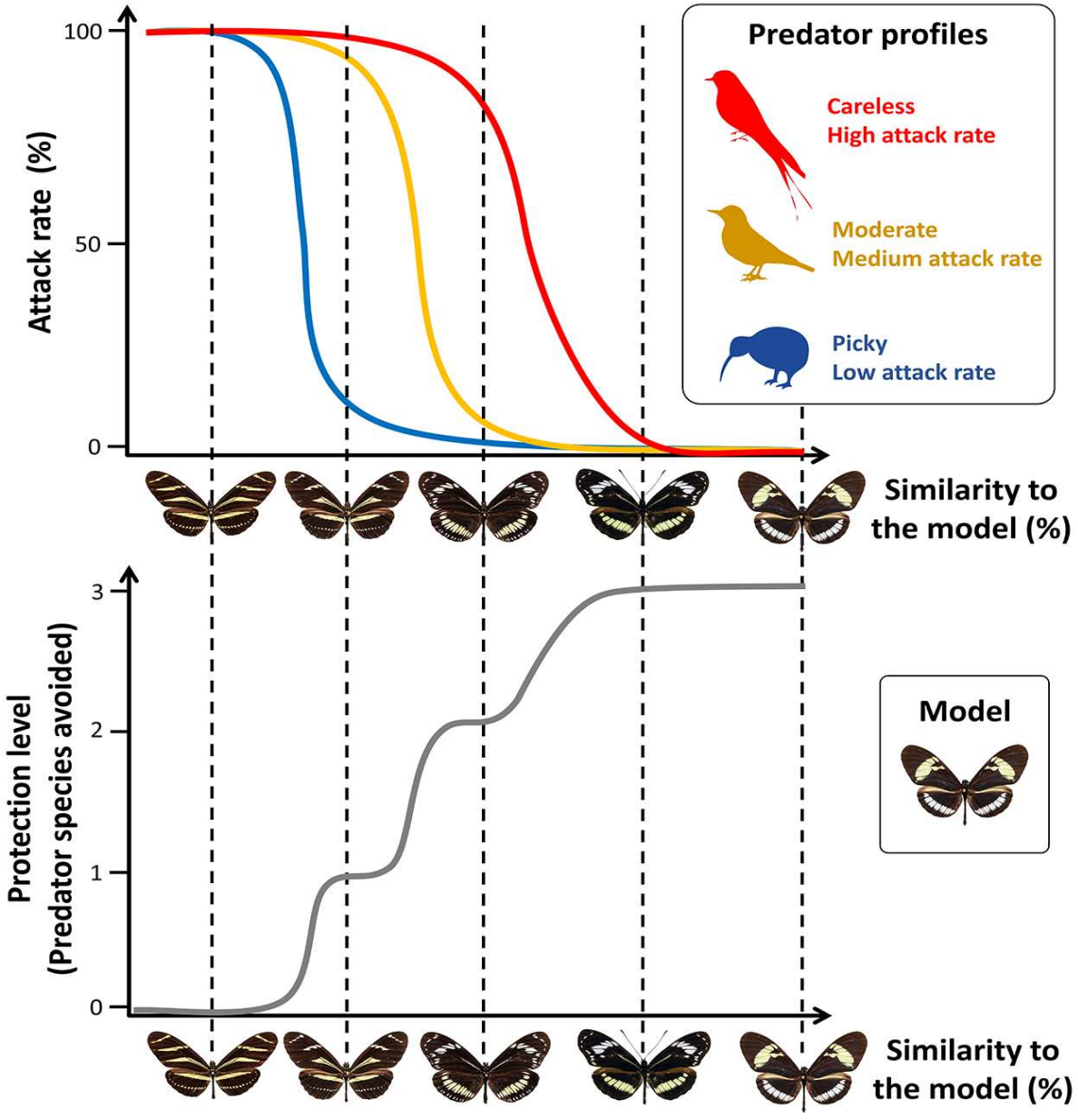

Figure 1: The continuous nature of ecological interactions illustrated by the non-binary levels of protection experienced by Müllerian mimetic species unknown to the predator community according to their similarity to the local model. While some careless predators (in red) with possibly a high ability to distinguish visual signals will attack most of the new forms, other picky predators with potentially lower ability to discriminate (or just wondering how they end up in the Amazonian forest, desperately trying to catch flying butterflies for a decent meal while they are stuck on the ground, illustrated with the kiwi bird as the blue predator) will attack only the most dissimilar new forms. As such, the fitness gains of the new forms from co-occurrence with the local model are not linear nor binary, and illustrate the fuzzy nature of boundaries between local mimicry rings aiming to describe mimetic interactions. For the sake of simplicity, this illustration ignores the effect of other factors such as relative densities and degrees of palatability.

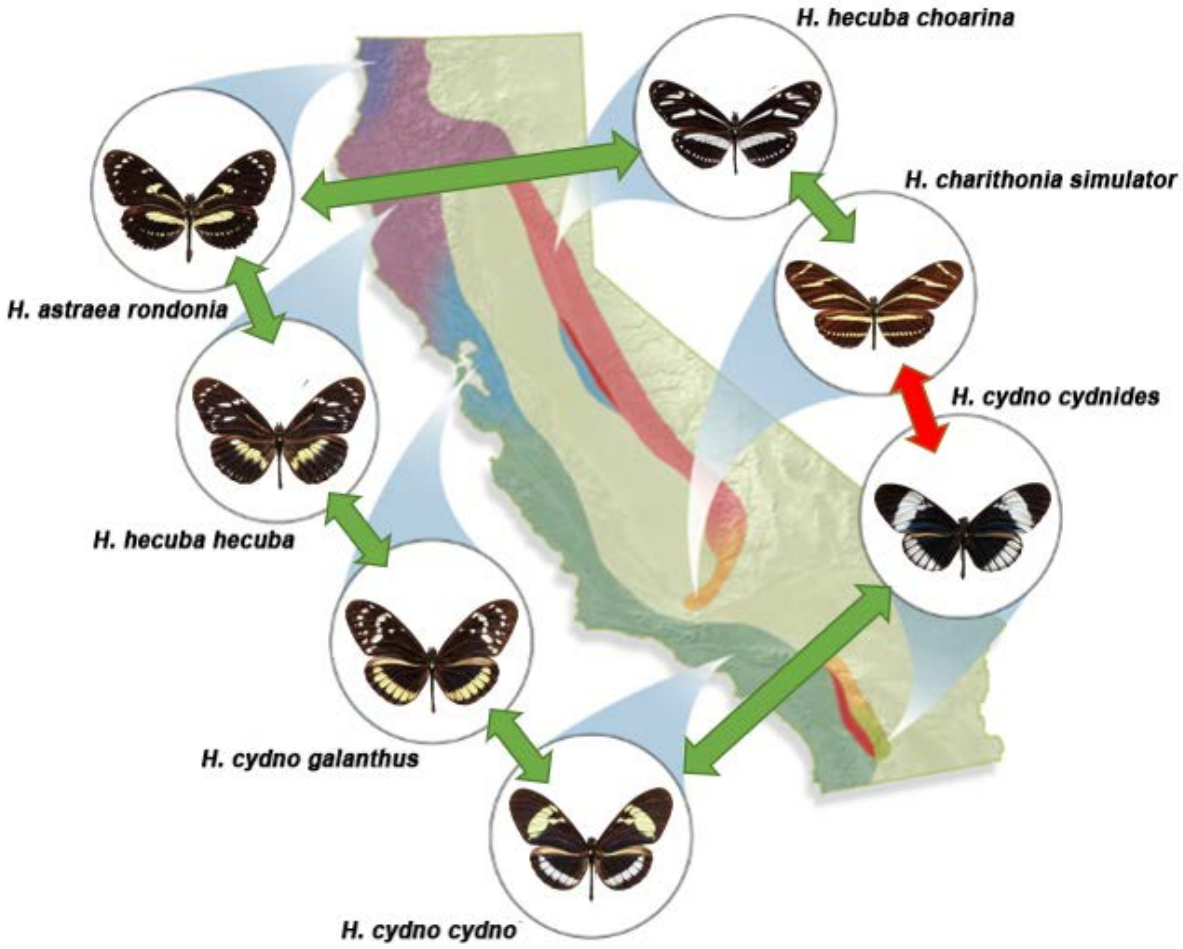

Figure 2: A fictional mimicry ring at regional scale reflecting the geographic organization of 'ring species'. Due to geographic drift, subspecies that show low level of phenotypic similarity (red arrow) could still be considered as part of the same mimicry ring since they are connected through a chain of partly overlapping pairs of species showing locally high similarity of patterns (green arrows). Subspecies patterns of heliconiine butterflies shown here are real but the locations are fictional and relate to the location of the species of the *Ensatina* complex, an emblematic case of ring species of salamanders found in California (Stebbins 1949).

1.2 A new hierarchical framework

Beyond the fuzziness entailed by the nature of mimicry rings, the concept itself seems to carry a degree of ambiguity since its emergence. The early reference to 'mimicry rings' or 'mimicry complexes' found in the literature regrouped species on the basis of phenotype similarity, independently from co-occurrence, and considered that local mimicry rings with similar patterns in different locations were the 'same' (Poole 1970; Papageorgis 1975). Other authors adopted an evolutionary perspective and described mimicry rings as "groups of unpalatable species, together with some palatable species, that have converged on the same warning color pattern" (Mallet & Gilbert 1995). Finally, other studies up to a recent review have described mimicry rings on the basis of local ecological interactions such as "a group of sympatric species sharing a common warning pattern" (Joron & Mallet 1998) or expressed in a more verbose manner as "communities that contain at least one well-defended prey species that has a warning signal and experiences reduced predation pressure owing to its aposematism and at least one more associated prey species that derives a fitness benefit from mimicking the well-established aposematic signal" (Kunte *et al.* 2021).

Despite these fundamental differences in definitions and their implications for the ecological and evolutionary levels, to my surprise no author seem to have yet discussed the conceptual blurriness surrounding the commonly applied idea of 'mimicry ring'. Here, I offer to clarify the situation and propose a hierarchical framework to clearly distinguish between the different levels of definition of the concept**S** of mimicry rings, and how to identify and support them.

I suggest that mimicry rings be defined through three different embedded frameworks according to available information and aims of the analyses (**Fig. 3**). I detail these frameworks here from the most inclusive, to the narrowest:

- 1/ **Phenotype-based mimicry rings** are defined on the basis of phenotypic similarity only (e.g., Poole 1970; Papageorgis 1975; Wilson *et al.* 2015; Joshi *et al.* 2017; Hoyal Cuthill *et al.* 2019; **Fig. 4.A**). They form groups of biological entities whose aposematic patterns can be perceived as similar in the eyes of the predator. As such, members of these groups can *potentially* be involved in mimetic interactions if they happen to co-occur. These groups of phenotypic similarity, defined as **"phenotypic mimicry rings"** can be seen as hypotheses of mimicry rings or "putative mimicry rings" (e.g., Symula *et al.* 2001; Sanders *et al.* 2006; Aubier & Elias 2020). They should be typically delineated by

investigating pattern variation at large scale, ideally pooling all patterns found within the geographical and taxonomic scope of the study. Our perceptual approach to the global variation of wing patterns in heliconiine butterflies is a good example of such design (See **Chapter 3**). These rings remain 'putative' in the sense that the occurrence of ecological interactions between their members remain to be tested and supported by a pattern of significance spatial co-occurrence as presented in **Chapter 4**.

- 2/ **Evolutionary-based mimicry rings** are defined in the evolutionary framework as groups of biological entities whose patterns have converged and/or have been maintained under common selective pressures incurred by predators (Mallet & Gilbert 1995). I labeled these groups as **"historical mimicry rings"**. Support for such types of mimicry rings can be explored with joint ancestral reconstruction of phenotypic patterns and ranges, a pattern of phenotypic similarity in the same ancestral area observed along the phylogeny being a correlative support for such rings (**Fig. 4.C)**. Because local pattern convergence can have arisen in the past, and patterns can be conserved along the phylogeny even following dispersal events, such mimicry rings may form disjunct areas in the present (**Fig. 4.D**), thus not qualifying as the last and narrower type of mimicry rings described below.
- 3/ **Interaction-based mimicry rings** are defined in the community ecology framework as groups of currently co-occurring biological entities with similar aposematic patterns *effectively* engaged in mimetic interactions (Joron & Mallet 1998; Kunte *et al.* 2021; **Fig. 4.B**). I labeled these groups as **"effective mimicry rings"**. It is worth noting that significant co-occurrence and phenotypic similarity in the present only provides correlative support for the existence of ecological interactions. Thus, experimental tests of predation and/or fieldwork observations remain necessary to provide empirical evidence of such interactions (e.g., Mallet & Barton 1989; Kapan 2001; Langham 2004).

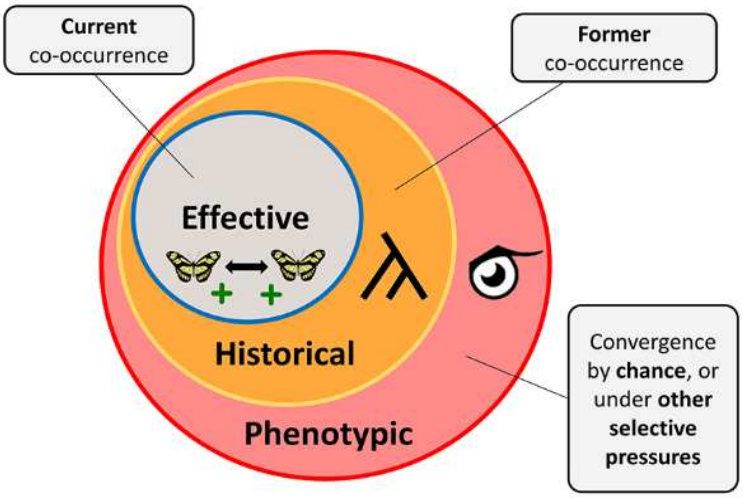

Figure 3: Hierarchy of mimicry ring definitions. Phenotypic mimicry rings (in red) are based on phenotype similarity. They encompass all biological entities with patterns perceived as similar in the eyes of the predator. **Historical mimicry rings** (in orange) are defined in an evolutionary framework. They represent groups of entities whose pattern similarity is due to convergence, and/or maintenance, under common selective pressures incurred by predators. **Effective mimicry rings** (in blue) are defined in a community ecology framework. They are limited to entities that are currently involved in mimetic interactions due to pattern similarity associated with local co-occurrence with a common cohort of predators. These definitions are hierarchical: phenotypic rings contain historical rings which contain effective rings.

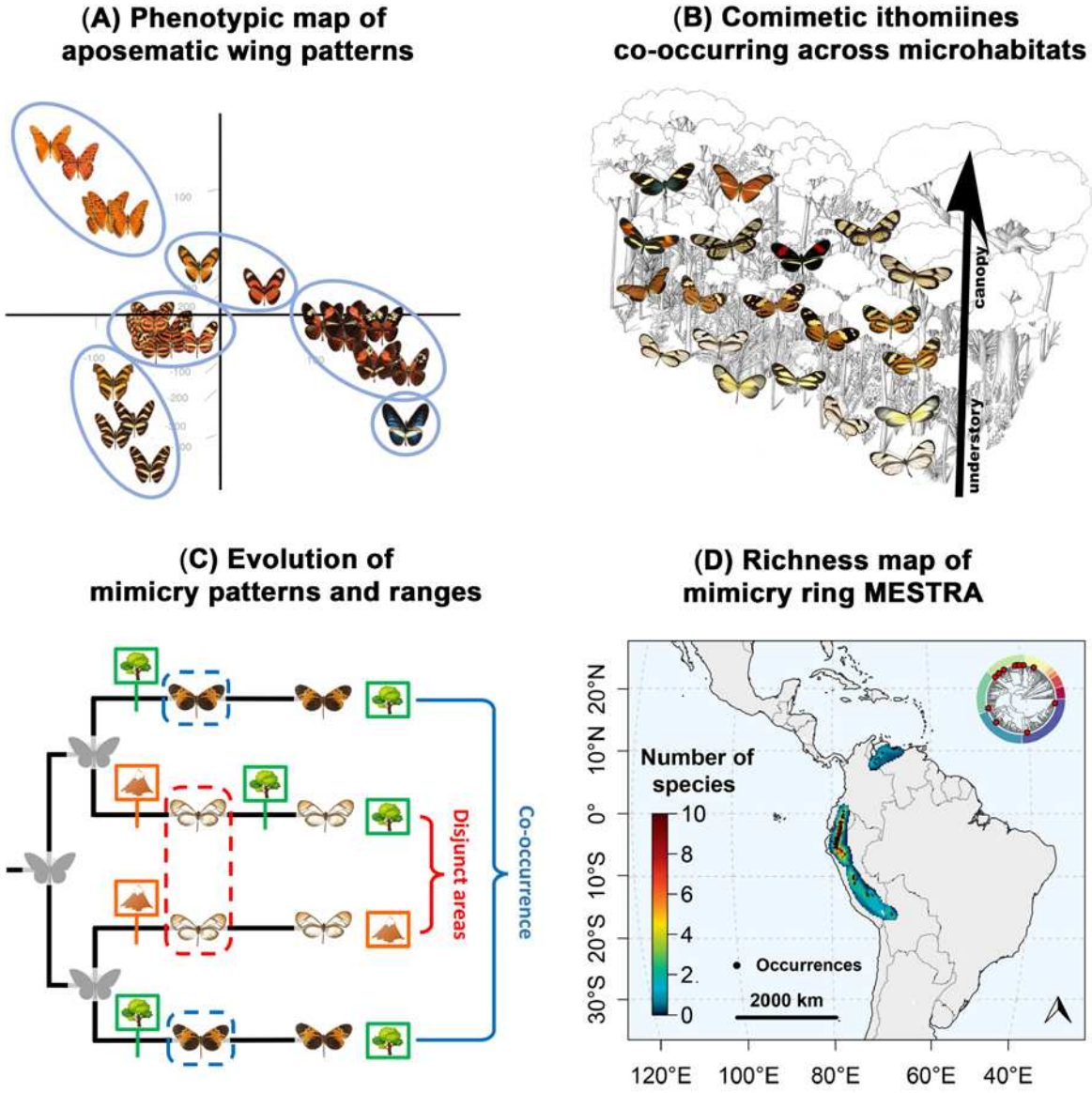

Figure 4: Evidence for the three embedded conceptual frameworks of 'mimicry rings'. **(A)** A phenotypic map of butterfly aposematic patterns that can be used to suggest hypotheses for "*phenotypic mimicry rings*" on the basis of phenotypic similarity. **(B)** An illustration of the local co-occurrence of comimetic butterflies across microhabitats (adapted from Birskis-Barros *et al.* 2021, with background art by Danilo B. Ribeiro and Rogério Lupo), depicting cases of "*effective mimicry rings*", where comimics effectively co-occur and interact in the present. **(C)** Evolution of mimicry patterns and habitats displaying cases of "*historical mimicry rings*" involving ancestral pattern convergence during species sympatry (in dashed frames), with (in blue) and without (in red) current co-occurrence. **(D)** Example of the ithomiine mimicry ring MESTRA with disjunct distribution that is defined as a "*phenotypic mimicry ring*" based on pattern similarity, but cannot be considered as an "*effective mimicry ring*" throughout all its range because some species do not co-occur currently, and may qualify as "*historical mimicry ring*" only if the similarity of patterns among comimetic species has arisen from common selective pressures incurred by predators during former local co-occurrence prior to species dispersal across mountain ranges.

The three types of mimicry rings are hierarchically embedded (**Fig. 3**). All mimicry rings are "phenotypic mimicry rings" since all biological entities in mimicry rings share a similar pattern. Thus, all "historical" and "effective" mimicry rings are "phenotypic rings". However, all "phenotypic mimicry rings" are not "historical mimicry rings", because similarity of patterns between species can arise simply by chance, or though adaptive convergence/conservatism not linked to mimicry as in the case of environmental filtering, or sexual selection. "Phenotypic mimicry rings" remain putative until sufficient evidence of pattern convergence/conservatism driven by selection linked to mimicry, and/or effective mimetic interactions in current communities, qualifies them as "historical mimicry rings" and/or "effective mimicry rings". Moreover, not all "historical mimicry rings" are "effective mimicry rings". In some cases, pattern convergence may have been achieved from common selective pressures incurred by predators during former local co-occurrence prior to species dispersal across different and currently disjunct areas (**Fig. 4D**). As such, these rings cannot qualify as "effective rings" since their entities are not currently involved in ecological (mimetic) interactions. Finally, all "effective mimicry rings" are "phenotypic rings" and "historical rings" since current mimetic interactions between sympatric species involve a frequency-dependent selection for the convergence and maintenance of pattern similarity.

Throughout my research work, I employed the concept of 'mimicry ring' and its different declinations according to the available information. In **Chapter 1**, I used a phenotype-based classification of mimicry rings in ithomiine butterflies to explore large-scale pattern of mimetic diversity as the number of mimicry rings predicted to be found within each grid cell. I was very thankful for Keith Willmott to have designed this operational classification from its immense expertise built from more than 30 years working with these inspiring butterflies. Yet, I was aiming for a more reproducible and quantitative approach to describe the variation in mimicry patterns. Thus, with Eddie Pérochon, the Master's student I supervised, and my collaborators on the project, we set to explore a new perceptual approach to quantify pattern variation in heliconiine butterflies. Our framework allowed us to design hypotheses for both putative phenotype-based mimicry rings at large scale and effective interaction-based mimicry rings in local communities (see **Chapter 3**). Finally, in **Chapter 4**, I described an analytic framework to question putative 'phenotype-based' mimicry rings and support their qualification as 'effective' mimicry rings in case of significant spatial congruence between the members of the ring. I hope this work will inspire researchers to apply this new framework for the concept**S** of mimicry rings in mimicry studies in the future.

2 Mimetic communities: a multi-taxon approach

2.1 On the limits of a unique group model

In **Chapter 1**, I presented how to produce distribution maps for ithomiines species and their mimicry rings, building on a comprehensive database of georeferenced occurrences and an expert-based classification of mimicry patterns. I aggregated these results to map biodiversity patterns at continental scale, including mimicry richness as the number of local mimicry rings found in each grid cell. Furthermore, in **Chapter 4,** I used these distribution maps to extrapolate local community composition and test for large scale spatial congruence among comimetic ithomiine taxa. I chose to focus initially on ithomiine butterflies because they are the numerically dominant group in Neotropical mimetic communities, encompassing up to half of the species richness, such as they are considered by some authors as the 'center' of attraction of their mimicry rings (Poole 1970; Beccaloni 1997a). Moreover, ithomiine butterflies have been proposed as indicator species for habitat quality and local butterfly diversity (Beccaloni & Gaston 1995; Brown Jr 1997; Uehara-Prado & Freitas 2009), making them an ideal candidate group for a first exploration of biodiversity patterns in Neotropical mimetic communities. However, mimetic communities ignore the taxonomic boundaries, and can drive phenotypic convergence across numerous distant butterfly taxa, and even damselfly (Beccaloni 1997a; Outomuro *et al.* 2013; Corral-lopez *et al.* 2021). Ignoring such diversity can have crucial effects on the study of mimetic communities.

In **Chapter 3**, I developed a perceptual approach to the study of ecological signal variation. Specifically, I built a perceptual space of heliconiine butterfly wing patterns, pooling all subspecies documented in the group in a unique macroecological perspective. This perceptual space can be used to design hypotheses of '*phenotype-based mimicry rings*' (see **section 1**). Then, it becomes possible to explore patterns of mimetic richness as the number of local mimicry rings (even if a quantitative approach like phenotypic clustering is likely to be favored, see Discussion in **Chapter 3**), or simply map the distribution of such mimicry rings in space. The crucial point here is that these hypotheses for phenotype-based mimicry rings, both at large and local scale, can be affected by the presence or absence of members of the broader mimetic community in the scope of the analyses. Indeed, if butterflies from other mimetic groups with an intermediate pattern exists, their inclusion can affect the clustering hypotheses raised during the process (**Fig. 5**). Accordingly, the quantification of phenotypic diversity, either from counts of mimicry rings or estimate of phenotypic clustering will be affected. The

distribution maps of mimicry rings will adjust to the taxa considered as part of each ring or not, potentially presenting a slightly different picture. Finally, as we showed, mimetic interactions can drive spatial distributions and niche evolution within the Ithomiini tribe (See **Chapter 4**), it seems highly relevant to explore how these effects extend beyond the ithomiines, and eventually affect them. More generally, tests for spatial congruence and niche convergence relying on mimicry classification would provide more robust results if a higher proportion of the members of the mimetic communities were included.

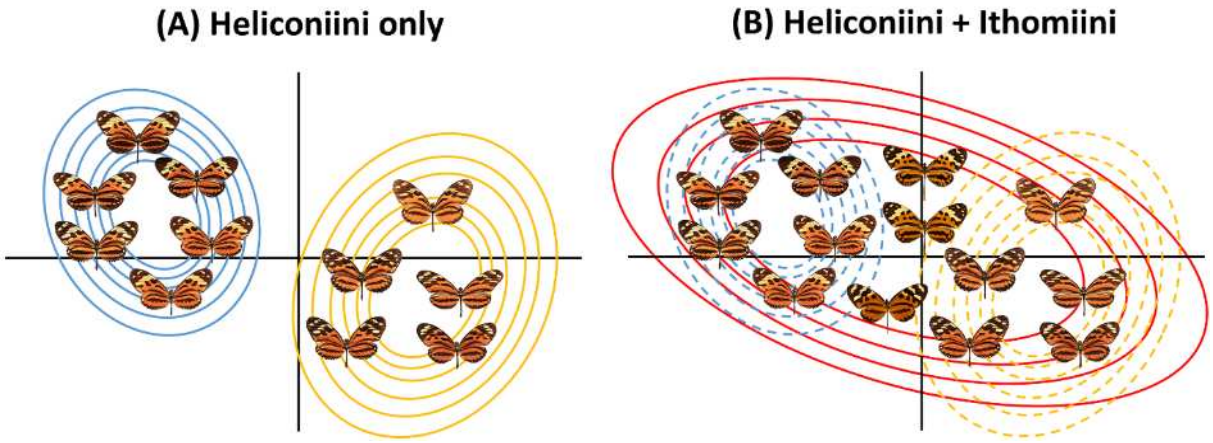

Figure 5: Hypothetical effect of the inclusion of external taxa to the delineation of mimicry rings. (A) Perceptual or phenotypic map of heliconiine butterflies displaying two relatively discrete groups of patterns. **(B)** Similar map including three additional ithomiine butterflies. Contour lines represent probability densities of clustering hypotheses. The addition of the three intermediate phenotypes of ithomiine butterflies lead to the reconsideration of the clustering hypotheses into a single mimetic group.

2.2 Heliconiini: the twin tribe

The natural candidate to explore the value of accounting for other members of the mimetic communities, beyond the focus on ithomiine butterflies, are the heliconiines butterflies. Heliconiines, similarly to ithomiines, form a diverse tribe of New World butterflies encompassing 77 species and 457 subspecies distributed across 8 genera (Kozak *et al.* 2015; Jiggins & Lamas 2016). They occur all across America, from Canada to Argentina, but share most of their range with ithomiines throughout the forests of the Neotropics, with highest diversity spotted in the Andes and Western Amazonia (Rosser *et al.* 2015). Their caterpillars feed on passionflower vines (Passifloraceae family) from which they obtain cyanogenic glucosides, the chemical compounds that provide them with protection against predators (Jiggins & Lamas 2016). More crucially for us, despite having diverged over 85 My ago from ithomiines (Chazot *et al.* 2021), heliconiine butterflies share numerous mimicry patterns with

them (see illustration in the **General Introduction**). Thus, both tribes are engaged in mutualistic interactions in the context of Müllerian mimicry within and between the two groups, throughout the rainforests of the New World.

In order to confront biodiversity patterns of heliconiine and ithomiine butterflies, and study the effects of mutualistic interactions in their respective spatial distributions and niche evolution, I supervised a Master's project led by Eddie Pérochon that aimed to explore these questions. Interestingly, this research project is what triggered in the first place the creation of a new reproducible method to classify wing patterns that later developed in the perceptual approach presented in **Chapter 3**. It resulted in the drafting of an on-going research article which I attached to this Thesis (Pérochon *et al.* 2023; see **ANNEXE 6**). Here, I outline some of the main results to highlight the value of a multi-taxon approach in mimetic studies.

First, we compared continental-scale biodiversity patterns between the two tribes. The two groups showed a peak of species and mimicry richness in the Andes, where the heterogeneity of landscapes, the elevation and environmental gradients, and the rigged topography is a perfect recipe for environmental structuration and geographic isolation fueling speciation (Weir 2006; Chaves *et al.* 2011; Hutter *et al.* 2013). However, while taxonomic and mimetic diversity of Ithomiini is highly concentrated in the Andes (**Fig. 6.A-C**), heliconiine butterflies show a relatively more balanced pattern with a secondary diversity hotspot found in the Amazonian basin with almost as much diversity of species and mimicry patterns (**Fig. 6.B-D**). Such differences could be explained by different biogeographic histories, with ithomiine butterflies predicted to have emerged in the eastern slopes of the Andes (Chazot *et al.* 2019b), while the heliconiines may have originated from the Amazon basin, hence the location of their secondary hotspot, even if studies are still lacking on the matter (Jiggins & Lamas 2016).

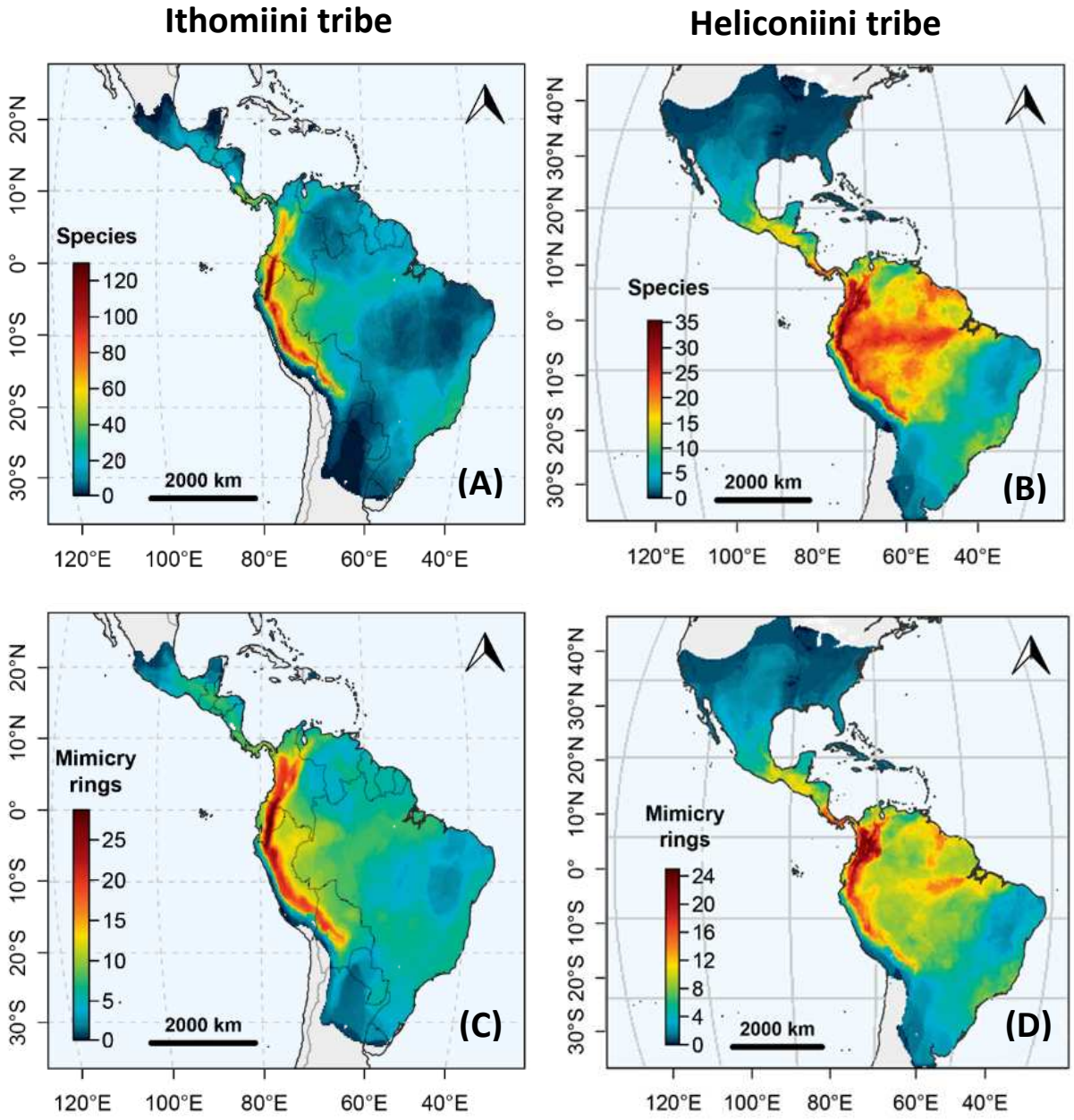

Figure 6: Biodiversity patterns of ithomiine and heliconiine butterflies showing global congruence. (A) Species richness of ithomiines. **(B)** Species richness of heliconiines. **(C)** Mimicry richness of ithomiines. **(D)** Mimicry richness of heliconiines. Mimicry richness are quantified as the local number or mimicry rings. Heliconiini maps are modified from Pérochon et al., 2023 (See **ANNEXE 6**).

Taxonomic and mimetic diversity patterns appear globally congruent, yet with interesting specificities for each tribe. However, the most significant patterns to explore in a context of mimicry are the spatial distributions of the phenotype-based mimicry rings. In particular, we showed that species harboring phenotypically similar patterns display a strong spatial association within, but also between the two tribes. For instance, species labeled under the mimicry ring MOTHONE are only found in the Andes in the two tribes, with strikingly

similar distributions (**Fig. 7.A-B**). Besides, the heliconiine species with the pattern MOTHONE show an apparently surprising disjunct distribution across Andean mountain ranges and the Amazon basin, which may be hard to explain without further information (**Fig. 7.D**). Meanwhile, the ithomiine species with the 'same' MAMERCUS pattern can be found almost in all the Neotropics, encompassing largely the whole disjunct distribution of their heliconiine twins (**Fig. 7.C**). As such, the heliconiines benefit from the co-occurrence with their more numerous ithomiine counterparts that also link indirectly the different areas where heliconiines with MAMERCUS patterns can be found. This phenomenon highlights remarkably the benefits of considering all members of the mimetic communities when trying to understand the processes driving their spatial distributions. Furthermore, such comparative approach can also help to clarify our hypotheses for putative 'phenotypic mimicry rings' since in a single case, we noted that the distribution of the species we labeled under the same ring MANTINEUS on the basis of phenotypic similarity were actually displaying widely divergent distributions that tend to disqualify our hypotheses (**Fig. 7.E-F**). Such similarity in wing pattern is thus likely due to chance alone, and does not qualify this group of species as an 'effective mimicry ring' crossing tribe boundaries.

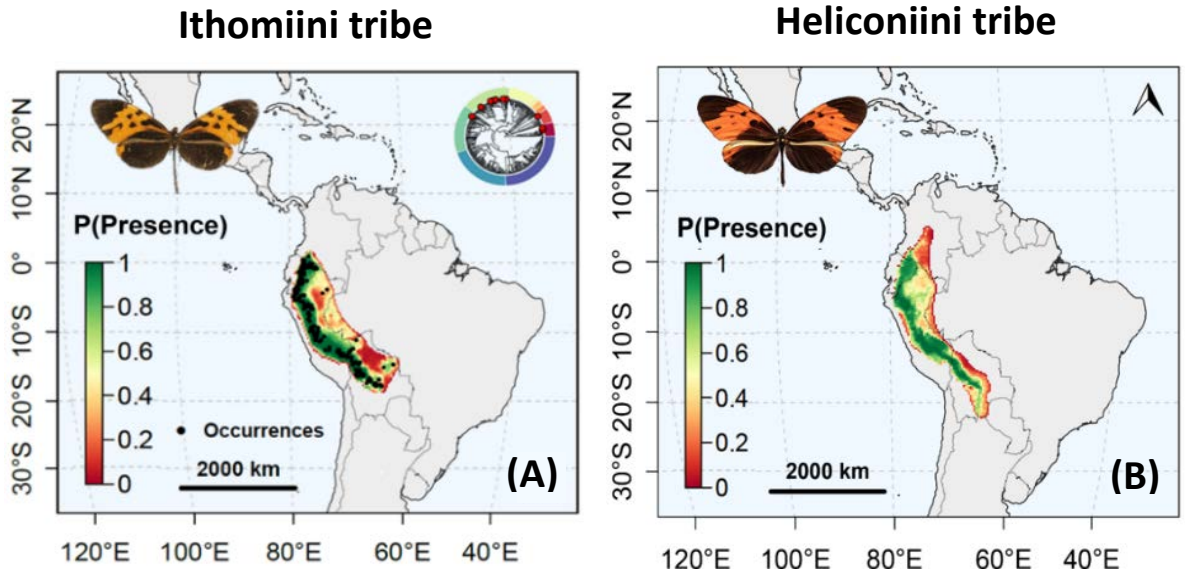

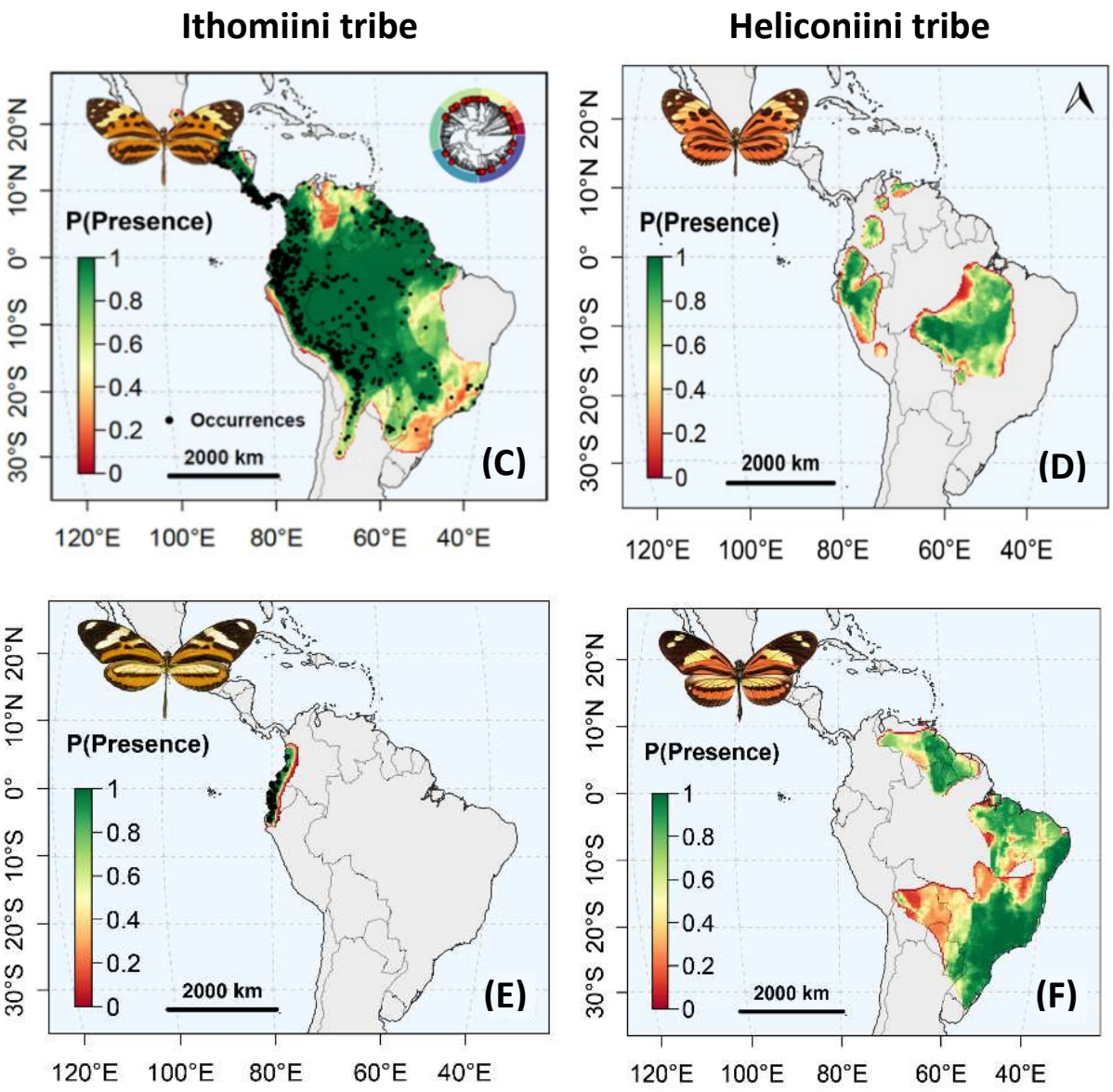

Figure 7: Spatial distributions of phenotype-based mimicry rings across the Ithomiini and Heliconiini tribes. (A-B) MOTHONE rings with a restricted Andean distribution (Ithomiini: 14 species; Heliconiini: 3 species). **(C-D)** MAMERCUS rings with a wide distribution and encompassing a disjunct distribution (Ithomiini: 64 species; Heliconiini: 4 species). **(E-F)** MANTINEUS rings with no overlap (Ithomiini: 5 species; Heliconiini: 3 species). Heliconiini maps are modified from Pérochon et al., 2023 (See **ANNEXE 6**).

Globally, we detected a significant signal for both spatial congruence and climatic niche convergence across species that we classified under the same phenotypic mimicry ring between the two tribes (Pérochon *et al.* 2023; see **ANNEXE 6**). These results highlight once again the importance of mutualistic interactions in shaping large spatial distributions and niche evolution. This conclusion is here boldly supported by large spatial and evolutionary associations between two clades separated by more than 85 My, that is as much as between us *Homo sapiens* (if you

are not a *Homo sapiens* and read those lines, I apologies for being so short-minded and anthropocentric) and for instance flying lemurs (Order: Dermoptera) (Upham *et al.* 2019).

2.3 Enlarging the taxonomic scope

Heliconiine and ithomiine butterflies are the most emblematic examples of Neotropical mimetic butterflies, largely because of their historical role in the emergence of the concept of mimicry in the second half of the 19th century (Bates 1862; Müller 1879). However, mimetic communities in the Neotropics can encompass a large diversity of distantly related groups of butterflies and moths (Poole 1970; Beccaloni 1997a). For instance, in the eastern slopes of the Andes in Ecuador, it is possible to find in the same locality a group of mimetic ithomiines and heliconiines harboring a 'tiger' pattern, as well as metalmark butterflies (Riodinidae: Riodininae) and even distantly related noctuid moths (Notodontidae: Dioptinae; Erebidae: Arctiinae) (**Fig. 8A**). Similarly, the common and widely-spread ithomiine species *Methona confusa* displaying large mostly transparent wings likely act as a model for many butterflies and moths in distant lineages across the Neotropics (**Fig. 8.B**).

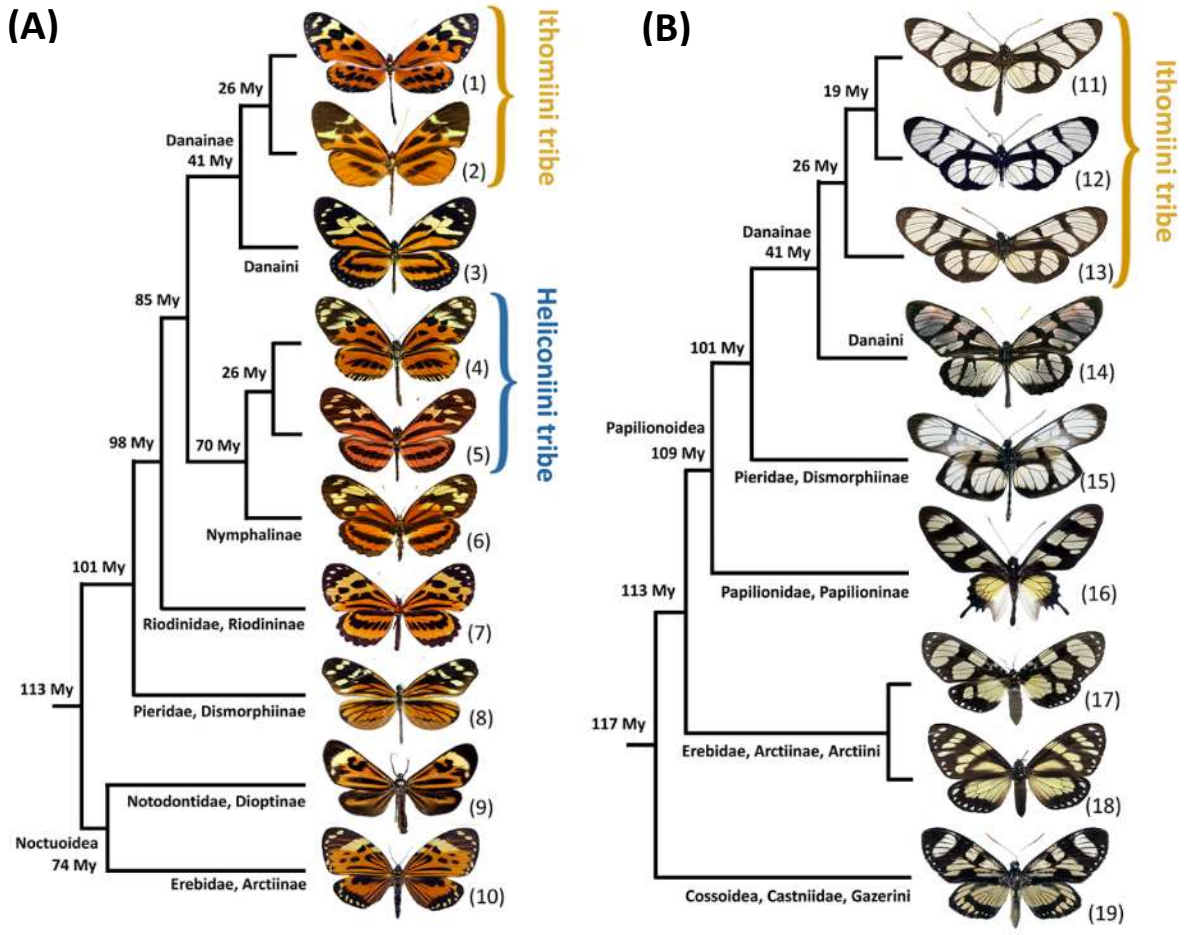

Figure 8: Phenotypic mimicry rings across neotropical butterflies and moths. (A) 'Tiger' ring across species found in the Eastern slopes of the Andes in Ecuador. (1) *Forbestra equicola equicoloides* (2) *Hypothyris fluonia berna* (3) *Lycorea halia fasciata* (4) *Heliconius numata laura*I (5) *Eueides isabella huebneri* (6) *Eresia eunice eunice* (7) *Stalachtis calliope voltumna* (8) *Dismorphia amphione* (9) *Phaeochlaena hazara hazara* (10) *Chetone histriomorpha*. **(B) 'Transparent' ring with the common and widely-spread *Methona confusa* (11) as main model.** (12) *Paititia neglecta* (13) *Thyridia psidii* (14) *Lycorea ilione* (15) *Patia orise* (16) *Parides hahneli* (17) *Notophyson heliconoides* (18) *Chetone physte* (19) *Gazera heliconioides*. Branch lengths are not strictly proportional to time. Node ages are approximated from Chazot *et al.* (2019, 2021) and Kawahara *et al.* (2019).

In the face of climate change, such network of interactions ranging all across the lepidopteran tree of Life may be critical. Indeed, the disappearance of key-members such as the numerically dominant ithomiines could potentially affect numerous lineages and have evolutionary far-reaching consequences. With the study of the interplay of spatial distributions and niche evolution between ithomiine and heliconiine butterflies, we have laid the first stone. Yet, how all these mimicry groups affects each other's distributions from local (e.g., microhabitat), regional (e.g., altitudinal gradient), to continental scale still remain to investigate. With the exponential growth of open-access biodiversity databases aiming to aggregate geographic, molecular and sometimes phenomic information across large sets if not all taxa (Benson *et al.* 2013; Parr *et al.* 2014; Antonelli 2017), it becomes possible to imagine designing and carrying out in the near future integrative studies aiming to investigate the whole mimetic communities of Neotropical insects, first at regional, and ultimately at the continental scale.

3 Assembly rules in mimetic communities: the 'saturation effect'

3.1 Saturation effect in ithomiine butterflies: a spatially structured pattern

Müller's famous model predicts the convergence of aposematic patterns between species cooccurring in local communities (Müller 1879). Yet, communities of neotropical butterflies are typically characterized by the presence of several if not dozens of local mimicry rings as illustrated on the map of mimicry richness in ithomiine butterflies across the Neotropics (see **Chapter 1**). This paradox is mostly explained by the fine-scale structuration of mimicry patterns along different ecological dimensions (Joron & Mallet 1998). Theoretical models have showed that heterogeneous communities of habitat-specialist predators that select locally for different optimal warning signals can induce the segregation of mimicry rings across

microhabitats (Gompert *et al.* 2011; Birskis-Barros *et al.* 2021). In the field, mimetic neotropical butterflies demonstrate significant degree of segregation of mimicry rings across nocturnal roosting habitat height (Mallet & Gilbert 1995), flight height (Beccaloni 1997b; DeVries *et al.* 1997), and forest structure (Elias *et al.* 2008). Since predators are also segregated by microhabitats (Willmott *et al.* 2017), selection for convergence across microhabitats is low, which explains the maintenance of local diversity of mimicry patterns (Gompert *et al.* 2011). Therefore, the number of local mimicry rings is expected to be restricted by the availability of ecological niches.

With the generation of continental maps for both species and mimicry richness in ithomiine butterflies (see **Chapter 1**), it becomes possible to explore how mimicry patterns can affect the assembly of species at large spatial scale. Beyond testing for a pattern of spatial congruence among comimetic species (see **Chapter 4**), we can also investigate the relationship between species and mimicry richness and how it is structured in space. Furthermore, we can now test for correlation between environmental factors depicting the local complexity of the available niche spaces and the extent of the local convergence of aposematic patterns (i.e., how much there is a higher or lower mimicry diversity than expected from the local number of species).

The theory predicts that the number of local mimicry patterns should saturate once all available niche spaces are occupied by distinct set of predators and prey (Gompert *et al.* 2011). Indeed, the global trend observed in ithomiine across 19,271 communities predicted from SDMs in 30 km × 30 km grid cells throughout the Neotropics (see **Chapter 1**) depicts the beginning of a saturation of local mimicry patterns as the number of species keeps increasing (**Fig. 9**). While the number of mimicry rings represented increase sharply across species-poor communities where we can presume that not all microhabitats are saturated, mimicry richness seems to increase more slowly across species-rich communities where most ecological dimensions may be occupied. However, this 'saturation effect' has not (yet) reached the asymptote, hinting that even in the richest communities, there may be still some perceptual/ecological/environmental space available for the emergence or colonization of new aposematic patterns. Alternatively, this pattern could support the idea that purifying selection acting against the emergence/colonization of new aposematic patterns is weaker than previously thought, or simply slower to act than the processes generating taxonomic diversity (Joron & Mallet 1998).

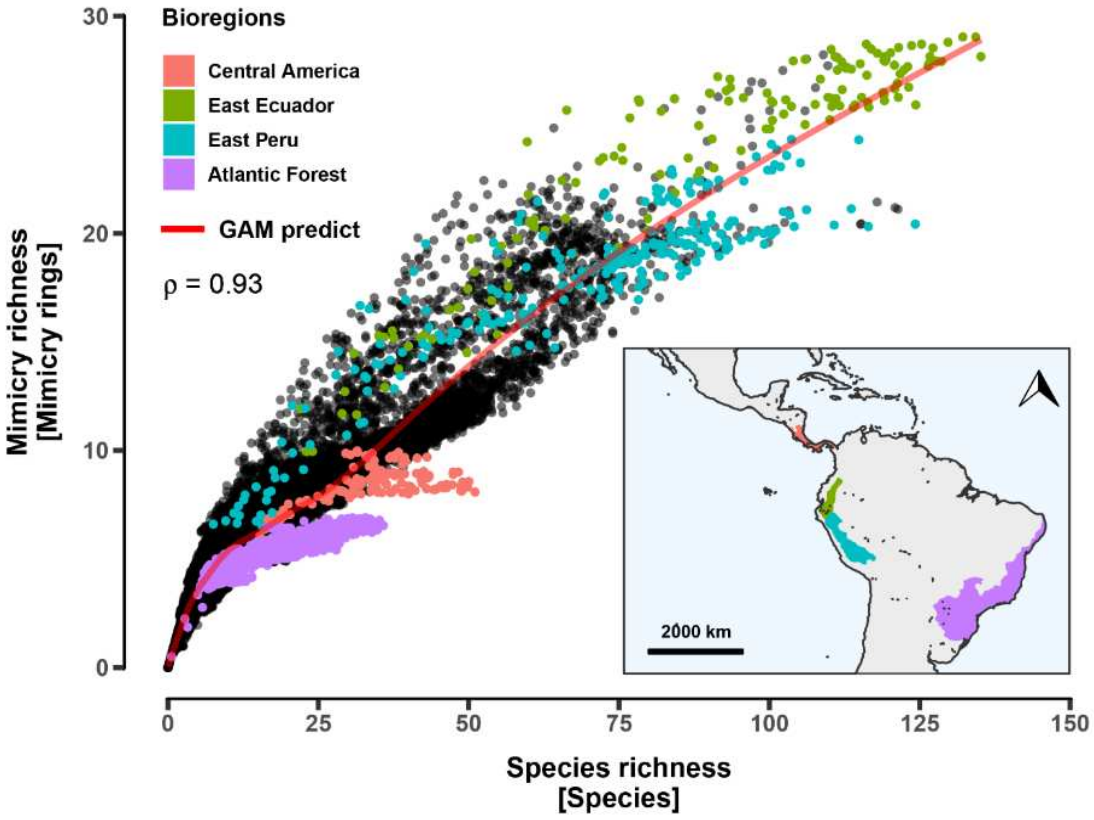

Figure 9: Relationship between predicted mimicry richness and predicted species richness among four bioregions. Each point represents a community as a 30 km × 30 km grid cell on the map. Four remarkable bioregions with patterns deviating from the overall trend are highlighted with colored points and shown on inset map with associated color. Black points correspond to all the other bioregions. ρ = Spearman's spatial rank correlation coefficient across all communities. Smooth red line represents the overall trend as predicted from a Generalized Additive Model. Points below the curve demonstrate lower levels of mimicry richness than expected from their species richness, and conversely.

Interestingly, the global 'saturation' trend in not homogenous and particular bioregions in the Neotropics, as defined by Olson *et al.* (2001), display a relationship between species and mimicry richness significantly divergent from the bulk of communities (**Fig. 9 & 10**). In particular, communities in the Brazilian Atlantic forest (BAF) and Central America (CA) show a strong saturation effect that appears to have reached a plateau of mimetic richness (**Fig. 9:** dots in red for CA, dots in purple for BAF). Such saturation produces lower levels of mimicry richness than expected relatively to their species richness, compared to other regions (**Fig. 9 & 10**; Wilcoxon tests: BAF: $W = 27 \times 10^6$, $p < 0.001$; CA: $W = 2.1 \times 10^6$, $p < 0.001$). Among species richness hotspots found on the eastern slopes of the Andes, the saturation effect seems less prominent. However, communities found in Peru were predicted to present lower mimicry richness than those found in Ecuador for similar species richness (**Fig. 9 & 10**; Wilcoxon test, $W = 32{,}564$, $p < 0.001$), highlighting regional differences in the size of local mimicry rings.

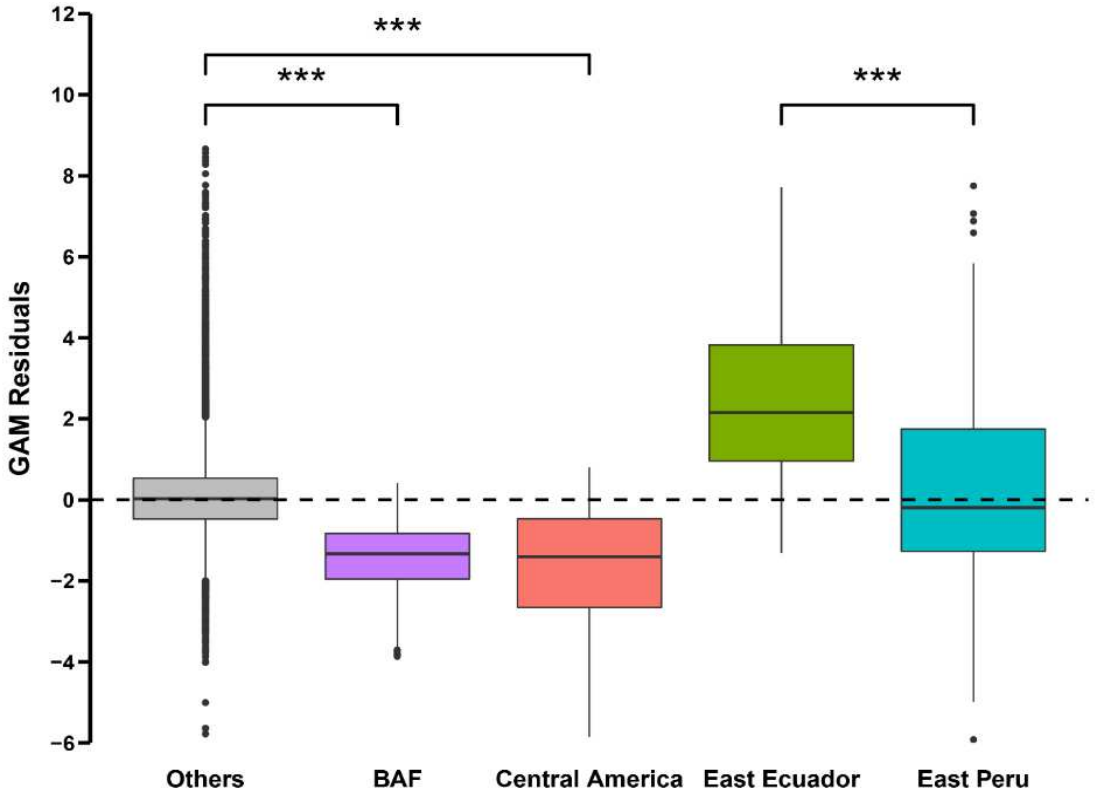

Figure 10: Comparison among bioregions of residuals from GAM fitting the relationship between mimicry richness and species richness. Residuals higher than zero correspond to communities with higher mimicry richness than expected from their species richness based on values observed among all communities. Conversely, residuals lower than zero correspond to communities with lower than expected mimicry richness. BAF = Brazilian Atlantic Forest. Asterisks represent the significance (i.e., $p < 0.001$) of pairwise comparisons between bioregions evaluated with pairwise Wilcoxon tests.

3.2 Hypotheses for mechanisms as directions for future investigations

This spatial structuration of the relationship between mimicry and species richness leading to significant differences across bioregions points to underlying assembly mechanisms that are also spatially structured at the continental scale. Here, I discuss several hypotheses relating to geographic, historical, ecological, and behavioral processes, that could act jointly to explain such a striking pattern.

A first possible explanation for the differences predicted among bioregions in the relationship between mimicry and species richness may lie in differences in habitat and topographic heterogeneity found within each community represented here by 30 km × 30 km grid cells. Indeed, partitioning of predators in a mosaic of habitats can lead to selection for different color patterns in each of these habitats and thus help maintain mimicry diversity (Gompert *et al.* 2011; Willmott *et al.* 2017; Birskis-Barros *et al.* 2021). Thus, areas with higher

topographic and habitat heterogeneity could favor the co-existence of higher richness in aposematic patterns if the local diversity of predators and prey is segregated among those habitats. As a preliminary analysis for this hypothesis, I compared levels of topographic ruggedness (TRI, Riley *et al.* 1999), presumed to favor habitat heterogeneity, between the four bioregions displaying a notable pattern. I showed that, contrary to predictions, the eastern Andean slopes present higher topographic heterogeneity in Peru than in Ecuador, despite hosting less mimicry rings for a similar species richness (**Fig. 11**; Wilcoxon test, $W = 12{,}782$, $p < 0.001$). Similarly, topographic heterogeneity could not explain the lower than expected mimicry richness predicted in Central America and the Brazilian Atlantic forest. Again, contrary to predictions, those bioregions harbored significantly higher topographic ruggedness than the rest of the communities, mostly represented by the relatively flat Amazonian basin which despite this topographic homogeneity harbors higher mimicry richness for a similar species richness (**Fig. 11**; Wilcoxon tests: BAF: $W = 25 \times 10^6$, $p < 0.001$; CA: $W = 2.1 \times 10^6$, $p < 0.001$). In first approximation, it seems that differences in landscape heterogeneity cannot explain differences in the intensity of the mimicry saturation effect observed across bioregions. However, further studies involving for instance habitat heterogeneity based on vegetation indices (e.g., Tuanmu & Jetz 2015), which may better describe the degree of structuration of local predator and prey communities, are still needed to assess thoroughly this hypothesis.

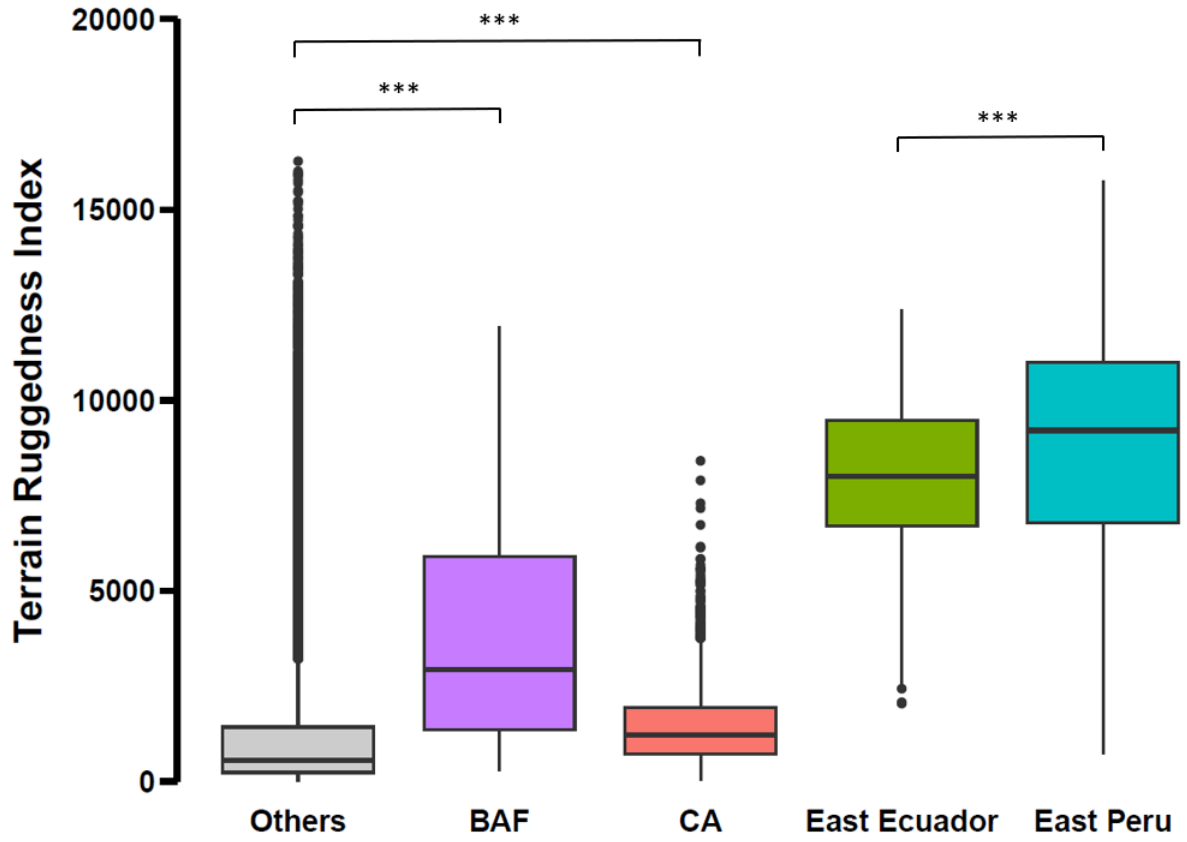

Figure 11: Comparison of topographic heterogeneity measured as the Terrain Ruggedness Index (TRI, Riley *et al.*, 1999) among bioregions. Asterisks represent the significance (i.e., $p < 0.001$) of pairwise comparisons between bioregions evaluated with pairwise Wilcoxon tests. Only the three comparisons of interest discussed in the text are showed. BAF = Brazilian Atlantic Forest. CA = Central America.

A second hypothesis to explain regional heterogeneity in the pattern of mimicry saturation focuses on a smaller spatial scale. Indeed, we already know that local mimicry richness is favored via the segregation of predators and prey along multiple ecological dimensions at local scale such as nocturnal roosting habitat height (Mallet & Gilbert 1995), flight height (Beccaloni 1997b; DeVries *et al.* 1997), and forest structures (Elias *et al.* 2008). Possibly, differences in forest microhabitat complexity could vary between bioregions and be a driver of differences in mimicry saturation. For instance, the high dense and complex forest of the Amazon basin could present a higher availability of microhabitats than the sparser forests of the Brazilian Atlantic coast or Central America. This hypothesis seems complex to test at large spatial scales, yet proxies such as local plant diversity and particularly forest height, linked to segregation among nocturnal roosting habitats and flight height, are readily available for continental scale exploration (Ter Steege *et al.* 2013; Potapov *et al.* 2021).

Third, the biogeographic history of the group could affect the pattern of mimicry saturation. Ithomiine butterflies are suspected to have emerged from the eastern slopes of the Andes (Chazot *et al.* 2019b) where their current hotspots of taxonomic and mimetic diversity lie (see **Chapter 1**). Following the cradle hypothesis, older communities would harbor higher species diversity, but also higher mimetic diversity, having benefited for more evolutionary time to witness both the local emergence of new patterns, and being colonized by species with initially foreign patterns (Kunte *et al.* 2021). As such, Andean communities may have benefited from more evolutionary time, as well as a central position for dispersal exchanges and multiple recolonizations (Chazot *et al.* 2016a). On the contrary, communities in Central America and the Atlantic forest lie on the outer range of Ithomiini distribution, and were more recently colonized (ca. 8-10 My; Chazot *et al.* 2019). Therefore, they have had less time to allow new mimicry rings to get established, while their relative isolation from other regions could have limited the recurrent permeation of other spatially distant mimicry rings, similarly to what is described in the relatively phenotypic-poor mimetic communities of butterflies in the Western Ghats in India (Joshi *et al.* 2017). However, in the context of mimicry, more time can also imply more opportunity for purifying selection to act on rare patterns and lead to more mature communities with fewer mimicry rings in the end. Moreover, the age hypothesis does not explain differences recorded between Peru and Ecuador. Further investigations based on joint inferences of ancestral ranges, colonization events and ancestral aposematic patterns are needed to clarify the picture.

Fourth, the characteristics of the prey species found in the different regional assemblages could influence the size of local mimicry rings, thus the spatial pattern of mimicry saturation. For instance, the level of prey defense abilities (e.g., toxicity and unpalability) can strongly affect the mimetic composition of communities. A highly defended prey is expected to trigger a faster associative learning and a stronger rejection of its aposematic pattern from predators (Goodale & Sneddon 1977; Lindstrom *et al.* 1997; but see Chouteau *et al.* 2019). As such, this species would benefit from an enhanced protection umbrella, offering a more efficient protection that potentially cover more species as predator would tend to generalize the aposematic pattern (Kunte *et al.* 2021). As a consequence, if the local prey community is mostly composed of highly unpalatable species, local mimicry rings may encompass more species than in community with mildly-defended models. In addition, the high availability of alternative prey is known to impose a relaxed selection on aposematic patterns since predators have less incentive to efficiently detect (un)palatable prey (Getty 1985; Lindström *et al.* 2004), leading

to potentially higher number of local mimicry rings with lesser degree of pattern convergence (Kunte *et al.* 2021).

Finally, the characteristics of predators found in the different regional assemblages could also affect the mimicry saturation effect. A higher diversity of predators implies higher diversity of perceptual systems potentially diverging in their ability to perceive and select specific aposematic patterns, leading to more discrete adaptive peaks in the perceptual space (see **Chapter 3**) associated with more local mimicry rings. For instance, the lower diversity in velvet ants' mimicry rings in Africa compared to North America has been attributed to lower diversity in predators and lower environmental heterogeneity (Wilson *et al.* 2018). The degree of generalization (i.e., to which extent species showing imperfect mimicry will be considered as a similar type of prey) can also vary among predators (Dittrich *et al.* 1993). As such a predator community composed mostly of acute predators with high discriminative abilities would potentially select for more mimicry rings than a community of predators with poorly discriminative predators.

Altogether, all factors, i.e., (1) regional and (2) local structuration, (3) age of communities, and ecological and behavioral characteristics of prey (4) and predators (5) could affect the assembly of mimetic species and the large-scale spatial heterogeneity observed in the relationship between species and mimetic richness. Most hypotheses remain to be investigated in ithomiine butterflies, and further so in other mimetic clades such as the heliconiines to disentangle between all possible factors at play and support the emergence of general assembly rules for mimetic communities. To this end, large-scale maps of taxonomic and mimetic biodiversity that allow to predict local community composition, such as those produced for ithomiines during this research work, offer an ideal sandbox to play around the question of species assembly at large spatial scale in the context of mimetic interactions.

4 Neotropical mimetic butterflies facing global changes

In **Chapter 1**, I identified areas of evolutionary and ecological importance for conservation based on hotspots of several facets of biodiversity in ithomiine butterflies, and I evaluated their overlap with current anthropogenic threats. I showed that tropical montane forests that host high species and mimetic diversity as well as rare species and mimicry rings appear particularly under threat. I also pointed out that remote parts of the Upper Amazon may act as refuges against current anthropogenic pressures for a limited portion of Ithomiini

diversity. However, it is likely that the current threat status of these regions will worsen with ongoing climate change and deforestation (Nobre *et al.* 2016; Armenteras *et al.* 2017; Bax *et al.* 2019; Escobar 2020), making these refugia potentially irrelevant in the near future (Keppel *et al.* 2015). Here, I want to emphasize on the consequences such changes could have on mutualistic communities as neotropical Müllerian mimetic butterflies and outline possible analyzes to predict if not prevent them.

4.1 Biodiversity hotspots in the Neotropics at risk

Climate change is one of the six main anthropogenic threats on biodiversity identified by the Intergovernmental Science-Policy Platform on Biodiversity and Ecosystem Services (IPBES) alongside habitat changes and fragmentation, direct exploitation, pollution, invasive alien species, and disease outbreaks (IPBES 2019a). It is affecting ecosystems and the living beings they host worldwide, perturbating biogeochemical cycles (Cusack *et al.* 2016; Mitchard 2018), converting habitats (Franklin *et al.* 2016; Segan *et al.* 2016), and triggering massive species dispersal following the displacement of their environmental envelop, and species extinction when the latter fail to follow up (Parmesan & Yohe 2003; Rosenzweig *et al.* 2008; Pecl *et al.* 2017; Nunez *et al.* 2019).

This threat is particularly prominent for species found in tropical mountainous regions which encompasses most of biodiversity hotspots on Earth, with the tropical Andes falling at the top seat (Myers *et al.* 2000; Hutter *et al.* 2017). Indeed, numerous well-studied plant and tetrapod groups show a peak of diversity and endemism in the western part of Amazonia and in the Andean foothills (Ter Steege *et al.* 2003; Grenyer *et al.* 2006; Morawetz & Raedig 2007; Kier *et al.* 2009; Jenkins *et al.* 2013; Roll *et al.* 2017; Gumbs *et al.* 2020). Among insect taxa, Cicindelinae beetles (Pearson & Carroll 2001), Adelpha butterflies (Mullen *et al.* 2011), Nymphidiina butterflies (Hall 2018), Heliconiini butterflies (Rosser *et al.* 2012; Pérochon *et al.* 2023; see **ANNEXE 6**) and, as showed in this research work, ithomiine butterflies (see **Chapter 1**), all show peaks of diversity in the Tropical Andes.

The outstanding biodiversity found in the tropical mountainous regions in general, and in the Tropical Andes in particular, is mostly explained by geological and climatic factors. The topographical complexity of recent mountain regions facilitates fine-spatial scale variation of environmental conditions and provides more opportunities for parapatric and allopatric speciation fueled by adaptive radiations across the diversity of environmental niches available (Särkinen *et al.* 2012; Bouchenak-Khelladi *et al.* 2015; Rangel *et al.* 2018). Moreover, Tropical

Andes have benefited from a relative historical climatic stability thought to reduce species extinction rate (Fine 2015) and allowing for the long-term persistence of high levels of species diversity and endemism (Araújo *et al.* 2008; Svenning *et al.* 2015; Harrison & Noss 2017). Meanwhile, current seasonal and diurnal climate variations in tropical mountain ranges are also relatively low, particularly in forested landscapes (Trew & Maclean 2021). This current climatic stability, combined with long-term stability and steep environmental gradients, permitted the accumulation of rare range-restricted species with narrow climatic niches and physiological tolerances (Kozak & Wiens 2010b; Antonelli 2015; Pintanel *et al.* 2019; Zuloaga *et al.* 2019).

As a consequence, an important proportion of species found in tropical mountains are poorly equipped to survive future climate changes with a low adaptive potential for climatic niche evolution (Harrison & Noss 2017; Saupe *et al.* 2019; Trew & Maclean 2021), and restricted geographic ranges making them particularly vulnerable (Malcolm *et al.* 2006; Ohlemüller *et al.* 2008; Mccain & Colwell 2011). Ironically, the geographic and environmental barriers that fueled diversification in the past now appear as obstacles to dispersal, impeding the abilities of most species to track climate changes. Indeed, mountainous species facing the extirpation of their climatic niche may suffer from the lack of available areas to disperse upward if they happen to be stuck at the top of a mountain range or in isolated valleys (Ohlemüller *et al.* 2008; Raxworthy *et al.* 2008; La Sorte & Jetz 2010). In addition, human activities above the tree line, such as cattle grazing and burning in the Andes, may prevent upslope dispersal, thereby increasing extinction risks (Peres *et al.* 2010).

Overall, species inhabiting hyper-diverse tropical mountain regions, many with narrow ranges, low adaptive potential for their climatic niche and limited dispersal opportunities, are likely to be exceptionally vulnerable to climate change (Laurance *et al.* 2011; Trew & Maclean 2021).

4.2 Müllerian mimetic communities at risk

Ithomiine and heliconiine butterflies are found throughout all the Neotropics, but their main hotspots of diversity are found in the Tropical Andes (see **Chapter 1**). Beyond being subjected to all the challenges associated to tropical mountain species, they also have to deal with the specificities of being mimetic in the face of global changes.

Müllerian mimicry represents mutualistic interactions since mimetic species benefit mutually from co-occurring by sharing the cost of educating local predators to avoid their

aposematic patterns (Sherratt 2008). Such positive interactions are beneficial for the individuals involved, allowing for instance to compensate for negative effects of competition (Aubier & Elias 2020), and fueling higher local richness (Gross 2008; Aubier *et al.* 2017). However, when mutualistic interactions are lost due to species extinction or community disassembly while facing global changes, their disappearance can fragilize the community stability and potentially trigger local extinction cascades (Dunn *et al.* 2009; Vidal *et al.* 2019). Since Müllerian mimetic species rely on local mutualistic interactions with co-mimics and host plants, the threat of community disassembly due to climate change is even more profound for them (Toby Kiers *et al.* 2010; Sheldon *et al.* 2011).

Moreover, the dispersal abilities of Müllerian mimetic species are impeded by the purifying selection acting on individuals harboring unknown phenotypes in the newly colonized areas. Indeed, local naïve predators that have not yet learnt to avoid a new aposematic pattern will apply stronger predation pressures on this rare phenotype and prevent its establishment in the community (Mallet & Barton 1989; Langham 2004). As a consequence, I showed that comimetic species of ithomiines display a significant spatial association throughout their ranges, beyond what could be expected from their phylogenetic relatedness. Similarly, comimetic species exhibit significant convergence in their climatic niches (see **Chapter 4**). Such pattern of niche convergence may limit community disassembly to a certain extent by allowing congruent dispersal trajectories in the face of climate change (**Fig. 12**). However, I also showed that climatic niche overlap between comimetic species is hardly ever complete (see **ANNEXE 5, *SI Appendix 9***). Moreover, despite relatively similar climatic niche optima, tolerance to climate change and extremes, as well as species dispersal abilities, may still differ among comimetic species, limiting opportunities for co-dispersal trajectories and leading to community disassembly (**Fig. 12**). Finally, the effects of climate change on biotic factors that affect local abundance, such as hostplants (Willmott & Mallet 2004) and parasitoids (Gentry 1998), may also differ among interacting species.

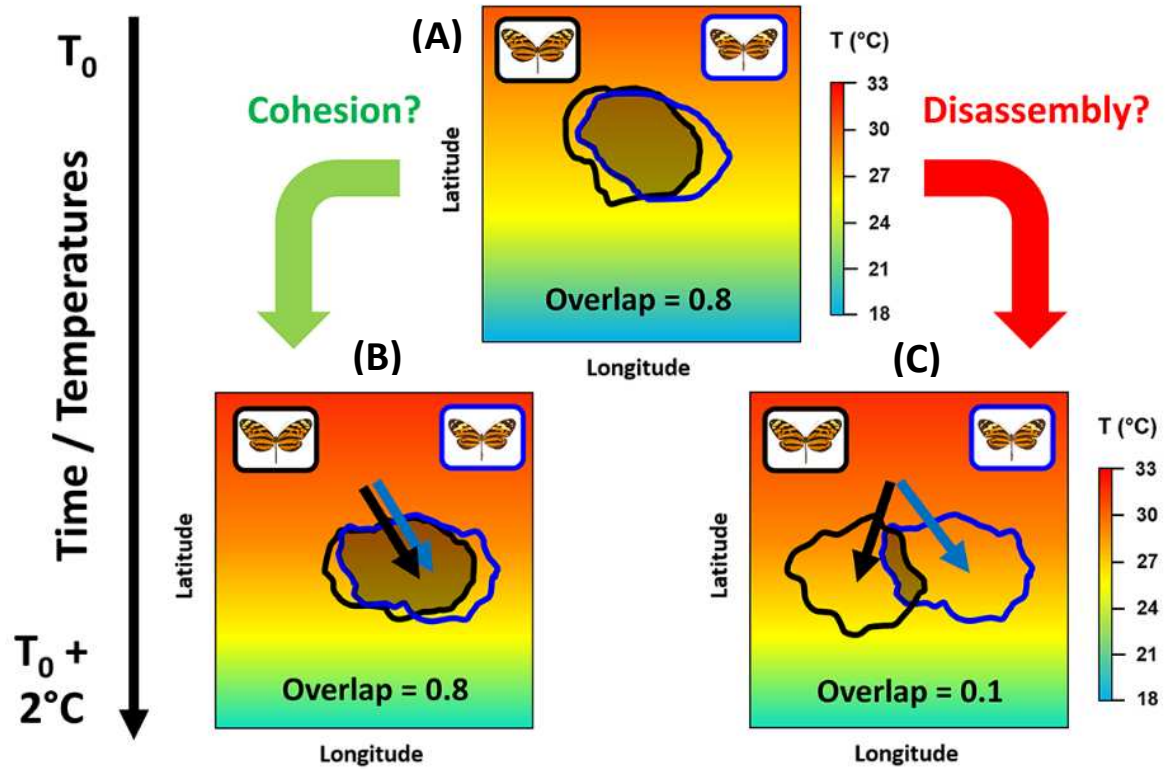

Figure 12: Two alternative scenarios for mimetic communities facing climate changes. (A) At T_0, the two mimetic species display a relatively important spatial overlap where they benefit from co-occurring. Following the increase of temperature and the migration of their environmental envelops southward, they demonstrate at T_0 + 2°C **(B)** joint dispersal trajectories ensuring the preservation of their spatial overlap, thus their mutualistic interactions in accordance with their niche similarity **(C)** diverging dispersal trajectories leading to the discrepancy of their spatial overlap, thus mutualistic interactions, illustrating the disassembly of the mimetic communities due to many factors including differences in tolerance to climate change and extremes, dispersal abilities, and/or availability of host plants.

Altogether, the consequences of climate changes on Müllerian mimetic communities remain uncertain. They form tightly coevolved assemblages tied by positive interactions, making them particularly vulnerable to global environmental changes (Tylianakis *et al.* 2008). However, the convergence of climatic niche among comimetic species may offer (limited) opportunities for congruent dispersal trajectories that would partly prevent community disassembly. This uncertainty stresses the need to produce predictions for future species distributions in order to better support the identification of refuge areas for biodiversity conservation that are resilient to climate changes (Keppel *et al.* 2015). Such predictions would ideally include species interactions in the modeling framework to account for the specificities of mutualistic communities illustrated by Neotropical mimetic butterflies (Brooker *et al.* 2007; Toby Kiers *et al.* 2010; Tylianakis *et al.* 2010; Staniczenko *et al.* 2017).

4.3 Species distribution modeling to the rescue?

In order to produce predictions for future species distributions of species involved in mimetic communities such as ithomiine and heliconiine butterflies, species distribution models (SDMs) appear as an ideal tool. In this research work, I employed SDMs to predict current distributions of ithomiines linking georeferenced occurrences data with current environmental conditions. Next avenue for this research agenda is to build upon such models to predict future distributions under several scenarios for climate changes associated with different Shared Socioeconomic Pathways (SSPs) depicting future global socioeconomic trajectories for the World and their impact on greenhouse gas emission (O'Neill *et al.* 2017). Each SSP typically involve predictions regarding regional demographic trends, energy consumption and economic growth, resulting, among other things, in increases in mean global temperature compared to pre-industrial levels. The most optimistic (and highly unlikely) scenario combining proactive environmental policies and sustainable production and consumption is labeled 'SSP1-1.9' and predicts temperature increases ranging from 1 to 1.8°C for the horizon 2100. The middle-of-the-road scenario labeled 'SSP2-4.5' implying some advances in the sustainability of our economic model, foresees an increase between 2.1°C to 3.5°C for 2100. The currently most likely scenario of rapid economic growth and low environmental regulation, labeled 'SSP5-8.5', leads to temperature increases ranging from 3.3°C to 5.7°C. Coupled with a set of General Circulation Models (GCMs) simulating the behavior of Earth's global climate system, aggregated and coordinated in the CMIP6 initiative (Eyring *et al.* 2016), it is now possible to produce sets of predictions under the different socioeconomic narratives integrating modeling uncertainty to multiple levels (Thuiller *et al.* 2019).

The most straightforward use for SDMs is to map changes is species richness across several scenarios (**Fig. 13.A-B**). Although, it is virtually possible to map changes in every facets of biodiversity (i.e., taxonomic, phylogenetic, mimetic, phenotypic, etc.) at different time-steps and for any given SSPs allowing to refine the identification of 'refuge' areas for biodiversity accounting for resilience to climate changes (Keppel *et al.* 2015). Interestingly in the context of mimetic communities, SDMs allow to predict and map changes in community composition. For instance, using Non-Metric Multidimensional Scaling methods, it is possible to represent in the same 2D space the dissimilarity in species and/or mimetic composition across current and future communities in order to highlight changes in community composition, detect the ones that will likely disappear, and foresee the assembly of new communities (**Fig. 13.C**). Moreover, it seems accessible to design a metric of global co-cooccurrence between mimetic

species (such as a mean spatial overlap computed with Schoener's D, see **Chapter 3**), and to plot its evolution across time-steps and scenarios (**Fig. 13.D**). Such analysis would provide a strong visual to assess and alert on the risks of community disassembly across mimetic, and more generally mutualistic communities.

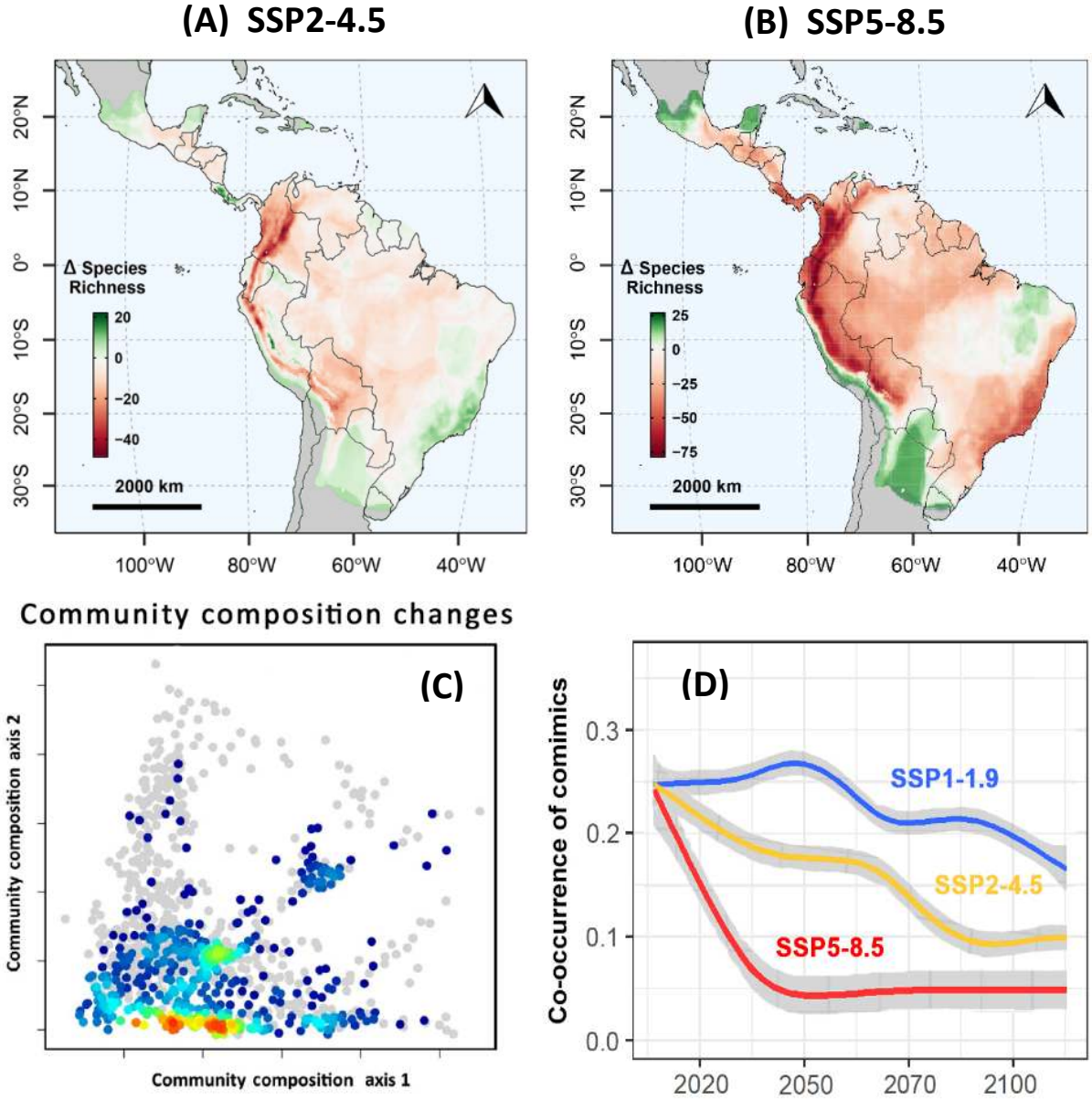

Figure 13: Illustrations of the potential of SDMs to predict changes in local species richness (A-B), community composition (C) and investigate the disassembly of mimetic communities (D). (A) Hypothetical changes in ithomiine species richness according to the most optimistic scenario SSP2-4.5 **(B)** Hypothetical changes in ithomiine species richness according to the most pessimistic scenario SSP5-8.5. **(C)** Hypothetical changes in community composition based on NMDS plot with color gradient representing the density of future communities with similar species and/or mimicry composition, and grey dots reflecting current composition that are not to be found in the future. Modified from Brown *et al.* (2020). **(D)** Hypothetical evolution of the index quantifying co-occurrence between co-mimetic species,

illustrating the degree of disassembly of mimetic communities according to several SSPs. All maps and graphs are illustrative and based on simulated made-up data. They do not represent real predicted trends.

Finally, a next generation of SDMs is currently paving the way to the direct integration of ecological interactions into the modeling framework. Joint Species Distribution Models (J-SDMs) offer to bridge the gap between community ecology and macroecology by providing a statistical framework to model the distribution of multiple species simultaneously while accounting for potential ecological interactions and environmental covariates (Pollock *et al.* 2014; Ovaskainen & Abrego 2020). As such, in a context of mimicry, they would theoretically allow to model simultaneously all species in the group of interest and highlight the competitive or mutualistic interactions at play depending on the sharing or not of aposematic patterns. Additionally, J-SDMs provide solutions to refine future projections by accounting for the exclusive or facilitative effects of the presence or absence of mimetic interactions between species on future distributions. These models are still in development and are, to my knowledge, mostly limited to hierarchical-GMM frameworks such as the HMSC (Ovaskainen *et al.* 2017). Such models do not provide (yet?) the flexibility in response curves I was aiming for my modeling approach, neither do they have (yet?) the ability to deal properly with low sampling data. However, they open an interesting perspective for the study of the fate of Neotropical mimetic butterflies, and ecological communities in general, under the ongoing climate changes.

SDMs are a powerful tool for researchers to open windows on the impacts of climate changes on biodiversity. They can be applied to design conservation status for species based on the IUCN Red List criteria (Gomes *et al.* 2019; IUCN 2020), or to generate powerful visuals of global biodiversity trends across socio-economic scenarios as a roadmap to follow or not as a globalized civilization (IPBES 2019a). Overall, they can be used to convey powerful narratives that alert the scientific community and ideally the public opinion, but without international political will and important adjustments to the current capitalist and productivist socio-economical paradigm, they will not yield real positive conservation outcomes.

ANNEXE 1

Supplementary Information for CHAPTER 1

Supplementary Information for

Anthropogenic pressures coincide with Neotropical biodiversity hotspots in a flagship butterfly group

Maël Doré[1,2], Keith Willmott[3], Boris Leroy[4], Nicolas Chazot[5], James Mallet[6], André V. L. Freitas[7], Jason P. W. Hall[8], Gerardo Lamas[9], Kanchon K. Dasmahapatra[10], Colin Fontaine[2], and Marianne Elias[1]

[1]*Institut de Systématique, Evolution, Biodiversité, MNHN-CNRS-Sorbonne Université-EPHE-Université des Antilles, Muséum national d'Histoire naturelle de Paris, 45 Rue Buffon, 75005, Paris, France*

[2]*Centre d'Ecologie et des Sciences de la Conservation, UMR 7204 MNHN-CNRS-Sorbonne Université, Muséum national d'Histoire naturelle de Paris, 45 rue Buffon, 75005, Paris, France*

[3]*McGuire Center for Lepidoptera and Biodiversity, Florida Museum of Natural History, University of Florida, Gainesville, FL, United States of America*

[4]*Unité Biologie des Organismes et Ecosystèmes Aquatiques (BOREA UMR 7208), Muséum National d'Histoire Naturelle, Sorbonne Universités, Université de Caen Normandie, Université des Antilles, CNRS, IRD, Paris, France*

[5]*Swedish University of Agricultural Sciences, Uppsala, Sweden*

[6]*Dept of Organismic and Evolutionary Biology, Harvard University, Cambridge, MA, United States of America*

[7]*Departamento de Biologia Animal and Museu da Biodiversidade, Instituto de Biologia, Universidade Estadual de Campinas, 13083-862 Campinas, São Paulo, Brazil*

[8]*Department of Entomology, National Museum of Natural History, Smithsonian Institution, Washington, DC 20560-0127, United States of America*

[9]*Museo de Historia Natural, Universidad Nacional Mayor de San Marcos, Lima, Peru*

[10]*Dept of Biology, University of York, Wentworth Way, Heslington, UK*

Appendix 1: Data sampling and bioregions

We compiled from multiple sources an initial dataset of 28,986 georeferenced occurrences of 388 ithomiine butterfly species in their natural habitats, out of the 396 known species (**Fig. S1.1a**). The dataset spans across 25 countries and many bioregions of the Neotropics (**Fig. S1.4**). It provided 19,271 species-grid-cell records for distribution modeling after removing duplicate records from single grid cells, which are available from Zenodo at 10.5281/zenodo.4696055. Data come from fieldwork data obtained by the authors over the past decades, and records from over 60 museums and private collections detailed in the online archive metadata.

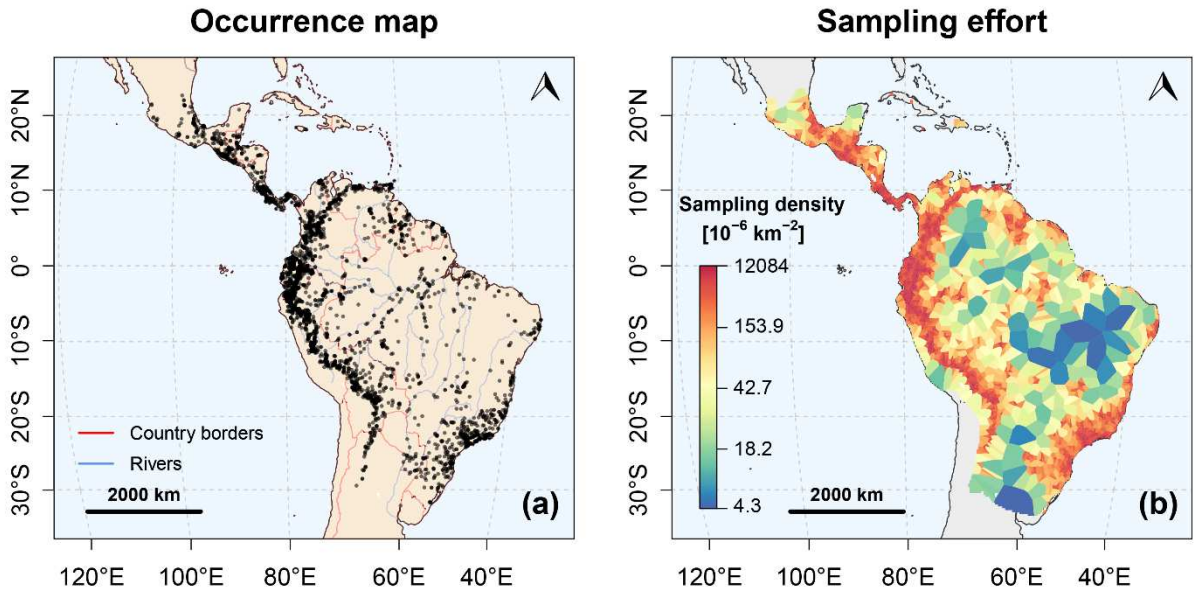

Figure S1.1: Occurrences and sampling effort of Ithomiini butterflies. (a) 28,986 georeferenced occurrences of Ithomiini recorded in their natural habitats in the Neotropics, encompassing 388 ithomiine butterfly species among the 396 known species. (b) Sampling effort illustrated as sampling density within Thiessen polygons. Each polygon is associated with a single sampling site and represents the area that is closer to the focal one than any other sample site. Color scale follows Jenks natural breaks.

Sampling effort is heterogeneous in geographical space and is higher in regions known for their high diversity and environmental heterogeneity, such as the Andes and Central America (**Fig. S1.1b**). As a result, sampling effort in environmental space is strongly correlated with the distribution of available environmental conditions in the Neotropics (**Fig. S1.2**) and reduces potential bias, due to sampling heterogeneity, in species distribution models based on such environmental conditions.

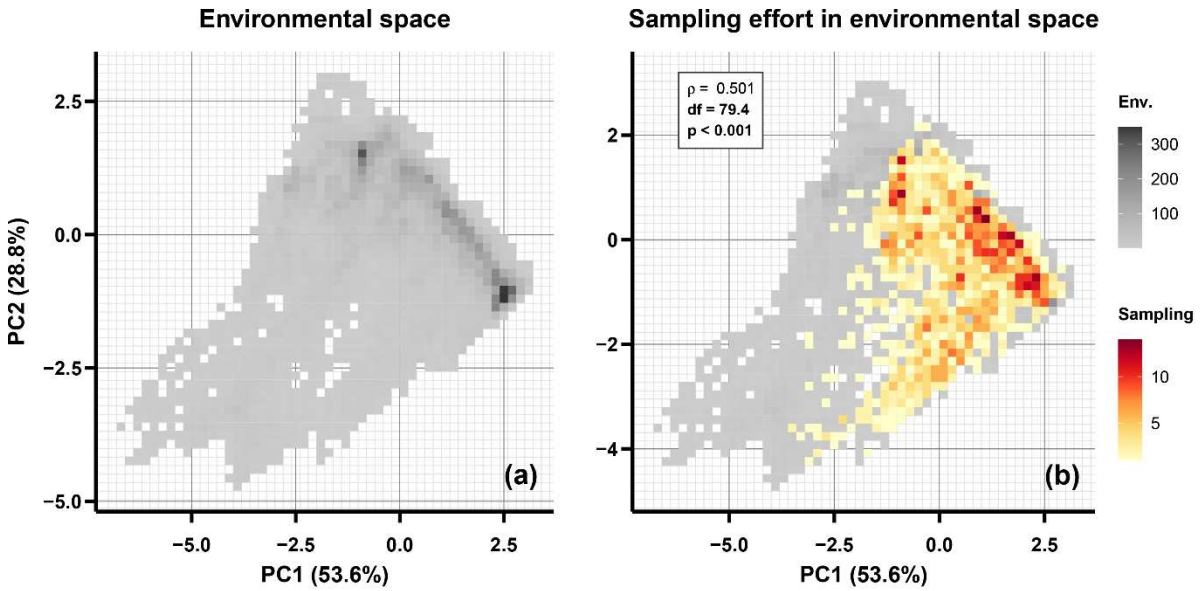

Figure S1.2: Sampling effort in environmental space. (a) Distribution of the 24 986 grid cells in the two first axes of the environmental space resulting from PCA. (b) Overlay of the distribution of the 1718 grid cells with Ithomiini occurrences in environmental space. Both distributions are strongly correlated (Spearman's rho = 0.501; df = 79.4 ; p < 0.001).

Additionally, we mapped sampling completeness as the proportion of species recorded in our dataset relative to the species richness estimated via bootstrap in each region (Smith & van Belle 1984), for 10° grid cells and for bioregions (**Fig. S1.3**). At the global scale, bootstrap estimates predicted 395.3 species, close to the 396 known species, for a completeness of 98.4%. We estimated an average completeness of 91.5 ± 6.5% within 10° grid cells, ranging from 77.1% to 100%. In parallel, we recorded an average completeness of 91.9 ± 4.7% within bioregions, ranging from 85.3% in the Chaco region to 98.9% in the Atlantic Forest.

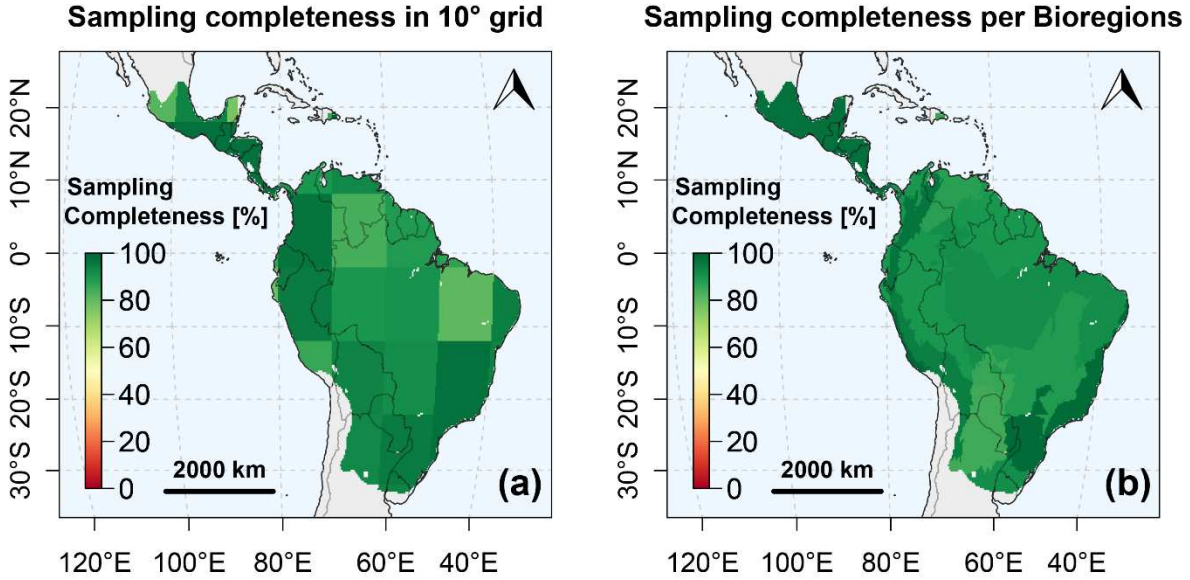

Figure S1.3: Sampling completeness. Proportion of species recorded in each region relative to the species richness estimated via bootstrap (Smith & van Belle 1984). (a) Sampling completeness within grid cells at 10° resolution. (b) Sampling completeness within bioregions.

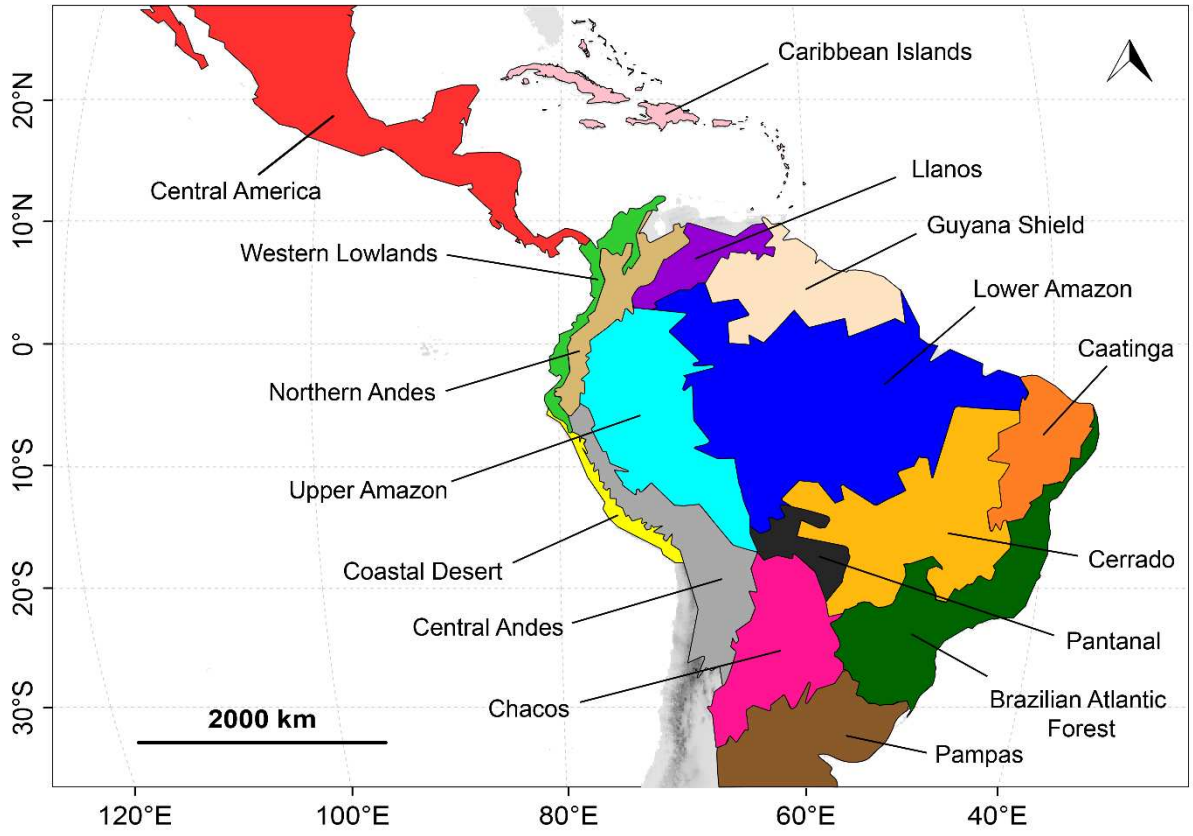

Figure S1.4: Map of bioregions cited throughout the manuscript and encompassing the range of Ithomiini, based on the aggregation of terrestrial ecoregions defined by Olson et al. (2001). Upper Amazon = Western Amazon. Lower Amazon = Central and Eastern Amazon.

Reference:

Olson, D. M., Dinerstein, E., Wikramanayake, E. D., Burgess, N. D., Powell, G. V. N., Underwood, E. C., Amico, J. A. D., Itoua, I., Strand, H. E., Morrison, J. C., Loucks, J., Allnutt, T. F., Ricketts, T. H., Kura, Y., Lamoreux, J. F., Wesley, W., Hedao, P., & Kassem, K. R. (2001). Terrestrial Ecoregions of the World: A New Map of Life on Earth: A new global map of terrestrial ecoregions provides an innovative tool for conserving biodiversity. *BioScience*, 51(11), 933–938. https://doi.org/https://doi.org/10.1641/0006-3568(2001)051[0933:TEOTWA]2.0.CO;2

Smith, E. P., & van Belle, G. (1984). Nonparametric estimation of species richness. *Biometrics*, 119-129.

Appendix 2: Mimicry ring classification of Ithomiini

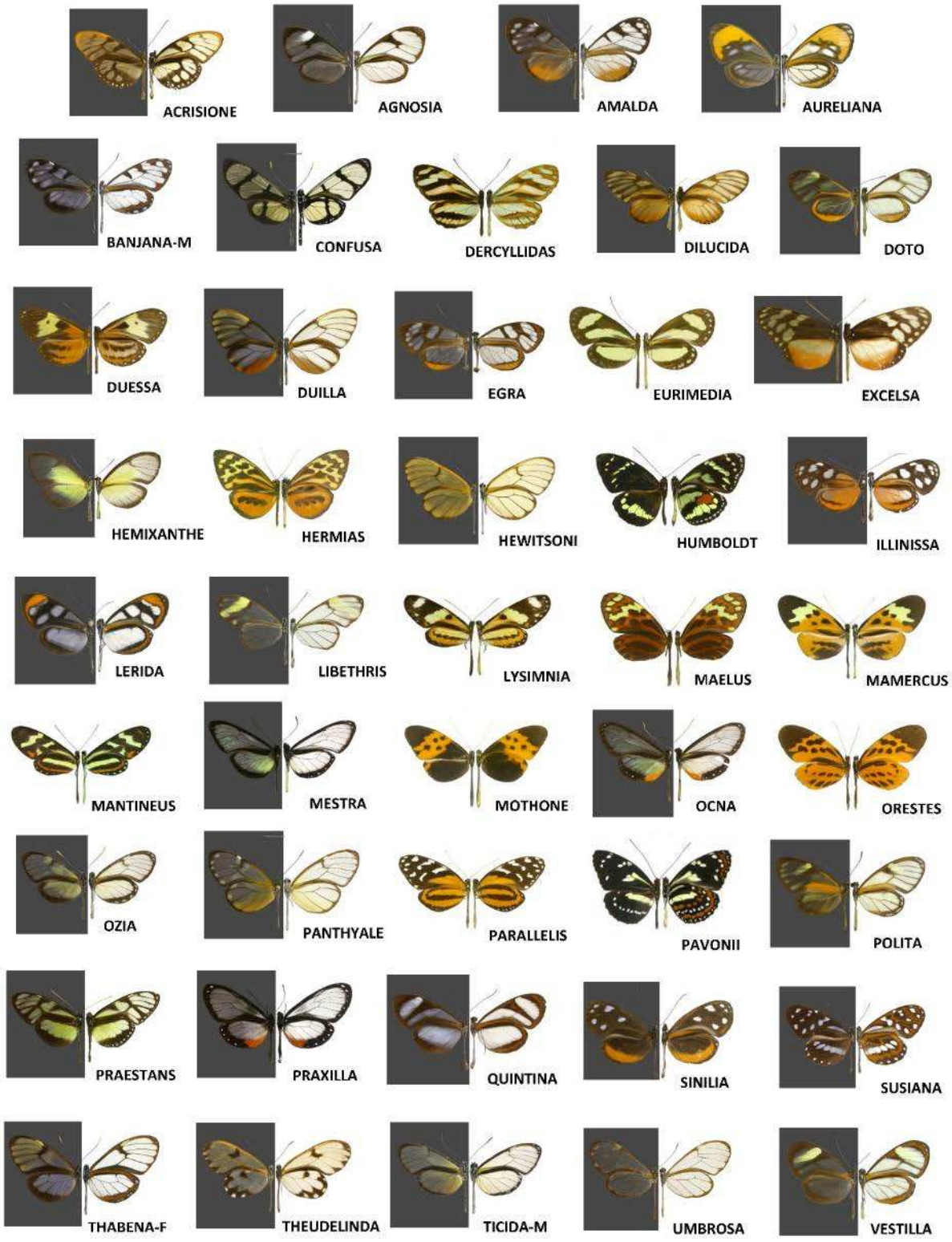

Figure S2.5: Illustration of mimicry ring classification for Ithomiini butterflies by Keith Willmott. Wing patterns are classified under 44 groups defined as mimicry rings. Dorsal view is shown on the left side against a dark background to highlight transparency when present. Ventral view is shown on the right side.

We based the nomenclature of mimicry rings on the epithet of the "type-taxa" chosen to represent each mimicry ring pattern. Suffix ‘M’ for males or ‘F’ for females is added when the pattern is displayed only by one sex. Specimens shown in **Figure S2.5** belong to these (sub-)species:

- **ACRISIONE**: *Athesis acrisione* ***acrisione*** Hewitson, 1869
- **AGNOSIA**: *Ithomia agnosia* ***agnosia*** Hewitson, [1855]
- **AMALDA**: *Oleria amalda* ***amalda*** (Hewitson, [1857])
- **AURELIANA**: *Hypoleria* ***aureliana*** (H. Bates, 1862)
- **BANJANA-M**: *Oleria athalina* ***banjana*** (Haensch, 1903)
- **CONFUSA**: *Methona confusa* ***confusa*** A. Butler, 1873
- **DERCYLLIDAS**: *Patricia dercyllidas* ***dercyllidas*** (Hewitson, 1864)
- **DILUCIDA**: *Eutresis* ***dilucida*** Staudinger, 1885
- **DOTO**: *Episcada doto* ***doto*** (Hübner, [1806])
- **DUESSA**: *Napeogenes duessa* ***duessa*** (Hewitson, [1859])
- **DUILLIA**: *Godyris* ***duillia*** (Hewitson, 1854)
- **EGRA**: *Oleria aegle* ***egra*** (Hewitson, [1852])
- **EURIMEDIA**: *Aeria eurimedia* ***eurimedia*** (Cramer, 1777)
- **EXCELSA**: *Hyalyris excelsa* ***excelsa*** (C. Felder & R. Felder, 1862)
- **HEMIXANTHE**: *Episcada* ***hemixanthe*** (C. Felder & R. Felder, 1865)
- **HERMIAS**: *Tithorea harmonia* ***hermias*** Godman & Salvin, 1898
- **HEWITSONI**: *Godyris hewitsoni* ***hewitsoni*** (Haensch, 1903)
- **HUMBOLDT**: *Elzunia humboldt* ***humboldt*** (Latreille, [1809])
- **ILLINISSA**: *Hyposcada illinissa* ***illinissa*** (Hewitson, [1852])
- **LERIDA**: *Oleria ilerdina* ***lerida*** (W. F. Kirby, 1878)
- **LIBETHRIS**: *Hypomenitis libethris* ***libethris*** (C. Felder & R. Felder, 1865)
- **LYSIMNIA**: *Mechanitis lysimnia* ***lysimnia*** (Fabricius, 1793)
- **MAELUS**: *Melinaea satevis* ***maelus*** (Hewitson, 1860)
- **MAMERCUS**: *Hypothyris mamercus* ***mamercus*** (Hewitson, 1869)
- **MANTINEUS**: *Mechanitis menapis* ***mantineus*** Hewitson, 1869
- **MESTRA**: *Hyalyris mestra* ***mestra*** (Hopffer, 1874)
- **MOTHONE**: *Melinaea marsaeus* ***mothone*** (Hewitson, 1860)
- **OCNA**: *Hyalyris ocna* ***ocna*** (Herrich-Schäffer, 1865)
- **ORESTES**: *Melinaea menophilus* ***orestes*** Salvin, 1871
- **OZIA**: *Pteronymia ozia* ***ozia*** (Hewitson, 1870)
- **PANTHYALE**: *Godyris panthyale* ***panthyale*** (C. Felder & R. Felder, 1862)
- **PARALLELIS**: *Melinaea lilis* ***parallelis*** A. Butler, 1873
- **PAVONII**: *Elzunia* ***pavonii*** (A. Butler, 1873)
- **POLITA**: *Episcada polita* ***polita*** Weymer, 1899
- **PRAESTANS**: *Olyras insignis* ***praestans*** Godman & Salvin, 1897
- **PRAXILLA**: *Hyalyris praxilla* ***praxilla*** (Hewitson, 1870)
- **QUINTINA**: *Oleria* ***quintina*** (C. Felder & R. Felder, 1865)
- **SINILIA**: *Hyposcada illinissa* ***sinilia*** (Herrich-Schäffer, 1865)

- **SUSIANA**: *Megoleria susiana* ***susiana*** (C. Felder & R. Felder, 1862)
- **THABENA-F**: *Pteronymia thabena* ***thabena*** (Hewitson, 1869)
- **THEUDELINDA**: *Hypomenitis theudelinda* ***theudelinda*** (Hewitson, [1861])
- **TICIDA-M**: *Pteronymia ticida* ***ticida*** (Hewitson, 1869)
- **UMBROSA**: *Hypomenitis depauperata* ***umbrosa*** (Haensch, 1903)
- **VESTILLA**: *Pteronymia vestilla* ***vestilla*** (Hewitson, [1853])

Appendix 3: Ithomiini phylogeny

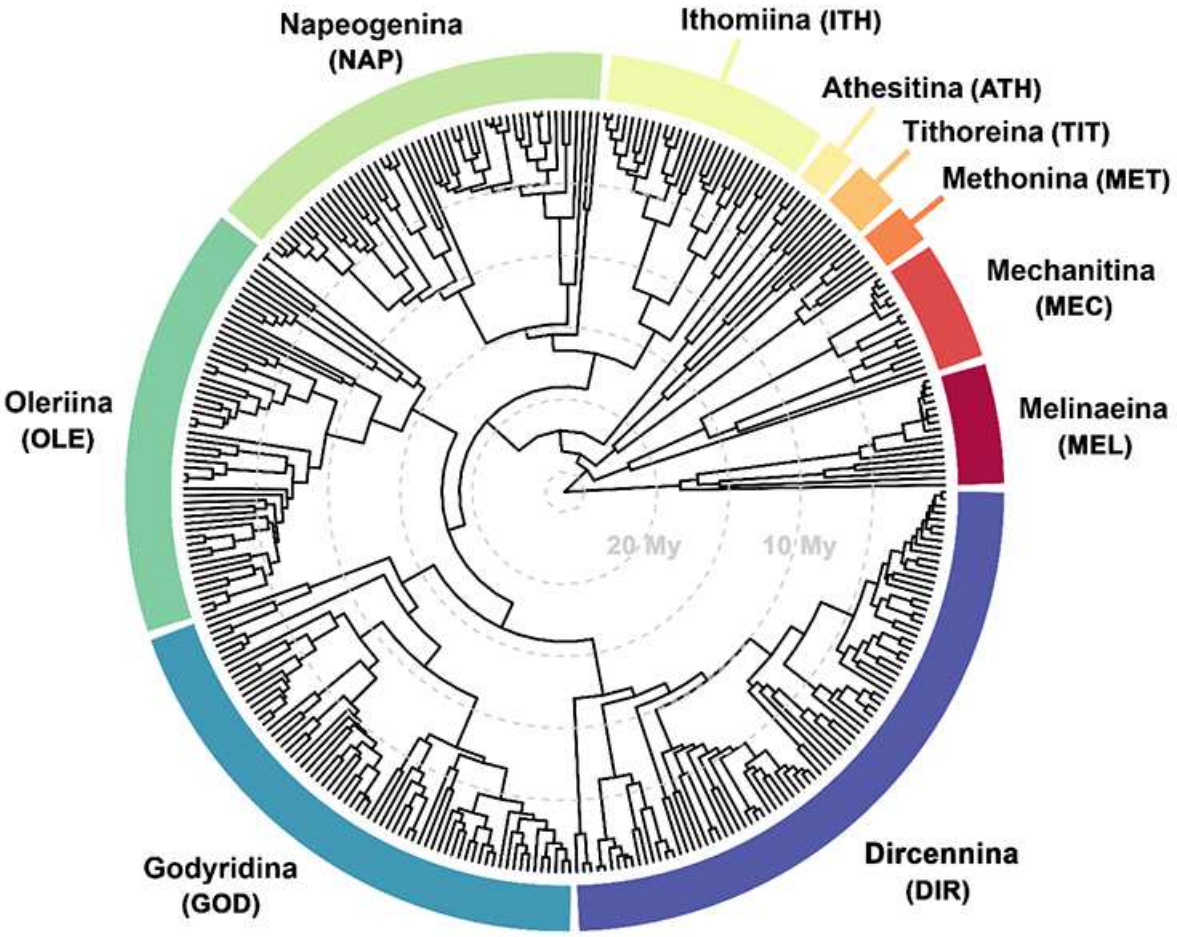

Figure S3.6: Time-calibrated phylogeny adapted from Chazot et al., 2019. It encompasses 339 species out of the 396 (85.6%) currently known in the group. Colors highlight the 10 subtribes. Dashed lines represent evolutionary time at intervals of 5 million years. Inset version of this phylogeny can be found in the distribution maps of each Operational Mimicry Unit, species and mimicry ring in **Appendix 5**.

Reference:

Chazot, N., Willmott, K. R., Lamas, G., Freitas, A. V. L., Piron-Prunier, F., Arias, C. F., Mallet, J., De-Silva, D. L., & Elias, M. (2019). Renewed diversification following Miocene landscape turnover in a Neotropical butterfly radiation. *Global Ecology and Biogeography*, 28(8), 1118–1132. https://doi.org/10.1111/geb.12919

Appendix 4: Taxonomic list

Taxonomic list of all 396 Ithomiini species with associated mimicry patterns (in CAPITAL LETTERS), grouped by subtribes. Subtribes are ordered as in the phylogeny. Species within subtribes are in alphabetic order. No georeferenced records for the eight species followed by an asterisk (*) were available at the time of analysis, and thus they are excluded from our study.

Ithomiini Godman & Salvin 1879

Melinaeina Clark, 1948

Athyrtis C. & R. Felder, 1862

Athyrtis mechanitis C. Felder & R. Felder, 1862
HERMIAS, ORESTES (2)

Eutresis Doubleday, 1847

Eutresis dilucida Staudinger, 1885
DILUCIDA (1)
Eutresis hypereia E. Doubleday, 1847
CONFUSA, DILUCIDA, EXCELSA (3)

Melinaea Hübner, 1816

Melinaea ethra (Godart, 1819)
HERMIAS (1)
Melinaea idae (C. Felder & R. Felder, 1862)
MAMERCUS (1)
Melinaea isocomma W. Forbes, 1948
MAMERCUS, MOTHONE (2)
Melinaea lilis (E. Doubleday, 1847)
HERMIAS, MAMERCUS, PARALLELIS (3)
Melinaea ludovica (Cramer, 1780)
HERMIAS (1)
Melinaea marsaeus (Hewitson, 1860)
MAELUS, MAMERCUS, MOTHONE, ORESTES (4)
Melinaea menophilus (Hewitson, [1856])
HERMIAS, MAELUS, MAMERCUS, ORESTES (4)
Melinaea mnasias (Hewitson, [1856])
HERMIAS, LYSIMNIA, MAMERCUS, ORESTES (4)
Melinaea mneme (Linnaeus, 1763)
HERMIAS, MAMERCUS (2)
Melinaea mnemopsis Berg, 1897
MAMERCUS (1)
Melinaea mothone (Hewitson, 1860)

MAMERCUS, MOTHONE (2)
Melinaea satevis (E. Doubleday, 1847)
HERMIAS, MAELUS, MAMERCUS, ORESTES (4)
Melinaea scylax Salvin, 1871
MAMERCUS (1)

Olyras E. Doubleday, 1847

Olyras crathis E. Doubleday, 1847
DILUCIDA, EXCELSA (2)
Olyras insignis Salvin, 1869
DILUCIDA, PRAESTANS (2)
Olyras theon H. Bates, 1866
DILUCIDA (1)

Paititia Lamas, 1979

Paititia neglecta Lamas, 1979
CONFUSA (1)

Mechanitina Fox, 1949

Forbestra Fox, 1967

Forbestra equicola (Cramer, 1780)
HERMIAS, MAMERCUS (2)
Forbestra olivencia (H. Bates, 1862)
HERMIAS, MAELUS, ORESTES (3)
Forbestra proceris (Weymer, 1883)
HERMIAS (1)

Mechanitis Fabricius, 1807

Mechanitis lysimnia (Fabricius, 1793)
HERMIAS, LYSIMNIA, MAMERCUS (3)
Mechanitis macrinus Hewitson, 1860
MAMERCUS (1)
Mechanitis mazaeus Hewitson, 1860
HERMIAS, MAELUS, MAMERCUS (3)
Mechanitis menapis Hewitson, [1856]
DILUCIDA, HERMIAS, MAMERCUS, MANTINEUS (4)
Mechanitis messenoides C. Felder & R. Felder, 1865
MAMERCUS, MOTHONE (2)
Mechanitis polymnia (Linnaeus, 1758)
DILUCIDA, EXCELSA, HERMIAS, MAELUS, MAMERCUS (5)

Sais Hübner, 1816

Sais browni (Takahashi, 1977) *
DOTO (1)
Sais rosalia (Cramer, 1779)
DILUCIDA, HERMIAS, MAELUS, MAMERCUS (4)

Scada Kirby, 1871

Scada karschina (Herbst, 1792)
EURIMEDIA, HEMIXANTHE (2)
Scada kusa (Hewitson, 1872)
EURIMEDIA (1)
Scada reckia (Hübner, [1808])
EURIMEDIA (1)
Scada zemira (Hewitson, 1856)
MANTINEUS (1)
Scada zibia (Hewitson, 1856)
EURIMEDIA (1)

Thyridia Hübner, 1816

Thyridia psidii (Linnaeus, 1758)
CONFUSA, DILUCIDA, EXCELSA (3)

Methonina Mielke & Brown, 1979

Methona Doubleday, 1847

Methona confusa A. Butler, 1873
CONFUSA (1)
Methona curvifascia Weymer, 1883
CONFUSA (1)
Methona grandior (W. Forbes, 1944)
CONFUSA (1)
Methona maxima (W. Forbes, 1944)
CONFUSA (1)
Methona megisto C. Felder & R. Felder, 1860
CONFUSA (1)
Methona singularis (Staudinger, [1884])
CONFUSA (1)
Methona themisto (Hübner, 1818)
CONFUSA (1)

Tithoreina Fox, 1940

Aeria Hübner, 1816

Aeria elara (Hewitson, 1855)
EURIMEDIA (1)
Aeria eurimedia (Cramer, 1777)
EURIMEDIA (1)
Aeria olena Weymer, 1875
EURIMEDIA (1)

Elzunia Bryk, 1937

Elzunia humboldt (Latreille, [1809])

HUMBOLDT, PAVONII (2)
Elzunia pavonii (A. Butler, 1873)
PAVONII (1)

Tithorea Doubleday, 1847

Tithorea harmonia (Cramer, 1777)
EXCELSA, HERMIAS, MAELUS, MAMERCUS, ORESTES (5)
Tithorea pacifica Willmott & Lamas, 2004
EXCELSA, HERMIAS (2)
Tithorea tarricina Hewitson, [1858]
EXCELSA, MAMERCUS (2)

Athesitina Brower et al. 2014

Athesis Doubleday, 1847

Athesis acrisione Hewitson, 1869
ACRISIONE, CONFUSA (2)
Athesis clearista E. Doubleday, 1847
DILUCIDA (1)
Athesis vitrala Kaye, 1918
HEWITSONI (1)

Patricia Fox, 1940

Patricia demylus (Godman & Salvin, 1879)
BANJANA-M, HEWITSONI (2)
Patricia dercyllidas (Hewitson, 1864)
DERCYLLIDAS, HEWITSONI, SUSIANA (3)
Patricia hewitsonii (Srnka, 1885)
HEWITSONI (1)
Patricia oligyrtis (Hewitson, 1877)
BANJANA-M, TICIDA-M (2)

Ithomiina Godman & Salvin, 1879

Ithomia Hübner, 1816

Ithomia adelinda Hewitson, 1868
CONFUSA, MESTRA, PRAXILLA (3)
Ithomia agnosia Hewitson, [1855]
AGNOSIA, LERIDA (2)
Ithomia amarilla Haensch, 1903
EURIMEDIA (1)
Ithomia arduinna R.F. d'Almeida, 1952
AGNOSIA (1)
Ithomia avella Hewitson, 1854
BANJANA-M, HEWITSONI, PANTHYALE, TICIDA-M (4)

Ithomia celemia Hewitson, [1854]
HERMIAS, PARALLELIS, MAMERCUS (3)
Ithomia cleora Hewitson, 1855
MANTINEUS, HERMIAS (2)
Ithomia diasia Hewitson, 1854
LERIDA, AMALDA (2)
Ithomia drymo Hübner, 1816
LERIDA (1)
Ithomia eleonora Haensch, 1905
BANJANA-M, SUSIANA (2)
Ithomia ellara Hewitson, 1874
BANJANA-M, SUSIANA (2)
Ithomia heraldica H. Bates, 1866
MAMERCUS (1)
Ithomia hyala Hewitson, [1856]
AGNOSIA, LERIDA (2)
Ithomia hymettia (Staudinger, 1885)
AGNOSIA, BANJANA-M (2)
Ithomia iphianassa E. Doubleday, 1847
POLITA, MAMERCUS, HERMIAS, DILUCIDA (4)
Ithomia jucunda Godman & Salvin, 1878
AMALDA, LERIDA (2)
Ithomia lagusa Hewitson, [1856]
DILUCIDA (1)
Ithomia leila Hewitson, 1852
LERIDA (1)
Ithomia lichyi R.F. d'Almeida, 1939
AGNOSIA, LERIDA (2)
Ithomia patilla Hewitson, 1852
LERIDA (1)
Ithomia praeithomia Vitale & Bollino, 2003
BANJANA-M, SUSIANA (2)
Ithomia pseudoagalla Rebel, 1902
DILUCIDA (1)
Ithomia salapia Hewitson, [1853]
AGNOSIA, EURIMEDIA (2)
Ithomia terra Hewitson, [1853]
AGNOSIA, LERIDA (2)
Ithomia terra EAST
BANJANA-M, AGNOSIA (2)
Ithomia xenos (H. Bates, 1866)
EXCELSA, DILUCIDA (2)

Pagyris Boisduval, 1870

Pagyris cymothoe (Hewitson, [1855])
AGNOSIA, DILUCIDA (2)

Pagyris priscilla Lamas, 1986
OZIA (1)
Pagyris renelichyi Neild, 2008 *
POLITA (1)
Pagyris ulla (Hewitson, [1857])
AGNOSIA, HEWITSONI, LIBETHRIS, PANTHYALE, TICIDA-M (5)

Placidina d'Almeida 1928

Placidina euryanassa (C. Felder & R. Felder, 1860)
LYSIMNIA (1)

Napeogenina Fox, 1956

Aremfoxia Real, 1971

Aremfoxia ferra (Haensch, 1909)
CONFUSA, MESTRA (2)

Epityches d'Almeida, 1938

Epityches eupompe (Geyer, 1832)
EURIMEDIA (1)

Hyalyris Boisduval, 1870

Hyalyris antea (Hewitson, 1869)
EURIMEDIA, MESTRA, OCNA, PRAXILLA (4)
Hyalyris coeno (E. Doubleday, 1847)
MAMERCUS, MESTRA, OCNA, OZIA (4)
Hyalyris excelsa (C. Felder & R. Felder, 1862)
EXCELSA (1)
Hyalyris fiammetta (Hewitson, 1852)
LYSIMNIA (1)
Hyalyris juninensis R. Fox & Real, 1971
EURIMEDIA (1)
Hyalyris lactea Willmott, Lamas & Hall 2020
MESTRA, PRAXILLA (2)
Hyalyris latilimbata (Weymer, 1890)
EURIMEDIA (1)
Hyalyris leptalina (C. Felder & R. Felder, 1865)
HEMIXANTHE (1)
Hyalyris mestra (Hopffer, 1874)
MESTRA, PRAXILLA (2)
Hyalyris ocna (Herrich-Schäffer, 1865)
MESTRA, OCNA (2)
Hyalyris oulita (Hewitson, [1859])
DUESSA, HERMIAS, MAMERCUS, OCNA (4)
Hyalyris praxilla (Hewitson, 1870)
PRAXILLA (1)
Hyalyris schlingeri Real, 1971

OCNA (1)

Hyalyris yasunina Willmott, Lamas & Hall 2020

HERMIAS (1)

Hypothyris Hübner, 1821

Hypothyris anastasia (H. Bates, 1862)

HERMIAS, ORESTES, MAELUS, MAMERCUS, MOTHONE (5)

Hypothyris cantobrica (Hewitson, 1876)

HERMIAS, MAMERCUS (2)

Hypothyris daphnis R.F. d'Almeida, 1945

HERMIAS, MAMERCUS (2)

Hypothyris euclea (Godart, 1819)

DOTO, HERMIAS, MAMERCUS, ORESTES, PARALLELIS (5)

Hypothyris fluonia (Hewitson, 1854)

HERMIAS, MAELUS, MAMERCUS, MOTHONE (4)

Hypothyris gemella R. Fox, 1971

DOTO (1)

Hypothyris leprieuri (Feisthamel, 1835)

DOTO, DUESSA, HERMIAS, MAMERCUS (4)

Hypothyris lycaste (Fabricius, 1793)

DILUCIDA, EXCELSA, HERMIAS, MAMERCUS (4)

Hypothyris maenas (Haensch, 1909)

MAMERCUS, MOTHONE (2)

Hypothyris mamercus (Hewitson, 1869)

MAMERCUS (1)

Hypothyris mansuetus (Hewitson, 1860)

MAMERCUS, MOTHONE (2)

Hypothyris moebiusi (Haensch, 1903)

MAMERCUS, MOTHONE (2)

Hypothyris ninonia (Hübner, [1806])

DOTO, HERMIAS, LYSIMNIA, MAELUS, MAMERCUS, MOTHONE, ORESTES (7)

Hypothyris nsp [n. sp.]

MOTHONE (1)

Hypothyris semifulva (Salvin, 1869)

HERMIAS, MAELUS, MAMERCUS, MOTHONE, ORESTES (5)

Hypothyris thea (Hewitson, 1852)

DUESSA, HERMIAS (2)

Hypothyris vallonia (Hewitson, [1853])

DOTO, HERMIAS (2)

Hypothyris xanthostola (H. Bates, 1862)

HERMIAS, MAMERCUS (2)

Napeogenes Bates, 1862

Napeogenes aethra (Hewitson, 1869)

HERMIAS (1)

Napeogenes apulia (Hewitson, 1858)
MESTRA, OCNA (2)
Napeogenes benigna Weymer, 1899
PANTHYALE, POLITA (2)
Napeogenes cranto C. Felder & R. Felder, 1865
DILUCIDA, EURIMEDIA (2)
Napeogenes duessa (Hewitson, [1859])
DOTO, DUESSA, MAMERCUS (3)
Napeogenes flossina A. Butler, 1873
PANTHYALE, TICIDA-M (2)
Napeogenes garwoodae Willmott & Hall, 2020
LERIDA (1)
Napeogenes glycera Godman, 1899
MESTRA, OCNA, PRAXILLA, SUSIANA (4)
Napeogenes gracilis Haensch, 1905
OZIA (1)
Napeogenes harbona (Hewitson, 1869)
BANJANA-M, EURIMEDIA, MESTRA, PANTHYALE, SUSIANA (5)
Napeogenes inachia (Hewitson, 1855)
DOTO, EURIMEDIA, HEMIXANTHE (3)
Napeogenes larilla (Hewitson, 1877)
HEWITSONI, PANTHYALE, THEUDELINDA (3)
Napeogenes larina (Hewitson, [1856])
HERMIAS (1)
Napeogenes lycora (Hewitson, 1870)
OZIA, PRAXILLA (2)
Napeogenes nsp1 [n. sp.]
OCNA, PRAXILLA (2)
Napeogenes nsp2 [n. sp.]
BANJANA-M, OCNA (2)
Napeogenes peridia (Hewitson, [1854])
DILUCIDA, EXCELSA, HERMIAS (3)
Napeogenes pharo (C. Felder & R. Felder, 1862)
CONFUSA, DOTO, EURIMEDIA, OZIA (4)
Napeogenes rhezia (Geyer, [1834])
DOTO, HEMIXANTHE, HERMIAS, MAMERCUS, MOTHONE (5)
Napeogenes sodalis Haensch, 1905
AGNOSIA (1)
Napeogenes stella (Hewitson, [1855])
HERMIAS (1)
Napeogenes sulphureophila Bryk, 1937
OCNA (1)
Napeogenes sylphis (Guérin-Méneville, [1844])
AGNOSIA, AURELIANA, EGRA, ILLINISSA, LERIDA (5)
Napeogenes tolosa (Hewitson, 1855)

DILUCIDA, EURIMEDIA, EXCELSA, MAMERCUS (4)
Napeogenes verticilla (Hewitson, 1874)
AGNOSIA (1)
Napeogenes zurippa (Hewitson, [1876])
HERMIAS, MAMERCUS, ORESTES (3)

Oleriina Fox, 1940

Hyposcada Godman & Salvin, 1879

Hyposcada anchiala (Hewitson, 1868)
ILLINISSA, MAELUS, MAMERCUS, MOTHONE, ORESTES, PARALLELIS (6)
Hyposcada attilodes Kaye, 1918
SUSIANA (1)
Hyposcada dujardini Brévignon, 1993
AGNOSIA, LERIDA (2)
Hyposcada gallardi Brévignon, 1993
MAMERCUS (1)
Hyposcada illinissa (Hewitson, [1852])
AGNOSIA, AURELIANA, ILLINISSA, LERIDA, PARALLELIS, QUINTINA, SINILIA (7)
Hyposcada kena (Hewitson, 1872)
AGNOSIA, BANJANA-M, LERIDA, QUINTINA, SINILIA (5)
Hyposcada nsp [n. sp.]
AGNOSIA, LERIDA (2)
Hyposcada schausi R. Fox, 1941
AMALDA, LERIDA (2)
Hyposcada taliata (Hewitson, 1874)
BANJANA-M, SUSIANA (2)
Hyposcada virginiana (Hewitson, [1855])
EXCELSA, HERMIAS, MAMERCUS, PARALLELIS (4)
Hyposcada zarepha (Hewitson, 1869)
AGNOSIA, EGRA, LERIDA (3)

Megoleria Constantino, 1999

Megoleria orestilla (Hewitson, 1867)
BANJANA-M, SUSIANA (2)
Megoleria susiana (C. Felder & R. Felder, 1862)
SUSIANA (1)

Oleria Hübner, 1816

Oleria aegle (Fabricius, 1776)
EGRA, LERIDA (2)
Oleria agarista (C. Felder & R. Felder, 1862)
LERIDA, SINILIA (2)
Oleria alexina (Hewitson, [1859])
AGNOSIA (1)

Oleria amalda (Hewitson, [1857])
AMALDA, LERIDA (2)
Oleria antaxis (Haensch, 1909)
EGRA, LERIDA, SINILIA (3)
Oleria aquata (Weymer, 1875)
LERIDA (1)
Oleria assimilis (Haensch, 1903)
AGNOSIA, LERIDA (2)
Oleria astrea (Cramer, 1775)
LERIDA (1)
Oleria athalina (Staudinger, [1884])
BANJANA-M, HEWITSONI, SUSIANA (3)
Oleria attalia (Hewitson, 1855)
BANJANA-M, MESTRA, SUSIANA (3)
Oleria baizana (Haensch, 1903)
BANJANA-M, HEWITSONI, SUSIANA (3)
Oleria bifurcata Willmott & Lamas, 2020
BANJANA-M (1)
Oleria bioculata (Haensch, 1905)
AGNOSIA (1)
Oleria boyeri Neild, 2008
AGNOSIA (1)
Oleria chimaera Willmott & Lamas, 2020 *
BANJANA-M (1)
Oleria cyrene (Latreille, [1809])
BANJANA-M, SUSIANA (2)
Oleria deronda (Hewitson, 1876)
BANJANA-M, PANTHYALE, SUSIANA, THABENA-F (4)
Oleria derondina (Haensch, 1909)
BANJANA-M, HEWITSONI, THABENA-F (3)
Oleria didymaea (Hewitson, 1876)
AGNOSIA, LERIDA (2)
Oleria enania (Haensch, 1909)
AGNOSIA, LERIDA (2)
Oleria estella (Hewitson, 1868)
AGNOSIA, QUINTINA (2)
Oleria fasciata (Haensch, 1903)
BANJANA-M, SUSIANA (2)
Oleria flora (Cramer, 1779)
EGRA, LERIDA (2)
Oleria fumata (Haensch, 1905)
BANJANA-M (1)
Oleria gunilla (Hewitson, 1858)
AGNOSIA, AURELIANA, ILLINISSA, LERIDA, QUINTINA, SINILIA (6)
Oleria ilerdina (Hewitson, 1858)

ILLINISSA, LERIDA (2)
Oleria makrena (Hewitson, 1854)
AGNOSIA, BANJANA-M (2)
Oleria nsp [n. sp.]
AGNOSIA (1)
Oleria nsp1 [n. sp.]
LERIDA (1)
Oleria onega (Hewitson, [1852])
AGNOSIA, AURELIANA, LERIDA, QUINTINA (4)
Oleria padilla (Hewitson, 1863)
AGNOSIA, BANJANA-M (2)
Oleria paula Weymer, 1883
AMALDA, LERIDA (2)
Oleria phenomoe (E. Doubleday, [1847])
AGNOSIA (1)
Oleria quadrata (Haensch, 1903)
LERIDA (1)
Oleria quintina (C. Felder & R. Felder, 1865)
QUINTINA (1)
Oleria radina (Haensch, 1909)
BANJANA-M, PANTHYALE, SUSIANA (3)
Oleria rubescens (A. Butler & H. Druce, 1872)
LERIDA (1)
Oleria santineza (Haensch, 1903)
AGNOSIA, BANJANA-M (2)
Oleria sexmaculata (Haensch, 1903)
LERIDA, SINILIA (2)
Oleria similigena R.F. d'Almeida, 1962
EGRA, LERIDA (2)
Oleria synnova (Hewitson, [1859])
SINILIA (1)
Oleria thiemei (Oberthür, 1879)
AMALDA (1)
Oleria tigilla (Weymer, 1899)
AGNOSIA, LERIDA (2)
Oleria tremona (Haensch, 1909)
BANJANA-M, PANTHYALE (2)
Oleria vicina (Salvin, 1869)
AGNOSIA (1)
Oleria victorine (Guérin-Méneville, [1844])
AGNOSIA, LERIDA (2)
Oleria zea (Hewitson, [1855])
AGNOSIA (1)
Oleria zelica (Hewitson, 1856)
EURIMEDIA (1)

Ollantaya Brown & Freitas, 1994

Ollantaya aegineta (Hewitson, 1869)
BANJANA-M, THABENA-F, THEUDELINDA (3)
Ollantaya canilla (Hewitson, 1874)
OZIA (1)
Ollantaya nsp [n. sp.]
SUSIANA (1)
Ollantaya olerioides (R.F. d'Almeida, 1952)
BANJANA-M, SUSIANA (2)

Godyridina d'Almeida, 1941

Brevioleria Lamas, 2004

Brevioleria aelia (Hewitson, 1852)
AURELIANA, ILLINISSA, LERIDA, SINILIA (4)
Brevioleria arzalia (Hewitson, 1876)
AGNOSIA, AURELIANA (2)
Brevioleria coenina (Hewitson, 1869)
OZIA (1)
Brevioleria nsp [n. sp.] *
Mimicry patterns not known
Brevioleria nsp1 [n. sp.]
LERIDA (1)
Brevioleria plisthenes (R.F. d'Almeida, 1958)
LERIDA (1)
Brevioleria seba (Hewitson, 1872)
AGNOSIA, AURELIANA, LERIDA (3)

Genus1 [n. genus]

*Genus*1 nsp1 [n. sp.]
BANJANA-M (1)

Genus2 [n. genus]

*Genus*2 *andromica* (Hewitson, [1855])
AGNOSIA (1)
*Genus*2 *annette* (Guérin-Méneville, [1844])
AGNOSIA (1)

Godyris Boisduval, 1870

Godyris crinippa (Hewitson, 1874)
PANTHYALE (1)
Godyris dircenna (C. Felder & R. Felder, 1865)
CONFUSA (1)
Godyris duillia (Hewitson, 1854)
DUILLIA (1)
Godyris hewitsoni (Haensch, 1903)
HEWITSONI, PANTHYALE (2)
Godyris kedema (Hewitson, [1855])

DILUCIDA, MAMERCUS (2)
Godyris lauta (Haensch, 1910)
BANJANA-M, UMBROSA (2)
Godyris nepos (Weymer, 1875)
LIBETHRIS (1)
Godyris nero (Hewitson, [1855])
AGNOSIA (1)
Godyris panthyale (C. Felder & R. Felder, 1862)
BANJANA-M, PANTHYALE (2)
Godyris sappho (Haensch, 1910)
BANJANA-M, PANTHYALE (2)
Godyris zavaleta (Hewitson, [1855])
DILUCIDA, DOTO, EURIMEDIA, EXCELSA, HERMIAS, MAMERCUS (6)

Greta Hemming, 1934

Greta clavijoi Neild, 2008
AGNOSIA (1)
Greta cubana (Herrich-Schäffer, 1862)
AGNOSIA (1)
Greta diaphanus (Drury, 1773)
AGNOSIA (1)
Greta morgane (Geyer, 1837)
AGNOSIA, LERIDA (2)

Heterosais Godman & Salvin, 1880

Heterosais edessa (Hewitson, [1855])
LERIDA (1)
Heterosais giulia (Hewitson, [1855])
DILUCIDA, LERIDA, POLITA (3)
Heterosais nephele (H. Bates, 1862)
AGNOSIA, LERIDA (2)

Hypoleria Godman & Salvin 1879

Hypoleria adasa (Hewitson, [1855])
LERIDA (1)
Hypoleria alema (Hewitson, [1857])
AGNOSIA, AURELIANA, EGRA, LERIDA, MESTRA, OCNA, PRAXILLA (7)
Hypoleria asellia (Hopffer, 1874)
AGNOSIA (1)
Hypoleria aureliana (H. Bates, 1862)
AURELIANA (1)
Hypoleria lavinia (Hewitson, [1855])
AGNOSIA, AMALDA, AURELIANA, LERIDA (4)
Hypoleria mulviana R.F. d'Almeida, 1958
EGRA (1)

Hypoleria ocalea (E. Doubleday, 1847)
DILUCIDA, HERMIAS (2)
Hypoleria sarepta (Hewitson, [1852])
AGNOSIA, AURELIANA, EGRA, LERIDA (4)
Hypoleria xenophis Haensch, 1909
EURIMEDIA (1)

Hypomenitis Fox, 1945

Hypomenitis alphesiboea (Hewitson, 1869)
DUILLIA (1)
Hypomenitis candida Lamas & Willmott, 2020
AGNOSIA (1)
Hypomenitis depauperata (Boisduval, 1870)
UMBROSA (1)
Hypomenitis dercetis (Doubleday & Hewitson, 1847)
LIBETHRIS (1)
Hypomenitis enigma (Haensch, 1905)
PANTHYALE (1)
Hypomenitis esula (Hewitson, 1855)
PANTHYALE (1)
Hypomenitis gabiglooris (Brabant & Bischler, 2005)
AGNOSIA (1)
Hypomenitis gardneri (Weeks, 1901)
BANJANA-M, PANTHYALE (2)
Hypomenitis hermana (Haensch, 1903)
HEWITSONI, THEUDELINDA (2)
Hypomenitis jamesiana Willmott, Lamas & Hall, 2020
PANTHYALE (1)
Hypomenitis libethris (C. Felder & R. Felder, 1865)
LIBETHRIS (1)
Hypomenitis lojana (Vitale & Bollino, 2001)
BANJANA-M (1)
Hypomenitis lydia (Weymer, 1899)
HEWITSONI (1)
Hypomenitis nsp [n. sp.]
BANJANA-M (1)
Hypomenitis nsp*4* [n. sp.] *
LIBETHRIS (1)
Hypomenitis nsp*C* [n. sp.]
AGNOSIA (1)
Hypomenitis nsp*D* [n. sp.]
PANTHYALE (1)
Hypomenitis nsp*E* [n. sp.]
LIBETHRIS (1)
Hypomenitis ochretis (Haensch, 1903)
UMBROSA (1)

Hypomenitis oneidodes (Kaye, 1918)
HEWITSONI, THEUDELINDA (2)
Hypomenitis ortygia (Weymer, 1890)
PANTHYALE (1)
Hypomenitis polissena (Hewitson, [1863])
AGNOSIA, LIBETHRIS (2)
Hypomenitis theudelinda (Hewitson, [1861])
HEWITSONI, PANTHYALE, THEUDELINDA (3)

Mcclungia Fox, 1940

Mcclungia cymo (Hübner, [1806])
AGNOSIA, EGRA, EURIMEDIA, MAMERCUS, SINILIA (5)

Pachacutia Willmott & Lamas, 2007

Pachacutia baroni Willmott & Lamas, 2007
DUILLIA (1)
Pachacutia cleomella (Hewitson, 1874)
OZIA, THABENA-F (2)
Pachacutia germaini Lamas & Willmott, 2007
OZIA (1)
Pachacutia mantura (Hewitson, 1876)
CONFUSA (1)

Pseudoscada Godman & Salvin, 1879

Pseudoscada acilla (Hewitson, 1867)
LERIDA (1)
Pseudoscada erruca (Hewitson, 1855)
LERIDA (1)
Pseudoscada florula (Hewitson, [1855])
AGNOSIA, AURELIANA, EGRA, LERIDA (4)
Pseudoscada timna COSTARICA
LERIDA (1)
Pseudoscada timna EASTERN
AGNOSIA, LERIDA (2)
Pseudoscada timna WESTERN
AMALDA, LERIDA (2)

Veladyris Fox, 1945

Veladyris cytharista (Hewitson, 1874)
PANTHYALE, THABENA-F (2)
Veladyris electrea (M. Brabant, 2004)
PANTHYALE (1)
Veladyris nsp [n. sp.]
HEWITSONI (1)
Veladyris pardalis (Salvin, 1869)
HEWITSONI, PANTHYALE, THEUDELINDA (3)

Velamysta Haensch, 1909

Velamysta desmondi Kell & Willmott, 2020
AGNOSIA (1)
Velamysta nsp [n. sp.]
PANTHYALE (1)
Velamysta peninna (Hewitson, 1855)
BANJANA-M, PANTHYALE, SUSIANA (3)
Velamysta phengites R. Fox, 1945
BANJANA-M, PANTHYALE (2)
Velamysta pupilla (Hewitson, 1874)
PANTHYALE, THEUDELINDA (2)

Dircennina d'Almeida, 1941

Callithomia Bates, 1862

Callithomia alexirrhoe H. Bates, 1862
HERMIAS, MAELUS, MAMERCUS (3)
Callithomia hezia (Hewitson, [1854])
EXCELSA, MAMERCUS, OCNA (3)
Callithomia hydra C. Felder & R. Felder, 1865
EXCELSA, MAMERCUS (2)
Callithomia lenea (Cramer, 1779)
CONFUSA, DILUCIDA, DOTO, HERMIAS, MAMERCUS (5)

Ceratinia Hübner, 1816

Ceratinia cayana (Salvin, 1869)
HERMIAS (1)
Ceratinia iolaia (Hewitson, [1856])
HERMIAS (1)
Ceratinia neso (Hübner, [1806])
DILUCIDA, DOTO, HERMIAS, MAELUS, MAMERCUS, ORESTES (6)
Ceratinia poecila (H. Bates, 1862)
HERMIAS, MAELUS, MAMERCUS, MOTHONE, ORESTES (5)
Ceratinia tutia (Hewitson, 1852)
HERMIAS, MAMERCUS, MANTINEUS (3)

Dircenna Doubleday, [1847]

Dircenna adina (Hewitson, [1855])
AGNOSIA, CONFUSA, DILUCIDA, HEWITSONI, LIBETHRIS, MESTRA, OCNA, OZIA (8)
Dircenna dero (Hübner, 1823)
CONFUSA, DILUCIDA, DOTO, MAMERCUS (4)
Dircenna jemina (Geyer, 1837)
DILUCIDA, MAMERCUS, POLITA (3)
Dircenna klugii (Geyer, 1837)

DILUCIDA (1)
Dircenna loreta Haensch, 1903
CONFUSA (1)
Dircenna olyras (C. Felder & R. Felder, 1865)
DILUCIDA, EXCELSA, MAMERCUS (3)

Episcada Godman & Salvin, 1879

Episcada apuleia (Hewitson, 1868)
HEWITSONI, PANTHYALE (2)
Episcada clausina (Hewitson, 1876)
EURIMEDIA, LIBETHRIS (2)
Episcada doto (Hübner, [1806])
DOTO, EURIMEDIA (2)
Episcada hemixanthe (C. Felder & R. Felder, 1865)
HEMIXANTHE (1)
Episcada hymen Haensch, 1905
EURIMEDIA (1)
Episcada hymenaea (Prittwitz, 1865)
EURIMEDIA, LERIDA, LIBETHRIS, POLITA (4)
Episcada mira (Hewitson, 1877)
AGNOSIA, LIBETHRIS (2)
Episcada nsp [n. sp.]
AGNOSIA (1)
Episcada nsp1 [n. sp.]
OZIA, PANTHYALE (2)
Episcada philoclea (Hewitson, [1855])
EURIMEDIA (1)
Episcada pichita Lamas & Willmott, 2020
LIBETHRIS (1)
Episcada polita Weymer, 1899
AGNOSIA, LIBETHRIS, POLITA (3)
Episcada salvinia (H. Bates, 1864)
AGNOSIA, BANJANA-M (2)
Episcada striposis Haensch, 1909
EURIMEDIA (1)
Episcada sulphurea Haensch, 1905
EURIMEDIA (1)
Episcada sylpha Haensch, 1905
POLITA (1)
Episcada sylvo (Geyer, 1832)
LERIDA (1)
Episcada ticidella (Hewitson, 1869)
PANTHYALE, TICIDA-M (2)
Episcada trapezula Brabant & Bischler, 2003
LIBETHRIS (1)
Episcada vitrea R.F. d'Almeida & O. Mielke, 1967

LERIDA (1)
Episcada zajciwi R.F. d'Almeida & O. Mielke, 1967
EURIMEDIA, HEMIXANTHE (2)

Haenschia Lamas, 2004

Haenschia derama (Haensch, 1905)
AGNOSIA, LIBETHRIS (2)
Haenschia nsp1 [n. sp.] *
Mimicry patterns not known
Haenschia nsp2 [n. sp.] *
OZIA (1) ; Mimicry pattern for females is not known
Haenschia sidonia (Haensch, 1905)
AGNOSIA, OZIA (2)

Hyalenna Forbes, 1942

Hyalenna alidella (Hewitson, 1869)
AGNOSIA, DILUCIDA, LIBETHRIS, OZIA, THABENA-F (5)
Hyalenna buckleyi Willmott & Lamas, 2006
PANTHYALE (1)
Hyalenna hugia (Lamas, 2004) *
OZIA (1) ; Mimicry pattern for females is not known
Hyalenna paradoxa (Staudinger, [1884])
BANJANA-M, PANTHYALE (2)
Hyalenna pascua (Schaus, 1902)
LERIDA (1)
Hyalenna perasippa (Hewitson, 1877)
PANTHYALE (1)
Hyalenna sulmona (Hewitson, 1877)
LIBETHRIS, PANTHYALE, TICIDA-M (3)

Pteronymia Butler & Druce, 1872

Pteronymia alcmena (Godman & Salvin, 1877)
AGNOSIA (1)
Pteronymia aletta (Hewitson, [1855])
DILUCIDA, MAMERCUS, MANTINEUS, POLITA (4)
Pteronymia alicia Neild, 2008
AGNOSIA (1)
Pteronymia alida (Hewitson, 1855)
BANJANA-M, HEWITSONI, LIBETHRIS, PANTHYALE, THABENA-F (5)
Pteronymia alina Haensch, 1909
BANJANA-M, HEWITSONI, PANTHYALE (3)
Pteronymia alissa (Hewitson, 1869)
AGNOSIA, LERIDA (2)
Pteronymia andreas (Weeks, 1901)
AGNOSIA (1)
Pteronymia artena (Hewitson, [1855])

AGNOSIA (1)
Pteronymia asopo (C. Felder & R. Felder, 1865)
AGNOSIA (1)
Pteronymia calgiria Schaus, 1902
OZIA (1)
Pteronymia carlia Schaus, 1902
LERIDA (1)
Pteronymia cotytto (Guérin-Méneville, [1844])
LERIDA (1)
Pteronymia cuneata Willmott, Lamas & Hall, 2020
HEWITSONI, TICIDA-M (2)
Pteronymia dispar Haensch, 1905
POLITA (1)
Pteronymia donella (C. Felder & R. Felder, 1865)
DILUCIDA, MAMERCUS (2)
Pteronymia dorothyae Neild, 2008
AGNOSIA (1)
Pteronymia euritea (Cramer, 1780)
HEMIXANTHE (1)
Pteronymia forsteri Baumann, 1985
AGNOSIA (1)
Pteronymia fulvimargo A. Butler & H. Druce, 1872
DILUCIDA (1)
Pteronymia fumida Schaus, 1913
DILUCIDA, HERMIAS (2)
Pteronymia gertschi R. Fox, 1945
OZIA (1)
Pteronymia glauca Haensch, 1903
LERIDA (1)
Pteronymia granica (Hewitson, 1877)
HEWITSONI (1)
Pteronymia hara (Hewitson, 1877)
AGNOSIA, BANJANA-M, HEWITSONI, LERIDA, LIBETHRIS, PANTHYALE (6)
Pteronymia inania Haensch, 1903
HEWITSONI, THABENA-F (2)
Pteronymia latilla (Hewitson, [1855])
DILUCIDA, HERMIAS, MAMERCUS, PARALLELIS (4)
Pteronymia laura (Staudinger, 1885)
AMALDA (1)
Pteronymia lonera (A. Butler & H. Druce, 1872)
EXCELSA (1)
Pteronymia luisa Willmott, Lamas & Hall, 2020
DILUCIDA (1)
Pteronymia mariannae Lamas, Willmott & Hall, 2020
AGNOSIA (1)

Pteronymia medellina Haensch, 1905
AGNOSIA, HEWITSONI (2)
Pteronymia nsp [n.sp.]
DILUCIDA (1)
Pteronymia nsp1 [n.sp.]
AGNOSIA (1)
Pteronymia obscuratus (Fabricius, 1793)
POLITA (1)
Pteronymia olimba Haensch, 1905
AGNOSIA, LIBETHRIS (2)
Pteronymia oneida (Hewitson, 1855)
HEWITSONI (1)
Pteronymia ozia (Hewitson, 1870)
MESTRA, OZIA (2)
Pteronymia parva (Salvin, 1869)
LERIDA (1)
Pteronymia peteri Neild, 2008
AGNOSIA (1)
Pteronymia picta (Salvin, 1869)
DILUCIDA, EURIMEDIA, MAMERCUS (3)
Pteronymia primula (H. Bates, 1862)
EURIMEDIA (1)
Pteronymia rufocincta (Salvin, 1869)
AGNOSIA (1)
Pteronymia sao (Hübner, [1813])
DOTO, EURIMEDIA (2)
Pteronymia serrata Haensch, 1903
HEWITSONI, PANTHYALE, THEUDELINDA (3)
Pteronymia sexpunctata (Bryk, 1953)
AGNOSIA (1)
Pteronymia simplex (Salvin, 1869)
AGNOSIA (1)
Pteronymia tamina Haensch, 1909
OZIA, THABENA-F (2)
Pteronymia teresita (Hewitson, 1863)
DILUCIDA (1)
Pteronymia thabena (Hewitson, 1869)
OZIA, THABENA-F (2)
Pteronymia ticida (Hewitson, 1869)
BANJANA-M, HEWITSONI, LIBETHRIS, OZIA, PANTHYALE, THABENA-F,
TICIDA-M (7)
Pteronymia tucuna (H. Bates, 1862)
EURIMEDIA (1)
Pteronymia veia EAST (Hewitson, [1853])
HEWITSONI, LIBETHRIS (2)

Pteronymia vestilla (Hewitson, [1853])
AGNOSIA, EURIMEDIA, VESTILLA (3)
Pteronymia zerlina (Hewitson, [1856])
AGNOSIA, BANJANA-M (2)

Appendix 5: ODMAP

See **ANNEXE 2**.

The ODMAP protocol for species distribution models (Zurell *et al.* 2020) provides a standard protocol to document and report all the modeling steps and decisions undertook during the analyses. It ensures transparency and reproducibility, and facilitates peer-review.

We include in our ODMAP report a more in-depth discussion on the potential caveats and limits inherent in SDMs, and provided additional maps to assess the uncertainties and robustness to modeling choices of our results.

Reference:

Zurell, D., Franklin, J., König, C., Bouchet, P. J., Dormann, C. F., Elith, J., Fandos, G., Feng, X., Guillera-Arroita, G., Guisan, A., Lahoz-Monfort, J. J., Leitão, P. J., Park, D. S., Peterson, A. T., Rapacciuolo, G., Schmatz, D. R., Schröder, B., Serra-Diaz, J. M., Thuiller, W., … Merow, C. (2020). A standard protocol for reporting species distribution models. Ecography, 1–17. https://doi.org/10.1111/ecog.04960

Appendix 6: Human Footprint map

Anthropogenic threats to Ithomiini biodiversity hotspots were estimated with the 2009 Human Footprint index (Venter et al., 2016a; **Fig. S6.17**). It combines eight variables which measure direct human impacts on the environment, namely, (1) human population density, (2) night-time light pollution, (3) extent of built environments, (4) crop landcover, (5) pasture landcover, (6) proximity to railways, (7) to major roadways, and (8) to navigable waterways. The following map was used to defined areas falling into categories of threats based on quantile distribution of Human Footprint across communities: very high (top 5%), high (top 25%), low (bottom 25%) and very low (bottom 5%).

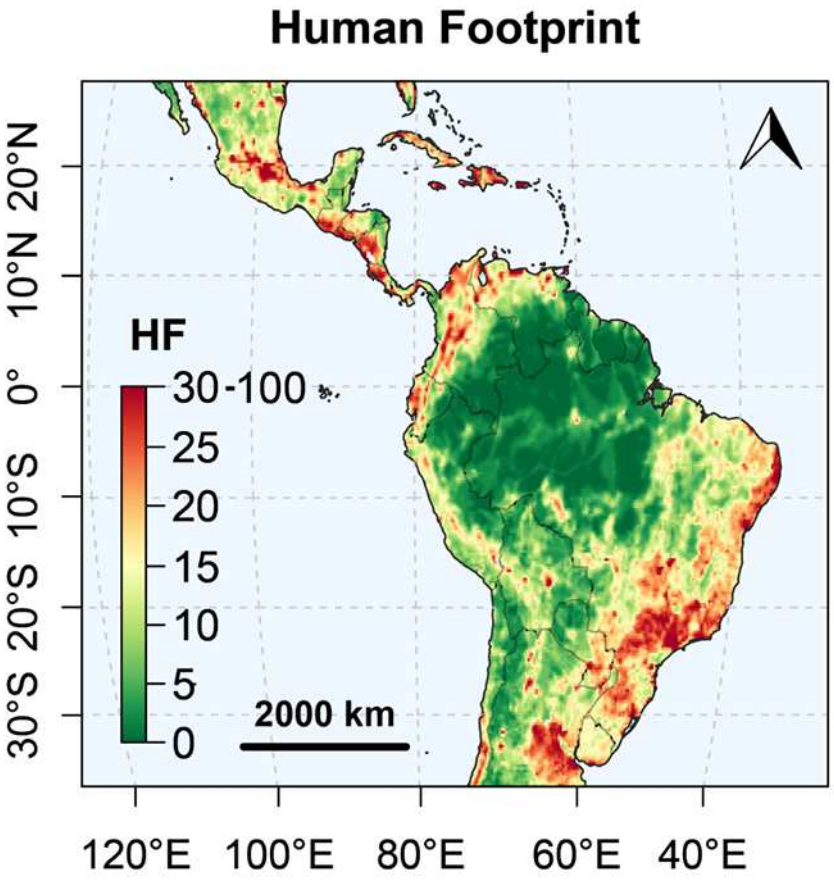

Figure S6.17: Human Footprint from Venter et al. (2016). Human Footprint represents cumulative human pressures on terrestrial ecosystems worldwide. Color scale is contrasted such that high values potentially as high as 100 are capped to 30.

Reference:

Venter, O., Sanderson, E. W., Magrach, A., Allan, J. R., Beher, J., Jones, K. R., Possingham, H. P., Laurance, W. F., Wood, P., Fekete, B. M., Levy, M. A., & Watson, J. E. M. (2016). Global terrestrial Human Footprint maps for 1993 and 2009. *Scientific Data*, 3(160067), 1–10. https://doi.org/doi: 10.1038/sdata.2016.67

Appendix 7: Examples of distribution maps

We provide here contrasting examples of distribution maps for four Operational Mimicry Units (**Fig. S7.18)**, four species (**Fig. S7.19)**, and four mimicry rings (**Fig. S7.20)** illustrating the diversity of biogeographic patterns found in Ithomiini. All maps of the 783 OMUs, 388 species, and 44 mimicry rings are available in an online archive at 10.5281/zenodo.4673446.

Dircenna dero pattern CONFUSA illustrates the example of a wide-ranging OMU extending from the Atlantic forest to the eastern slopes of the Central Andes, up to Central America, but showing low habitat suitability in the Northern cordilleras (**Fig. S7.18a)**. It is part of a complex of four OMUs belonging to the same species *Dircenna dero*, yet showing different wing patterns. In contrast, *Dircenna dero* pattern DILUCIDA presents a smaller range, encompassing Central America and the Northern Cordilleras in Colombia (**Fig. S7.18b)**. As such, these maps show that OMUs from the same species can present different niches with different local suitability in a region (i.e., in the Northern Cordilleras), and yet show some degree of environmental and spatial overlap in another (i.e., in the highlands of Central America). *Hyalenna alidella* pattern LIBETHRIS is strictly Andean but shows a disjointed distribution between the Central Andes in Peru and the Northern Andes in Colombia (**Fig. S7.18c)**. Its environmental niche appears similar in both regions and our modeling process allows to discriminate between suitable highlands and unsuitable lowlands in the two areas of distribution. *Oleria similigena* pattern EGRA presents a continuous range restricted to the region around the mouth of the Amazon river (**Fig. S7.18d)**.

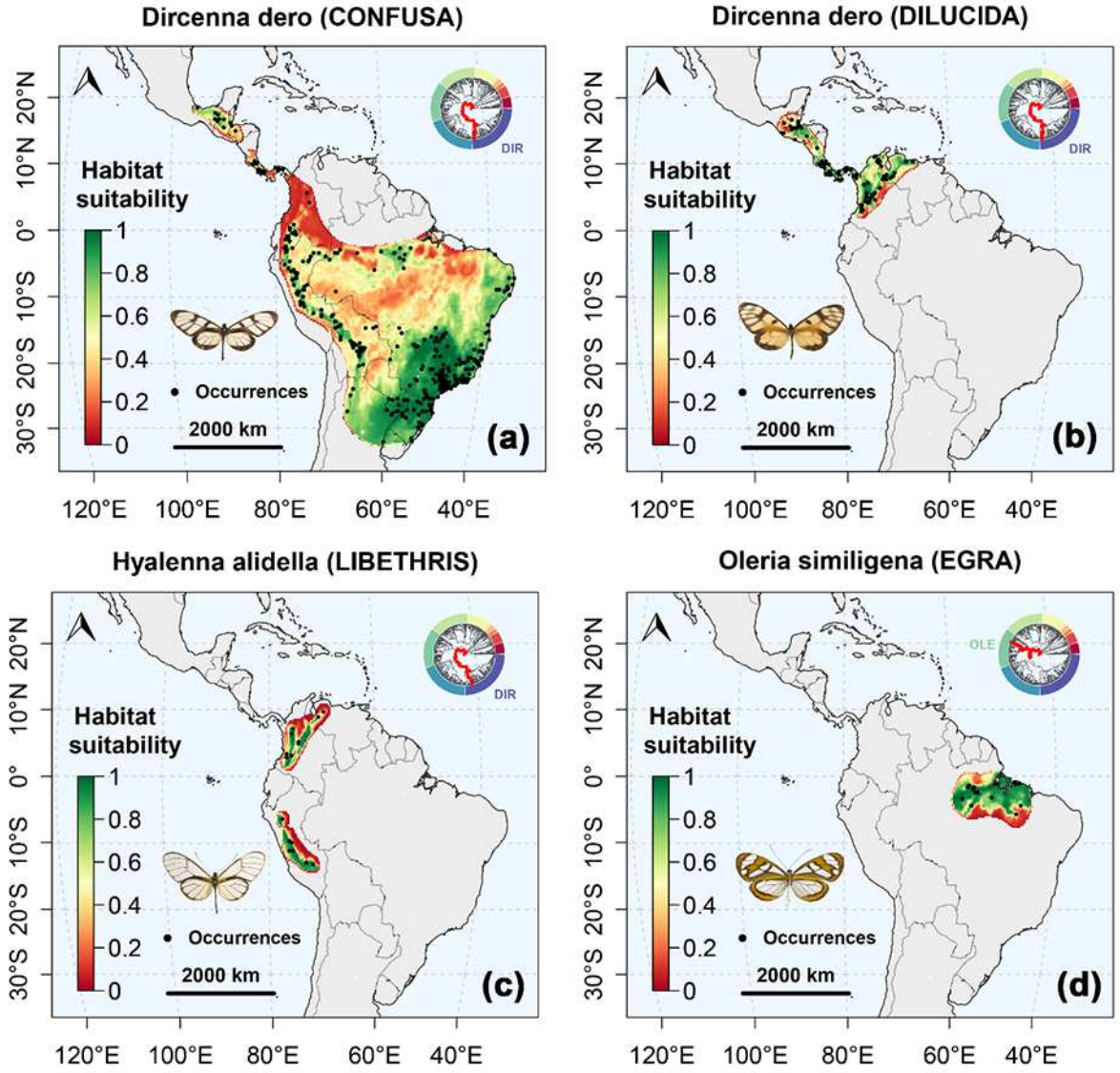

Figure S7.18: Four examples of distribution maps for Operational Mimicry Units (OMUs) resulting from our environmental niche ensemble modeling process. Position in the phylogeny is represented in the top-right corner. **(a)** = A wide-spread OMU: *Dircenna dero* pattern CONFUSA. **(b)** = An OMU from Central America and the Northern cordilleras: *Dircenna dero* pattern DILUCIDA. **(c)** = An Andean OMU with disjointed distribution: *Hyalenna alidella* pattern LIBETHRIS. **(d)** = A lower Amazonian OMU: *Oleria similigena* pattern EGRA. Photo credits: Nicolas Chazot, 2015.

Dircenna adina is the ithomiine species that displays the most diversity in mimicry patterns with up to eight different patterns (**Fig. S7.19a**). These patterns (i.e., OMUs) shows some degrees of overlap in the highly diverse region of Ecuador and Northern Peru, but overall, patterns remained clustered in space along the area of distribution of the species along the Andes, in the highlands, from Bolivia to Venezuela and the Guyana shield. In contrast, *Hypomenitis ortygia*, which is also restricted to the highlands along the Andes, displays a single

pattern all along its range (**Fig. S7.19c).** Its mimicry ring itself (PANTHYALE) is restricted to these Andean highland habitats. Other species demonstrate a wider environmental niche, yet can be restricted to a geographic area. For instance, *Greta morgane* is found in Central America, with high habitat suitability in all conditions, from lowlands to highlands, from the coast to central areas (**Fig. S7.19b)**. Finally, *Epityches eupompe* is widely spread in the Atlantic forest (**Fig. S7.19d)**, but restricted to this region despite harboring a mimicry pattern (EURIMEDIA) that can be found within the whole range of Ithomiini.

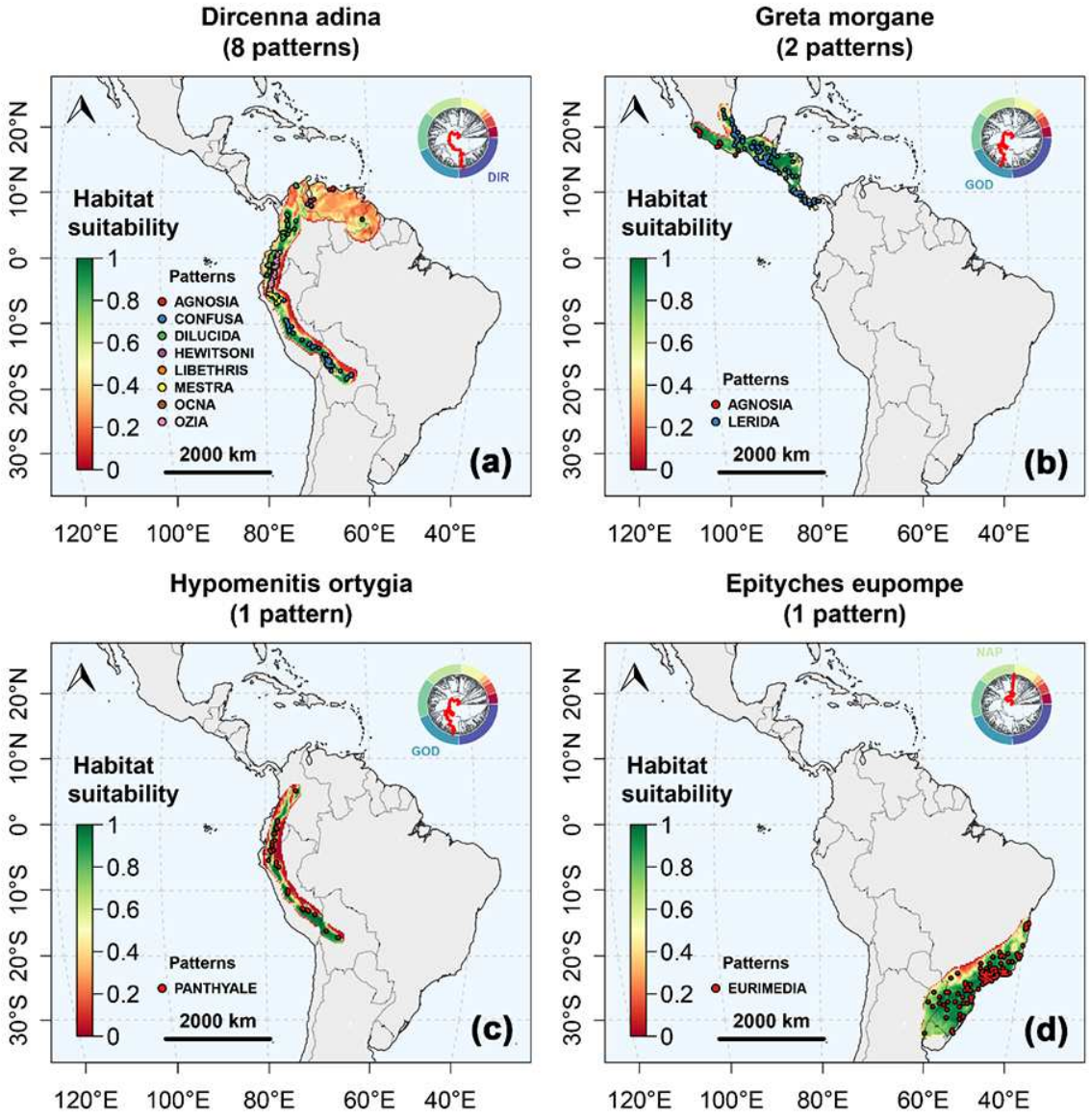

Figure S7.19: Four examples of distribution maps for species resulting from our environmental niche ensemble modeling process. Position in the phylogeny is represented in the top-right corner. **(a)** = An Andean species with multiple mimicry wing patterns: *Dircenna adina*. **(b)** = A species from Central America: *Greta morgane*. **(c)** = An Andean species with a single mimicry wing pattern: *Hypomenitis ortygia*. **(d)** = A species from the Atlantic forest: *Epityches eupompe*. Photo credits: Nicolas Chazot, 2015.

The mimicry ring LERIDA is widely spread in the entire range of Ithomiini. Its species richness reflects the global pattern of diversity, with hotspots in the Andes, the Atlantic forest, and Central America (**Fig. S7.20a)**. In contrast, the mimicry ring HEWITSONI is endemic to the highlands in the Central Andes (**Fig. S7.20c)**. Yet, it shows the same maximum local species richness (around 15 species) as the widespread LERIDA pattern, despite being represented by half as many species (30 species vs. 66 species). The mimicry ring LYSIMNIA is endemic to the Atlantic forest (**Fig. S7.20b)**, while the mimicry ring MAELUS is found only in the Amazonian forest (**Fig. S7.20d)**. Its species richness peaks in the Upper Amazon, which may suggest it originated and spread from this region.

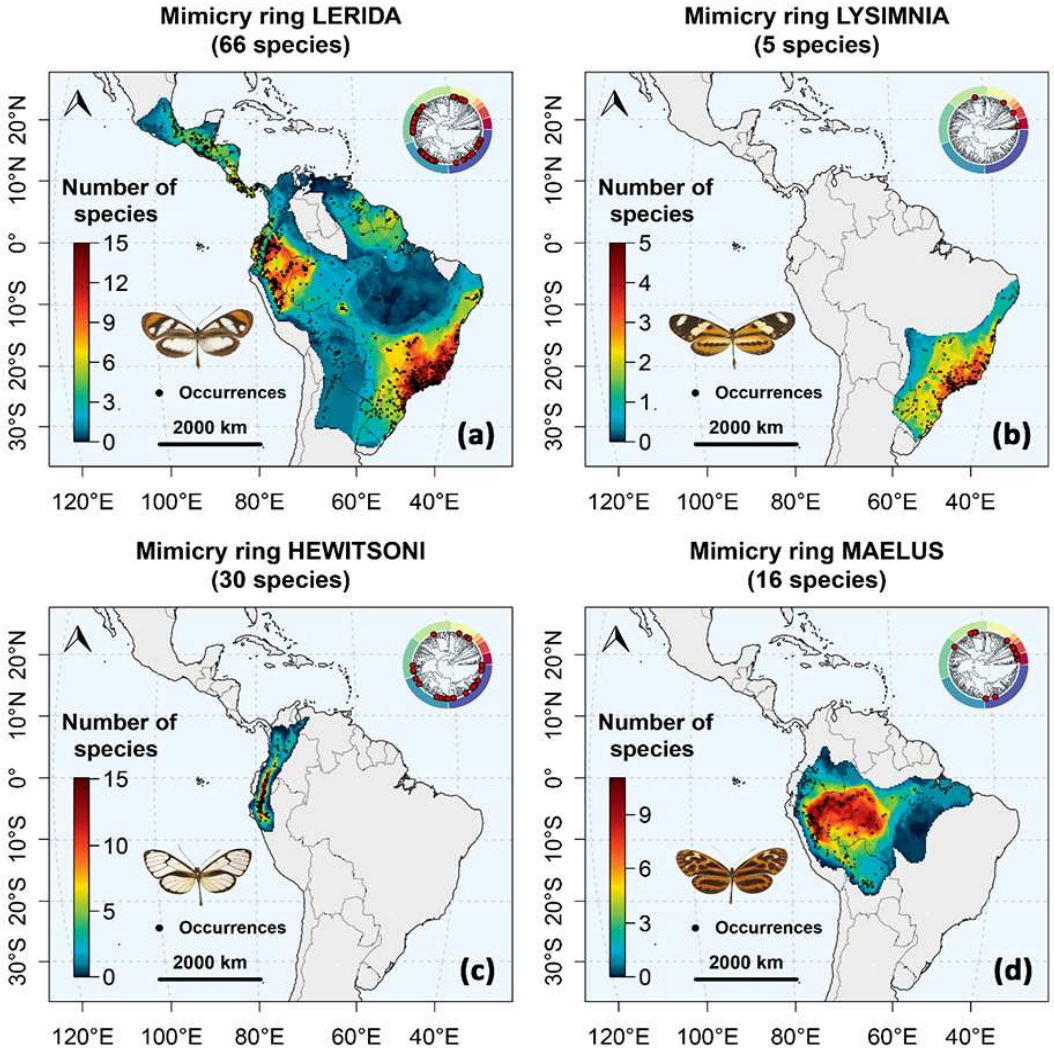

Figure S7.20: Four examples of distribution maps for species resulting from our environmental niche ensemble modeling process. Position in the phylogeny of species harboring the pattern is represented in the top-right corner. **(a)** = A wide-ranging mimicry ring: pattern LERIDA. **(b)** = A mimicry ring endemic to the Atlantic forest: pattern LYSIMNIA. **(c)** = An Andean mimicry ring: pattern HEWISTONI. **(d)** = An Amazonian mimicry ring: pattern MAELUS. Photo credits: Nicolas Chazot, 2015.

Appendix 8: Biodiversity indices: flowchart and details on computation

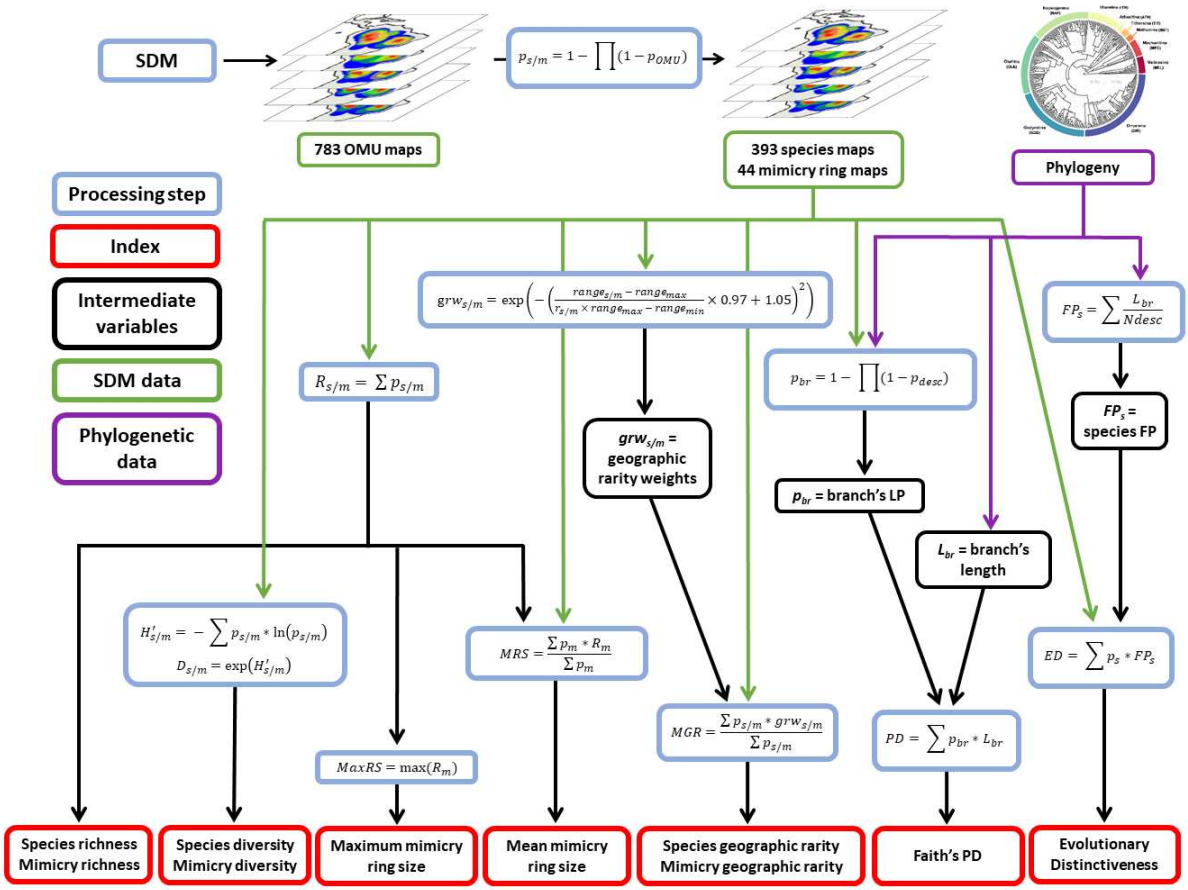

Figure S8.21: Flowchart of index computation from Species Distribution Models (SDM) outputs. p_{OMU} = proxy of probability of presence of an Operational Mimicry Unit (OMU) derived from environmental suitability outputs from SDMs. $p_{s/m}$ = proxy of the likelihood of presence (LP) of a species or a mimicry ring. $R_{s/m}$ = richness indices. $H'_{s/m}$ = Shannon's diversity indices. *MaxRS* = maximum mimicry ring size. *MRS* = Mean mimicry ring size. $grw_{s/m}$ = geographic rarity weights from Leroy *et al.* (2013) with $r_{s/m}$ as rarity thresholds. *MGR* = Mean geographic rarity indices. p_{br} = likelihood of presence of the phylogenetic tree's branch in a community. p_{desc} = likelihood of presence of all descending species from a specific branch. L_{br} = branch's length. *PD* = Faith's Phylogenetic Diversity. *FPs* = Species Fair-Proportion indices. N_{desc} = Number of species descending from a specific branch. *ED* = Evolutionary Distinctiveness. Phylogeny based on Chazot et al. (2019).

We stacked all modeled distribution maps of OMUs in order to obtain in each pixel the predicted occurrence of OMUs. Then, we computed a series of ten indices aiming to describe Ithomiini diversity in various facets. Thresholding can introduce bias leading to overestimation of species richness (Calabrese *et al.* 2014; Guillera-Arroita *et al.* 2015), and thus we did not

apply any threshold to produce binary outputs from the continuous outputs of modeled distribution maps, taken as proxies of likelihood of presence.

We computed species richness and mimicry richness indices ($R_{s/m}$) by summing all proxies of likelihood of presence of species or mimicry rings in a community ($p_{s/m}$) to reach an expected richness estimation.

$$R_{s/m} = \sum p_{s/m} \quad \text{(Eqn. 1)}$$

We estimated species and mimicry diversity firstly as Shannon's diversity index (H'; Shannon 1948)

$$H'_{s/m} = -\sum p_{s/m} \times \ln(p_{s/m}) \quad \text{(Eqn. 2)}$$

where $p_{s/m}$ is the relative frequency of each species or mimicry pattern in the community. For species diversity (D_s), the continuous output of each species modeled distribution map was used as proxy for the relative abundances of each species since environmental suitability can be a reasonable proxy for species abundance (VanDerWal *et al.* 2009). For mimicry diversity (D_m), the number of species/OMUs in each mimicry ring was directly used to compute the relative frequencies. Secondly, we transformed our H' indices following Jost's (2006) recommendations, applying an exponential function as

$$D_{s/m} = \exp(H'_{s/m}) \quad \text{(Eqn. 3)}$$

in order to obtain an effective species or mimicry richness comparable with the richness indices computed previously based on the expected number of species and mimicry rings. Diversity indices reflect the number of species or mimicry rings in equiprobability (*i.e.*, equal relative frequencies) needed to reach such an H' score. Thus, the more unequal the distribution of abundances among the species/mimicry ring in the community, the further from the richness index the effective richness value will fall.

Traditionally, the rarity of a biological entity is evaluated along three dimensions: abundance, geographic range, and habitat specificity (Rabinowitz 1981; Gaston 1997). Among these three, we only had access to geographic range. Thus, we computed species and mimicry geographic rarity based on geographic ranges ($range_{s/m}$) as the sum of all environmental suitability values representing likelihood of presence within each pixel, times the area of pixels (*i.e.*, 27.8 × 27.8 = 772.84 km²). Then, we assigned a relative geographic rarity weight (grw_i)

to each species and mimicry ring following a threshold-dependent exponentially decaying weighting scheme as in Eqn. 4 from Leroy *et al.* (2013). This method assigns weights that exponentially increase below the chosen rarity threshold ($r_{s/m}$), and weights rapidly decay to zero above the threshold, which limits the impact of common species on community indices. We chose the rarity threshold at which the average proportion of rare species in communities was 25%, as detailed in Leroy *et al.* (2012). The rarity threshold (r_s) for species representing the inflexion point of the weights/range curve was 0.125, corresponding to a total range of 983 x 10^3 km². Likewise, the threshold for mimicry rings (r_m) was 0.332, corresponding to a total range of 4,441 x 10^3 km².

$$grw_i = \exp\left(-\left(\frac{range_{s/m} - range_{max}}{r_{s/m} \times range_{max} - range_{min}} \times 0.97 + 1.05\right)^2\right) \quad \text{(Eqn. 4)}$$

Those weights are normalized between 0 and 1 using the maximum range ($range_{max}$) and minimum range ($range_{min}$) observed in the data. Therefore, species/mimicry rings with range close to the rarity threshold value scored 0.05. Species/mimicry rings with a more restricted range scored exponentially higher, up to a score of 1 for the rarest species/mimicry ring. Species/mimicry rings with a wider range showed a score close to 0. For our final mean geographic rarity (*MGR*) maps, we computed the weighted mean of the geographic rarity indices in communities (weighted by the proxy of likelihood of presence of all species/mimicry ring as $p_{s/m}$).

$$MGR = \frac{\sum p_{s/m} \times grw_{s/m}}{\sum p_{s/m}} \quad \text{(Eqn. 5)}$$

We computed two indices of phylogenetic diversity based on the phylogeny of Ithomiini (Chazot *et al.* 2019b) containing 339 species and 719 OMUs. Tree and branch manipulations were conducted with the R packages *ape* 5.3 (Paradis & Schliep 2019) and *geiger* 2.0.6.1 (Harmon *et al.* 2008).

The Fair-Proportion index (FP; Redding, 2003) is a species evolutionary distinctiveness metric calculated first at species level. It aims to represent the portion of the tree attributable to a species. It is computed by summing branch lengths (L_{br}) as shared branches are apportioned equally among all descendant species (N_{desc}).

$$FP_s = \sum \frac{L_{br}}{N_{desc}} \quad \text{(Eqn. 6)}$$

In this community-level analysis, we used the sum of species Fair-Proportion (FP_s) weighted by the proxy of species likelihood of presence (p_s) as our measurement of Evolutionary Distinctiveness (*ED*).

$$ED = \sum p_s \times FP_s \quad \text{(Eqn. 7)}$$

Faith's Phylogenetic Diversity (Faith 1992) was computed as the total length of branches connecting all the species in a given community. In our framework, the proxy of the likelihood of presence of each branch in the community (p_{br}) was estimated as

$$p_{br} = 1 - \prod(1 - p_{desc}) \quad \text{(Eqn. 8)}$$

where p_{desc} is the proxy of the likelihood of presence of all species descending from each specific branch in the global tree. Thus, we used these values to weight the sum of branch' lengths and retrieve the Faith's Phylogenetic Diversity.

$$PD = \sum p_{br} \times L_{br} \quad \text{(Eqn. 9)}$$

To quantify the importance of mutualistic interactions within our communities, we estimated the mean size (*MRS*) of mimicry rings among each community as the weighted mean of mimicry ring richness (R_m), weighted by the likelihood of presence of each mimicry ring (p_m).

$$MRS = \frac{\sum p_m \times R_m}{\sum p_m} \quad \text{(Eqn. 10)}$$

Besides, we also recorded the maximum mimicry ring size (*MaxRS*) found within each community as the highest value for mimicry ring richness (R_m) predicted among all mimicry rings.

$$MaxRS = \max(R_m) \quad \text{(Eqn. 11)}$$

We tested the robustness of the patterns obtained by computing the same indices only for OMUs included in the phylogeny, only for OMUs with niche models, with different thresholds for model selection, and with a different buffer to distribution maps (**see Appendix 5: ODMAP**). Results showed no qualitative differences with the results presented in the main text.

References:

Calabrese, J. M., Certain, G., Kraan, C., & Dormann, C. F. (2014). Stacking species distribution models and adjusting bias by linking them to macroecological models. *Global Ecology and Biogeography*, 23(1), 99–112. https://doi.org/10.1111/geb.12102

Chazot, N., Willmott, K. R., Lamas, G., Freitas, A. V. L., Piron-Prunier, F., Arias, C. F., Mallet, J., De-Silva, D. L., & Elias, M. (2019). Renewed diversification following Miocene landscape turnover in a Neotropical butterfly radiation. *Global Ecology and Biogeography*, 28(8), 1118–1132. https://doi.org/10.1111/geb.12919

Faith, D. P. (1992). Conservation evaluation and phylogenetic diversity. *Biological Conservation*, 61, 1–10. https://doi.org/https://doi.org/10.1016/0006-3207(92)91201-3

Gaston, K. J. (1997). What is rarity? In *The Biology of Rarity* (Vol. 1, Issue 1981, pp. 30–47). Springer Netherlands. https://doi.org/10.1007/978-94-011-5874-9_3

Guillera-Arroita, G., Lahoz-Monfort, J. J., Elith, J., Gordon, A., Kujala, H., Lentini, P. E., Mccarthy, M. A., Tingley, R., & Wintle, B. A. (2015). Is my species distribution model fit for purpose? Matching data and models to applications. *Global Ecology and Biogeography*, 24(3), 276–292. https://doi.org/10.1111/geb.12268

Harmon, L. J., Weir, J. T., Brock, C. D., Glor, R. E., & Challenger, W. (2008). GEIGER: Investigating evolutionary radiations. *Bioinformatics*, 24(1), 129–131. https://doi.org/10.1093/bioinformatics/btm538

Jost, L. (2006). Entropy and diversity. *Oikos*, 113(2), 363–375. https://doi.org/10.1111/j.2006.0030-1299.14714.x

Leroy, B., Canard, A., & Ysnel, F. (2013). Integrating multiple scales in rarity assessments of invertebrate taxa. *Diversity and Distributions*, 19(7), 794–803. https://doi.org/10.1111/ddi.12040

Leroy, B., Petillon, J., Gallon, R., Canard, A., & Ysnel, F. (2012). Improving occurrence-based rarity metrics in conservation studies by including multiple rarity cut-off points. *Insect Conservation* and Diversity, 5(2), 159–168. https://doi.org/10.1111/j.1752-4598.2011.00148.x

Paradis, E., & Schliep, K. (2019). Ape 5.0: An environment for modern phylogenetics and evolutionary analyses in R. *Bioinformatics*, 35(3), 526–528. https://doi.org/10.1093/bioinformatics/bty633

Rabinowitz, D. (1981). Seven forms of rarity. In H. Synge (Ed.), *Biological Aspects of Rare Plant Conservation* (pp. 205–217). Wiley.

Redding, D. W. (2003). Incorporating genetic distinctness and reserve occupancy into a conservation priorisation approach. Master's Thesis. University Of East Anglia, Norwich, UK.

Shannon, C. E. (1948). A mathematical theory of communication. *Bell System Technical Journal*, 27(3), 379–423.

VanDerWal, J., Shoo, L. P., Johnson, C. N., & Williams, S. E. (2009). Abundance and the environmental niche: Environmental suitability estimated from niche models predicts the upper limit of local abundance. *American Naturalist*, 174(2), 282–291. https://doi.org/10.1086/600087

Appendix 9: Alternative index maps and correlations

In addition to the six main indices presented in main text, we computed four additional indices representing similar facets of diversity with alternative methods to explore the robustness of our analyses to index selection (**Fig. S9.22**).

Complementarily to richness, we calculated diversity indices based on Shannon indices (Shannon 1948), thereby also considering the relative frequencies of species or mimicry rings. We applied Jost's transformation (Jost 2006) to obtain diversity indices as effective richness indices (**see Appendix 8**). The more unbalanced the frequencies of species or mimicry rings are, the smaller the diversity indices are compared to richness indices. We computed Shannon diversity indices for species (**Fig. S9.22a**) and mimicry rings (**Fig. S9.22b**). Both maps appeared very similar to the patterns observed for classic species and mimicry richness as presented in the main text (**Fig. 3a & 3d**), with peaks of diversity found in the eastern slopes of the Andean mountain range, and secondary hotspots of species richness in the Atlantic forest and Central America.

We computed an index closely related to Faith's phylogenetic diversity (Faith 1992), the Fair-Proportion index (FP; Redding, 2003). It is an Evolutionary Distinctiveness metric calculated first at species level. It aims to represent the portion of evolutionary history attributable to a species within a phylogenetic tree. By summing species Fair-Proportions, we retrieve the proportion of evolutionary history attributable to the whole community as its Evolutionary Distinctiveness index. As such, conversely to the Faith's phylogenetic diversity index, the length of branches representing evolutionary time are not included fully but apportioned relatively to the proportion of descending species found in the focal community. Overall, its pattern is highly similar to Faith's phylogenetic diversity, and the richness indices, with again peaks in the eastern slopes of the Andean mountain range, and secondary hotspots in the Atlantic forest and Central America (**Fig. S9.22c**).

As a complement to the mean mimicry ring size, we computed the maximum ring size as a measurement of the importance of the potentially most robust group of mutualistically interacting species in each community. As well as for mean ring size, we predicted that the most locally speciose mimicry rings occur in Central America in Panama and Costa Rica, on the eastern slopes of the Andes in Ecuador and Peru, along the Amazon river, and in the Atlantic Forest (**Fig. S9.22d**).

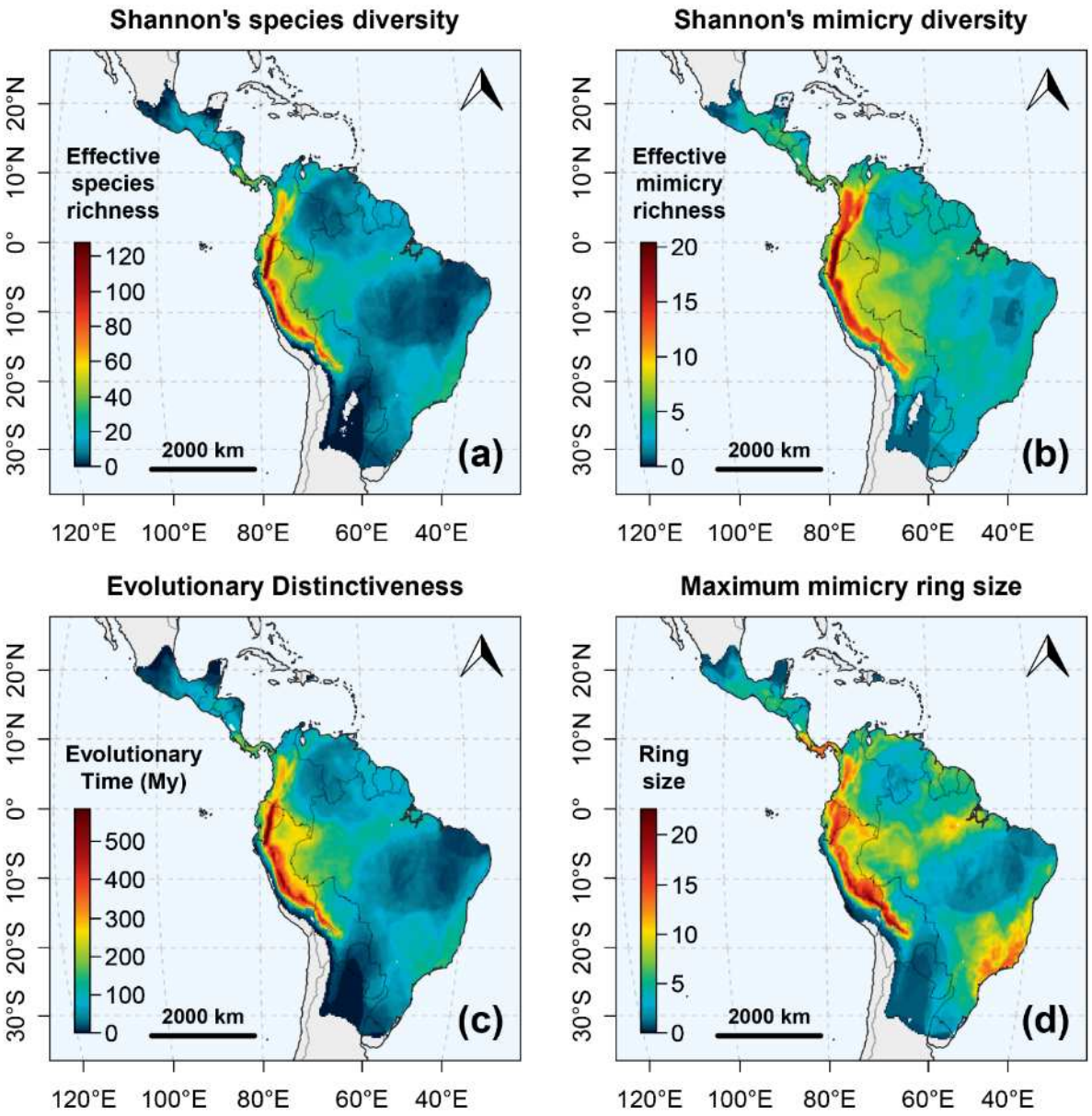

Figure S9.22: Heatmaps of alternative metrics for Ithomiini diversity in the Neotropics at quarter-degree resolution. (a) Shannon's species diversity estimated as effective species richness following Jost's transformation (Jost 2006). (b) Shannon's mimicry diversity estimated as effective mimicry richness following Jost's transformation (Jost 2006). (c) Evolutionary Distinctiveness based on the sum of species Fair-Proportion indices (Redding 2003). (d) Maximum mimicry ring size as the number of species harboring the most common wing pattern locally. Political boundaries are displayed in light grey. All maps are projected under Mollweide's projection, centered on the meridian 75°E.

Overall, these alternative methods to estimate facets of Ithomiini diversity yielded similar results to the ones we presented in the main text. Correlation among indices reinforced our classification of four groups of indices (**Fig. S9.23**).

Shannon's diversity indices, when converted to represent effective richness, correlate very strongly with their respective richness index (**Tables S10.26 & S10.27**: $\rho = 0.999$, $t = 169.8$, Clifford's $df = 57.8$, $p < 0.001$ for species indices ; $\rho = 0.981$, $t = 36.4$, Clifford's $df = 52$, $p < 0.001$ for mimicry indices). Since the effective richness combines the original richness and the distribution of species environmental suitability, it implies that the distribution of species environmental suitability does not vary widely among communities. Likewise, the distribution of species across mimicry rings, which is involved in the computation of the Shannon's mimicry diversity, does not vary widely among communities since the effective mimicry richness also correlates strongly with the original mimicry richness. As such, we grouped species diversity with the group of indices strongly correlated with species richness, while mimicry diversity formed a separated group with mimicry richness (**Fig. S9.23**).

Similarly, the Faith's Phylogenetic Diversity and the Evolutionary Distinctiveness also correlate strongly between each other (**Tables S10.26 & S10.27**: $\rho = 0.993$, $t = 61.6$, Clifford's $df = 53.8$, $p < 0.001$) and with species richness (**Tables S10.26 & S10.27**: $\rho = 0.993$, $t = 61.9$, Clifford's $df = 54.3$, $p < 0.001$ between species richness and Evolutionary Distinctiveness). Those indices estimate phylogenetic diversity as a sum of branches depicting the total evolutionary time represented in a community defined as a sum of species. Since the richest communities comprise a large portion of the total species pool (i.e., up to 135 out of 393 species, around a third of the entire tribe), they tend to encompass a larger part of the evolutionary history of the Ithomiini tribe, and thus drive a strong correlation between these indices of phylogenetic diversity and species richness. As such, they are grouped together with species richness (**Fig. S9.23**).

Finally, the maximum ring size correlated strongly with the mean ring size (**Tables S10.26 & S10.27**: $\rho = 0.957$, $t = 25.6$, Clifford's $df = 60.5$, $p < 0.001$), and is also correlated with species richness (**Tables S10.26 & S10.27**: $\rho = 0.948$, $t = 23.75$, Clifford's $df = 63.6$, $p < 0.001$). Thus, communities harboring the most speciose mimicry ring on average, are also the ones harboring the most speciose mimicry rings in absolute, and the highest species richness. Indeed, since the positive correlation between mimicry richness and species richness tends to saturate in the richest communities (**Fig. S10.24c**), it is expected that the most speciose communities also host the largest mimicry rings. As such, the maximum ring size index is also grouped with species richness, alongside the mean mimicry ring size index (**Fig. S9.23**).

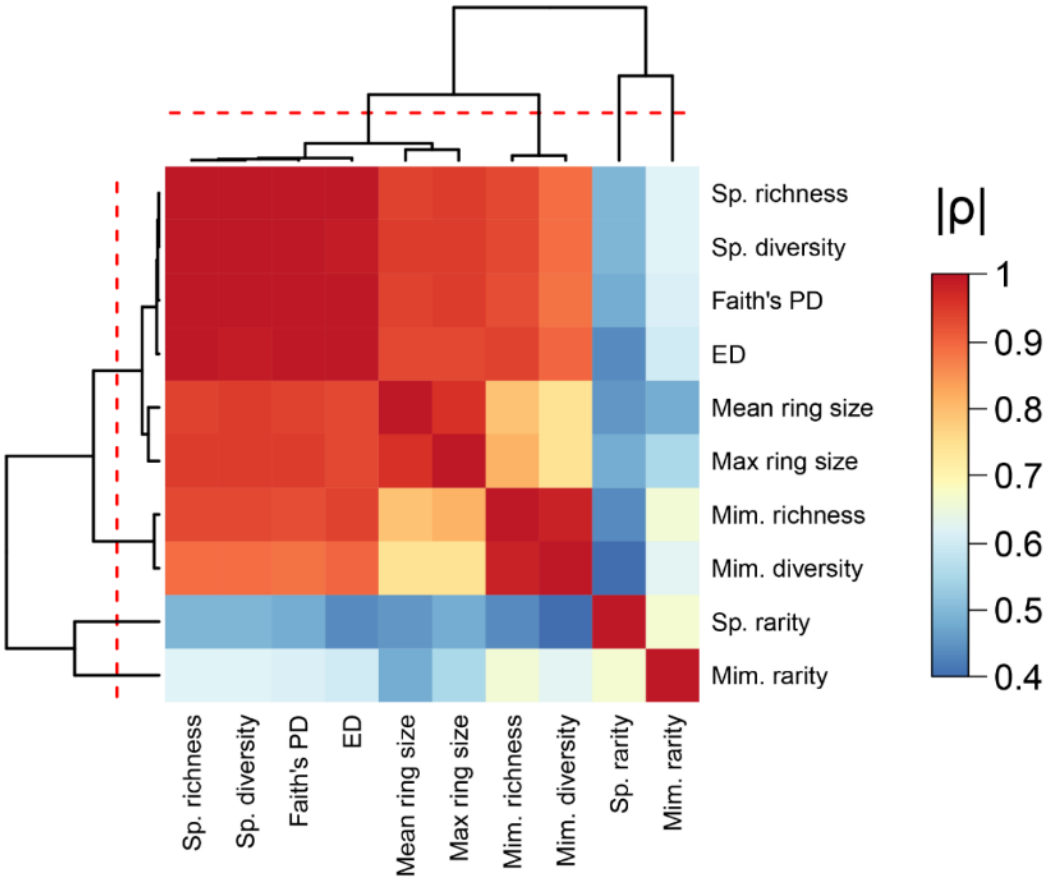

Figure S9.23: Heatmap of index correlations based on the absolute values of Spearman's rho statistics (ρ). Dendrogram built with a complete link method. Red dashed lines represent the threshold used to regroup indices with strong correlation (|ρ| = 0.94). Sp. = Species. Mim. = Mimicry. PD = Phylogenetic Diversity. ED = Evolutionary Distinctiveness as sum of species Fair-Proportions (Redding 2003). Ring as mimicry ring. Rarity as geographic rarity.

References:

Jost, L. (2006). Entropy and diversity. *Oikos*, 113(2), 363–375. https://doi.org/10.1111/j.2006.0030-1299.14714.x

Redding, D. W. (2003). Incorporating genetic distinctness and reserve occupancy into a conservation priorisation approach. Master's Thesis. University Of East Anglia, Norwich, UK.

Appendix 10: Correlation between indices

Overall, relationships between the different facets of Ithomiini diversity show a high degree of spatial congruence reflected by significant and high correlation coefficients (**Fig. S10.25).** Yet, this global pattern can hide more subtle relationships that differ for low scoring and high scoring communities.

For instance, species-rich communities tended to present high mean geographic rarity values, while species-poor communities exhibited the entire range of relative levels of species and mimicry ring endemism (**Fig. S10.24a & S10.24b**). Similarly, communities with high mimicry richness showed high mean mimicry geographic rarity, while communities with few mimicry rings could exhibit the entire range of relative levels of mimicry endemism (**Fig. S10.24d**). Despite being positively correlated with species richness, our indices of geographic rarity allowed us to highlight communities of high conservation interest harboring few species and/or mimicry rings, yet hosting some of the rarest biological features in ithomiine butterflies. As such, we classified our two indices of geographic rarity in independent groups in order to investigate threats on their hotspots separately, and reveal potential differences in threat levels across these different facets of Ithomiini diversity.

Moreover, a more careful investigation of the relationship between species richness and mimicry richness revealed it was not strictly linear: some communities with the highest number of mimicry rings are not the most speciose, and the positive correlation between mimicry richness and species richness tends to saturate in the richest communities (**Fig. S10.24c**). As discussed, in the main-text, this pattern of 'mimicry' saturation is expected from Müllerian mimicry theory that predicts the local convergence of wing patterns. Yet, the relationship appeared only slightly saturated, which suggests that even in species-rich communities there is some free ecological space, or that the effect of selection for wing pattern convergence is weaker than thought in Müllerian mimetic communities.

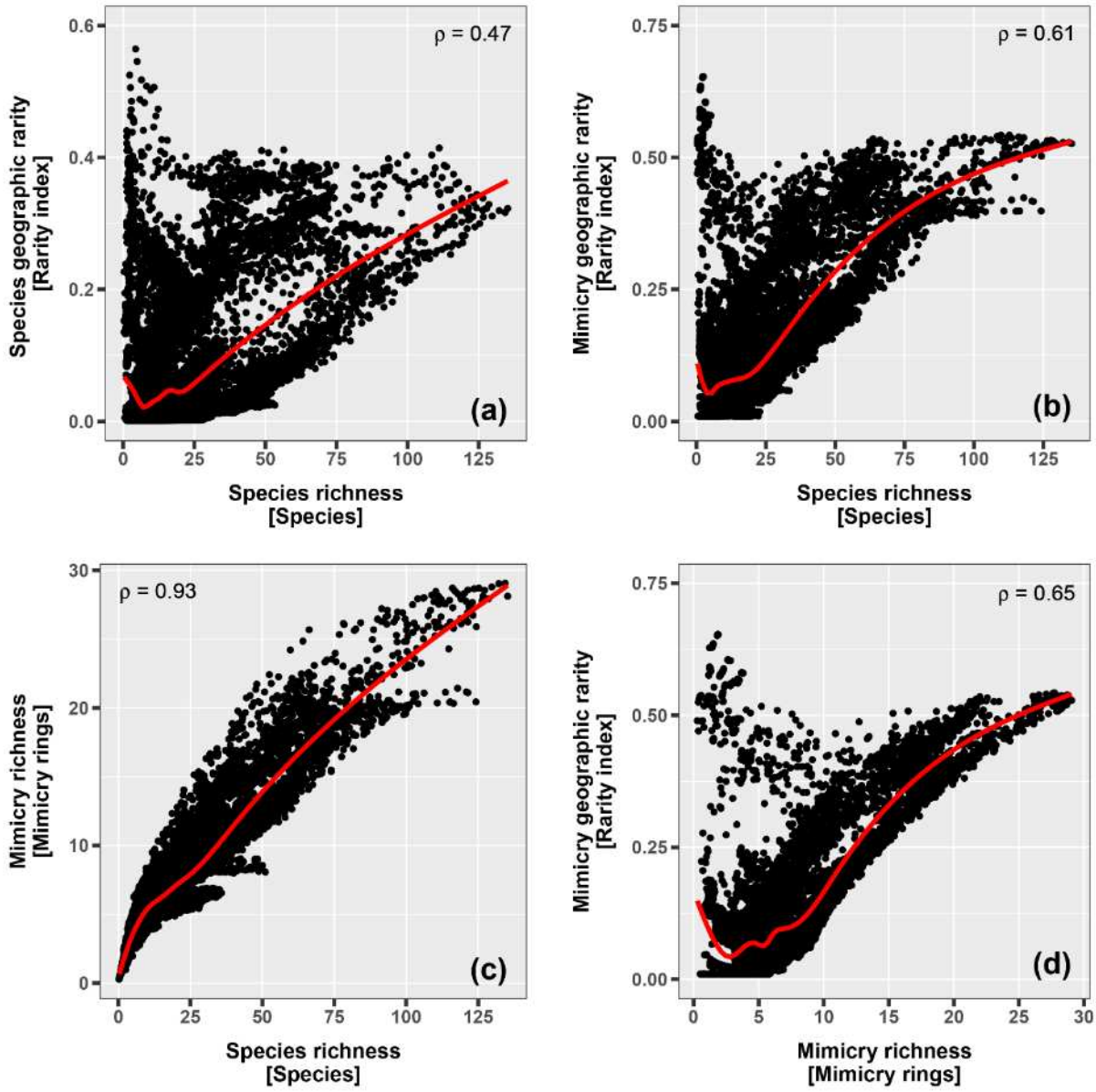

Figure S10.24: Relationships between diversity and geographic rarity indices in Ithomiini communities in the Neotropics. Each point represents a community (i.e., a pixel on the map). Smooth curves obtained from GAM fits with cubic regression splines as smoothing basis. ρ = Spearman's spatial rank correlation coefficient.

All pairwise scatterplots with associated Spearman's rho correlation coefficients to estimate the spatial congruence across indices are presented in **Fig. S10.25**. Details on the correlation tests for significance with corrected degrees of freedom accounting for the positive spatial autocorrelation among observations (Clifford *et al.* 1989; Haining 1991) can be found in **Tables S10.26 & S10.27**.

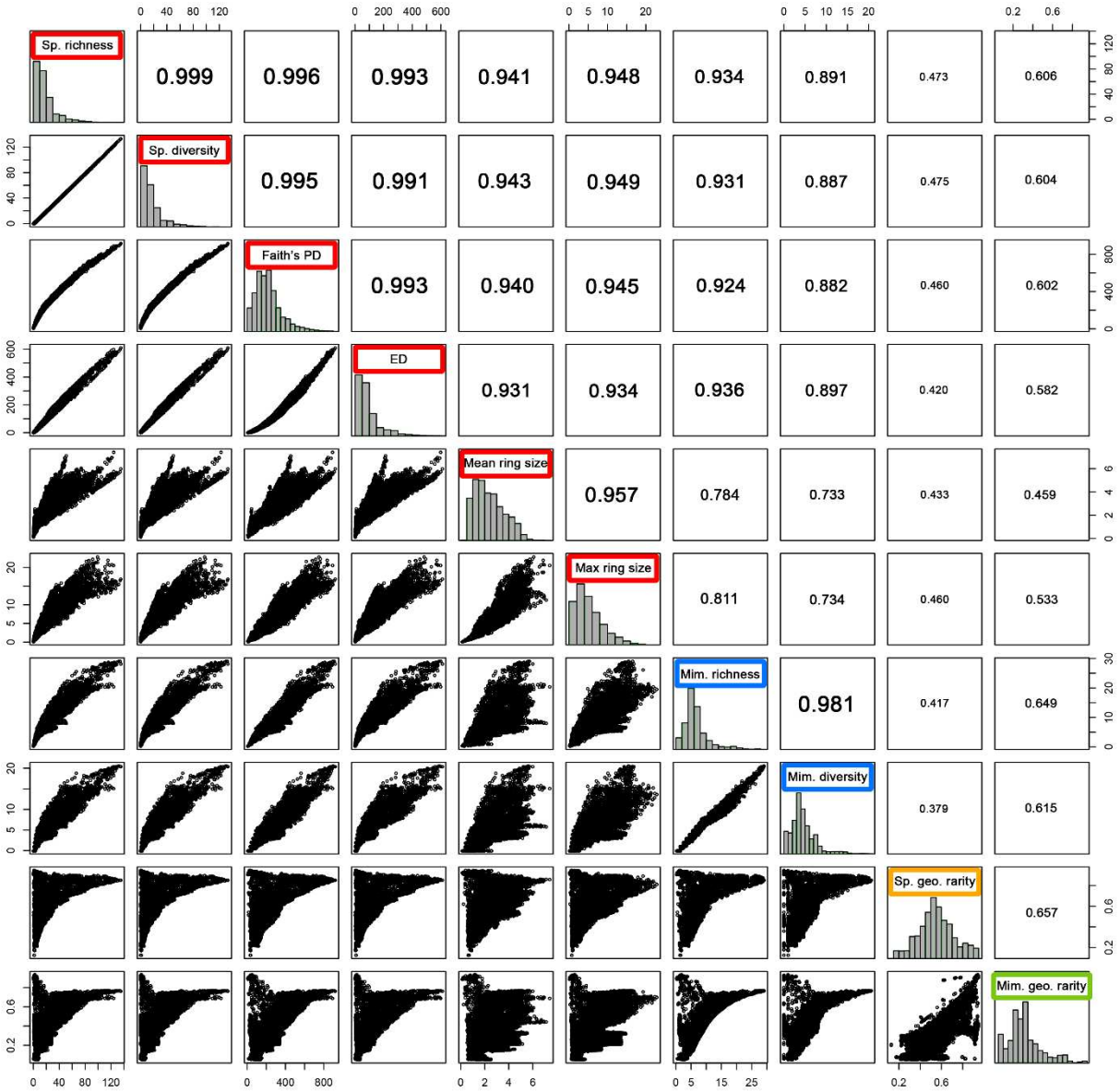

Figure S10.25: Relationships between all pairs of biodiversity indices. Each point in the scatter plots in the lower triangle represents a community (i.e., a pixel on the map). Upper triangle represents Spearman's spatial rank correlation coefficients (ρ). Colored labels correspond to index groups as defined on the dendrogram in Figure S9.18.

Table S10.26: Spearman's rho coefficients (lower triangle) and associated p-value (upper triangle) for pairwise evaluation of spatial correlation among indices. All values are significant (** $p < 0.01$, *** $p < 0.001$). Bold indices are the one presented in main text. Bold values correspond to indices belonging to the same group.

		p-values									
		Sp. richness	Sp. diversity	**Faith's PD**	ED	**Mean ring size**	Max ring size	**Mim. richness**	Mim. diversity	**Sp. rarity**	**Mim. rarity**
Rho coefficients	**Sp. richness**	-	**< 0.001*** **	**< 0.001*** **	**< 0.001*** **	**< 0.001*** **	**< 0.001*** **	< 0.001***	< 0.001***	< 0.001***	< 0.001***
	Sp. diversity	**0.999**	-	**< 0.001*** **	**< 0.001*** **	**< 0.001*** **	**< 0.001*** **	< 0.001***	< 0.001***	< 0.001***	< 0.001***
	Faith's PD	**0.996**	**0.995**	-	**< 0.001*** **	**< 0.001*** **	**< 0.001*** **	< 0.001***	< 0.001***	< 0.001***	< 0.001***
	ED	**0.993**	**0.991**	**0.993**	-	**< 0.001*** **	**< 0.001*** **	< 0.001***	< 0.001***	0.001**	< 0.001***
	Mean ring size	**0.941**	**0.943**	**0.94**	**0.931**	-	**< 0.001*** **	< 0.001***	< 0.001***	< 0.001***	< 0.001***
	Max ring size	**0.948**	**0.949**	**0.945**	**0.934**	**0.957**	-	< 0.001***	< 0.001***	< 0.001***	< 0.001***
	Mim. richness	0.934	0.931	0.924	0.936	0.784	0.811	-	**< 0.001*** **	0.001**	< 0.001***
	Mim. diversity	0.891	0.887	0.882	0.897	0.733	0.734	**0.981**	-	0.002**	< 0.001***
	Sp. rarity	0.473	0.475	0.46	0.42	0.433	0.46	0.417	0.379	-	< 0.001***
	Mim. rarity	0.606	0.604	0.602	0.582	0.459	0.533	0.649	0.615	0.657	-

Table S10.27: T-statistics (lower triangle) and corrected degrees of freedom (upper triangle) for pairwise spatial correlation test among indices. Bold indices are the ones presented in main text. Bold values correspond to indices belonging to the same group.

		Clifford's corrected degrees of freedom									
		Sp. richness	Sp. diversity	**Faith's PD**	ED	**Mean ring size**	Max ring size	**Mim. richness**	Mim. diversity	**Sp. rarity**	**Mim. rarity**
T-statistics	**Sp. richness**	-	**57.8**	**56.7**	**54.3**	**57.9**	**63.6**	56.6	57	65.4	61.5
	Sp. diversity	**169.84**	-	**57.3**	**54.8**	**58.3**	**64**	57.3	57.7	66.1	62.4
	Faith's PD	**83.96**	**75.38**	-	**53.8**	**57**	**62.7**	56.5	56.8	65.2	61.6
	ED	**61.93**	**54.8**	**61.65**	-	**55**	**60.6**	53.5	53.7	62.2	58.1
	Mean ring size	**21.16**	**21.63**	**20.8**	**18.92**	-	**60.5**	62.1	63.4	69.6	71.9
	Max ring size	**23.75**	**24.08**	**22.89**	**20.34**	**25.65**	-	66.9	68.3	74.5	76
	Mim. richness	19.67	19.31	18.16	19.45	9.95	11.34	-	**52**	62.2	54.2
	Mim. diversity	14.82	14.6	14.11	14.88	8.58	8.93	**36.45**	-	62.5	53.5
	Sp. rarity	4.34	4.39	4.18	3.65	4.01	4.47	3.62	3.24	-	65.5
	Mim. rarity	5.98	5.99	5.92	5.45	4.38	5.49	6.28	5.7	7.05	-

References:

Clifford, P., Richardson, S., & Hemon, D. (1989). Assessing the Significance of the Correlation between Two Spatial Processes. *Biometrics*, 45(1), 123–134. https://www.jstor.org/stable/2532039

Haining, R. (1991). Bivariate Correlation with Spatial Data. *Geographical Analysis*, 23(3), 210–227. https://doi.org/10.1111/j.1538-4632.1991.tb00235.x

Appendix 11: Threats on biodiversity hotspots: threshold-independent analysis

In our analyses, we estimated mean species geographic rarity hotspots to be relatively more threatened than the other facets of Ithomiini diversity, and their level of threats to deviate positively from those expected from a random distribution of anthropogenic threats (**Fig. 5c-d & 6**). We based our conclusion on analyses based on the top 5% and 25% of communities defined as hotspots. To support this finding, we investigated the evolution of the mean threat level undergone by communities ranked following their biodiversity scores for several indices, independently from the use of a threshold to discriminate biodiversity hotspots. We found a similar trend with communities hosting the rarest species showing on average the highest levels of anthropogenic threats (higher Human Footprint levels) independently from the threshold applied to defined hotspots (**Fig. S11.28)**. Additionally, communities hosting the rarest mimicry rings also demonstrated higher levels of threats than expected from a random distribution of anthropogenic pressures in space (i.e., the curve remain above the mean threat level within the Ithomiini range). In contrast, the communities with the most species did not appear particularly under threat, except from the top 5% ones, as previously found in our main analyses.

Overall, this complementary investigation confirms that ithomiine communities hosting the geographically rarest (i.e., with a small range) species and mimicry rings are currently facing high levels of anthropogenic threats. This situation is of particular concern since species with small distribution ranges are known to face higher risks of extinction (Purvis *et al.* 2000; Cardillo *et al.* 2008; Böhm *et al.* 2016), thereby also impacting the narrowly distributed mimicry rings they represent.

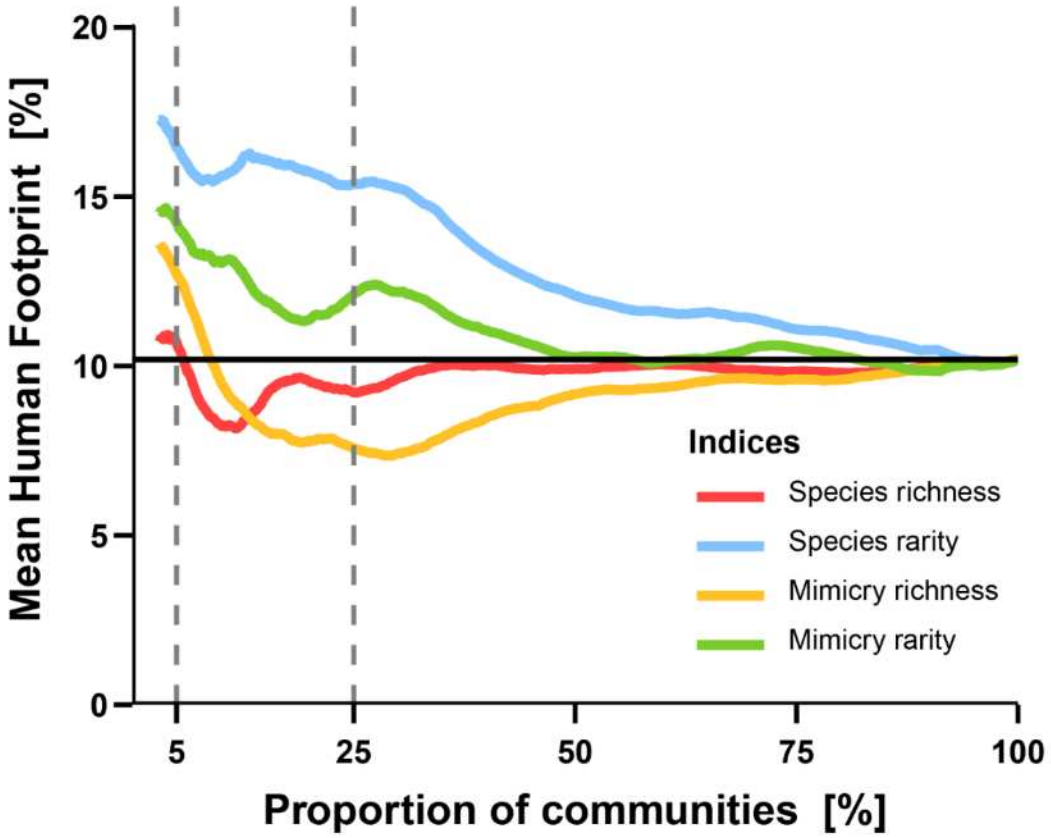

Figure S11.28: Anthropogenic pressures in ranked communities. Evolution of the mean Human Footprint level (HF; Venter *et al.* 2016) undergone by communities (i.e., quarter-degree grid cells). Communities are aggregated iteratively following their biodiversity scores starting from the higher scores down to the minimum scores to encompass all ithomiine communities. Each curve represents the evolution of mean Human Footprint levels following rank based on species richness (red), species rarity (blue), mimicry richness (orange), and mimicry rarity (green). Horizontal line represents the mean level of anthropogenic threats undergone by all Ithomiine communities: mean HF = 10.2 %. As such, this illustrates the expected level of threat undergone by any group of communities if the Human Footprint was distributed randomly in space. Vertical dashed lines represent thresholds used to designed our two levels of hotspots (Top 5% and top 25%) investigated in Fig. 5 & 6 in the main text.

References:

Böhm, M., Williams, R., Bramhall, H.R., Mcmillan, K.M., Davidson, A.D., Garcia, A., et al. (2016). Correlates of extinction risk in squamate reptiles: The relative importance of biology, geography, threat and range size. *Glob. Ecol. Biogeogr.*, 25, 391–405.

Cardillo, M., MacE, G.M., Gittleman, J.L., Jones, K.E., Bielby, J. & Purvis, A. (2008). The predictability of extinction: Biological and external correlates of decline in mammals. *Proc. R. Soc. B Biol. Sci.*, 275, 1441–1448.

Purvis, A., Gittleman, J.L., Cowlishaw, G. & Mace, G.M. (2000). Predicting extinction risk in declining species. *Proc. R. Soc. B Biol. Sci.*, 267, 1947–1952.

ANNEXE 2

ODMAP for CHAPTER 1

Anthropogenic pressures coincide with Neotropical biodiversity hotspots in a flagship butterfly group

Maël Doré*[1,2], Keith Willmott[3], Boris Leroy[4], Nicolas Chazot[5], James Mallet[6], André V. L. Freitas[7], Jason P. W. Hall[8], Gerardo Lamas[9], Kanchon K. Dasmahapatra[10], Colin Fontaine[2], and Marianne Elias[1]

[1]*Institut de Systématique, Evolution, Biodiversité, MNHN-CNRS-Sorbonne Université-EPHE-Université des Antilles, Muséum national d'Histoire naturelle de Paris, 45 Rue Buffon, 75005, Paris, France*

[2]*Centre d'Ecologie et des Sciences de la Conservation, UMR 7204 MNHN-CNRS-Sorbonne Université, Muséum national d'Histoire naturelle de Paris, 45 rue Buffon, 75005, Paris, France*

[3]*McGuire Center for Lepidoptera and Biodiversity, Florida Museum of Natural History, University of Florida, Gainesville, FL, United States of America*

[4]*Unité Biologie des Organismes et Ecosystèmes Aquatiques (BOREA UMR 7208), Muséum National d'Histoire Naturelle, Sorbonne Universités, Université de Caen Normandie, Université des Antilles, CNRS, IRD, Paris, France*

[5]*Swedish University of Agricultural Sciences, Uppsala, Sweden*

[6]*Dept of Organismic and Evolutionary Biology, Harvard University, Cambridge, MA, United States of America*

[7]*Departamento de Biologia Animal and Museu da Biodiversidade, Instituto de Biologia, Universidade Estadual de Campinas, 13083-862 Campinas, São Paulo, Brazil*

[8]*Department of Entomology, National Museum of Natural History, Smithsonian Institution, Washington, DC 20560-0127, United States of America*

[9]*Museo de Historia Natural, Universidad Nacional Mayor de San Marcos, Lima, Peru*

[10]*Dept of Biology, University of York, Wentworth Way, Heslington, UK*

– ODMAP Protocol –

2021-01-27

1 Overview

1.1 Authorship

Authors: Maël Doré, Keith Willmott, Boris Leroy, Nicolas Chazot, James Mallet, André V. L. Freitas, Jason P. W. Hall, Gerardo Lamas, Kanchon K. Dasmahapatra, Colin Fontaine, and Marianne Elias

Contact: Maël Doré ; mael.dore@gmail.com

Title: Anthropogenic pressures coincide with Neotropical biodiversity hotspots in a flagship butterfly group

1.2 Model objective

Model objectives: Mapping and interpolation. We mapped current potential distribution of species and mimicry rings. Additionally, we mapped current potential patterns of different facets of rarity and diversity (taxonomic, phylogenetic, and mimicry) for the whole Ithomiini tribe.

Target output: Meeting our objectives required several steps in the post-processing of model outputs. (i) We obtained environmental suitability maps depicting potential distributions from SDM for each modeling unit (Operational Mimicry Unit, OMU). (ii) We predicted species and mimicry ring distribution maps as likelihood of presence of at least one OMU from the species/ring. (iii) We obtained richness maps as stacked-SDMs from species and mimicry-ring maps. (iv) We computed various taxonomic, phylogenetic and mimicry diversity and rarity indices from the previous richness maps.

1.3 Focal Taxon

Focal Taxon: Our study group was the Neotropical clearwing butterfly tribe Ithomiini Godman & Salvin, 1879 (Nymphalidae: Danainae). This clade represents the most diverse radiation of mimetic butterflies known, with 1,511 subspecies distributed among 396 species, 42 genera, and 10 subtribes (Chazot *et al.* 2019b). Our study includes the 388 species with available georeferenced occurrences. Our base modeling units were the 783 Operational Mimicry Units (OMU) defined as group of subspecies of a unique species sharing the same mimicry pattern.

1.4 Location

Location: Neotropics, from Argentina to Mexico, including the Caribbean region, encompassing the whole range of the Ithomiini tribe.

1.5 Scale of Analysis

Spatial extent: Longitude 120° E - 30° E, Latitude 37° S – 28° S

Spatial resolution:

Community boundaries were defined as grid cell of 0.25° x 0.25° = 27.8km x 27.8km.

As a methodological point, this resolution is appropriate for developing niche models based on large scale predictors such as climate (McGill 2010). Furthermore, it has been previously identified as suitable for reducing the effects of commission errors (where species are thought to be present but are not) when working with species range maps (Di Marco *et al.* 2017), while limiting possibilities for individual butterfly ranges to overlap two cells.

As a practical point, this resolution is sufficient to identify broad geographic patterns of diversity at a scale relevant to biodiversity conservation (e.g., Roll *et al.* 2017; Gumbs *et al.* 2020; Abreu-Jardim *et al.* 2021; Robuchon *et al.* 2021). For example, it enables identification of high priority areas even within specific regions of countries, at a scale comparable, for example, to that of individual national protected areas that may span a range of habitats.

Temporal extent: Field surveys were conducted from 1988 to 2020. The dataset is complemented with historical records that span from 1826 to present, with the majority within the last 50 years. Considering the scale of spatial resolution of this study, we assumed that visits to historical localities (i.e., sites within the same grid cell) would result in finding the same species.

Temporal resolution: We modeled distributions under current environmental conditions: we retrieved bioclimatic data for the 2000's decade, and forest cover data for the year 2010.

Boundary: We constrained the study area to the spatial extent provided in previous subsection in order to encompass the distribution range of the whole Ithomiini tribe.

1.6 Biodiversity data

Observation type: Georeferenced occurrences from field surveys and museum collections

Response data type: An initial set of 28,986 species-locality records as presence data were screened to yield 19,271 species-grid-cell records after removing duplicate records from single grid cells. We drew pseudo-absences from those occurrences in a target group strategy. See details in Data.

1.7 Predictors

Predictor types: bioclimatic, topographic (elevation), and habitat (forest cover)

1.8 Hypotheses

Hypotheses:

Ithomiini inhabit mainly moist forest in the Neotropics (Brown, 1979). Thus, their distribution is expected to be widely influenced by the local availability of forest cover. Likewise, elevation has been shown to shape the species and mimetic composition of Ithomiini communities (Chazot *et al.* 2014). We also used climatic layers as predictors in an exploratory way because

climate is known to be an important driver of species distributions at a continental scale in general (Thomas *et al.* 2004).

1.9 Assumptions

Model assumptions: We assumed that (i) relevant ecological drivers (or proxies) of species distributions are included, (ii) detectability does not change across environmental gradients, (iii) predictor measurements are free of error, (iv) the species are at equilibrium with their environment, (v) sampling is sufficient and representative, and (vi) environmental suitability outputs are valuable proxies to estimate potential distributions.

1.10 Algorithms

Modelling techniques: The main issue with our dataset is the low sample size of many modeling units. Thus, we chose to limit our methods to machine learning algorithms since, unlike regression methods, those algorithms do not rely on parameter estimates burning degrees of freedom, thus they have no restriction regarding the sample size vs. the number of predictors involved in the modeling process. We employed three different algorithms: Random Forest (RF), Generalized Boosted Models (GBM) also known as Boosted Regression Trees (BRT), and Artificial Neural Networks (ANN).

Model complexity: We kept model settings to the default settings in *biomod2* v.3.4.6, keeping a balance between flexibility of the response curves and overfitting (Merow *et al.* 2014). The only exceptions were the minimum size of leaves that was lowered to two instead of five, and the fraction of observations used at each step (0.7 instead of 0.5) to allow tentative runs in GBM for OMUs with low sample size.

Model ensembles: We stacked all models meeting our validation thresholds to produce a single "ensemble" model per unit. We computed the ensemble as the median rather than the mean to limit influence of models with extreme outputs. We did not use a weighting scheme since we considered our evaluation metric (i.e., Jaccard index) a suitable metric to discard low quality models, but not adequate to rank best models in the context of pseudo-absences data (Leroy *et al.* 2018).

1.11 Workflow

Model workflow: We fitted SDMs for 563 OMUs (72%) representing 325 species (84%), for which we had at least six occurrences available. We included the remaining OMUs in stacks as binary raster of presence-absences. Workflow also differed between the 361 OMUs with restricted sample size ($6 \leq N < 30$) and the 202 OMUs with large sample size ($N \geq 30$). For restricted sample size, we kept all occurrences for calibration and validation and draw 10 independent pseudo-absences sets. For large sample sizes, we drew three independent pseudo-absences sets combined with 3-fold spatial block cross-validation to assess predictive model performance. We selected valid models for ensemble based on maximized Jaccard indices and plausibility checks. Ensemble predictions were derived using ensemble medians. We clipped final outputs with OMU-specific buffered alpha-hulls and Andean region masks to constrain the extent of possible distributions to reasonable areas. We derived species and mimicry rings maps from the OMU maps as the likelihood to find at least one of the related OMU in the community. Final post-processing step consisted in the computation of nine diversity and rarity

indices based directly on the species or mimicry ring maps. This workflow is depicted in as a chart in Figure 2 in the main text, reproduced in **Figure S5.5** below.

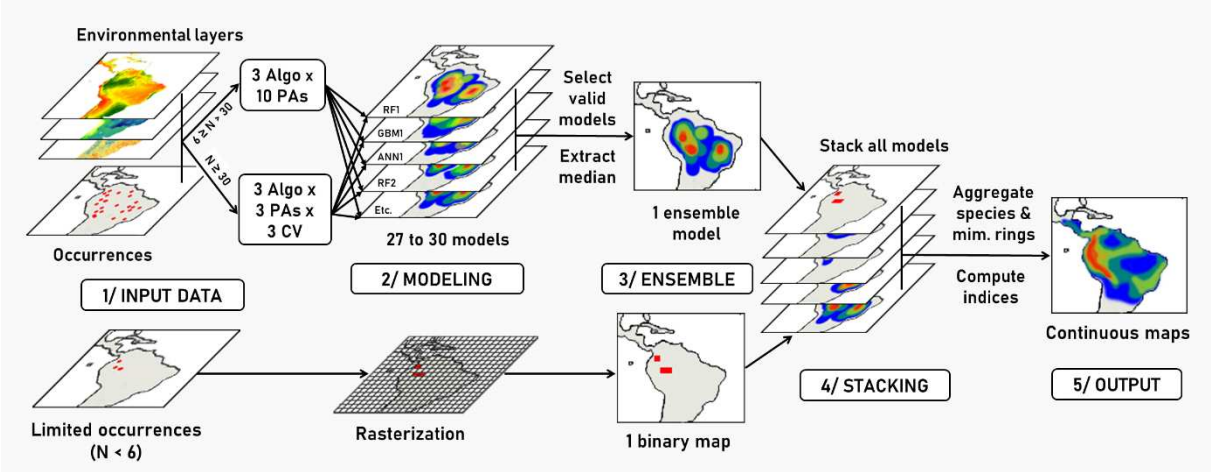

Figure S5.7: SDM workflow chart depicting the different steps of the analysis performed in this study. Depending on sample size, modeling steps and settings differed. Clipping step to constrain SDM projections to plausible distribution ranges is not shown on the chart. Algo = algorithms used in the study, namely random forest (RF), gradient boosting models (GBM), and artificial neural networks (ANN); PAs = pseudo-absences sets; CV = cross-validation folds.

1.12 Software

Software: R version 3.6.2 (R Core Team 2019) with packages *raster* 3.0-12 (Hijmans 2020), *biomod2* 3.4.6 (Thuiller *et al.* 2020), *sf* 0.9-0 (Pebesma 2018), *blockCV* 2.1.1 (Valavi *et al.* 2019), *alphahull* 2.2 (Pateiro-Lopez & Rodriguez-Casal 2019), and others.

Code availability: All scripts are provided on GitHub at https://github.com/MaelDore/ithomiini_diversity

Data availability: Occurrences data and mimicry ring delimitation used for modeling are available from Zenodo at 10.5281/zenodo.4696055 and 10.5281/zenodo.5497876. All OMU/species/mimicry ring modeled distribution maps are available from Zenodo at 10.5281/zenodo.4673446.

2 Data

2.1 Biodiversity data

Taxon names: Ithomiini tribe (All species and OMUs are listed in the taxonomic list in **Appendix 4**).

Taxonomic reference system: Current names in use in the most recent published phylogeny of the group (Chazot *et al.* 2019b).

Ecological level: Operational Mimicry Units (OMU) as subspecies of a unique species sharing the same mimicry pattern. We chose to model at OMU-level because (i) we aimed to investigate patterns of mimicry rings, and (ii) we suspected OMUs of the same species to show rapid divergent evolution of their niche since Müllerian mimicry theory predicts spatial overlap of species variants to be selected against (Sherratt 2006). In case of sexual dimorphism (i.e., male and females displaying different mimicry patterns), the occurrences were duplicated and the output models were assigned to their respective mimicry ring for mimicry ring-level models. There are 783 OMUs representing the whole Ithomiini tribe.

Data sources: Dataset of georeferenced occurrences is a compilation of fieldwork data from G. Lamas (Museo de Historial Natural, UNMSM, Peru), K. Willmott (University of Florida, USA), A.V.L. Freitas (University of Campinas, Brazil), J. Mallet (UCL, UK), and M. Elias (MNHN, France), obtained over the past five decades.

Additionally, the dataset comprises records from more than 60 museums and private collections compiled by K. Willmott and G. Lamas over several decades of research on Ithomiini. The main contributors (>200 records each) are the Natural History Museum, London (NHMUK), the Museo de Historia Natural, Universidad Mayor de San Marcos, Lima (MUSM), the McGuire Center, Florida Museum of Natural History, Gainesville (FLMNH), the United States National Museum, Washington D.C. (USNM), the American Museum of Natural History, New York (AMNH), and the Zoological Collection of the "Museu da Biodiversidade" at the University of Campinas (ZUEC).

The dataset of the 19,271 species-grid-cell records for distribution modeling is available from Zenodo at 10.5281/zenodo.4696055. A map of all occurrences and sampling effort is provided in **Fig. S1.1**.

Sampling design: During fieldwork, we mainly collected specimens following the same protocol: collectors focused efforts on areas of the forest were Ithomiini were observed to be abundant, often in tall forest near streams, using hand nets and attempting to collect all individuals encountered (Chazot et al., 2014; for further details see Willmott et al., 2020).

Sample size: Sample size for each OMU, after spatial filtering, varied widely from 1 to 316. We employed a different modeling scheme for OMUs falling into different sample size categories. We classified the 202 OMUs (28.1%) with sample size lower than six as "rasterized" and did not go through the SDM process. We labelled as "restricted" the 361 OMUs (46.1%) with sample size between 6 and 29. We modeled these "restricted" OMUs without cross-validation. The 202 OMUs (25.8%) with sample size greater or equal to 30 underwent the full SDM process. See workflow in **Fig. S5.7** and distribution of occurrences across OMUs in **Fig. S5.8**.

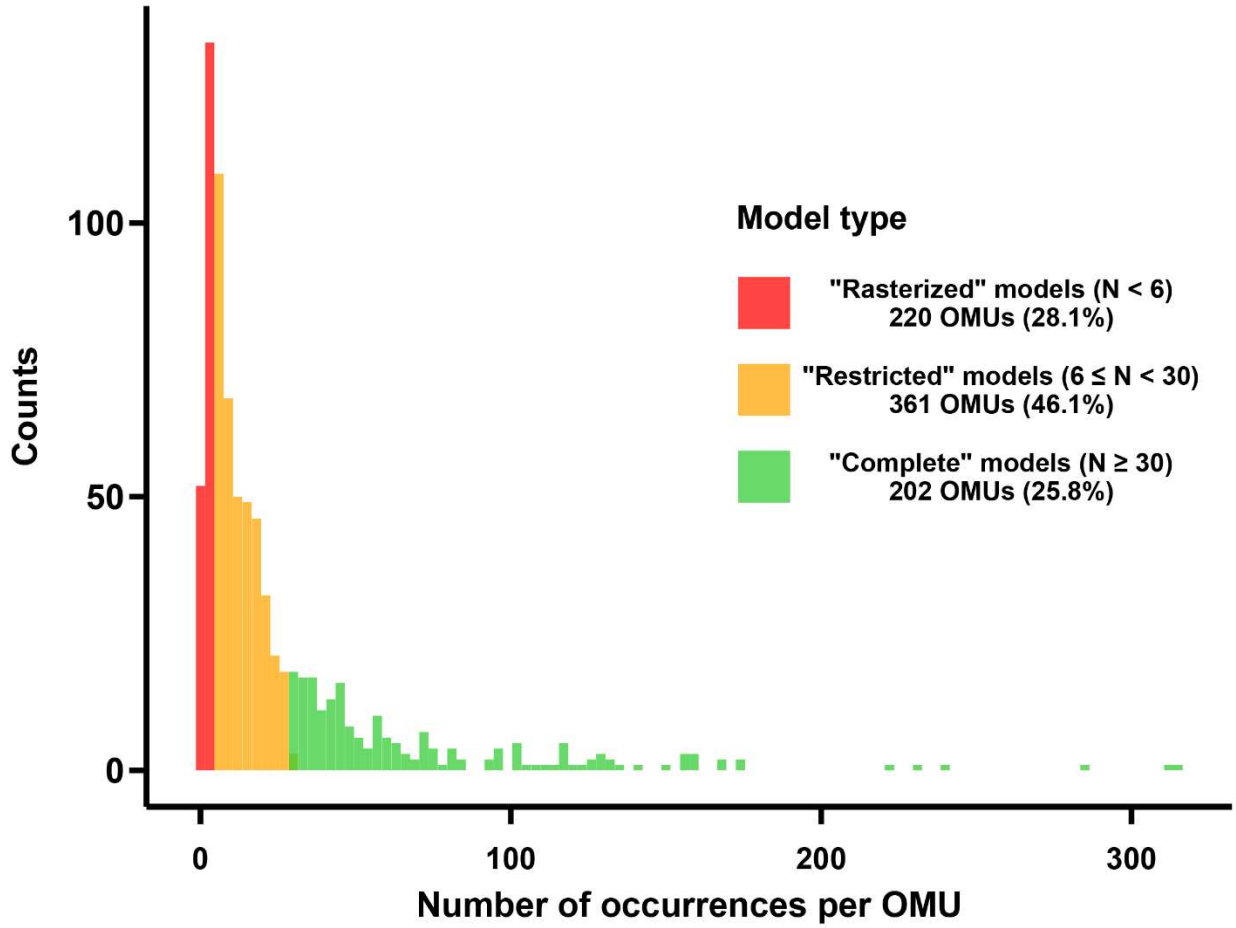

Figure S5.8: Distribution of occurrences across Operational Mimicry Units (OMUs). Three groups of model types are defined by sample size (N). Bin width = 3, excluding superior values.

Scaling: We removed spatial duplicates by applying spatial filtering on a 0.25° x 0.25° grid used as final modeling resolution whose pixels defined our virtual communities.

Cleaning: We examined the presence of geographic and environmental outliers prior modeling. We considered as geographic outliers all occurrences of a specific OMU with no other neighboring points in a 1000km buffer area. These outliers were further scrutinized to decide case by case to retain or discard those points from the dataset if considered erroneous or not.

We automatically removed occurrences with significant Mahalanobis distance (Mahalanobis 1936) from other points in the environmental space. Those points could be either errors, or real abnormal occurrences, due to temporary migration of individuals following an extreme climatic event (e.g., individuals migrating temporarily up mountain slopes following an extreme heat event). In any case, those occurrences cannot be considered helpful to model the global species distribution based on the local average climate, and were therefore discarded.

Pseudo-absence data: We generated pseudo-absences using a target-group strategy (Mateo *et al.* 2010), employing sampling sites where other OMUs have been detected but not the targeted OMUs as a pool for drawing pseudo-absences. In doing so, we increased the likelihood for the targeted OMUs to be effectively not present in our pseudo-absence sites, a critical aspect in order to produce quantities that approach the actual probability of occurrence of the entity modeled as output, as we intended to do (Guillera-Arroita *et al.* 2015). This approach also

allowed us to use confidently the Jaccard index as an evaluation metric to discard poorly performing models from the ensemble models despite this measurement being based on confusion matrix, thus designed primarily for presence-absence data.

Additionally, in order to minimize even more the risk of assigning wrongly a pseudo-absence in an actual occupied site we applied a minimum buffer of 1° (111.32km at the equator) to discard all sites within this minimum range of a presence point from the potential pseudo-absence pool. Finally, to prevent selecting pseudo-absences too far from any presence points while avoiding to have to decide a global arbitrary maximum threshold, we weighted the probability for sites to be selected by their inverse distance to any presence point. Therefore, we ensure our pseudo-absences were likely to represent real absences, while at the same time avoiding to extensively sample too far beyond the range of a species, where absences are likely to occur due to non-bioclimatic reasons (e.g., Biber et al., 2020).

Following recommendations from Barbet-Massin et al. (2012) for machine-learning algorithms, we drew a number of new pseudo-absences equal to the number of presences recorded for the target OMU, for each run. For each OMU model with a restricted sample size ($6 \leq N < 30$), we ran ten independent replicates for each algorithm leading to a total of 30 models per OMU. For each OMU model with a large enough sample size ($N \geq 30$), we ran three independent replicates for each algorithm leading to a total of 27 models per OMU (i.e., 3 algorithms * 3 pseudo-absence sets * 3 CV-folds), once the 3-fold spatial blocks CV was applied.

2.2 Data partitioning

Validation data: We split data between training set and validation sets only for OMUs with sample size ≥ 30.

For models with limited sample size ($6 \leq N < 30$), we decided to keep all data points in our calibration set in order to yield better estimates from SDMs with low sample size. Using a partition scheme would have left fewer points for calibration, decreasing the already scarce information available to yield proper SDMs, and even fewer for validation which would have become meaningless (Hallman & Robinson 2020). Thus, we evaluated model performances with the same dataset used for calibration (« resubstitution » in Roberts et al., 2017). To compensate for non-independence between our calibration sets and validation sets, we used conservative high thresholds to select models with valid performance to keep for the final ensemble.

For models with sufficient sample size (N >= 30), we applied a 3-folds cross-validation (CV) strategy with spatial blocks to define our calibration and validation sets. Spatial blocks CV allows to partition dataset into spatially independent blocks that ensure the predictive error of the model is not underestimated due to spatial autocorrelation between calibration and validation sets (Roberts *et al.* 2017). We defined our folds for each OMU dataset of presences combined with each independent draw of pseudo-absences using the *spatialBlock* function in the R package *blockCV* 2.1.1 (Valavi *et al.* 2019).

Test data: No truly independent dataset was available.

2.3 Predictor variables

Predictor variables:

Climate is known to widely influence large-scale patterns of species distribution (McGill 2010). We selected as predictors four bioclimatic variables among the 19 available in the MERRAclim online database (Vega *et al.* 2017): mean annual temperature, mean annual specific humidity, temperature seasonality, and specific humidity seasonality. We selected this subset of climate predictors following two aims : (1) representativity of the whole variance in our study region, and (2) ease of ecological interpretations. Each variable was included in a different group of intercorrelated variables when performing hierarchical clustering. Within each group, we selected the most adequate variables for ease of ecological interpretation of effects of climate on species distribution. Additionally, we checked that those four variables represented 94.1% of the whole climatic variance in the Neotropics (RDA, F-test with 1000 permutations: $F = 39974$, $df = 4, 9995$, $p < 0.001$), which is expected since most additional variables in the dataset are constructed from the one we selected (Vega *et al.* 2017).

We used elevation as our topographic predictor since it is known to structure ithomiine community composition (Chazot *et al.* 2014).

We used percentage of forest cover as our habitat/land use type predictor since Ithomiini species are known to be forest specialists (Beccaloni 1997a).

Data sources:

For bioclimatic predictors, we downloaded data from MERRAclim v.2.0 (Vega et al., 2017; https://doi.org/10.5061/dryad.s2v81, accessed on 04/02/2020). Contrary to WorldClim v2.1 (Fick & Hijmans 2017), which uses data from land-based meteorological stations to extrapolate information, MERRAclim uses hourly measurements from satellite images to produce high resolution maps of bioclimatic variables averaged over time. We favored this database since we believe they offer more reliable climatic inferences for regions lacking a high-density network of meteorological stations (typically the remoted parts of the Andes and the Amazon regions), and provide more recent estimates.

We retrieved elevation from the SRTM Dataset v.4.1 (Farr et al., 2007; http://srtm.csi.cgiar.org/, accessed on 03/26/2019).

We extracted the percentage of land cover per pixel from the Landsat Tree Cover Continuous Fields dataset (Sexton *et al.* 2013) for the year 2010, accessible through Google Earth Engine (GLCF: Landsat Tree Cover Continuous Fields in the Earth Engine Data Catalog, accessed on 03/26/2019). The GLCF tree cover layers contain estimates of the percentage of horizontal ground covered by woody vegetation.

Spatial extent: We clipped all rasters to our study area: Longitude 120° E - 30° E, Latitude 37° S – 28° S.

Spatial resolution: We obtained GLCF and MERRAclim data at a resolution of 5min of arc, while SRTM had a resolution of 90m. We aggregated all predictor variables to our final model resolution (0.25°) prior to modeling.

Coordinate reference system: All data were stored under WGS84 (EPSG:4326)

Temporal extent:

We downloaded MERRAclim data averaged for the 2000s decade, and GLCF for the year 2010.

Data processing: We aggregated all predictor variables to our final model resolution (0.25°) prior to modeling. We harmonized final predictor rasters to display missing data in pixels where

at least one predictor was lacking information to avoid modeling points with partial environmental information.

Dimension reduction: We selected four bioclimatic variables among the 19 bioclimatic variables available in MERRAclim in order to reduce multicollinearity among bioclimatic predictors, and limit the complexity of the models to a reasonable number of predictors (six in total).

We selected bioclimatic variables as the results of a hierarchical agglomerative clustering on Spearman's rho correlation coefficients, using a complete linkage method with the function *hclust* in R base package. We applied a cutoff of $|\rho| > 0.7$ (Dormann *et al.* 2013; Brun *et al.* 2020) on the resulting dendrogram to highlight groups of multicorrelated variables (Leroy *et al.* 2014). Then, we selected only one variable in each group. Selection criteria for retaining variables were (1) their ease to interpret as an ecological factor (e.g., "mean temperature" rather than the "mean temperature of the driest quarter") and (2) their high correlation with the axis of a global PCA run on all 19 variables. The final four variables included in the models were mean annual temperature, mean annual specific humidity, temperature seasonality, and specific humidity seasonality.

2.4 Transfer data

We interpolated our final maps of environmental suitability depicting potential distributions with the same environmental rasters as the one used for modeling. Thus, the transfer data is the same as the predictors.

3 Model

3.1 Variable pre-selection

See Dimension reduction in Data section in Predictor variables (***2.3***).

3.2 Multicollinearity

See Dimension reduction in Data section in Predictor variables (***2.3***).

3.3 Model settings

We did not apply a weighting scheme to our presence data since we ignored the relative sampling effort associated with each collection of individuals.

Model complexity: We kept model settings to the default settings in *biomod2* v.3.4.6, since models with intermediate levels of complexity have been shown to perform best (Brun *et al.* 2020), keeping a balance between flexibility of the response curves and overfitting (Merow *et al.* 2014). The only exceptions to default settings were the minimum size of leaves that was lowered to two instead of five, and the fraction of observations used at each step (0.7 instead of 0.5) to allow tentative runs in GBM for OMUs with low sample size.

BRT/GBM settings: distribution (bernoulli), nTrees (2500), interactionDepth (7), shrinkage (0.001), bagFraction (0.7), trainFraction (1), n.minobsinnode (2), CV.folds (3)

randomForest settings: ntree (500), mtry (2), maxnodes (n.obs), sampsize (n.obs), replace (TRUE)

ANN settings: nbCV (5), maxit (200)
size = 2, 4, 6, or 8. Optimized by CV for best AUC.
decay = 0.001, 0.01, 0.05, or 0.1. Optimized by CV for best AUC.

Model extrapolation: Extrapolation was possible but remain limited since we constrained final outputs inside the buffer around known presence points.

3.4 Model estimates

Variable importance: We assessed variable importance for each calibrated model within the R package *biomod2* 3.4.6 (Thuiller *et al.* 2020) by looking at the correlation between predictions obtained from the real data and predictions from data with randomized values for each variable evaluated.

3.5 Model selection - model averaging - ensembles

Model selection: We discarded all models that did not reach our thresholds for model quality prior to ensemble (See Performance statistics in Assessment section for details on evaluation metric choice). We set our threshold to a minimum Jaccard index of 0.6 for complete models (N >= 30), and 0.95 for restricted models ($6 \leq N < 30$). The threshold for OMU with "restricted" sample size was more conservative since they were evaluated on the calibration set, while complete models were evaluated on spatially independent validation sets. We chose those thresholds since they ensured each OMU retained at least 5 models for the ensemble, while keeping quality standard to a relatively high value. We conducted additional plausibility checks by inspecting the response curves of each variable for each model following an automatic procedure, completed with manual checks (See plausibility checks in Assessment for details). We discarded from the ensemble models holding at least one response curve with a non-ecologically plausible shape.

Model ensembles: We stacked all models meeting our validation thresholds to produce a single "ensemble" model per OMU. We computed the ensemble as the median rather than the mean to limit influence of models with extreme outputs. We did not use a weighting scheme since we considered our evaluation metric (i.e., Jaccard index) a suitable metric to discard low quality models, but not adequate to rank best models in the context of pseudo-absence data (Leroy *et al.* 2018).

3.6 Analysis and Correction of non-independence

Spatial autocorrelation: We applied spatial blocks CV to account for spatial autocorrelation among calibration and validation sets for models with sufficient sample size (N >= 30).

3.7 Threshold selection

Threshold selection: We did not apply a threshold on the final continuous outputs prior stacking since it has been proven that thresholding could introduce bias leading to overestimation of species richness (Calabrese *et al.* 2014). For instance, we simply estimated species richness as the sum of species environmental suitability maps depicting potential distributions as proxies of occurrence probabilities.

4 Assessment

4.1 Performance statistics

Metric choice: In order to evaluate model performance, we chose to use the Jaccard index, an ecological index of similarity which can be directly interpreted as the spatial overlap between the observed distribution (valid predicted presences as true positives (TP), and missed presences as false negatives (FN)) and predicted distribution (valid predicted presences as true positives (TP), and erroneous predicted presences as false positives (FP)). Thus, for each model we retained the maximum Jaccard index obtained for a model specific optimized threshold, and computed as TP/(TP + FN + FP). Contrary to the TSS, the Jaccard index prevents overestimation of model performance due to the inflation of true negatives based on pseudo-absences drawn far from presences, and appeared to be not biased by prevalence (Leroy *et al.* 2018).

Additionally, despite being primarily designed for presence-absence data, we used the Jaccard index as evaluation metric because: (1) we did not have enough occurrence data to use presence-only evaluation metrics such as the Boyce index (Hirzel *et al.* 2006) or the hyperTest (Jiménez & Soberón 2020) for most of our OMU; (2) we carefully selected our pseudo-absences in a target-group strategy (Mateo et al., 2010) to maximize the probability for our pseudo-absences to be real absences, thus we are confident the Jaccard index remains informative to discard poorly performing models.

Performance on training data: We set to 0.95 the threshold to meet required quality for "restricted" models evaluated directly on the calibration set due to low sample size.

Performance on validation data: We set to 0.6 the threshold to meet required quality for "complete" models (N >= 30) evaluated using spatial CV-blocks.

Following our criteria, we retained 87.3% of sub-models run with Random Forest algorithms, 96.0% of Gradient Boosted Models, and 56.7% of Artificial Neural Networks (**Fig. S5.9**). All OMU ensemble models retained at least five sub-models, allowing to provide final predictions based on ensemble models accounting for uncertainties associated with modeling choices.

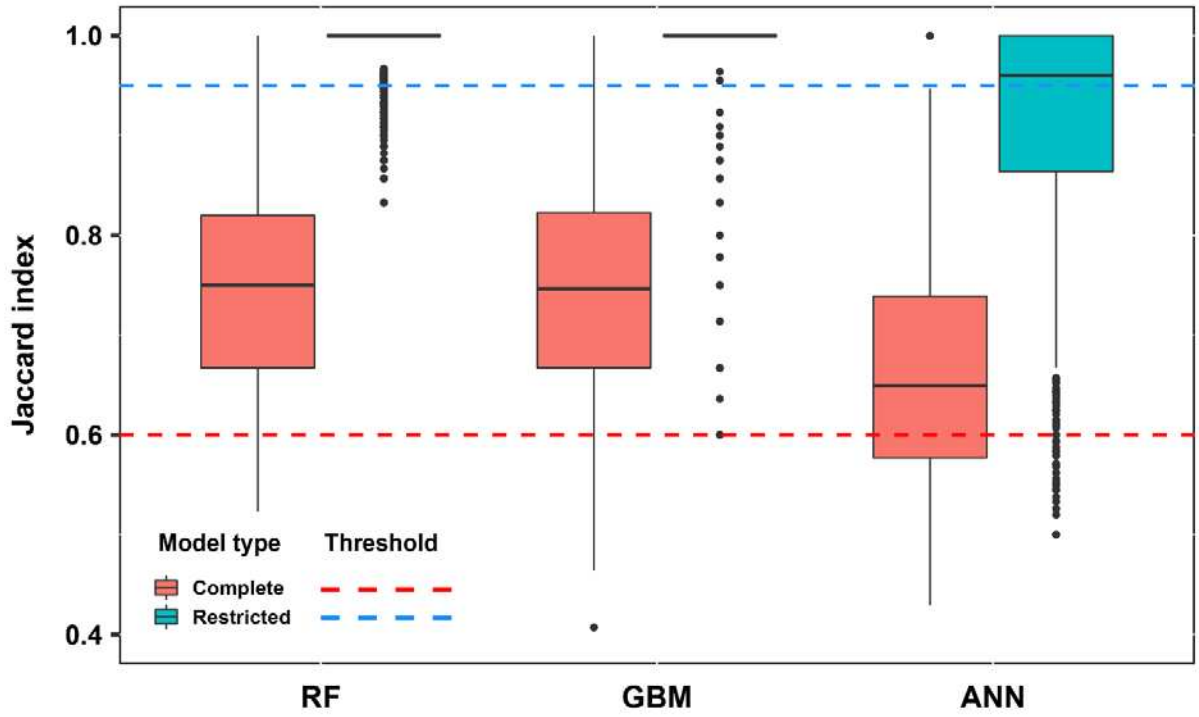

Figure S5.9: Evaluation of sub-model performances based on Jaccard indices. Sub-models are grouped by type of algorithms: Random Forest (RF), Gradient Boosted Models (GBM), and Artificial Neural Networks (ANN). Two distinct thresholds (dashed lines) were used to discard from ensemble models the sub-models with insufficient performance depending on the type of evaluation set used: 0.95 when evaluated on the training set data ("restricted models", in blue), 0.6 when evaluated on a validation set designed from spatial CV-blocks ("complete models", in red).

4.2 Plausibility check

Response shapes: We designed an automatic procedure to check for multimodality and positive quadratic relationships in the response curve of all variables for all models since such relationships would have low ecological plausibility. We assessed multimodality through Hartigan's dip test using the R package *diptest* 0.75-7 (Maechler 2016). We inspected case by case the response curves highlighted by the automatic procedure and then manually removed models holding non-plausible response curves based on expert judgement.

5 Prediction

5.1 Prediction output

Prediction unit: Models produced environmental suitability maps depicting potential distribution for each OMU.

Clipping: We clipped all final ensemble model per unit using a unit-specific buffer.

We clipped all final ensemble models to constrain the extent of possible distribution of each OMU to a reasonable area accordingly to the limited migration abilities of our butterflies, and the degree of certainty we had about the range of the species based on the spread of occurrence

points. Thus, we computed alpha-hulls (α = 1000 km) using the function *ahull* from the R package *alpha-hull* 2.2 (Pateiro-Lopez & Rodriguez-Casal 2019) encompassing all occurrence points for each OMU in order to design a smooth surface able to engulf occurrences points but that could also generate automatically disjointed distributions when needed. We choose an alpha parameter of 1000 km (diameter of the circles used to draw the alpha-hull) to be coherent with our threshold for detection of outliers. In parallel, we computed the 80% quantile for the distance to the closest occurrence points among occurrence points of each OMU. This measure is to be seen as measurement of how confident we are that our records cover extensively the range of the OMU studied. The rationale is that an OMU with a clustered set of occurrences is more likely to describe accurately the global range of this OMU, while an OMU with a more dispersed set of occurrence points could signal a lack of information, or an OMU with a wide range. Therefore, we added to our alpha-hull a buffer corresponding to the max value between this unit-specific parameter and a distance of 1° assumed to represent a conservative limit for Ithomiini dispersion abilities. We used these final polygons to restrict our SDMs predictions for each OMU.

In the specific case of the Andean region, strong environmental gradients can be found following the slopes, leading to potentially suitable areas on both sides of the Cordillera across limited distances. To avoid false predictions of OMUs known with reasonable confidence to be restricted to one side of the Cordillera, we cropped the final maps applying a set of two polygons corresponding respectively to each side of the mountain range. We built those polygons by aggregating watersheds retrieved from a Digital Elevation Model in ArcGIS. In practice, if an OMU presented occurrences falling only in one of the two polygons, we used the other to crop out the final map of this OMU.

Aggregating to higher level: Exploiting the 783 environmental suitability maps depicting potential distributions for each OMU, we built potential distribution maps at species and mimicry ring levels.

We assumed outputs from SDMs relate to likelihood of presence of each OMU. Then, for each community, the likelihood of presence of a species, or a mimicry ring was computed as the likelihood to find at least one of the related OMU in the community such as

$$p_{s/m} = 1 - \prod(1 - p_i) \quad (1)$$

where $p_{s/m}$ is the likelihood of presence of the species or the mimicry ring, and p_i the likelihood of presence of each OMUs of this species or mimicry ring.

Index computation: A final post-processing step consisted in the computation of ten diversity and rarity indices based directly on the species or mimicry ring maps. For all computation, we used the continuous outputs from SDM since binarization to presence-absences usually degrades inference and can introduces bias in community richness evaluation (Calabrese *et al.* 2014; Guillera-Arroita *et al.* 2015). Details on indices computation are provided in **Appendix 8**.

5.2 Uncertainty quantification

Algorithmic uncertainty: We accounted for algorithmic uncertainty by applying an ensemble approach averaging over three different SDM algorithms.

Input data uncertainty: We accounted for uncertainty in input data by applying an ensemble approach averaging over three (for OMU with additional spatial blocks CV) or ten (for OMU without CV) different pseudo-absences draws.

Global uncertainty: We quantified global modeling uncertainty in two ways.

We computed standard deviation in ensemble model for each OMU. Then, we mapped the mean standard deviation among all OMU models to highlight areas of high model **uncertainties (see Fig. S5.10** in the 'Uncertainty maps' section below). Uncertainties were the highest in the Andes but remained fairly low (maximum = 0.08) in comparison to the range of outputs (0-1).

Additionally, we quantified uncertainties associated with our species richness map due to the whole modeling process (i.e., algorithm choices, pseudo-absences draws, and CV). We built 100 alternative richness maps based on a random selection among all valid models for each OMU rather than their ensemble, prior to aggregating to species level, and built S-SDM for species richness. Finally, we mapped the standard deviation among those alternative richness maps (see **Fig. S5.11** in the 'Uncertainty maps' section below). In doing so, we quantified the uncertainties associated with our modeling choices, including selecting different algorithms, drawing different pseudo-absences, or calibrating and evaluating models under different spatial CV-block strategies. Again, uncertainties were the highest in the Andes but were negligible compared to local estimated richness (maximum around 3, compared to local richness around 100).

Novel environments: Predictions to novel environments were limited since we interpolate maps inside a buffer encompassing known presence points.

Robustness assessment: We explored several other modeling options to assess the robustness of our results. For instance, we produced two alternative sets of indices. First, a set without species not included in the phylogeny. Second, a set without OMUs with no SDMs ($N < 6$). We alternatively selected valid models for ensemble modeling based on TSS rather than Jaccard indices, and allowed a wider buffer for clipping using a 0.95 quantile instead of 0.8. Finally, we built maps for a higher resolution of 0.083° (ca. 9.3km x 9.3km), applying a simplified workflow with a single model per OMU based on Random Forest algorithm, with a unique random pseudo-absence draw and no cross-validation. All options explored yielded qualitatively similar results for our final diversity and rarity maps (see **Fig. S5.12 to S5.16** in the 'Robustness assessment: index maps from alternative stacks' section below).

6 Additional remarks on SDM caveats and limits:

We acknowledge outputs from SDM based on presence-only data do not represent direct estimation of probability of presences (Guillera-Arroita *et al.* 2015). Thus, we designed a specific protocol to draw carefully pseudo-absences in order to maximize the likelihood of selecting real absences and to be able to use confidently our SDM outputs depicting the potential distribution of our OMUs as proxy for their likelihood of presence.

Additionally, we quantified the uncertainties associated with our different modeling techniques, which did not prove to be an issue (**Fig. S5.10 & S5.11**). We also applied a buffer

surrounding the known occurrences of each OMU to limit potential overestimation due to the fact that SDMs predict distributions based on the fundamental niche in the environmental space, when in reality we believe the realized niche, and actual distribution of OMUs, to also be constrained by competitive interactions with OMU from a different ring. Therefore, we expect most of our richness and diversity indices to be overestimated as it is commonly the case in stack-SDM procedures, due for instance to underestimation of habitat saturation effects (Guisan & Rahbek 2011, but see Biber et al., 2020; Calabrese et al., 2014). However, we remain confident that the relative patterns we describe are robust and provided meaningful insights regarding spatial correlation among indices and human impacts on hotspots. Future work should aim at fine-tuning predictions employing joint-SDMs and clipping ithomiine distribution with that of their host-plants, but more occurrences and knowledge about ithomiine-hostplant interactions are still required.

7 Uncertainty maps

In this section, we provide maps to quantify the uncertainties associated with our model predictions.

We computed standard deviation in ensemble model for each Operational Mimicry Unit (OMU). Then, we mapped the mean standard deviation among all OMU models to highlight areas of high model uncertainties **(Fig. S5.10)**. Uncertainties were the highest in the Andes but remained fairly low (maximum = 0.08) in comparison to the range of outputs (0-1).

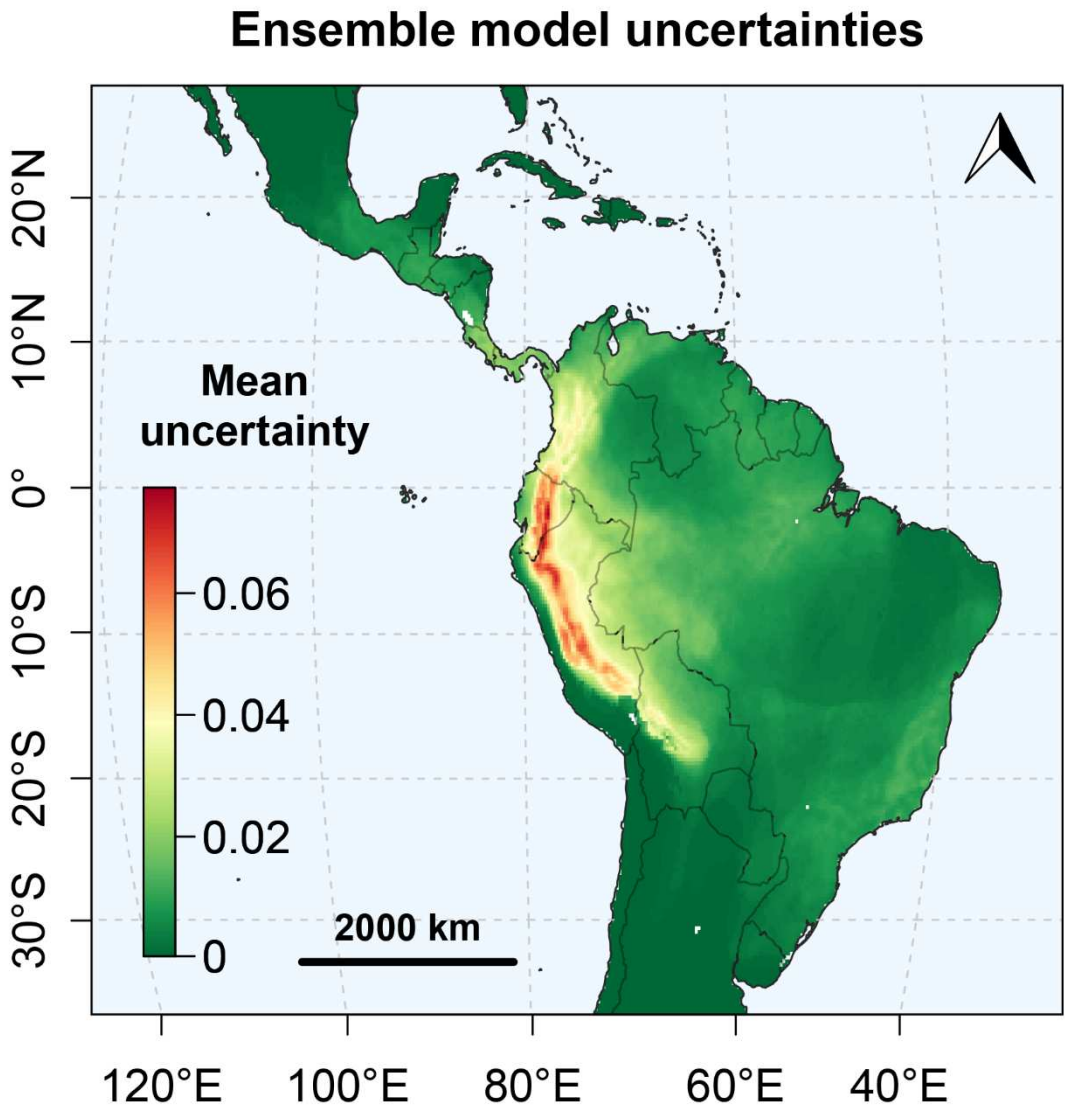

Figure S5.10: Mean uncertainties in ensemble models for OMU. Within each pixel, the mean uncertainty represents the mean standard deviation of predictions from ensemble models of each OMU with a range encompassing the pixel.

Additionally, we quantified uncertainties associated with our species richness map due to the whole modeling process (i.e., algorithm choices, pseudo-absences draws, and CV). We built 100 alternative richness maps based on a random selection among all valid models for each OMU rather than their ensemble model, prior to aggregating to species level and computing species richness. Finally, we mapped the standard deviation among those alternative richness maps **(Fig. S5.11)**. In doing so, we quantified the uncertainties associated with our modeling choices, if we had selected different algorithms, drawn different pseudo-absences, or calibrated and evaluated models under different spatial CV-block strategies. Again, uncertainties were the highest in the Andes but were negligible compared to local estimated richness (maximum around 3, compared to local richness around 100).

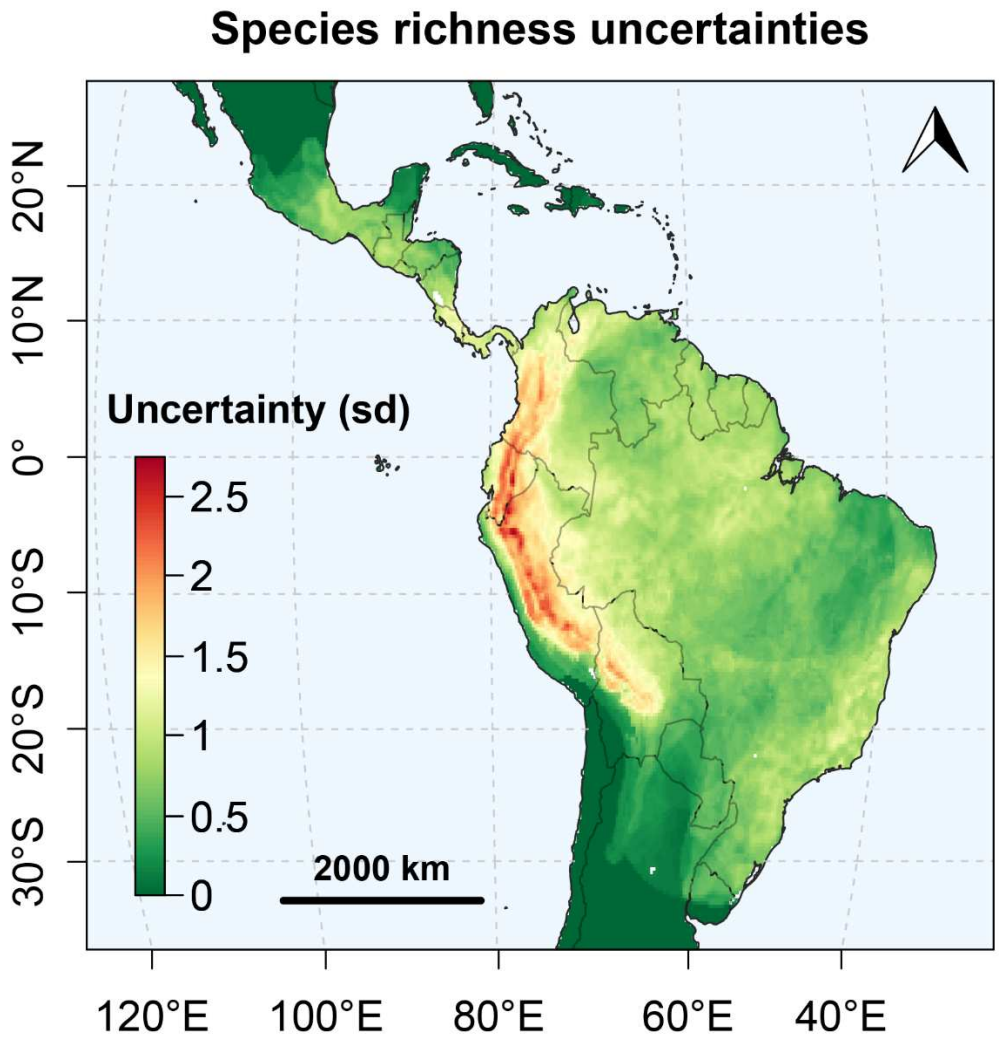

Figure S5.11: Uncertainties in species richness predictions based on modeling alternatives. Uncertainties represents the standard deviation of predicts from 1000 species richness maps built from a random sample of sub-models extracted from ensemble models (1 random sub-model used per OMU).

8 Robustness assessment: index maps from alternative stacks

The robustness of index maps was tested with several sensitivity analyses. Results showed no qualitative difference with the results presented in the main text (see **Fig. 3**).

First, we computed index maps only for the 339 species present in the phylogeny used to compute the phylogenetic diversity (**Fig. S5.12**). No qualitative differences can be observed with indices computed on the whole dataset encompassing 388 species. Hence, our results appear robust to taxonomic subsampling.

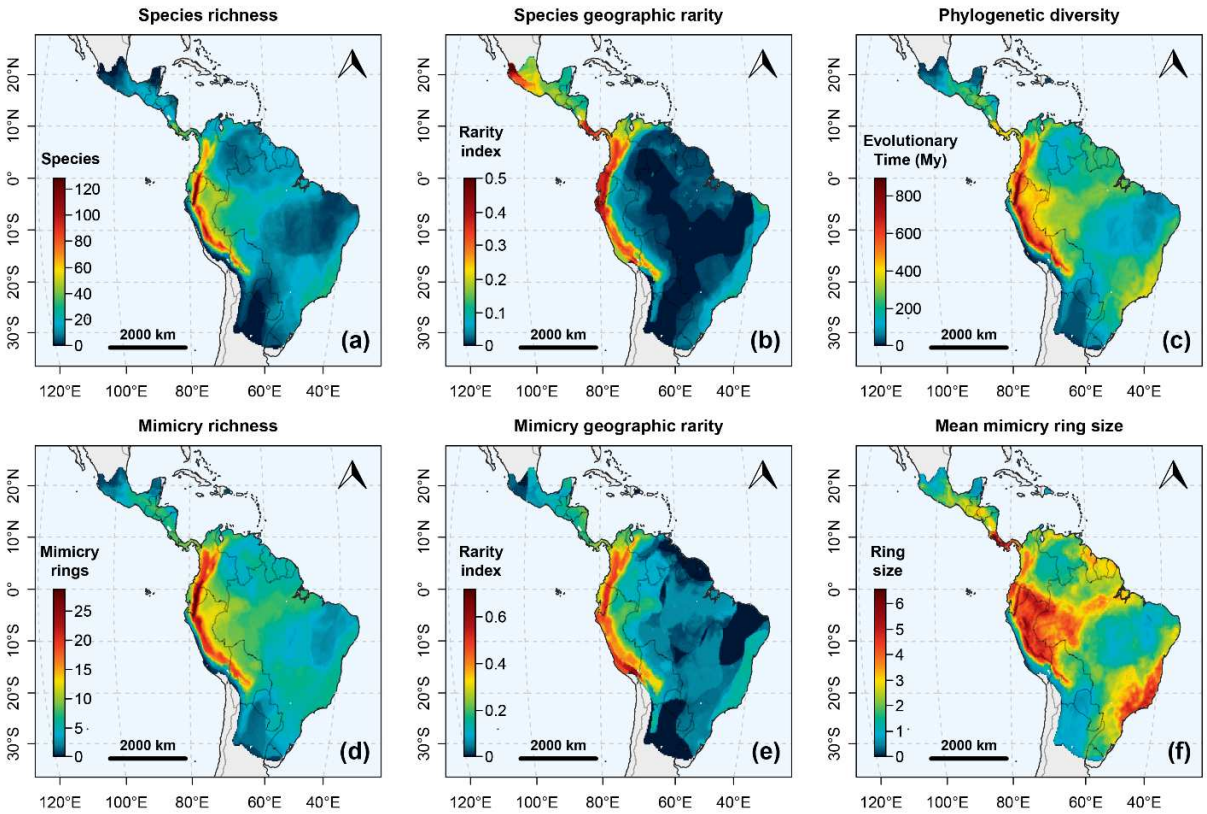

Figure S5.12: Heatmaps of the different facets of Ithomiini diversity in the Neotropics for quarter-degree grid cells, including only the 339 species present in the phylogeny (Chazot *et al.* 2019b)**.** a = Species richness. b = Mean species geographic rarity based on species range. c = Faith's Phylogenetic Diversity (Faith 1992). d = Mimicry richness (*i.e.*, number of mimicry rings). e = Mean mimicry geographic rarity based on mimicry ring range. f = Mean mimicry ring size as mean number of species per mimicry ring. Political boundaries are displayed in light grey. All maps are projected under Mollweide's projection, centered on the meridian 75°E.

Second, we built maps including only OMUs that have undergone SDM process, discarding OMUs with low sample size (N < 6) which distribution was only rasterized (**Fig. S5.13**). No qualitative differences can be observed with indices including OMUs with only rasterized occurrences. The maximum species richness appeared relatively lower, with ca. 80 species in the most speciose communities against ca. 120 species when all OMUs are included. However, general patterns of distribution and associated biodiversity hotspots remained highly similar. Hence, our results appear robust to the inclusion or exclusion of sample-restricted OMUs and species.

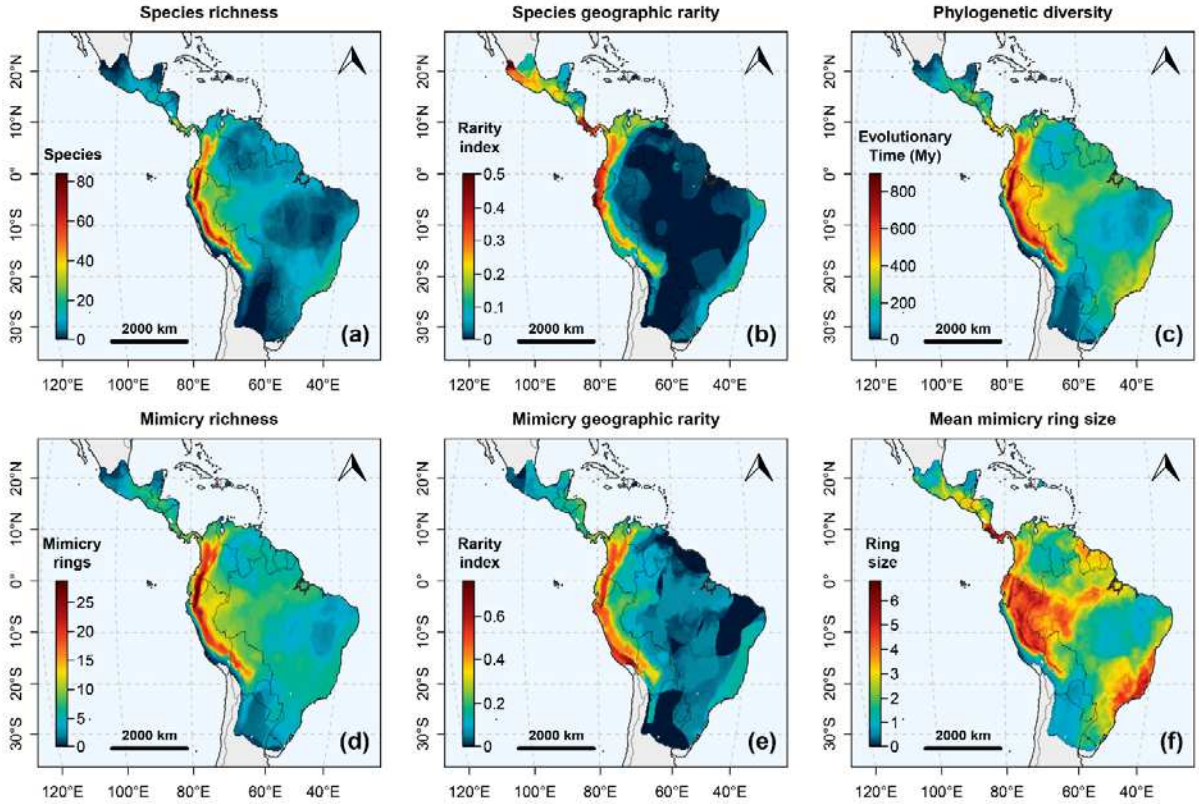

Figure S5.13: Heatmaps of the different facets of Ithomiini diversity in the Neotropics for quarter-degree grid cells, including only Operational Mimicry Units with more than five occurrences those distribution was modeled following our SDM workflow. a = Species richness. b = Mean species geographic rarity based on species range. c = Faith's Phylogenetic Diversity (Faith 1992). d = Mimicry richness (*i.e.*, number of mimicry rings). e = Mean mimicry geographic rarity based on mimicry ring range. f = Mean mimicry ring size as mean number of species per mimicry ring. Political boundaries are displayed in light grey. All maps are projected under Mollweide's projection, centered on the meridian 75°E.

Third, we built maps using the True Skill Statistics (TSS) instead of the Jaccard index to discard poorly performing models from the ensemble models of OMUs. We applied a threshold of TSS > 0.5 for complete models with spatial-block CV, and a threshold of TSS > 0.95 for restricted models with no CV, evaluated directly on the calibration set (**Fig. S5.14**). Almost no difference was observed with indices computed on ensemble models with selection based on Jaccard indices. Indeed, sub-models retained for ensemble under the TSS thresholds were almost always the same than the ones retained under the Jaccard thresholds. Hence, our analysis appears robust to the choice of evaluation metric to select sub-models to include in ensemble models.

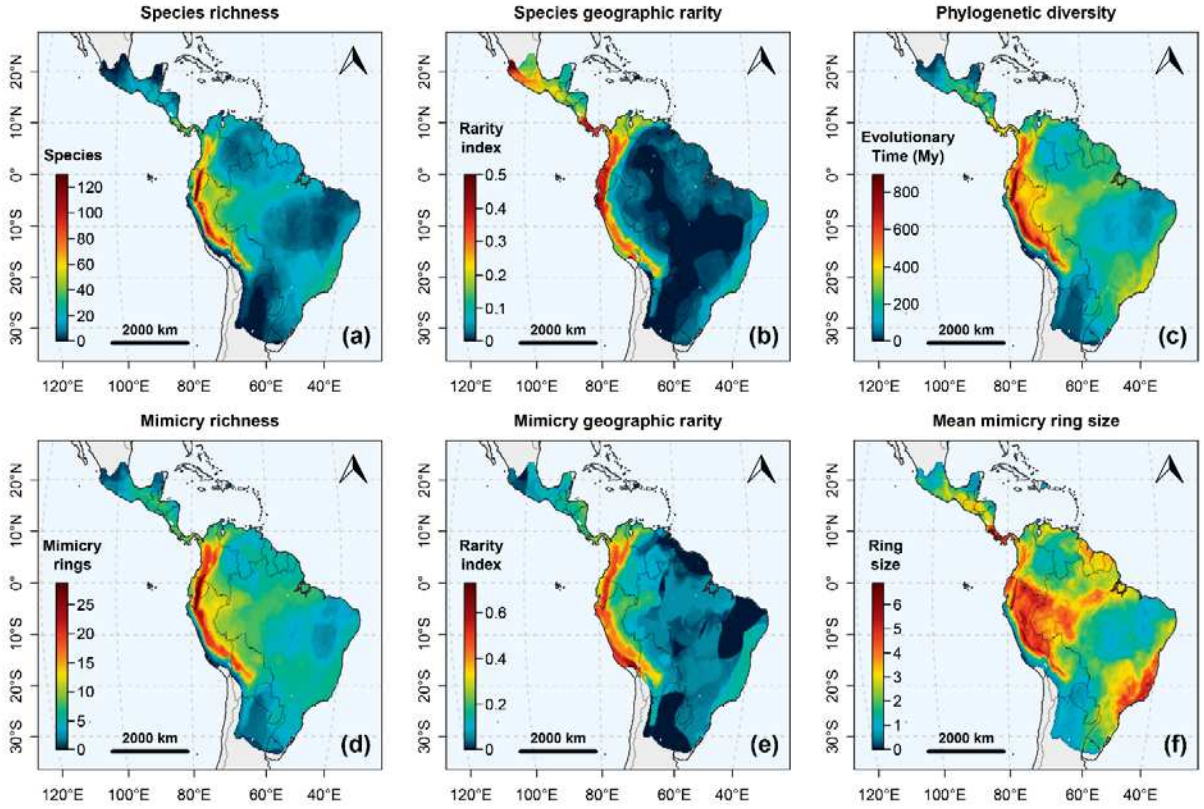

Figure S5.14: Heatmaps of the different facets of Ithomiini diversity in the Neotropics for quarter-degree grid cells, with sub-model selection for ensemble models based on TSS thresholds. a = Species richness. b = Mean species geographic rarity based on species range. c = Faith's Phylogenetic Diversity (Faith 1992). d = Mimicry richness (*i.e.*, number of mimicry rings). e = Mean mimicry geographic rarity based on mimicry ring range. f = Mean mimicry ring size as mean number of species per mimicry ring. Political boundaries are displayed in light grey. All maps are projected under Mollweide's projection, centered on the meridian 75°E.

Fourth, we built maps using a larger buffer to delineate the area of potential distribution for each taxon. We computed the 95% quantile for the distance to the closest occurrence points among occurrence points of each OMU to be used as additional buffer distance around our alpha-hulls, compare to the 80% quantile used in the main text. This alternative buffer allows a wider estimation of the possible range of each OMU, especially when occurrences are sparse and widely spread (**Fig. S5.15**). Again, results showed relatively few qualitative differences with the results presented in the main text. The larger buffer size tended to increase slightly biodiversity metrics based on overlap of distributions such as species richness, mimicry richness, and mean mimicry ring size. This method led to the prediction of occurrence of rare ithomiine butterflies along the coast of the dry Peruvian desert which is not known to host ithomiine butterflies due to its lack of forest cover. Thus, we decided to present in the main text results with the buffer size based on the 80% quantile. Our results may be slightly driven by the

choice of buffer size at a small regional scale, but overall, the main patterns remain highly similar between the two methods.

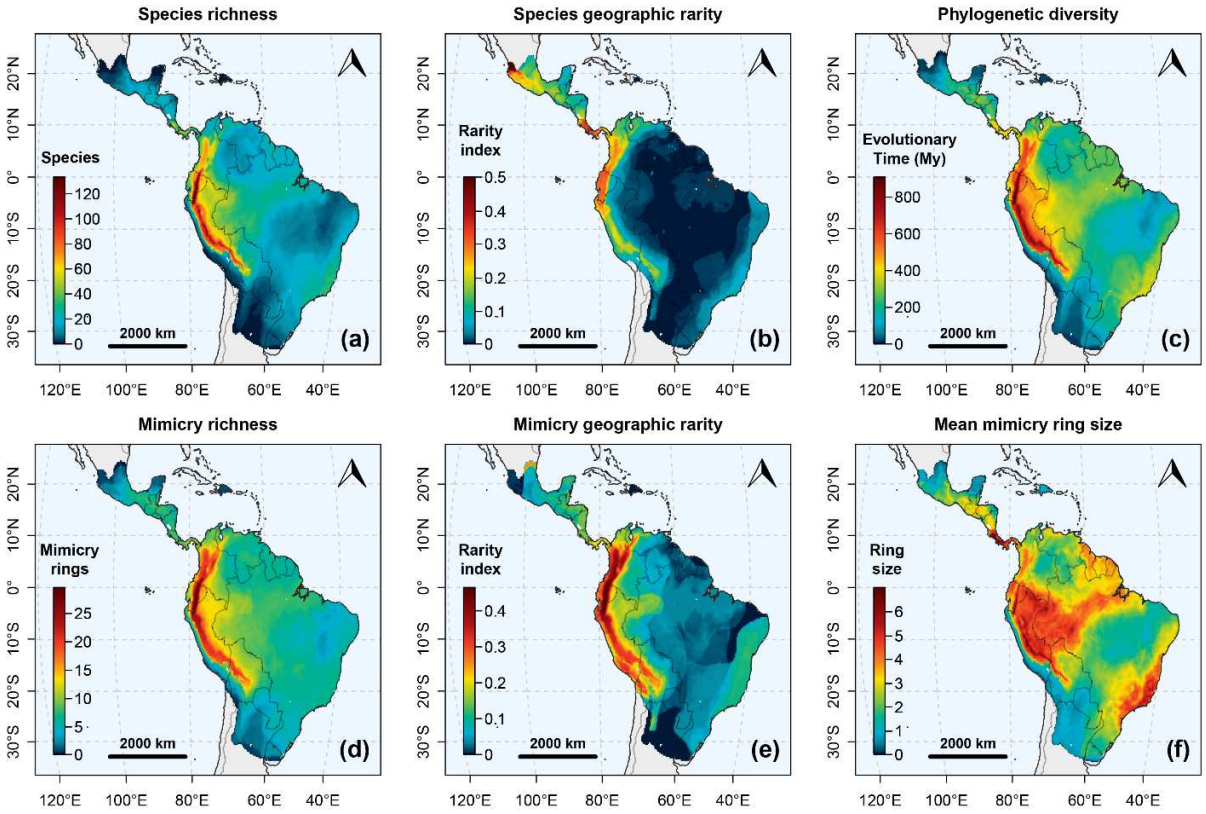

Figure S5.15: Heatmaps of the different facets of Ithomiini diversity in the Neotropics for quarter-degree grid cells, with buffers for OMU distributions based on 95% quantile for the distance to the closest occurrence points among occurrence points. a = Species richness. b = Mean species geographic rarity based on species range. c = Faith's Phylogenetic Diversity (Faith 1992). d = Mimicry richness (*i.e.*, number of mimicry rings). e = Mean mimicry geographic rarity based on mimicry ring range. f = Mean mimicry ring size as mean number of species per mimicry ring. Political boundaries are displayed in light grey. All maps are projected under Mollweide's projection, centered on the meridian 75°E.

Lastly, we built maps at a higher resolution of 0.083° (ca. 9.3km x 9.3km), applying a simplified workflow with a single model per OMU based on Random Forest algorithm, with a unique random pseudo-absence draw and no cross-validation (**Fig. S5.16**). Results showed almost no difference with the results presented in the main text for the lower resolution of 0.25° (ca. 27.8km x 27.8km). As such our results do not appear to be sensitive to the grid resolution used throughout the modeling workflow.

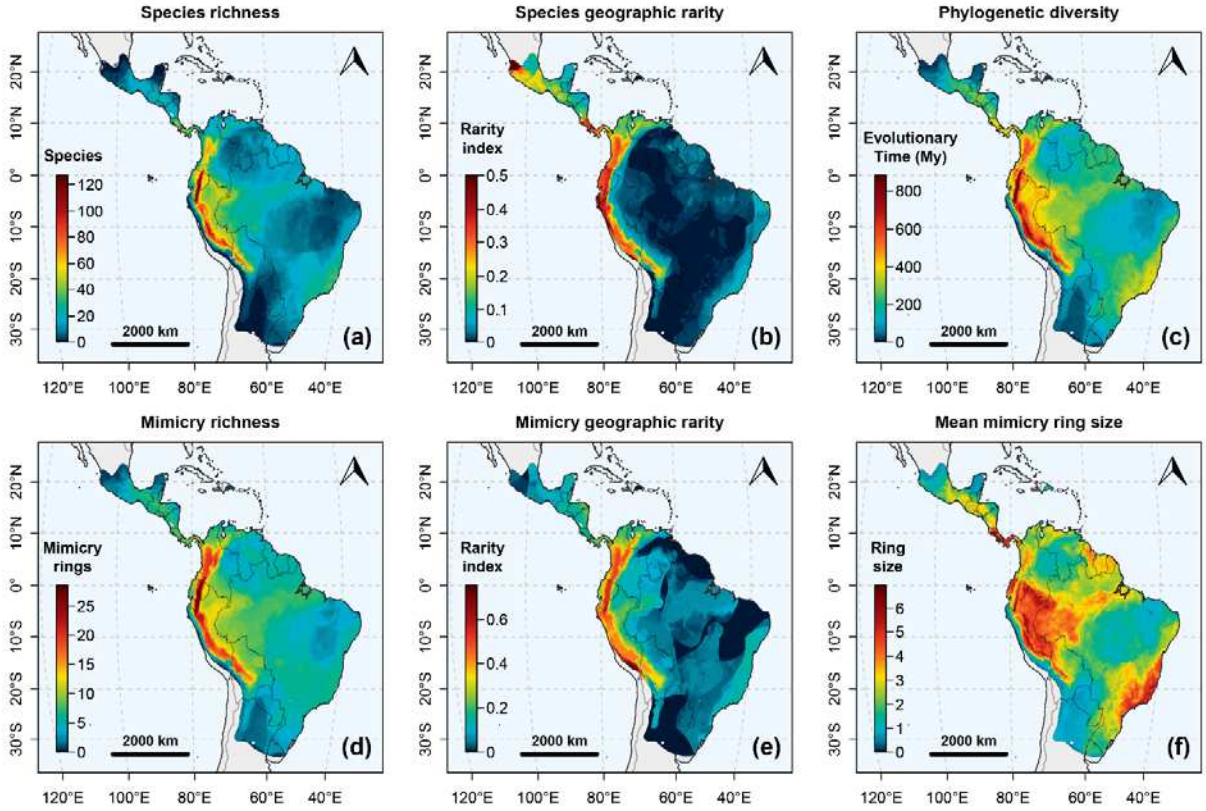

Figure S5.16: Heatmaps of the different facets of Ithomiini diversity in the Neotropics for twelfth-degree grid cells built with a simplified workflow with a unique model per OMU. a = Species richness. b = Mean species geographic rarity based on species range. c = Faith's Phylogenetic Diversity (Faith 1992). d = Mimicry richness (*i.e.*, number of mimicry rings). e = Mean mimicry geographic rarity based on mimicry ring range. f = Mean mimicry ring size as mean number of species per mimicry ring. Political boundaries are displayed in light grey. All maps are projected under Mollweide's projection, centered on the meridian 75°E.

9 References

Abreu-Jardim, T. P. F., Jardim, L., Ballesteros-Mejia, L., Maciel, N. M., & Collevatti, R. G. (2021). Predicting impacts of global climatic change on genetic and phylogeographical diversity of a Neotropical treefrog. *Diversity and Distributions*, 27(8), 1519–1535. https://doi.org/10.1111/ddi.13299

Barbet-Massin, M., Jiguet, F., Albert, C. H., & Thuiller, W. (2012). Selecting pseudo-absences for species distribution models: How, where and how many? *Methods in Ecology and Evolution*, 3(2), 327–338. https://doi.org/10.1111/j.2041-210X.2011.00172.x

Beccaloni, G. W. (1997). Ecology, Natural History and Behaviour of Ithomiine Butterflies and their Mimics in Ecuador. *Tropical Lepidoptera*, 8(2), 103–124.

Biber, M. F., Voskamp, A., Niamir, A., Hickler, T., & Hof, C. (2020). A comparison of macroecological and stacked species distribution models to predict future global terrestrial

vertebrate richness. *Journal of Biogeography*, 47(1), 114–129. https://doi.org/10.1111/jbi.13696

Brown Jr, K. S. (1979). Ecologia Geográfica e Evolução nas Florestas Neotropicais. Universidade Estadual de Campinas, Campinas, Brazil.

Brun, P., Thuiller, W., Chauvier, Y., Pellissier, L., Wüest, R. O., Wang, Z., & Zimmermann, N. E. (2020). Model complexity affects species distribution projections under climate change. *Journal of Biogeography*, 47(1), 130–142. https://doi.org/10.1111/jbi.13734

Calabrese, J. M., Certain, G., Kraan, C., & Dormann, C. F. (2014). Stacking species distribution models and adjusting bias by linking them to macroecological models. *Global Ecology and Biogeography*, 23(1), 99–112. https://doi.org/10.1111/geb.12102

Chazot, N., Willmott, K. R., Lamas, G., Freitas, A. V. L., Piron-Prunier, F., Arias, C. F., Mallet, J., De-Silva, D. L., & Elias, M. (2019). Renewed diversification following Miocene landscape turnover in a Neotropical butterfly radiation. *Global Ecology and Biogeography*, 28(8), 1118–1132. https://doi.org/10.1111/geb.12919

Chazot, N., Willmott, K. R., Santacruz Endara, P. G., Toporov, A., Hill, R. I., Jiggins, C. D., & Elias, M. (2014). Mutualistic Mimicry and Filtering by Altitude Shape the Structure of Andean Butterfly Communities. *The American Naturalist*, 183(1), 26–39. https://doi.org/10.1086/674100

Di Marco, M., Watson, J. E. M., Possingham, H. P., & Venter, O. (2017). Limitations and trade-offs in the use of species distribution maps for protected area planning. *Journal of Applied Ecology*, 54(2), 402–411. https://doi.org/10.1111/1365-2664.12771

Dormann, C. F., Elith, J., Bacher, S., Buchmann, C., Carl, G., Carré, G., Marquéz, J. R. G., Gruber, B., Lafourcade, B., Leitão, P. J., Münkemüller, T., Mcclean, C., Osborne, P. E., Reineking, B., Schröder, B., Skidmore, A. K., Zurell, D., & Lautenbach, S. (2013). Collinearity: A review of methods to deal with it and a simulation study evaluating their performance. *Ecography*, 36(1), 27–46. https://doi.org/10.1111/j.1600-0587.2012.07348.x

Faith, D. P. (1992). Conservation evaluation and phylogenetic diversity. *Biological Conservation*, 61, 1–10. https://doi.org/https://doi.org/10.1016/0006-3207(92)91201-3

Farr, T. G., Rosen, P. A., Caro, E., Crippen, R., Duren, R., Hensley, S., Kobrick, M., Paller, M., Rodriguez, E., Roth, L., Seal, D., Shaffer, S., Shimada, J., Umland, J., Werner, M., Oskin, M., Burbank, D., & Alsdorf, D. (2007). The Shuttle Radar Topography Mission. *Reviews of Geophysics*, 45(2), RG2004. https://doi.org/10.1029/2005RG000183

Fick, S. E., & Hijmans, R. J. (2017). WorldClim 2: new 1-km spatial resolution climate surfaces for global land areas. *International Journal of Climatology*, 37(12), 4302–4315. https://doi.org/10.1002/joc.5086

Guillera-Arroita, G., Lahoz-Monfort, J. J., Elith, J., Gordon, A., Kujala, H., Lentini, P. E., Mccarthy, M. A., Tingley, R., & Wintle, B. A. (2015). Is my species distribution model fit for purpose? Matching data and models to applications. *Global Ecology and Biogeography*, 24(3), 276–292. https://doi.org/10.1111/geb.12268

Guisan, A., & Rahbek, C. (2011). SESAM - a new framework integrating macroecological and species distribution models for predicting spatio-temporal patterns of species assemblages.

Journal of Biogeography, 38(8), 1433–1444. https://doi.org/10.1111/j.1365-2699.2011.02550.x

Gumbs, R., Gray, C. L., Böhm, M., Hoffmann, M., Grenyer, R., Meiri, S., Roll, U., Owen, N. R., & Rosindell, J. (2020). Global priorities for conservation of reptilian phylogenetic diversity in the face of human impacts. *Nature Communications*, 11(2616), 1–13. https://doi.org/10.1038/s41467-020-16410-6

Hallman, T. A., & Robinson, W. D. (2020). Deciphering ecology from statistical artefacts: Competing influence of sample size, prevalence and habitat specialization on species distribution models and how small evaluation datasets can inflate metrics of performance. *Diversity and Distributions*, 26(3), 315–328. https://doi.org/10.1111/ddi.13030

Hijmans, R. J. (2020). raster: Geographic Data Analysis and Modeling. R package version 3.0-12. https://cran.r-project.org/package=raster

Hirzel, A. H., Le Lay, G., Helfer, V., Randin, C., & Guisan, A. (2006). Evaluating the ability of habitat suitability models to predict species presences. *Ecological Modelling*, 199(2), 142–152. https://doi.org/10.1016/j.ecolmodel.2006.05.017

Jiménez, L., & Soberón, J. (2020). Leaving the area under the receiving operating characteristic curve behind: An evaluation method for species distribution modelling applications based on presence-only data. *Methods in Ecology and Evolution*, 11(12), 1571–1586. https://doi.org/10.1111/2041-210X.13479

Leroy, B., Bellard, C., Dubos, N., Colliot, A., Vasseur, M., Courtial, C., Bakkenes, M., Canard, A., & Ysnel, F. (2014). Forecasted climate and land use changes, and protected areas: The contrasting case of spiders. *Diversity and Distributions*, 20(6), 686–697. https://doi.org/10.1111/ddi.12191

Leroy, B., Delsol, R., Hugueny, B., Meynard, C. N., Barhoumi, C., Barbet-Massin, M., & Bellard, C. (2018). Without quality presence–absence data, discrimination metrics such as TSS can be misleading measures of model performance. *Journal of Biogeography*, 45(9), 1994–2002. https://doi.org/10.1111/jbi.13402

Maechler, M. (2016). diptest: Hartigan's Dip Test Statistic for Unimodality - Corrected. R package version 0.75-7. https://cran.r-project.org/package=diptest

Mahalanobis, P. C. (1936). On the generalised distance in statistics. *Proceedings of the National Institute of Science of India*, 2(1), 49–55.

Mateo, R. G., Croat, T. B., Felicísimo, Á. M., & Muñoz, J. (2010). Profile or group discriminative techniques? Generating reliable species distribution models using pseudo-absences and target-group absences from natural history collections. *Diversity and Distributions*, 16(1), 84–94. https://doi.org/10.1111/j.1472-4642.2009.00617.x

McGill, B. J. (2010). Matters of scale. *Science*, 328(5978), 575–576. https://doi.org/10.1126/science.1188528

Merow, C., Smith, M. J., Edwards, T. C., Guisan, A., Mcmahon, S. M., Normand, S., Thuiller, W., Wüest, R. O., Zimmermann, N. E., & Elith, J. (2014). What do we gain from simplicity versus complexity in species distribution models? *Ecography*, 37(12), 1267–1281. https://doi.org/10.1111/ecog.00845

Pateiro-Lopez, B., & Rodriguez-Casal, A. (2019). alphahull: Generalization of the Convex Hull of a Sample of Points in the Plane. R package version 2.2. https://cran.r-project.org/package=alphahull

Pebesma, E. (2018). Simple Features for R: Standardized Support for Spatial Vector Data. *The R Journal*, 10(1), 439–446. https://doi.org/https://doi.org/10.32614/RJ-2018-009

R Core Team. (2019). R: A Language and Environment for Statistical Computing. R Foundation for Statistical Computing. https://www.r-project.org/

Roberts, D. R., Bahn, V., Ciuti, S., Boyce, M. S., Elith, J., Guillera-Arroita, G., Hauenstein, S., Lahoz-Monfort, J. J., Schröder, B., Thuiller, W., Warton, D. I., Wintle, B. A., Hartig, F., & Dormann, C. F. (2017). Cross-validation strategies for data with temporal, spatial, hierarchical, or phylogenetic structure. *Ecography*, 40(8), 913–929. https://doi.org/10.1111/ecog.02881

Robuchon, M., Pavoine, S., Véron, S., Delli, G., Faith, D. P., Mandrici, A., Pellens, R., Dubois, G., & Leroy, B. (2021). Revisiting species and areas of interest for conserving global mammalian phylogenetic diversity. *Nature Communications*, 12(1), 1–11. https://doi.org/10.1038/s41467-021-23861-y

Roll, U., Feldman, A., Novosolov, M., Allison, A., Bauer, A. M., Bernard, R., Böhm, M., Castro-Herrera, F., Chirio, L., Collen, B., Colli, G. R., Dabool, L., Das, I., Doan, T. M., Grismer, L. L., Hoogmoed, M., Itescu, Y., Kraus, F., Lebreton, M., … Meiri, S. (2017). The global distribution of tetrapods reveals a need for targeted reptile conservation. *Nature Ecology and Evolution*, 1(11), 1677–1682. https://doi.org/10.1038/s41559-017-0332-2

Sexton, J. O., Song, X. P., Feng, M., Noojipady, P., Anand, A., Huang, C., Kim, D. H., Collins, K. M., Channan, S., DiMiceli, C., & Townshend, J. R. (2013). Global, 30-m resolution continuous fields of tree cover: Landsat-based rescaling of MODIS vegetation continuous fields with lidar-based estimates of error. *International Journal of Digital Earth*, 6(5), 427–448. https://doi.org/10.1080/17538947.2013.786146

Sherratt, T. N. (2006). Spatial mosaic formation through frequency-dependent selection in Müllerian mimicry complexes. *Journal of Theoretical Biology*, 240(2), 165–174. https://doi.org/10.1016/j.jtbi.2005.09.017

Thomas, C. D., Cameron, A., Green, R. E., Bakkenes, M., Beaumont, L. J., Collingham, Y. C., Erasmus, B. F. N., De Siqueira, M. F., Grainger, A., Hannah, L., Hughes, L., Huntley, B., Van Jaarsveld, A. S., Midgley, G. F., Miles, L., Ortega-Huerta, M. A., Townsend Peterson, A., Phillips, O. L., & Williams, S. E. (2004). Extinction risk from climate change. *Nature*, 427(6970), 145–148. https://doi.org/10.1038/nature02121

Thuiller, W., Georges, D., Engler, R., & Breiner, F. (2020). biomod2: Ensemble Platform for Species Distribution Modeling. R package version 3.4.6. https://cran.r-project.org/package=biomod2

Valavi, R., Elith, J., Lahoz-Monfort, J. J., & Guillera-Arroita, G. (2019). blockCV: An r package for generating spatially or environmentally separated folds for k-fold cross-validation of species distribution models. *Methods in Ecology and Evolution*, 10(2), 225–232. https://doi.org/10.1111/2041-210X.13107

Vega, G. C., Pertierra, L. R., & Olalla-Tárraga, M. Á. (2017). Data Descriptor: MERRAclim, a high-resolution global dataset of remotely sensed bioclimatic variables for ecological modelling. *Scientific Data*, 4(170078), 1–11. https://doi.org/10.1038/sdata.2017.78

Willmott, K. R., Lamas, G., Hall, J. P. W., Mota, L., Kell, T. (2020). The common, the rare, and the lost: Descriptions of twelve new species and three new subspecies of equatorial Ithomiini (Lepidoptera, Nymphalidae, Danainae). *Tropical Lepidoptera Research*, 30(Supplement 1), 1-49. https://doi.org/10.5281/zenodo.3990663

ANNEXE 3

Supplementary Information for CHAPTER 2

Supplementary Information for

Phylogenomics resolve deep evolutionary relationships in clearwing butterflies

Maël Doré[1,2], Jérémy Gauthier[3], Rémi Allio[4], Nick Grishin[5], Joana Meier[6,7], Nicolas Chazot[8], Keith Willmott[9], and Marianne Elias[1,10]

[1]*Institut de Systématique, Evolution, Biodiversité, MNHN-CNRS-Sorbonne Université-EPHE-Université des Antilles, Muséum national d'Histoire naturelle de Paris, 45 Rue Buffon, 75005, Paris, France*

[2]*Centre d'Ecologie et des Sciences de la Conservation, UMR 7204 MNHN-CNRS-Sorbonne Université, Muséum national d'Histoire naturelle de Paris, 45 rue Buffon, 75005, Paris, France*

[3]*Natural History Museum of Geneva, Geneva, Switzerland*

[4]*Centre de Biologie pour la Gestion des Populations, INRAE, CIRAD, IRD, Montpellier SupAgro, Université de Montpellier, Montpellier, France*

[5]*Department of Biochemistry, University of Texas Southwestern Medical Center, Dallas, TX, United States of America*

[6]*Department of Zoology, University of Cambridge, Cambridge, CB2 3EJ, United Kingdom*

[7]*Tree of Life Programme, Wellcome Sanger Institute, United Kingdom*

[8]*Swedish University of Agricultural Sciences, Uppsala, Sweden*

[9]*McGuire Center for Lepidoptera and Biodiversity, Florida Museum of Natural History, University of Florida, Gainesville, FL, United States of America*

[10]*Smithsonian Tropical Research Institute, Panamá, Panamá*

Appendix 1: Metadata and summary statistics for specimens employed in WGS analyses

Table S1: Metadata and summary statistics for the 155 specimens employed in WGS analyses

This table provides summary information for each specimen involved in the WGS datasets regarding its identification, field sampling, NovaSeq sequencing, genome assembly, mDNA assembly, CDS annotation, cross-contamination checks, orthology assignment, and summary statistics (i.e., number of genes, sites, missing data, undefined nucleotides, etc.) in the *Inclusive* and *Conservative* dataset. Such table is too vast to be provided here in this document but can be found in the GitHub repository: https://github.com/MaelDore/Ithomiini_phylogenomics.

Appendix 2: Metadata and summary statistics for specimens used in the taxa-rich alignments for comprehensive phylogenetic inferences

Table S2: Metadata and summary statistics for the 368 specimens used in the taxa-rich alignments for comprehensive phylogenetic inferences

This table provides summary information for each specimen involved in the *Comprehensive dataset* regarding its identification, field sampling, NCBI deposit, taxonomic update, and summary statistics (i.e., number of genes, sites, missing data, undefined nucleotides, etc.) in the *Comprehensive* dataset. Such table is too vast to be provided here in this document but can be found in the GitHub repository: https://github.com/MaelDore/Ithomiini_phylogenomics.

Appendix 3: Sample-specific similarity threshold to reconstruct CDS sequences from genome assemblies

In order to reconstruct CDS sequences from multiple samples with variable degrees of divergence with respect to the reference genome, we used sample-specific similarity thresholds to filter scaffolds that matched with the reference protein sequences using the *blastn* tool. Indeed, if we were using a unique similarity threshold for all samples, we would likely miss a lot of potentially matching sequences from distant species with lower global similarity, while we may not be conservative enough to avoid the matching of recently duplicated genes on the same reference protein in closely related species.

To define such sample-specific threshold, we ran preliminary tests on four samples selected for their particular status. The *Hyposcada illinissa* sample (Voucher: 05-409) showed a high quality assembly that recovered 87.7% of complete genes from the BUSCO reference set. The *Dircenna dero* sample (Voucher: 19011C03) showed a low assembly quality with only 11.2% of complete reference genes recovered. The *Hypomenitis theudelinda* sample (Voucher: 19097G09) showed virtually no recovery of complete genes from the BUSCO set while producing a very small and fragmented assembly (300K sites and 686 scaffolds) being the extreme case of low quality in our dataset. Conversely, we used the chromosome-scale assembly of *Bombyx mori* (NBCI assembly reference: 014905235.1; 460M sites for 697 scaffolds) as the positive extremum of the quality spectrum, but also as an example for distant species.

We explored how the number of reference proteins that registered a matching scaffold via *tblastn* evolved according to the similarity threshold used to filter hits. By construct, the lower the similarity threshold, the more reference proteins register a match, and conversely. Thus, we also explored changes in the distribution of the number of scaffolds matching each reference proteins with the idea that if some proteins were matching with numerous scaffolds, this was likely a source of error as a sign of matching paralogous sequences due to duplication or simply noisy short elements matching incorrect reference proteins. We found that the distribution changed qualitatively and qualitatively according to the sample. In general, we observed that after a particular threshold value, which depends on the quality of the assembly and the distance of the sample to the reference species, the number of proteins with a single hit do not increase much. Meanwhile, the new hits that passed a lower filter mostly matched on

reference proteins with multiple hits, likely adding noise to our sequences (**Figure S1)**. In detail, we found this inflexion point to be lower for distant species such as the *Bombyx mori* (**Figure S1.D)** reflecting its need for a lower similarity threshold to retrieve more sequences. Among similarly distant samples, the two assemblies with high and low quality showed relatively similar patterns (**Figure S1.A & S1.B),** while the sample with the lowest quality needed a lower similarity threshold to start showing a potentially problematic accumulation of hits on the same references. Altogether, as a conservative rule to avoid potential issues with duplicated genes, we decided to use as sample-specific similarity threshold the value for which no more than 25% of matched proteins show 6 or more hits.

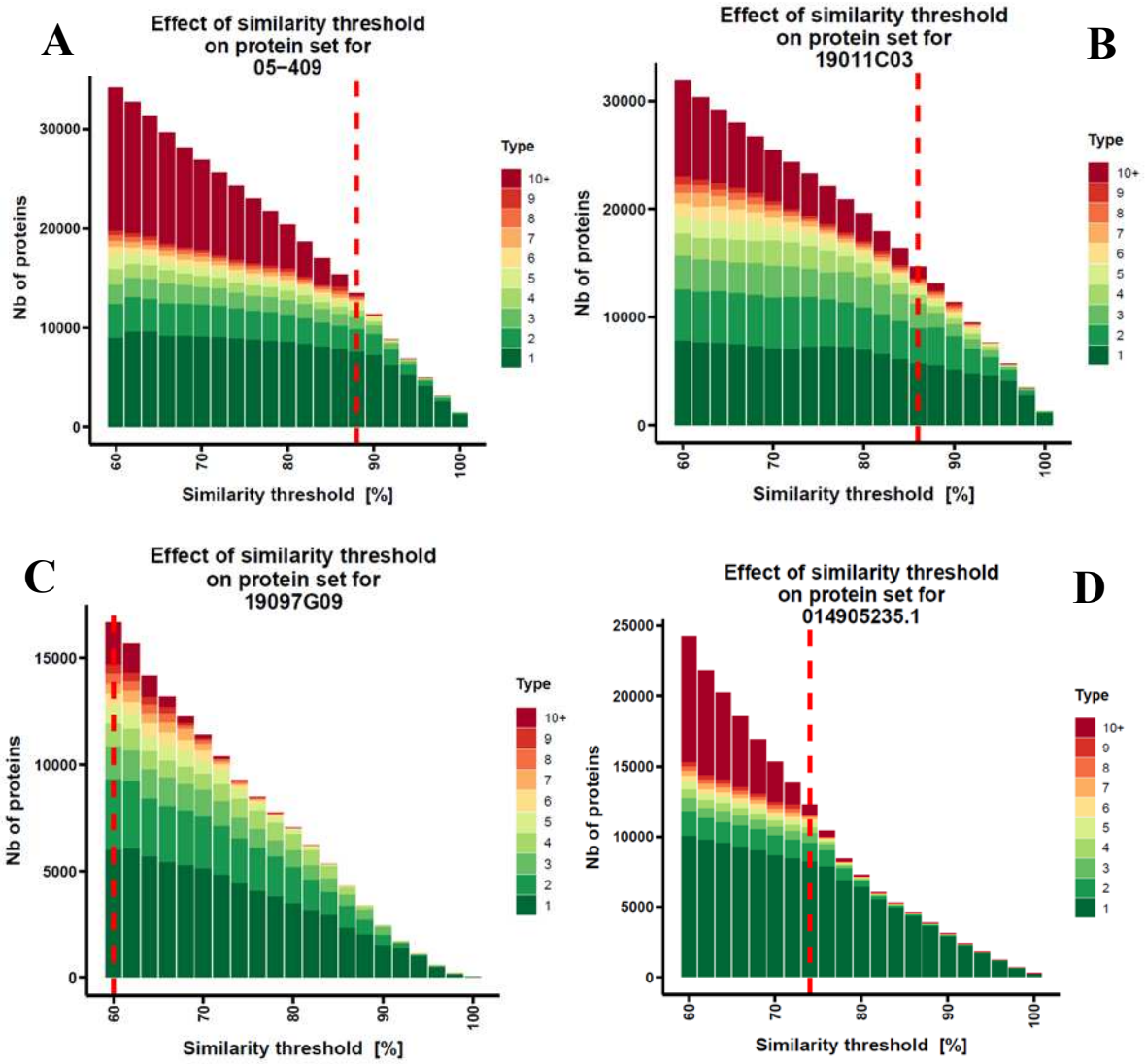

Figure S1: Changes in the distribution of numbers of scaffolds matched across each reference protein according to the similarity threshold employed to filter hits. (A) High quality sample (BUSCO = 87.7%). **(B)** Low quality sample (BUSCO = 11.2%). **(C)** Extremely poor quality sample (BUSCO = 0%). **(D)** Chromosome-scale assembly. Sample-specific similarity detected with our rule are represented with the dashed vertical red lines.

Appendix 4: Cross-contamination cleaning step

As we used multiplexed runs to sequences our samples, we were exposed to the risk of cross-contamination (i.e., sequenced identified to the wrong sample (Ballenghien *et al.* 2017)). Thus, we used CroCo 1.1 (Simion *et al.* 2018) to investigate potential cross-contamination in our CDS dataset and filter out all dubious sequences that displayed a higher match with raw reads from other samples that from its original read pool.

Contrary to expectations (see Allio *et al.* 2021), this cross-contamination step did not allowed us to identify a higher number of orthogroups, but it efficiently cleaned sequences initially forming dubious small putative orthogroups with very few sequences/taxa involved. Indeed, we observed a high decrease in the frequencies of orthogroups involving few taxa obtained from OrthoFinder after the cross-contamination step compared to what is obtained without cross-contamination checks (**Fig. S2**). As such, cross-contamination checking may still be a useful and conservative step to integrate in phylogenomic pipelines in order to limit errors in the final alignments.

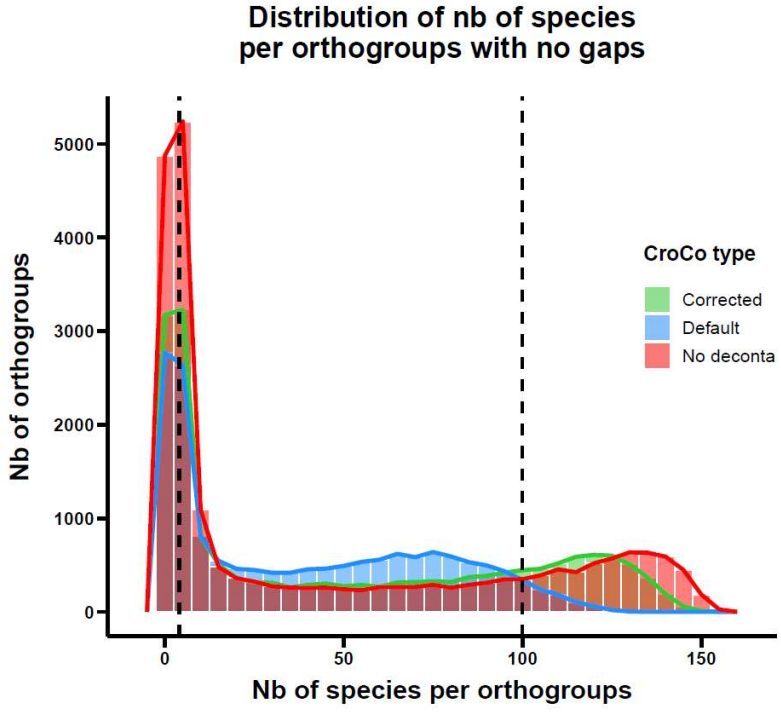

Figure S2: Distribution of the number of genes found in the final putative orthogroups detected by OrthoFinder with or without a preliminary step filtering for potential cross-contamination. Red distribution represents the putative orthogroups obtained from OrthoFinder without the cross-contamination checks. Green and blue distributions represent the distributions obtained after cross-contamination checks using different degrees of scrutiny regarding what is considered a potential contamination (Default = very conservative; Corrected = less conservative).

Appendix 5: WGS dataset selection

After all the curation steps, we were left with 16,859 alignments of single-copy orthologous genes including from 2 to 153 taxa distributed across 163 species (151 ithomiines + 12 outgroups). Histograms showed a high heterogeneity of coverage across both genes and taxa, with a very few gene alignments encompassing more than 120 species (i.e., 75% of available taxa; **Fig. S3**).

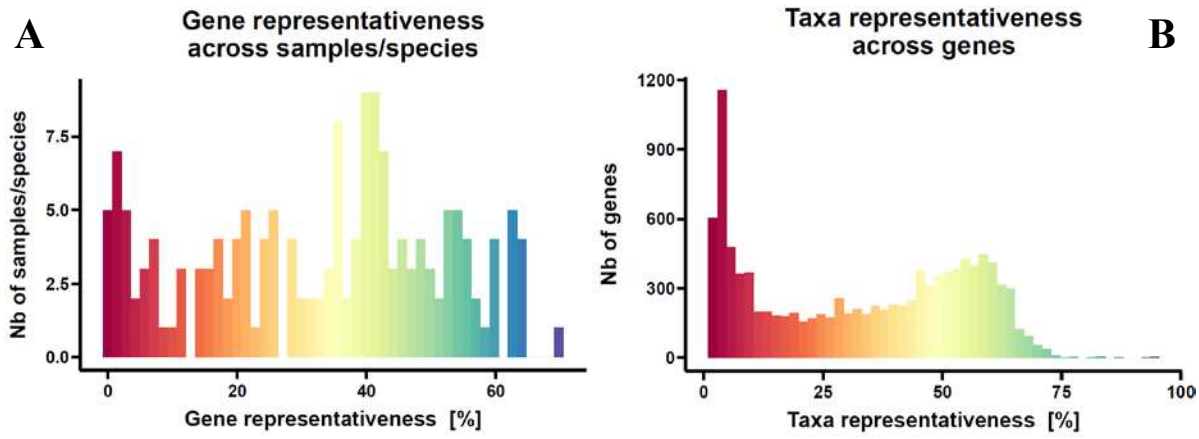

Figure S3: Histograms of gene representativeness across samples/species (A) and taxa representativeness across genes (B) showing the heterogeneity of coverage across both taxa and single-copy orthologous genes.

We used AMAS (Borowiec 2016) to concatenate genes into datasets with a combination of gene and taxa representativeness thresholds, and computed the number of remaining genes, taxa, and informative sites in datasets obtained from each threshold combination (**Fig. S4**). To build the *Inclusive dataset*, we tried to maximize both the number of taxa and genes involved since the percentage of informative sites remained reasonable in any case with a minimum of 30% even with the least representative taxa involved (**Fig. S4.C)**. For the *Conservative dataset*, we tried to find a balance between reducing the proportion of missing data (i.e., increasing the proportion of informative sites) while keeping a maximum of taxa. Since we detected the number of remaining genes and informative sites showed a sharp drop beyond a threshold of 60% for taxa representativeness (**Fig. S4.B & 4.C)**, we decided to use only genes with at least 50% of taxa representativeness (i.e., 82 species), which corresponded roughly to the top 30% of genes ranked according to the number of taxa in their alignment (i.e., 3,518 genes).

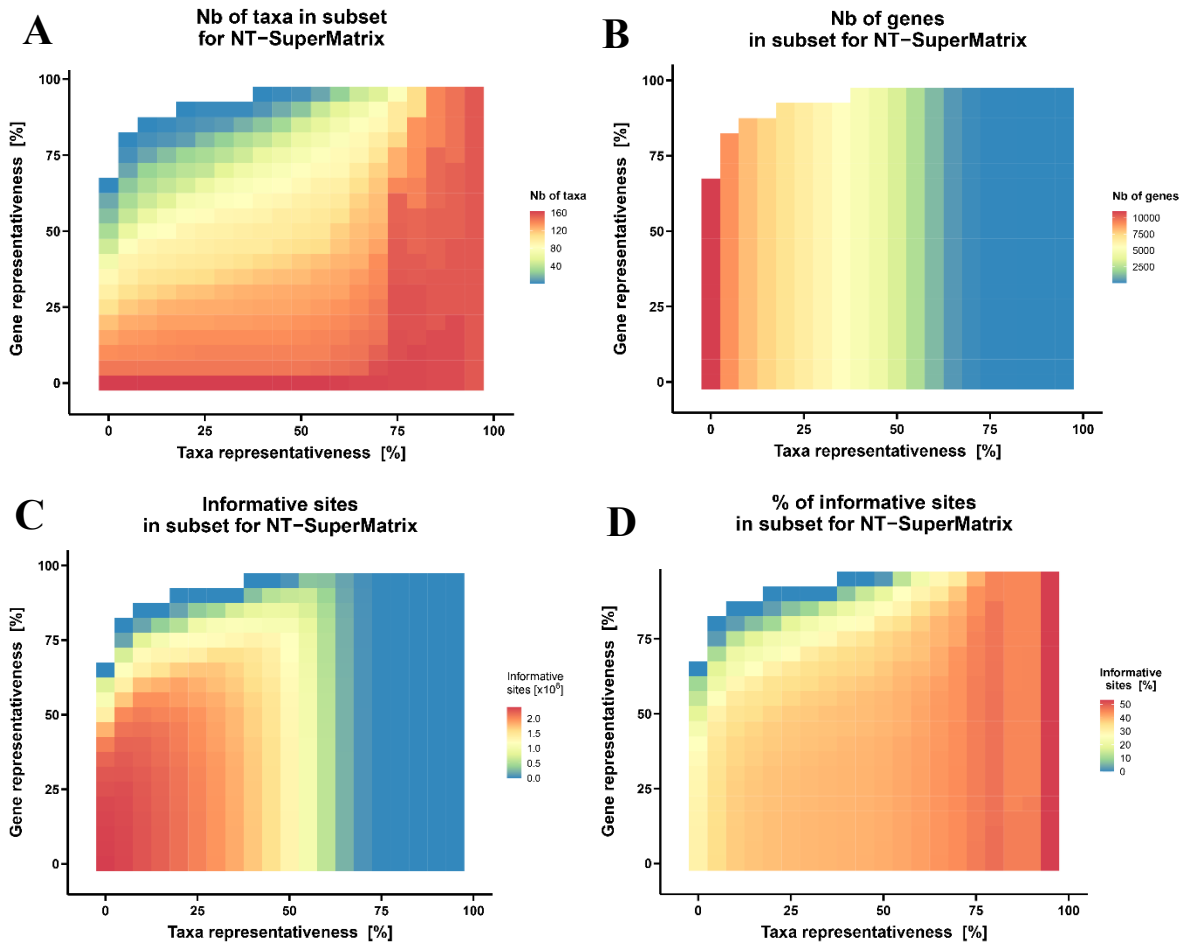

Figure S4 : Heatmaps of dataset contents obtained when applying a range of gene and taxa representativeness thresholds to select respectively the taxa and the genes to incorporate in the final dataset. (A) Number of taxa. **(B)** Number of genes. **(C)** Number of informative sites. **(D)** Percentage of informative sites.

Appendix 6: Selection of substitution models for ML gene tree inferences

In order to infer the gene trees needed to generate the final species trees using a summary approach with ASTRAL-III 5.7.8 (Zhang *et al.* 2018), we first estimated the best fitted gene tree for each gene alignment with IQ-TREE 2.2.0.3 (Minh *et al.* 2020b) using maximum likelihood optimization. We performed a full model selection across all available nucleotide substitution models including free rate categories (Parameter settings: -m MFP -mrate R) with ModelFinder (Kalyaanamoorthy *et al.* 2017). We visualized the heterogeneity in complexity of gene evolution by summarizing the best models selected across all genes according to their number of parameters used to model substitution rates across nucleotides. We found that the complexity of gene evolution in our dataset was relatively low with only 3 parameters needed in average and less than 10% of best models involving a complete substitution matrix as in a GTR or SYM model (**Fig. S5.A**). Additionally, the heterogeneity of substitution rates across sites within a single gene alignment appeared also relatively low, with most best models selecting only for two or three categories of free rates, while less than 5% of best models suggesting 6 or more categories (**Fig. S5.B**). As such, we concluded that we did not need to carry out codon partition models since most gene evolution revealed to be properly accounted with simple substitution models and with few substitution rate categories.

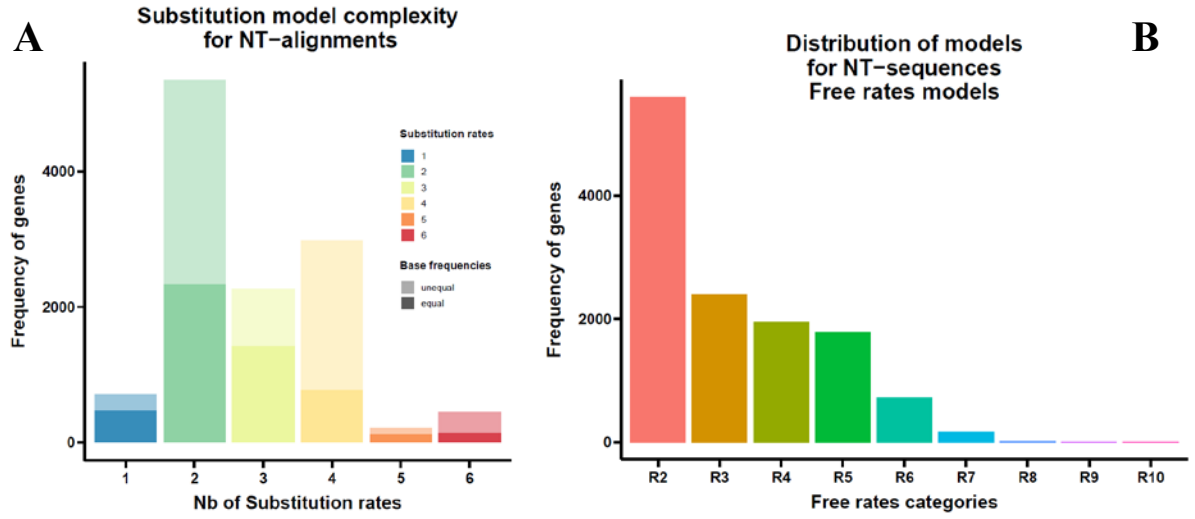

Figure S5: Evaluation of the complexity of best models selected for gene tree inferences using free rates to account for substitution rate heterogeneity across sites. (A) Distribution of the number of parameters in substitution rate matrices used in best models across all genes. Median = 3 substitution rate parameters. **(B)** Distribution of the number of free rate categories selected in best models across all genes. Median = 3 categories.

In order to make computationally feasible in a reasonable time the inference of species trees from ML approaches based on SuperMatrix, we aimed to obtain a partition grouping genes according to similarity in their evolution models. Such grouping is more likely to be achieved if authorizing a limited shared set of models across genes. As such, we opted for using GTR models with varying degree of free rates (GTR + R) across all genes, but we first investigated if individual gene trees inferred with GTR + R models were similar enough to the ones obtained with the best selected models typically involving less parameters, thus potentially sensitive to overparameterization. We computed the pairwise Robinson-Foulds distances and Normalized Quartet distances between gene trees obtained from both full model selection, and selection between GTR + R models across all genes. We showed differences in the final topologies were low with most pairwise distances below 0.1 for both metrics (**Fig. S6**). Meanwhile, such comparisons also highlighted the important differences with gene trees retrieved from the homologous alignments using amino-acids and LG + Γ4 models (Le & Gascuel 2008). We concluded that GTR + R models were suitable to model the evolution of all genes, and therefore performed a partition merging run (Parameter settings: -m MF+MERGE) with a limited set of GTR models with free rates categories ranging from 2 to 6 to cover most of best model options selected from individual gene tree inferences (**Fig. 5.B**). We obtained 332 partitions for the 11,012 genes in the *Inclusive dataset* and 178 partitions for 3,518 genes in the *Conservative dataset* saving us important computation time for species tree inferences.

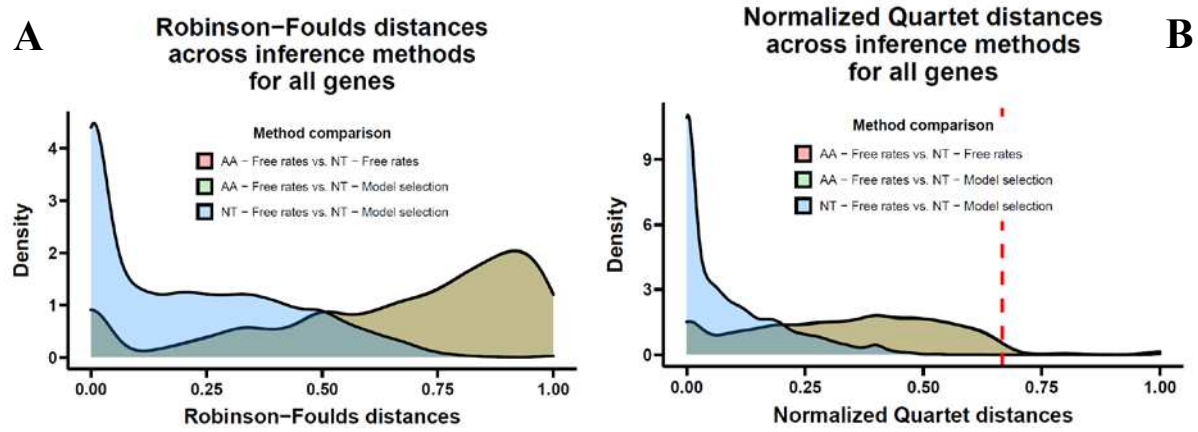

Figure S6: Evaluation of differences of gene tree topologies between different model selections and datasets. (A) Robinson-Foulds distances based on comparison of bipartitions. **(B)** Normalized Quartet distances based on quartet comparisons. 'Free rates' refer to selection across GTR + R models while 'Model selection' found the best model across all available substitution models in IQ-TREE. We also inferred gene trees from homologous amino-acid (AA) alignments. Both nucleotide-based (NT) models showed little difference in gene topology while they differ largely with topologies inferred from AA-alignments. Both distributions against the AA-based gene trees are confounded. The red dashed vertical line signals the random expectation for Normalize Quartet distances between two random trees encompassing the same species (i.e., 2/3).

Appendix 7: Congruence between gene trees and ASTRAL SuperTrees

ASTRAL-III is a summary algorithm aiming to find the species tree topology that optimizes its congruency with the phylogenetic signal found in individual gene trees and evaluated trough comparison of quartets (Zhang *et al.* 2018).

First, we explored the levels of incongruency across gene trees to evaluate if they were suitable for summary methods such as ASTRAL-III. We computed the mean distance of each gene tree to all other gene tree topologies in the dataset. If this mean distance is low, it implies a high level of congruence, and likely a strong phylogenetic signal shared across the gene trees. Conversely, if this mean distance is high, it means gene trees topologies tend to disagree and may suffer from high degree of incomplete lineage sorting, or simply errors of inferences. We observed a medium congruency within gene tree topologies for trees inferred with best substitution models and GTR + R models that did not fundamentally preclude to opt for summary-based approach to infer our species trees (**Fig. 7**). The high similarity in the distribution of their mean distances confirmed gene tree topologies were only slightly affected by the substitution model used. On the other end, gene trees inferred from amino-acid alignments showed high degree of incongruency signaling a poor phylogenetic signal, or difficulty to carry out correct gene tree inferences (**Fig. 7**).

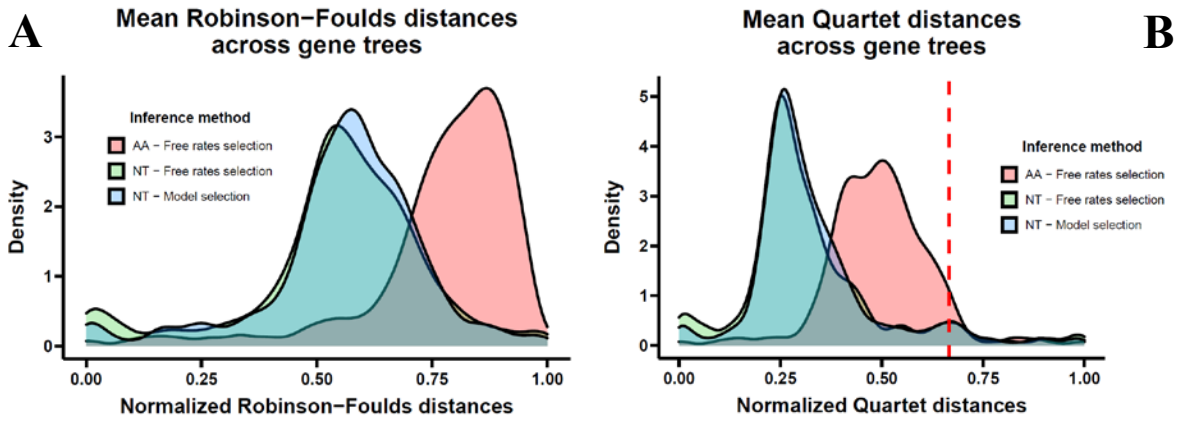

Figure S7: Distributions of mean distance of each gene tree relative to all other gene tree topologies in the dataset obtained through different model selections and datasets. (A) Robinson-Foulds distances based on comparison of bipartitions. **(B)** Normalized Quartet distances based on quartet comparisons. The red dashed vertical line signals the random expectation for Normalize Quartet distances between two random trees encompassing the same species (i.e., 2/3).

Second, we compared *a posteriori* the quality of our SuperTree inferences by computing the normalized quartet distances between each SuperTree and the set of gene trees used to produce this SuperTree. We found that SuperTrees based on the *Inclusive* and *Conservative datasets* showed relatively similar and moderate levels of congruence with their initial set of gene trees (**Fig. S8**; Normalized Quartet distance modes around 0.12). As such, we may suspect that the inclusion of ca. 6,500 additional genes in the *Inclusive dataset* compared to the *Comprehensive dataset* did not improve nor affected drastically the quality of the phylogenetic signal in the dataset. Moreover, we found that the SuperTrees inferred from gene trees based on amino-acid sequences showed a low congruency towards their set of gene trees, likely because such gene trees showed initially low congruency between each other (**Fig. S7**). Due to this lack of phylogenetic signal and global congruency, analyses based on amino-acid sequences were discarded from our analytic framework.

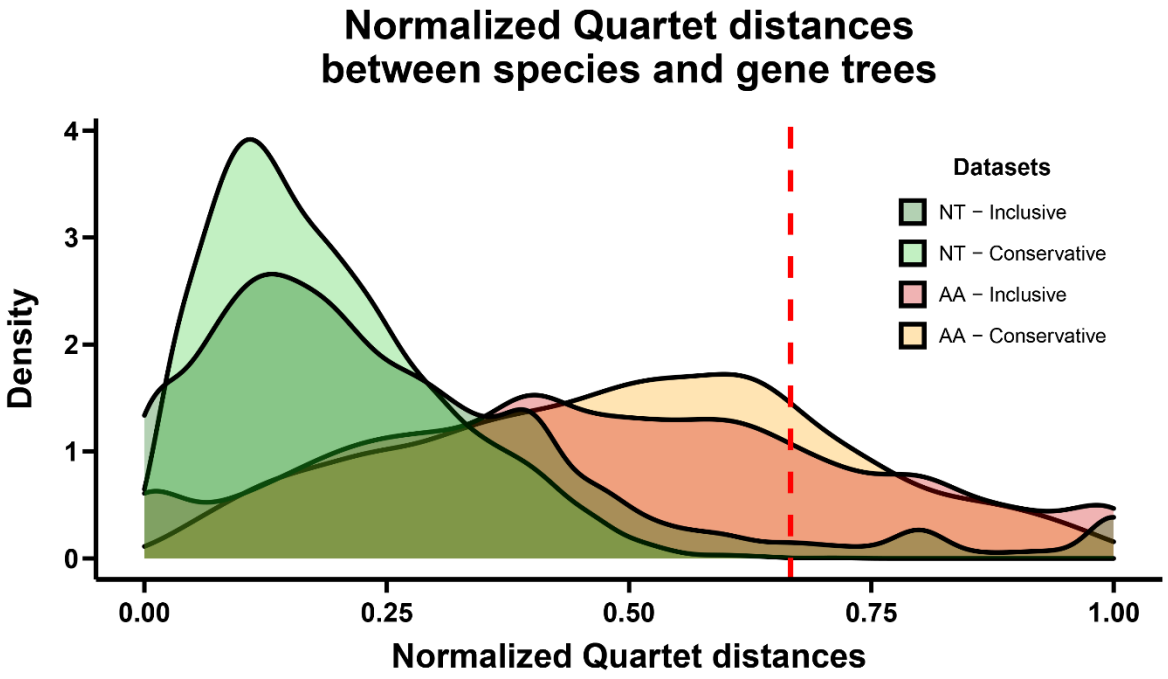

Figure S8: Distributions of pairwise Normalized Quartet distances between species-level SuperTree and their respective sets of individual gene trees from which they have been previously inferred. Right-skewed distributions indicate low distances, thus high congruency reflecting a strong phylogenetic signal and potentially a better supported species tree. The red dashed vertical line signals the random expectation for Normalize Quartet distances between two random trees encompassing the same species (i.e., 2/3).

Appendix 8: Secondary calibrations for node age estimates

We ran Bayesian inferences for time-calibration in order to estimate nod ages in our phylogenies. Since no fossil are available for ithomiine butterflies, we applied five secondary calibrations on ingroup (Ithomiini) internal nodes as uniform priors with upper bounds based on the maximum estimated age of the Solanaceae hostplant lineage associated with each ithomiine clade, as retrieved from De-Silva *et al.* (2017). We applied ten additional secondary calibrations on outgroup nodes based on larger phylogenies of Nymphalidae (Chazot *et al.* 2021), Papilionoidea (Chazot *et al.* 2019a), and Lepidoptera as a whole (Kawahara *et al.* 2019). These calibrations consisted in normal priors adjusted such as their 95% confidence interval matched with the 95% Height Posterior Density (HPD) of node age posterior distributions reported in these higher phylogenies. The complete list with associated node is presented in **Table S3**.

Table S3: Secondary calibrations used for Bayesian inferences of node ages. The first five calibrations are uniform priors with upper bounds based on the maximum estimated age of the Solanaceae hostplant lineage associated with each ithomiine clade. The next ten calibrations are normal priors adjusted such as their 95% confidence interval matched with the 95% Height Posterior Density (HPD) of node age posterior distributions reported from higher-level reference phylogenies.

Node	Upper bound (My)	Lower bound (My)	host-plant group OR higher-taxa phylogeny	Reference
Ollantaya + *Oleria*	0	32	*Lycianthes*	De-Silva, *et al.*, 2017
Melinaeina	0	37.2	*Schultesianthus*	De-Silva, *et al.*, 2017
Methonina	0	41.3	*Brunfelsia*	De-Silva, *et al.*, 2017
Athesitina	0	24.8	*Capsicum*	De-Silva, *et al.*, 2017
Placidina + *Pagyris*	0	17.3	*Brugmansia*	De-Silva, *et al.*, 2017
Ithomiini	21.8	27.8	Nymphalidae	Chazot *et al.*, 2021
Ithomiini + Danaiini	36.1	46.9	Nymphalidae	Chazot *et al.*, 2021
Heliconius + *Dryas*	21.4	28.8	Nymphalidae	Chazot *et al.*, 2021
Heliconiini + Argynnini	42.8	52.9	Nymphalidae	Chazot *et al.*, 2021

Nymphalini + Melitaeini	38.5	47.1	Nymphalidae	Chazot *et al.*, 2021
Heliconiinae + Nymphalinae	63.8	76.8	Nymphalidae	Chazot *et al.*, 2021
Maniola + Pararge	41.9	50.5	Nymphalidae	Chazot *et al.*, 2021
Nymphalidae + Lycaenidae	80.4	116.5	Papilionoidea	Chazot *et al.*, 2019a
Nymphalidae + Lycaenidae + Papilionidae	89.5	129.5	Papilionoidea	Chazot *et al.*, 2019a
Papilionoidea + Bombycoidea + Zygaenoidea	94.3	117.3	Lepidoptera	Kawahara *et al.*, 2019

Appendix 9: Backbone phylogenies inferred from WGS datasets

We obtained four different phylogenetic hypotheses based on WGS data for the backbone topology crossing our two datasets (*Inclusive vs. Conservative*) vs. two phylogenetic inference methods (SuperMatrix with IQ-TREE vs. SuperTree with ASTRAL). The deep relationships between subtribes were similar for the two SuperMatrix-based phylogenies (**Fig. S9 & S10**), while the two datasets led to different deep topologies for the SuperTrees (**Fig. S11 & S12**). All four topologies suggested the existence of a clade formed by Mechanitina and the core-group, which encompasses all subtribes with members feeding on the diverse *Solanum* genus, and having lost their subdorsal filaments in the last instar caterpillar (Willmott & Freitas 2006). However, the branching of the remaining four subtribes (i.e., Melinaeina, Athesitina, Tithoreina, and Methonina) varies across topologies. The two SuperTree topologies suggested an unusual (i.e., never suspected in previous systematic explorations) unique clade for these four tribes, sister to the 'Solanum-feeders' clade, while the SuperMatrix topologies both featured the Melinaeina tribe as sister to all other ithomiines (**Fig. S11 & S12**). Additionally, the SuperTree topology based on the *Inclusive* dataset (**Fig. S11**) did not retrieve the well-established Tithoreina/Methonina clade found in all modern propositions (Brower *et al.* 2006, 2014; Willmott & Freitas 2006; Chazot *et al.* 2019b).

Based on the comparison of node support metrics, and the plausibility of proposed topologies, we selected the two topologies based on the *Inclusive* and *Conservative datasets* inferred with IQ-TREE from the concatenated SuperMatrices as the best supported topologies. Therefore, we built the final backbone topology as the strict consensus between these two selected topologies (**Fig. S9 & S10**).

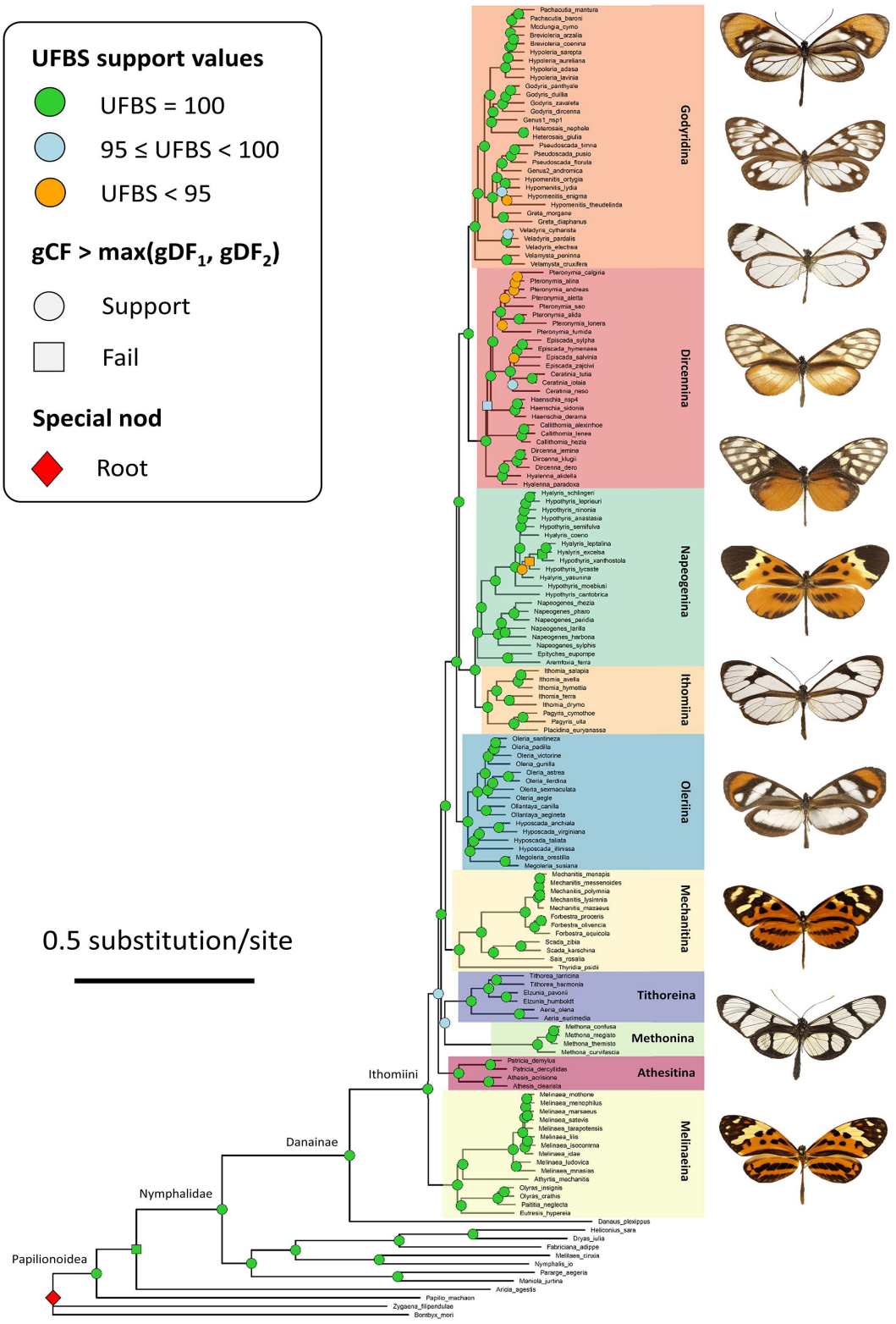

Figure S9: Phylogenetic hypothesis inferred from SuperMatrix with IQ-TREE based on the *Inclusive dataset.* Branch lengths relate to the inferred mean number of substitutions per site along each branch. Colored clades correspond to the ten known subtribes. Node support values are illustrated with colored symbols according to UFBS scores and gene concordance factor (gCF) tests against support for alternative local topologies (i.e., gDF = discordance factors).

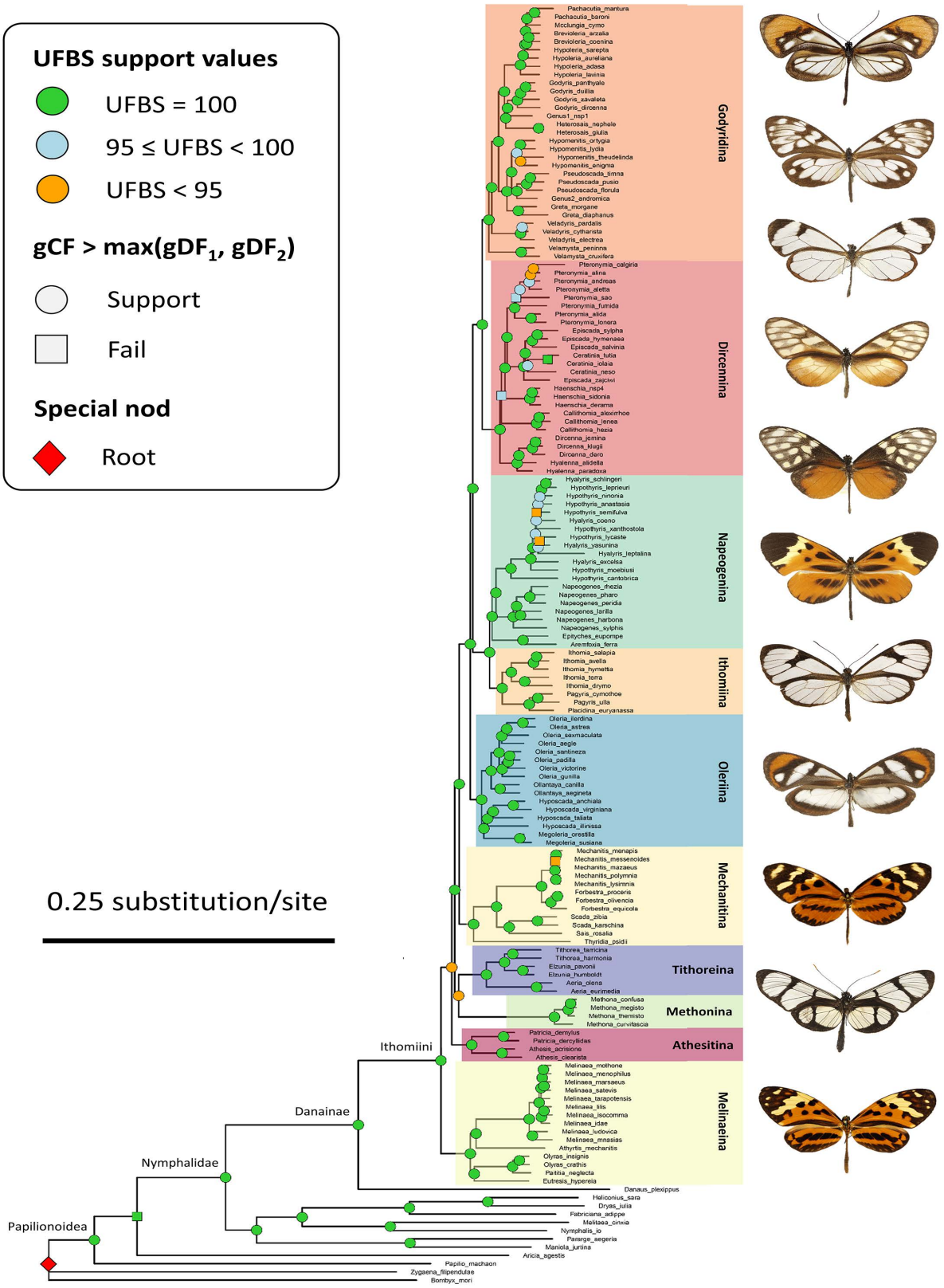

Figure S10: Phylogenetic hypothesis inferred from SuperMatrix with IQ-TREE based on the *Conservative dataset*. Branch lengths relate to the inferred mean number of substitutions per site along each branch. Colored clades correspond to the ten known subtribes. Node support values are illustrated with colored symbols according to UFBS scores and gene concordance factor (gCF) tests against support for alternative local topologies (i.e., gDF = discordance factors).

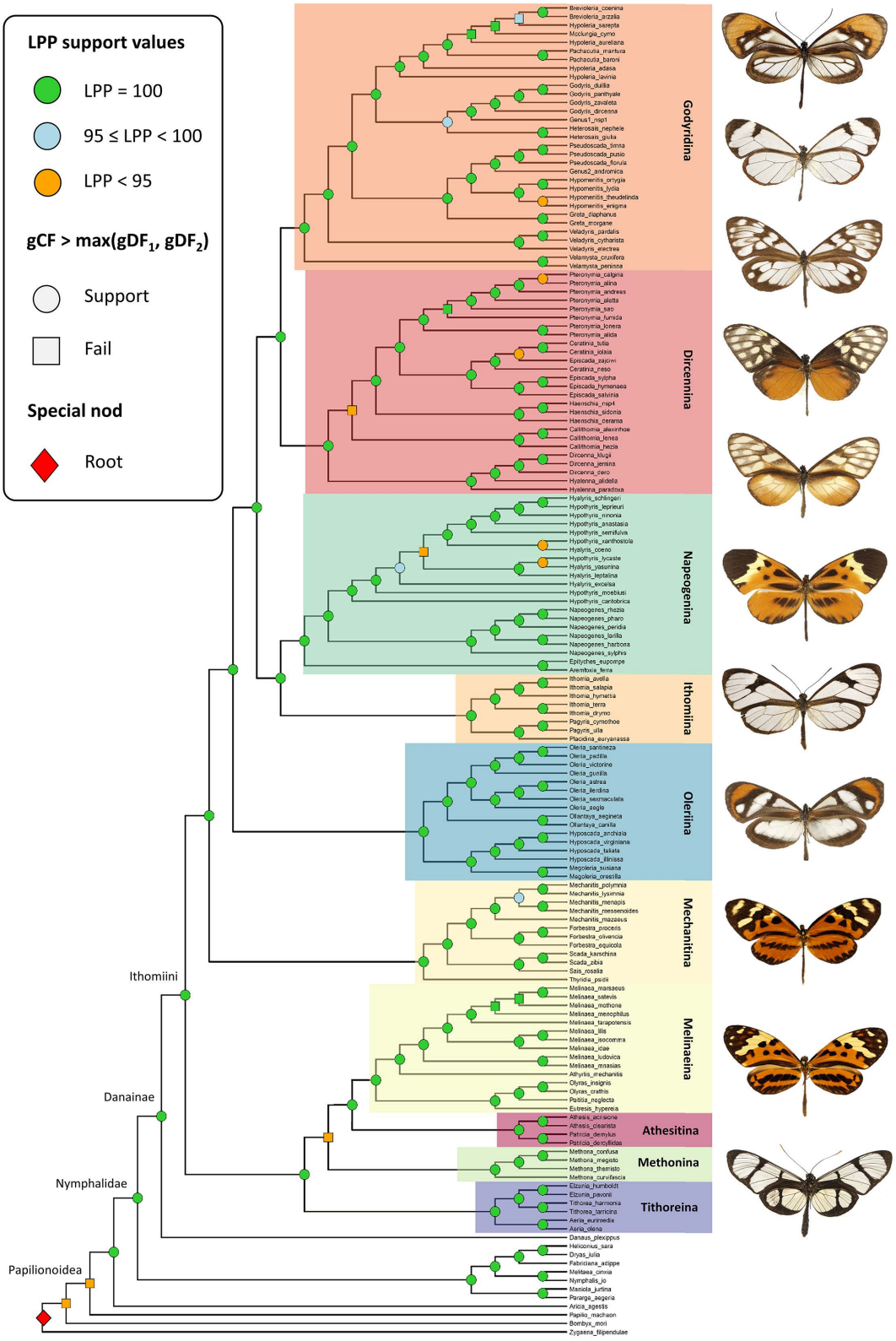

Figure S11: Phylogenetic hypothesis inferred with ASTRAL from a set of 11,012 individual gene trees based on the *Inclusive dataset*. Branch lengths are uniformly distributed to obtain an ultrametric tree for visualization but do not relate to estimated phylogenetic distances. Colored clades correspond to the ten known subtribes. Node support values are illustrated with colored symbols according to local posterior probabilities (LPP) and gene concordance factor (gCF) tests against support for alternative local topologies (i.e., gDF = discordance factors).

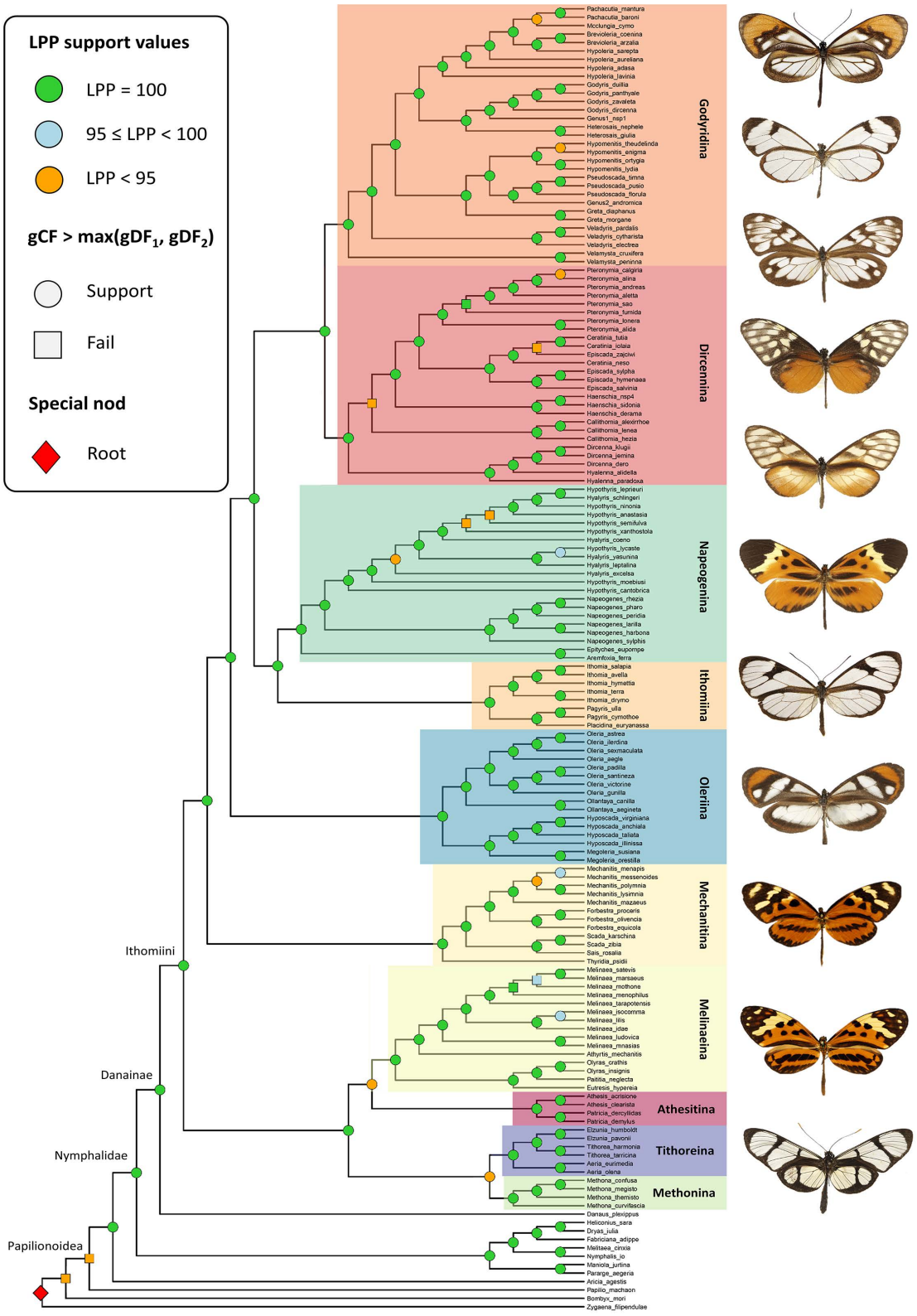

Figure S12: Phylogenetic hypothesis inferred with ASTRAL from a set of 3,518 individual gene trees based on the *Conservative dataset*. Branch lengths are uniformly distributed to obtain an ultrametric tree for visualization but do not relate to estimated phylogenetic distances. Colored clades correspond to the ten known subtribes. Node support values are illustrated with colored symbols according to local posterior probabilities (LPP) and gene concordance factor (gCF) tests against support for alternative local topologies (i.e., gDF = discordance factors).

Appendix 10: Time-calibrated phylogenies: clade-level

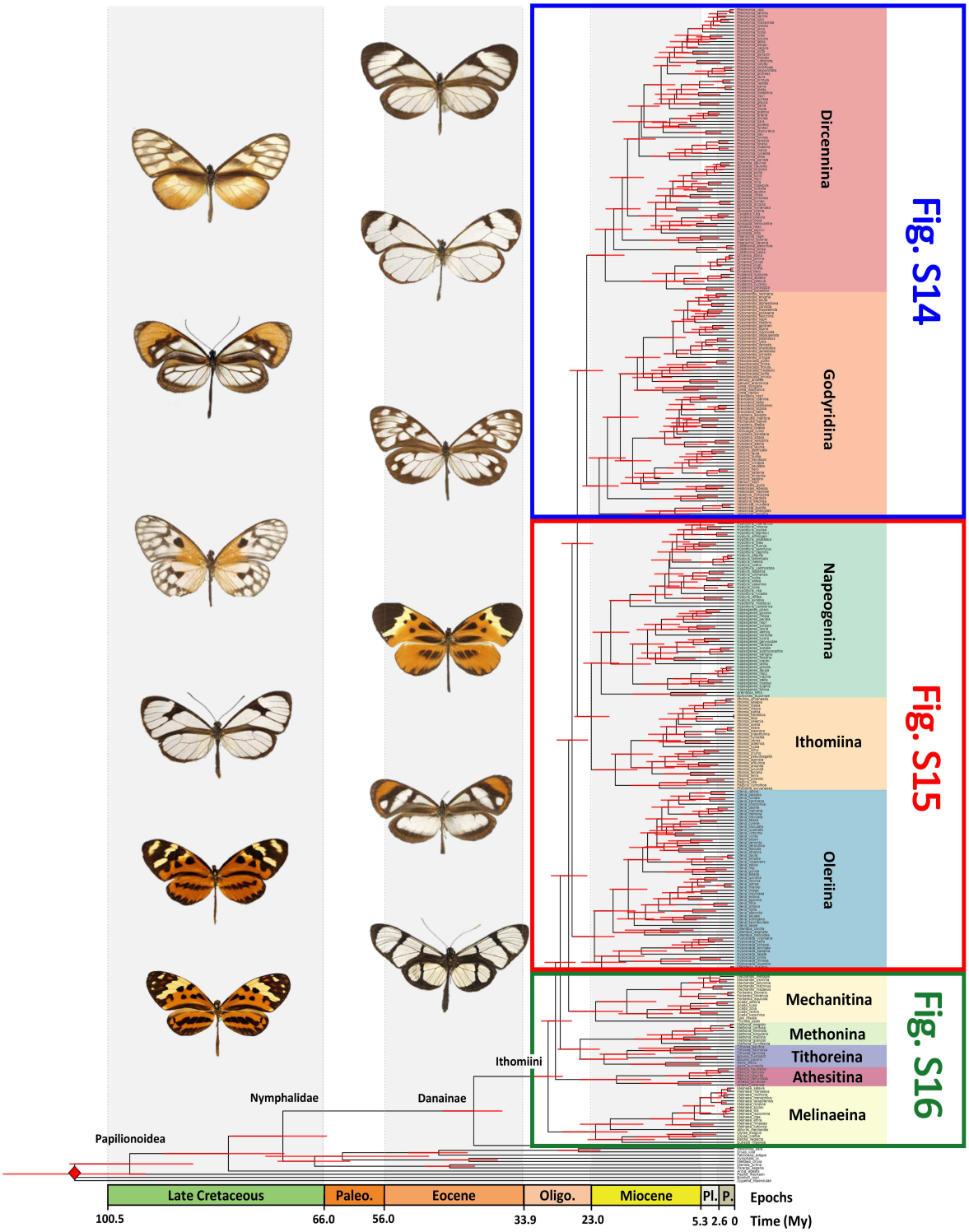

Figure S13: Comprehensive time-calibrated species-level phylogeny encompassing 356 ithomiine species and 12 outgroups. Node ages were estimated from Bayesian inference with BEAST using secondary calibrations from hostplant and higher-level phylogenies. Median node ages are shown inside their 95% Height Posterior Density intervals obtained through Bayesian inference (red bars).Colored clades correspond to the ten known subtribes. Detailed time-calibrated phylogenies zooming on specific clades are available in **Fig. S14, S15 & S16**.

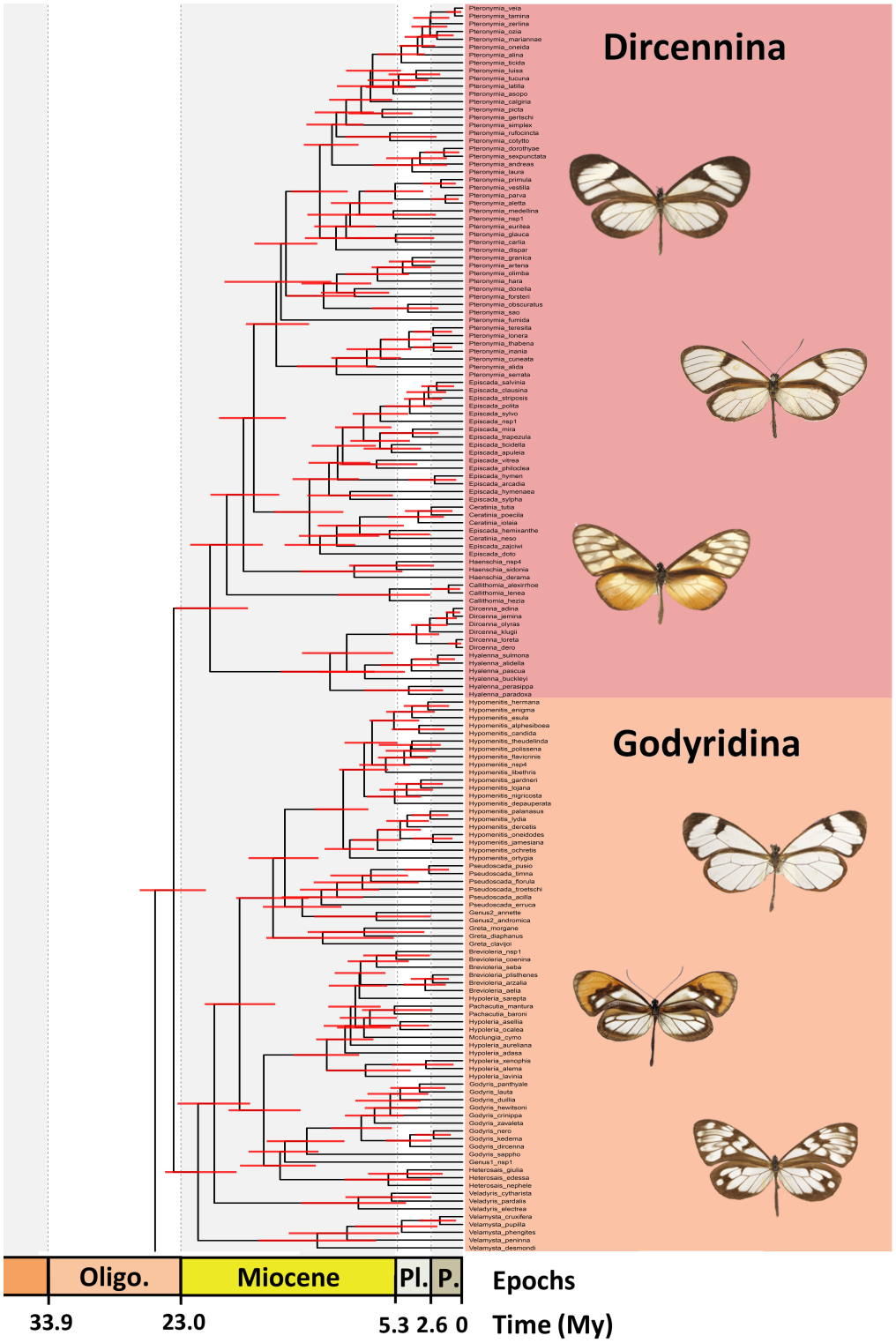

Figure S14: Time-calibrated species-level phylogeny zooming on Dircennina and Godyridina subtribes. Node ages were estimated from Bayesian inference with BEAST using secondary calibrations from hostplant and higher-level phylogenies. Median node ages are shown inside their 95% Height Posterior Density intervals obtained through Bayesian inference (red bars). Colored clades correspond to the Dircennina and Godyridina subtribes.

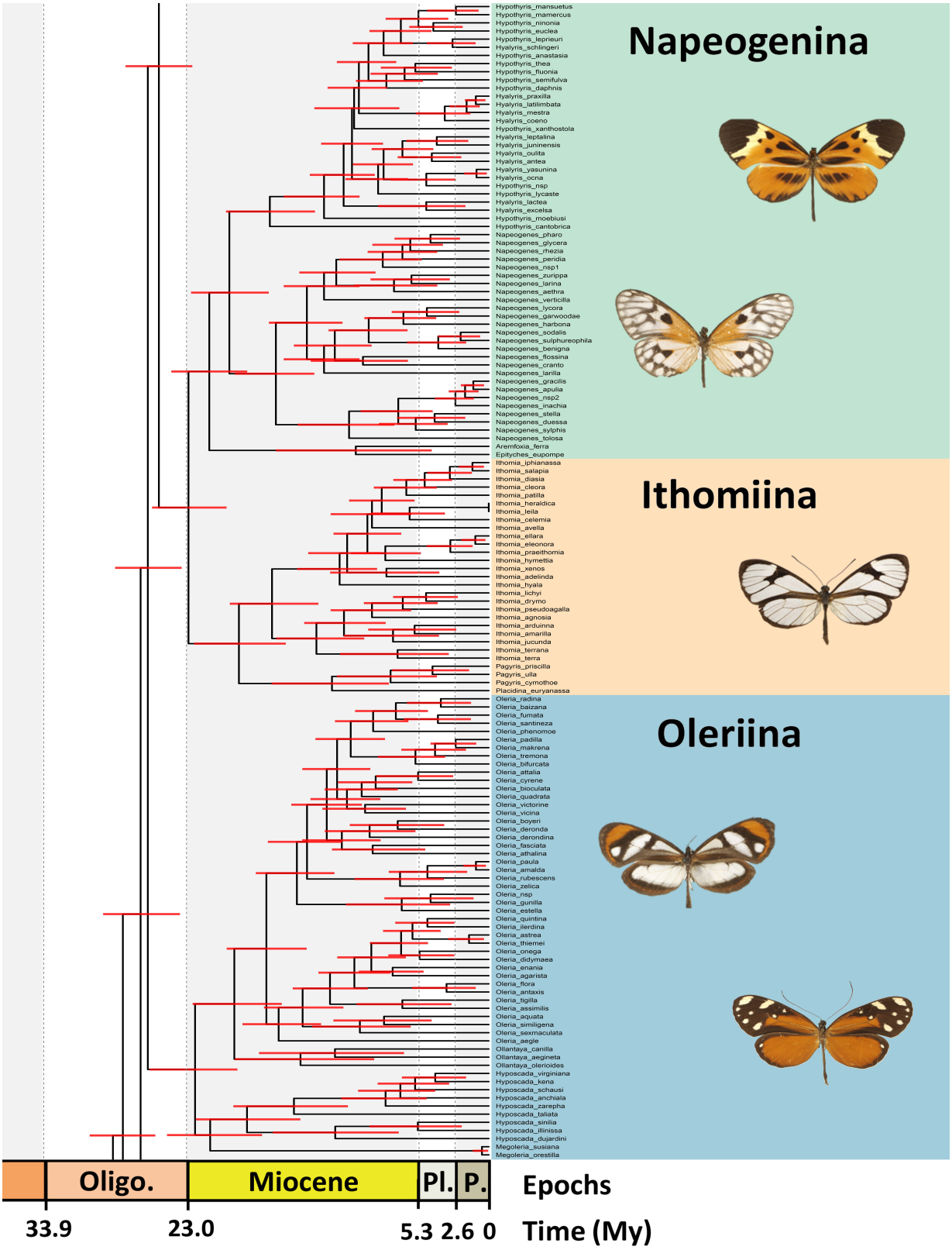

Figure S15: Time-calibrated species-level phylogeny zooming on Napeogenina, Ithomiina, and Oleriina subtribes. Node ages were estimated from Bayesian inference with BEAST using secondary calibrations from hostplant and higher-level phylogenies. Median node ages are shown inside their 95% Height Posterior Density intervals obtained through Bayesian inference (red bars). Colored clades correspond to the Napeogenina, Ithomiina, and Oleriina subtribes.

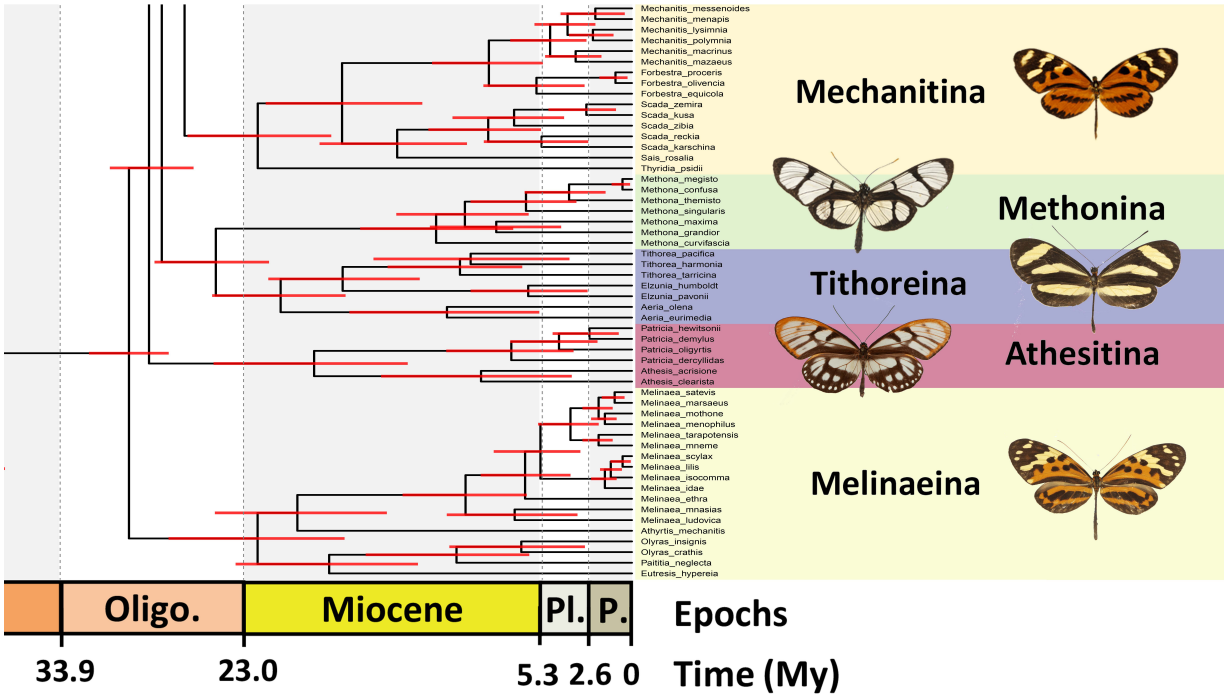

Figure S16: Time-calibrated species-level phylogeny zooming on the basal subtribes: Mechanitina, Methonina, Tithoreina, Athesitina, Melinaeina subtribes. Node ages were estimated from Bayesian inference with BEAST using secondary calibrations from hostplant and higher-level phylogenies. Median node ages are shown inside their 95% Height Posterior Density intervals obtained through Bayesian inference (red bars). Colored clades correspond to the Mechanitina, Methonina, Tithoreina, Athesitina, Melinaeina subtribes.

ANNEXE 4

Supplementary Information for CHAPTER 3

Supplementary Information for

Perceptual maps: a new tool to investigate mimicry patterns from Citizen Science to individual perception

Maël Doré[1,2], Eddie Pérochon[1,3], Thomas Aubier[4], Mathieu Joron[5*], and Marianne Elias[1,6*]

[1]*Institut de Systématique, Evolution, Biodiversité, MNHN-CNRS-Sorbonne Université-EPHE-Université des Antilles, Muséum national d'Histoire naturelle de Paris, 45 Rue Buffon, 75005, Paris, France*

[2]*Centre d'Ecologie et des Sciences de la Conservation, UMR 7204 MNHN-CNRS-Sorbonne Université, Muséum national d'Histoire naturelle de Paris, 45 rue Buffon, 75005, Paris, France*

[3]*Department of Ecology and Evolution, University of Lausanne, Lausanne, Switzerland.*

[4]*Laboratoire Évolution & Diversité Biologique, Université Paul Sabatier Toulouse III, UMR 5174, CNRS/IRD, 31077 Toulouse, France*

[5]*Centre d'Ecologie Fonctionnelle et Evolutive, Université de Montpellier, CNRS, EPHE, IRD, Montpellier, France*

[6]*Smithsonian Tropical Research Institute, Panamá, Panamá*

**Co-last authors*

Appendix 1: Metadata for images of subspecies

Table S1: Source for images used to represent the 432 heliconiine subspecies in the online survey.

ID	Genus	Species	Subspecies	Source	Author(s)
1	Agraulis	vanillae	galapagensis	BOA	Gerardo Lamas
2	Agraulis	vanillae	incarnata	Boyer_Collection	Pierre Boyer
3	Agraulis	vanillae	insularis	Boyer_Collection	Pierre Boyer
4	Agraulis	vanillae	lucina	Boyer_Collection	Pierre Boyer
5	Agraulis	vanillae	maculosa	FLMNH	Chris Jiggins
6	Agraulis	vanillae	nigrior	BOA	Andrew D Warren
7	Agraulis	vanillae	vanillae	Boyer_Collection	Pierre Boyer
8	Dione	glycera		FLMNH	Chris Jiggins
9	Dione	juno	andicola	BOA	Gerardo Lamas
10	Dione	juno	huascuma	Boyer_Collection	Pierre Boyer
11	Dione	juno	juno	FLMNH	Chris Jiggins
12	Dione	juno	miraculosa	Boyer_Collection	Pierre Boyer
13	Dione	moneta	butleri	BOA	Gerardo Lamas
14	Dione	moneta	poeyii	FLMNH	Chris Jiggins
15	Dryadula	phaetusa		FLMNH	Chris Jiggins
16	Dryas	iulia	alcionea	FLMNH	Chris Jiggins
17	Eueides	aliphera	aliphera	FLMNH	Chris Jiggins
18	Eueides	aliphera	cyllenella	FLMNH	Chris Jiggins
19	Eueides	aliphera	gracilis	Michel_Cast_website	Michel Cast
20	Eueides	emsleyi	emsleyi	Boyer_Collection	Pierre Boyer
21	Eueides	heliconioides	eanes	FLMNH	Chris Jiggins
22	Eueides	heliconioides	heliconioides	FLMNH	Chris Jiggins
23	Dione	moneta	moneta	FLMNH	Augusto H. B. Rosa
24	Eueides	isabella	dissoluta	FLMNH	Chris Jiggins
25	Eueides	isabella	ecuadorensis	FLMNH	Chris Jiggins
26	Eueides	isabella	hippolinus	Boyer_Collection	Pierre Boyer
27	Eueides	isabella	huebneri	FLMNH	Chris Jiggins
28	Eueides	isabella	isabella	FLMNH	Chris Jiggins
29	Eueides	isabella	melphis	Boyer_Collection	Pierre Boyer
30	Eueides	isabella	nigricornis	BOA	Andrew D Warren
31	Eueides	lampeto	acacetes	FLMNH	Chris Jiggins
32	Dryas	iulia	delila	FLMNH	Augusto H. B. Rosa
33	Dryas	iulia	dominicana	Boyer_Collection	Pierre Boyer
34	Eueides	lampeto	nigrofulva	FLMNH	Chris Jiggins
35	Eueides	libitina	libitina	MNHN_Collection	Maël Doré
36	Eueides	libitina	malleti	Michel_Cast_website	Michel Cast
37	Eueides	lineata		FLMNH	Chris Jiggins
38	Eueides	lybia	lybia	FLMNH	Chris Jiggins

39	Eueides	lybia	lybioides	MNHN_Collection	Maël Doré
40	Eueides	lybia	olympia	FLMNH	Chris Jiggins
41	Eueides	isabella	dianasa	Boyer_Collection	Pierre Boyer
42	Eueides	isabella	eva	Boyer_Collection	Pierre Boyer
43	Eueides	tales	michaeli	FLMNH	Augusto H. B. Rosa
44	Eueides	pavana		FLMNH	Chris Jiggins
45	Heliconius	demeter	subspnov	FLMNH	Keith Willmott
46	Eueides	procula	edias	FLMNH	Chris Jiggins
47	Eueides	procula	eurysaces	FLMNH	Chris Jiggins
48	Dryas	iulia	nudeola	Boyer_Collection	Pierre Boyer
49	Eueides	procula	procula	FLMNH	Chris Jiggins
50	Eueides	procula	vulgiformis	Boyer_Collection	Pierre Boyer
51	Dryas	iulia	fucatus	Boyer_Collection	Pierre Boyer
52	Eueides	tales	calathus	FLMNH	Chris Jiggins
53	Dryas	iulia	martinica	MNHN_Collection	Maël Doré
54	Eueides	tales	franciscus	Boyer_Collection	Pierre Boyer
55	Eueides	lybia	orinocensis	FLMNH	Augusto H. B. Rosa
56	Eueides	tales	pseudeanes	Boyer_Collection	Pierre Boyer
57	Eueides	tales	pythagoras	FLMNH	Chris Jiggins
58	Eueides	tales	surdus	FLMNH	Chris Jiggins
59	Eueides	procula	asidia	FLMNH	Augusto H. B. Rosa
60	Eueides	tales	tales	MNHN_Collection	Maël Doré
61	Dryas	iulia	moderata	Boyer_Collection	Pierre Boyer
62	Eueides	vibilia	unifasciatus	FLMNH	Chris Jiggins
63	Eueides	vibilia	vialis	FLMNH	Chris Jiggins
64	Eueides	vibilia	vibilia	FLMNH	Chris Jiggins
65	Eueides	vibilia	vicinalis	Boyer_Collection	Pierre Boyer
66	Heliconius	antiochus	antiochus	FLMNH	Chris Jiggins
67	Heliconius	antiochus	aranea	FLMNH	Chris Jiggins
68	Heliconius	antiochus	araneides	Boyer_Collection	Pierre Boyer
69	Heliconius	antiochus	salvinii	FLMNH	Chris Jiggins
70	Heliconius	aoede	aliciae	FLMNH	Chris Jiggins
71	Heliconius	aoede	aoede	FLMNH	Chris Jiggins
72	Heliconius	aoede	astydamia	FLMNH	Chris Jiggins
73	Heliconius	aoede	ayacuchensis	FLMNH	Chris Jiggins
74	Heliconius	aoede	bartletti	FLMNH	Chris Jiggins
75	Heliconius	aoede	centurius	FLMNH	Chris Jiggins
76	Heliconius	aoede	cupidineus	FLMNH	Chris Jiggins
77	Heliconius	aoede	emmelina	Boyer_Collection	Pierre Boyer
78	Heliconius	aoede	eurycleia	Boyer_Collection	Pierre Boyer
79	Heliconius	aoede	faleria	Heliconius.net	NA
80	Heliconius	aoede	lucretius	FLMNH	Chris Jiggins
81	Heliconius	aoede	manu	FLMNH	Chris Jiggins
82	Heliconius	aoede	philipi	FLMNH	Chris Jiggins

83	Heliconius	astraea	astraea	FLMNH	Chris Jiggins
84	Heliconius	astraea	rondonia	FLMNH	Chris Jiggins
85	Heliconius	atthis		FLMNH	Chris Jiggins
86	Heliconius	besckei		FLMNH	Chris Jiggins
87	Heliconius	burneyi	ada	Boyer_Collection	Pierre Boyer
88	Heliconius	burneyi	anjae	FLMNH	Chris Jiggins
89	Heliconius	burneyi	burneyi	FLMNH	Chris Jiggins
90	Heliconius	burneyi	catharinae	FLMNH	Chris Jiggins
91	Heliconius	burneyi	huebneri	FLMNH	Chris Jiggins
92	Heliconius	burneyi	jamesi	FLMNH	Chris Jiggins
93	Heliconius	burneyi	lindigii	MNHN_Collection	Maël Doré
94	Agraulis	vanillae	forbesi	FLMNH	Keith Willmott
95	Heliconius	burneyi	skinneri	FLMNH	Chris Jiggins
96	Heliconius	charithonia	bassleri	FLMNH	Chris Jiggins
97	Heliconius	charithonia	charithonia	FLMNH	Chris Jiggins
98	Heliconius	charithonia	churchi	FLMNH	Chris Jiggins
99	Heliconius	charithonia	ramsdeni	FLMNH	Chris Jiggins
100	Heliconius	charithonia	simulator	FLMNH	Chris Jiggins
101	Heliconius	charithonia	tuckeri	FLMNH	Chris Jiggins
102	Heliconius	charithonia	vazquezae	FLMNH	Chris Jiggins
103	Heliconius	clysonymus	clysonymus	FLMNH	Chris Jiggins
104	Heliconius	clysonymus	hygiana	FLMNH	Chris Jiggins
105	Heliconius	clysonymus	montanus	FLMNH	Chris Jiggins
106	Philaethria	dido	panamensis	Remi_Mauxion	Remi Mauxion
107	Heliconius	congener	aquilionaris	MNHN_Collection	Maël Doré
108	Heliconius	congener	congener	FLMNH	Chris Jiggins
109	Philaethria	dido	dido	FLMNH	Chris Jiggins
110	Heliconius	cydno	alithea	FLMNH	Chris Jiggins
111	Heliconius	cydno	barinasensis	FLMNH	Chris Jiggins
112	Heliconius	cydno	chioneus	FLMNH	Chris Jiggins
113	Heliconius	cydno	cordula	FLMNH	Chris Jiggins
114	Heliconius	cydno	cydnides	FLMNH	Chris Jiggins
115	Heliconius	cydno	cydno	FLMNH	Chris Jiggins
116	Heliconius	cydno	gadouae	FLMNH	Chris Jiggins
117	Heliconius	cydno	galanthus	FLMNH	Chris Jiggins
118	Heliconius	cydno	hermogenes	FLMNH	Chris Jiggins
119	Heliconius	cydno	lisethae	FLMNH	Chris Jiggins
120	Heliconius	cydno	wanningeri	FLMNH	Chris Jiggins
121	Heliconius	cydno	weymeri	FLMNH	Chris Jiggins
122	Heliconius	cydno	zelinde	FLMNH	Chris Jiggins
123	Philaethria	dido	chocoensis	Boyer_Collection	Pierre Boyer
124	Heliconius	demeter	bouqueti	FLMNH	Chris Jiggins
125	Heliconius	demeter	demeter	FLMNH	Chris Jiggins
126	Heliconius	demeter	joroni	Michel_Cast_website	Michel Cast

127	Heliconius	demeter	karinae	FLMNH	Chris Jiggins
128	Heliconius	demeter	neildi	FLMNH	Chris Jiggins
129	Heliconius	demeter	terrasanta	FLMNH	Chris Jiggins
130	Heliconius	demeter	titan	FLMNH	Chris Jiggins
131	Heliconius	demeter	turneri	FLMNH	Chris Jiggins
132	Philaethria	diatonica		FLMNH	Chris Jiggins
133	Heliconius	doris	dives	Boyer_Collection	Pierre Boyer
134	Heliconius	doris	doris	FLMNH	Chris Jiggins
135	Heliconius	doris	obscurus	FLMNH	Chris Jiggins
136	Heliconius	doris	viridis	FLMNH	Chris Jiggins
137	Heliconius	egeria	egeria	FLMNH	Chris Jiggins
138	Heliconius	egeria	egerides	Boyer_Collection	Pierre Boyer
139	Heliconius	egeria	homogena	FLMNH	Chris Jiggins
140	Heliconius	egeria	hyas	FLMNH	Chris Jiggins
141	Heliconius	egeria	keithbrowni	FLMNH	Chris Jiggins
142	Heliconius	eleuchia	eleuchia	FLMNH	Chris Jiggins
143	Heliconius	eleuchia	eleusinus	FLMNH	Chris Jiggins
144	Heliconius	eleuchia	primularis	FLMNH	Chris Jiggins
145	Heliconius	elevatus	bari	Michel_Cast_website	Michel Cast
146	Heliconius	elevatus	elevatus	FLMNH	Chris Jiggins
147	Heliconius	elevatus	lapis	FLMNH	Chris Jiggins
148	Heliconius	elevatus	perchlora	FLMNH	Chris Jiggins
149	Heliconius	elevatus	pseudocupidineus	FLMNH	Chris Jiggins
150	Heliconius	elevatus	roraima	FLMNH	Chris Jiggins
151	Heliconius	elevatus	schmassmanni	FLMNH	Chris Jiggins
152	Heliconius	elevatus	taracuanus	FLMNH	Chris Jiggins
153	Heliconius	elevatus	tumatumari	FLMNH	Keith Willmott
154	Heliconius	elevatus	zoelleri	FLMNH	Chris Jiggins
155	Heliconius	erato	adana	FLMNH	Chris Jiggins
156	Heliconius	erato	amalfreda	FLMNH	Chris Jiggins
157	Heliconius	erato	amazona	FLMNH	Chris Jiggins
158	Heliconius	erato	amphitrite	FLMNH	Chris Jiggins
159	Heliconius	erato	chestertonii	FLMNH	Chris Jiggins
160	Heliconius	erato	colombina	Boyer_Collection	Pierre Boyer
161	Philaethria	constantinoi		FLMNH	Chris Jiggins
162	Heliconius	erato	cyrbia	FLMNH	Chris Jiggins
163	Heliconius	erato	demophoon	FLMNH	Chris Jiggins
164	Heliconius	erato	dignus	FLMNH	Chris Jiggins
165	Heliconius	erato	emma	FLMNH	Chris Jiggins
166	Heliconius	erato	erato	FLMNH	Chris Jiggins
167	Heliconius	erato	estrella	Boyer_Collection	Pierre Boyer
168	Heliconius	erato	etylus	FLMNH	Chris Jiggins
169	Heliconius	erato	favorinus	FLMNH	Chris Jiggins
170	Heliconius	erato	guarica	FLMNH	Chris Jiggins

171	Heliconius	erato	hydara	FLMNH	Chris Jiggins
172	Heliconius	erato	lativitta	FLMNH	Chris Jiggins
173	Heliconius	erato	lichyi	FLMNH	Chris Jiggins
174	Heliconius	erato	luscombei	FLMNH	Chris Jiggins
175	Heliconius	erato	magnifica	FLMNH	Chris Jiggins
176	Heliconius	erato	microclea	FLMNH	Chris Jiggins
177	Heliconius	erato	notabilis	FLMNH	Chris Jiggins
178	Heliconius	erato	phyllis	FLMNH	Chris Jiggins
179	Heliconius	erato	reductimacula	FLMNH	Chris Jiggins
180	Heliconius	erato	tobagoensis	FLMNH	Chris Jiggins
181	Heliconius	erato	venus	FLMNH	Chris Jiggins
182	Heliconius	erato	venustus	FLMNH	Chris Jiggins
183	Philaethria	andrei	andrei	BOA	Christian Brevignon
184	Heliconius	eratosignis	tambopata	FLMNH	Keith Willmott
185	Heliconius	eratosignis	ucayalensis	FLMNH	Chris Jiggins
186	Heliconius	eratosignis	ulysses	FLMNH	Chris Jiggins
187	Heliconius	ethilla	adela	FLMNH	Chris Jiggins
188	Heliconius	ethilla	aerotome	FLMNH	Chris Jiggins
189	Heliconius	ethilla	cephallenia	Boyer_Collection	Pierre Boyer
190	Heliconius	ethilla	chapadensis	FLMNH	Chris Jiggins
191	Heliconius	ethilla	claudia	FLMNH	Chris Jiggins
192	Heliconius	ethilla	ethilla	FLMNH	Chris Jiggins
193	Heliconius	ethilla	eucoma	FLMNH	Chris Jiggins
194	Heliconius	ethilla	flavofasciatus	FLMNH	Augusto H. B. Rosa
195	Heliconius	ethilla	flavomaculatus	FLMNH	Chris Jiggins
196	Heliconius	ethilla	hyalina	FLMNH	Keith Willmott
197	Heliconius	ethilla	jaruensis	FLMNH	Chris Jiggins
198	Heliconius	ethilla	latona	FLMNH	Chris Jiggins
199	Heliconius	ethilla	mentor	Boyer_Collection	Pierre Boyer
200	Heliconius	ethilla	metalilis	FLMNH	Chris Jiggins
201	Heliconius	ethilla	michaelianius	FLMNH	Chris Jiggins
202	Heliconius	ethilla	narcaea	FLMNH	Chris Jiggins
203	Heliconius	xanthocles	zamora	FLMNH	Chris Jiggins
204	Heliconius	ethilla	numismaticus	FLMNH	Chris Jiggins
205	Heliconius	ethilla	penthesilea	FLMNH	Chris Jiggins
206	Heliconius	ethilla	polychrous	FLMNH	Chris Jiggins
207	Heliconius	ethilla	semiflavidus	FLMNH	Chris Jiggins
208	Heliconius	ethilla	thielei	FLMNH	Chris Jiggins
209	Heliconius	ethilla	tyndarus	FLMNH	Chris Jiggins
210	Heliconius	ethilla	yuruani	FLMNH	Chris Jiggins
211	Heliconius	godmani		FLMNH	Chris Jiggins
212	Heliconius	hecale	anderida	FLMNH	Chris Jiggins
213	Heliconius	hecale	annetta	FLMNH	Chris Jiggins
214	Heliconius	hecale	australis	FLMNH	Chris Jiggins

215	Heliconius	hecale	barcanti	MNHN_Collection	Maël Doré
216	Heliconius	hecale	clearei	FLMNH	Chris Jiggins
217	Heliconius	hecale	ennius	FLMNH	Chris Jiggins
218	Heliconius	hecale	felix	FLMNH	Chris Jiggins
219	Heliconius	hecale	fornarina	FLMNH	Chris Jiggins
220	Heliconius	hecale	hecale	FLMNH	Chris Jiggins
221	Heliconius	hecale	holcophorus	FLMNH	Chris Jiggins
222	Heliconius	hecale	humboldti	FLMNH	Chris Jiggins
223	Heliconius	hecale	ithaca	FLMNH	Chris Jiggins
224	Heliconius	hecale	latus	FLMNH	Chris Jiggins
225	Heliconius	hecale	melicerta	FLMNH	Chris Jiggins
226	Heliconius	hecale	metellus	FLMNH	Chris Jiggins
227	Heliconius	hecale	nigrofasciatus	FLMNH	Chris Jiggins
228	Heliconius	hecale	novatus	FLMNH	Chris Jiggins
229	Heliconius	hecale	paraensis	FLMNH	Keith Willmott
230	Heliconius	hecale	paulus	FLMNH	Chris Jiggins
231	Heliconius	hecale	quitalena	FLMNH	Chris Jiggins
232	Heliconius	hecale	rosalesi	FLMNH	Keith Willmott
233	Heliconius	hecale	shanki	FLMNH	Chris Jiggins
234	Heliconius	hecale	sisyphus	FLMNH	Chris Jiggins
235	Heliconius	hecale	sulphureus	FLMNH	Chris Jiggins
236	Heliconius	hecale	vetustus	FLMNH	Chris Jiggins
237	Heliconius	hecale	zuleika	FLMNH	Chris Jiggins
238	Heliconius	hecalesia	eximius	Boyer_Collection	Pierre Boyer
239	Heliconius	hecalesia	formosus	FLMNH	Chris Jiggins
240	Heliconius	hecalesia	gynaesia	FLMNH	Chris Jiggins
241	Heliconius	hecalesia	hecalesia	FLMNH	Chris Jiggins
242	Heliconius	hecalesia	longarena	FLMNH	Chris Jiggins
243	Heliconius	hecalesia	octavia	FLMNH	Chris Jiggins
244	Heliconius	hecalesia	romeroi	FLMNH	Chris Jiggins
245	Heliconius	hecuba	cassandra	Boyer_Collection	Pierre Boyer
246	Heliconius	hecuba	choarina	FLMNH	Chris Jiggins
247	Heliconius	hecuba	creusa	FLMNH	Chris Jiggins
248	Heliconius	xanthocles	xanthocles	FLMNH	Chris Jiggins
249	Heliconius	hecuba	flava	FLMNH	Chris Jiggins
250	Heliconius	hecuba	hecuba	FLMNH	Chris Jiggins
251	Heliconius	hecuba	tolima	FLMNH	Chris Jiggins
252	Heliconius	hermathena	curua	FLMNH	Augusto H. B. Rosa
253	Heliconius	hermathena	duckei	FLMNH	Augusto H. B. Rosa
254	Heliconius	hermathena	hermathena	FLMNH	Chris Jiggins
255	Heliconius	hermathena	renatae	FLMNH	Chris Jiggins
256	Heliconius	hermathena	sabinae	FLMNH	Chris Jiggins
257	Heliconius	hermathena	sheppardi	FLMNH	Augusto H. B. Rosa
258	Heliconius	hermathena	vereatta	FLMNH	Augusto H. B. Rosa

259	Heliconius	heurippa		FLMNH	Chris Jiggins
260	Heliconius	hewitsoni		FLMNH	Chris Jiggins
261	Heliconius	hierax	hierax	FLMNH	Chris Jiggins
262	Heliconius	xanthocles	vala	FLMNH	Chris Jiggins
263	Heliconius	himera		FLMNH	Chris Jiggins
264	Heliconius	hortense		FLMNH	Chris Jiggins
265	Heliconius	ismenius	boulleti	FLMNH	Chris Jiggins
266	Heliconius	ismenius	clarescens	FLMNH	Chris Jiggins
267	Heliconius	ismenius	fasciatus	MNHN_Collection	Maël Doré
268	Heliconius	ismenius	ismenius	FLMNH	Chris Jiggins
269	Heliconius	ismenius	metaphorus	FLMNH	Chris Jiggins
270	Heliconius	ismenius	occidentalis	FLMNH	Chris Jiggins
271	Heliconius	ismenius	telchinia	FLMNH	Chris Jiggins
272	Heliconius	ismenius	tilletti	FLMNH	Keith Willmott
273	Heliconius	lalitae		FLMNH	Chris Jiggins
274	Heliconius	leucadia	leucadia	FLMNH	Chris Jiggins
275	Heliconius	leucadia	pseudorhea	FLMNH	Chris Jiggins
276	Heliconius	xanthocles	similatus	FLMNH	Chris Jiggins
277	Heliconius	luciana	watunna	FLMNH	Chris Jiggins
278	Heliconius	melpomene	aglaope	FLMNH	Chris Jiggins
279	Heliconius	melpomene	amandus	FLMNH	Chris Jiggins
280	Heliconius	melpomene	amaryllis	FLMNH	Chris Jiggins
281	Heliconius	melpomene	anduzei	FLMNH	Chris Jiggins
282	Heliconius	melpomene	bellula	FLMNH	Chris Jiggins
283	Heliconius	melpomene	burchelli	FLMNH	Chris Jiggins
284	Heliconius	melpomene	cythera	FLMNH	Chris Jiggins
285	Heliconius	melpomene	ecuadorensis	FLMNH	Chris Jiggins
286	Heliconius	melpomene	euryades	FLMNH	Keith Willmott
287	Heliconius	melpomene	flagrans	FLMNH	Chris Jiggins
288	Heliconius	melpomene	intersectus	FLMNH	Keith Willmott
289	Heliconius	melpomene	madeira	Boyer_Collection	Pierre Boyer
290	Heliconius	melpomene	malleti	FLMNH	Chris Jiggins
291	Heliconius	melpomene	martinae	Michel_Cast_website	Michel Cast
292	Heliconius	melpomene	melpomene	FLMNH	Chris Jiggins
293	Heliconius	melpomene	meriana	Boyer_Collection	Pierre Boyer
294	Heliconius	melpomene	michellae	FLMNH	Chris Jiggins
295	Heliconius	melpomene	nanna	FLMNH	Chris Jiggins
296	Heliconius	melpomene	penelope	FLMNH	Chris Jiggins
297	Heliconius	melpomene	plesseni	FLMNH	Chris Jiggins
298	Heliconius	melpomene	pyrforus	FLMNH	Chris Jiggins
299	Heliconius	melpomene	rosina	FLMNH	Chris Jiggins
300	Heliconius	melpomene	schunkei	FLMNH	Chris Jiggins
301	Heliconius	melpomene	tessa	FLMNH	Chris Jiggins
302	Heliconius	melpomene	thelxiope	FLMNH	Chris Jiggins

303	Heliconius	melpomene	thelxiopeia	Boyer_Collection	Pierre Boyer
304	Heliconius	melpomene	vicina	FLMNH	Chris Jiggins
305	Heliconius	melpomene	vulcanus	FLMNH	Chris Jiggins
306	Heliconius	melpomene	xenoclea	FLMNH	Chris Jiggins
307	Heliconius	metharme	makiritare	FLMNH	Chris Jiggins
308	Heliconius	metharme	metharme	FLMNH	Chris Jiggins
309	Heliconius	metharme	perseis	FLMNH	Chris Jiggins
310	Philaethria	ostara	ostara	BOA	Keith Willmott
311	Heliconius	nattereri		FLMNH	Chris Jiggins
312	Heliconius	numata	arcuella	FLMNH	Chris Jiggins
313	Heliconius	numata	aristiona	FLMNH	Chris Jiggins
314	Heliconius	numata	aulicus	FLMNH	Chris Jiggins
315	Heliconius	numata	aurora	FLMNH	Chris Jiggins
316	Heliconius	numata	bicoloratus	FLMNH	Chris Jiggins
317	Heliconius	numata	elegans	Boyer_Collection	Pierre Boyer
318	Heliconius	numata	ethra	FLMNH	Chris Jiggins
319	Heliconius	numata	euphone	FLMNH	Chris Jiggins
320	Heliconius	numata	euphrasius	Boyer_Collection	Pierre Boyer
321	Heliconius	numata	geminatus	Boyer_Collection	Pierre Boyer
322	Heliconius	numata	holzingeri	FLMNH	Chris Jiggins
323	Heliconius	numata	ignotus	FLMNH	Chris Jiggins
324	Heliconius	numata	illustris	FLMNH	Chris Jiggins
325	Heliconius	numata	isabellinus	NHMUK	B. Huertas & R. Crowther
326	Heliconius	numata	jiparanaensis	FLMNH	Chris Jiggins
327	Heliconius	numata	laura	Boyer_Collection	Pierre Boyer
328	Heliconius	numata	lenaeus	FLMNH	Chris Jiggins
329	Heliconius	numata	lyrcaeus	FLMNH	Chris Jiggins
330	Heliconius	numata	mavors	FLMNH	Chris Jiggins
331	Heliconius	numata	messene	FLMNH	Chris Jiggins
332	Heliconius	numata	mirus	FLMNH	Chris Jiggins
333	Heliconius	numata	nubifer	FLMNH	Chris Jiggins
334	Heliconius	numata	numata	FLMNH	Chris Jiggins
335	Heliconius	numata	peeblesi	Boyer_Collection	Pierre Boyer
336	Heliconius	numata	pratti	FLMNH	Chris Jiggins
337	Heliconius	numata	robigus	FLMNH	Chris Jiggins
338	Heliconius	numata	silvana	FLMNH	Chris Jiggins
339	Heliconius	numata	sourensis	FLMNH	Chris Jiggins
340	Heliconius	numata	superioris	FLMNH	Chris Jiggins
341	Heliconius	numata	talboti	FLMNH	Chris Jiggins
342	Heliconius	numata	tarapotensis	Boyer_Collection	Pierre Boyer
343	Heliconius	numata	timaeus	Boyer_Collection	Pierre Boyer
344	Heliconius	numata	zobrysi	FLMNH	Chris Jiggins
345	Heliconius	pachinus		FLMNH	Chris Jiggins
346	Podotricha	telesiphe	telesiphe	FLMNH	Chris Jiggins

347	Heliconius	pardalinus	butleri	Boyer_Collection	Pierre Boyer
348	Heliconius	pardalinus	dilatus	Boyer_Collection	Pierre Boyer
349	Podotricha	telesiphe	tithraustes	BOA	Gerardo Lamas
350	Heliconius	pardalinus	lucescens	MNHN_Collection	Maël Doré
351	Heliconius	pardalinus	maeon	FLMNH	Chris Jiggins
352	Heliconius	pardalinus	orteguaza	FLMNH	Keith Willmott
353	Heliconius	pardalinus	pardalinus	FLMNH	Chris Jiggins
354	Heliconius	pardalinus	radiosus	FLMNH	Keith Willmott
355	Heliconius	pardalinus	sergestus	FLMNH	Chris Jiggins
356	Heliconius	pardalinus	tithoreides	FLMNH	Chris Jiggins
357	Heliconius	peruvianus		FLMNH	Chris Jiggins
358	Heliconius	ricini	insulanus	FLMNH	Chris Jiggins
359	Heliconius	ricini	ricini	FLMNH	Chris Jiggins
360	Heliconius	sapho	candidus	FLMNH	Chris Jiggins
361	Heliconius	sapho	chocoensis	FLMNH	Chris Jiggins
362	Heliconius	sapho	leuce	FLMNH	Chris Jiggins
363	Heliconius	sapho	sapho	FLMNH	Chris Jiggins
364	Heliconius	sara	apseudes	FLMNH	Chris Jiggins
365	Heliconius	sara	brevimaculata	Boyer_Collection	Pierre Boyer
366	Heliconius	sara	elektra	FLMNH	Chris Jiggins
367	Heliconius	sara	fulgidus	FLMNH	Chris Jiggins
368	Heliconius	sara	magdalena	FLMNH	Chris Jiggins
369	Heliconius	sara	sara	FLMNH	Chris Jiggins
370	Heliconius	sara	sprucei	FLMNH	Chris Jiggins
371	Heliconius	sara	theudela	FLMNH	Chris Jiggins
372	Heliconius	sara	veraepacis	FLMNH	Chris Jiggins
373	Heliconius	sara	williami	FLMNH	Chris Jiggins
374	Heliconius	telesiphe	cretacea	FLMNH	Chris Jiggins
375	Heliconius	telesiphe	sotericus	FLMNH	Chris Jiggins
376	Heliconius	telesiphe	telesiphe	FLMNH	Chris Jiggins
377	Philaethria	wernickei		Boyer_Collection	Pierre Boyer
378	Podotricha	judith	straminea	Boyer_Collection	Pierre Boyer
379	Heliconius	timareta	thelxinoe	Boyer_Collection	Pierre Boyer
380	Heliconius	timareta	timareta	FLMNH	Chris Jiggins
381	Podotricha	judith	caucana	Boyer_Collection	Pierre Boyer
382	Podotricha	judith	judith	Boyer_Collection	Pierre Boyer
383	Podotricha	judith	mellosa	BOA	Gerardo Lamas
384	Heliconius	wallacei	colon	Boyer_Collection	Pierre Boyer
385	Heliconius	wallacei	flavescens	FLMNH	Chris Jiggins
386	Heliconius	wallacei	kayei	FLMNH	Chris Jiggins
387	Heliconius	wallacei	mimulinus	Boyer_Collection	Pierre Boyer
388	Heliconius	wallacei	wallacei	FLMNH	Chris Jiggins
389	Heliconius	xanthocles	buechei	FLMNH	Chris Jiggins
390	Heliconius	xanthocles	cleoxanthe	FLMNH	Chris Jiggins

391	Heliconius	xanthocles	donatia	Boyer_Collection	Pierre Boyer
392	Heliconius	xanthocles	explicata	FLMNH	Chris Jiggins
393	Heliconius	xanthocles	hippocrene	FLMNH	Chris Jiggins
394	Heliconius	xanthocles	melete	FLMNH	Chris Jiggins
395	Heliconius	xanthocles	melior	FLMNH	Chris Jiggins
396	Heliconius	xanthocles	melittus	FLMNH	Chris Jiggins
397	Heliconius	xanthocles	napoensis	FLMNH	Chris Jiggins
398	Heliconius	xanthocles	paraplesius	FLMNH	Chris Jiggins
399	Heliconius	xanthocles	quindecim	FLMNH	Chris Jiggins
400	Heliconius	xanthocles	rindgei	FLMNH	Chris Jiggins
401	Eueides	isabella	cleobaea	MNHN_Collection	Maël Doré
402	Heliconius	hecuba	crispus	MNHN_Collection	Maël Doré
403	Heliconius	erato	petiverana	MNHN_Collection	Maël Doré
404	Dione	juno	suffumata	NHMUK	B. Huertas & R. Crowther
405	Dryas	iulia	carteri	NHMUK	B. Huertas & R. Crowther
406	Dryas	iulia	framptoni	NHMUK	B. Huertas & R. Crowther
407	Dryas	iulia	warneri	NHMUK	B. Huertas & R. Crowther
408	Dryas	iulia	lucia	NHMUK	B. Huertas & R. Crowther
409	Eueides	lampeto	apicalis	NHMUK	B. Huertas & R. Crowther
410	Eueides	lampeto	lampeto	NHMUK	B. Huertas & R. Crowther
411	Eueides	procula	kuenowii	NHMUK	B. Huertas & R. Crowther
412	Eueides	tales	barcellinus	NHMUK	B. Huertas & R. Crowther
413	Eueides	tales	cognata	NHMUK	B. Huertas & R. Crowther
414	Eueides	tales	tabernula	NHMUK	B. Huertas & R. Crowther
415	Eueides	tales	xenophanes	NHMUK	B. Huertas & R. Crowther
416	Heliconius	luciana	luciana	NHMUK	B. Huertas & R. Crowther
417	Heliconius	pardalinus	julia	NHMUK	B. Huertas & R. Crowther
418	Heliconius	wallacei	araguaia	NHMUK	B. Huertas & R. Crowther
419	Eueides	emsleyi	esmeraldensis	Michel_Cast_website	Yves Lever
420	Eueides	heliconioides	koenigi	Michel_Cast_website	Yves Lever
421	Eueides	lampeto	brownsbergensis	10.18473/lepi.v64i3.a7	H. Gernaat
422	Eueides	procula	browni	Michel_Cast_website	Yves Lever
423	Eueides	vibilia	louisi	Michel_Cast_website	Yves Lever
424	Heliconius	aoede	auca	Michel_Cast_website	Michel Cast
425	Heliconius	burneyi	boliviensis	Michel_Cast_website	Michel Cast
426	Heliconius	burneyi	koenigi	Michel_Cast_website	Michel Cast
427	Heliconius	burneyi	mirtarosa	Michel_Cast_website	Michel Cast
428	Heliconius	hecuba	lamasi	Michel_Cast_website	Pierre Boyer
429	Heliconius	metis		ISSN 0723-9912	G. Moreira & C. Mielke
430	Heliconius	timareta	florencia	10.1186/1471-2148-8-324	Chris D. Jiggins
431	Heliconius	timareta	linaresi	IIRB	Chris D. Jiggins
432	Heliconius	timareta	tristero	Michel_Cast_website	D. Lacomme

Appendix 2: Online survey of wing pattern perception from similarity triplets

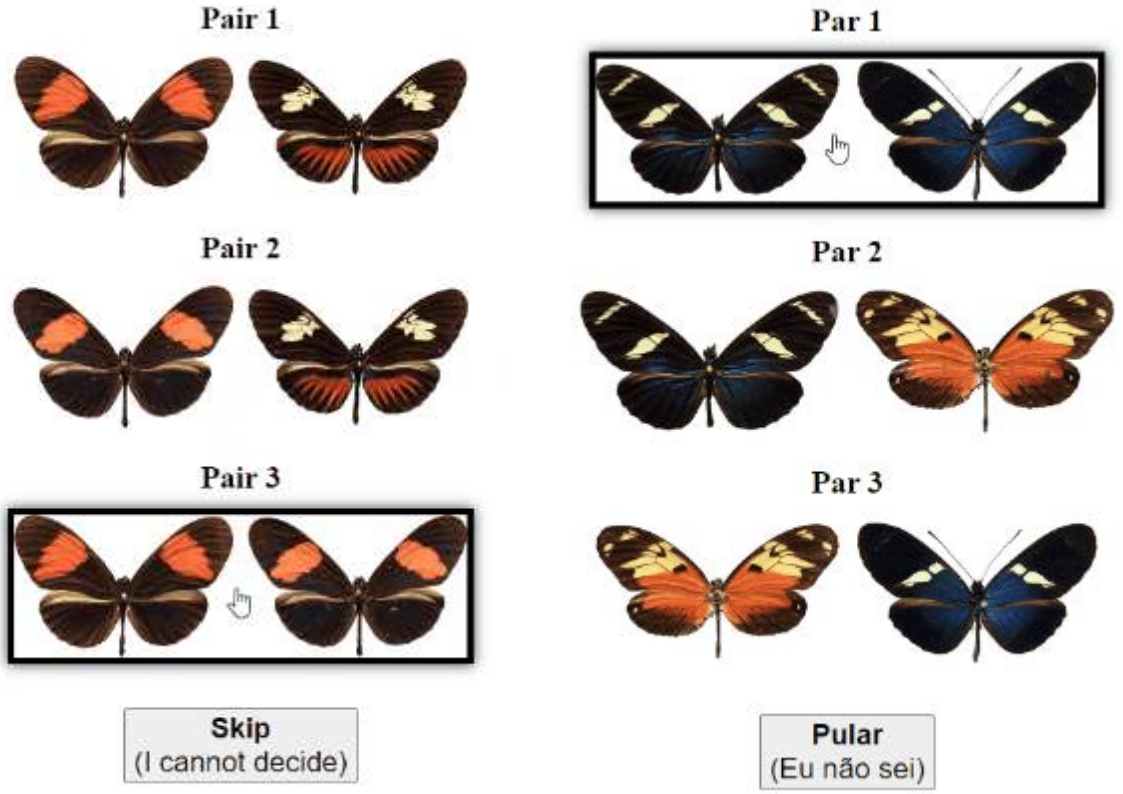

Figure S1: Interface for triplet selection in the online Citizen Science survey. The player is invited to select the pair of butterflies that displays the more similar color patterns according to its own perception. A skip button is available in case the player is undecided about a particular triplet. The website was made available in multiple languages. Left: English interface. Right: Brazilian Portuguese interface.

Appendix 3: Controlled trials of similarity triplets for the online survey

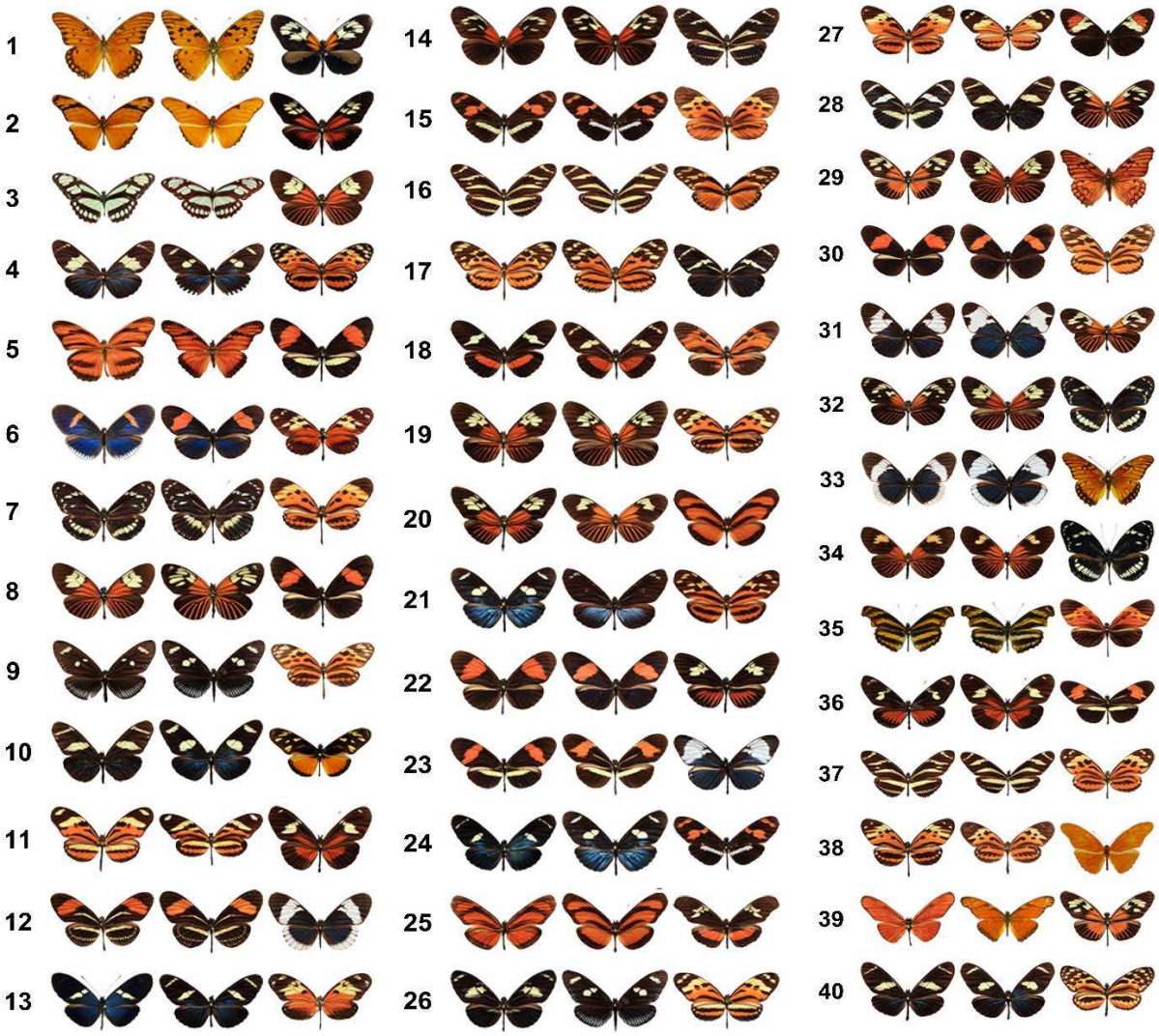

Figure S2: Triplets of images used as controlled trials in the online survey. For each game session, two random controlled trials were presented. The expected chosen pair for maximum similarity are the first two columns of each triplet. Images in a controlled trial are displayed at random to avoid positional bias. Game session that failed at least one controlled trial were removed from the triplet dataset.

Appendix 4: Online survey: demographics and game analytics

Website logs:

During the course of the online survey, we recorded 1,422 game sessions from 1,242 distinct players in 474 locations across 53 countries in 5 continents (**Fig. S3**), including 337 locations in 22 countries within Europe (**Fig. S4**).

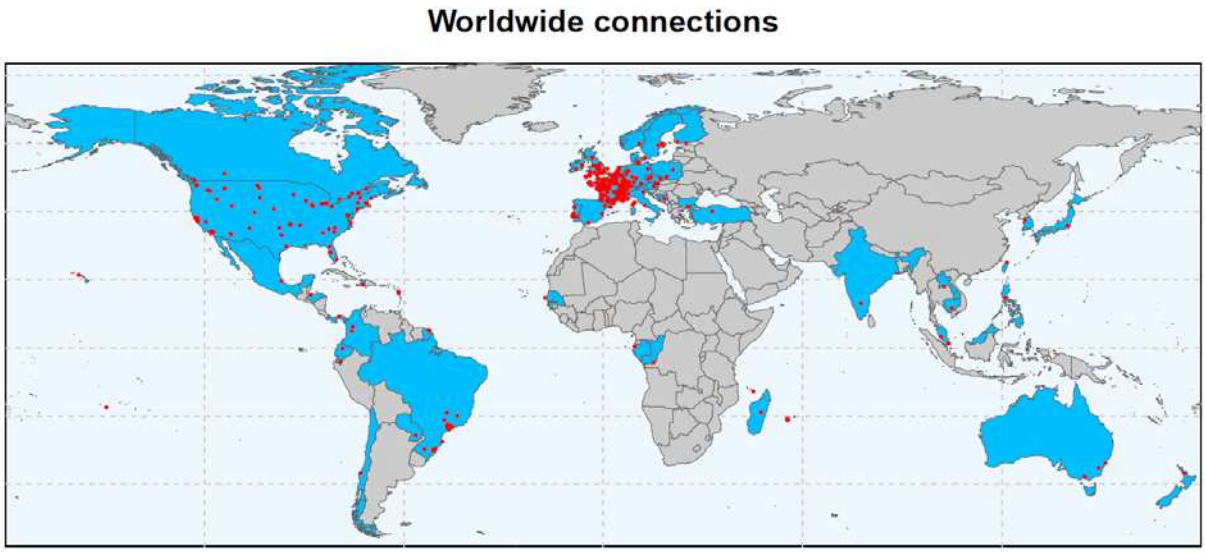

Figure S3: Location of the 1,422 connections recorded across 474 cities in 53 countries worldwide.

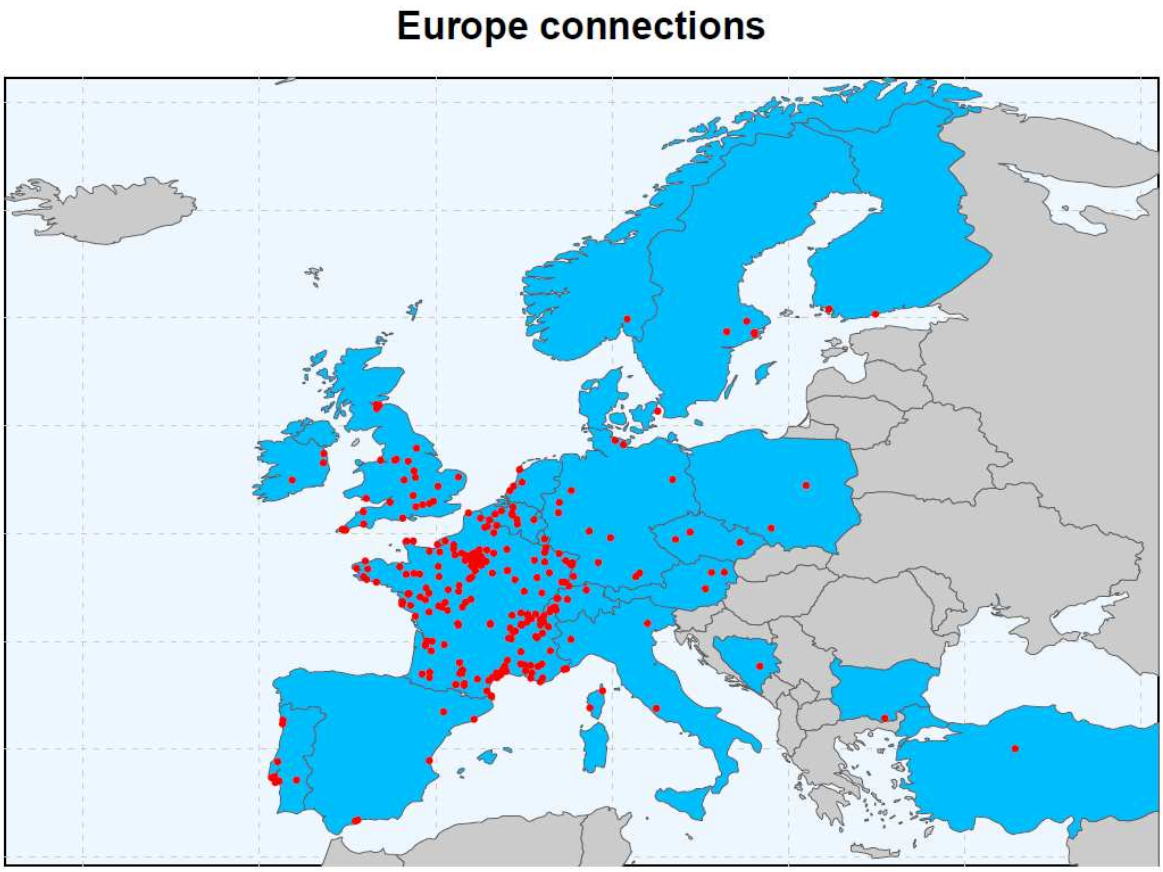

Figure S4: Location of the 1,010 connections recorded across 337 cities in 22 countries within Europe.

Data collection was open for six weeks from November 09th to December 18th 2022. We recorded two massive peaks of connections associated with the diffusion of the project to important French and international mailing lists of the community of evolutionary biologists (**Fig. S5**). Clearly, the effect of online publication did not last in time with a poor repeatability of play.

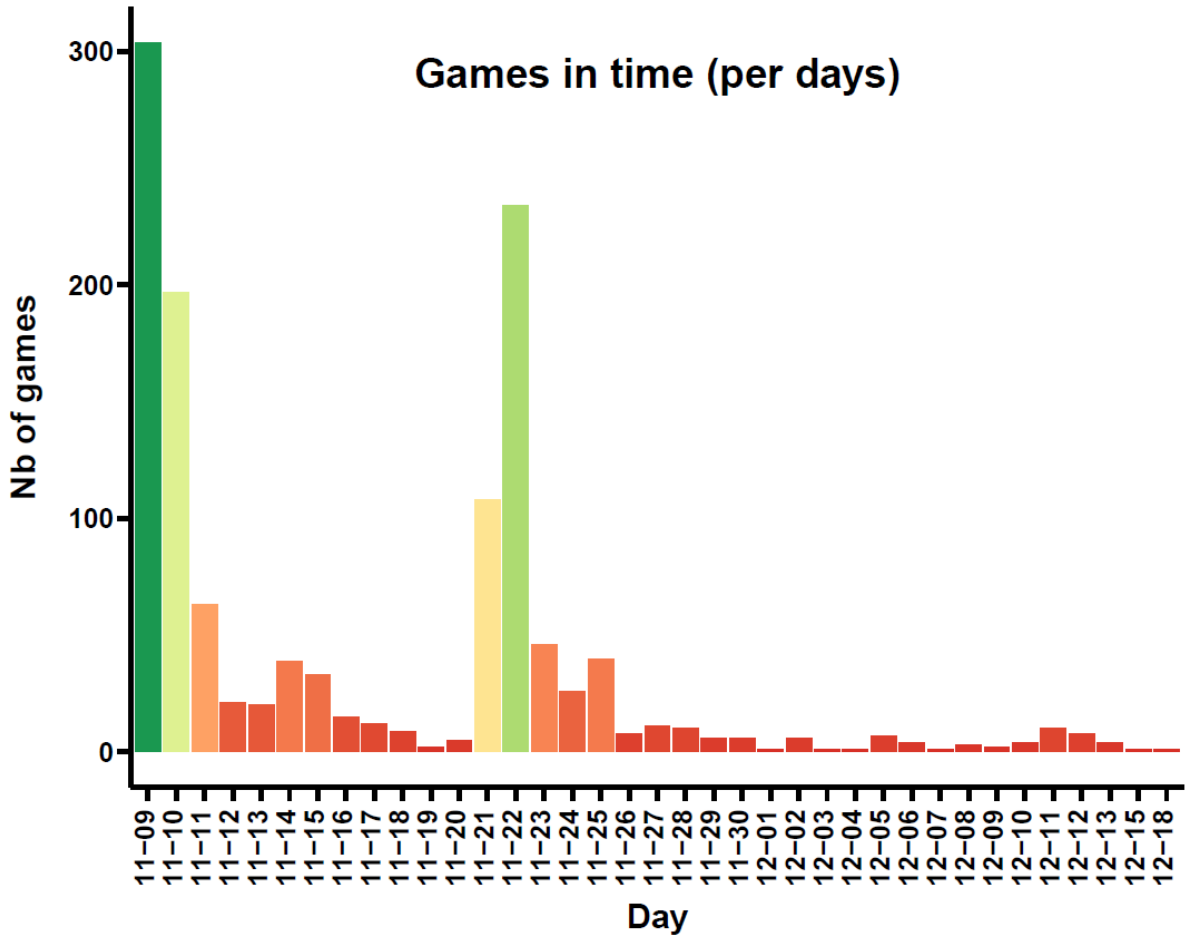

Figure S5: Frequencies of connections to the online survey (http://memometic.cleverapps.io/). Records show two massive peaks associated with the timing of publications advertising the project on important French and international mailing lists for evolutionary biologists.

Playstyle:

The repeatability of play was fairly poor with a fast majority of players playing only once despite incentive to play multiple times displayed in the online survey. The median number of games was 1.1 (**Fig. S6.a**). This low fidelity is likely due to the fact we decided not to provide any direct feedback such as a score at the end of a game session because we did not want to influence the play style of people by guiding them towards more average choices rewarded with an increasing score measuring the degree of closeness to the norm. We recorded time spent per triplet showing most players took around 5 to 10 seconds to examine a triplet (**Fig. S6.b**). Most people rarely use the 'Skip option' with 4.4 skips per game in average (**Fig. S6.c**), with an important proportion of games without any skip (643 games = 46.1%). It seems likely players perceived the Skip option as a negative action, while it actually can help to

eliminate noise in the dataset. A next version of the survey interface should emphasize on the benefits from using skips as it is shown to decrease the degree of abnormal triplets recorded (see **Fig. S9.a**: normality-score increases with number of skips). Finally, only 45 game sessions (3.2%) failed at least one controlled trial (**Fig. S6.d**) and were subsequently removed from the triplet dataset.

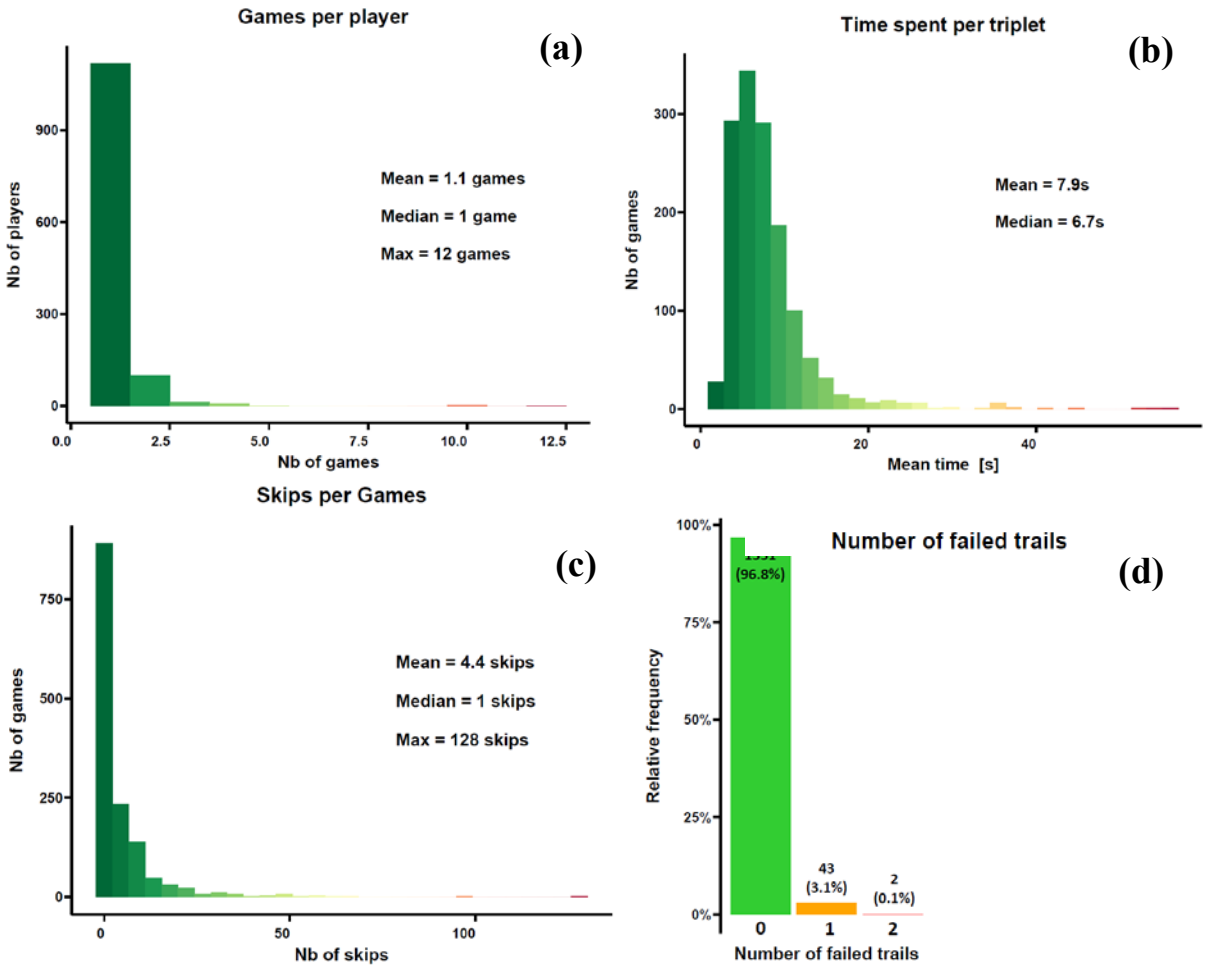

Figure S6: Analytics for game sessions. (a) Number of games per player. **(b)** Mean time spent to examine each triplet in a game session **(c)** Number of uses of the 'skip' option per game session. **(d)** Percentage of game sessions according to the number of failed controlled trials in the game session.

Player diversity: age, background, geography, language

We reached a diverse audience of surrogate 'predators' with declared age ranging from 4 years old to 92 years old. The distribution of age shows the survey reached mostly adults, likely students, researchers, and their family members (**Fig. S7.a**). The four different languages of the interface were used with varying degrees of success. The Spanish and Portuguese interfaces were rarely used (< 4% ; **Fig. S7.b**), also because native speakers who played were

researchers familiar with English who likely used the English interface. Most players had a biological scientific background (785 players = 55.2%; **Fig. S7.c**) due to the use of scientific diffusion channels to advertise the game. However, having almost half of players who do not have a biological scientific background is a nice pointer to the fairly efficient diffusion of the survey outside of the scientific community despite not having being targeted during diffusion.

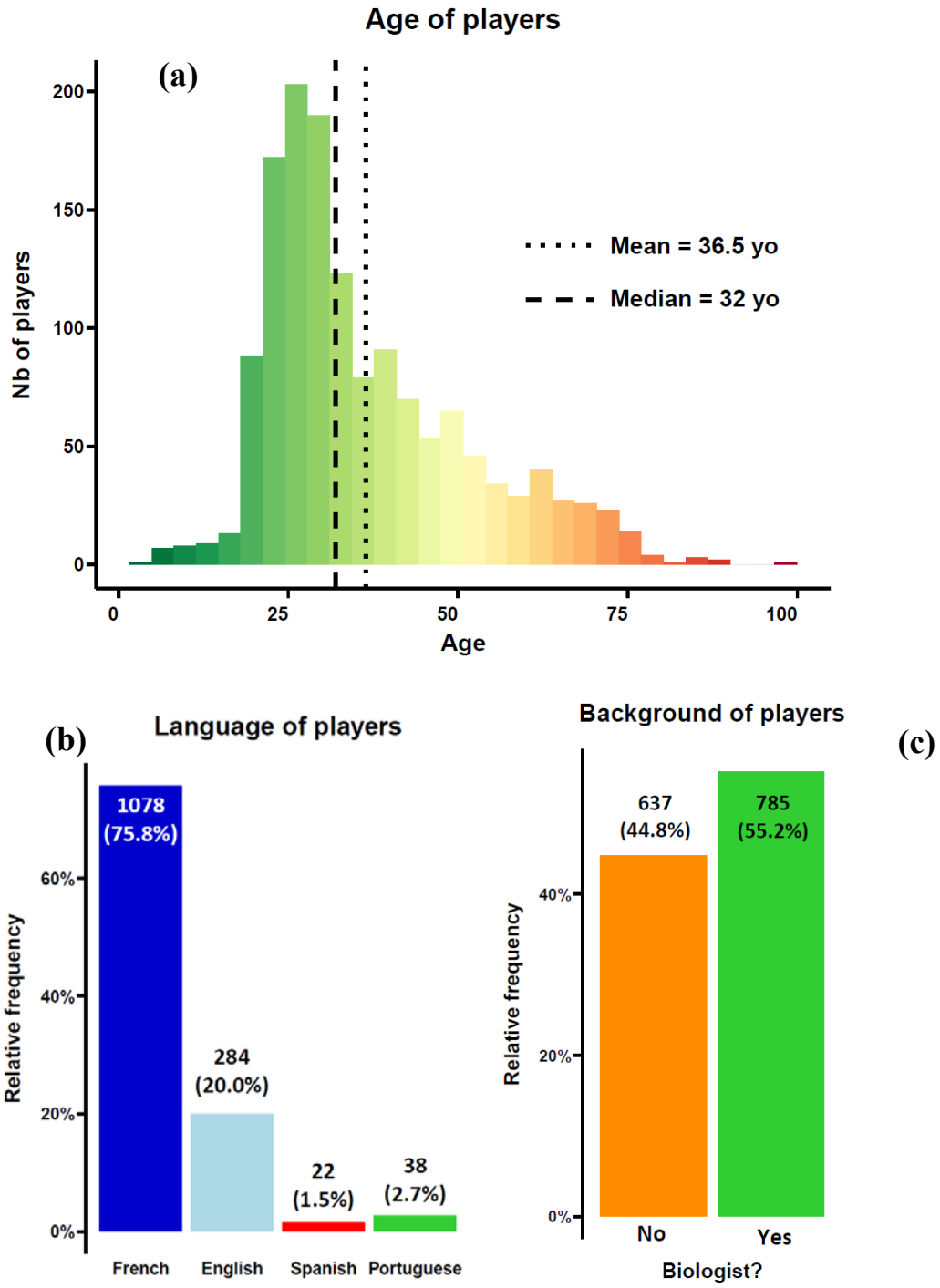

Figure S7: Analytics for player demographics. (a) Distribution of age of players. **(b)** Language interface used in game sessions **(c)** Biological scientific background of players.

Normality scores:

In order to evaluate the dissimilarities across game sessions, we designed two normality scores reflecting the degree of agreement between the set of similarity triplets provided during a game session, and the final perceptual space built on all similarity triplets. The triplet-based score simply quantifies the percentage of triplets whose distance between images A and B, perceived as the most similar pair, is indeed inferior to the distance between images A and C in the final perceptual space (i.e., $d_{A\text{-}B} > d_{A\text{-}C}$). The distance-weighted score adjusts the triplet-based score according to relative distances of the images in each triplet as follows:

$$S_{triplet} = \min\left(\frac{d_{A-C}}{d_{A-B}}, 1\right) \quad \text{(Eqn. 4)}$$

where $d_{A\text{-}B}$ is the distance between the images perceived as the most similar and $d_{A\text{-}C}$ is the distance between the images not labeled as the most similar. As such, satisfied triplets score one and unsatisfied triplets with a high relative difference in pairwise distances score lower to account for the high abnormality of this triplet compared to the global perceptual space. The score for a game session is the sum of score for each triplet and range from 0 to the number of triplets. Final scores were converted in percentages. Importantly, they are not scores of performance but scores of similarity to the norm, thus we coined them as "normality scores".

In average, a game session provided 86.1% of similarity triplets in agreement with the coordinates of images in the final perceptual space built on all similarity triplets (**Fig. 8.a**). Once weighted for relative differences in distances, the mean score increase to 96.3% (**Fig. 8.b**) which hints that most unsatisfied triplets show a small relative distance in the final perceptual space, reflecting small variation in perception.

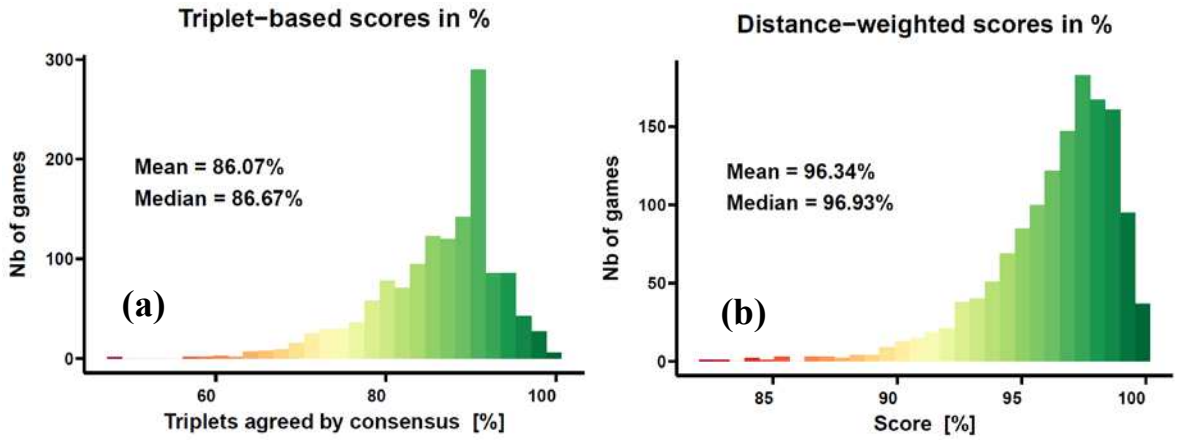

Figure S8: Distribution of normality scores across games. (a) Triplet-based score evaluating the percentage of triplets provided during a game session in accordance with the final perceptual space produced using all similarity triplets. **(b)** Distance-weighted score adjusting the triplet-based score according to pairwise distances of the image in each triplet. Unsatisfied triplets with a high relative difference in pairwise distances score lower to account for the high abnormality of this triplet compared to the global perceptual space.

Effects of skip option and controlled trials:

Using the distance-weighted normality scores, we explored the effect of the skip option and the number of failed controlled trials on the score of a game session. We showed the usefulness of the skip option by highlighting a positive correlation between the number of skips and the normality score (Spearman's $\rho = 0.292$, $p < 0.001$; **Fig. S9.a**) reflecting a higher number of abnormal triplets recorded in games with low to no skip uses. Games with failed controlled trials appeared to score significantly lower than games without fails (Kruskal-Wallis, $\chi = 59.9$, $p < 0.001$; **Fig. S9.b**) illustrating the ability of controlled trials to detect abnormal game sessions. Altogether, both features seem to fulfill their purpose of filtering triplets and game sessions which are strong suspicious outliers relative to the global perception of players.

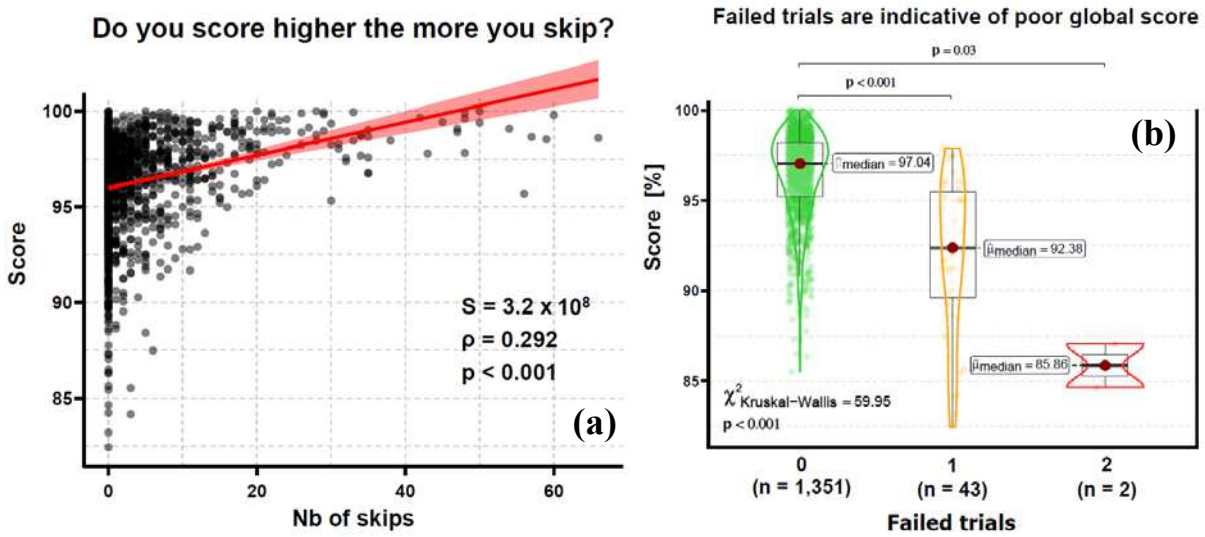

Figure S9: Tests for the effects of the skip option and the number of failed controlled trials on normality scores. (a) Positive correlation between normality scores and number of skips in a game session. **(b)** Negative relationship between normality scores and number of failed controlled trials in a game session.

Effects of Age and Colorblindness:

We explored the effect of age and colorblindness on game performance. Age did not have any significant effect on normality scores (Spearman's $\rho = 0.009$, $p = 0.741$; **Fig. S10.a**),

neither on the mean time taken to answer a triplet (Spearman's ρ = -0.021, p = 0.431; **Fig. S10.b**). However, older players tended to use more the skip option than younger players (Spearman's ρ = 0.077, p = 0.033; **Fig. S10.c**). This mild trend could reflect the idea that older players trust less their perceptual abilities, or are more careful in their choices. A few colorblind people participated in the survey (N = 17). This low number of games did not allow to find a statistically significant difference in normality scores, however we visualized a slight tendency for the few colorblind players to score lower reflecting their particular visual perception (Mann-Whitney, W = 9395, p = 0.16; **Fig. S10.d**).

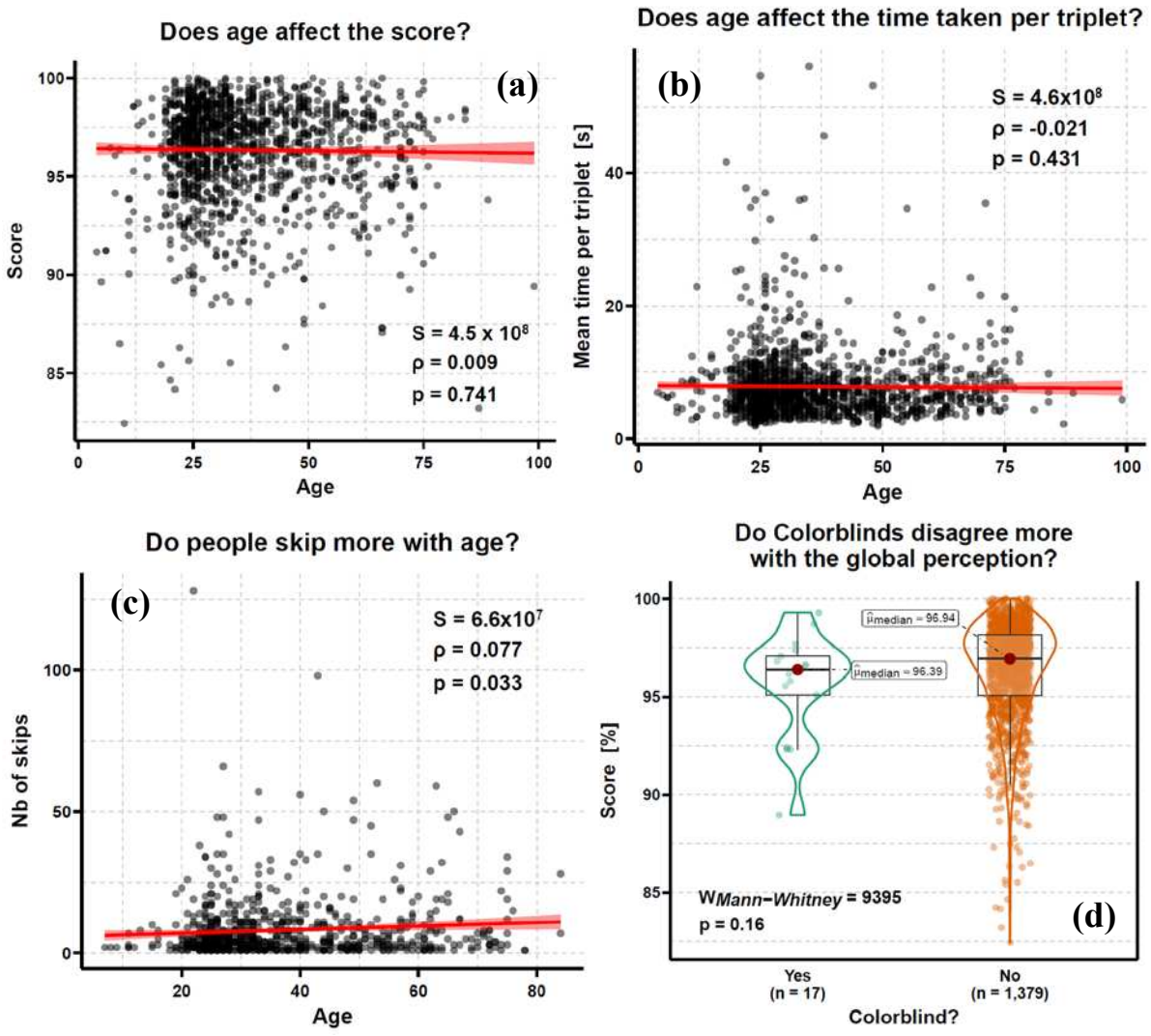

Figure S10: Tests for the effects of age and colorblindness on game performances. (a) No effect of age on normality scores. **(b)** No effect of age on the mean time taken to answer a triplet. **(c)** Positive correlation between age and number of skips. **(d)** No significant effect of colorblindness on normality score, yet we detect a slight tendency for the few colorblind players to score lower reflecting their particular visual perception.

Effects of cultural and scientific background:

We explored the effect of cultural and scientific background on game performance. Biologists appeared to play quicker (Mann-Whitney: W = 21,812, p < 0.001; **Fig. S11.a**) and score significantly higher than non-biologists (Mann-Whitney: W = 29,743, p < 0.001; **Fig. S11.c**), but they did not show any difference in their frequency of use of the skip option (Mann-Whitney: W = 66,464, p = 0.48; **Fig. S11.c**). Since scores are normality scores and not performance scores, these results mostly tell us that experience affects the perception of similarity in wing patterns and that non-biologists tend to perceive similarity patterns that are outside the norm more frequently than trained biologists are. In parallel, Brazilian-Portuguese speakers were scoring significantly higher than other languages (Kruskal-Wallis: $\chi = 14.7$, p < 0.001; **Fig. S11.d**). This trend is likely due again to the effect of experience: almost all respondents for this language were scientists working with neotropical butterflies, native to their country (i.e., Brazil). Altogether, these results hint for a strong effect of experience in task requiring abilities to detect differences in neotropical butterflies. However, this conclusion need to be tempered by the significantly lower scores obtained by Spanish speaking speakers, mostly from Latin America, for which the same positive effect of experience could have been expected (**Fig. S11.d**).

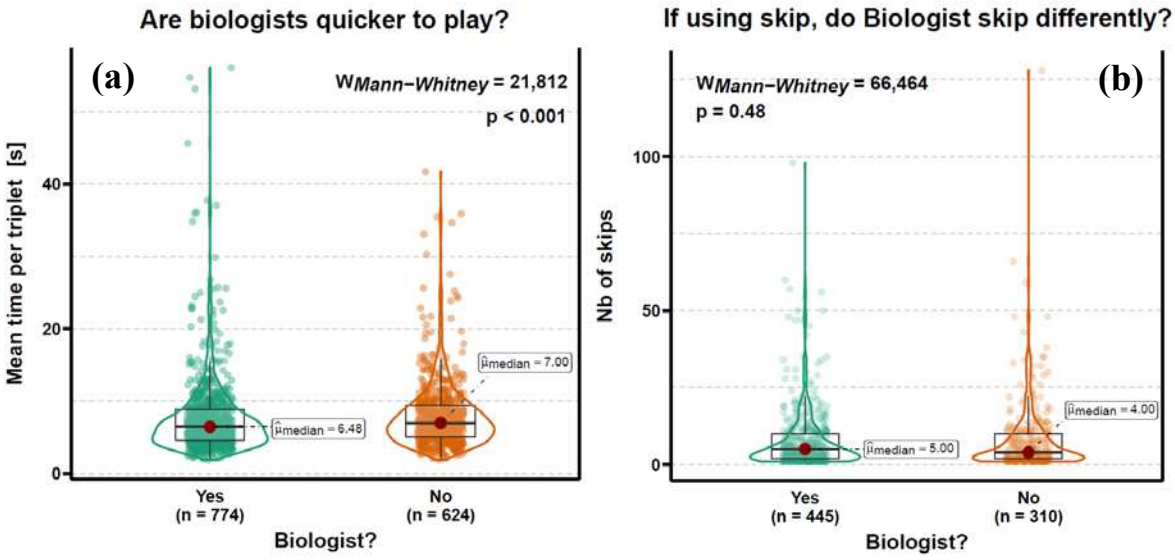

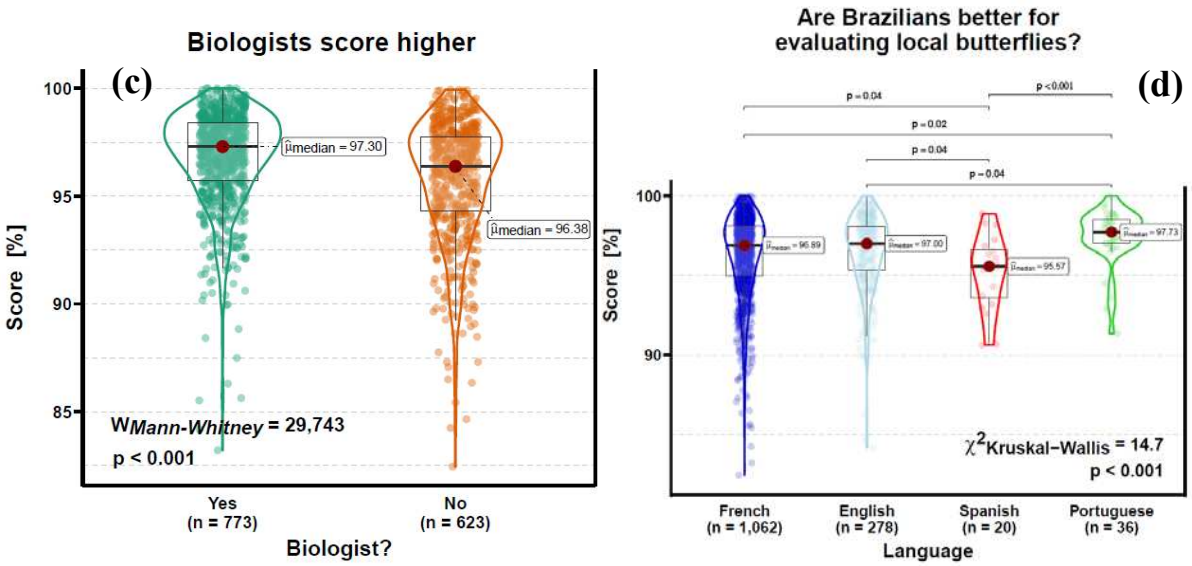

Figure S11: Tests for the effects of cultural and scientific background on game performances. (a) The scientific background affects the response time: biologists are significantly faster to answer. **(b)** No effect of scientific background on the use of the skip option. **(c)** Positive relationship between scientific background and normality scores: biologists score higher. **(d)** Significant effect of the language on normality scores with Brazilian-Portuguese speakers scoring significantly higher than other languages, hinting for an effect of experience in task requiring abilities to detect differences in native neotropical butterflies.

Effect of learning:

We explored the effect of learning through multiple game sessions on game performance. Globally, first game sessions were slower than the next game sessions (Mann-Whitney: $W = 17{,}205$, $p < 0.001$; **Fig. S12.a**). This effect persisted when comparing for a given player the time taken during the first game session and the average time for the next game sessions (Wilcoxon $V = 3{,}42848$, $p < 0.001$; **Fig. S12.b**). As such, players seems to learn to be more efficient (and maybe more confident) at selecting the pair they perceived as the most similar highlighting the importance of memorization and experience in perception. Globally, first game sessions provide lower normality scores than the next game sessions (Mann-Whitney: $W = 11{,}928$, $p = 0.003$; **Fig. S12.c**). However, at player-level, we detected no significant increase of the normality score between the first game session and the average of all next sessions (Wilcoxon $V = 2{,}865$, $p = 0.24$; **Fig. S12.d**). Thus, players who play the most were the ones the least susceptible to show a perception out of the ordinary, but they did not seem to provide similarity triplet closer to the global average as much as they played. Altogether, we did not show a clear effect of training experience on the evolution of perception towards the norm during game sessions, but trained players definitely played faster.

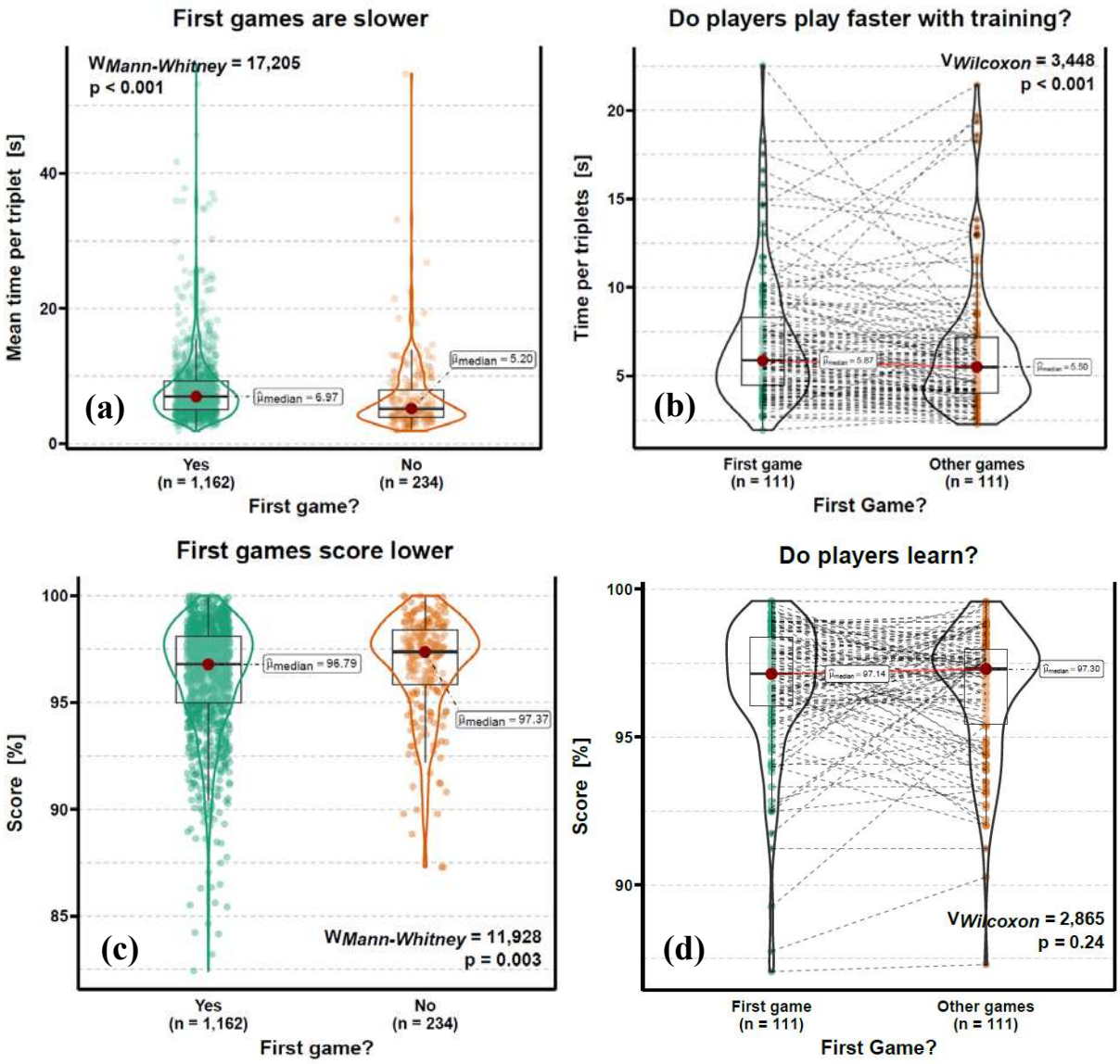

Figure S12: Tests for the effects of learning through multiple game sessions on game performance. (a) Globally, first game sessions are slower than the next game sessions **(b)** At the player level, first game sessions are slower than the next game sessions. **(c)** Globally, first game sessions provide lower normality scores than the next game sessions. **(d)** At player-level, there is no significant increase of the normality score between the first game session and the average of all next sessions.

Appendix 5: Visual lists of subspecies in local communities

We produced analyses of perceived wing pattern variation in five local communities. We present here the subspecies found in each of this community: Cayenne, French Guyana (**Fig. S13**), Gamboa, Panama (**Fig. S14**), Jatun Sacha, Napo, Ecuador (**Fig. S15**), Manaus, Amazonas, Brazil (**Fig. S16**), and Santa Teresa, Espírito Santo, Brazil (**Fig. S17**).

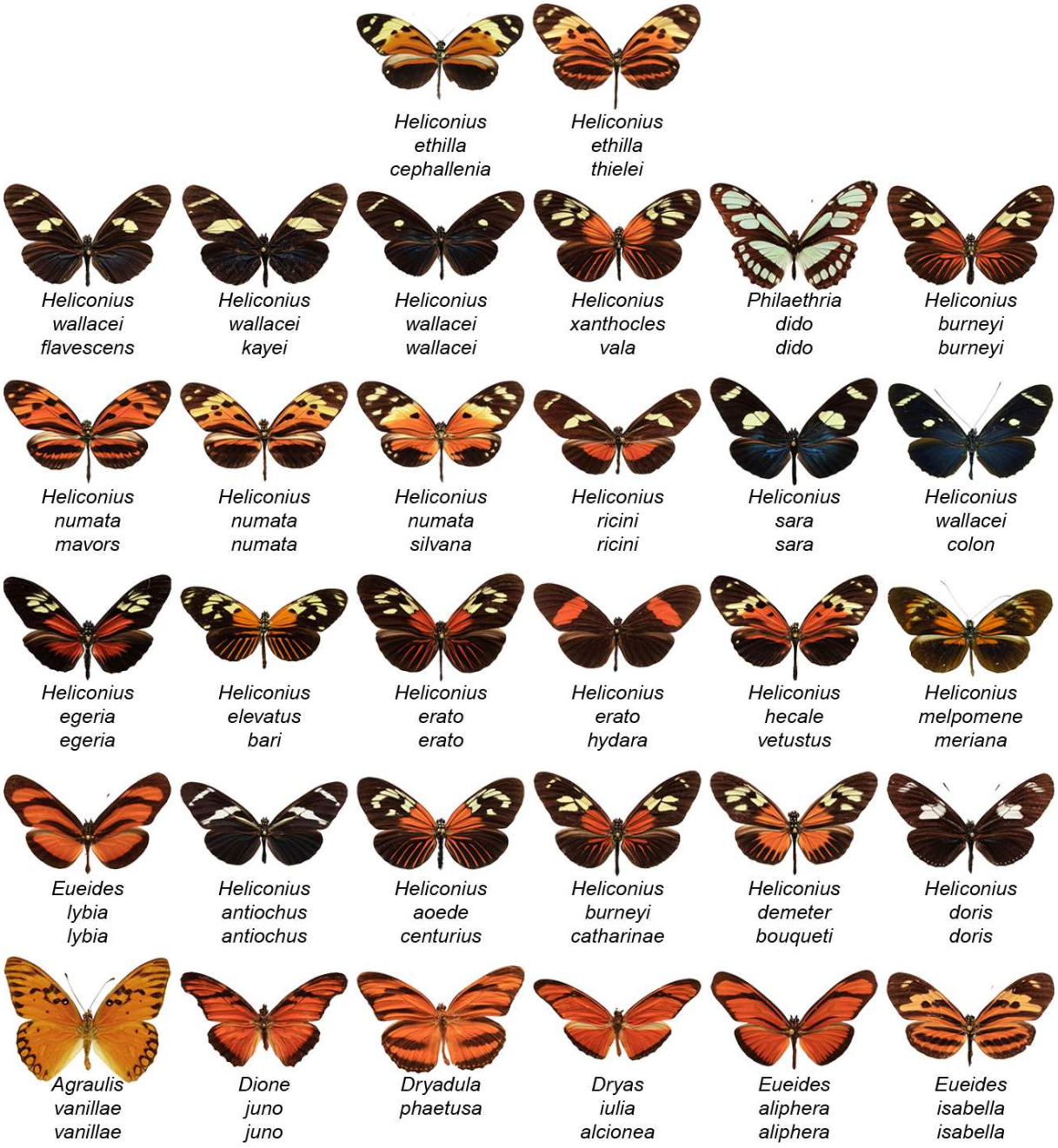

Figure S13: Visual taxonomic list of the 32 subspecies of heliconiine butterflies found in Cayenne, French Guyana.

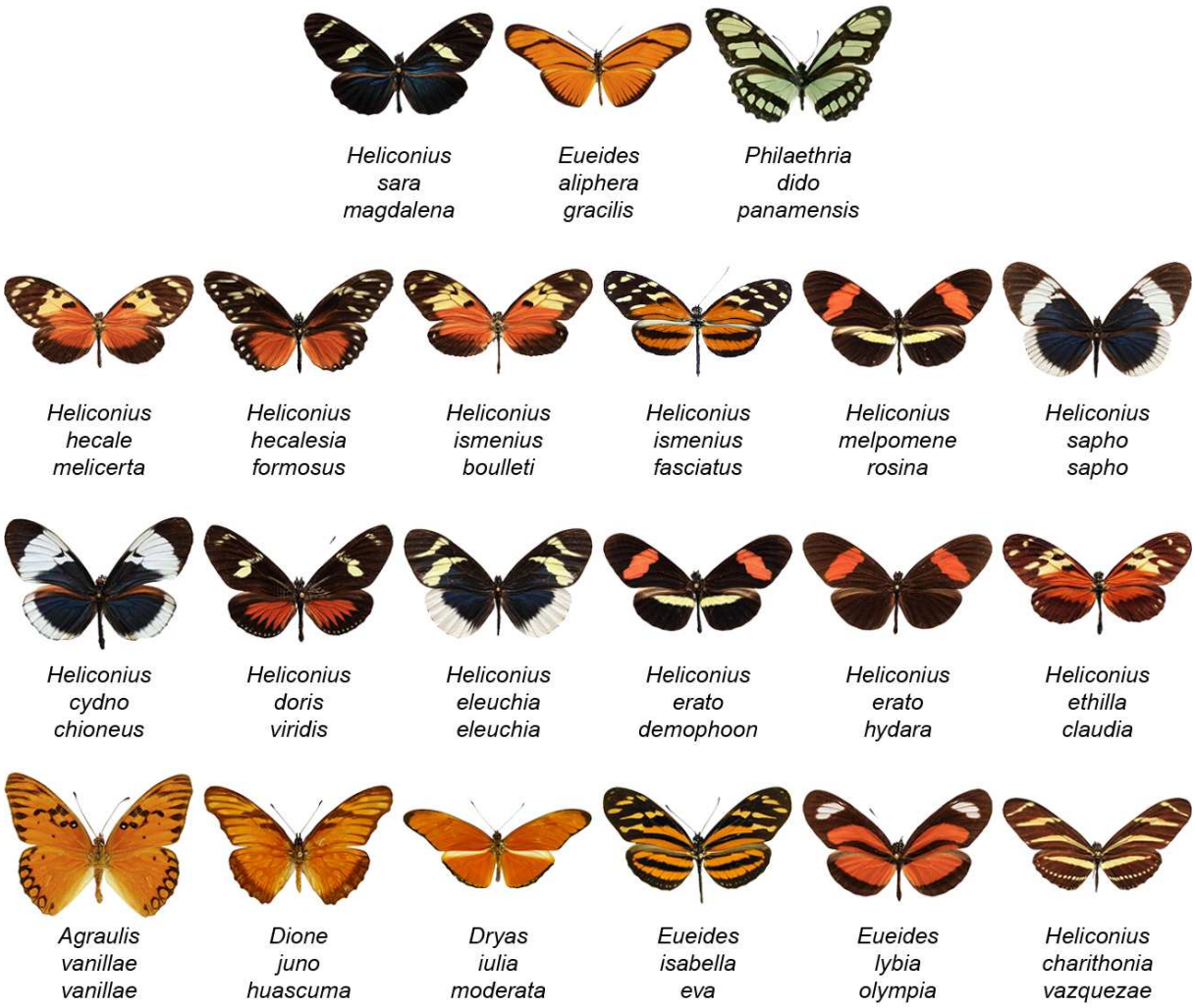

Figure S14: Visual taxonomic list of the 21 subspecies of heliconiine butterflies found in Gamboa, Panama.

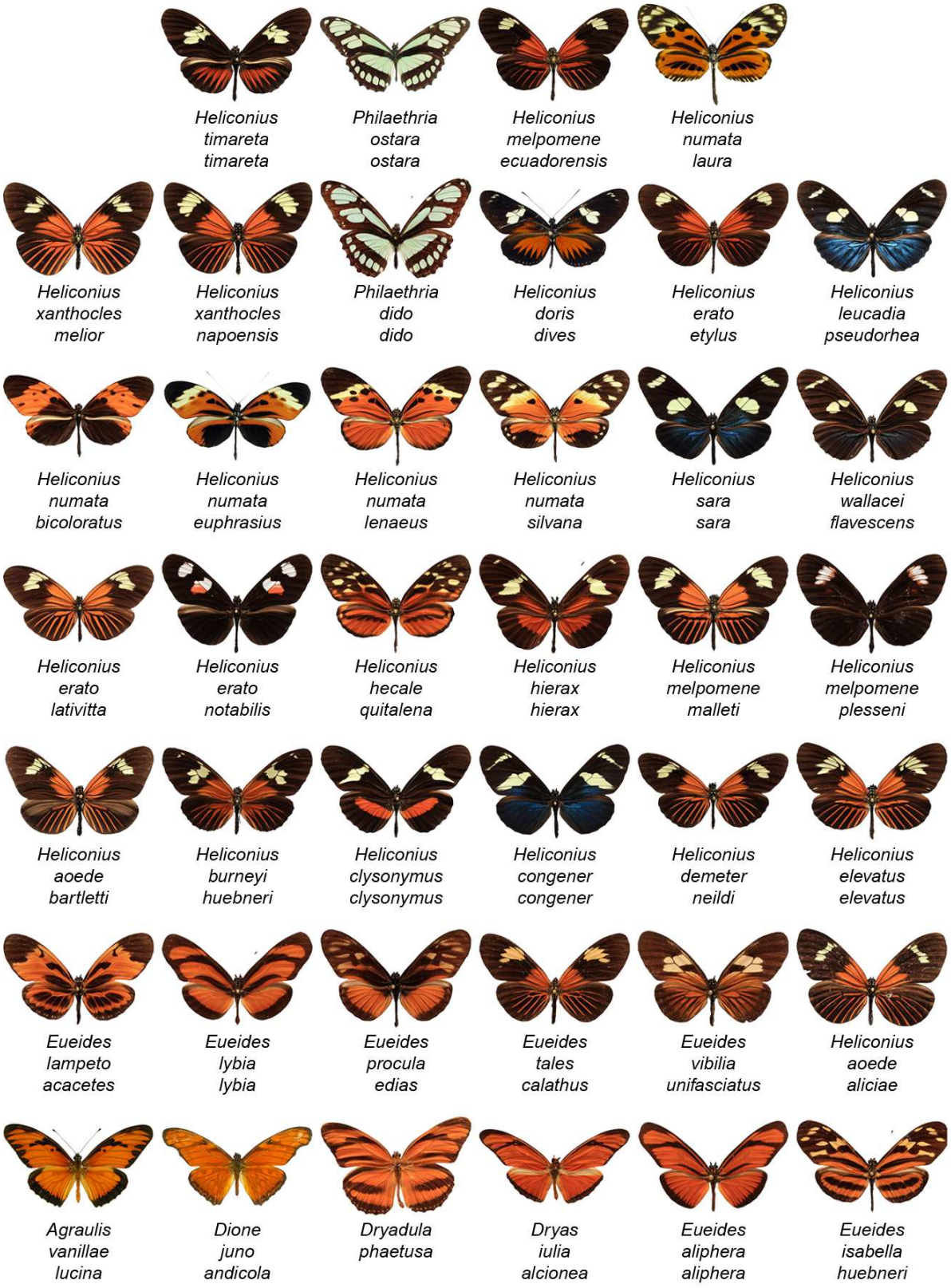

Figure S15: Visual taxonomic list of the 40 subspecies of heliconiine butterflies found in Jatun Sacha, Napo, Ecuador.

Figure S16: Visual taxonomic list of the 44 subspecies of heliconiine butterflies found in Manaus, Amazonas, Brazil.

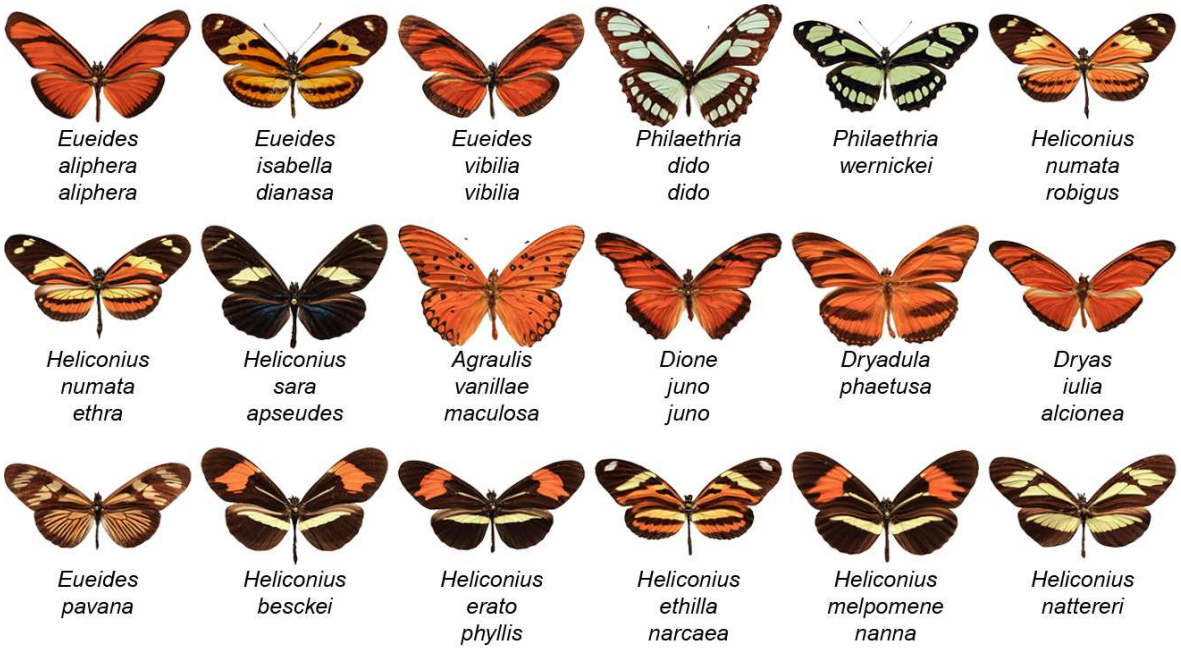

Figure S17: Visual taxonomic list of the 18 subspecies of heliconiine butterflies found in Santa Teresa, Espírito Santo, Brazil.

Appendix 6: How many triplets to obtain a stable perceptual space?

In order to assess whether our sampling effort was sufficient to obtain a proper representation of the average global perception of wing pattern similarity, we designed a criterion to study the stability of the perceptual space across sampling effort as the number of similarity triplets incorporated in the dataset increased. We computed the degree of similarity between the topologies of perceptual space obtained for different levels of sampling effort using the Procrustes's correlation index (See **Eqn. 3** in main text). Then, we plotted the evolution of the Procrustes's correlation along sampling effort in order to detect a plateau of stability which would reflect the stability of the final perceptual space obtained. The stability threshold represented the minimal sampling effort needed to obtain a proper representation of global perception since adding more triplets would not change much the final output. We considered stability reached once adding any number of triplets will not decrease Procrustes's correlation below 0.95.

In the Citizen Science dataset, the stability threshold was reached for 22 572 triplets (30% of the total available number of triplets), demonstrating our sampling effort was sufficient to guarantee a suitable representation of global perception and support reproducibility of the results (**Fig. S18**).

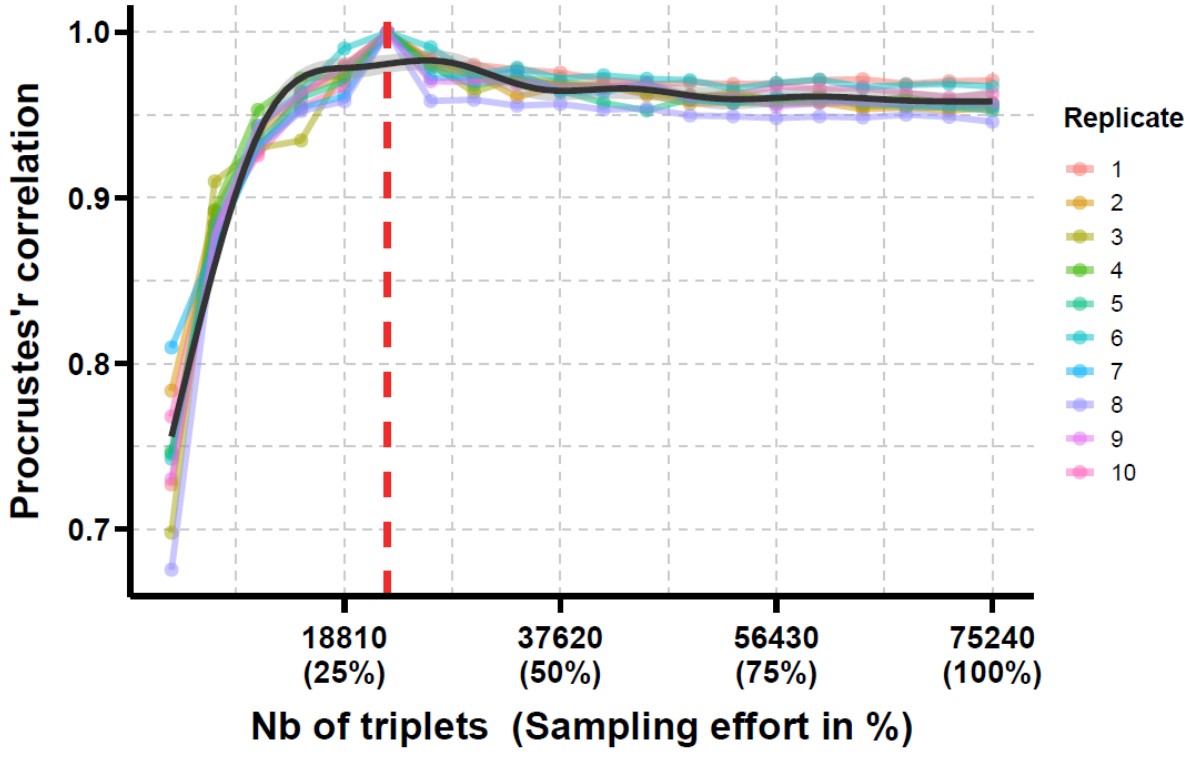

Figure S18: Evaluation plot to define stability threshold across sampling effort for the Citizen Science dataset. N images = 432, N triplets = 75,240. Evaluation was made on 10 independent series of random nested subsets of triplets. Stability, symbolized by the vertical red dashed line, was reached for 22 572 triplets (30%) since in average Procrustes's correlation never decrease below 0.95 beyond this point, independently of the number of similarity triplets added to the triplet dataset.

We used the same protocol to evaluate stability and define the minimum number of triplets needed to produce the individual perceptual maps of local community based on sets of similarity triplets provided by a single expert. First, we ran a test set with 1000 triplets and plotted the evolution of Procrustes's correlation along sampling effort for series of random nested subsets. We observed the large fulfillment of the stability criterion after 600 triplets (**Fig. S19**). Thus, we used 600 triplets as our sampling effort for individual local perceptual maps.

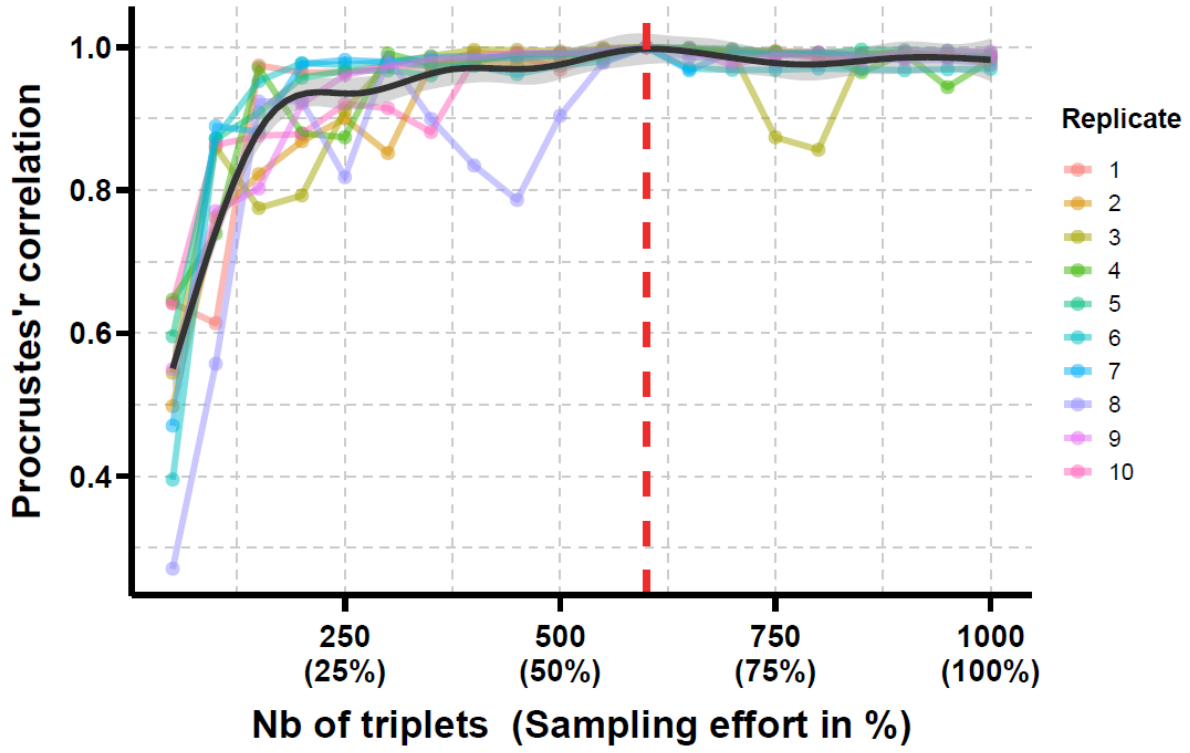

Figure S19: Evaluation plot to define stability threshold across sampling effort for local individual maps. Local community = Jatun Sacha, N images = 40, N triplets = 1,000. Evaluation was made on 10 independent series of random nested subsets of triplets. Stability, symbolized by the vertical red dashed line, was largely reached for 600 triplets (60%) since in average Procrustes's correlation never decrease below 0.98 beyond this point, independently of the number of similarity triplets added to the triplet dataset.

Appendix 7: Test the limits of the method via simulations

We designed simulation tests to explore the limits of the t-STE in the context of the perceptual approach. Specifically, we aimed to:

(1) Define the minimal number of triplets needed to reach stability according to the size of the dataset (i.e., the number of images to evaluate)

(2) Quantify the levels of inconsistency (i.e., percentage of unsatisfied triplets) inherent to the method *vs.* accounting for true inconsistency in the dataset of triplet similarity reflecting diversity of perceptions that are sometimes contradictory

(3) Study the learning effort (i.e., number of iterations) needed to reach stability during the running of the t-STE algorithm.

We designed three types of simulations. The first types are labeled as 'Informative'. These datasets are subsets of images drawn randomly from our collection of 432 images. For each random subset of images, we extracted the available similarity triplets that encompass the selected images from our Citizen Science collection of 75,240 informative triplets. Then, we created random nested subsets of triplets for different levels of sampling effort (i.e., for different number/percentage of triplets). We used ten replicates per image set size, and five replicates per sampling effort for a given image set. This approach was limited by the availability of similarity triplets for small subsets of images. Indeed, below 200 images, we were not able to retrieve enough similarity triplets encompassing only the focal subset of images to create meaningful subsets and study effects of sampling effort.

Therefore, we designed in parallel a second types of simulations labeled as 'Perfect triplets' with the aim of representing situations where there is no inconsistency in the set of similarity triplets (i.e., it exists a perceptual space topology that satisfies all triplets at once). In these datasets, the similarity triplets were not drawn from our Citizen Science collection of 75,240 informative triplets, but they were created directly from our Citizen Science-based perceptual space. We used the coordinates of images in this perceptual space to draw random set of triplets that were all satisfied by this topology. Similarly to 'Informative' datasets, we made replicates for ten image set size across five replicates per sampling effort. Since we were not limited by the number of triplets, we used subsampled datasets with the maximum size (i.e., all possible triplets) or a maximum of 75,240 triplets as in our Citizen Science dataset. Those datasets are labeled as 'full'. Complementarily, we designed subsampled triplet datasets with

size adjusted to the one of 'Informative datasets so we could compare directly their results while accounting for variation in triplet dataset size. Those later datasets are labeled as 'adjusted'.

Finally, we complemented this analysis with a 'Null model' using sets of random triplets with no information (i.e., in those triplets, images and their order were selected randomly), producing random nested subsampled dataset with 'full' size and 'adjusted' size.

We showed the number of images to evaluate and the level of inconsistency across similarity triplets affect the number of triplets needed to obtain a stable perceptual space. Indeed, datasets of perfect triplets reach stability faster than the informative datasets inherently including some degree of true inconsistency. For instance, for 200 images, stability was reached in 2,800 perfect triplets *vs.* 7,500 informative triplets. For 400 images, around 20,000 informative triplets were need while only 7,000 perfect triplets could achieve stability (**Fig. S20 & S21**). The relation appeared almost linear for perfect triplets with around 15 triplets per image needed. For informative triplets, the relation was also relatively linear for the range we could explored with our data (from 200 to 432 images), with around 60 triplets per additional image needed. It is worth noted we also recorded stability to be reached for 600 triplets on the 40 images of local communities (see **Fig. S19** in **SI Appendix 6**), hinting than the relationship get close to the one observed for perfect triplets (i.e., 15 triplets per image) when the number of images is low, since less true inconsistency is expected in the set of similarity triplets. Null models showed no stability as the sampling effort increase, as expected from dataset which contains no congruent information across triplets (**Fig. S20 & S21**).

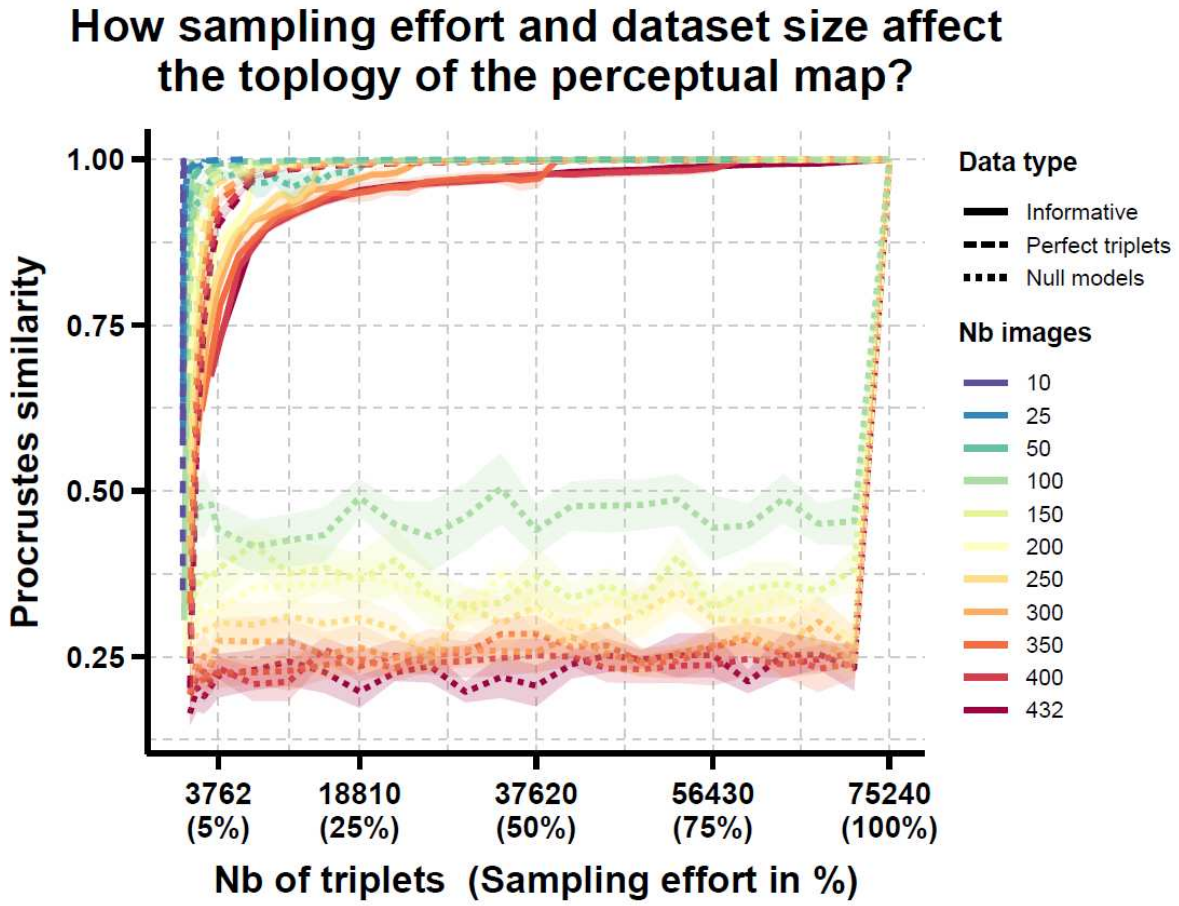

Figure S20: Evaluation plot to define stability threshold across sampling effort and image set size for simulated data. Plain lines refers to subsets of informative triplets drawn from the Citizen Science data collection. Dashed lines refers to subsets of perfect triplets with no inconsistency. Dotted lines refers to null model of random triplets with no coherent information. Each curve shows the evolution of the Procrustes's correlation of the current perceptual space relative to the final space built with all triplets, with increasing sampling effort (i.e., number of triplets), for a given type of simulation and number of images, aggregated over all ten replicates. Color represents the range of image set size from 10 to 432 images.

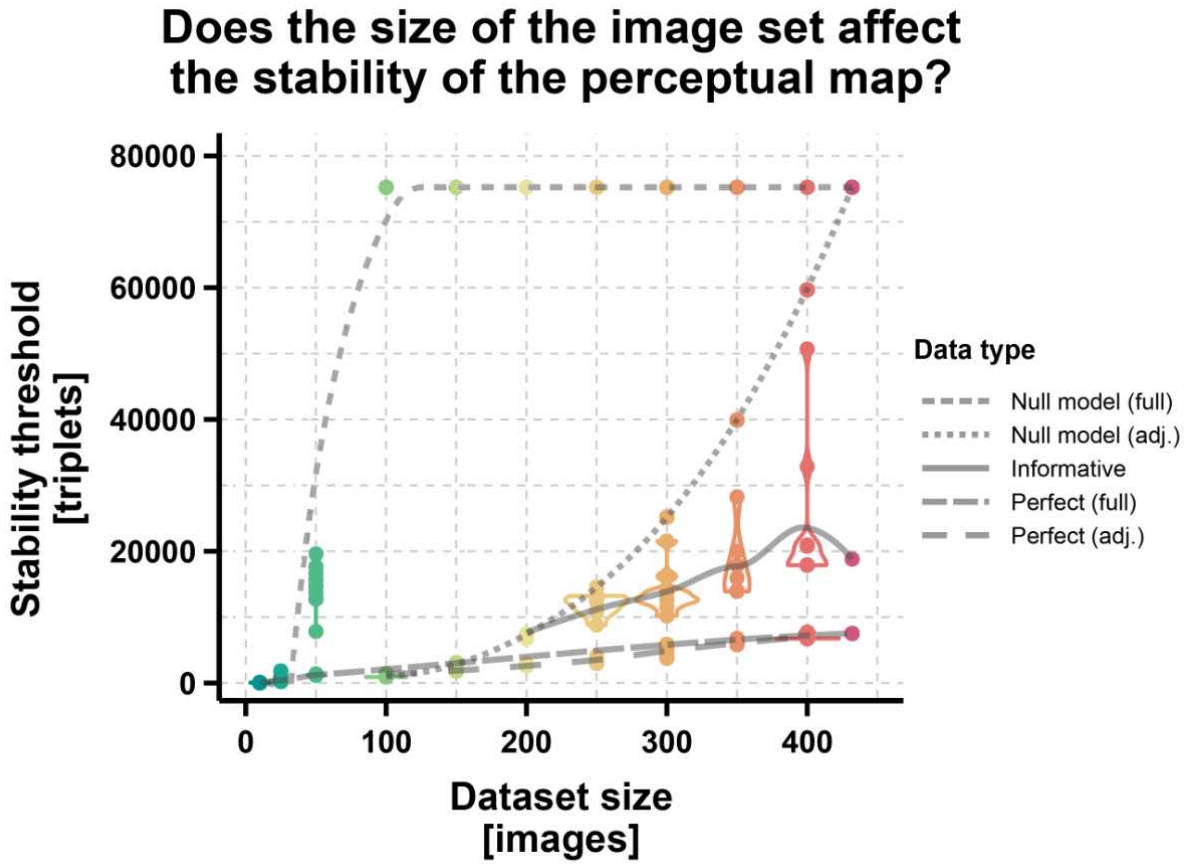

Figure S21: Evaluation of stability threshold across image set size for simulated data in datasets with 100% of triplets. Plain lines refers to subsets of informative triplets drawn from the Citizen Science data collection. Long-dashed lines refers to subsets of perfect triplets with no inconsistency using full triplet datasets and adjusted triplet datasets which size is similar to those for informative triplets. Short-dashed and dotted lines refers to null model of random triplets with no coherent information, using again full and adjusted datasets. Null-model datasets never reach stability, and the points show on the graph refer only to the size of their triplet sets. Color represents the range of image set size from 10 to 432 images.

Parallelly, we explored the influence of sampling effort and image set size on the degree of inconsistency in the final perceptual space quantified as the percentage of unsatisfied triplets. We showed the number of images evaluated had relatively light impacts on the final degree of inconsistency in the perceptual space once a stable topology is reached, contrary to the degree of conflictual information across similarity triplets. Indeed, informative datasets, with triplets drawn from the Citizen Science data collection, tend to reach a maximum percentage of 15% of unsatisfied triplets beyond 250 images (**Fig. S22 & S23**). On the other hand, datasets of perfect triplets led to 5% of unsatisfied triplets in the final perceptual space for any number of images, despite being 100% consistent by design (**Fig. S22 & S23**). Null models with no coherent information showed relatively low inconsistency for any number of images (below

2.5%; **Fig. S22 & S23**), reflecting the fact we had enough dimensions to accommodate triplets that describe random similarity patterns. As such, it seems the t-STE have an inherent 5% error rate when it comes to accommodate informative triplets, even if they present no internal inconsistency such as our 'perfect' triplets. We conclude there is around 10% of natural inconsistency in our informative dataset which reflect true differences across individual perception, while the remaining 5% are due to the resolution limit of the algorithm in our specific context.

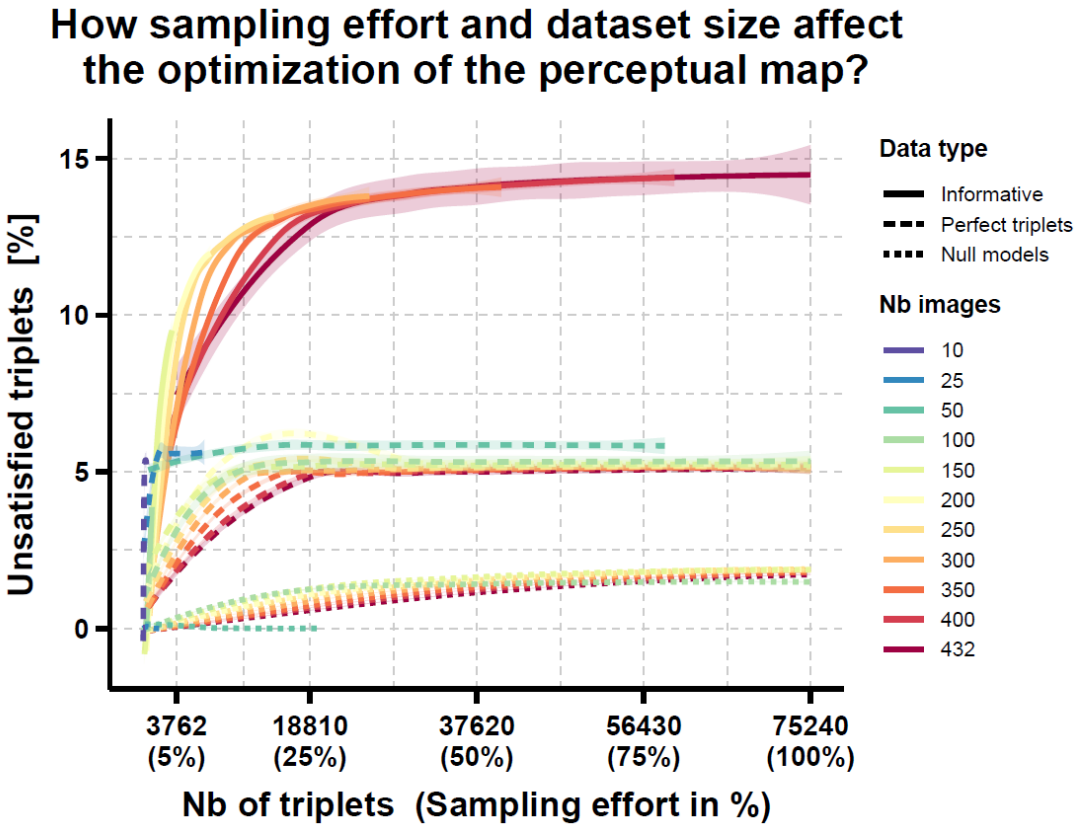

Figure S22: Evolution of the percentage of unsatisfied triplets in the final perceptual spaces across sampling effort and image set size for simulated data. Plain lines refers to subsets of informative triplets drawn from the Citizen Science data collection. Dashed lines refers to subsets of perfect triplets with no inconsistency. Dotted lines refers to null model of random triplets with no coherent information. Each curve shows the evolution of the percentage of unsatisfied triplets of the current perceptual space with increasing sampling effort (i.e., number of triplets) for a given type of simulation and number of images, aggregated over all ten replicates. Color represents the range of image set size from 10 to 432 images.

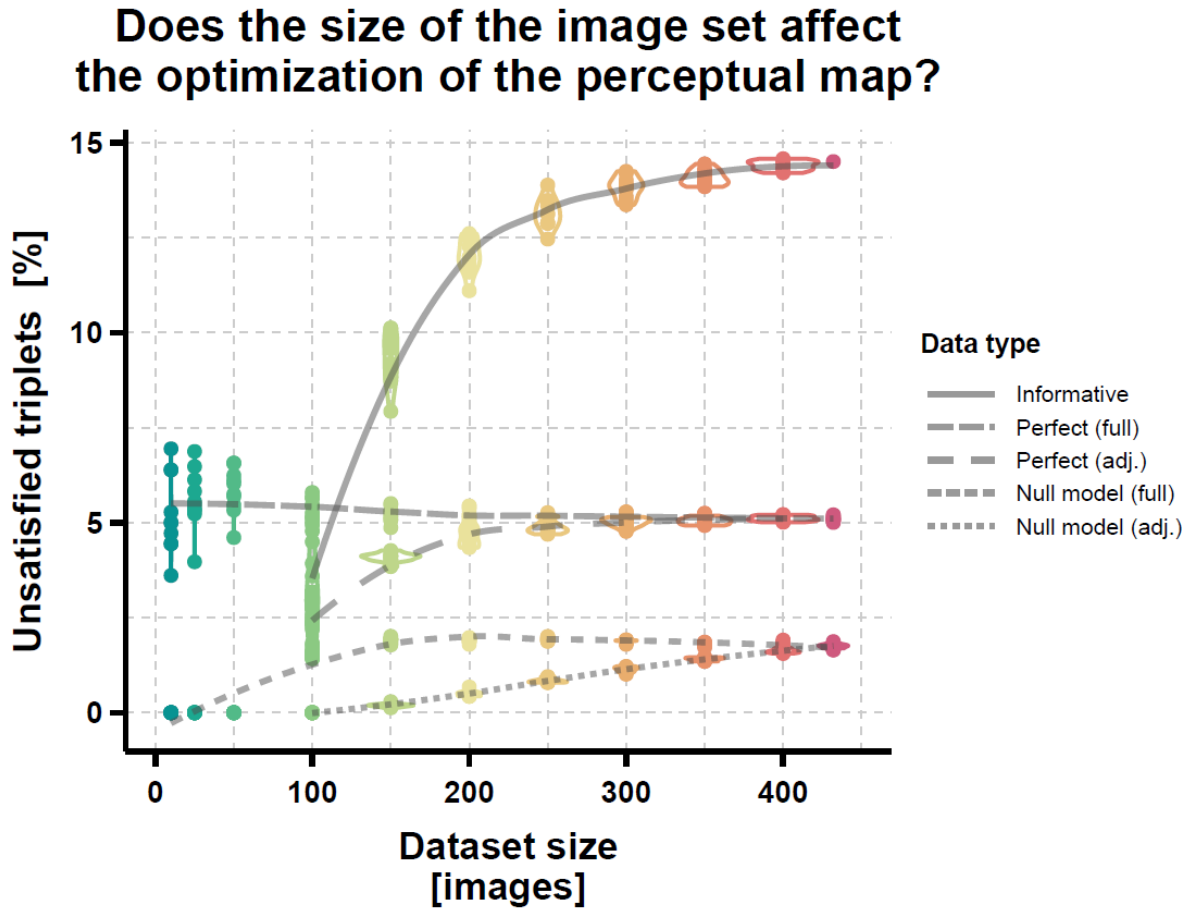

Figure S23: Evaluation of the percentage of unsatisfied triplets in the final perceptual spaces across image set size for simulated data in datasets with 100% of triplets. Plain lines refers to subsets of informative triplets drawn from the Citizen Science data collection. Long-dashed lines refers to subsets of perfect triplets with no inconsistency using full triplet datasets and adjusted triplet datasets which size is similar to those for informative triplets. Short-dashed and dotted lines refers to null model of random triplets with no coherent information, using again full and adjusted datasets. Color represents the range of image set size from 10 to 432 images.

Finally, we explored the effect of learning effort (i.e., number of iterations) on the stability of the perceptual space topology. At each iteration of the t-STE, the algorithm tries to optimize the coordinates of images so a maximum of triplet are satisfied, following a stochastic cost function providing more weights to improvement of short distances than long distances (i.e., optimizing clustering and local topologies). Therefore, the algorithm learns iteratively the best embedding to optimize the distances of images in the reduced space satisfying the initial set of similarity triplets.

We compared the evolution of the Procrustes's correlation between the current topology and the final one obtained after 30,000 iterations for the complete Citizen Science dataset with

75,240 triplets. We showed that stability is reached fairly quickly with almost no perceptible differences after 200 iterations (**Fig. S24**). In practice, the algorithm was observed to proceed in distinct steps. First, it initialized with random agglomerated coordinates for all images. Second, it pushed far away the images that are considered different by most triplets since it is the easiest way to decrease the cost function quickly at first, when all images are agglomerated. Third, it aggregated core groups and tuned distances of highly dissimilar images. Forth, it adjusted individual images that were not yet well optimized, maybe due to conflicting triplets. Fifth, it reached a state of sub-stability by dangling around but keeping global structure highly similar (i.e., coordinates can rotate but the topology remains the same).

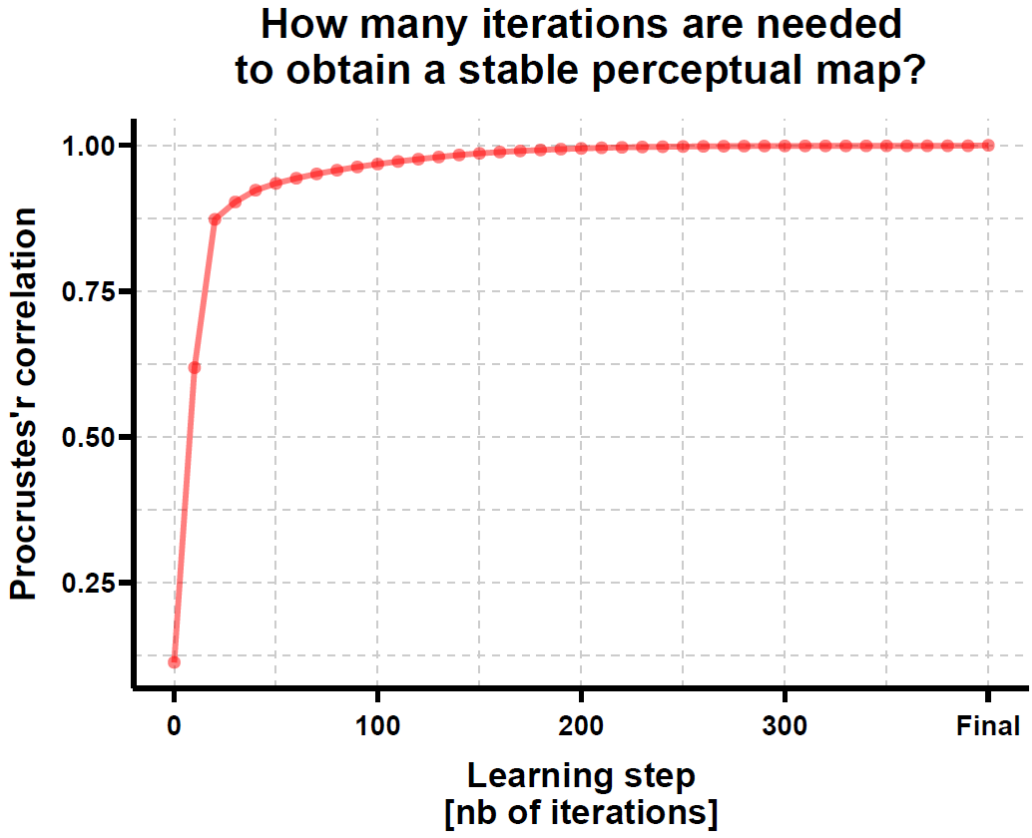

Figure S24: Evolution of the global topology of the perceptual space during learning process of the t-STE for the Citizen Science dataset of 75,240 similarity triplets for 432 images. Procrustes's correlations are computed between the current topology and the final one reached after 30,000 iterations. Stability is reached fairly quickly after 200 iterations.

Appendix 8: Categorical tests for effect of sympatry on perceptual distances

Müller's theory of mimicry (Müller 1879) predicted the convergence of local toxic prey towards a similar aposematic pattern. To evaluate if this prediction could influence large-scale patterns of phenotypic distributions, we tested if the perceptual distances between subspecies were correlated with the geographic distances between their spatial distributions. Complementary to analyses based on Schoener's D as a continuous measurement of geographic distances, we designed analyses based on sympatric and allopatric categories for geographic status of pair of subspecies. We defined as sympatric all pairs of subspecies with a Schoener's D higher than 0.2 (thus a geographic distance lower than 0.8). All other pairs were considered allopatric.

First, we tested for differences in perceptual distances across geographic status of pair of heliconiine subspecies. To test for higher perceived similarity between sympatric species than allopatric species, we used non-parametric Wilcox tests to compare perceptual distances across geographic status. In order to account for the effect of phylogeny, we ran the same tests on the residuals of perceptual distances regressed on phylogenetic distances. We computed phylogenetic distances as the pairwise patristic distances on the phylogeny of Heliconiini (Kozak *et al.* 2015) with terminal branches of null length to describe the relative position of subspecies in their associated species.

Second, we designed permutation tests aiming to test for a signal of perceived similarity and convergence higher than expected at random, if patterns were distributed randomly along the phylogeny. Thus, we computed the mean perceptual distance (for similarity) and residual perceptual distances (for convergence) in sympatric and allopatric pairs. We compared the observed statistics with a null distribution obtained from random permutation of distances across pairs of subspecies. As such, an observed statistic falling in the lower tail of the null distribution relates to a significant signal of perceived similarity/convergence in the group, and conversely.

As a result, we showed that subspecies in sympatry have significantly lower perceived similarity than allopatric species (Wilcox test: $W = 210 \times 10^6$, $p < 0.001$; **Fig. S25.a**), and lower than if patterns were distributed randomly (Permutation test: $D_{obs} = 104.0$, $Q5\% = 113.1$, $p < 0.001$; **Fig. S25.b**). Once accounted for evolutionary relationships across subspecies, we showed that subspecies in sympatry have significantly lower perceived residual similarity than

allopatric species (Wilcox test: $W = 214 \times 10^6$, $p < 0.001$; **Fig. S25.c**), and lower than if patterns were distributed randomly (Permutation test: Dobs = -11.2, Q5% = -3.33, $p < 0.001$; **Fig. S25.d**). Altogether, these results comfort our conclusion from the continuous analyses presented in the main text: spatially congruent species show significant degree of pattern similarity that goes beyond expectation from phylogenetic relatedness, hinting for the local convergence of aposematic patterns following Müller's predictions (Müller 1879).

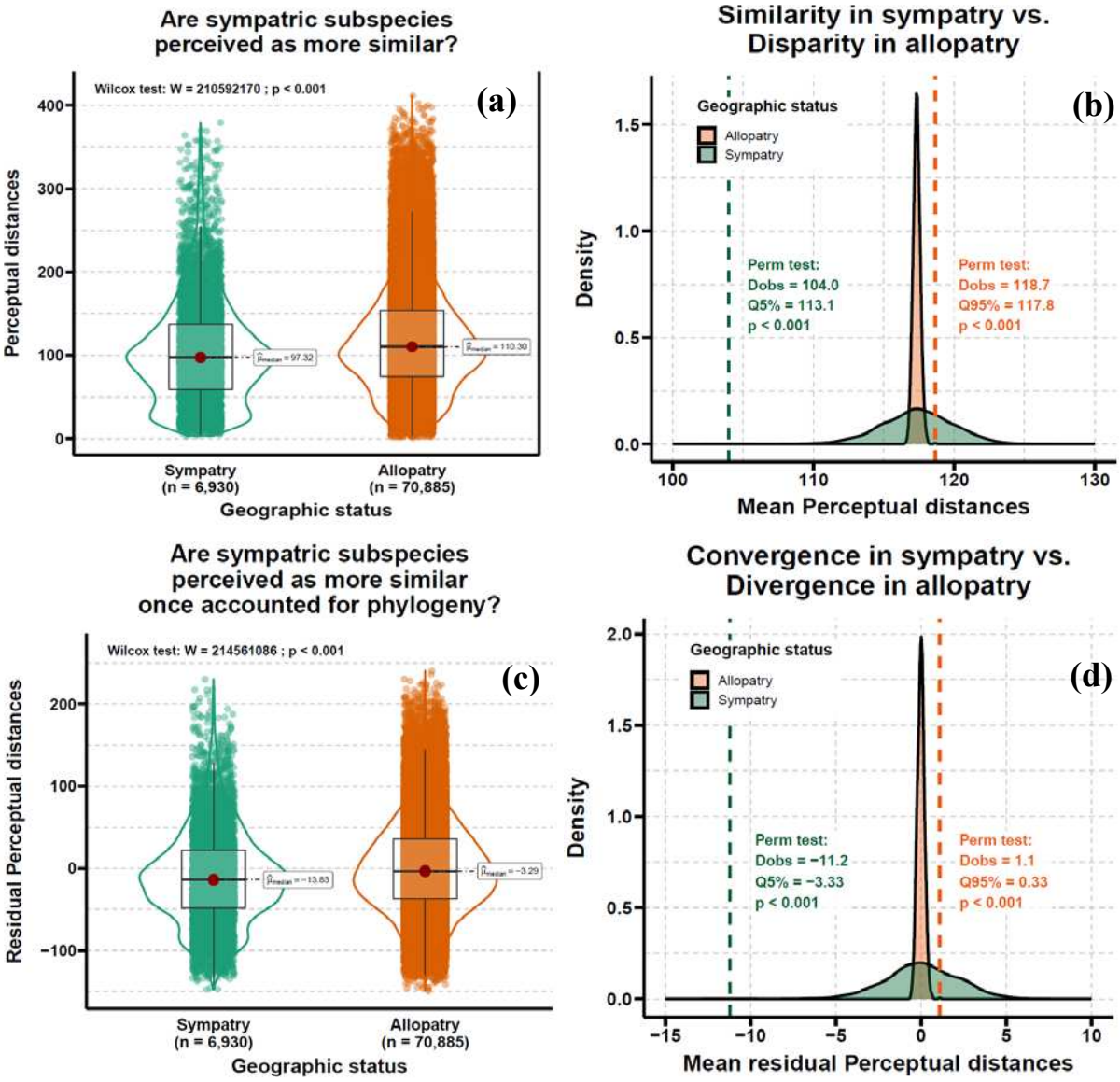

Figure S25: Tests for similarity (a-b) and convergence (c-d) of perceived wing patterns in sympatry. (a) Comparison of perceptual distances between pair of subspecies according to their geographic status. **(b)** Null distribution of mean perceptual distances in sympatric and allopatric pairs of species obtained through random permutation of perceptual distances. **(c)** Comparison of residual perceptual distances accounting for phylogeny between pair of subspecies according to their geographic status. **(d)** Null distribution of mean residual perceptual distances accounting for phylogeny in sympatric and allopatric pairs of species obtained through random permutation of perceptual distances.

Appendix 9: How many players to obtain a stable perceptual space?

When exploring the ability of the perceptual method to build a perceptual space illustrating the perceived variance in wing patterns of heliconiine butterflies for local communities, we aggregated sets of similarity triplets provided by five independent experts into a shared triplet dataset (3,000 triplets per local community as 600 triplets × 5 experts). The maps built from such aggregated sets of triplets were labeled as 'Aggregated-triplets' and were used as the reference to compute Procrustes's correlation and Cohen's Kappa dissimilarity with the CS-based maps and the individual maps.

Here, we explored the effect of aggregating individual perceptions from different people. Specifically, we inspect how many independent perceptions are needed to obtain a stable perceptual space and an associated classification such as adding more individual perception data will not change significantly the final output, supporting the idea that the final space and classification are fairly representative.

By aggregating perceptions across a range of number of players, we showed that five players were already enough to reach stability in the perceptual space for all but one local community (**Fig. S26**). The only exception was the community from Cayenne in which the location in the perceptual space of the outlier pattern/subspecies *Philaethria dido dido* was relatively conflictual across the five experts leading to an absence of stability (**Fig. S26**).

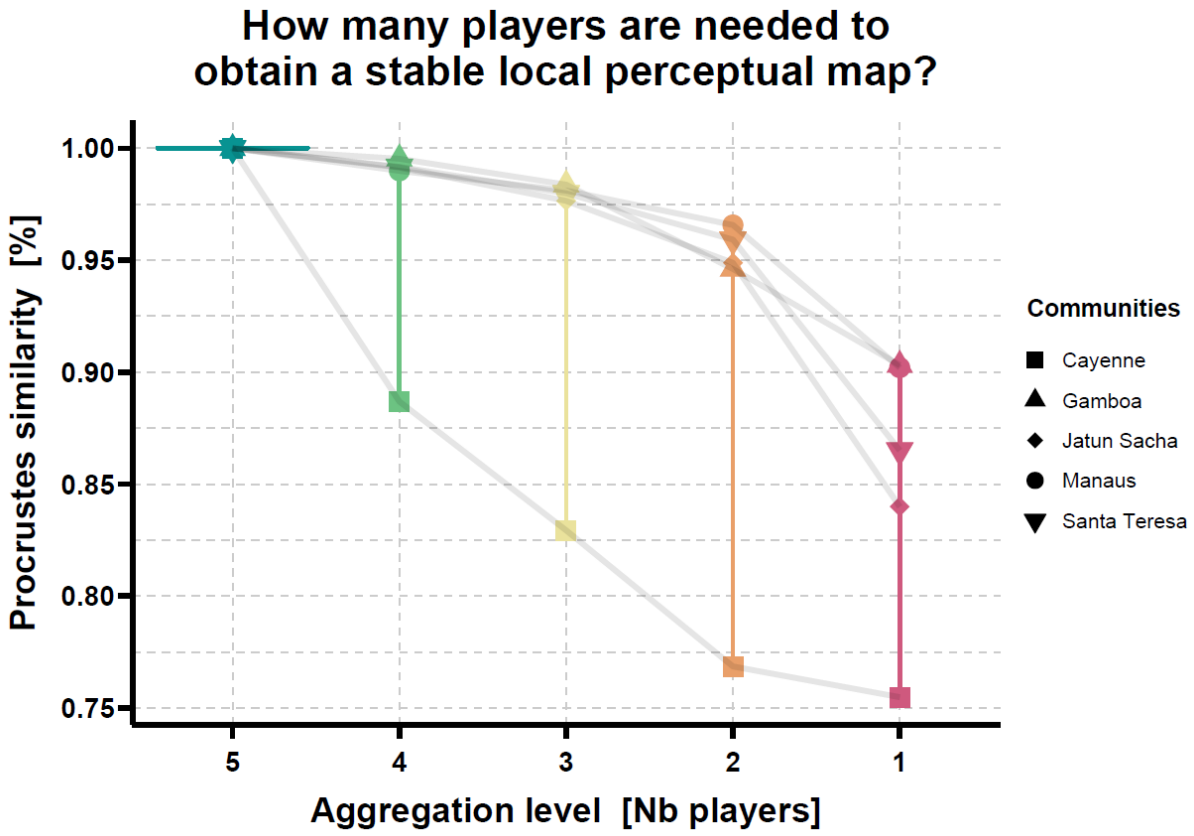

Figure S26: Evaluation plot for the stability of the local perceptual space while aggregating an increasing number of sets of similarity triplets provided by independent experts. Topological similarity of the perceptual spaces was evaluated with Procrustes's correlation. The dataset encompassing all five independent perceptions was used as the reference. Grey lines link scores obtained for a given local community. Scores are averaged across all possible combinations of experts for a given number of players for a given community.

Similarly, we showed that five players were already enough to reach stability in the mimetic classifications obtained for all local communities (**Fig. S27**). Cohen's Kappa scores were not perfect, but already reflected a strong agreement (all scores above 0.5). More importantly, similarity to the reference classification using data from all five experts did not seems to improve much beyond three players (**Fig. S27**).

Altogether, these results support the idea that gathering perception data from five independent people may be sufficient to produce rather stable and representative local perceptual spaces and associated classifications.

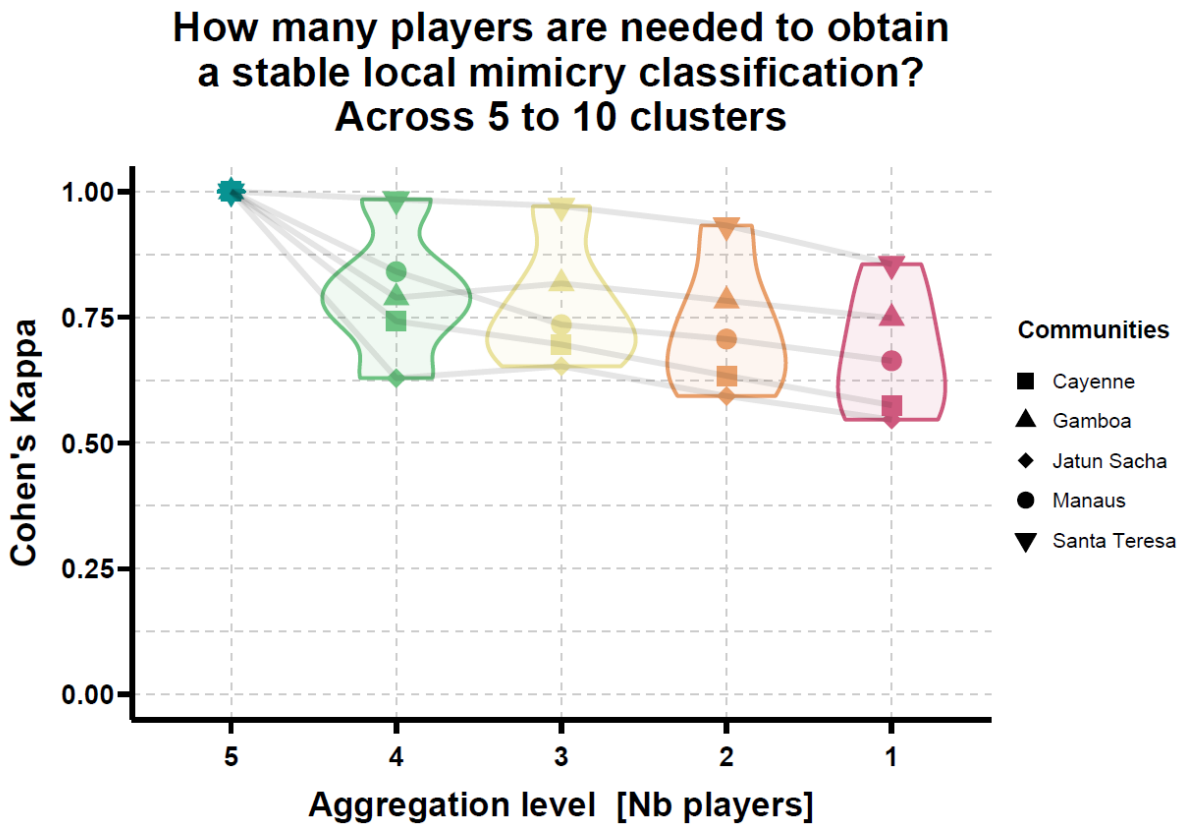

Figure S27: Evaluation plot for the stability of the local mimetic classification while aggregating an increasing number of sets of similarity triplets provided by independent experts. Classification agreement was evaluated with Cohen's Kappa. The dataset encompassing all five independent perceptions was used as the reference. Grey lines link scores obtained for a given local community. Scores are averaged across all possible combinations of experts for k ranging from 5 to 10 groups, for a given number of players for a given community.

Appendix 10: Lists of local mimetic groups

We built mimetic classifications of wing patterns in local community from GMM clustering applied on different perceptual maps. 'Triplet-aggregated' maps were obtained from the aggregation of similarity triplets provided by a panel of experts evaluating only the patterns of local taxa. 'CS' maps were obtained by extracting coordinates of those same local patterns from the macro-scale perceptual map involving all 432 subspecies patterns. We present here the mimicry classification resulting from such clustering for each local community: Cayenne, French Guyana (**Fig. S28**), Gamboa, Panama (**Fig. S29**), Jatun Sacha, Napo, Ecuador (**Fig. S30**), Manaus, Amazonas, Brazil (**Fig. S31**), and Santa Teresa, Espírito Santo, Brazil (**Fig. S32**).

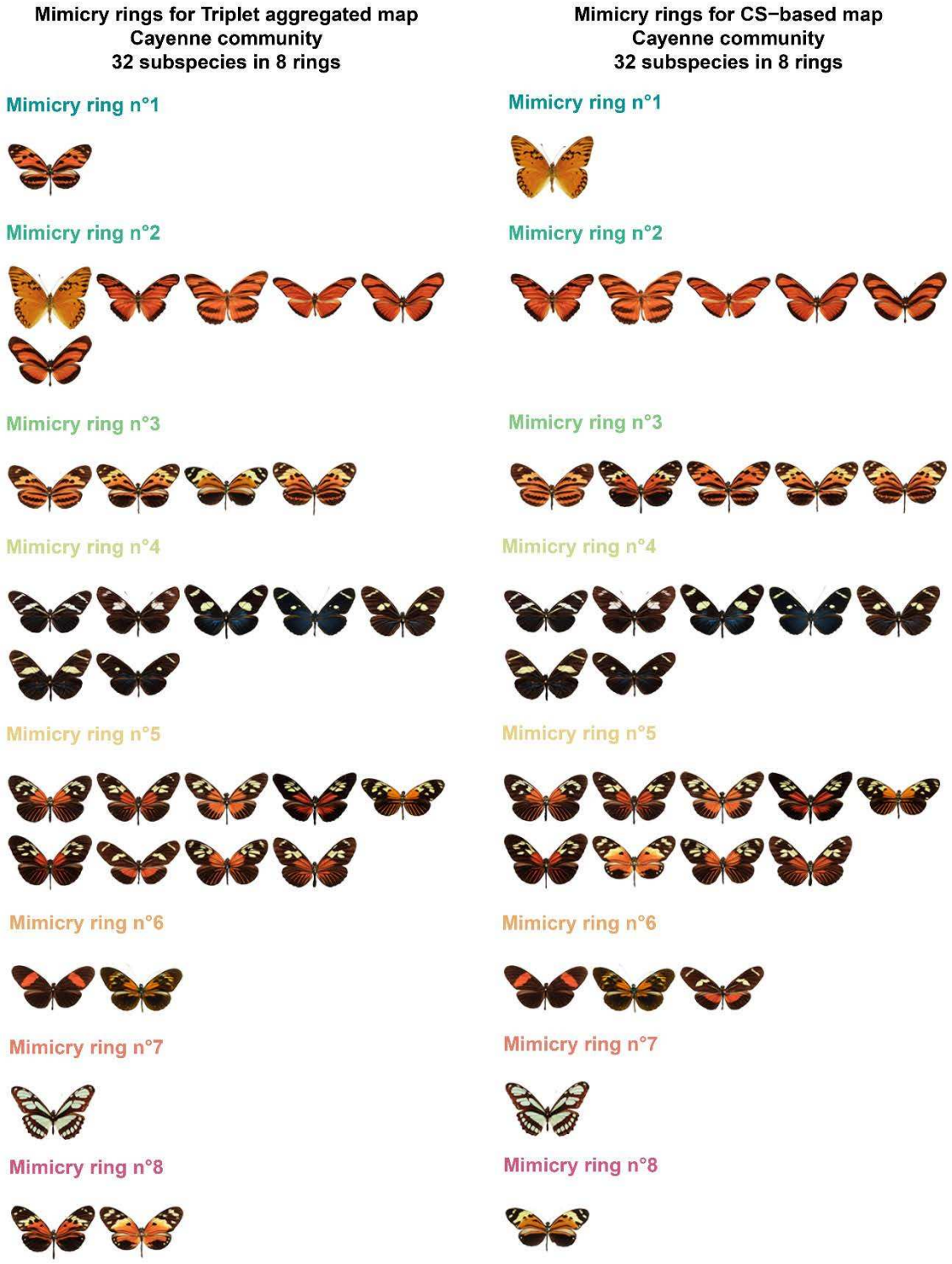

Figure S28: Visual list of local mimetic groups in Cayenne, French Guyana. Left: From the 'triplet-aggregated' perceptual space. **Right:** From the 'CS' perceptual space. The eight mimetic groups are ordered by similarity but they may not be equivalent.

Figure S29: Visual list of local mimetic groups in Gamboa, Panama. Left: From the 'triplet-aggregated' perceptual space. **Right:** From the 'CS' perceptual space. The eight mimetic groups are ordered by similarity but they may not be equivalent.

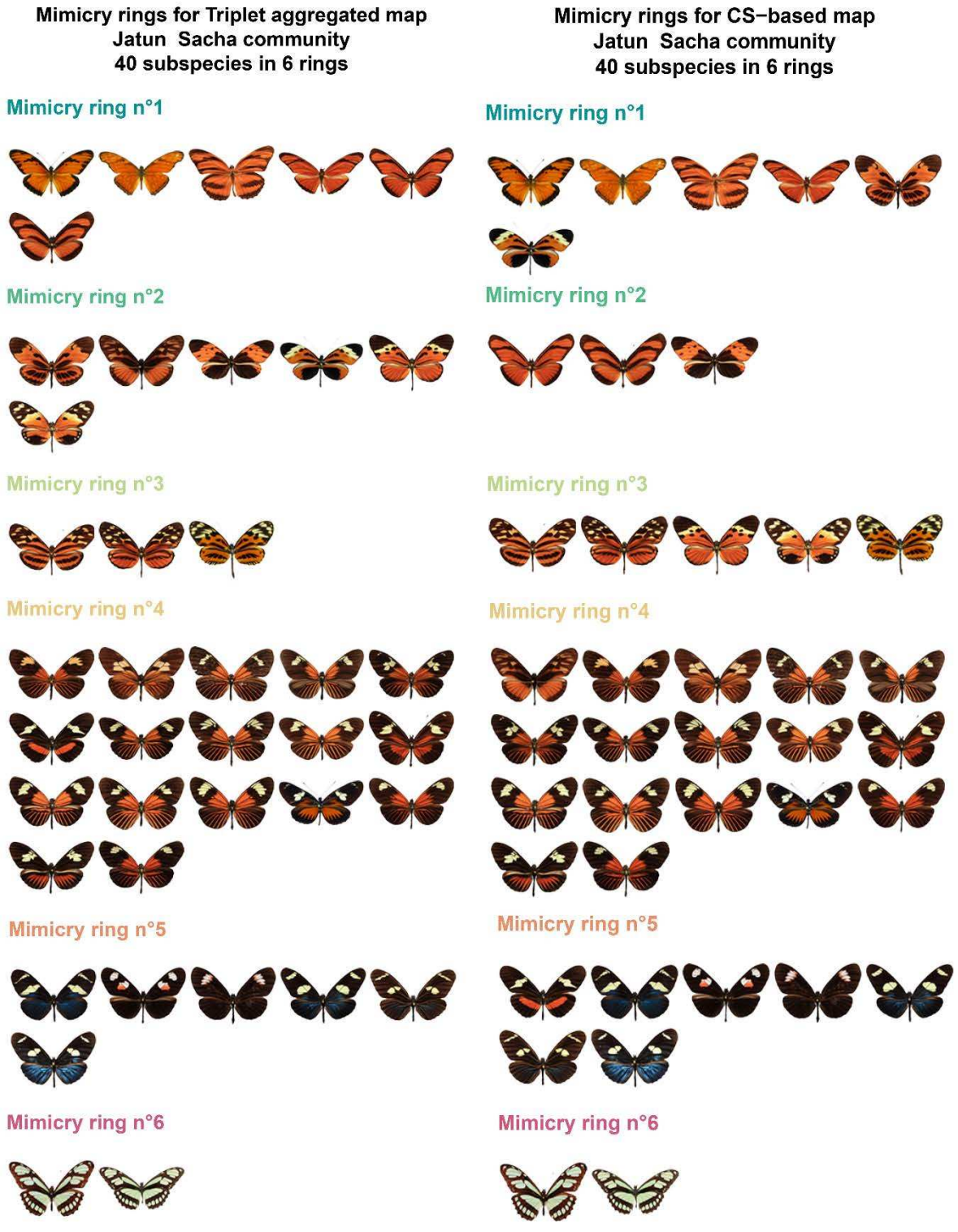

Figure S30: Visual list of local mimetic groups in Jatun Sacha, Napo, Ecuador. Left: From the 'triplet-aggregated' perceptual space. **Right:** From the 'CS' perceptual space. The six mimetic groups are ordered by similarity but they may not be equivalent.

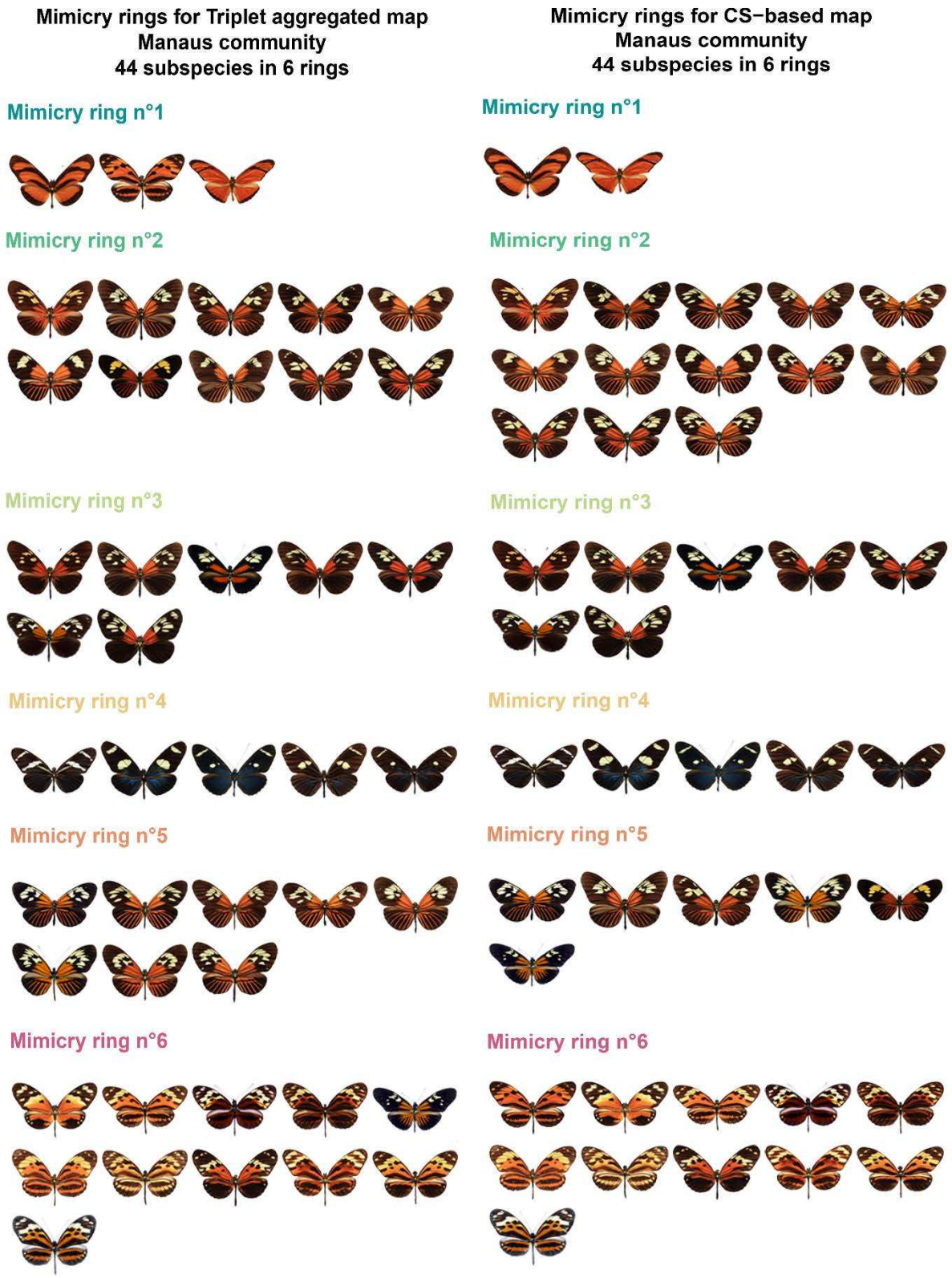

Figure S31: Visual list of local mimetic groups in Manaus, Amazonas, Brazil. Left: From the 'triplet-aggregated' perceptual space. **Right:** From the 'CS' perceptual space. The six mimetic groups are ordered by similarity but they may not be equivalent.

Figure S32: Visual list of local mimetic groups in Santa Teresa, Espírito Santo, Brazil. Left: From the 'triplet-aggregated' perceptual space. **Right:** From the 'CS' perceptual space. The seven mimetic groups are ordered by similarity but they may not be equivalent.

ANNEXE 5

Supplementary Information for CHAPTER 4

Supplementary Information for

Mutualistic interactions shape global spatial congruence and climatic niche evolution in Neotropical mimetic butterflies

Maël Doré[1,2], Keith Willmott[3], Sebastien Lavergne[4], Nicolas Chazot[5], André V. L. Freitas[6], Colin Fontaine[2], and Marianne Elias[1,7]

[1]*Institut de Systématique, Evolution, Biodiversité, MNHN-CNRS-Sorbonne Université-EPHE-Université des Antilles, Muséum national d'Histoire naturelle, 45 Rue Buffon, 75005, Paris, France*

[2]*Centre d'Ecologie et des Sciences de la Conservation, UMR 7204 MNHN-CNRS-Sorbonne Université, Muséum national d'Histoire naturelle, 45 rue Buffon, 75005, Paris, France*

[3]*McGuire Center for Lepidoptera and Biodiversity, Florida Museum of Natural History, University of Florida, Gainesville, FL, United States of America*

[4]*Laboratoire d'Ecologie Alpine, Université Grenoble Alpes, Université Savoie Mont Blanc, CNRS, FR-38000 Grenoble, France*

[5]*Swedish University of Agricultural Sciences, Uppsala, Sweden*

[6]*Departamento de Biologia Animal and Museu de Diversidade Biológica, Instituto de Biologia, Universidade Estadual de Campinas, 13083-862 Campinas, São Paulo, Brazil*

[7]*Smithsonian Tropical Research Institute, Panamá, Panamá*

Appendix 1: Phylogeny of Ithomiini butterflies

Figure S1: Time-calibrated phylogeny adapted from Chazot *et al.*, 2019. The tree includes 339 species out of the 396 species (85.6%) currently known in the group. Colors highlight the 10 subtribes. Dashed lines represent evolutionary time at intervals of 5 million years.

Reference:

Chazot, N., Willmott, K. R., Lamas, G., Freitas, A. V., Piron-Prunier, F., Arias, C. F., ... & Elias, M. (2019). Renewed diversification following Miocene landscape turnover in a Neotropical butterfly radiation. Global Ecology and Biogeography, 28(8), 1118-1132. https://doi.org/10.1111/geb.12919

Appendix 2: Definition of Operational Mimicry Units (OMUs)

In this study, we aimed to investigate the interplay between Müllerian mimicry and the distribution and climatic niche of ithomiine butterflies. As such, we defined Operational Mimicry Units (OMUs) as the set of conspecific butterflies that share the same mimicry pattern. Therefore, a species may either be equivalent to an OMU, if all individuals of both sexes and all subspecies of that species share the same pattern (Species A in **Figure S2**), or may be represented by multiple OMUs if different subspecies belong to different putative mimicry rings, or if there is sexual dimorphism (Species B in **Figure S2**). Cases of sexual dimorphism are rare occurrences in Ithomiini (70 cases across the 1542 subspecies = 4.5%), while species polymorphism is common (202 cases across the 396 species = 51%). We employed the 783 currently known OMUs in the Ithomiini tribe as the ecological units for our analyses (Doré *et al.* 2022). For the sake of simplicity, we use "comimetic species" in the main text to refer to the OMUs sharing the same mimicry pattern.

Members of a putative mimicry ring are all the OMUs displaying its associated aposematic pattern. It could include OMU representing entire monomorphic species (OMU A - LYSIMNIA in **Figure S2**), or OMUs that are part of polymorphic species (OMU B - LYSIMNIA in **Figure S2**). Therefore, a putative mimicry ring encompasses all individuals displaying its associated aposematic pattern.

Reference:

Doré, M., Willmott, K., Leroy, B., Chazot, N., Mallet, J., Freitas, A. V. L., Hall, J. P. W., Lamas, G., Dasmahapatra, K. K., Fontaine, C., & Elias, M. (2022). Anthropogenic pressures coincide with Neotropical biodiversity hotspots in a flagship butterfly group. Diversity and Distributions, 28(12), 2912–2930. https://doi.org/10.1111/ddi.13455

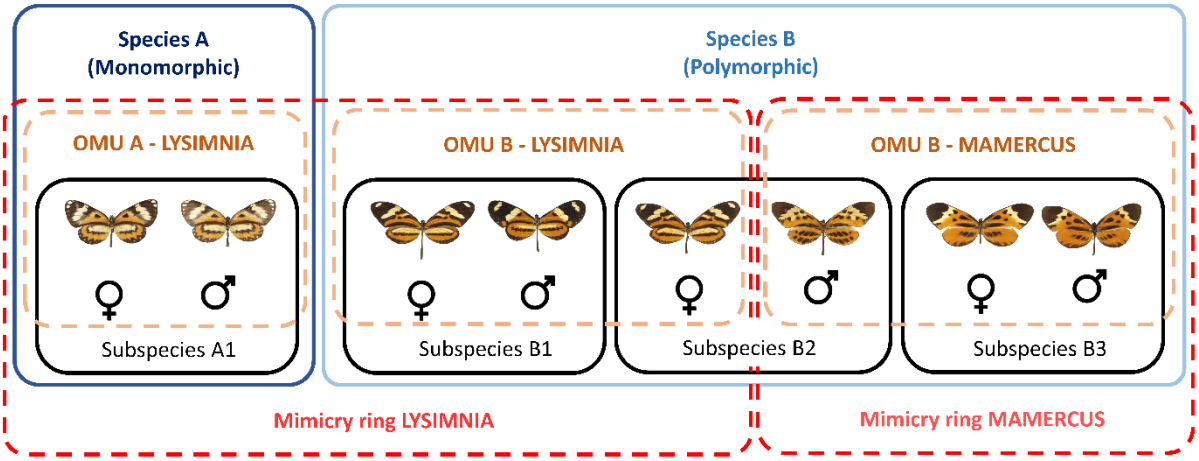

Figure S2: Hierarchal relationships between taxonomic groups in plain lines with four subspecies and two species, and mimicry groups in dashed lines with three Operational Mimicry Units (OMUs) and two mimicry rings. Subspecies B2 displays a case of sexual dimorphism with both sexes belonging to different OMUs and mimicry rings.

Appendix 3: Map of Ithomiini species richness

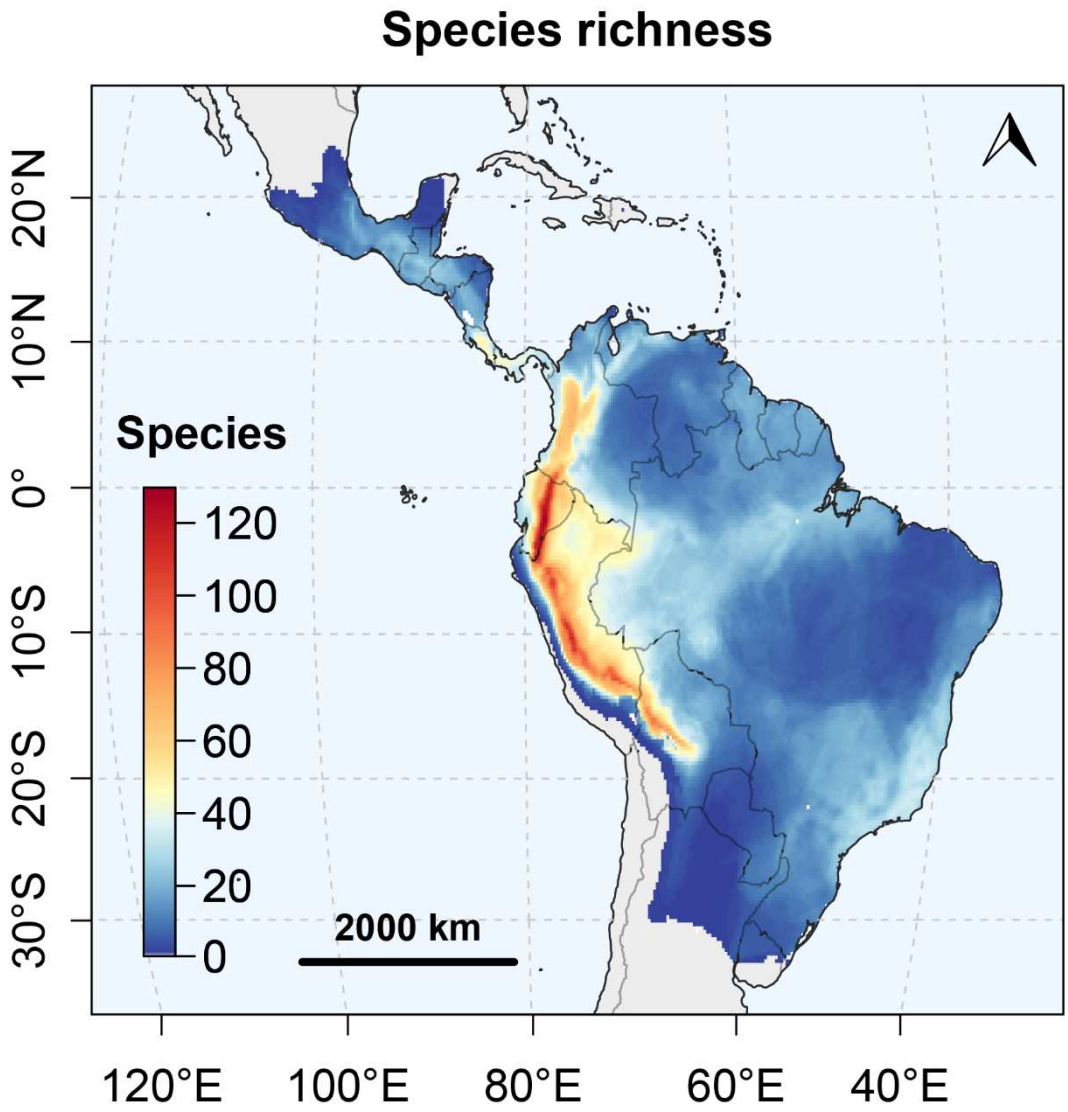

Figure S3: Map of Ithomiini predicted species richness. The map was built from the distribution maps of 393 species produced by Doré *et al.* 2021.

Reference:

Doré, M., Willmott, K., Leroy, B., Chazot, N., Mallet, J., Freitas, A. V. L., Hall, J. P. W., Lamas, G., Dasmahapatra, K. K., Fontaine, C., & Elias, M. (2022). Anthropogenic pressures coincide with Neotropical biodiversity hotspots in a flagship butterfly group. Diversity and Distributions, 28(12), 2912–2930. https://doi.org/10.1111/ddi.13455

Appendix 4: Distribution of OMUs among mimicry rings

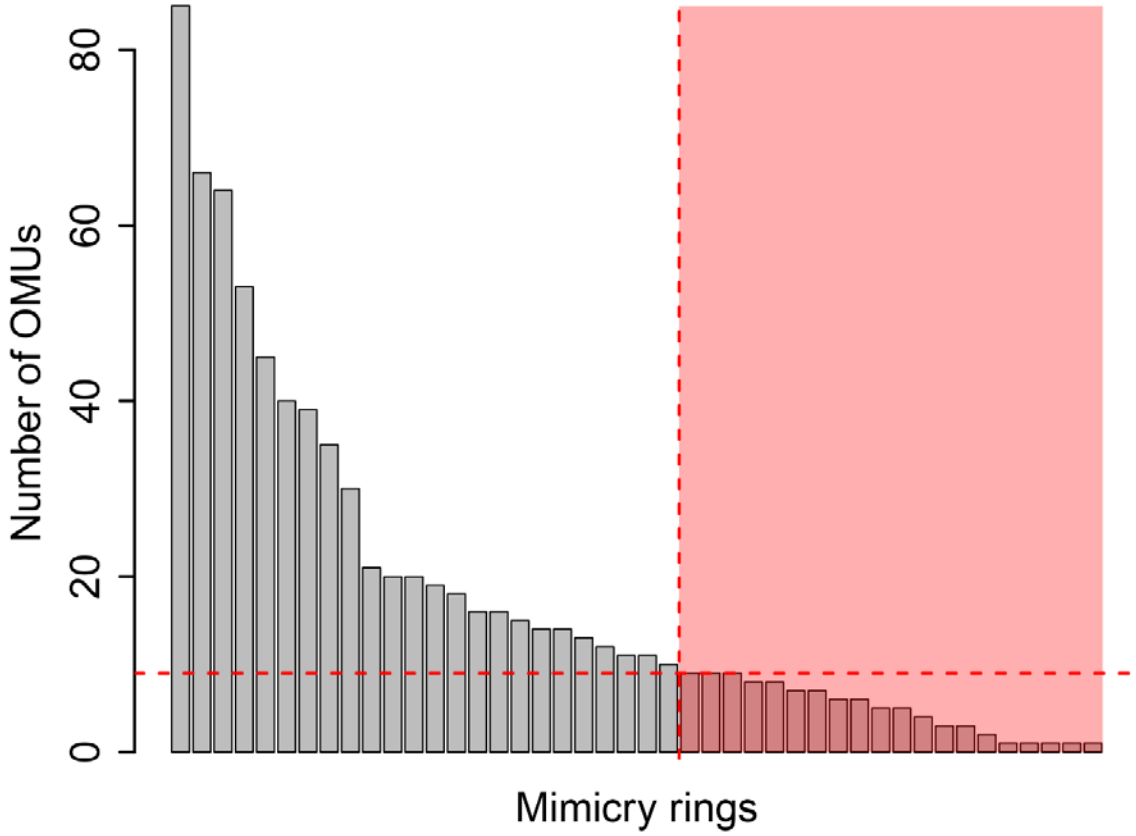

Figure S4: Distribution of Operational Mimicry Units (OMUs) among the 44 putative mimicry rings. Small mimicry rings (i.e., with less than 10 OMUs) inside the red area were discarded from the perMANOVA and phylogenetic MANOVA analysis because of their reduced sample size. As a result, 24 out of 44 mimicry rings (54.5%) were retained in the analysis, encompassing 322 species (95.0%) and 619 OMUs (86.1%) among the 339 species and 719 OMUs represented in the phylogeny.

Appendix 5: Histograms of null distributions for statistical tests

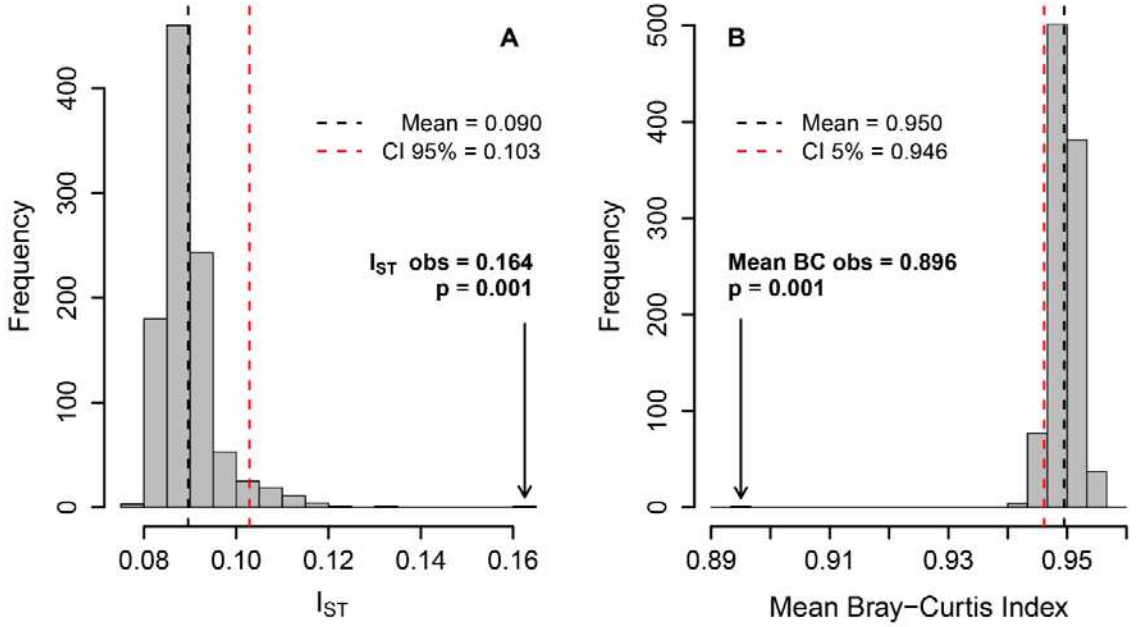

Figure S5: Tests for community structure. (A) Distribution of global I_{ST} under 999 randomizations of mimicry patterns among species in communities. CI 95% = threshold of significance for this test. Black arrow indicates the position of the observed value. (B) Distribution of the mean Bray-Curtis distance among all comimetic species under 999 randomizations of mimicry patterns among species in communities. CI 5% = threshold of significance for this test. Black arrow indicates the position of the observed value.

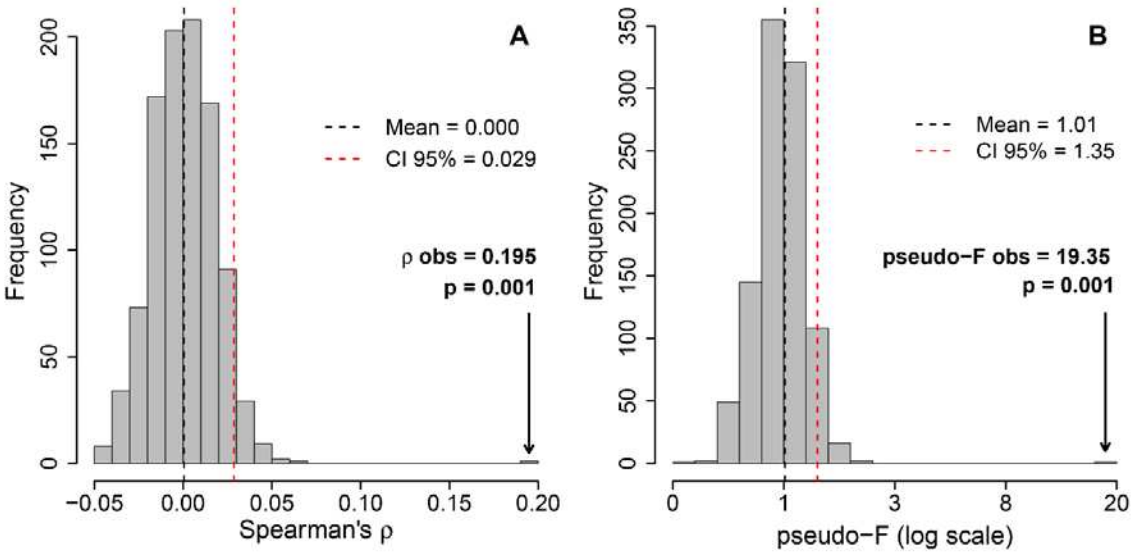

Figure S6: Test for association between climate and mimicry patterns: mimicry turnover (pairwise I_{ST}) correlates with climatic distances beyond the effect of geographic distance (A) while species climatic niches are segregated among mimicry rings (B). (A) Null distribution of

the Spearman's rho correlation statistics generated during the permutation process for the partial Mantel test investigating the relationship between mimicry turnover (pairwise I_{ST}) and climatic distances accounting for effects of geographic distance. We performed this partial Mantel test on a random sample of 1000 communities to limit spatial autocorrelation. (B) Distribution of the pseudo-F generated during the permutation process (n = 999) of the perMANOVA which tests for the significance of the relationship between mimicry rings and climatic niches. X-axis is on log-scale. The observed pseudo-F is higher than all the pseudo-F values in the null distribution (pseudo-F obs = 19.35, $p \leq 0.001$), thus indicating a significant divergence between the climatic niche of species belonging to different putative mimicry rings, compared to a random association of mimicry patterns to species and their climatic niche.

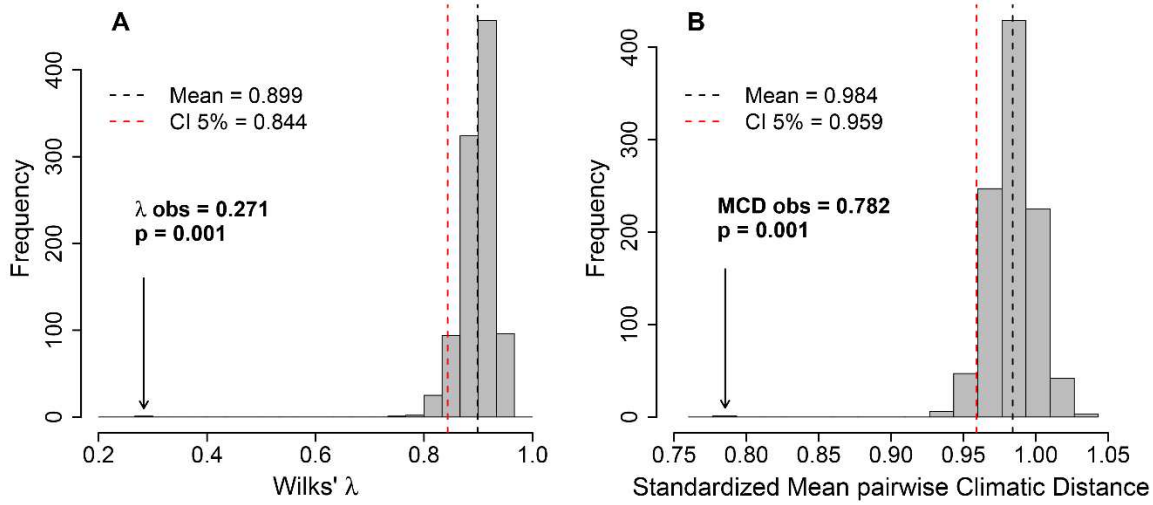

Figure S7: Tests for niche convergence among mimicry rings. (A) Null distribution of the Wilks' λ statistic of the phylogenetic MANOVA testing for divergence of climatic niches among putative mimicry rings while the evolution of niche is simulated 999 times on the phylogeny. An observed Wilks' λ lower than the 5% quantile shows that the climatic niches of the different mimicry rings diverge more than expected under a neutral model of evolution. (B) Null distribution of the mean climatic distance (MCD) among comimetic species while climatic niches are simulated 999 times on the phylogeny. An observed MCD lower than the 5% quantile shows that the evolutionary convergence between climatic niche and mimicry patterns of species is greater than expected under a neutral model of evolution.

Appendix 6: Bray-Curtis distances per mimicry ring

In order to investigate if the dissimilarity between spatial distributions of species was lower for phenotypically similar species, we computed pairwise Bray-Curtis distances (Bray & Curtis 1957) across the distributions of all pairs of OMUs with the R package *vegan* 2.5-4 (Oksanen *et al.* 2019). The pairwise Bray-Curtis distances were computed as follows:

$$BC_{jk} = 1 - \frac{2\sum_{i=1}^{p} min(N_{ij}, N_{ik})}{\sum_{i=1}^{p}(N_{ij} + N_{ik})} \qquad \text{(Eqn. 1)}$$

where *j* and *k* are two species evaluated, *i* is one community among *p* communities, and N is the species likelihood of presence (traditionally, the species abundance). Bray-Curtis distances range from 0 to 1 and can be interpreted as the opposite of a proportion of overlap weighted by the likelihood of presence of both species within grid-cells across their range. As such, a high Bray-Curtis value correspond to a large dissimilarity in species spatial distributions, while a low value relates to an important spatial overlap (**Fig. 2**).

We evaluated the significance of the mean value obtained for pairs of phenotypically similar species (i.e., putative co-mimics) by permutation of mimicry patterns among the OMUs. We carried out this analysis for 39 putative mimicry rings for which the analysis could be performed since they hosted more than one species (**Fig. 1**: mimicry rings showing significant spatial congruence are associated with a 'Co' symbol in green ; **Table S1**: statistical summary for species spatial congruence within each putative mimicry ring).

References:

Bray, J. R., & Curtis, J. T. (1957). An ordination of the upland forest communities of southern Wisconsin. *Ecological monographs*, 27(4), 326-349. https://www.jstor.org/stable/1942268

Oksanen, J. R., et al. (2019). vegan: Community Ecology Package. R package version 2.5-4. https://cran.r-project.org/package=vegan

Table S1: Summary of randomization tests for community composition based on mean Bray-Curtis distance among comimetic Operational Mimicry Units (OMUs) from each putative mimicry ring. N OMUs = Number of OMUs in the mimicry ring. N pairs = Number of pairs tested for this mimicry ring. Mean BC obs = Mean Bray-Curtis distance among comimetic OMUs observed. Mean null BC = Average mean Bray-Curtis distance among comimetic OMUs for 999 randomizations of mimicry patterns among OMUs. CI 2.5% = Bray-Curtis value for quantile 2.5% in the null distribution. CI 97.5% = Bray-Curtis value for quantile 2.5% in the null distribution. Bold p-values are significant for an $\alpha = 0.05$.

Mimicry ring	N OMUs	N pairs	Mean BC obs	Mean null BC	CI 2.5%	CI 97.5%	p-value
ACRISIONE	1	0	NA	NA	NA	NA	NA
AGNOSIA	85	3570	0.924	0.95	0.932	0.964	**0.004**
AMALDA	9	36	0.849	0.949	0.877	0.994	**0.009**
AURELIANA	12	66	0.74	0.948	0.885	0.986	**0.001**
BANJANA-M	45	990	0.899	0.949	0.923	0.969	**0.002**
CONFUSA	20	190	0.843	0.949	0.904	0.98	**0.001**
DERCYLLIDAS	1	0	NA	NA	NA	NA	NA
DILUCIDA	40	780	0.844	0.95	0.922	0.969	**0.001**
DOTO	15	105	0.922	0.949	0.894	0.985	0.127
DUESSA	4	6	0.96	0.948	0.802	1	0.477
DUILLIA	3	3	0.829	0.949	0.728	1	0.093
EGRA	11	55	0.872	0.95	0.884	0.99	**0.014**
EURIMEDIA	35	595	0.906	0.949	0.918	0.972	**0.007**
EXCELSA	18	153	0.844	0.949	0.901	0.981	**0.001**
HEMIXANTHE	7	21	0.543	0.948	0.857	0.998	**0.001**
HERMIAS	53	1378	0.918	0.949	0.925	0.968	**0.006**
HEWITSONI	30	435	0.807	0.948	0.915	0.974	**0.001**
HUMBOLDT	1	0	NA	NA	NA	NA	NA
ILLINISSA	6	15	0.585	0.947	0.826	1	**0.001**
LERIDA	66	2145	0.925	0.95	0.929	0.966	**0.015**
LIBETHRIS	21	210	0.901	0.949	0.905	0.978	**0.022**
LYSIMNIA	5	10	0.787	0.95	0.806	1	**0.017**
MAELUS	16	120	0.662	0.949	0.901	0.983	**0.001**
MAMERCUS	64	2016	0.916	0.95	0.929	0.968	**0.002**
MANTINEUS	5	10	0.315	0.949	0.826	1	**0.001**
MESTRA	14	91	0.741	0.949	0.894	0.986	**0.001**
MOTHONE	14	91	0.802	0.95	0.896	0.986	**0.001**
OCNA	13	78	0.902	0.951	0.896	0.986	**0.036**
ORESTES	16	120	0.695	0.95	0.902	0.983	**0.001**
OZIA	19	171	0.894	0.949	0.908	0.978	**0.014**
PANTHYALE	39	741	0.908	0.95	0.921	0.972	**0.005**
PARALLELIS	7	21	0.694	0.951	0.856	0.999	**0.001**
PAVONII	2	1	1	0.95	0.552	1	1
POLITA	10	45	0.877	0.949	0.875	0.992	**0.03**

PRAESTANS	1	0	NA	NA	NA	NA	NA
PRAXILLA	9	36	0.768	0.949	0.868	0.994	**0.001**
QUINTINA	6	15	0.88	0.95	0.843	1	0.066
SINILIA	9	36	0.883	0.951	0.881	0.994	**0.028**
SUSIANA	20	190	0.829	0.949	0.903	0.978	**0.001**
THABENA-F	11	55	0.875	0.95	0.884	0.99	**0.018**
THEUDELINDA	8	28	0.686	0.951	0.875	0.997	**0.001**
TICIDA-M	8	28	0.285	0.95	0.867	0.996	**0.001**
UMBROSA	3	3	0.876	0.949	0.73	1	0.162
VESTILLA	1	0	NA	NA	NA	NA	NA

Appendix 7: Investigating the effect of random subsampling on Mantel tests and Multiple Regression on distance Matrices

To examine whether mimetic interactions have led to the similarity of climatic niches between phenotypically similar species, thereby reinforcing their pattern of spatial congruence, we explored the relationship between mimetic turn-over (i.e., pairwise I_{ST}) and climatic distances (i.e., Euclidian distances in a standardized multivariate climatic space formed by our four bioclimatic variables) between pairs of communities. We randomly subsampled 1000 communities in order to limit spatial autocorrelation and reduce computation time. We applied partial Mantel tests and Multiple Regressions on distance Matrices (MRM ; Legendre *et al.* 1994) between pairwise I_{ST} and climatic distances taking into account a possible confounding effect of geographic distances. We performed these analyses a hundred times to ensure random subsampling of communities had no effect on our results. **Table S2** summarizes the distribution of Spearman's rho statistics and p-values obtained from the hundred replicates of Mantel tests. **Table S3** summarizes the distribution of β-coefficients quantifying the strength of the relationship between distance matrices, and their associated p-values, obtained from the hundred replicates of MRM tests. Variability in the results appeared low in both cases (i.e., between 3.3 and 12.4% of variation in estimates of Spearman's ρ and β-coefficients) and tests always led to high significance (all p-values ≤ 0.001), which ensures that the significance of the Mantel tests and MRM tests presented in the main text (**Fig. 4**) is robust to the random subsampling of communities applied prior the analyses.

Reference:

Legendre, P., Lapointe, F. J., & Casgrain, P. (1994). Modeling brain evolution from behavior: a permutational regression approach. *Evolution*, 48(5), 1487-1499. https://doi.org/10.1111/j.1558-5646.1994.tb02191.x

Table S2: Summary statistics of Spearman's ρ correlation coefficients and associated p-values for the 100 replicates of Mantel tests performed on different subsamples of Ithomiini communities (n = 1000). I_{ST} = pairwise mimicry turnover. D_{clim} = standardized climatic distances. D_{geo} = geographic distances. SD = Standard deviation. CV = coefficient of variation. Q = quantile.

	$I_{ST} \sim D_{clim}$ (n = 100)		**$I_{ST} \sim D_{geo}$** (n = 100)		**$I_{ST} \sim D_{clim} + cov(D_{geo})$** (n = 100)	
Summary stats	Spearman's ρ	p-value	Spearman's ρ	p-value	Spearman's ρ	p-value
In Fig. 4	0.351	0.001	0.517	0.001	0.195	0.001
mean ± SD	0.362 ± 0.016	0.001	0.534 ± 0.016	0.001	0.204 ± 0.022	0.001
CV (%)	4.3	0	3.3	0	10.7	0
Q 2.5%	0.333	0.001	0.504	0.001	0.159	0.001
Q 97.5%	0.393	0.001	0.572	0.001	0.249	0.001
min	0.316	0.001	0.492	0.001	0.156	0.001
max	0.403	0.001	0.575	0.001	0.252	0.001

Table S3: Summary statistics of β-coefficients quantifying the strength of the relationship between distance matrices, and their associated p-values for the 100 replicates of Multiple Regressions on distance Matrices (MRM) tests performed on different subsamples of Ithomiini communities (n = 1000). I_{ST} = pairwise mimicry turnover. D_{clim} = standardized climatic distances. D_{geo} = geographic distances. SD = Standard deviation. CV = coefficient of variation. Q = quantile. § β-coefficients for $I_{ST} \sim D_{clim} + cov(D_{geo})$ relates to the effect of climatic distances while accounting for the effect of geographic distances.

	$I_{ST} \sim D_{clim}$ (n = 100)		**$I_{ST} \sim D_{geo}$** (n = 100)		**$I_{ST} \sim D_{clim} + cov(D_{geo})$** (n = 100)	
Summary stats	β-coefficient	p-value	β-coefficient	p-value	β-coefficient §	p-value
In Fig. 4	0.367	0.001	0.598	0.001	0.216	0.001
mean ± SD	0.382 ± 0.020	0.001	0.632 ± 0.020	0.001	0.216 ± 0.027	0.001
CV (%)	5.4	0	4.6	0	12.4	0
Q 2.5%	0.344	0.001	0.583	0.001	0.165	0.001
Q 97.5%	0.418	0.001	0.693	0.001	0.270	0.001
min	0.336	0.001	0.567	0.001	0.161	0.001
max	0.447	0.001	0.712	0.001	0.283	0.001

Appendix 8: Heatmap of climatic niche (dis)similarities among mimicry rings

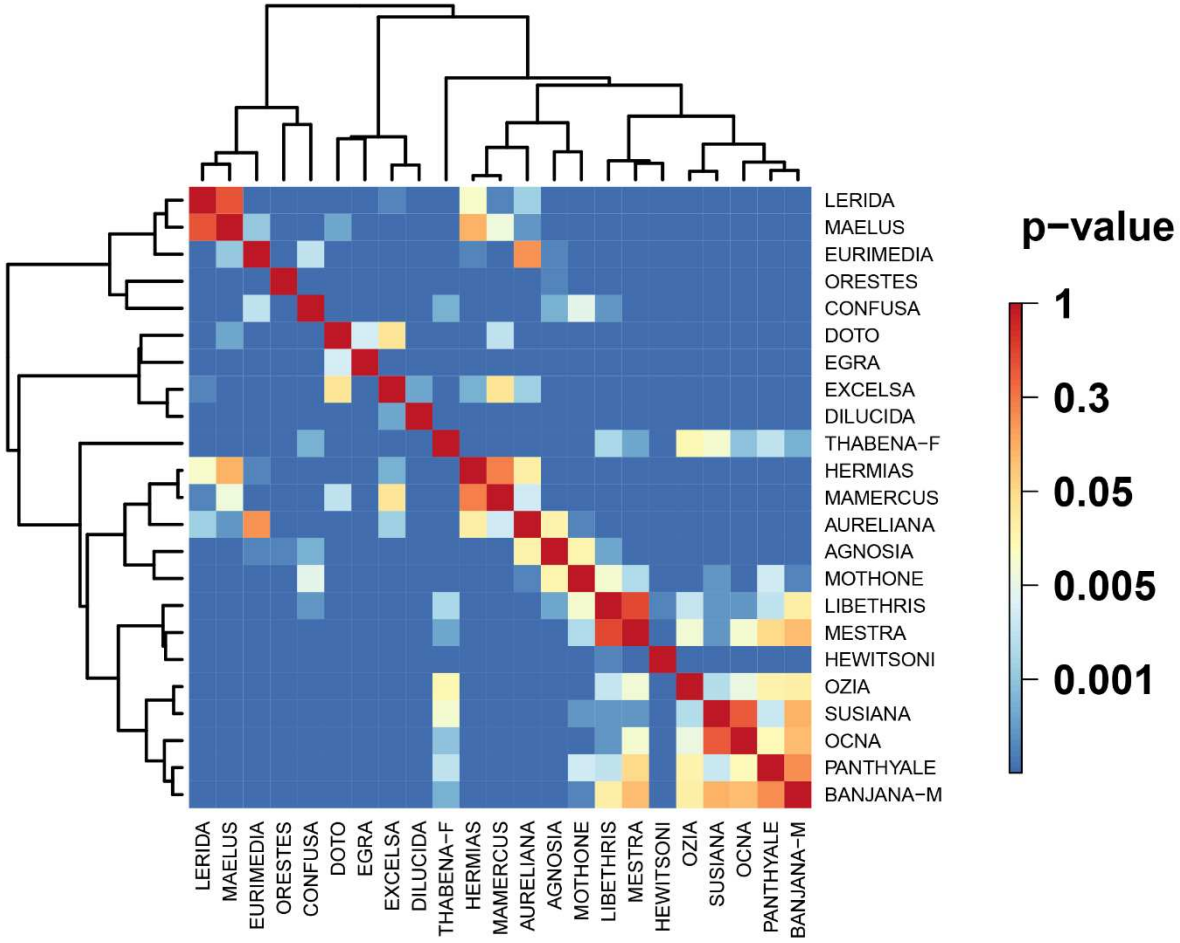

Figure S8: Heatmap of the p-values resulting from the post-hoc pairwise perMANOVA assessing the dissimilarity between the climatic niche of mimicry rings. The lower the p-value, the more dissimilar the climatic niches of the two mimicry rings. Scale has been transformed as $y = x^{5.8}$ to increase the contrast among low p-values. 186 out of 253 pairs (73.5%) show a p-value ≤ 0.001 (in blue); 210 (83.0%) show a p-value lower than 0.01; 226 (89.3%) show a p-value lower than 0.05. The dendrogram represents relationships between the mimicry rings based on their climatic niche. It was obtained with the *hclust* function, based on the standardized climatic Euclidian distances and a complete linkage method.

Appendix 9: Niche overlap among mimicry rings

Complementarily to analyses of niche dissimilarity based on Euclidean centroid distances (**Fig. 4.D** ; **SI Appendix 5, Fig. S6.B ; SI Appendix 8, Fig. S8**), we explored differences in climatic niche overlap between co-mimetic OMUs.

First, we applied a PCA on environmental data extracted from the entire Ithomiini range in order to build a 2D orthogonal environmental space. We projected occurrences from OMUs in this environmental space. Then, we applied gaussian kernel density smoother on the occurrence points of each OMU using the R package *hypervolume* 3.1.0 (Blonder *et al.* 2022) in order to build a density function that model the environmental niche of each OMU (Broennimann *et al.* 2012). We applied a 95% probability threshold to delineate each hypervolume. We estimated niche overlap between pairs of OMUs as the Jaccard index which in this context represents the weighted portion of overlap across two hypervolumes.

In order to test for the similarity of niche between comimetic OMUs, we compared the observed pairwise mean Jaccard index of niche overlap (i.e., Euclidean distances between niche centroids) between the niche optimum of pairs of co-mimetic OMUs with the null distribution of that same statistic obtained from 999 permutations of mimicry patterns across OMUs. A higher observed Jaccard index than the values in the null distribution would indicate that co-mimetic OMUs display more similar climatic niche (i.e., show higher niche overlap) than expected at random. We conducted this test globally for all co-mimics, and per putative mimicry ring.

As a result, we showed that, similarly to PerMANOVA based on centroid distances, climatic niche overlap is significantly more important between co-mimetic OMUs than expected at random (**Figure S9** ; Jobs = 0.230, CI 95% = 0.154, p-value $\leq$ 0.001). Moreover, 28 putative mimicry rings (i.e., 71.8%) out of the 39 rings for which the test could be performed showed a significant pattern of niche similarity (**Table S4**). Altogether, this complementary analysis is in accordance with what was observed for niche dissimilarity based on Euclidean centroid distances (**Fig. 4.D ; SI Appendix 5, Fig. S6.B**: PerMANOVA : R^2 = 0.416, Pseudo-F = 19.35, p $\leq$ 0.001 ; **SI Appendix 8, Fig. S8**).

References:

Blonder, B., et al. (2022). hypervolume: High Dimensional Geometry, Set Operations, Projection, and Inference Using Kernel Density Estimation, Support Vector Machines, and Convex Hulls. R package version 3.1.0. https://CRAN.R-project.org/package=hypervolume

Broennimann, O., Fitzpatrick, M. C., Pearman, P. B., Petitpierre, B., Pellissier, L., Yoccoz, N. G., ... & Guisan, A. (2012). Measuring ecological niche overlap from occurrence and spatial environmental data. *Global ecology and biogeography*, 21(4), 481-497. https://doi.org/10.1111/j.1466-8238.2011.00698.x

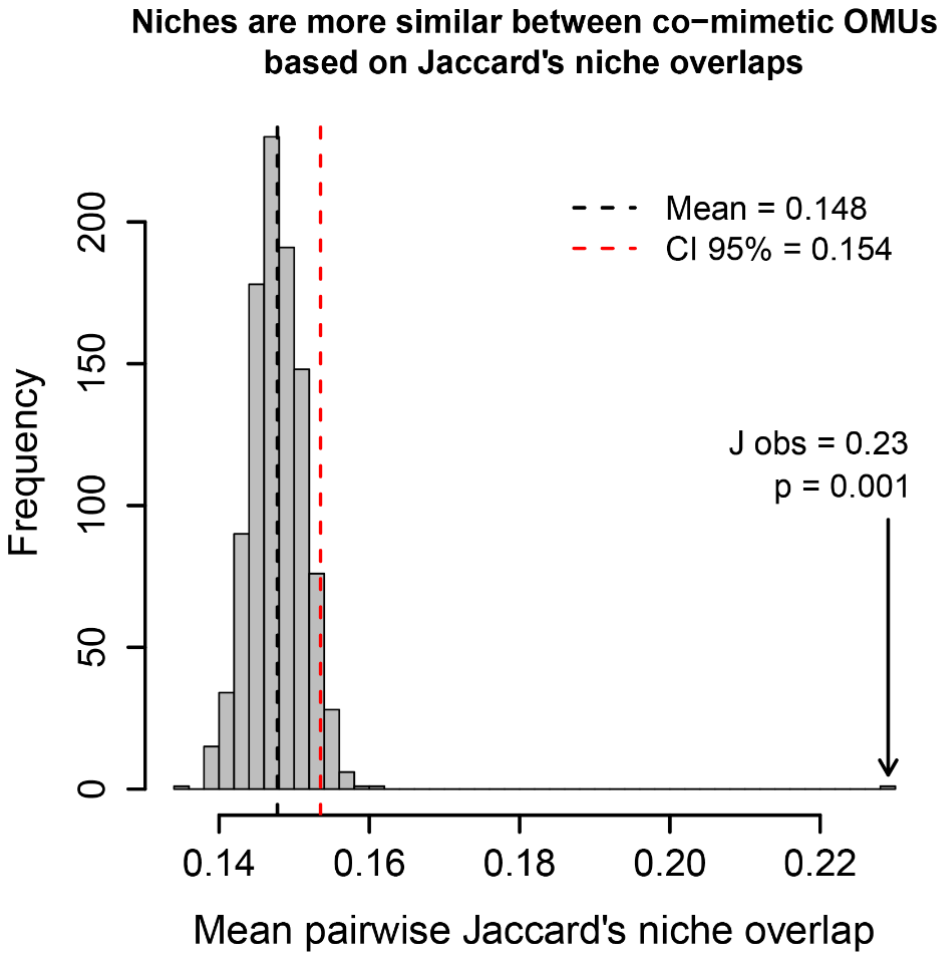

Figure S9: Distribution of global mean Jaccard's niche overlap between co-mimetic OMUs under 999 randomizations of mimicry patterns. CI 95% = threshold of significance for this test. Black arrow indicates the position of the observed value (J obs).

Table S4: Summary of permutation tests for the similarity of the climatic niche following mimicry patterns based on Jaccard's niche overlap (J) among comimetic Operational Mimicry Units (OMUs) from each mimicry ring. N OMUs = Number of OMUs in the mimicry ring. N pairs = Number of pairs tested for this mimicry ring. Mean J_{obs} = Mean Jaccard's niche overlap among comimetic OMUs observed. Mean J_{null} = Average mean Jaccard's niche overlap among comimetic OMUs for 999 permutations of mimicry patterns across OMUs. Q 5% = Jaccard's niche overlap for quantile 5% in the null distribution. Q 95% = Jaccard's niche overlap for quantile 95% in the null distribution. Bold p-values are significative for an $\alpha = 0.05$. P-values are computed for a right-tail test assessing niche similarity, except for p-values with an asterisk which are computed for a left-tail test assessing dissimilarity of the climatic niche.

Mimicry ring	N OMUs	N pairs	Mean J_{obs}	Mean J_{null}	Q 5%	Q 95%	p-value	Pattern
ACRISIONE	1	0	NA	NA	NA	NA	NA	NA
AGNOSIA	85	3570	0.191	0.147	0.126	0.17	**0.002**	**similarity**
AMALDA	9	36	0.282	0.147	0.075	0.237	**0.016**	**similarity**
AURELIANA	12	66	0.324	0.149	0.085	0.225	**0.001**	**similarity**
BANJANA-M	45	990	0.194	0.148	0.115	0.182	**0.013**	**similarity**
CONFUSA	20	190	0.279	0.147	0.098	0.204	**0.001**	**similarity**
DERCYLLIDAS	1	0	NA	NA	NA	NA	NA	NA
DILUCIDA	40	780	0.345	0.148	0.113	0.187	**0.001**	**similarity**
DOTO	15	105	0.223	0.149	0.094	0.214	**0.034**	**similarity**
DUESSA	4	6	0.036	0.145	0.026	0.306	0.079	**dissimilarity**
DUILLIA	3	3	0.374	0.149	0.006	0.368	**0.046**	**similarity**
EGRA	11	55	0.221	0.148	0.081	0.228	0.066	**similarity**
EURIMEDIA	35	595	0.216	0.147	0.112	0.185	**0.001**	**similarity**
EXCELSA	18	153	0.288	0.148	0.097	0.209	**0.001**	**similarity**
HEMIXANTHE	7	21	0.414	0.148	0.064	0.253	**0.001**	**similarity**
HERMIAS	53	1378	0.254	0.147	0.119	0.178	**0.001**	**similarity**
HEWITSONI	30	435	0.244	0.148	0.106	0.191	**0.001**	**similarity**
HUMBOLDT	1	0	NA	NA	NA	NA	NA	NA
ILLINISSA	6	15	0.181	0.151	0.054	0.273	0.312	**similarity**
LERIDA	66	2145	0.222	0.148	0.121	0.176	**0.001**	**similarity**
LIBETHRIS	21	210	0.187	0.15	0.103	0.205	0.132	**similarity**
LYSIMNIA	5	10	0.268	0.144	0.043	0.284	0.067	**similarity**
MAELUS	16	120	0.277	0.146	0.092	0.208	**0.003**	**similarity**
MAMERCUS	64	2016	0.233	0.147	0.12	0.177	**0.001**	**similarity**
MANTINEUS	5	10	0.48	0.147	0.048	0.281	**0.001**	**similarity**
MESTRA	14	91	0.247	0.149	0.09	0.22	**0.014**	**similarity**
MOTHONE	14	91	0.303	0.147	0.086	0.218	**0.001**	**similarity**
OCNA	13	78	0.216	0.149	0.084	0.221	0.066	**similarity**
ORESTES	16	120	0.386	0.146	0.093	0.205	**0.001**	**similarity**
OZIA	19	171	0.166	0.147	0.098	0.207	0.266	**similarity**
PANTHYALE	39	741	0.205	0.148	0.113	0.185	**0.012**	**similarity**
PARALLELIS	7	21	0.359	0.147	0.065	0.256	**0.005**	**similarity**

PAVONII	2	1	0.141	0.145	0	0.469	0.384*	**dissimilarity**
POLITA	10	45	0.221	0.151	0.081	0.236	0.088	**similarity**
PRAESTANS	1	0	NA	NA	NA	NA	NA	NA
PRAXILLA	9	36	0.245	0.15	0.072	0.245	**0.048**	**similarity**
QUINTINA	6	15	0.325	0.148	0.051	0.267	**0.013**	**similarity**
SINILIA	9	36	0.113	0.146	0.074	0.233	0.285*	**dissimilarity**
SUSIANA	20	190	0.252	0.148	0.103	0.209	**0.005**	**similarity**
THABENA-F	11	55	0.231	0.148	0.085	0.228	**0.044**	**similarity**
THEUDELINDA	8	28	0.395	0.147	0.072	0.242	**0.001**	**similarity**
TICIDA-M	8	28	0.525	0.147	0.069	0.247	**0.001**	**similarity**
UMBROSA	3	3	0.243	0.153	0.006	0.361	0.188	**similarity**
VESTILLA	1	0	NA	NA	NA	NA	NA	NA

Appendix 10: Phylogenetic signal in the evolution of climatic niches and mimetic wing patterns

The pattern of correlation between climatic conditions and mimicry rings could arise from phylogenetic inertia in both the evolution of mimicry patterns and the climatic niche of species (Losos 2008). Therefore, we tested for the presence of phylogenetic signal in those two ecological aspects.

To test for phylogenetic signal in wing patterns, we computed the mean phylogenetic distance (MPD) among comimetic Operational Mimicry Units (OMUs). To assess the significance of the MPD, we generated via permutations a null distribution of this statistic modeling the absence of phylogenetic signal. The p-value of this test corresponds to the probability of obtaining a lower value for the MPD of comimetic OMUs than the values in the null distribution. Mimicry patterns did indeed show a significant phylogenetic signal. The mean pairwise phylogenetic distance between comimetic OMUs was lower than expected at random (i.e., when mimicry patterns are shuffled among OMUs; **Fig. S10.A**. MPD = 34.43 My, 999 permutations, $p \leq 0.001$). Twenty-three putative mimicry rings among the 39 for which the analysis could be performed (i.e., those having more than one OMU and thus with at least one pair) showed a significant phylogenetic signal in the distribution of their pattern in the phylogeny. Six mimicry rings showed the opposite pattern of significant phylogenetic overdispersion. A detailed summary for each mimicry ring is available in **Table S5**.

To assess the presence of phylogenetic signal in the evolution of climatic niche, we computed the generalized version of Blomberg's K statistic for multivariate traits (K_{mult} ; Blomberg *et al.* 2003; Adams 2014) using the R package *geomorph* (Adams *et al.* 2018). The original univariate statistic estimates the phylogenetic signal as the ratio of observed to expected phenotypic variation, given the phylogeny and a Brownian motion (BM) model of evolution (Blomberg *et al.* 2003). Its expected value under BM is K = 1, while a lower value indicates higher phenotypic variation among closely related species and a higher value shows phylogenetic conservatism (i.e., when traits across closely related species are even more similar than expected following evolution under BM). Its multivariate counterpart, the K_{mult}, takes into account the covariation between the different dimensions of a trait (i.e., the bioclimatic variables defining the climatic niche). Similarly to the K statistic, the significance of the K_{mult} is assessed by permuting data on the tips of the phylogeny and generating a null distribution that models the absence of phylogenetic signal. The p-value of this test corresponds to the

probability of obtaining a higher value for K_{mult} in the null distribution than the observed value, thereby indicating that the climatic niche is more similar among closely related species than expected at random (Adams 2014). The K_{mult} appeared to be higher than expected under the null hypothesis (i.e., permutations of climatic niches among species on the phylogeny; **Fig. S10.B**. K_{mult} obs = 0.120, 999 permutations, p = 0.013). Similarly, the likelihood ratio test between a macroevolutionary model of the climatic niche with an optimized λ (H_1) and a null model with a λ fixed to zero (H_0) revealed a low (λ = 0.41) yet significant phylogenetic signal (LRT - Khi² test, $\chi = 20.57$, df = 1, $p < 0.001$).

References:

Adams, D. C. (2014). A generalized K statistic for estimating phylogenetic signal from shape and other high-dimensional multivariate data. Systematic biology, 63(5), 685-697. https://doi.org/10.1093/sysbio/syu030

Adams, D. C., Collyer, M. L., Kaliontzopoulou, A. (2018) R package geomorph: Software for geometric morphometric analyses. R package version 3.0.6. https://cran.r-project.org/package=geomorph

Blomberg, S. P., Garland Jr, T., & Ives, A. R. (2003). Testing for phylogenetic signal in comparative data: behavioral traits are more labile. Evolution, 57(4), 717-745. https://doi.org/10.1111/j.0014-3820.2003.tb00285.x

Losos, J. B. (2008). Phylogenetic niche conservatism, phylogenetic signal and the relationship between phylogenetic relatedness and ecological similarity among species. Ecology letters, 11(10), 995-1003. https://doi.org/10.1111/j.1461-0248.2008.01229.x

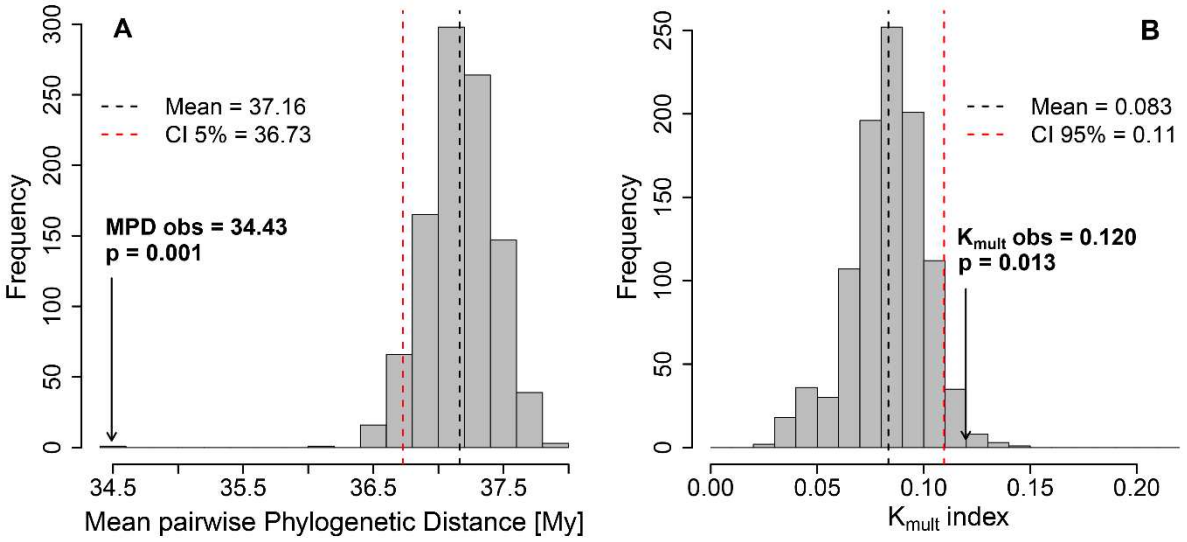

Figure S10: Tests for phylogenetic signal in the evolution of mimicry pattern and climatic niche. **(A)** Null distribution of the mean pairwise phylogenetic distance (MPD) among comimetic species with mimicry pattern randomized 999 times on the phylogeny. An observed MPD lower than the 5% quantile shows the presence of phylogenetic signal in the evolution of mimicry patterns. **(B)** Null distribution of the K_{mult} statistic (103) with 999 permutations of climatic niche on the phylogeny. An observed K_{mult} higher than the 95% quantile shows the presence of phylogenetic signal in the evolution of climatic niche.

Table S5: Permutation tests for phylogenetic signal in the evolution of each mimicry ring. Tests were based on mean pairwise phylogenetic distance (MPD) among comimetic Operational Mimicry Units (OMUs) within each mimicry ring. N OMUs = Number of OMUs in the mimicry ring. N pairs = Number of pairs tested for this mimicry ring. Mean MPD obs = Average mean pairwise phylogenetic distance among comimetic OMUs observed. Mean null MPD = Average mean pairwise phylogenetic distance among comimetic OMUs for 999 randomizations of mimicry patterns among OMUs. CI 2.5% = MPD value for quantile 2.5% in the null distribution. CI 97.5% = MPD value for quantile 97.5% in the null distribution. Bold p-values are significative for an $\alpha = 0.05$. p-values with an asterisk are computed for a right-tail test (i.e., p-value* = 1 – p-value) meaning they are assessing presence or absence of phylogenetic overdispersion in the mimicry ring pattern, while initial p-values are assessing presence or absence of phylogenetic clustering (i.e., phylogenetic signal). Green p-values are significant for clustering. Blue p-values are significant for overdispersion.

Mimicry ring	N OMUs	N pairs	Mean MPD obs	Mean null MPD	CI 2.5%	CI 97.5%	p-value
ACRISIONE	1	0	NA	NA	NA	NA	NA
AGNOSIA	74	2701	31.784	37.16	34.928	39.277	**0.001**
AMALDA	9	36	33.275	37.104	30.327	43.517	0.158
AURELIANA	12	66	25.939	37.213	31.697	42.859	**0.001**
BANJANA-M	43	903	32.787	37.127	34.193	39.974	**0.001**

CONFUSA	19	171	41.67	37.176	32.699	41.654	**0.025***
DERCYLLIDAS	1	0	NA	NA	NA	NA	NA
DILUCIDA	35	595	37.864	37.14	33.967	40.138	0.334*
DOTO	12	66	31.553	37.152	31.552	42.729	**0.025**
DUESSA	3	3	23.002	37.393	23.579	50.981	**0.023**
DUILLIA	3	3	20.439	37.415	24.417	48.155	**0.018**
EGRA	10	45	30.232	37.213	30.583	43.369	**0.023**
EURIMEDIA	33	528	36.452	37.074	33.566	40.189	0.358
EXCELSA	17	136	43.615	37.025	32.305	41.653	**0.001***
HEMIXANTHE	5	10	38.464	37.206	27.681	46.539	0.439*
HERMIAS	47	1081	41.073	37.129	34.444	39.866	**0.001***
HEWITSONI	27	351	30.914	37.117	33.227	40.707	**0.001**
HUMBOLDT	1	0	NA	NA	NA	NA	NA
ILLINISSA	6	15	32.855	37.302	29.033	45.084	0.157
LERIDA	63	1953	31.529	37.144	34.774	39.366	**0.001**
LIBETHRIS	20	190	24.444	37.071	32.763	41.437	**0.001**
LYSIMNIA	4	6	48.133	37.373	25.917	48.543	**0.033***
MAELUS	15	105	42.965	37.132	32.389	42.117	**0.008***
MAMERCUS	56	1540	40.479	37.246	34.894	39.602	**0.003***
MANTINEUS	5	10	41.883	37.042	27.626	46.551	0.192
MESTRA	14	91	31.47	37.321	32.281	42.597	**0.012**
MOTHONE	12	66	36.728	37.22	31.793	42.728	0.441
OCNA	13	78	28.457	37.026	31.595	42.333	**0.001**
ORESTES	15	105	41.555	37.127	32.248	42.221	0.05*
OZIA	16	120	30.628	37.183	32.688	42.132	**0.001**
PANTHYALE	38	703	30.591	37.199	34.053	40.232	**0.001**
PARALLELIS	7	21	39.086	37.394	29.93	45.421	0.339*
PAVONII	2	1	12.271	37.314	11.078	52.878	**0.028**
POLITA	9	36	29.048	37.128	30.806	43.569	**0.011**
PRAESTANS	1	0	NA	NA	NA	NA	NA
PRAXILLA	9	36	27.626	37.395	30.661	44.486	**0.003**
QUINTINA	6	15	22.756	37.264	28.592	45.14	**0.001**
SINILIA	8	28	28.209	37.473	31.015	44.202	**0.005**
SUSIANA	18	153	31.503	37.219	32.761	41.624	**0.006**
THABENA-F	10	45	27.166	37.217	30.94	43.474	**0.002**
THEUDELINDA	8	28	30.391	37.113	30.351	44.293	**0.028**
TICIDA-M	8	28	35.186	37.339	30.189	44.34	0.325
UMBROSA	3	3	16.834	36.915	21.843	48.056	**0.012**
VESTILLA	1	0	NA	NA	NA	NA	NA

Appendix 11: Simulation of neutral evolution of the climatic niche

In order to disentangle similarity in wing patterns and climatic niches due to shared ancestry from that due to evolutionary convergence (i.e., exceeding expectations from shared ancestry alone), we took phylogeny into account in our analyses. We used comparative phylogenetic methods based on the simulation of stochastic evolution of continuous characters (Elias *et al.* 2008; Chazot *et al.* 2014) to simulate random evolution of the mean bioclimatic conditions of our species with the R package *phylocurve* 2.1.1 (Goolsby 2015). We applied first a phylogenetic PCA transformation (pPCA; Revell 2009) on our four bioclimatic variables in order to limit the number of dimensions and reduce risks of model misspecification (Adams & Collyer 2018). Then, we used the R package *motmot.2.0* 1.1.2 (Puttick *et al.* 2018) to test for the fit of several neutral multivariate macroevolutionary models.

A classic Brownian Motion model (BM) simulating evolution in random direction of the niche space may not be optimal to model the neutral evolution of the climatic niche. For instance, punctuated evolution patterns can arise from the interaction between geographic barriers and dispersal (Boucher *et al.* 2014). Therefore we tested fits for models involving branch length transformations on the phylogenetic tree by implementing Pagel's Lambda (λ) and/or Pagel's Kappa (κ ; Pagel 1994, 1999) parameters. λ quantifies the intensity of phylogenetic signal in the data. In practice, all internal branches are multiplied by λ, and the value providing the best fit to the trait data is estimated. λ close to 1 (i.e., no transformation) equals a BM and is a sign of phylogenetic signal, while λ close to 0 illustrates the absence of phylogenetic structure. κ models the extent of punctuated evolution associated with cladogenesis. In practice, all branch lengths are raised to the power κ, and the value best fitting the trait data is estimated. For κ close to 0, all branch lengths are equal to 1 and trait evolution is strictly associated with cladogenesis. For κ close to 1, trait evolution follows a BM. All model fits were compared using AICc and Likelihood Ratio Tests. The best model according to the minimum AIC was the model including both a κ and a λ parameter for branch lengths transformation (**Table S6**).

Table S6: Comparison of the fit and estimated parameters of multivariate macroevolutionary models to the first two principal components of the pPCA applied on our four bioclimatic variables. BM = Brownian Motion model. p = number of parameters additionally to a BM, included in the AICc penalization. AICc = Akaike's corrected Information Criterion.

Evolutionary model	p	Likelihood	AICc	lambda (λ)	kappa (κ)
BM	0	-1689.36	3382.756	-	-
Lambda	1	-1506.043	3018.158	0.408	-
Kappa	1	-1553.857	3113.786	-	0.169
Kappa - Lambda	2	-1503.552	3015.224	0.01	0.39

The likelihood ratio test between the Lambda model (H_0) and the Kappa – Lambda model (H_1) confirmed the significance of the improvement achieved by the inclusion of a kappa parameter (LRT - Khi² test, $\chi = 4.18$, df = 1, $p = 0.041$). However, since the optimal λ parameter estimated for the Kappa – Lambda model tended to be very close to zero (i.e., $\lambda = 0.01$) and would have led to a phylogenetic tree harboring a unique basal polytomy denying the existence of phylogenetic signal in climatic niche, we decided to keep the Lambda model for our simulations.

The reason behind the odd value for the estimated λ in the Kappa-Lambda model can be found in the topography of the likelihood landscape of the Kappa-Lambda model, since this model presents a wide plateau of optimality (**Fig. S11**). In consequence, combination of $\lambda = 0.4$ and $\kappa = 0.8$ were nearly suboptimal in comparison to the actual estimated optimum for $\lambda = 0.01$ and $\kappa = 0.39$. However, those two combinations of parameters describe a very different macroevolutionary reality, the former showing rather strong phylogenetic signal while the latter, and optimal one denies the presence of phylogenetic signal. Therefore, because of this plateau in the optimization of the likelihood, we cannot be confident in the estimation of the lambda and kappa parameters for this model. This exploration confirms our choice to keep the simpler Lambda model (with $\lambda = 0.408$) rather than this uncertain Kappa – Lambda model.

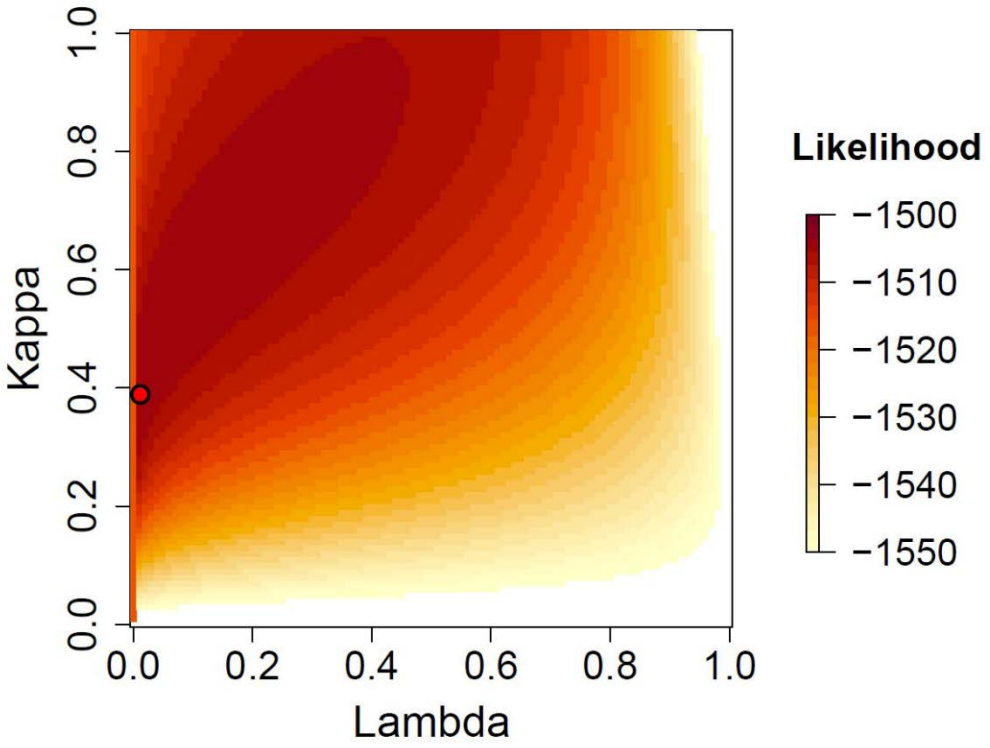

Figure S11: Likelihood landscape of the Lambda-Kappa multivariate macroevolutionary model while varying the lambda (x-axis) and kappa (y-axis) parameters. The red dot represents the estimated optimal combination of parameters to maximize the likelihood (i.e., lambda = 0.01 & kappa = 0.39).

Finally, we selected a Brownian Motion with an additional Pagel's λ parameter (λ = 0.408) to simulate the neutral evolution of the climatic niche accounting for the intensity of the phylogenetic signal. To account for differences between OMUs of the same polymorphic species, we first simulated data at species-level on the phylogeny then added an intra-species variance component drawn for gaussian distributions based on observed variance of niches within each species to simulate data for each OMU.

References:

Adams, D. C., & Collyer, M. L. (2018). Multivariate phylogenetic comparative methods: evaluations, comparisons, and recommendations. Systematic biology, 67(1), 14-31. https://doi.org/10.1093/sysbio/syx055

Boucher, F. C., Thuiller, W., Davies, T. J., & Lavergne, S. (2014). Neutral biogeography and the evolution of climatic niches. The American Naturalist, 183(5), 573-584. https://doi.org/10.1086/675506

Chazot, N., Willmott, K. R., Santacruz Endara, P. G., Toporov, A., Hill, R. I., Jiggins, C. D., & Elias, M. (2014). Mutualistic mimicry and filtering by altitude shape the structure of Andean butterfly communities. The American Naturalist, 183(1), 26-39. https://doi.org/10.1086/674100

Elias, M., Gompert, Z., Jiggins, C., & Willmott, K. (2008). Mutualistic interactions drive ecological niche convergence in a diverse butterfly community. PLoS biology, 6(12), e300. https://doi.org/10.1371/journal.pbio.0060300

Goolsby, E. W. (2015). Phylogenetic comparative methods for evaluating the evolutionary history of function-valued traits. Systematic biology, 64(4), 568-578. https://doi.org/10.1093/sysbio/syv012

Pagel, M. (1994). Detecting correlated evolution on phylogenies: a general method for the comparative analysis of discrete characters. Proceedings of the Royal Society of London. Series B: Biological Sciences, 255(1342), 37-45. https://doi.org/10.1098/rspb.1994.0006

Pagel, M. (1999). Inferring the historical patterns of biological evolution. Nature, 401(6756), 877-884. https://doi.org/10.1038/44766

Puttick, M., Thomas, G., Freckleton, R., Ingram, T., Paradis, E., Orme, D. (2018) motmot.2.0: Models of Trait Macroevolution on Trees. R package version 1.1.2. https://cran.r-project.org/package=motmot.2.0

Revell, L. J. (2009). Size-correction and principal components for interspecific comparative studies. Evolution: International Journal of Organic Evolution, 63(12), 3258-3268. https://doi.org/10.1111/j.1558-5646.2009.00804.x

Appendix 12: Climatic niche convergence per mimicry ring

Table S7: Summary of simulation tests for the convergence of the climatic niche following mimicry patterns based on standardized climatic distance (MCD) among comimetic Operational Mimicry Units (OMUs) from each mimicry ring. N OMUs = Number of OMUs in the mimicry ring. N pairs = Number of pairs tested for this mimicry ring. Mean MCD obs = Mean climatic distance among comimetic OMUs observed. Mean null MCD = Average Mean climatic distance among comimetic OMUs for 999 simulations of climatic niche evolution. CI 2.5% = MCD value for quantile 2.5% in the null distribution. CI 97.5% = MCD value for quantile 97.5% in the null distribution. Bold p-values are significative for an $\alpha = 0.05$. The p-value with an asterisk is computed for a right-tail test (i.e., p-value* = 1 – p-value) meaning it is assessing divergence of the climatic niche, while initial p-values are assessing convergence. Green p-values are significant for convergence.

Mimicry ring	N OMUs	N pairs	Mean MCD obs	Mean null MCD	CI 2.5%	CI 97.5%	p-value
ACRISIONE	1	0	NA	NA	NA	NA	NA
AGNOSIA	74	2701	0.913	0.954	0.851	1.069	0.239
AMALDA	9	36	0.439	0.92	0.615	1.244	**0.002**
AURELIANA	12	66	0.657	1.01	0.726	1.362	**0.008**
BANJANA-M	43	903	0.673	0.934	0.795	1.09	**0.001**
CONFUSA	19	171	0.867	0.984	0.761	1.242	0.17
DERCYLLIDAS	1	0	NA	NA	NA	NA	NA
DILUCIDA	35	595	0.366	0.986	0.817	1.149	**0.001**
DOTO	12	66	0.616	1.086	0.789	1.425	**0.001**
DUESSA	3	3	0.823	0.992	0.358	1.696	0.339
DUILLIA	3	3	0.159	0.913	0.355	1.61	**0.002**
EGRA	10	45	0.319	1.035	0.68	1.419	**0.001**
EURIMEDIA	33	528	0.947	0.976	0.799	1.156	0.387
EXCELSA	17	136	0.588	1.049	0.785	1.31	**0.001**
HEMIXANTHE	5	10	0.14	1.153	0.63	1.776	**0.001**
HERMIAS	47	1081	0.771	1.054	0.898	1.212	**0.001**
HEWITSONI	27	351	0.404	0.951	0.773	1.146	**0.001**
HUMBOLDT	1	0	NA	NA	NA	NA	NA
ILLINISSA	6	15	0.31	1.188	0.682	1.804	0.001
LERIDA	63	1953	1.014	0.953	0.834	1.074	0.173*
LIBETHRIS	20	190	0.733	0.905	0.704	1.139	**0.049**
LYSIMNIA	4	6	0.481	1.177	0.542	1.942	**0.013**
MAELUS	15	105	0.628	1.132	0.839	1.45	**0.002**
MAMERCUS	56	1540	0.867	1.076	0.928	1.22	**0.003**
MANTINEUS	5	10	0.286	0.948	0.494	1.451	**0.001**
MESTRA	14	91	0.42	0.917	0.687	1.16	**0.001**
MOTHONE	12	66	0.532	1.054	0.728	1.377	**0.001**

OCNA	13	78	0.535	0.922	0.656	1.184	**0.001**
ORESTES	15	105	0.428	1.115	0.825	1.438	**0.001**
OZIA	16	120	0.62	0.917	0.68	1.159	**0.006**
PANTHYALE	38	703	0.574	0.949	0.8	1.116	**0.001**
PARALLELIS	7	21	0.478	1.089	0.668	1.548	**0.003**
PAVONII	2	1	0.63	0.864	0.156	1.884	0.339
POLITA	9	36	0.583	0.885	0.597	1.224	**0.019**
PRAESTANS	1	0	NA	NA	NA	NA	NA
PRAXILLA	9	36	0.357	0.873	0.577	1.199	**0.002**
QUINTINA	6	15	0.349	1.05	0.576	1.598	**0.001**
SINILIA	8	28	0.234	1.146	0.732	1.633	**0.001**
SUSIANA	18	153	0.489	0.902	0.692	1.125	**0.001**
THABENA-F	10	45	0.502	0.973	0.656	1.322	**0.001**
THEUDELINDA	8	28	0.098	1.001	0.632	1.444	**0.001**
TICIDA-M	8	28	0.114	0.993	0.626	1.427	**0.001**
UMBROSA	3	3	0.595	0.819	0.318	1.469	0.233
VESTILLA	1	0	NA	NA	NA	NA	NA

Appendix 13: Distribution of mimicry patterns on the phylogeny

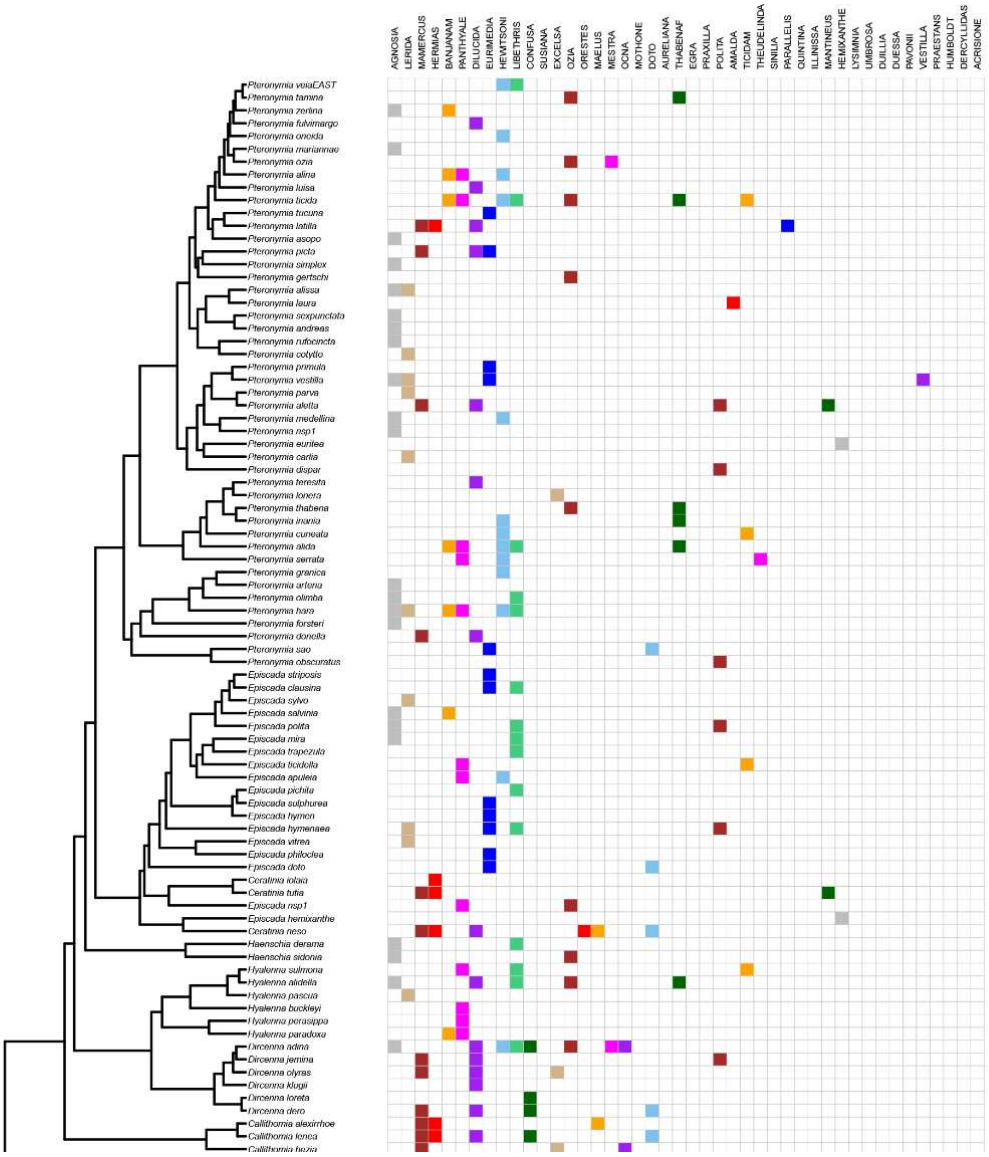

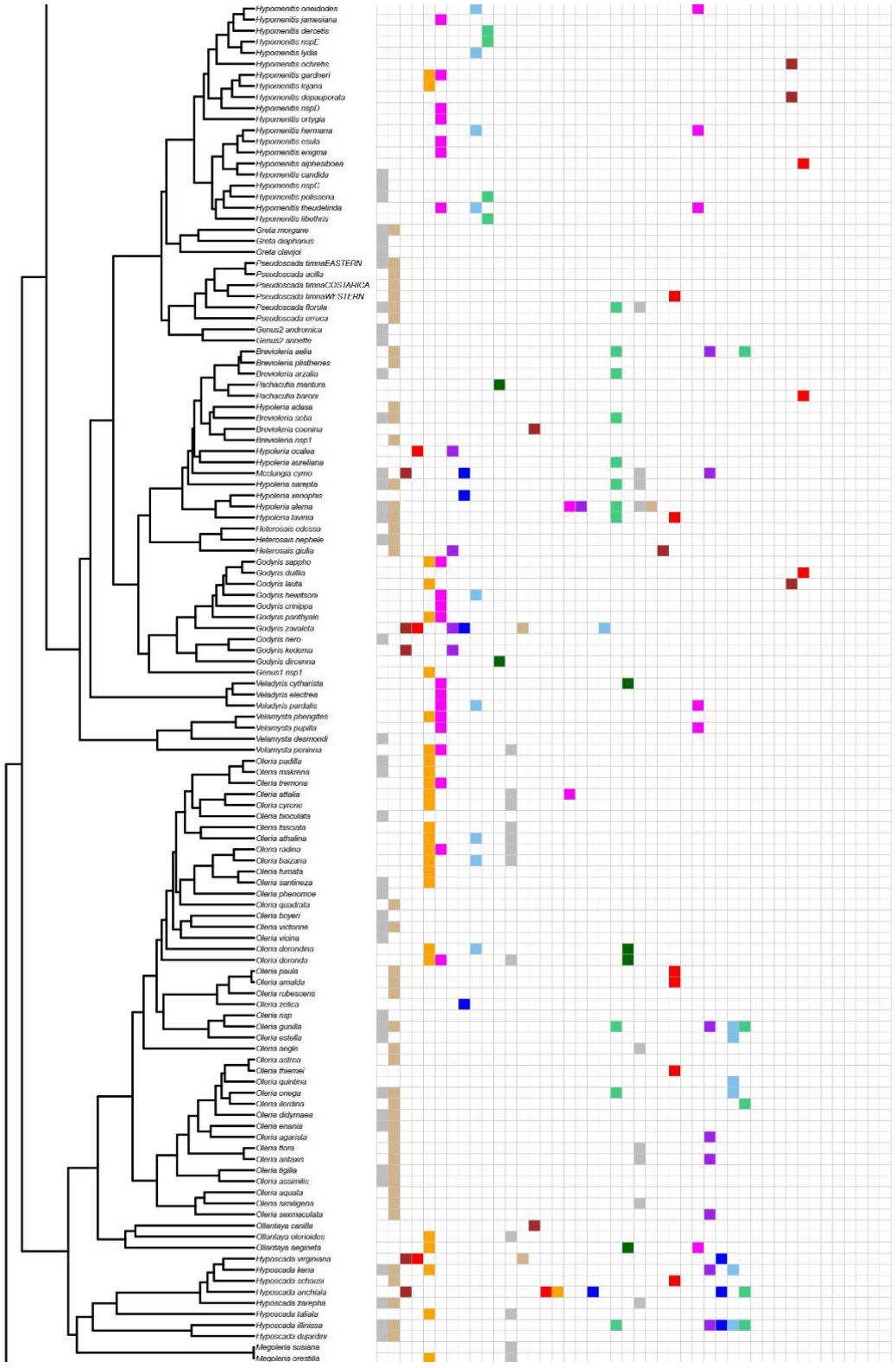
Hypomenitis oneidodes
Hypomenitis jamesiana
Hypomenitis dercetis
Hypomenitis nspE
Hypomenitis lydia
Hypomenitis ochretis
Hypomenitis gardneri
Hypomenitis lojana
Hypomenitis dopauporata
Hypomenitis nspD
Hypomenitis ortygia
Hypomenitis hermana
Hypomenitis esala
Hypomenitis enigma
Hypomenitis alpheiboea
Hypomenitis candida
Hypomenitis nspC
Hypomenitis polissena
Hypomenitis theudelinda
Hypomenitis libetheis
Greta morgane
Greta diaphanus
Greta clavijoi
Pseudoscada timnaEASTERN
Pseudoscada acilla
Pseudoscada timnaCOSTARICA
Pseudoscada timnaWESTERN
Pseudoscada florula
Pseudoscada erruca
Genus2 andromica
Genus2 annette
Brevioleria aelia
Brevioleria plisthenes
Brevioleria arzalia
Pachacutia mantuna
Pachacutia banoni
Hypoleria adasa
Brevioleria soba
Brevioleria coenina
Brevioleria nsp1
Hypoleria ocalea
Hypoleria aureliana
Mcclungia cymo
Hypoleria sarepta
Hypoleria xenophis
Hypoleria alema
Hypoleria lavinia
Heterosais odossa
Heterosais nephele
Heterosais giulia
Godyris sappho
Godyris duilia
Godyris lauta
Godyris hewitsoni
Godyris crinippa
Godyris panthyale
Godyris zavaleta
Godyris niero
Godyris lederna
Godyris dircenna
Genus1 nsp1
Veladyris cytharista
Veladyris electrea
Veladyris pardalis
Velamysta phengites
Velamysta pupita
Velamysta desmondi
Velamysta peninna
Oleria padilla
Olena makrena
Oleria tremona
Oleria attalia
Oleria cyrene
Olena bioculata
Olena fasciata
Oleria athalina
Oleria radina
Oleria baizana
Olena fumata
Oleria santineza
Oleria phenomoe
Oleria quadrata
Olena boyeri
Olena victorine
Oleria vicina
Oleria dorondina
Oleria doronda
Olena paula
Oleria amalda
Oleria rubescens
Oleria zelica
Oleria nsp
Olena gunilla
Oleria estella
Olena aegle
Oleria astrea
Olena thiemei
Oleria quintina
Oleria onega
Olena lerdina
Oleria didymaea
Oleria enania
Oleria agarista
Olena flora
Olena antaxes
Oleria tigilla
Oleria assimilis
Oleria aquala
Olena similgena
Oleria sexmaculata
Ollantaya canille
Ollantaya olerioides
Ollantaya aegineta
Hyposcada virginiana
Hyposcada kena
Hyposcada schausi
Hyposcada anchiala
Hyposcada zarepha
Hyposcada taliata
Hyposcada illinissa
Hyposcada dujardini
Megoleria susiana
Megoleria orestilla

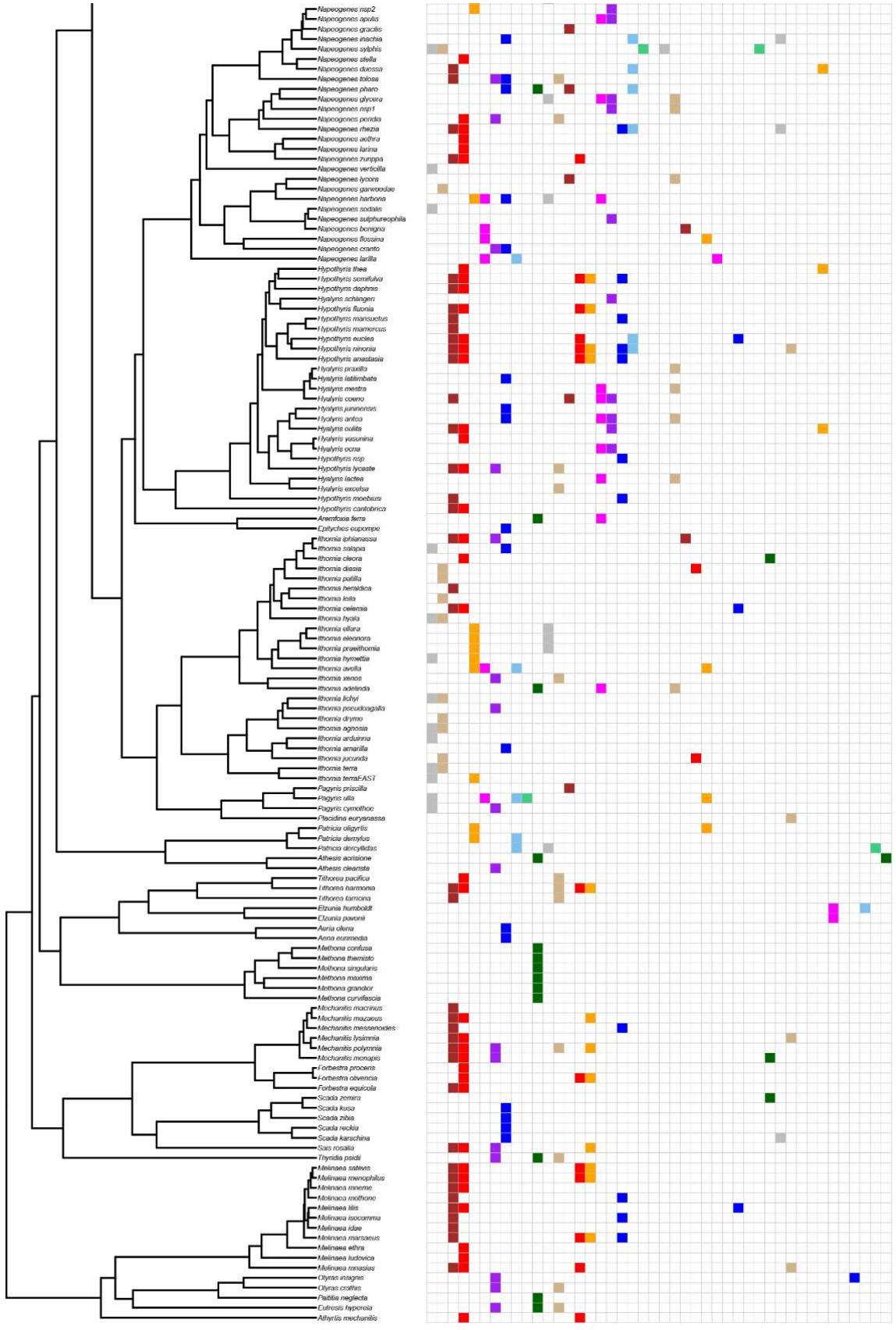
Napeogenes nsp2
Napeogenes apula
Napeogenes gracilis
Napeogenes inachia
Napeogenes sylphis
Napeogenes stella
Napeogenes duessa
Napeogenes tolosa
Napeogenes pharo
Napeogenes glycera
Napeogenes nsp1
Napeogenes peridia
Napeogenes rhezia
Napeogenes aothra
Napeogenes larina
Napeogenes zunippa
Napeogenes verticilla
Napeogenes lycora
Napeogenes garwoodae
Napeogenes harbona
Napeogenes sodalis
Napeogenes sulphureophila
Napeogenes boniqna
Napeogenes flossina
Napeogenes cranto
Napeogenes larilla
Hypothyris thea
Hypothyris semifulva
Hypothyris daphnis
Hyalyris schlingeri
Hypothyris fluonia
Hypothyris mansuetus
Hypothyris mamercus
Hypothyris euclea
Hypothyris ninonia
Hypothyris anastasia
Hyalyris praxilla
Hyalyris latimbata
Hyalyris mestra
Hyalyris coeno
Hyalyris junonnes
Hyalyris antea
Hyalyris oulita
Hyalyris yasunina
Hyalyris ocna
Hypothyris nsp
Hypothyris lycaste
Hyalyris lactea
Hyalyris excelsa
Hypothyris moebius
Hypothyris cantobrica
Aremfoxia ferra
Epityches eupompe
Ithomia iphianassa
Ithomia salapia
Ithomia cleora
Ithomia diasia
Ithomia patilla
Ithomia heraldica
Ithomia leila
Ithomia celemia
Ithomia hyala
Ithomia ellara
Ithomia eleonora
Ithomia praeithomia
Ithomia hymettia
Ithomia ovolla
Ithomia xenos
Ithomia adelinda
Ithomia lichyi
Ithomia pseudagalla
Ithomia drymo
Ithomia agnosia
Ithomia arduinna
Ithomia amarilla
Ithomia jucunda
Ithomia terra
Ithomia terraEAST
Pagyris priscilla
Pagyris ulla
Pagyris cymothoe
Placidina euryanassa
Patricia oligyrtis
Patricia demylus
Patricia dercyllidas
Athesis acrisione
Athesis cleansta
Tithorea pacifica
Tithorea harmonia
Tithorea tarricina
Elzunia humboldt
Elzunia pavonii
Aeria olena
Aeria eurimedia
Methona confusa
Methona themisto
Methona singularis
Methona maxima
Methona grandior
Methona curvifascia
Mechanitis macrinus
Mechanitis mazaeus
Mechanitis messenoides
Mechanitis lysimnia
Mechanitis polymnia
Mechanitis menapis
Forbestra procera
Forbestra olivencia
Forbestra equicola
Scada zemira
Scada kusa
Scada zibia
Scada reckia
Scada karschina
Sais rosalia
Thyridia psidii
Melinaea satevis
Melinaea menophilus
Melinaea mneme
Melinaea mothone
Melinaea lilis
Melinaea isocomma
Melinaea idae
Melinaea marsaeus
Melinaea ethra
Melinaea ludovica
Melinaea mnasias
Oleras insignis
Oleras crathis
Paititia neglecta
Eutresis hyperoia
Athyrtis mechanitis

Figure S12: Heatmap of the 44 mimicry patterns on the phylogeny of the tribe Ithomiini.

The phylogeny from Chazot et al., 2019 includes 339 out of the 396 known species (85.6%).

Mimicry rings are ordered from left to right by frequency of occurrences across the species.

Reference:

Chazot, N., Willmott, K. R., Lamas, G., Freitas, A. V., Piron-Prunier, F., Arias, C. F., Mallet, J., ... & Elias, M. (2019). Renewed diversification following Miocene landscape turnover in a Neotropical butterfly radiation. *Global Ecology and Biogeography*, 28(8), 1118-1132. https://doi.org/10.1111/geb.12919

ANNEXE 6

Müllerian mimicry : one ring to bring them all, and in the jungle bind them

The draft article presented here is the product of an on-going collaboration that followed the completion of a Master's project led by Eddie Pérochon under my supervision during the course of my own PhD research. The project aimed to build upon my findings regarding the patterns of distribution of ithomiine butterflies presented in **Chapter 1** to enlarge the taxonomic scope of the study to another emblematic clade of Neotropical mimetic butterflies involved in mutualistic interactions with ithomiines: the heliconiines (Nymphalidae: Heliconiinae: Heliconiini tribe). Specifically, we confronted biodiversity patterns of heliconiine and ithomiine butterflies throughout the Neotropics, and studied the effects of mutualistic interactions in their respective spatial distributions and niche evolution.

Interestingly, this research project is what triggered in the first place the creation of a new reproducible method to classify wing patterns that later developed in the perceptual approach presented in **Chapter 3**. It resulted in the drafting of a research article which I present below in its current on-going progress.

Müllerian mimicry: one mimicry ring to bring them all, and in the jungle bind them

Eddie Pérochon[1,2], Neil Rosser[3,4], Krzysztof Kozak[5,6], Owen McMillan[5], Marianne Elias[1,5], Maël Doré[1,7]

[1]*Institut de Systématique, Evolution, Biodiversité, MNHN-CNRS-Sorbonne Université-EPHE-Université des Antilles, Muséum national d'Histoire naturelle de Paris, 45 Rue Buffon, 75005, Paris, France*

[2]*Department of Ecology and Evolution, University of Lausanne, Lausanne, Switzerland.*

[3]*Department of Organismic and Evolutionary Biology, Harvard University, Cambridge, Massachusetts, USA*

[4]*Department of Biology, University of York, York, UK*

[5]*Smithsonian Tropical Research Institute, Panamá, Panamá*

[6]*Museum of Vertebrate Zoology, UC Berkeley, USA*

[7]*Centre d'Ecologie et des Sciences de la Conservation, UMR 7204 MNHN-CNRS-Sorbonne Université, Muséum national d'Histoire naturelle de Paris, 45 rue Buffon, 75005, Paris, France*

Reference:

Pérochon, E., Rosser, N., Kozak, K., McMillan O., Elias, M. & Doré, M. (2023). Müllerian mimicry: one mimicry ring to bring them all, and in the jungle bind them. *In prep.*

Author contributions:

EP, ME and MD conceived the study and designed the analyses. NR, KK, & OMM provided occurrence data. KK provided the phylogenetic trees. MD aggregated the database. EP curated the database. EP & MD wrote the R scripts. EP carried out the analyses, produced all maps, results and figures, and led the manuscript writing.

Abstract

In the face of global change, understanding the mechanisms underlying species distributions and coexistence is essential to predict and prevent future disturbances, even more so for biodiversity hotspots such as the Neotropics. In particular, the effect of biotic interactions may be challenging to investigate at large spatial scales. Taking advantage of the well-characterized Müllerian mimetic systems of neotropical butterflies, we investigated the effects of mutualistic mimetic interactions on large-scale spatial distributions and species niche evolution within and between two emblematic tribes of unpalatable neotropical butterflies separated by 85 My of evolutionary time, yet harbouring similar warning signals: the Heliconiini (Nymphalidae: Heliconiinae) and the Ithomiini (Nymphalidae: Danainae).

We showed that both tribes display high diversity and concentration of rare species and mimicry patterns in the Tropical Andes, where anthropogenic pressures levels are high. Although, we detected differences in global biodiversity patterns between the two tribes likely due to differences in biogeographic histories, we showed that mimicry drives large scale spatial association among phenotypically similar species, both within and between tribes, providing new empirical evidence for the unfolding of Müller's model at a macroecological scale. Furthermore, comparative phylogenetic analyses suggested that mimetic interactions drive the evolutionary convergence of the climatic niche of comimetic species within and even across tribes, thereby strengthening their co-occurrence.

Altogether, our study highlights the power of mutualistic interactions in shaping large scale distribution patterns and driving species niche convergence across evolutionary distant lineages. Critically, our findings emphasize the vulnerability of mutualistic communities tied by positive interactions to community disassembly induced by climate change.

Keywords

biodiversity hotspots, comparative phylogenetic analyses, heliconiines, ithomiines, mimicry rings, Müllerian mimicry, Neotropical butterflies, niche convergence, spatial co-occurrence.

1 Introduction

Biotic interactions known to structure ecological communities (Bascompte 2009) but, counterintuitively, their impact on biodiversity patterns remains difficult to quantify, especially at large spatial scales (Gaüzère *et al.* 2022; Windsor *et al.* 2023). There is a large diversity of biotic interactions, typically characterized by their effects on the fitness of interacting partners with negative effects such as exploitative competition, positive effects such as facilitation, or both such as predation. Ecologists also distinguish between intra-guild interactions occurring among species from the same ecological guild (i.e., sharing similar ecological roles or functions in the ecosystem) such as competition between predators for a similar prey resource, and interguild interactions occurring between species from different ecological guilds, such as predators and prey. Ecological interactions underlies numerous complex ecological and evolutionary processes that involves virtually all organisms on Earth forming what have been labeled as the web of Life (Bascompte 2009).

Among this diversity of ecological interactions, intraguild mutualistic interactions remains some of the most understudied ones, particularly compared to other interactions such as predation and competition (Elias *et al.* 2009a). Such interactions within communities may involve from two unique individuals, such as a grouper and a moray eel patrolling the coral reef together, taking advantage of the complementary nature of their hunting abilities (Bshary *et al.* 2006), to entire communities such as multispecies assemblages of frugivorous monkeys in the African equatorial forest, cooperating for food detection and predator warning (Stensland *et al.* 2003). Despite their relative oversight, intraguild mutualistic interactions can have important consequences on both trait evolution and geographic distributions of involved organisms. They are predicted to favor evolutionary convergence of traits that enhance the co-occurrence of species, hence increasing benefits from such positive interactions, and leading to higher species ecological similarity in communities (Bruno *et al.* 2003; Thompson 2005; Elias *et al.* 2009a; Nuismer *et al.* 2013; Aubier & Elias 2020; Doré *et al.* 2023) in contrast to spatial and phenotypical divergence driven by negative intraguild interactions (Brown & Wilson 1956; Webb *et al.* 2002; Dayan & Simberloff 2005).

The sampling of ecological interactions involved substantial costs in time and resources associated with the detection and characterization of the interactions such as in gut content analyses for trophic networks, records of flower visitation for pollination networks, curation of camera trap videos to identify plant-seed dispersers networks, etc. Although we witnessed

recent international efforts to aggregate and standardize ecological interactions datasets in openly accessible databases (GloBI: Poelen *et al.* (2014); Interaction Web DataBase: www.ecologia.ib.usp.br/iwdb/; Web of Life: www.web-of-life.es), there are still many gaps in our global knowledge of the biogeography of ecological interactions (Poisot *et al.* 2021).

In order to partly fill this gap, and address the effect of intraguild mutualistic interactions at large spatial scales, Müllerian mimicry appears as an ideal case study. Müllerian mimicry is a type of mutualistic interactions that involves species that evolved similarity in traits associated with predator deceiving characteristics. This similarity is characterized by shared visual, behavioral, chemical or acoustic signals, which are labeled as "honest" because they are used to warn predators for existing predatory-deceiving traits such as unpalatability, harmfulness, and evasiveness (Ruxton *et al.* 2004; Sherratt 2008). Species that interact through mimicry form groups called 'mimicry rings' (Papageorgis 1975; Joron & Mallet 1998). Such interactions are considered mutualistic because the species involved are sharing the cost of educating predators to avoid their pattern. The more abundant are the individuals that are sharing warning patterns, the less the cost for each species (Müller 1879). Müllerian mimicry has been described in many groups including birds, several taxonomic orders of insects, snakes, fishes, and amphibians (Dumbacher & Fleischer 2001; Symula *et al.* 2001; Williams 2007; Alexandrou *et al.* 2011; Wilson *et al.* 2015; Muñoz-Ramírez *et al.* 2016; Motyka *et al.* 2021). This wide taxonomic distribution and numerous independent emergences reinforce the idea that Mullerian mimicry represents a selective advantage for defended prey (Sherratt 2008). Contrary to many ecological interactions, Müllerian mimicry relatively straightforward to characterize: in a given community, individuals sharing their warning signal (i.e., from the same mimicry ring) are engaged in mimetic interactions with each other, while individuals from different mimicry rings do not interact, at least through mimicry. Therefore, in this study we offer to use Müllerian mimicry as a case study to investigate the consequences of intraguild mutualistic interactions on community structures and species niche evolution at large spatial scales.

Both founders of the theoretical background for the two main documented types of defensive mimicry, Fritz Müller (Müllerian mimicry) and Henri Walter Bates (Batesian mimicry), studied the neotropical Heliconiine and Ithomiine butterflies (Nymphalidae: Heliconiini & Ithomiini tribes), which were instrumental in building their respective theories. All species in these tribes appear unpalatable to predators. They acquire this defensive ability through the accumulation of toxic chemical compounds retrieved as caterpillars from their Passifloraceae host plants in the case of heliconiines (Castro & Zurano 2019), and from feeding

on decaying Boraginaceae and Asteraceae flowers for Ithomiini (Brown Jr 1984). Both tribes are widely distributed across the American continent, from Canada (Heliconiini) and Mexico (Ithomiini) to the North of Argentina. Throughout this wide range, many species are interacting via Müllerian mimicry harboring locally similar wing patterns making them ideal candidates to study the effects of intraguild mutualistic interactions at large spatial scales.

The tribe Heliconiini contains 8 genera, 77 species and 457 subspecies (Kozak *et al.* 2015; Jiggins & Lamas 2016). There is a large diversity of wing patterns in this tribe and some species like *Heliconius erato* shows a striking intra-specific diversity of forms (**Fig. 1.a**). The tribe Ithomiini contains 42 genera, 396 species and 1542 subspecies (Chazot *et al.* 2019b). They are well-known for some species like *Greta morgane* which possess partly transparent wings (**Fig. 1.a**). Despite being phylogenetically distant by approximately 86 My (**Fig. 1.b;** Espeland *et al.* 2018; Chazot *et al.* 2019a), the same distance from humans to flying lemurs (Order: Dermoptera; Upham *et al.* 2019), the two tribes share numerous warning patterns, thus still interact through mimetic interactions (**Fig. 1.a**).

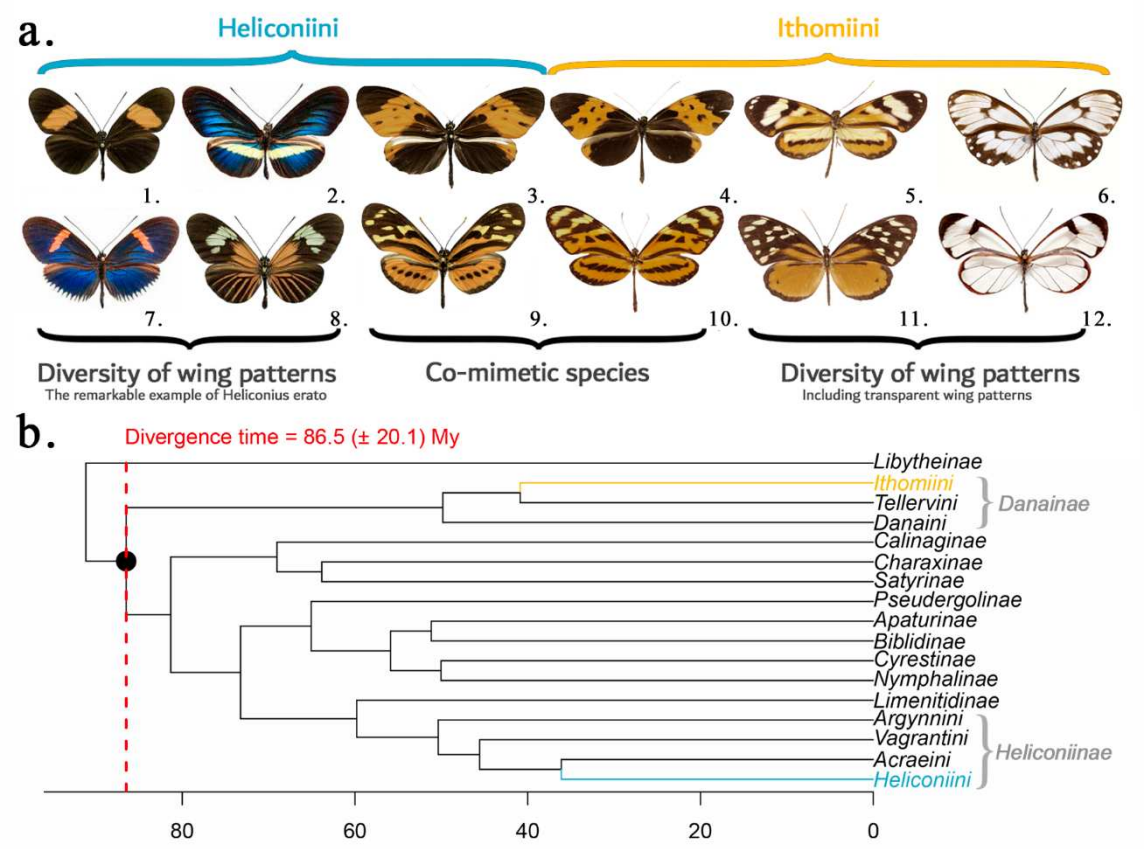

Figure 1. (a) Illustration of the diversity of wing patterns within and between tribes for Ithomiini and Heliconiini. The four central subspecies represent examples of subspecies that share similar wing patterns and take part into Müllerian mimicry interactions. From 1 to 12 : *Heliconius erato adana*, *Heliconius erato chestertonii*, *Heliconius numata bicoloratus, Melinaea isocomma simulator*,

Hypothyris ninonia daeta, *Veladyris pardalis christina*, *Heliconius erato cyrbia*, *Heliconius erato luscombei*, *Eueides isabella dissoluta*, *Mechanitis lysimnia utemaia, Tithorea harmonia helicaon*, *Greta morgana oto*. **(b)** Phylogeny of the Nymphalidae family (Espeland *et al.* 2018). Tip labels represent butterfly subfamilies except for Danainae and Heliconiinae which are divided in tribes. The red-dotted line represents the estimated divergence time between Heliconiini and Ithomiini tribes.

Previous studies have investigated independently the macroecological patterns of diversity in ithomiine (Doré *et al.* 2022) and heliconiine butterflies. A recent study on Ithomiini showed that mutualistic interactions has led to both large scale spatial associations and climatic niche evolutionary convergences between co-mimetic species (i.e., species that are in the same mimicry ring) in this clade (Doré *et al.* 2023). Nevertheless, no study has yet investigated in an integrated framework the two tribes, a crucial step to jointly define mimicry rings, and to understand the role of mimetic interactions into shaping the continental-scale distribution of interacting species, as such defining the structure and composition of communities.

Considering the lack of knowledge in the importance of mutualistic interactions in shaping global diversity patterns, the present study aims to:

(1) Map Heliconiini diversity patterns and to investigate potential differences and similarities with Ithomiini.

(2) Test whether mutualistic interactions between Heliconiini and Ithomiini shape co-occurrence of co-mimetic species at large spatial scales, within and between tribes.

(3) Test whether mutualistic interactions jointly drives the convergence of the climatic niche of co-mimetic species within and between tribes.

2 Materials and Methods

2.1 Mimicry classification

We classified butterfly wing patterns in groups of phenotypically similar patterns (i.e., hypothesized phenotypic mimicry rings as in Doré *et al.* 2023). Such mimicry rings may not represent mutualistic interactions, because the members of the ring may not actually cooccur. As such, they are hypotheses of 'putative mimicry rings'. If a significant signal of spatial co-occurrence is detected, then they can qualify as 'effective mimicry rings' tentatively depicting true ecological interactions (Sanders *et al.* 2006; Wilson *et al.* 2022). We collected at least one picture of dorsal wing patterns for 435 out of 457 subspecies of Heliconiini, taken from Museum and private collection specimens thanks to our network of collaborators. We ordinated and clustered visually all Heliconiini pictures based on perceived similarity in their dorsal wing

similarity of color, patterns, and shape. Geographic distributions of taxa were not taken into account during this process. For Ithomiini, we used the currently accepted classification of mimicry patterns (Doré *et al.* 2022), built following the same rationale of phenotypic similarity independent from geographical distributions. Then, we matched the identity of 'phenotype-based mimicry rings' represented in the two tribes. The comprehensive mimicry classification of heliconiine subspecies is available in Supplementary (**Table SX** in SM).

2.2 Occurrence database and phylogenies

In order to map biodiversity patterns of heliconiine butterflies, we employed a database of 77,577 georeferenced occurrences collected on the field and complemented by records from Museum collections. We updated the taxonomic identity of records in agreement with the latest publications (Kozak *et al.* 2015; Jiggins & Lamas 2016). This database covered 73 out of 77 species of the tribe (94.8 %) and 418 out of 457 subspecies (91.4 %).

To estimate indices of phylogenetic diversity and evaluate niche convergence we merged three phylogenies: the Heliconiini phylogeny by Kozak *et al.* (2015) that encompasses 67 of the 77 species (87 %) of the tribe; the Ithomiini phylogeny by Chazot *et al.* (2019b) that encompasses 339 of the 396 species (85.6 %); and the Nymphalidae phylogeny by Espeland *et al.* (2018) as the backbone used to graft the two tribe-level phylogenies.

2.3 Species Distribution Modeling (SDM)

To predict spatial distributions, we performed independently Species Distribution Modeling (SDM) for each subspecies of Heliconiini. The output of the SDM process was a single consensus model (Ensemble model) for each subspecies that quantifies habitat suitability on a realistic taxa-specific range and provides a proxy of likelihood of presence of each subspecies in each grid cell (i.e., community).

As predictors of species distributions, we used environmental variables that are relevant for butterfly ecology according to literature. Temperatures and precipitation are known to influence the development of host plants for butterflies (Boggs *et al.* 2003), while elevation (Chazot *et al.* 2014; Montejo-Kovacevich *et al.* 2020) and forest cover (Brown Jr 1997) are important factors shaping heliconiine butterfly distribution. We extracted annual mean temperature, mean diurnal range, annual precipitation levels, and precipitation seasonality from WorldClim bioclimatic variables dataset (v2.1, accessed 02/2021; Fick & Hijmans 2017) and from forest cover from the Landsat Tree Cover Continuous Fields dataset (Sexton *et al.* 2013) aggregated at a quarter-degree cell resolution (i.e., pixel of ca. 30 km × 30 km).

We performed modelling for each subspecies by using three different algorithms (Random Forest, Gradient Tree Boosting and Artificial Neural Network) crossed with three independent sets of pseudo-absences and three spatially-structured cross-validation blocks. . We calculated the median of all models that passed our quality evaluation process to create an ensemble model for each subspecies. We cropped each subspecies predicted distribution to a relevant area according to its occurrences using a taxa-specific buffered alpha-hull. Finally, we merged ensemble models to acquire predicted distribution maps for species, mimicry rings, and Operational Mimicry Units (OMUs). OMUs are defined as all individuals of a unique species, eventually spread among several sub-species, that belong to the same mimicry ring (Doré *et al.* 2022).

More details about the modelling process are available in the ODMAP form (Zurell *et al.* 2020) in Supplementary Materials (**Appendix X** in SM). Similar models were already performed for Ithomiini at the OMU-level in Doré *et al.* (2022). These predictions were used to compare diversity patterns and investigate spatial associations between the two tribes.

2.4 Diversity indices

We computed a series of indices for each community (represented by 30 km × 30 km grid cell) and mapped for the whole distribution range of the two tribes:

- Species & mimicry richness as the number of predicted species/mimicry ring per community.

- Faith's Phylogenetic Diversity (Faith 1992) as the sum of branch lengths of the phylogenetic tree including all taxa found in a community.

- Mean species & mimicry ring geographic rarity (Leroy *et al.* 2012) as the weighted proportion of species or mimicry ring with small geographical range per community. These indices inform on the areas where species/mimicry ring with the smallest range are concentrated.

- Mean ring size as the mean number of species per mimicry ring for each community. This index provides insights on the degree of pattern convergence in the community as a high mean ring size implies high number of species harboring the same mimicry patterns locally.

2.5 Test for spatial association among comimetic species

In order to detect effects of mimicry ring membership, thus of mutualistic interactions, on the spatial distribution of Heliconiini and Ithomiini, we investigated the degree of co-

occurrence of co-mimetic species (species of the same mimicry ring) across grid cells. We computed pairwise Bray-Curtis (Bray & Curtis, 1957) distances, an index that quantifies dissimilarity between the distribution of two entities, in our case between pairs of OMUs. Thus, we calculated the mean Bray-Curtis distance of all co-mimetic OMUs and within each mimicry ring, representing the average degree of co-occurrence of co-mimetic units. To test the significance of these statistics, we used permutation tests under the null hypothesis that mimicry ring membership has no effect on co-occurrence. Therefore, for each permutation, we randomized the mimicry ring membership of all OMUs to investigate whether co-mimics species co-occur more than expected at random globally, and within each mimicry ring. As such, an observed BC lower than 95% of null statistics indicates a significant signal for spatial congruence. These analyses were performed for Ithomiini and Heliconiini independently and for pairs of comimetic OMUs formed between the two tribes (labeled as 'Inter' in subsequent analyses).

2.6 Test for niche evolution among co-mimetic species

In order to investigate whether mimicry led to niche convergence between co-mimetic species (i.e., Ithomiini only, Heliconiini only and Inter-tribe comimics), we performed comparative phylogenetic analyses. Climatic niche was described as the centroid of OMUs occurrences using bioclimatic variables employed during niche modeling (i.e., annual mean temperature, mean diurnal range, annual precipitation levels, precipitation seasonality).

First, we fit multivariate neutral evolution models to explain the distribution of niche centroid values on the phylogeny. We compared AICc of a Brownian motion model with models implementing additional Pagel's lambda or/and Pagel's kappa parameters accounting respectively for presence of phylogenetic signal and punctuated evolution associated with cladogenesis (Pagel 1994, 1999), to select for the best fitted option. Additionally, we tested for the presence of phylogenetic signal in the evolution of the climatic niche, and mimetic patterns.

We used mean climatic distances (MCD) as the pairwise Euclidean distances in the climatic space to measure the similarity of niches between co-mimetic species. To test for an effect of mimicry membership of climatic niche evolution, we simulated the evolution of the climatic niche under the neutral evolutionary model (n = 999) to obtain a null distribution for MCD between co-mimetic OMUs. As such, an observed MCD lower than 95% of null statistics indicates a significant signal for niche convergence.

3 Results

3.1 Diversity patterns

We mapped several diversity indices that represent different facets of Heliconiini and Ithomiini diversity (**Fig. 2**). As a reference, a map of South American regions mentioned in this study are available in Supplementary (**Fig. SX** in SM).

We predicted a peak of species richness in the Andes for Heliconiini with up to 35 species (**Fig. 2.a**), which is almost half of the total species count in the group (35 out of 77 species; 45.5%). We also observed a high richness in the Amazon basin (especially along the Amazon River) and in the south of Central America. The regions of Cerrado, Northern Argentina, Northern Central America, Caribbean islands, and the United States appeared less rich with generally the presence of one to six species predicted. Zooming on the Andean region, we observed that the most important species richness is found at mid-elevation, between 500 and 2,500 meters, with a significant drop beyond 2,500 meters (**Fig. SX** in SM). These biodiversity patterns are close to what was predicted for Ithomiini that present also a peak of richness in Andes and Southern Central America, but proportionally less species along the Amazon River and more in the Atlantic Forest. Also, Heliconiini are present in North America where Ithomiini do not go higher than Mexico.

We predicted a high geographical rarity (i.e., many species with restricted geographical ranges) not only in the Andes, but also in the North of Argentina and in the Caatinga in Brazil (**Fig. 2.b**). In this last region, up to 50% of the species present are among those considered as rare regarding of their restricted geographic range. The minimum geographic rarity is found in the United States because they host few species (e.g., *Agraulis vanillae* and *Dryas iulia*) with wide geographical distributions. Proportionally, more rare species are present at higher altitudes, especially above 2,500 meters, in contrast to species richness that declines sharply above that limit (**Fig. SX** in SM). In contrast, Ithomiini species with restricted ranges are concentrated along the Andes and in Central America.

Phylogenetic diversity was highly correlated with species richness for both tribes with peaks in the Andes and around the Amazon River (**Fig. 2.c**). However, a more homogeneous phylogenetic diversity is predicted in the Amazon basin for Heliconiini, not only around the Amazon river and main streams, but also in the heart of the forest. Phylogenetic diversity is also high in Central America and near the Atlantic Forest.

Mimetic richness (i.e., the number of mimicry rings present at a given location) has a pattern close to that of species richness. However, there is an even higher contrast between the Andes and the rest of America, the maximum richness being reached in the Northern Andes where 24 of the 39 Heliconiini mimicry rings and 29 of the 44 Ithomiini mimicry rings are predicted to cooccur. The mimicry richness of the Amazon basin stands out much less for Heliconiini due to an average ring size estimated between 1.5 and 3 species per ring, more important in the Amazon basin compared to the Andes with up to 1.5 species per ring only (**Fig. 2.f**). Furthermore, mimetic rarity shows rings with smaller distribution ranges in these regions compared to the rest of the continent (**Fig. 2.e**). Ithomiini patterns are quite different in terms of mimicry ring size. Species are forming larger mimicry rings in Eastern Andes, Western Amazon, Panama, Guyana Shield and Atlantic Forest, with between 3.5 to 7 species per ring in average. However, it is similar in terms of mimicry rings rarity with largely distributed mimicry rings in Amazonia and rings with restricted distributions in the Andes.

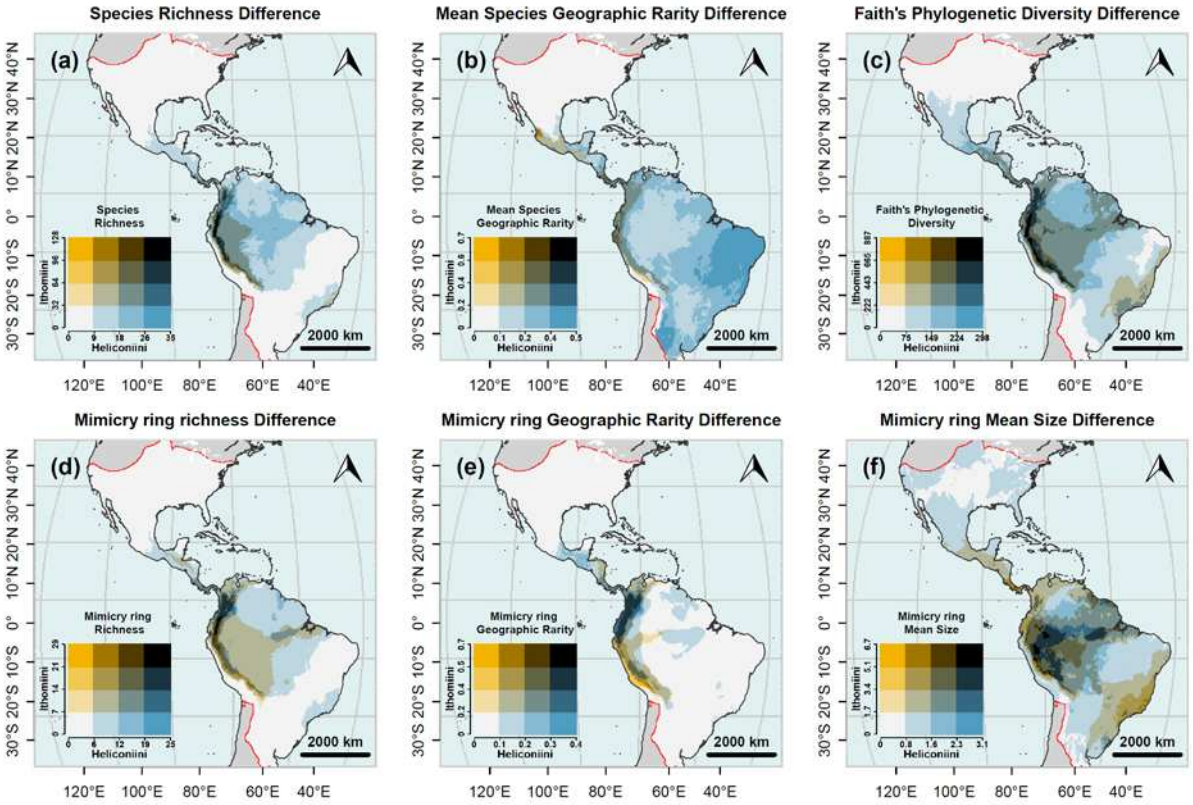

Figure 2: Heatmaps of the different facets of Heliconiini and Ithomiini diversity at the continental scale. (a) Species richness. **(b)** Mean species rarity. Rarity index based on species range. **(c)** Faith's Phylogenetic Diversity (Faith, 1992). **(d)** Mimicry richness (i.e., number of mimicry rings). **(e)** Mean mimicry rarity. Rarity index based on mimicry ring range. **(f)** Mean mimicry ring size (i.e., mean number of species per ring).

3.2 Mimicry drives spatial congruence of comimetic species

To explore whereas mutualistic interactions have an effect on species distributions we used the Bray Curtis index to measure large-scale co-occurrence of comimetic species. We detected that Heliconiini (BC_{obs} = 0.892, BC_{null} 5% = XXX, p ≤ 0.001), Ithomiini (BC_{obs} = 0.724, BC_{null} 5% = XXX, p ≤ 0.001) and inter-tribe comimics (BC_{obs} = 0.882, BC_{null} 5% = XXX, p ≤ 0.001) all display significant congruent spatial distributions. Hence, comimetic species tend to cooccur more than at random at large spatial scale, within and between tribes.

At mimicry ring-level, we observed that our hypothesized phenotypic mimicry rings display a variety of spatial distributions, mostly supporting their qualification as 'effective mimicry rings' in case of significant signal for spatial congruence. For instance, the MOTHONE ring showed an important and significant overlap between the tribes (**Fig. 3.a**; Permutation test: BC_{obs} = XXX, BC_{null} Q5% = XXX, p ≤ 001), with most species found in the Andes. On the contrary, the ring MANTINEUS showed no overlap between the two tribes (**Fig. 3.b**; Permutation test: BC_{obs} = 0, BC_{null} Q5% = XXX, p = 1), with Ithomiini species only found in the Western lowlands across Ecuador and Colombia, and Heliconiini species found in contrast in the Atlantic Forest, the Caatinga, the Lower Amazon and the Guyana Shield. The MAMERCUS ring presented a remarkable pattern where Ithomiini taxa showed a wide range from Central America to Argentina, covering almost the entirely the disjunct distribution of Heliconiini species spread between the Lower Amazon and several mountain ranges in the Andes (**Fig. 3.c**). Despite this important overlap, the non-significance of the spatial congruence test for this mimicry ring hypothesis (Permutation test: BC_{obs} = 0, BC_{null} Q5% = XXX, p > 0.05) was likely due to the small number of Heliconiini taxa (4) compared to Ithomiini (64) limiting the power of permutation tests.

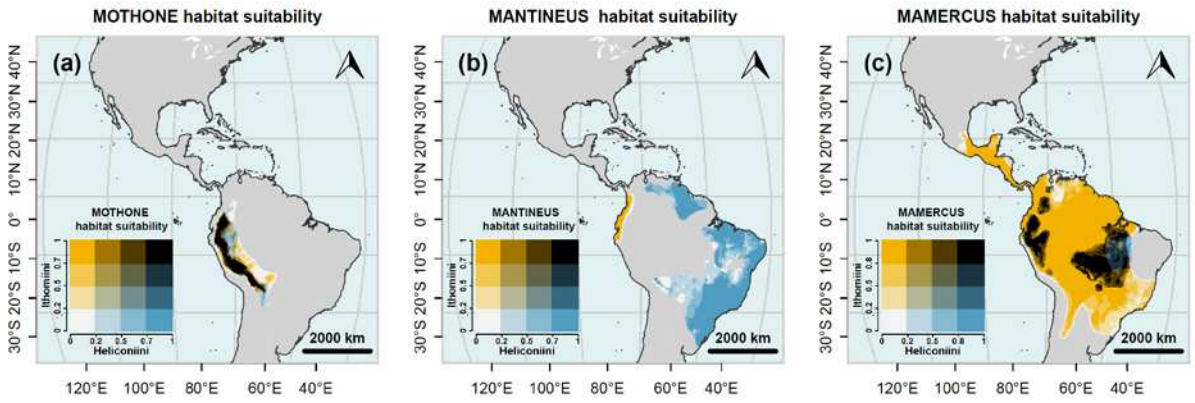

Figure 3: Comparative maps of predicted habitat suitability for Heliconiini and Ithomiini putative phenotypic mimicry rings. (a) MOTHONE ring. **(b)** MANTINEUS ring. **(c)** MAMERCUS ring.

Overall, we observe that 14 out of 31 (45.2%) of our phenotypic mimicry ring hypotheses are supported by the spatial congruence test for Heliconiini (8 patterns were not tested because only one species harbors it). This proportion rise to 32 out of 39 (82.1%) rings supported for Ithomiini (5 patterns not tested for similar reasons). For Inter-tribe mimicry ring hypotheses, 6 out of 8 (75%) are supported by our tests (**Table SX** in SM).

3.3 Mimicry is associated with niche convergence of comimetic species

We investigated the significance of niche convergence between phenotypically similar species by computing MCD for each group of comimetic species (Heliconiini, Ithomiini, Inter-tribe comimics). Mean climatic niche similarity (i.e., MCD) in Ithomiini, Heliconiini and Inter-tribe was significantly lower than the distribution of climatic distances simulated under our null evolution model, for all three groups (Ithomiini only: MCD_{obs} = 0.788, MCD_{null} Q5% = XXX, p ≤ 001; Heliconiini only: MCD_{obs} = 0.670, MCD_{null} Q5% = XXX, p ≤ 001; Inter-tribe: MCD_{obs} = 0.782, MCD_{null} Q5% = XXX, p = 0.024). Therefore, comimetic species in all three groups tends to have more similar climatic niches than expected if niche evolution was neutral. As such, climatic niche of comimetic species tend to converge within and between tribes.

Overall, we observed that XX out of 31 (XX%) of our phenotypic mimicry ring hypotheses showed significant niche convergence in Heliconiini, and 33 out of 39 (84.6%) rings in Ithomiini. For Inter-tribe mimicry ring hypotheses, niche convergence was supported for XX out of 8 (XX%) mimicry rings (**Table SX** in SM).

4 Discussion

Taking advantage of the well-characterized Müllerian mimetic systems of neotropical butterflies, we investigated the effects of mutualistic mimetic interactions on large-scale spatial distributions and species niche evolution within and between two emblematic tribes of unpalatable neotropical butterflies separated by 85 My of evolutionary time, yet harbouring similar warning signals: the Heliconiini (Nymphalidae: Heliconiinae) and the Ithomiini (Nymphalidae: Danainae). We showed that both tribes display high diversity and concentration of rare species and mimicry patterns in the Tropical Andes, where anthropogenic pressures levels are high. Although, we detected differences in global biodiversity patterns between the two tribes likely due to differences in biogeographic histories, we showed that mimicry drives large scale spatial association among phenotypically similar species, both within and between tribes, providing new empirical evidence for the unfolding of Müller's model at a

macroecological scale. Furthermore, comparative phylogenetic analyses suggested that mimetic interactions drive the evolutionary convergence of the climatic niche of comimetic species within and even across tribes, thereby strengthening their co-occurrence.

Altogether, our study highlights the power of mutualistic interactions in shaping large scale distribution patterns and driving species niche convergence across evolutionary distant lineages. Critically, our findings emphasize the vulnerability of mutualistic communities tied by positive interactions to community disassembly induced by climate change.

4.1 Biogeographic history, topographic heterogeneity, and host plant distributions may explain global biodiversity patterns

The species richness and phylogenetic diversity of Heliconiini are particularly high around the Amazon River and in the eastern Andes (**Fig. 2**), which is consistent with previous study about Heliconiini (Rosser et al., 2012, 2021). It also correlates with biodiversity patterns observed in other taxa including angiosperms (Ter Steege *et al.* 2003), beetles (Pearson & Carroll 2001), birds (Orme *et al.* 2005), mammals (Kaufman & Willig 1998), reptiles (Roll *et al.* 2017), and amphibians (Hutter *et al.* 2017). As such, the Amazon basin and Tropical Andes are one of the highest, if not the highest biodiversity hotspot on Earth (Myers *et al.* 2000; Hutter *et al.* 2017). This outstanding biodiversity can mostly be explained by geological and climatic factors. The topographical complexity of recent mountain regions such as the Tropical Andes facilitates fine-spatial scale variation of environmental conditions and provides more opportunities for parapatric and allopatric speciation fueled by adaptive radiations across the diversity of environmental niches available (Särkinen *et al.* 2012; Bouchenak-Khelladi *et al.* 2015; Rangel *et al.* 2018). Moreover, Tropical Andes and the Amazon basin have benefited from a relative historical climatic stability thought to reduce species extinction rate (Fine 2015) and allowing for the long-term persistence of high levels of species diversity and endemism (Araújo *et al.* 2008; Svenning *et al.* 2015; Harrison & Noss 2017). Noticeably, the Brazilian Atlantic forest that, although far away from the other hotspots, presents a relatively important diversity, which could be explained by multiple colonization events followed by local diversification facilitated by an adequate environment (i.e., dense forest cover, similar to the Amazon forest).

While both the Andes and the area surrounding the Amazon River harbor a high species richness, mimicry richness is reduced in the Amazon compared to that of the Andes. Thus, mimicry rings comprise more species along the Amazon River than in the Andes, while also

having larger geographic ranges, as illustrated by the low geographic rarity index in this region. Although there are more mimicry rings in the Andes, they tend to harbor fewer species per ring and smaller distribution ranges (**Fig. 2**). This mimicry richness and distribution pattern suggests two contrasting evolutionary histories for those two regions. In the Amazon forest, a few large-range mimicry rings dominate heliconiine communities, which may advocate for important convergence of wing patterns, and an efficient frequency-dependent selection purging less frequent rings at large scale. In the Andes, where mimicry rings have a smaller area and are composed of fewer species, there is no dominance of a few large-range patterns. This is likely due to important environmental gradients and geographic barriers present in these regions that favor local scale partitioning of predator communities and consequently the presence of local scale selection of various mimicry patterns.

Altogether, Heliconiini large-scale diversity patterns show some disparities with are those of Ithomiini (Doré *et al.* 2022). Overall, Ithomiini diversity is more important all over the continent with more species and mimicry patterns. Ithomiini present very dominant richness and rarity hotspots in the Andes while heliconiines show relatively high richness in the Amazon forest too. This disparity could be explained by the different origin of those lineages: Ithomiini in the Andes (Chazot *et al.* 2019b) and Heliconiini in the Amazon basin (Rosser *et al.* 2012) where they had more time to speciate and accumulate richness respectively. Moreover, both tribes are composed of highly specialized species which typically nest on a single host plant species (Willmott & Mallet 2004; Jiggins & Lamas 2016). However, heliconiines and ithomiines are specialized on two distinct families of plants, respectively the Passifloraceae and the Solanaceae, with which they are suspected to have tightly coevolved (Willmott & Mallet 2004; Jiggins & Lamas 2016). Thus, differences in the biogeographic histories of the two hostplant lineages could partly explained the current dissimilarities observed between global biodiversity patterns of heliconiine and ithomiine butterflies. Overall, further investigations based on joint inferences of ancestral ranges of butterflies and their respective hostplants, colonization events and ancestral aposematic patterns are needed to clarify the picture.

4.2 Strong spatial and climatic niche associations over 85 My of independent evolution

Despite showing some disparities in global biodiversity patterns, the two tribes are still strongly linked through mimetic interactions. We showed an important proportion of the phenotypic mimicry rings we hypothesized within and between both tribes are actually showing significant spatial congruence (e.g., MOTHONE ring in **Fig. 3.a**), thus are likely involved in

mutualistic interactions in local communities where they share the cost of educating predators to their unpalability.

Our study also highlighted the importance of considering the whole mimetic community into account when investigating how mutualistic interactions shape the distribution of species, even when those are evolutionary distantly related. For example, when studying the Heliconiini mimicry ring MAELUS, we found no evidence of co-occurrence nor climatic niche convergence among species for this hypothesized ring. Yet, once accounting for the Ithomiini members of such inter-tribe phenotypic ring, we detected an overall significant signal for spatial congruence and niche convergence. Similarly, the Heliconiini mimicry ring MAMERCUS presented a disjunct distribution pattern (**Fig. 3.c**) that seemed hardly coherent at first sight. Yet, once studied in relation to its Ithomiini counterpart, it formed a continuous coherent pattern since the range of comimetic ithomiine species encompasses the different patches of heliconiines (**Fig. 3.c**).

Moreover, we found a significant pattern of climatic niche convergence within and between phenotypically similar species that unfolds at continental scale. A pattern of niche convergence across comimetic species of mimetic neotropical butterflies had already been detected for ecological dimensions acting at local scales, such as nocturnal roosting habitat height (Mallet & Gilbert 1995), flight height (Beccaloni 1997b; DeVries *et al.* 1997), and forest structure (Elias *et al.* 2008). Yet, here we show such convergence can arise for niche dimensions (i.e., climatic niche) that affect directly large scale biodiversity patterns and link the faith of two tribes separated by over 85 My of independent evolution. Indeed, mimetic interactions appeared powerful enough that even species that have diverged in a time where *Tyrannosaurid* were still on Earth (Brusatte *et al.* 2010), are currently sharing very similar phenotype, spatial distributions and climatic niches.

Such strong adaptive bounding going across millions of years of evolution may have crucial consequences in the face of the ongoing climate change. Indeed, Müllerian mimicry represents mutualistic interactions that are beneficial for the individuals involved, allowing for instance to compensate for negative effects of competition (Aubier & Elias 2020), and fueling higher local richness (Gross 2008; Aubier *et al.* 2017). However, when mutualistic interactions are lost due to species extinction or community disassembly while facing global changes, their disappearance can fragilize the community stability and potentially trigger local extinction cascades (Dunn *et al.* 2009; Vidal *et al.* 2019). Since Müllerian mimetic species rely on local

mutualistic interactions with co-mimics and host plants, the threat of community disassembly due to climate change is even more profound for them (Toby Kiers *et al.* 2010; Sheldon *et al.* 2011). The dispersal abilities of Müllerian mimetic species are impeded by the purifying selection acting on individuals harboring unknown phenotypes in the newly colonized areas (Mallet & Barton 1989; Langham 2004). Moreover, despite relatively similar climatic niche optima, tolerance to climate change and extremes, as well as species dispersal abilities, may still differ among comimetic species, limiting opportunities for co-dispersal trajectories and leading to community disassembly. Finally, the effects of climate change on biotic factors that affect local abundance, such as hostplants (Willmott & Mallet 2004) and parasitoids (Gentry 1998), may also differ among interacting species.

Altogether, the consequences of climate changes on Müllerian mimetic communities remain uncertain. They form tightly coevolved assemblages tied by positive interactions, making them particularly vulnerable to global environmental changes (Tylianakis *et al.* 2008). However, the convergence of climatic niche among comimetic species may offer (limited) opportunities for congruent dispersal trajectories that would partly prevent community disassembly. This uncertainty stresses the need to produce predictions for future species distributions in order to better support the identification of refuge areas for biodiversity conservation that are resilient to climate changes (Keppel *et al.* 2015). Such predictions would ideally include species interactions in the modeling framework (Brooker *et al.* 2007; Toby Kiers *et al.* 2010; Tylianakis *et al.* 2010; Staniczenko *et al.* 2017) to account for their importance in shaping large biodiversity patterns as illustrated here with Neotropical mimetic butterflies.

4.3 Limits and perspectives

Despite a high proportion of putative phenotypic ring showing significant spatial co-occurrence, thus likely representing current mimetic interactions among members of the rings, there are groups of species that we hypothesized to cooccur because of similarity in wing patterns that actually displayed disjunct distribution areas (i.e., MANTINEUS ring in **Fig 3.b**). In these cases, the similarity of patterns could tentatively be explained by cooccurrence in the past that led to local pattern convergence followed by different dispersal trajectories leading to current disjunct areas. However, this is unlikely for the MANTINEUS rings considering the important geographic distances and topographic barriers separating the two groups. Thus, the similarity in phenotypes may have arisen by chance.

Such similarity observed between geographically separated group of species could also illustrate the limit of our mimetic classification approach. Indeed, our classification is based on expert decision and perception which may differ from those of the communities of predators that are selecting the patterns of these butterflies. What is perceived has similar by the expert, may not be considered as such by a wild predator (e.g., Dittrich *et al.* 1993). Research about mimicry would greatly benefit from a standardized and reproducible analytic framework to classify patterns. Recent advances in machine learning-based algorithms adapted to visual signal treatment could pave the way for such standards (e.g., Ezray *et al.* 2019; Hoyal Cuthill *et al.* 2019).

Finally, this study has highlighted the importance of accounting for the whole community of interacting species when investigating mutualistic interactions. This is particularly true for macroecological studies that are often focused on specific taxonomic groups and tend to overlook the ecological and evolutionary importance of interactions (Windsor *et al.* 2023). Heliconiines and ithomiines forms the bulk of the insect mimetic communities in the Neotropics (Poole 1970; Beccaloni 1997a), yet they also interact with a wide range of other mimetic butterflies and moths such as the Dismorphiinae (Poulton 1898), the Dioptinae (DeVries 1994), the Pericopina (Brown Jr 1979), and even damselflies (Outomuro *et al.* 2013; Corral-lopez *et al.* 2021). How these relatively less explored components of mimetic communities affect the whole distribution and niche evolution of interacting species is virtually unknown. Thus, future directions on this research topic may aim to enlarge the taxonomic scope and shed an even brighter light on the importance of mimetic interactions into shaping large spatial biodiversity patterns across evolutionary distantly related lineages.

BIBLIOGRAPHY

Abreu-Jardim, T.P.F., Jardim, L., Ballesteros-Mejia, L., Maciel, N.M. & Collevatti, R.G. (2021). Predicting impacts of global climatic change on genetic and phylogeographical diversity of a Neotropical treefrog. *Divers. Distrib.*, 27, 1519–1535.

Ackery, P.R. (1987). The danaid genus Tellervo (Lepidoptera, Nymphalidae)—a cladistic approach. *Zool. J. Linn. Soc.*, 89, 203–274.

Ackery, P.R. & Vane-Wright, R.I. (1984). *Milkweed butterflies, their cladistics and biology, being an account of the natural history of the Danainae, a subfamily of the Lepidoptera, Nymphalidae.* British Museum (Natural History).

Adams, D.C. (2014). A Generalized K Statistic for Estimating Phylogenetic Signal from Shape and other High-dimensional Multivariate Data. *Syst. Biol.*, 63, 685–697.

Adams, D.C. & Collyer, M.L. (2018). Multivariate Phylogenetic Comparative Methods : Evaluations, Comparisons, and Recommendations. *Syst. Biol.*, 67, 14–31.

Adams, D.C., Collyer, M.L. & Kaliontzopoulou, A. (2018). Geomorph: Software for geometric morphometric analyses.

Agarwal, S., Lanckriet, G., Wills, J., Kriegman, D., Cayton, L. & Belongie, S. (2007). Generalized non-metric multidimensional scaling. *J. Mach. Learn. Res.*, 2, 11–18.

Akcali, C.K., Kikuchi, D.W. & Pfennig, D.W. (2018). Coevolutionary arms races in Batesian mimicry? A test of the chase-away hypothesis. *Biol. J. Linn. Soc.*, 124, 668–676.

Albert, J.S. & Antonelli, A. (2017). Society for the study of systematic biology symposium: Frontiers in parametric biogeography. *Syst. Biol.*, 66, 125–127.

Albouy, C., Delattre, V.L., Mérigot, B., Meynard, C.N. & Leprieur, F. (2017). Multifaceted biodiversity hotspots of marine mammals for conservation priorities. *Divers. Distrib.*, 23, 615–626.

Alexandrou, M.A., Oliveira, C., Maillard, M., McGill, R.A.R., Newton, J., Creer, S., *et al.* (2011). Competition and phylogeny determine community structure in Müllerian co-mimics. *Nature*, 469, 84–89.

Allan, J.R., Watson, J.E.M., Di Marco, M., O'Bryan, C.J., Possingham, H.P., Atkinson, S.C., *et al.* (2019). Hotspots of human impact on threatened terrestrial vertebrates. *PLoS Biol.*, 17, 1–18.

Allio, R., Nabholz, B., Wanke, S., Chomicki, G., Pérez-Escobar, O.A., Cotton, A.M., *et al.* (2021). Genome-wide macroevolutionary signatures of key innovations in butterflies colonizing new host plants. *Nat. Commun.*, 12.

Allio, R., Schomaker-Bastos, A., Romiguier, J., Prosdocimi, F., Nabholz, B. & Delsuc, F. (2020a). MitoFinder: Efficient automated large-scale extraction of mitogenomic data in target enrichment phylogenomics. *Mol. Ecol. Resour.*, 20, 892–905.

Allio, R., Scornavacca, C., Nabholz, B., Clamens, A.L., Sperling, F.A.H. & Condamine, F.L. (2020b). Whole genome shotgun phylogenomics resolves the pattern and timing of swallowtail butterfly evolution. *Syst. Biol.*, 69, 38–60.

Allouche, O., Tsoar, A. & Kadmon, R. (2006). Assessing the accuracy of species distribution models: Prevalence, kappa and the true skill statistic (TSS). *J. Appl. Ecol.*, 43, 1223–1232.

Antonelli, A. (2015). Multiple origins of mountain life. *Nature*, 524, 300–301.

Antonelli, A. (2017). Comparative biogeography, big data and common myths. *Trop. plant Collect. legacies from past? Essent. tools Futur. Sci.*, 6, 41–52.

Araújo, M.B., Nogués-Bravo, D., Diniz-Filho, J.A.F., Haywood, A.M., Valdes, P.J. & Rahbek, C. (2008). Quaternary climate changes explain diversity among reptiles and amphibians. *Ecography (Cop.).*, 31, 8–15.

Arias, M., Mappes, J., Desbois, C., Gordon, S., McClure, M., Elias, M., *et al.* (2019). Transparency reduces predator detection in mimetic clearwing butterflies. *Funct. Ecol.*

Armbruster, W.S. & Herzig, A.L. (1984). Partitioning and Sharing of Pollinators by Four Sympatric Species of Dalechampia (Euphorbiaceae) in Panama. *Ann. Missouri Bot. Gard.*, 71, 1.

Armenteras, D., Espelta, J.M., Rodríguez, N. & Retana, J. (2017). Deforestation dynamics and drivers in different forest types in Latin America: Three decades of studies (1980–2010). *Glob. Environ. Chang.*, 46, 139–147.

Aronsson, M. & Gamberale-Stille, G. (2012). Colour and pattern similarity in mimicry: Evidence for a hierarchical discriminative learning of different components. *Anim. Behav.*, 84, 881–887.

Aubier, T.G. & Elias, M. (2020). Positive and negative interactions jointly determine the structure of Müllerian mimetic communities. *Oikos*, 129, 983–997.

Aubier, T.G., Elias, M., Llaurens, V. & Chazot, N. (2017). Mutualistic mimicry enhances species diversification through spatial segregation and extension of the ecological niche space. *Evolution (N. Y).*, 71, 826–844.

Bai, X., Ramos, M.R. & Fiske, S.T. (2020). As diversity increases, people paradoxically perceive social groups as more similar. *Proc. Natl. Acad. Sci. U. S. A.*, 117, 12741–12749.

Ballenghien, M., Faivre, N. & Galtier, N. (2017). Patterns of cross-contamination in a multispecies population genomic project: Detection, quantification, impact, and solutions. *BMC Biol.*, 15, 1–16.

Balogh, A.C.V., Gamberale-Stille, G. & Leimar, O. (2008). Learning and the mimicry spectrum: from quasi-Bates to super-Müller. *Anim. Behav.*, 76, 1591–1599.

Bankevich, A., Nurk, S., Antipov, D., Gurevich, A.A., Dvorkin, M., Kulikov, A.S., *et al.* (2012). SPAdes: A New Genome Assembly Algorithm and Its Applications to Single-Cell Sequencing. *J. Comput. Biol.*, 19, 455–477.

Barbet-Massin, M., Jiguet, F., Albert, C.H. & Thuiller, W. (2012). Selecting pseudo-absences for species distribution models: How, where and how many? *Methods Ecol. Evol.*, 3,

327–338.

Barnagaud, J., Barbet-massin, M., Viol, I. Le, Devictor, V., Jiguet, F. & Archaux, F. (2012). Relating Habitat and Climatic Niches in Birds. *PLoS One*, 7, 1–10.

Barnosky, A.D., Matzke, N., Tomiya, S., Wogan, G.O.U., Swartz, B., Quental, T.B., *et al.* (2011). Has the Earth's sixth mass extinction already arrived? *Nature*, 471, 51–57.

Barua, M., Gurdak, D.J., Ahmed, R.A. & Tamuly, J. (2012). Selecting flagships for invertebrate conservation. *Biodivers. Conserv.*, 21, 1457–1476.

Bascompte, J. (2009). Disentangling the Web of Life. *Science (80-.).*, 325, 416–419.

Bascompte, J. & Jordano, P. (2007). Plant-animal mutualistic networks: the architecture of biodiversity. *Annu. Rev. Ecol. Evol. Syst.*, 38, 567–593.

Bastolla, U., Fortuna, M.A., Pascual-García, A., Ferrera, A., Luque, B. & Bascompte, J. (2009). The architecture of mutualistic networks minimizes competition and increases biodiversity. *Nature*, 458, 1018–1020.

Bates, H.W. (1862). XXXII. Contributions to an insect fauna of the Amazon Valley. Lepidoptera: Heliconidæ. *Trans. Linn. Soc. London*, XXIII, 495–566.

Bax, V., Francesconi, W. & Delgado, A. (2019). Land-use conflicts between biodiversity conservation and extractive industries in the Peruvian Andes. *J. Environ. Manage.*, 232, 1028–1036.

Beatty, C.D., Bain, R.S. & Sherratt, T.N. (2005). The evolution of aggregation in profitable and unprofitable prey. *Anim. Behav.*, 70, 199–208.

Beauchamp, G. (2004). Reduced flocking by birds on islands with relaxed predation. *Proc. R. Soc. B Biol. Sci.*, 271, 1039–1042.

Beccaloni, G.W. (1997a). Ecology, Natural History and Behaviour of Ithomiine Butterflies and their Mimics in Ecuador. *Trop. Lepid.*, 8, 103–124.

Beccaloni, G.W. (1997b). Vertical stratification of ithomiine butterfly (Nymphalidae: Ithomiinae) mimicry complexes: The relationship between adult flight height and larval host-plant height. *Biol. J. Linn. Soc.*, 62, 313–341.

Beccaloni, G.W. & Gaston, K.J. (1995). Predicting the species richness of neotropical forest butterflies: Ithomiinae (Lepidoptera: Nymphalidae) as indicators. *Biol. Conserv.*, 71, 77–86.

Beccaloni, G.W., Viloria, A.L., Hall, S.K. & Robinson, G.S. (2008). *Catalogue of the hostplants of the Neotropical butterflies*. Sociedad Entomológica Aragonesa., Zaragoza, Spain.

Van Belleghem, S.M., Papa, R., Ortiz-Zuazaga, H., Hendrickx, F., Jiggins, C.D., Owen McMillan, W., *et al.* (2018). patternize: An R package for quantifying colour pattern variation. *Methods Ecol. Evol.*, 9, 390–398.

Benson, D.A., Cavanaugh, M., Clark, K., Karsch-Mizrachi, I., Lipman, D.J., Ostell, J., *et al.* (2013). GenBank. *Nucleic Acids Res.*, 41, 36–42.

Bentley, D.R., Balasubramanian, S., Swerdlow, H.P., Smith, G.P., Milton, J., Brown, C.G., *et al.* (2008). Accurate whole human genome sequencing using reversible terminator

chemistry. *Nature*, 456, 53–59.

Bergmann, C. (1848). *Ueber die Verhältnisse der Wärmeökonomie der Thiere zu ihrer Größe*. *1848*. Vandenhoeck und Ruprecht, Göttingen.

Biber, M.F., Voskamp, A., Niamir, A., Hickler, T. & Hof, C. (2020). A comparison of macroecological and stacked species distribution models to predict future global terrestrial vertebrate richness. *J. Biogeogr.*, 47, 114–129.

Bilder, R.M., Sabb, F.W., Cannon, T.D., London, E.D., Jentsch, J.D., Parker, D.S., *et al.* (2009). Phenomics: the systematic study of phenotypes on a genome-wide scale. *Neuroscience*, 164, 30–42.

Binetti, V.R., Schiffman, J.D., Leaffer, O.D., Spanier, J.E. & Schauer, C.L. (2009). The natural transparency and piezoelectric response of the Greta oto butterfly wing. *Integr. Biol.*, 1, 324–329.

Birskis-Barros, I., Freitas, A.V.L. & Guimarães, P.R. (2021). Habitat generalist species constrain the diversity of mimicry rings in heterogeneous habitats. *Sci. Rep.*, 11, 5072.

Bisby, F.A. (2000). The quiet revolution: Biodiversity informatics and the internet. *Science (80-.).*, 289, 2309–2312.

Blomberg, S.P., Garland, T. & Ives, A.R. (2003). Testing For Phylogenetic Signal In Comparative Data: Behavioral Traits Are More Labile. *Evolution (N. Y).*, 57, 717–745.

Blonder, B., Morrow, B., Harris, D.J., Brown, S., Butruille, G., Laini, A., *et al.* (2022). hypervolume: High Dimensional Geometry, Set Operations, Projection, and Inference Using Kernel Density Estimation, Support Vector Machines, and Convex Hulls. https://CRAN.R-project.org/package=hypervolume.

Boeye, J., Travis, J.M.J., Stoks, R. & Bonte, D. (2013). More rapid climate change promotes evolutionary rescue through selection for increased dispersal distance. *Evol. Appl.*, 6, 353–364.

Boggs, C.L., Watt, W.B., Ehrlich, P.R. & Ehrlich, P.R. (Eds.). (2003). *Butterflies: ecology and evolution taking flight*. University of Chicago Press.

Bogoni, J.A., Carvalho-Rocha, V., Ferraz, K.M.P.M.B. & Peres, C.A. (2021). Interacting elevational and latitudinal gradients determine bat diversity and distribution across the Neotropics. *J. Anim. Ecol.*, 90, 2729–2743.

Böhm, M., Williams, R., Bramhall, H.R., Mcmillan, K.M., Davidson, A.D., Garcia, A., *et al.* (2016). Correlates of extinction risk in squamate reptiles: The relative importance of biology, geography, threat and range size. *Glob. Ecol. Biogeogr.*, 25, 391–405.

Bolger, A.M., Lohse, M. & Usadel, B. (2014). Trimmomatic: A flexible trimmer for Illumina sequence data. *Bioinformatics*, 30, 2114–2120.

Borowiec, M.L. (2016). AMAS: A fast tool for alignment manipulation and computing of summary statistics. *PeerJ*, 2016.

Bosch, N.E., Wernberg, T., Langlois, T.J., Smale, D.A., Moore, P.J., Franco, J.N., *et al.* (2021). Niche and neutral assembly mechanisms contribute to latitudinal diversity gradients in reef fishes. *J. Biogeogr.*, 48, 2683–2698.

Bosque, R.J., Lawrence, J.P., Buchholz, R., Colli, G.R., Heppard, J. & Noonan, B. (2018). Diversity of warning signal and social interaction influences the evolution of imperfect mimicry. *Ecol. Evol.*, 8, 7490–7499.

Bouchenak-Khelladi, Y., Onstein, R.E., Xing, Y., Schwery, O. & Linder, H.P. (2015). On the complexity of triggering evolutionary radiations. *New Phytol.*, 207, 313–326.

Boucher, F.C., Thuiller, W., Davies, T.J. & Lavergne, S. (2014). Neutral Biogeography and the Evolution of Climatic Niches. *Am. Nat.*, 183, 573–584.

Bouckaert, R., Vaughan, T.G., Barido-Sottani, J., Duchêne, S., Fourment, M., Gavryushkina, A., *et al.* (2019). BEAST 2.5: An advanced software platform for Bayesian evolutionary analysis. *PLoS Comput. Biol.*, 15, 1–28.

Bray, J.R. & Curtis, J.T. (1957). An ordination of the upland forest communities of southern Wisconsin. *Ecol. Monogr.*, 27, 325–349.

Broennimann, O., Fitzpatrick, M.C., Pearman, P.B., Petitpierre, B., Pellissier, L., Yoccoz, N.G., *et al.* (2012). Measuring ecological niche overlap from occurrence and spatial environmental data. *Glob. Ecol. Biogeogr.*, 21, 481–497.

Bronstein, J.L. (1994). Conditional outcomes in mutualistic interactions. *Trends Ecol. Evol.*, 9, 214–217.

Brooker, R.W., Maestre, F.T., Callaway, R.M., Lortie, C.L., Cavieres, L.A., Kunstler, G., *et al.* (2008). Facilitation in plant communities: The past, the present, and the future. *J. Ecol.*, 96, 18–34.

Brooker, R.W., Travis, J.M.J., Clark, E.J. & Dytham, C. (2007). Modelling species' range shifts in a changing climate: The impacts of biotic interactions, dispersal distance and the rate of climate change. *J. Theor. Biol.*, 245, 59–65.

Brooks, T.M., Mittermeier, R.A., Da Fonseca, G.A.B., Gerlach, J., Hoffmann, M., Lamoreux, J.F., *et al.* (2006). Global biodiversity conservation priorities. *Science (80-.).*, 313, 58–61.

Brower, A.V.Z. (1996). Parallel race formation and the evolution of mimicry in Heliconius butterflies: A phylogenetic hypothesis from mitochondrial DNA sequences. *Evolution (N. Y).*, 50, 195–221.

Brower, A.V.Z., Freitas, A.V.L., Lee, M.-M., Silva-Brandão, K.L., Whinnett, A. & Willmott, K.R. (2006). Phylogenetic relationships among the Ithomiini (Lepidoptera: Nymphalidae) inferred from one mitochondrial and two nuclear gene regions. *Syst. Entomol.*, 31, 288–301.

Brower, A.V.Z., Willmott, K.R., Silva-Brandão, K.L., Garzón-Orduña, I.J. & Freitas, A.V.L. (2014). Phylogenetic relationships of ithomiine butterflies (Lepidoptera: Nymphalidae: Danainae) as implied by combined morphological and molecular data. *Syst. Biodivers.*, 12, 133–147.

Brown, J.H. & Maurer, B.A. (1989). Macroecology: The Division of Food and Space Among Species on Continents. *Science (80-.).*, 243, 1145–1150.

Brown, J.L., Paz, A., Reginato, M., Renata, C.A., Assis, C., Lyra, M., *et al.* (2020). Seeing the forest through many trees: Multi-taxon patterns of phylogenetic diversity in the Atlantic Forest hotspot. *Divers. Distrib.*, 26, 1160–1176.

Brown Jr., K.S. (2005). Geologic, evolutionary and ecological bases of the diversification of neotropical butterflies: implications for conservation. In: *Tropical rain- forest: past, present and future* (ed. Bermingham, E. et al.). Univ. of Chicago Press, pp. 166–201.

Brown Jr., K.S. & Benson, W.W. (1974). Adaptive Polymorphism Associated with Multiple Müllerian Mimicry in Heliconius numata. *Biotropica*, 6, 205–228.

Brown Jr., K.S. & Freitas, A.V.L. (1994). Juvenile Stages of Ithomiinae: Overview and Systematics (Lepidoptera: Nymphalidae). *Trop. Lepid.*, 5, 9–20.

Brown Jr., K.S. & Freitas, A.V.L. (2002). Diversidade Biológica no Alto Juruá: Avaliação, Causas e Manutenção. In: *Enciclopédia da floresta. O Alto Juruá: Práticas e conhecimentos das populações* (eds. Carneiro da Cunha, M.M. & Almeida, M.B.). Companhia das Letras, São Paulo, p. 735pp.

Brown Jr, K.S. (1977). Centros de evolução, refúgios quaternários e conservação de patrimônios genéticos na região neotropical: padrões de diferenciação em Ithominae (Lepidoptera: Nymphalidae). *Acta Amaz.*, 7, 75–137.

Brown Jr, K.S. (1979). Ecologia Geográfica e Evolução nas Florestas Neotropicais. Universidade Estadual de Campinas, Campinas, Brazil.

Brown Jr, K.S. (1982). Historical and ecological factors in the biogeography of aposematic neotropical butterflies. *Integr. Comp. Biol.*, 22, 453–471.

Brown Jr, K.S. (1984). Adult obtained pyrrolizidine alkaloids defend ithomiine butterflies against a spider predator. *Nature*, 309, 707–709.

Brown Jr, K.S. (1987). Chemistry at the Solanaceae/Ithomiinae Interface. *Ann. Missouri Bot. Gard.*, 74, 359.

Brown Jr, K.S. (1988). Mimicry, aposematism and crypsis in neotropical Lepidoptera: the importance of dual signals. *Bull. la Société Zool. Fr.*, 113, 83–101.

Brown Jr, K.S. (1997). Diversity, disturbance, and sustainable use of Neotropical forests: insects as indicators for conservation monitoring. *J. Insect Conserv.*, 1, 25–42.

Brown Jr, K.S. & Freitas, A.V.L. (2000). Atlantic Forest Butterflies : Indicators for Landscape Conservation. *Biotropica*, 32, 934–956.

Brown Jr, K.S., Von Schoultz, B. & Suomalainen, E. (2004). Chromosome evolution in Neotropical Danainae and Ithomiinae (Lepidoptera). *Hereditas*, 141, 216–236.

Brown Jr, K.S., Sheppard, P.M. & Turner, J.R.G. (1974). Quaternary Refugia in Tropical America : Evidence from Race Formation in Heliconius Butterflies. *Proc. R. Soc. London. Ser. B Biol. Sci.*, 187, 369–378.

Brown, K.S. & Henriques, S.A. (1991). Chemistry, co-evolution, and colonisation of Solanaceae leaves by ithomiine butterflies. In: *Solanaceae III: Taxonomy, Chemistry, Evolution* (eds. Hawkes & J.G., Lester, R.N., Nee, M., Estrada, N.). Linnean Society of London, London, pp. 51–68.

Brown, W.L.J. & Wilson, E.O. (1956). Character displacement. *Syst. Zool.*, 5, 49–64.

Brun, P., Thuiller, W., Chauvier, Y., Pellissier, L., Wüest, R.O., Wang, Z., *et al.* (2020). Model complexity affects species distribution projections under climate change. *J.*

Biogeogr., 47, 130–142.

Bruno, J.F., Stachowicz, J.J. & Bertness, M.D. (2003). Inclusion of facilitation into ecological theory. *Trends Ecol. Evol.*, 18, 119–125.

Brusatte, S.L., Norell, M.A., Carr, T.D., Erickson, G.M., Hutchinson, J.R., Balanoff, A.M., *et al.* (2010). Tyrannosaur Paleobiology :, 329, 1481–1486.

Bshary, R., Hohner, A., Ait-el-djoudi, K. & Fricke, H. (2006). Interspecific Communicative and Coordinated Hunting between Groupers and Giant Moray Eels in the Red Sea, 4.

Burki, F., Roger, A.J., Brown, M.W. & Simpson, A.G.B. (2020). The New Tree of Eukaryotes. *Trends Ecol. Evol.*, 35, 43–55.

Bybee, S.M., Yuan, F., Ramstetter, M.D., Llorente-Bousquets, J., Reed, R.D., Osorio, D., *et al.* (2012). UV photoreceptors and UV-yellow wing pigments in heliconius butterflies allow a color signal to serve both mimicry and intraspecific communication. *Am. Nat.*, 179, 38–51.

Cadotte, M.W. & Davies, J.T. (2010). Rarest of the rare: Advances in combining evolutionary distinctiveness and scarcity to inform conservation at biogeographical scales. *Divers. Distrib.*, 16, 376–385.

Calabrese, J.M., Certain, G., Kraan, C. & Dormann, C.F. (2014). Stacking species distribution models and adjusting bias by linking them to macroecological models. *Glob. Ecol. Biogeogr.*, 23, 99–112.

Capella-Gutiérrez, S., Silla-Martínez, J.M. & Gabaldón, T. (2009). trimAl: A tool for automated alignment trimming in large-scale phylogenetic analyses. *Bioinformatics*, 25, 1972–1973.

Cardillo, M. (2011). Phylogenetic structure of mammal assemblages at large geographical scales: Linking phylogenetic community ecology with macroecology. *Philos. Trans. R. Soc. B Biol. Sci.*, 366, 2545–2553.

Cardillo, M., MacE, G.M., Gittleman, J.L., Jones, K.E., Bielby, J. & Purvis, A. (2008). The predictability of extinction: Biological and external correlates of decline in mammals. *Proc. R. Soc. B Biol. Sci.*, 275, 1441–1448.

Cardoso, P., Barton, P.S., Birkhofer, K., Chichorro, F., Deacon, C., Fartmann, T., *et al.* (2020). Scientists' warning to humanity on insect extinctions. *Biol. Conserv.*, 242.

Carvalho, W.D., Mustin, K., Hilário, R.R., Vasconcelos, I.M., Eilers, V. & Fearnside, P.M. (2019). Deforestation control in the Brazilian Amazon: A conservation struggle being lost as agreements and regulations are subverted and bypassed. *Perspect. Ecol. Conserv.*, 17, 122–130.

Castro-Insua, A., Gómez-Rodríguez, C., Wiens, J.J. & Baselga, A. (2018). Climatic niche divergence drives patterns of diversification and richness among mammal families. *Sci. Rep.*, 8, 1–12.

Castro, É.C.P. De & Zurano, J.P. (2019). Sequestration and biosynthesis of cyanogenic glucosides in passion vine butterflies and consequences for the diversification of their host plants, 5079–5093.

Ceballos, G., Ehrlich, P.R., Barnosky, A.D., García, A., Pringle, R.M. & Palmer, T.M. (2015).

Accelerated modern human-induced species losses: Entering the sixth mass extinction. *Sci. Adv.*, 1, 9–13.

Chai, P. (1986). Field observations and feeding experiments on the responses of rufous-tailed jacamars (Galbula ruficauda) to free-flying butterflies in a tropical rainforest. *Biol. J. Linn. Soc.*, 29, 161–189.

Chan, W.P., Rabideau Childers, R., Ashe, S., Tsai, C.C., Elson, C., Keleher, K.J., *et al.* (2022). A high-throughput multispectral imaging system for museum specimens. *Commun. Biol.*, 5, 1–13.

Chatelain, P., Elias, M., Fontaine, C., Villemant, C., Dajoz, I. & Perrard, A. (2023). Müllerian mimicry among bees and wasps: a review of current knowledge and future avenues of research. *Biol. Rev.*, 4.

Chaves, J.A., Weir, J.T. & Smith, T.B. (2011). Diversification in Adelomyia hummingbirds follows Andean uplift. *Mol. Ecol.*, 20, 4564–4576.

Chazot, N., Condamine, F.L., Dudas, G., Peña, C., Kodandaramaiah, U., Matos-Maraví, P., *et al.* (2021). Conserved ancestral tropical niche but different continental histories explain the latitudinal diversity gradient in brush-footed butterflies. *Nat. Commun.*, 12, 5717.

Chazot, N., De-Silva, D.L., Willmott, K.R., Freitas, A.V.L., Lamas, G., Mallet, J., *et al.* (2018). Contrasting patterns of Andean diversification among three diverse clades of Neotropical clearwing butterflies. *Ecol. Evol.*, 8, 3965–3982.

Chazot, N., Wahlberg, N., Freitas, A.V.L., Mitter, C., Labandeira, C., Sohn, J.C., *et al.* (2019a). Priors and Posteriors in Bayesian Timing of Divergence Analyses: The Age of Butterflies Revisited. *Syst. Biol.*, 68, 797–813.

Chazot, N., Willmott, K.R., Condamine, F.L., De-Silva, D.L., Freitas, A.V.L., Lamas, G., *et al.* (2016a). Into the Andes: multiple independent colonizations drive montane diversity in the Neotropical clearwing butterflies Godyridina. *Mol. Ecol.*, 25, 5765–5784.

Chazot, N., Willmott, K.R., Freitas, A.V.L., de Silva, D.L., Pellens, R. & Elias, M. (2016b). Patterns of Species, Phylogenetic and Mimicry Diversity of Clearwing Butterflies in the Neotropics. In: *Biodiversity Conservation and Phylogenetic Systematics*. Springer, pp. 333–354.

Chazot, N., Willmott, K.R., Lamas, G., Freitas, A.V.L., Piron-Prunier, F., Arias, C.F., *et al.* (2019b). Renewed diversification following Miocene landscape turnover in a Neotropical butterfly radiation. *Glob. Ecol. Biogeogr.*, 28, 1118–1132.

Chazot, N., Willmott, K.R., Santacruz Endara, P.G., Toporov, A., Hill, R.I., Jiggins, C.D., *et al.* (2014). Mutualistic Mimicry and Filtering by Altitude Shape the Structure of Andean Butterfly Communities. *Am. Nat.*, 183, 26–39.

Chen, I.-C., Shiu, H.-J., Benedick, S., Holloway, J.D., Chey, V.K., Barlow, H.S., *et al.* (2009). Elevation increases in moth assemblages over 42 years on a tropical mountain. *Proc. Natl. Acad. Sci.*, 106, 1479–1483.

Chouteau, M., Dezeure, J., Sherratt, T.N., Llaurens, V. & Joron, M. (2019). Similar predator aversion for natural prey with diverse toxicity levels. *Anim. Behav.*, 153, 49–59.

Clifford, P., Richardson, S. & Hemon, D. (1989). Assessing the Significance of the Correlation between Two Spatial Processes. *Biometrics*, 45, 123–134.

Clusella-Trullas, S. & Nielsen, M. (2020). The evolution of insect body coloration under changing climates. *Curr. Opin. Insect Sci.*, 41, 25–32.

Clusella Trullas, S., van Wyk, J.H. & Spotila, J.R. (2007). Thermal melanism in ectotherms. *J. Therm. Biol.*, 32, 235–245.

Cohen, J. (1960). A coefficient of agreement for nominal scales. *Educ. Psychol. Meas.*, XX, 37–46.

Committee of the IUCN Species Survival Commission and IUCN World Commission on Protected Areas. (2020). *Guidelines for using A Global Standard for the Identification of Key Biodiversity Areas. Version 1.1. Prepared by the KBA Standards and Appeals Committee of the IUCN Species Survival Commission and IUCN World Commission on Protected Areas.* Gland, Switzerland.

Cook, L.M., Grant, B.S., Saccheri, I.J. & Mallet, J. (2012). Selective bird predation on the peppered moth: The last experiment of Michael Majerus. *Biol. Lett.*, 8, 609–612.

Cooney, C.R., Bright, J.A., Capp, E.J.R., Chira, A.M., Hughes, E.C., Moody, C.J.A., *et al.* (2017). Mega-evolutionary dynamics of the adaptive radiation of birds. *Nature*, 542, 344–347.

Corral-lopez, A., Edo, J., Yiselle, V., Losada, R., Realpe, E. & Outomuro, D. (2021). Field evidence for colour mimicry overshadowing morphological mimicry, 698–709.

Costello, M.J., DeWalt, R.E., Orrell, T.M. & Banki, O. (2022). Two million species catalogued by 500 experts. *Nature*, 601, 191–191.

Crowley, P.H. & Cox, J.J. (2011). Intraguild mutualism. *Trends Ecol. Evol.*, 26, 627–633.

Cusack, D.F., Karpman, J., Ashdown, D., Cao, Q., Ciochina, M., Halterman, S., *et al.* (2016). Global change effects on humid tropical forests: Evidence for biogeochemical and biodiversity shifts at an ecosystem scale. *Rev. Geophys.*, 54, 523–610.

Cuthill, I.C. & Bennett, A.T.D. (1993). Mimicry and the eye of the beholder. *Proc. R. Soc. B Biol. Sci.*, 253, 203–204.

D'Almeida, R.F. (1941). Contribução ao estudo dos Mechanitidae (Lep. Rhopalocera) (4a. nota). *Pap. Avulsos do Dep. Zool. Secr. da Agric.*, 1, 79–85.

Darwin, C. (1859). *On the origin of species by means of natural selection, or the preservation of favoured races in the struggle for life*. 1st Editio. John Murray, London.

Dayan, T. & Simberloff, D. (2005). Ecological and community-wide character displacement: The next generation. *Ecol. Lett.*, 8, 875–894.

Dayrat, B. (2005). Towards integrative taxonomy. *Biol. J. Linn. Soc.*, 85, 407–415.

De-Silva, D.L., Elias, M., Willmott, K., Mallet, J. & Day, J.J. (2016). Diversification of clearwing butterflies with the rise of the Andes. *J. Biogeogr.*, 43, 44–58.

De-Silva, D.L., Mota, L.L., Chazot, N., Mallarino, R., Silva-Brandão, K.L., Piñerez, L.M.G., *et al.* (2017). North Andean origin and diversification of the largest ithomiine butterfly genus. *Sci. Rep.*, 7.

Delsuc, F., Brinkmann, H. & Philippe, H. (2005). Phylogenomics and the reconstruction of the tree of life. *Nat. Rev. Genet.*, 6, 361–375.

Devictor, V., Mouillot, D., Meynard, C., Jiguet, F., Thuiller, W. & Mouquet, N. (2010). Spatial mismatch and congruence between taxonomic, phylogenetic and functional diversity: The need for integrative conservation strategies in a changing world. *Ecol. Lett.*, 13, 1030–1040.

DeVries, P.J. (1994). Patterns of butterfly diversity and promising topics in natural history and ecology. In: *La Selva: ecology and natural history of a Neotropical rain forest.* University of Chicago Press, pp. 187–194.

DeVries, P.J., Lande, R. & Murray, D. (1999). Associations of co-mimetic ithomiine butterflies on small spatial and temporal scales in a neotropical rainforest. *Biol. J. Linn. Soc.*, 67, 73–85.

DeVries, P.J., Murray, D. & Lande, R. (1997). Species diversity in vertical, horizontal, and temporal dimensions of a fruit-feeding butterfly community in an Ecuadorian rainforest. *Biol. J. Linn. Soc.*, 62, 343–364.

Díaz, S., Kattge, J., Cornelissen, J.H.C., Wright, I.J., Lavorel, S., Dray, S., *et al.* (2016). The global spectrum of plant form and function. *Nature*, 529, 167–171.

Díaz, S. & Malhi, Y. (2022). Biodiversity : Concepts , Patterns , Trends , and Perspectives.

Dittrich, W., Gilbert, F., Green, P., Mcgregor, P. & Grewcock, D. (1993). Imperfect mimicry: A pigeon's perspective. *Proc. R. Soc. B Biol. Sci.*, 251, 195–200.

Doré, M., Willmott, K., Lavergne, S., Chazot, N., Freitas, A.V.L., Fontaine, C., *et al.* (2023). Mutualistic interactions shape global spatial congruence and climatic niche evolution in Neotropical mimetic butterflies. *Ecol. Lett.*, 1–16.

Doré, M., Willmott, K., Leroy, B., Chazot, N., Mallet, J., Freitas, A.V.L., *et al.* (2022). Anthropogenic pressures coincide with Neotropical biodiversity hotspots in a flagship butterfly group. *Divers. Distrib.*, 28, 2912–2930.

Dormann, C.F., Elith, J., Bacher, S., Buchmann, C., Carl, G., Carré, G., *et al.* (2013). Collinearity: A review of methods to deal with it and a simulation study evaluating their performance. *Ecography (Cop.).*, 36, 27–46.

Doubleday, E. (1847). *The Genera of Diurnal Lepidoptera: Comprising their Generic Characters, a Notice of their Habits and Transformations, and a Catalogue of the Species of Each Genus 1*. Longman, Brown, Green & Longmans, London.

Douglas, J., Zhang, R. & Bouckaert, R. (2021). Adaptive dating and fast proposals: Revisiting the phylogenetic relaxed clock model. *PLoS Comput. Biol.*, 17, 1–30.

Dracxler, C.M. & Kissling, W.D. (2022). The mutualism – antagonism continuum in Neotropical palm – frugivore interactions : from interaction outcomes to ecosystem dynamics, 31, 527–553.

Drew, G.C., Stevens, E.J. & King, K.C. (2021). Microbial evolution and transitions along the parasite–mutualist continuum. *Nat. Rev. Microbiol.*, 19, 623–638.

Drummond, B.A. (1986). Coevolution of ithomiine butterflies and solanaceous plants. In: *Solanaceae: Biology and Systematics* (ed. D'Arcy, W.G.). Columbia University Press, New York, pp. 307– 327.

Drummond, B.A. & Brown Jr, K.S. (1987). Ithomiinae (Lepidoptera: Nymphalidae):

Summary of Known Larval Food Plants. *Ann. Missouri Bot. Gard.*, 74, 341.

Drury, J.P., Cowen, M.C. & Grether, G.F. (2020). Competition and hybridization drive interspecific territoriality in birds. *Proc. Natl. Acad. Sci.*, 117, 12923–12930.

Duffy, K.J. & Johnson, S.D. (2017). Specialized mutualisms may constrain the geographical distribution of flowering plants. *Proc. R. Soc. B Biol. Sci.*, 284.

Dufour, P.C., Willmott, K.R., Padrón, P.S., Xing, S., Bonebrake, T.C. & Scheffers, B.R. (2018). Divergent melanism strategies in Andean butterfly communities structure diversity patterns and climate responses. *J. Biogeogr.*, 45, 2471–2482.

Dumbacher, J.P. & Fleischer, R.C. (2001). Phylogenetic evidence for colour pattern convergence in toxic pitohuis: Müllerian mimicry in birds? *Proc. R. Soc. B Biol. Sci.*, 268, 1971–1976.

Dunn, C.W., Hejnol, A., Matus, D.Q., Pang, K., Browne, W.E., Smith, S.A., *et al.* (2008). Broad phylogenomic sampling improves resolution of the animal tree of life. *Nature*, 452, 745–749.

Dunn, R.R., Harris, N.C., Colwell, R.K., Koh, L.P. & Sodhi, N.S. (2009). The sixth mass coextinction: Are most endangered species parasites and mutualists? *Proc. R. Soc. B Biol. Sci.*, 276, 3037–3045.

Dupin, J., Matzke, N.J., Särkinen, T., Knapp, S., Olmstead, R.G., Bohs, L., *et al.* (2017). Bayesian estimation of the global biogeographical history of the Solanaceae. *J. Biogeogr.*, 44, 887–899.

Durán, S.M., Martin, R.E., Díaz, S., Maitner, B.S., Malhi, Y., Salinas, N., *et al.* (2019). Informing trait-based ecology by assessing remotely sensed functional diversity across a broad tropical temperature gradient. *Sci. Adv.*, 5, 1–12.

Edgar, R.C. (2022). Muscle5: High-accuracy alignment ensembles enable unbiased assessments of sequence homology and phylogeny. *Nat. Commun.*, 13, 1–9.

Eggleton, P. (2020). The State of the World's Insects. *Annu. Rev. Environ. Resour.*, 61–82.

Ehrlich, P.R. & Raven, P.H. (1964). Butterflies and Plants: a Study in Coevolution. *Evolution (N. Y).*, 18, 586–608.

Ekblom, R. & Wolf, J.B.W. (2014). A field guide to whole-genome sequencing, assembly and annotation. *Evol. Appl.*, 7, 1026–1042.

Elias, M., Gompert, Z., Jiggins, C. & Willmott, K. (2008). Mutualistic interactions drive ecological niche convergence in a diverse butterfly community. *PLoS Biol.*, 6.

Elias, M., Gompert, Z., Willmott, K. & Jiggins, C. (2009a). Phylogenetic community ecology needs to take positive interactions into account: Insights from colorful butterflies. *Commun. Integr. Biol.*, 2, 113–116.

Elias, M., Joron, M., Willmott, K., Silva-Brandão, K.L., Kaiser, V., Arias, C.F., *et al.* (2009b). Out of the Andes: Patterns of diversification in clearwing butterflies. *Mol. Ecol.*, 18, 1716–1729.

Ellegren, H. (2014). Genome sequencing and population genomics in non-model organisms. *Trends Ecol. Evol.*, 29, 51–63.

Ellis, E.C. (2019). Evolution: Biodiversity in the Anthropocene. *Curr. Biol.*, 29, R831–R833.

Elsen, P.R., Monahan, W.B. & Merenlender, A.M. (2020). Topography and human pressure in mountain ranges alter expected species responses to climate change. *Nat. Commun.*, 11, 1–10.

Elton, C.S. (1927). *Animal ecology*. Sidgwick & Jackson.

Emms, D.M. & Kelly, S. (2019). OrthoFinder: phylogenetic orthology inference for comparative genomics. *Genome Biol.*, 20, 238.

Endler, J.A. (1992). Signals, Signal Conditions, and the Direction of Evolution. *Am. Nat.*, 139, S125–S153.

Escobar, H. (2020). Deforestation in the Brazilian Amazon is still rising sharply. *Science (80-.).*, 369, 613–613.

Espeland, M., Breinholt, J., Willmott, K.R., Warren, A.D., Vila, R., Toussaint, E.F.A., *et al.* (2018). A Comprehensive and Dated Phylogenomic Analysis of Butterflies. *Curr. Biol.*, 28, 770-778.e5.

Esquerré, D., Keogh, J.S., Demangel, D., Morando, M., Avila, L.J., Sites, J.W., *et al.* (2022). Rapid Radiation and Rampant Reticulation: Phylogenomics of South American Liolaemus Lizards. *Syst. Biol.*, 71, 286–300.

Eude, A., Roddaz, M., Brichau, S., Brusset, S., Calderon, Y., Baby, P., *et al.* (2015). Controls on timing of exhumation and deformation in the northern Peruvian eastern Andean wedge as inferred from low-temperature thermochronology and balanced cross section. *Tectonics*, 34, 715–730.

Eyring, V., Bony, S., Meehl, G.A., Senior, C.A., Stevens, B., Stouffer, R.J., *et al.* (2016). Overview of the Coupled Model Intercomparison Project Phase 6 (CMIP6) experimental design and organization. *Geosci. Model Dev.*, 9, 1937–1958.

Ezray, B.D., Wham, D.C., Hill, C.E. & Hines, H.M. (2019). Unsupervised machine learning reveals mimicry complexes in bumblebees occur along a perceptual continuum. *Proc. R. Soc. B Biol. Sci.*, 286.

Faith, D.P. (1992). Conservation evaluation and phylogenetic diversity. *Biol. Conserv.*, 61, 1–10.

Faith, D.P. (2018). Phylogenetic Diversity and Conservation Evaluation: Perspectives on Multiple Values, Indices, and Scales of Application. In: *Phylogenetic Diversity: Applications and Challenges in Biodiversity Science* (eds. Scherson, R.A. & Faith, D.P.). Springer International Publishing, Cham, pp. 1–26.

Farber, P.L. (2000). *Finding order in nature: the naturalist tradition from Linnaeus to EO Wilson*. JHU Press.

Farina, A., Bogaert, J. & Schipani, I. (2005). Cognitive landscape and information: New perspectives to investigate the ecological complexity. *BioSystems*, 79, 235–240.

Farr, T.G., Rosen, P.A., Caro, E., Crippen, R., Duren, R., Hensley, S., *et al.* (2007). The Shuttle Radar Topography Mission. *Rev. Geophys.*, 45, RG2004.

Fearnside, P. (2017). *Deforestation of the Brazilian Amazon*. *Oxford Res. Encycl. Environ.*

Sci.

Felsenstein, J. (1981). Evolutionary trees from DNA sequences: A maximum likelihood approach. *J. Mol. Evol.*, 17, 368–376.

Felsenstein, J. (1985). Confidence Limits on Phylogenies: An Approach Using the Bootstrap. *Evolution (N. Y).*, 39, 783.

Feng, S., Bai, M., Rivas-González, I., Li, C., Liu, S., Tong, Y., *et al.* (2022). Incomplete lineage sorting and phenotypic evolution in marsupials. *Cell*, 185, 1646-1660.e18.

Fick, S.E. & Hijmans, R.J. (2017). WorldClim 2: new 1-km spatial resolution climate surfaces for global land areas. *Int. J. Climatol.*, 37, 4302–4315.

Fine, P.V.A. (2015). Ecological and Evolutionary Drivers of Geographic Variation in Species Diversity. *Annu. Rev. Ecol. Evol. Syst.*, 46, 369–392.

Flores-Tolentino, M., García-Valdés, R., Saénz-Romero, C., Ávila-Díaz, I., Paz, H. & Lopez-Toledo, L. (2020). Distribution and conservation of species is misestimated if biotic interactions are ignored: the case of the orchid Laelia speciosa. *Sci. Rep.*, 10, 1–14.

Fox, R.M.. (1940). A Generic Review of the Ithomiinae (Lepidoptera, Nymphalidae). *Trans. Am. Entomol. Soc.*, 66, 161–207.

Fox, R.M. (1956). A monograph of the Ithomiidae (Lepidoptera). Part I. *Bull. Am. Museum Nat. Hist.*, 111, 1–76.

Di Franco, A., Poujol, R., Baurain, D. & Philippe, H. (2019). Evaluating the usefulness of alignment filtering methods to reduce the impact of errors on evolutionary inferences. *BMC Evol. Biol.*, 19, 1–17.

Franklin, J., Serra-Diaz, J.M., Syphard, A.D. & Regan, H.M. (2016). Global change and terrestrial plant community dynamics. *Proc. Natl. Acad. Sci. U. S. A.*, 113, 3725–3734.

Franks, D.W., Ruxton, G.D. & Sherratt, T.N. (2009). Warning signals evolve to disengage batesian mimics. *Evolution (N. Y).*, 63, 256–267.

Freitas, A.V.L. (1999). Nymphalidae (Lepidoptera), filogenia com base em caracteres de imaturos, com experimentos de troca de plantas hospedeiras. Universidade Estadual de Campinas, Campinas.

Fritz, S.A., Bininda-Emonds, O.R.P. & Purvis, A. (2009). Geographical variation in predictors of mammalian extinction risk: Big is bad, but only in the tropics. *Ecol. Lett.*, 12, 538–549.

Fürst von Lieven & Alexander Humar, M. (2008). A Cladistic Analysis of Aristotle's Animal Groups in the "Historia animalium." *Hist. Philos. Life Sci.*, 30, 227–262.

Garzón-Orduña, I.J., Silva-Brandão, K.L., Willmott, K.R., Freitas, A.V.L. & Brower, A.V.Z. (2015). Incompatible Ages for Clearwing Butterflies Based on Alternative Secondary Calibrations. *Syst. Biol.*, 64, 752–767.

Gaston, K.J. (1997). What is rarity? In: *The Biology of Rarity*. Springer Netherlands, Dordrecht, pp. 30–47.

Gauthier, J., Meier, J., Legeai, F., McClure, M., Whibley, A., Bretaudeau, A., *et al.* (2023). First chromosome scale genomes of ithomiine butterflies (Nymphalidae: Ithomiini):

Comparative models for mimicry genetic studies. *Mol. Ecol. Resour.*, 23, 872–885.

Gaüzère, P., O'Connor, L., Botella, C., Poggiato, G., Münkemüller, T., Pollock, L.J., *et al.* (2022). The diversity of biotic interactions complements functional and phylogenetic facets of biodiversity. *Curr. Biol.*, 32, 2093-2100.e3.

Gentry, G.L. (1998). Mutualistic Interactions Between Parasitoids and a Neotropical Extrafloral Nectary Plant in the Solanaceae. University of California, Los Angeles.

Gerts, E.M., Yu, Y.K., Agarwala, R., Schäffer, A.A. & Altschul, S.F. (2006). Composition-based statistics and translated nucleotide searches: Improving the TBLASTN module of BLAST. *BMC Biol.*, 4, 1–14.

Getty, T. (1985). Discriminability and the Sigmoid Functional Response : How Optimal Foragers Could Stabilize Model-Mimic Complexes. *Am. Nat.*, 125, 239–256.

Godoy-Bürki, A.C., Ortega-Baes, P., Sajama, J.M. & Aagesen, L. (2014). Conservation priorities in the Southern Central Andes: Mismatch between endemism and diversity hotspots in the regional flora. *Biodivers. Conserv.*, 23, 81–107.

Goldberg, E.E., Lancaster, L.T. & Ree, R.H. (2011). Phylogenetic inference of reciprocal effects between geographic range evolution and diversification. *Syst. Biol.*, 60, 451–465.

Gomes, V.H.F., Vieira, I.C.G., Salomão, R.P. & ter Steege, H. (2019). Amazonian tree species threatened by deforestation and climate change. *Nat. Clim. Chang.*, 9, 547–553.

Gompert, Z., Willmott, K. & Elias, M. (2011). Heterogeneity in predator micro-habitat use and the maintenance of Müllerian mimetic diversity. *J. Theor. Biol.*, 281, 39–46.

Goodale, M.A. & Sneddon, I. (1977). The effect of distastefulness of the model on the predation of artificial batesian mimics. *Anim. Behav.*, 25, 660–665.

Goolsby, E.W. (2015). Phylogenetic Comparative Methods for Evaluating the Evolutionary History of Function-Valued Traits. *Syst. Biol.*, 64, 568–578.

Gouveia, S.F., Hortal, J., Tejedo, M., Duarte, H., Cassemiro, F.A.S., Navas, C.A., *et al.* (2014). Climatic niche at physiological and macroecological scales: The thermal tolerance-geographical range interface and niche dimensionality. *Glob. Ecol. Biogeogr.*, 23, 446–456.

Gower, J.C. (1975). Generalized procrustes analysis. *Psychometrika*, 40, 33–51.

Grenyer, R., Orme, C.D.L., Jackson, S.F., Thomas, G.H., Davies, R.G., Davies, T.J., *et al.* (2006). Global distribution and conservation of rare and threatened vertebrates. *Nature*, 444, 93–96.

Grime, J.P. (1997). Biodiversity and Ecosystem Function : The Debate Deepens. *Science (80-.).*, 277, 1260–1261.

Grinnell, J. (1917). The Niche-Relationships of the California Thrasher. *Auk*, 34, 427–433.

Gross, K. (2008). Positive interactions among competitors can produce species-rich communities. *Ecol. Lett.*, 11, 929–936.

Guillera-Arroita, G., Lahoz-Monfort, J.J., Elith, J., Gordon, A., Kujala, H., Lentini, P.E., *et al.* (2015). Is my species distribution model fit for purpose? Matching data and models to applications. *Glob. Ecol. Biogeogr.*, 24, 276–292.

Guimarães, P.R., Jordano, P. & Thompson, J.N. (2011). Evolution and coevolution in mutualistic networks. *Ecol. Lett.*, 14, 877–885.

Guimarães, P.R., Pires, M.M., Jordano, P., Bascompte, J. & Thompson, J.N. (2017). Indirect effects drive coevolution in mutualistic networks. *Nature*, 550, 511–514.

Guindon, S., Dufayard, J.F., Lefort, V., Anisimova, M., Hordijk, W. & Gascuel, O. (2010). New algorithms and methods to estimate maximum-likelihood phylogenies: Assessing the performance of PhyML 3.0. *Syst. Biol.*, 59, 307–321.

Guisan, A. & Rahbek, C. (2011). SESAM - a new framework integrating macroecological and species distribution models for predicting spatio-temporal patterns of species assemblages. *J. Biogeogr.*, 38, 1433–1444.

Guisan, A. & Thuiller, W. (2005). Predicting species distribution: Offering more than simple habitat models. *Ecol. Lett.*, 8, 993–1009.

Gumbs, R., Gray, C.L., Böhm, M., Hoffmann, M., Grenyer, R., Meiri, S., *et al.* (2020). Global priorities for conservation of reptilian phylogenetic diversity in the face of human impacts. *Nat. Commun.*, 11, 1–13.

Hahsler, M., Piekenbrock, M. & Doran, D. (2019). Dbscan: Fast density-based clustering with R. *J. Stat. Softw.*, 91.

Haining, R. (1991). Bivariate Correlation with Spatial Data. *Geogr. Anal.*, 23, 210–227.

Hale, K.R.S., Valdovinos, F.S. & Martinez, N.D. (2020). Mutualism increases diversity, stability, and function of multiplex networks that integrate pollinators into food webs. *Nat. Commun.*, 11, 2182.

Hall, J.P.W. (2018). *A Monograph of the Nymphidiina (Lepidoptera: Riodinidae: Nymphidiini): Phylogeny, Taxonomy, Biology and Biogeography*. The Entomological Society of Washington, Washington, DC.

Hallman, T.A. & Robinson, W.D. (2020). Deciphering ecology from statistical artefacts: Competing influence of sample size, prevalence and habitat specialization on species distribution models and how small evaluation datasets can inflate metrics of performance. *Divers. Distrib.*, 26, 315–328.

Hallmann, C.A., Sorg, M., Jongejans, E., Siepel, H., Hofland, N., Schwan, H., *et al.* (2017). More than 75 percent decline over 27 years in total flying insect biomass in protected areas. *PLoS One*, 12.

Hallmann, C.A., Zeegers, T., van Klink, R., Vermeulen, R., van Wielink, P., Spijkers, H., *et al.* (2020). Declining abundance of beetles, moths and caddisflies in the Netherlands. *Insect Conserv. Divers.*, 13, 127–139.

Hansen, M.C., Potapov, P. V., Moore, R., Hancher, M., Turubanova, S.A., Tyukavina, A., *et al.* (2013). High-Resolution Global Maps of 21st-Century Forest Cover Change. *Science (80-.).*, 342, 850–853.

Hardy, O.J. & Senterre, B. (2007). Characterizing the phylogenetic structure of communities by an additive partitioning of phylogenetic diversity. *J. Ecol.*, 95, 493–506.

Harmon, L.J., Weir, J.T., Brock, C.D., Glor, R.E. & Challenger, W. (2008). GEIGER: Investigating evolutionary radiations. *Bioinformatics*, 24, 129–131.

Harrison, S. & Noss, R. (2017). Endemism hotspots are linked to stable climatic refugia. *Ann. Bot.*, 119, 207–214.

Hennig, W. (1950). *Grundzüge einer Theorie der phylogenetischen Systematik*. Deutscher Zentralverlag, Berlin.

Hennig, W. (1965). Phylogenetic Systematics. *Annu. Rev. Entomol.*, 10, 97–116.

Hijmans, R.J. (2020). raster: Geographic Data Analysis and Modeling. R package version 3.0-12.

Hilborn, A., Pettorelli, N., Orme, C.D.L. & Durant, S.M. (2012). Stalk and chase: How hunt stages affect hunting success in Serengeti cheetah. *Anim. Behav.*, 84, 701–706.

Hill, R.I. (2010). Habitat segregation among mimetic ithomiine butterflies (Nymphalidae). *Evol. Ecol.*, 24, 273–285.

Hill, R.I., Gilbert, L.E. & Kronforst, M.R. (2013). Cryptic genetic and wing pattern diversity in a mimetic Heliconius butterfly. *Mol. Ecol.*, 22, 2760–2770.

Hines, H.M., Counterman, B.A., Papa, R., De Moura, P.A., Cardoso, M.Z., Linares, M., *et al.* (2011). Wing patterning gene redefines the mimetic history of Heliconius butterflies. *Proc. Natl. Acad. Sci. U. S. A.*, 108, 19666–19671.

Hirzel, A.H., Le Lay, G., Helfer, V., Randin, C. & Guisan, A. (2006). Evaluating the ability of habitat suitability models to predict species presences. *Ecol. Modell.*, 199, 142–152.

Hof, C., Rahbek, C. & Araújo, M.B. (2010). Phylogenetic signals in the climatic niches of the world's amphibians. *Ecography (Cop.).*, 33, 242–250.

Hoorn, C. & Wesselingh, F.P. (Eds.). (2010). *Amazonia - Landscape and species evolution: A look into the past*. Wiley-Blackwell, New York.

Hoyal Cuthill, J.F., Guttenberg, N., Ledger, S., Crowther, R. & Huertas, B. (2019). Deep learning on butterfly phenotypes tests evolution's oldest mathematical model. *Sci. Adv.*, 5, 1–12.

Huang, S.Q. & Shi, X.Q. (2013). Floral isolation in Pedicularis: How do congeners with shared pollinators minimize reproductive interference? *New Phytol.*, 199, 858–865.

Huelsenbeck, J.P. & Rannala, B. (2004). Frequentist properties of bayesian posterior probabilities of phylogenetic trees under simple and complex substitution models. *Syst. Biol.*, 53, 904–913.

Hughes, C.E., Pennington, R.T. & Antonelli, A. (2013). Neotropical Plant Evolution: Assembling the Big Picture. *Bot. J. Linn. Soc.*, 171, 1–18.

Huheey, J.E. (1976). Studies in Warning Coloration and Mimicry. VII. Evolutionary Consequences of a Batesian-Mullerian Spectrum: A Model for Mullerian Mimicry. *Evolution (N. Y).*, 30, 86.

Hutchinson, G.E. (1957). Population studies - Animal ecology and demography - Concluding Remarks. In: *Cold Spring Harbor Symposia on Quantitative Biology*.

Hutter, C.R., Guayasamin, J.M. & Wiens, J.J. (2013). Explaining Andean megadiversity: The evolutionary and ecological causes of glassfrog elevational richness patterns. *Ecol. Lett.*, 16, 1135–1144.

Hutter, C.R., Lambert, S.M. & Wiens, J.J. (2017). Rapid Diversification and Time Explain Amphibian Richness at Different Scales in the Tropical Andes, Earth's Most Biodiverse Hotspot. *Am. Nat.*, 190, 828–843.

IPBES. (2019a). *Global assessment report on biodiversity and ecosystem services of the Intergovernmental Science-Policy Platform on Biodiversity and Ecosystem Services*. IPBES secretariat, Bonn, Germany.

IPBES. (2019b). *Summary for policymakers of the global assessment report on biodiversity and ecosystem services of the Intergovernmental Science-Policy Platform on Biodiversity and Ecosystem Services*. Bonn, Germany.

Irisson, J.O., Ayata, S.D., Lindsay, D.J., Karp-Boss, L. & Stemmann, L. (2022). Machine Learning for the Study of Plankton and Marine Snow from Images. *Ann. Rev. Mar. Sci.*, 14, 277–301.

Irwin, D.E., Bensch, S. & Price, T.D. (2001). Speciation in a ring, 409, 333–337.

Isaac, N.J.B., Turvey, S.T., Collen, B., Waterman, C. & Baillie, J.E.M. (2007). Mammals on the EDGE: Conservation priorities based on threat and phylogeny. *PLoS One*, 2.

Jain, M., Olsen, H.E., Paten, B. & Akeson, M. (2016). The Oxford Nanopore MinION: delivery of nanopore sequencing to the genomics community. *Genome Biol.*, 17, 1–11.

Janz, N. & Nylin, S. (2008). The oscillation hypothesis of host-plant range and speciation. *Spec. Speciation, Radiat. Evol. Biol. Herbiv. Insects*, 203–215.

Jenkins, C.N., Pimm, S.L. & Joppa, L.N. (2013). Global patterns of terrestrial vertebrate diversity and conservation. *Proc. Natl. Acad. Sci.*, 110, E2602–E2610.

Jetz, W., McPherson, J.M. & Guralnick, R.P. (2012). Integrating biodiversity distribution knowledge: Toward a global map of life. *Trends Ecol. Evol.*, 27, 151–159.

Jetz, W., Thomas, G.H., Joy, J.B., Redding, D.W., Hartmann, K. & Mooers, A.O. (2014). Global Distribution and Conservation of Evolutionary Distinctness in Birds. *Curr. Biol.*, 24, 919–930.

Jezkova, T. & Wiens, J.J. (2016). Rates of change in climatic niches in plant and animal populations are much slower than projected climate change. *Proc. R. Soc. B Biol. Sci.*, 283.

Jiggins, C.D. & Lamas, G. (2016). *The Ecology and Evolution of Heliconius Butterflies*. Oxford University Press.

Jiggins, C.D., Mallarino, R., Willmott, K.R. & Bermingham, E. (2006). The Phylogenetic Pattern of Speciation and Wing Pattern Change in Neotropical Ithomia Butterflies (Lepidoptera: Nymphalidae). *Evolution (N. Y).*, 60, 1454–1466.

Jiménez, L. & Soberón, J. (2020). Leaving the area under the receiving operating characteristic curve behind: An evaluation method for species distribution modelling applications based on presence-only data. *Methods Ecol. Evol.*, 11, 1571–1586.

Johnston, A., Matechou, E. & Dennis, E.B. (2023). Outstanding challenges and future directions for biodiversity monitoring using citizen science data. *Methods Ecol. Evol.*, 14, 103–116.

Jones, K.E., Bielby, J., Cardillo, M., Fritz, S.A., O'Dell, J., Orme, C.D.L., *et al.* (2009). PanTHERIA: a species-level database of life history, ecology, and geography of extant and recently extinct mammals. *Ecology*, 90, 2648–2648.

Joron, M. & Iwasa, Y. (2005). The evolution of a Müllerian mimic in a spatially distributed community. *J. Theor. Biol.*, 237, 87–103.

Joron, M. & Mallet, J.L.B. (1998). Diversity in mimicry: Paradox or paradigm? *Trends Ecol. Evol.*, 13, 461–466.

Joshi, J., Prakash, A. & Kunte, K. (2017). Evolutionary assembly of communities in butterfly mimicry rings. *Am. Nat.*, 189, E58–E76.

Jost, L. (2006). Entropy and diversity. *Oikos*, 113, 363–375.

Jousselin, E. & Elias, M. (2019). Testing host-plant driven speciation in phytophagous insects : a phylogenetic perspective. *Peer Community Evol. Biol.*, 1–35.

Kalyaanamoorthy, S., Minh, B.Q., Wong, T.K.F., Von Haeseler, A. & Jermiin, L.S. (2017). ModelFinder: Fast model selection for accurate phylogenetic estimates. *Nat. Methods*, 14, 587–589.

Kang, C., Im, S., Lee, W.Y., Choi, Y., Stuart-Fox, D. & Huertas, B. (2021). Climate predicts both visible and near-infrared reflectance in butterflies. *Ecol. Lett.*, 24, 1869–1879.

Kantsa, A., Raguso, R.A., Dyer, A.G., Sgardelis, S.P., Olesen, J.M. & Petanidou, T. (2017). Community-wide integration of floral colour and scent in a Mediterranean scrubland. *Nat. Ecol. Evol.*, 1, 1502–1510.

Kapan, D.D. (2001). Three-butterfly system provides a field test of müllerian mimicry. *Nature*, 409, 338–340.

Karatzoglou, A., Smola, A., Hornik, K. & Zeileis, A. (2004). kernlab - An S4 Package for Kernel Methods in R. *J. Stat. Softw.*, 11, 389–393.

Kass, J.M., Guenard, B., Dudley, K.L., Jenkins, C.N., Azuma, F., Fisher, B.L., *et al.* (2022). The global distribution of known and undiscovered ant biodiversity. *Sci. Adv.*, 8.

Katz, K., Shutov, O., Lapoint, R., Kimelman, M., Rodney Brister, J. & O'Sullivan, C. (2022). The Sequence Read Archive: A decade more of explosive growth. *Nucleic Acids Res.*, 50, D387–D390.

Kaufman, D.M. & Willig, M.R. (1998). Latitudinal patterns of mammalian species richness in the New World: the effects of sampling method and faunal group. *J. Biogeogr.*, 25, 795–805.

Kawahara, A.Y., Plotkin, D., Espeland, M., Meusemann, K., Toussaint, E.F.A., Donath, A., *et al.* (2019). Phylogenomics reveals the evolutionary timing and pattern of butterflies and moths. *Proc. Natl. Acad. Sci.*, 116, 22657–22663.

KBA Standards and Appeals Committee. (2020). *Guidelines for using A Global Standard for the Identification of Key Biodiversity Areas. Version 1.1. Prepared by the KBA Standards and Appeals Committee of the IUCN Species Survival Commission and IUCN World Commission on Protected Areas.* Gland, Switzerland.

Keppel, G., Mokany, K., Wardell-Johnson, G.W., Phillips, B.L., Welbergen, J.A. & Reside,

A.E. (2015). The capacity of refugia for conservation planning under climate change. *Front. Ecol. Environ.*, 13, 106–112.

Kier, G., Kreft, H., Tien, M.L., Jetz, W., Ibisch, P.L., Nowicki, C., *et al.* (2009). A global assessment of endemism and species richness across island and mainland regions. *Proc. Natl. Acad. Sci. U. S. A.*, 106, 9322–9327.

Kikuchi, D.W. & Pfennig, D.W. (2013). Imperfect mimicry and the limits of natural selection. *Q. Rev. Biol.*, 88, 297–315.

Kindlmann, P., Schödelbauerová, I. & Dixon, A.F.G. (2012). Inverse latitudinal gradients in species diversity. In: *Scaling Biodiversity*. pp. 246–257.

Kitching, I.J. (1985). Early stages and the classification of the milkweed butterflies (Lepidoptera: Danainae). *Zool. J. Linn. Soc.*, 85, 1–97.

Knapp, S. (2002). Assessing Patterns of Plant Endemism in Neotropical Uplands. *Bot. Rev.*, 68, 22–37.

Kokko, H., Mappes, J. & Lindström, L. (2003). Alternative prey can change model-mimic dynamics between parasitism and mutualism. *Ecol. Lett.*, 6, 1068–1076.

König, C., Wüest, R.O., Graham, C.H., Karger, D.N., Sattler, T., Zimmermann, N.E., *et al.* (2021). Scale dependency of joint species distribution models challenges interpretation of biotic interactions. *J. Biogeogr.*, 48, 1541–1551.

Kozak, K.H. & Wiens, J.J. (2010a). Accelerated rates of climatic-niche evolution underlie rapid species diversification. *Ecol. Lett.*, 13, 1378–1389.

Kozak, K.H. & Wiens, J.J. (2010b). Niche conservatism drives elevational diversity patterns in appalachian salamanders. *Am. Nat.*, 176, 40–54.

Kozak, K.M., Wahlberg, N., Neild, A.F.E., Dasmahapatra, K.K., Mallet, J. & Jiggins, C.D. (2015). Multilocus Species Trees Show the Recent Adaptive Radiation of the Mimetic Heliconius Butterflies. *Syst. Biol.*, 64, 505–524.

Kozlov, A.M., Darriba, D., Flouri, T., Morel, B. & Stamatakis, A. (2019). RAxML-NG: a fast, scalable and user-friendly tool for maximum likelihood phylogenetic inference. *Bioinformatics*, 35, 4453–4455.

Kraft, N.J.B., Cornwell, W.K., Webb, C.O. & Ackerly, D.D. (2007). Trait Evolution, Community Assembly, and the Phylogenetic Structure of Ecological Communities. *Am. Nat.*, 170, 271–283.

Kunte, K. (2008). Competition and species diversity: Removal of dominant species increases diversity in Costa Rican butterfly communities. *Oikos*, 117, 69–76.

Kunte, K., Kizhakke, A.G. & Nawge, V. (2021). Evolution of Mimicry Rings as a Window into Community Dynamics. *Annu. Rev. Ecol. Evol. Syst.*, 52, 315–341.

Kuzniar, A., van Ham, R.C.H.J., Pongor, S. & Leunissen, J.A.M. (2008). The quest for orthologs: finding the corresponding gene across genomes. *Trends Genet.*, 24, 539–551.

Lampa, S., Dahlö, M., Olason, P.I., Hagberg, J. & Spjuth, O. (2013). Lessons learned from implementing a national infrastructure in Sweden for storage and analysis of next-generation sequencing data. *Gigascience*, 2, 9.

Langham, G.M. (2004). Specialized avian predators repeatedly attack novel color morphs of Heliconius butterflies. *Evolution (N. Y).*, 58, 2783–2787.

Larget, B. & Simon, D.L. (1999). Markov chain Monte Carlo algorithms for the Bayesian analysis of phylogenetic trees. *Mol. Biol. Evol.*, 16, 750–759.

Laurance, W.F., Carolina Useche, D., Shoo, L.P., Herzog, S.K., Kessler, M., Escobar, F., *et al.* (2011). Global warming, elevational ranges and the vulnerability of tropical biota. *Biol. Conserv.*, 144, 548–557.

Lawler, J.J., White, D., Sifneos, J.C. & Master, L.L. (2003). Rare species and the use of indicator groups for conservation planning. *Conserv. Biol.*, 17, 875–882.

Le, S.Q. & Gascuel, O. (2008). An improved general amino acid replacement matrix. *Mol. Biol. Evol.*, 25, 1307–1320.

Legendre, P., Lapointe, F.-J. & Casgrain, P. (1994). Modeling Brain Evolution from Behavior: A Permutational Regression Approach. *Evolution (N. Y).*, 48, 1487.

Legendre, P. & Legendre, L. (2012). *Numerical ecology. Developments in environmental modeling*. *Dev. Environ. Model.*

Leroy, B. (2016). Rarity: Calculation of Rarity Indices for Species and Assemblages of Species. R package version 1.3-6.

Leroy, B., Bellard, C., Dubos, N., Colliot, A., Vasseur, M., Courtial, C., *et al.* (2014). Forecasted climate and land use changes, and protected areas: The contrasting case of spiders. *Divers. Distrib.*, 20, 686–697.

Leroy, B., Canard, A. & Ysnel, F. (2013). Integrating multiple scales in rarity assessments of invertebrate taxa. *Divers. Distrib.*, 19, 794–803.

Leroy, B., Delsol, R., Hugueny, B., Meynard, C.N., Barhoumi, C., Barbet-Massin, M., *et al.* (2018). Without quality presence–absence data, discrimination metrics such as TSS can be misleading measures of model performance. *J. Biogeogr.*, 45, 1994–2002.

Leroy, B., Petillon, J., Gallon, R., Canard, A. & Ysnel, F. (2012). Improving occurrence-based rarity metrics in conservation studies by including multiple rarity cut-off points. *Insect Conserv. Divers.*, 5, 159–168.

Lindström, L., Alatalo, R. V., Lyytinen, A. & Mappes, J. (2004). The effect of alternative prey on the dynamics of imperfect Batesian and Müllerian mimicries. *Evolution (N. Y).*, 58, 1294–1302.

Lindstrom, L., Alatalo, R. V. & Mappes, J. (1997). Imperfect Batesian mimicry - The effects of the frequency and the distastefulness of the model. *Proc. R. Soc. B Biol. Sci.*, 264, 149–153.

Linnæus, C. V. (1753). *Species Plantarum*.

Linnæus, C. V. (1758). *Systema Naturae*.

Lomolino, M. V. (2004). Conservation Biogeography. In: *Frontiers of Biogeography: new directions in the geography of nature* (eds. Lomolino, M.V. & Heaney, L.R.). Sinauer Associates, Sunderland, Massachusetts, pp. 293–296.

Lomolino, M. V. (2016). *Biogeography, History of*. *Encycl. Evol. Biol.* Elsevier Ltd.

Lomolino, M. V., Riddle, B.R. & Whittaker, R.J. (2016). *Biogeography : biological diversity across space and time*. Oxford University Press.

Losos, J.B. (2008). Phylogenetic niche conservatism, phylogenetic signal and the relationship between phylogenetic relatedness and ecological similarity among species. *Ecol. Lett.*, 11, 995–1003.

Lürig, M.D., Donoughe, S., Svensson, E.I., Porto, A. & Tsuboi, M. (2021). Computer Vision, Machine Learning, and the Promise of Phenomics in Ecology and Evolutionary Biology. *Front. Ecol. Evol.*, 9.

van der Maaten, L. & Weinberger, K. (2012). Stochastic triplet embedding. In: *2012 IEEE International Workshop on Machine Learning for Signal Processing*. IEEE, pp. 1–6.

MacArthur, R. & Levins, R. (1964). COMPETITION, HABITAT SELECTION, AND CHARACTER DISPLACEMENT IN A PATCHY ENVIRONMENT. *Proc. Natl. Acad. Sci.*, 51, 1207–1210.

Maechler, M. (2016). diptest: Hartigan's Dip Test Statistic for Unimodality - Corrected. R package version 0.75-7.

Mahalanobis, P.C. (1936). On the generalised distance in statistics. *Proc. Natl. Inst. Sci. India*, 2, 49–55.

Maiorano, L., Montemaggiori, A., Ficetola, G.F., O'Connor, L. & Thuiller, W. (2020). TETRA-EU 1.0: A species-level trophic metaweb of European tetrapods. *Glob. Ecol. Biogeogr.*, 29, 1452–1457.

Malcolm, J.R., Liu, C., Neilson, R.P., Hansen, L. & Hannah, L. (2006). Global warming and extinctions of endemic species from biodiversity hotspots. *Conserv. Biol.*, 20, 538–548.

Malhi, Y., Roberts, J.T., Betts, R.A., Killeen, T.J., Li, W. & Nobre, C.A. (2008). Climate change, deforestation, and the fate of the Amazon. *Science (80-.).*, 319, 169–172.

Mallet, J. (1993). Speciation, Raciation, and Color Pattern Evolution in Heliconius Butterflies: The Evidence from Hybrid Zones. In: *Hybrid Zones and the Evolutionary Process* (ed. Harrison, R.G.). Oxford University Press.

Mallet, J. (1999). Causes and Consequences of a Lack of Coevolution in Müllerian mimicry. *Evol. Ecol.*, 13, 777–806.

Mallet, J. (2001). Mimicry: An interface between psychology and evolution. *Proc. Natl. Acad. Sci. U. S. A.*, 98, 8928–8930.

Mallet, J. & Barton, N.H. (1989). Strong natural selection in a warning-color hybrid zone. *Evolution (N. Y).*, 43, 421–431.

Mallet, J. & Gilbert, L.E. (1995). Why are there so many mimicry rings? Correlations between habitat, behaviour and mimicry in Heliconius butterflies. *Biol. J. Linn. Soc.*, 55, 159–180.

Manni, M., Berkeley, M.R., Seppey, M., Simão, F.A. & Zdobnov, E.M. (2021a). BUSCO Update: Novel and Streamlined Workflows along with Broader and Deeper Phylogenetic Coverage for Scoring of Eukaryotic, Prokaryotic, and Viral Genomes. *Mol. Biol. Evol.*, 38, 4647–4654.

Manni, M., Berkeley, M.R., Seppey, M. & Zdobnov, E.M. (2021b). BUSCO: Assessing Genomic Data Quality and Beyond. *Curr. Protoc.*, 1.

Mannion, P.D., Upchurch, P., Benson, R.B.J. & Goswami, A. (2014). The latitudinal biodiversity gradient through deep time. *Trends Ecol. Evol.*, 29, 42–50.

Mappes, J., Marples, N. & Endler, J.A. (2005). The complex business of survival by aposematism. *Trends Ecol. Evol.*, 20, 598–603.

Di Marco, M., Venter, O., Possingham, H.P. & Watson, J.E.M. (2018). Changes in human footprint drive changes in species extinction risk. *Nat. Commun.*, 9, 4621.

Di Marco, M., Watson, J.E.M., Possingham, H.P. & Venter, O. (2017). Limitations and trade-offs in the use of species distribution maps for protected area planning. *J. Appl. Ecol.*, 54, 402–411.

Maritz, B., Penner, J., Martins, M., Crnobrnja-Isailović, J., Spear, S., Alencar, L.R.V., *et al.* (2016). Identifying global priorities for the conservation of vipers. *Biol. Conserv.*, 204, 94–102.

Maron, M., Simmonds, J.S., Watson, J.E.M., Sonter, L.J., Bennun, L., Griffiths, V.F., *et al.* (2020). Global no net loss of natural ecosystems. *Nat. Ecol. Evol.*, 4, 46–49.

Martínez-Freiría, F., Toyama, K.S., Freitas, I. & Kaliontzopoulou, A. (2020). Thermal melanism explains macroevolutionary variation of dorsal pigmentation in Eurasian vipers. *Sci. Rep.*, 10, 1–10.

Mateo, R.G., Croat, T.B., Felicísimo, Á.M. & Muñoz, J. (2010). Profile or group discriminative techniques? Generating reliable species distribution models using pseudo-absences and target-group absences from natural history collections. *Divers. Distrib.*, 16, 84–94.

Mäyrä, J., Keski-Saari, S., Kivinen, S., Tanhuanpää, T., Hurskainen, P., Kullberg, P., *et al.* (2021). Tree species classification from airborne hyperspectral and LiDAR data using 3D convolutional neural networks. *Remote Sens. Environ.*, 256.

Mazel, F., Guilhaumon, F., Mouquet, N., Devictor, V., Gravel, D., Renaud, J., *et al.* (2014). Multifaceted diversity-area relationships reveal global hotspots of mammalian species, trait and lineage diversity. *Glob. Ecol. Biogeogr.*, 23, 836–847.

Mccain, C.M. & Colwell, R.K. (2011). Assessing the threat to montane biodiversity from discordant shifts in temperature and precipitation in a changing climate. *Ecol. Lett.*, 14, 1236–1245.

McClure, M., Clerc, C., Desbois, C., Meichanetzoglou, A., Cau, M., Bastin-Héline, L., *et al.* (2019). Why has transparency evolved in aposematic butterflies? Insights from the largest radiation of aposematic butterflies, the Ithomiini. *Proc. R. Soc. B Biol. Sci.*, 286, 20182769.

McClure, M., Dutrillaux, B., Dutrillaux, A.M., Lukhtanov, V. & Elias, M. (2018). Heterozygosity and Chain Multivalents during Meiosis Illustrate Ongoing Evolution as a Result of Multiple Holokinetic Chromosome Fusions in the Genus Melinaea (Lepidoptera, Nymphalidae). *Cytogenet. Genome Res.*, 153, 213–222.

McClure, M. & Elias, M. (2016). Unravelling the role of host plant expansion in the diversification of a Neotropical butterfly genus. *BMC Evol. Biol.*, 16, 128.

McDonald-Madden, E., Sabbadin, R., Game, E.T., Baxter, P.W.J., Chadès, I. & Possingham, H.P. (2016). Using food-web theory to conserve ecosystems. *Nat. Commun.*, 7, 1–8.

McGill, B.J. (2010). Matters of scale. *Science (80-.).*, 328, 575–576.

Melo, A.S., Rangel, T.F.L.V.B. & Diniz-Filho, J.A.F. (2009). Environmental drivers of beta-diversity patterns in New-World birds and mammals. *Ecography (Cop.).*, 32, 226–236.

Merow, C., Smith, M.J., Edwards, T.C., Guisan, A., Mcmahon, S.M., Normand, S., *et al.* (2014). What do we gain from simplicity versus complexity in species distribution models? *Ecography (Cop.).*, 37, 1267–1281.

Mikheenko, A., Prjibelski, A., Saveliev, V., Antipov, D. & Gurevich, A. (2018). Versatile genome assembly evaluation with QUAST-LG. *Bioinformatics*, 34, i142–i150.

Millennium Ecosystem Assessment. (2005). *Ecosystems and Human Well-being: Synthesis*. Island Press, Washington, DC.

Minh, B.Q., Hahn, M.W. & Lanfear, R. (2020a). New methods to calculate concordance factors for phylogenomic datasets. *Mol. Biol. Evol.*, 37, 2727–2733.

Minh, B.Q., Nguyen, M.A.T. & Von Haeseler, A. (2013). Ultrafast approximation for phylogenetic bootstrap. *Mol. Biol. Evol.*, 30, 1188–1195.

Minh, B.Q., Schmidt, H.A., Chernomor, O., Schrempf, D., Woodhams, M.D., von Haeseler, A., *et al.* (2020b). IQ-TREE 2: New Models and Efficient Methods for Phylogenetic Inference in the Genomic Era. *Mol. Biol. Evol.*, 37, 1530–1534.

Mirarab, S., Reaz, R., Bayzid, M.S., Zimmermann, T., S. Swenson, M. & Warnow, T. (2014). ASTRAL: Genome-scale coalescent-based species tree estimation. *Bioinformatics*, 30, 541–548.

Mishler, B.D. (2023). Spatial Phylogenetics. *50 th Anniv. Perspect. Biogeogr.*, 1–10.

Mitchard, E.T.A. (2018). The tropical forest carbon cycle and climate change. *Nature*, 559, 527–534.

Moeller, D.A. (2004). Facilitative interactions among plants via shared pollinators. *Ecology*, 85, 3289–3301.

Molloy, E.K. & Warnow, T. (2018). To Include or Not to Include: The Impact of Gene Filtering on Species Tree Estimation Methods. *Syst. Biol.*, 67, 285–303.

Montejo-Kovacevich, G., Martin, S.H., Meier, J.I., Bacquet, C.N., Monllor, M., Jiggins, C.D., *et al.* (2020). Microclimate buffering and thermal tolerance across elevations in a tropical butterfly. *J. Exp. Biol.*

Montgomery, G.A., Dunn, R.R., Fox, R., Jongejans, E., Leather, S.R., Saunders, M.E., *et al.* (2020). Is the insect apocalypse upon us? How to find out. *Biol. Conserv.*, 241.

Mora, C., Tittensor, D.P., Adl, S., Simpson, A.G.B. & Worm, B. (2011). How many species are there on earth and in the ocean? *PLoS Biol.*, 9, 1–8.

Morawetz, W. & Raedig, C. (2007). Angiosperm Biodiversity, Endemism and Conservation in the Neotropics. *Taxon*, 56, 1245.

Motyka, M., Kusy, D., Masek, M., Bocek, M., Li, Y. & Bilkova, R. (2021). Conspicuousness,

phylogenetic structure, and origins of Müllerian mimicry in 4000 lycid beetles from all zoogeographic regions. *Sci. Rep.*, 1–19.

Mougi, A. & Kondoh, M. (2012). Diversity of interaction types and ecological community stability. *Science (80-.).*, 337, 349–351.

Mouillot, D., Bellwood, D.R., Baraloto, C., Chave, J., Galzin, R., Harmelin-Vivien, M., *et al.* (2013). Rare Species Support Vulnerable Functions in High-Diversity Ecosystems. *PLoS Biol.*, 11.

Mullen, S.P., Savage, W.K., Wahlberg, N. & Willmott, K.R. (2011). Rapid diversification and not clade age explains high diversity in neotropical Adelpha butterflies. *Proc. R. Soc. B Biol. Sci.*, 278, 1777–1785.

Müller, F. (1879). Ituna and Thyridia; a remarkable case of mimicry in butterflies. *Trans. Entomol. Soc. Lond.*, xx–xxix.

Mullis, K., Faloona, F., Scharf, S., Saiki, R., Horn, G. & Erlich, H. (1992). Specific enzymatic amplification of DNA in vitro: the polymerase chain reaction. 1986. *Biotechnology*.

Muñoz-Ramírez, C.P., Bitton, P.-P., Doucet, S.M. & Knowles, L.L. (2016). Mimics here and there, but not everywhere: Müllerian mimicry in Ceroglossus ground beetles? . *Biol. Lett.*, 12, 20160429.

Murali, G., Gumbs, R., Meiri, S. & Roll, U. (2021). Global determinants and conservation of evolutionary and geographic rarity in land vertebrates. *Sci. Adv.*, 7, 1–15.

Myers, N., Mittermeier, R.A., Mittermeier, C.G., da Fonseca, G.A.B. & Kent, J. (2000). Biodiversity hotspots for conservation priorities. *Nature*, 403, 853–858.

Nahrstedt, A. & Davis, R.H. (1983). Occurrence, variation and biosynthesis of the cyanogenic glucosides linamarin and lotaustralin in species of the Heliconiini (Insecta: Lepidoptera). *Comp. Biochem. Physiol. -- Part B Biochem.*, 75, 65–73.

Nevado, B., Atchison, G.W., Hughes, C.E. & Filatov, D.A. (2016). Widespread adaptive evolution during repeated evolutionary radiations in New World lupins. *Nat. Commun.*, 7, 1–9.

Newbold, T., Hudson, L.N., Hill, S.L.L., Contu, S., Lysenko, I., Senior, R.A., *et al.* (2015). Global effects of land use on local terrestrial biodiversity. *Nature*, 520, 45–50.

Newman, E., Manning, J. & Anderson, B. (2014). Matching floral and pollinator traits through guild convergence and pollinator ecotype formation. *Ann. Bot.*, 113, 373–384.

Nobre, C.A., Sampaio, G., Borma, L.S., Castilla-Rubio, J.C., Silva, J.S. & Cardoso, M. (2016). Land-use and climate change risks in the amazon and the need of a novel sustainable development paradigm. *Proc. Natl. Acad. Sci. U. S. A.*, 113, 10759–10768.

Nuismer, S.L., Jordano, P. & Bascompte, J. (2013). Coevolution and the architecture of mutualistic networks. *Evolution (N. Y).*, 67, 338–354.

Nunez, S., Arets, E., Alkemade, R., Verwer, C. & Leemans, R. (2019). Assessing the impacts of climate change on biodiversity: is below 2 °C enough? *Clim. Change*, 154, 351–365.

O'Brien, A.M., Jack, C.N., Friesen, M.L. & Frederickson, M.E. (2021). Whose trait is it anyways? Coevolution of joint phenotypes and genetic architecture in mutualisms. *Proc.*

R. Soc. B Biol. Sci., 288, 20202483.

O'Neill, B.C., Kriegler, E., Ebi, K.L., Kemp-Benedict, E., Riahi, K., Rothman, D.S., *et al.* (2017). The roads ahead: Narratives for shared socioeconomic pathways describing world futures in the 21st century. *Glob. Environ. Chang.*, 42, 169–180.

Ohlemüller, R., Anderson, B.J., Araújo, M.B., Butchart, S.H.M., Kudrna, O., Ridgely, R.S., *et al.* (2008). The coincidence of climatic and species rarity: High risk to small-range species from climate change. *Biol. Lett.*, 4, 568–572.

Oksanen, J.F., Blanchet, G., Friendly, M., Kindt, R., Legendre, P., McGlinn, D., *et al.* (2019). vegan: Community Ecology Package.

Okuyama, T. & Holland, J.N. (2008). Network structural properties mediate the stability of mutualistic communities. *Ecol. Lett.*, 11, 208–216.

Olson, D.M., Dinerstein, E., Wikramanayake, E.D., Burgess, N.D., Powell, G.V.N., Underwood, E.C., *et al.* (2001). Terrestrial Ecoregions of the World: A New Map of Life on Earth: A new global map of terrestrial ecoregions provides an innovative tool for conserving biodiversity. *Bioscience*, 51, 933–938.

Orme, C.D.L., Davies, R.G., Burgess, M., Eigenbrod, F., Pickup, N., Olson, V.A., *et al.* (2005). Global hotspots of species richness are not congruent with endemism or threat. *Nature*, 436, 1016–1019.

Orr, M.C., Hughes, A.C., Chesters, D., Pickering, J., Zhu, C.D. & Ascher, J.S. (2021). Global Patterns and Drivers of Bee Distribution. *Curr. Biol.*, 31, 451-458.e4.

Ortiz-Acevedo, E., Gomez, J.P., Espeland, M., Toussaint, E.F.A. & Willmott, K.R. (2020). The roles of wing color pattern and geography in the evolution of Neotropical Preponini butterflies. *Ecol. Evol.*, 10, 12801–12816.

Osborne, P. (2012). Mountains, zonation and community gradients. In: *Tropical Ecosystems and Ecological Concepts*. Cambridge University Press, pp. 315–333.

Outomuro, D., Angel-giraldo, P., Corral-lopez, A. & Realpe, E. (2013). Multitrait aposematic signal in Batesian, 1–13.

Ovaskainen, O. & Abrego, N. (2020). *Joint Distribution Modelling (with applications in R)*.

Ovaskainen, O., Tikhonov, G., Norberg, A., Guillaume Blanchet, F., Duan, L., Dunson, D., *et al.* (2017). How to make more out of community data? A conceptual framework and its implementation as models and software. *Ecol. Lett.*, 20, 561–576.

Owens, I.P.F. & Short, R. V. (1995). Hormonal basis of sexual dimorphism in birds: implications for new theories of sexual selection. *Trends Ecol. Evol.*, 10, 44–47.

Pagel, M. (1994). Detecting correlated evolution on phylogenies: a general method for the comparative analysis of discrete characters. *Proc. R. Soc. London. Ser. B Biol. Sci.*, 255, 37–45.

Pagel, M. (1999). Inferring the historical patterns of biological evolution. *Nature*, 401, 877.

Papageorgis, C. (1975). Mimicry in Neotropical butterflies. *Am. Sci.*, 63, 522–532.

Paradis, E. & Schliep, K. (2019). Ape 5.0: An environment for modern phylogenetics and evolutionary analyses in R. *Bioinformatics*, 35, 526–528.

Pareek, C.S., Smoczynski, R. & Tretyn, A. (2011). Sequencing technologies and genome sequencing. *J. Appl. Genet.*, 52, 413–435.

Parmesan, C. & Yohe, G. (2003). A globally coherent fingerprint of climate change impacts across natural systems. *Nature*, 421, 37–42.

Parr, C.L., Dunn, R.R., Sanders, N.J., Weiser, M.D., Photakis, M., Bishop, T.R., *et al.* (2017). GlobalAnts: a new database on the geography of ant traits (Hymenoptera: Formicidae). *Insect Conserv. Divers.*, 10, 5–20.

Parr, C.S., Wilson, N., Leary, P., Schulz, K.S., Lans, K., Walley, L., *et al.* (2014). The Encyclopedia of Life v2: Providing Global Access to Knowledge About Life on Earth. *Biodivers. Data J.*, 2.

Parr, M.J., Bennun, L., Boucher, T., Brooks, T., Chutas, C.A., Dinerstein, E., *et al.* (2009). Why we should aim for zero extinction. *Trends Ecol. Evol.*, 24, 181.

Pascual-García, A. & Bastolla, U. (2017). Mutualism supports biodiversity when the direct competition is weak. *Nat. Commun.*, 8, 14326.

Pateiro-Lopez, B. & Rodriguez-Casal, A. (2019). alphahull: Generalization of the Convex Hull of a Sample of Points in the Plane. R package version 2.2.

Pearson, D.L. & Carroll, S.S. (2001). Predicting patterns of tiger beetle (Coleoptera: Cicindelidae) species richness in northwestern south america. *Stud. Neotrop. Fauna Environ.*, 36, 125–136.

Pearson, R.G. (2006). Climate change and the migration capacity of species. *Trends Ecol. Evol.*, 21, 111–113.

Pebesma, E. (2018). Simple Features for R: Standardized Support for Spatial Vector Data. *R J.*, 10, 439–446.

Pecl, G.T., Araújo, M.B., Bell, J.D., Blanchard, J., Bonebrake, T.C., Chen, I.C., *et al.* (2017). Biodiversity redistribution under climate change: Impacts on ecosystems and human well-being. *Science (80-.).*, 355.

Peña, C. & Espeland, M. (2015). Diversity Dynamics in Nymphalidae Butterflies: Effect of Phylogenetic Uncertainty on Diversification Rate Shift Estimates. *PLoS One*, 10, e0120928.

Penney, H.D., Hassall, C., Skevington, J.H., Abbott, K.R. & Sherratt, T.N. (2012). A comparative analysis of the evolution of imperfect mimicry. *Nature*, 483, 461–464.

Peres, C.A., Gardner, T.A., Barlow, J., Zuanon, J., Michalski, F., Lees, A.C., *et al.* (2010). Biodiversity conservation in human-modified Amazonian forest landscapes. *Biol. Conserv.*, 143, 2314–2327.

Pérochon, E., Rosser, N., Kozak, K.M., Elias, M. & Doré, M. (2023). Müllerian mimicry: one ring to bring them all, and in the jungle bind them.

Pianka, E.R. (1981). Competition and niche theory. In: *Theoretical ecology: Principles and applications* (ed. May, R.M.). Blackwell, Oxford, Sunderland, Mass.

Pigot, A.L., Sheard, C., Miller, E.T., Bregman, T.P., Freeman, B.G., Roll, U., *et al.* (2020). Macroevolutionary convergence connects morphological form to ecological function in

birds. *Nat. Ecol. Evol.*, 4, 230–239.

Pinna, C.S., Vilbert, M., Borensztajn, S., De Marcillac, W.D., Piron-Prunier, F., Pomerantz, A., *et al.* (2021). Mimicry can drive convergence in structural and light transmission features of transparent wings in Lepidoptera. *Elife*, 10, 1–25.

Pintanel, P., Tejedo, M., Ron, S.R., Llorente, G.A. & Merino-Viteri, A. (2019). Elevational and microclimatic drivers of thermal tolerance in Andean Pristimantis frogs. *J. Biogeogr.*, 46, 1664–1675.

Poelen, J.H., Simons, J.D. & Mungall, C.J. (2014). Global biotic interactions: An open infrastructure to share and analyze species-interaction datasets. *Ecol. Inform.*, 24, 148–159.

Poisot, T., Bergeron, G., Cazelles, K., Dallas, T., Gravel, D., MacDonald, A., *et al.* (2021). Global knowledge gaps in species interaction networks data. *J. Biogeogr.*, 48, 1552–1563.

Pollock, L.J., O'Connor, L.M.J., Mokany, K., Rosauer, D.F., Talluto, M. V. & Thuiller, W. (2020). Protecting Biodiversity (in All Its Complexity): New Models and Methods. *Trends Ecol. Evol.*, 35, 1119–1128.

Pollock, L.J., Thuiller, W. & Jetz, W. (2017). Large conservation gains possible for global biodiversity facets. *Nature*, 546, 141–144.

Pollock, L.J., Tingley, R., Morris, W.K., Golding, N., O'Hara, R.B., Parris, K.M., *et al.* (2014). Understanding co-occurrence by modelling species simultaneously with a Joint Species Distribution Model (JSDM). *Methods Ecol. Evol.*, 5, 397–406.

Pomerantz, A.F., Siddique, R.H., Cash, E.I., Kishi, Y., Pinna, C., Hammar, K., *et al.* (2021). Developmental, cellular and biochemical basis of transparency in clearwing butterflies. *J. Exp. Biol.*, 224.

Poole, R.W.. (1970). Habitat Preferences of Some Species of a Müllerian-Mimicry Complex in Northern Venezuela , and Their Effects on Evolution of Mimic-Wing Pattern. *J. New York Entomol. Soc.*, 78, 121–129.

Porto, A. & Voje, K.L. (2020). ML-morph: A fast, accurate and general approach for automated detection and landmarking of biological structures in images. *Methods Ecol. Evol.*, 11, 500–512.

Posada, D. & Buckley, T.R. (2004). Model selection and model averaging in phylogenetics: Advantages of akaike information criterion and bayesian approaches over likelihood ratio tests. *Syst. Biol.*, 53, 793–808.

Potapov, P., Li, X., Hernandez-Serna, A., Tyukavina, A., Hansen, M.C., Kommareddy, A., *et al.* (2021). Mapping global forest canopy height through integration of GEDI and Landsat data. *Remote Sens. Environ.*, 253, 1–30.

Le Poul, Y., Whibley, A., Chouteau, M., Prunier, F., Llaurens, V. & Joron, M. (2014). Evolution of dominance mechanisms at a butterfly mimicry supergene. *Nat. Commun.*, 5, 1–8.

Poulton, E.B. (1890). *The colours of animals: their meaning and use, especially considered in the case of insects.* D. Appleton.

Poulton, E.B. (1898). Natural Selection the Cause of Mimetic Resemblance and Common Warning Colours. *Zool. J. Linn. Soc.*, 26, 558–612.

Prendergast, J.R., Quinn, R.M., Lawton, J.H., Eversham, B.C. & Gibbons, D.W. (1993). Rare species, the coincidence of diversity hotspots and conservation strategies. *Nature*, 365, 335–337.

Purvis, A., Gittleman, J.L., Cowlishaw, G. & Mace, G.M. (2000). Predicting extinction risk in declining species. *Proc. R. Soc. B Biol. Sci.*, 267, 1947–1952.

Putnam, N.H., O'Connell, B.L., Stites, J.C., Rice, B.J., Blanchette, M., Calef, R., *et al.* (2016). Chromosome-scale shotgun assembly using an in vitro method for long-range linkage. *Genome Res.*, 26, 342–350.

Puttick, M., Thomas, G., Freckleton, R., Ingram, T., Paradis, E. & Orme, D. (2018). motmot.2.0: Models of Trait Macroevolution on Trees.

R Core Team. (2019). R: A Language and Environment for Statistical Computing.

Rabinowitz, D. (1981). Seven forms of rarity. In: *Biological Aspects of Rare Plant Conservation* (ed. Synge, H.). Wiley, New York, pp. 205–217.

Rajão, R., Soares-Filho, B., Nunes, F., Börner, J., Machado, L., Assis, D., *et al.* (2020). The rotten apples of Brazil's agribusiness. *Science (80-.).*, 369, 246–248.

Rangel, T.F., Edwards, N.R., Holden, P.B., Diniz-Filho, J.A.F., Gosling, W.D., Coelho, M.T.P., *et al.* (2018). Modeling the ecology and evolution of biodiversity: Biogeographical cradles, museums, and graves. *Science (80-.).*, 361.

Raxworthy, C.J., Pearson, R.G., Rabibisoa, N., Rakotondrazafy, A.M., Ramanamanjato, J.B., Raselimanana, A.P., *et al.* (2008). Extinction vulnerability of tropical montane endemism from warming and upslope displacement: A preliminary appraisal for the highest massif in Madagascar. *Glob. Chang. Biol.*, 14, 1703–1720.

Redding, D.W. (2003). Incorporating genetic distinctness and reserve occupancy into a conservation priorisation approach. Master's Thesis. *Univ. East Anglia, Norwich, UK*.

Ree, R.H. & Smith, S.A. (2008). Maximum likelihood inference of geographic range evolution by dispersal, local extinction, and cladogenesis. *Syst. Biol.*, 57, 4–14.

Revell, L.J. (2009). Size-correction and principal components for interspecific comparative studies. *Evolution (N. Y).*, 63, 3258–3268.

Revell, L.J. & Harmon, L.J. (2022). *Phylogenetic comparative methods in R*. PRINCETON UNIVERSITY PRESS.

Reynolds, D. (2015). Gaussian Mixture Models. *Encycl. Biometrics*, 827–832.

Reznick, D.N. & Ricklefs, R.E. (2009). Darwin's bridge between microevolution and macroevolution. *Nature*, 457, 837–842.

Ribeiro, M.C., Metzger, J.P., Martensen, A.C., Ponzoni, F.J. & Hirota, M.M. (2009). The Brazilian Atlantic Forest: How much is left, and how is the remaining forest distributed? Implications for conservation. *Biol. Conserv.*, 142, 1141–1153.

Riley, S.J., DeGloria, S.D. & Elliot, R. (1999). A terrain ruggedness index that quantifies topographic heterogeneity. *Intermt. J. Sci.*

Roberts, D.R., Bahn, V., Ciuti, S., Boyce, M.S., Elith, J., Guillera-Arroita, G., *et al.* (2017). Cross-validation strategies for data with temporal, spatial, hierarchical, or phylogenetic structure. *Ecography (Cop.).*, 40, 913–929.

Robuchon, M., Pavoine, S., Véron, S., Delli, G., Faith, D.P., Mandrici, A., *et al.* (2021). Revisiting species and areas of interest for conserving global mammalian phylogenetic diversity. *Nat. Commun.*, 12, 1–11.

Roll, U., Feldman, A., Novosolov, M., Allison, A., Bauer, A.M., Bernard, R., *et al.* (2017). The global distribution of tetrapods reveals a need for targeted reptile conservation. *Nat. Ecol. Evol.*, 1, 1677–1682.

Rolland, J., Condamine, F.L., Jiguet, F. & Morlon, H. (2014). Faster Speciation and Reduced Extinction in the Tropics Contribute to the Mammalian Latitudinal Diversity Gradient. *PLoS Biol.*, 12.

Rolland, J., Silvestro, D., Schluter, D., Guisan, A., Broennimann, O. & Salamin, N. (2018). The impact of endothermy on the climatic niche evolution and the distribution of vertebrate diversity. *Nat. Ecol. Evol.*, 2, 459–464.

Rosenzweig, C., Karoly, D., Vicarelli, M., Neofotis, P., Wu, Q., Casassa, G., *et al.* (2008). Attributing physical and biological impacts to anthropogenic climate change. *Nature*, 453, 353–357.

Rosser, N., Kozak, K.M., Phillimore, A.B. & Mallet, J. (2015). Extensive range overlap between heliconiine sister species: Evidence for sympatric speciation in butterflies? *BMC Evol. Biol.*, 15, 1–13.

Rosser, N., Phillimore, A.B., Huertas, B., Willmott, K.R. & Mallet, J. (2012). Testing historical explanations for gradients in species richness in heliconiine butterflies of tropical America. *Biol. J. Linn. Soc.*, 105, 479–497.

Rosser, N., Shirai, L.T., Dasmahapatra, K.K., Mallet, J. & Freitas, A.V.L. (2021). The Amazon river is a suture zone for a polyphyletic group of co-mimetic heliconiine butterflies. *Ecography (Cop.).*, 44, 177–187.

Rothberg, J.M., Hinz, W., Rearick, T.M., Schultz, J., Mileski, W., Davey, M., *et al.* (2011). An integrated semiconductor device enabling non-optical genome sequencing. *Nature*, 475, 348–352.

Le Roy, C., Roux, C., Authier, E., Parrinello, H., Bastide, H., Debat, V., *et al.* (2021). Convergent morphology and divergent phenology promote the coexistence of Morpho butterfly species. *Nat. Commun.*, 12, 1–9.

Rueda, M., Rodríguez, M.Á. & Hawkins, B.A. (2013). Identifying global zoogeographical regions: Lessons from Wallace. *J. Biogeogr.*, 40, 2215–2225.

Ruxton, G.D., Speed, M. & Sherratt, T.N. (2004). Evasive mimicry: when (if ever) could mimicry based on difficulty of capture evolve? *Proc. R. Soc. London. Ser. B Biol. Sci.*, 271, 2135–2142.

Sakai, S. (2002). General flowering in lowland mixed dipterocarp forests of south-east Asia. *Biol. J. Linn. Soc.*, 75, 233–247.

Salcido, D.M., Forister, M.L., Garcia Lopez, H. & Dyer, L.A. (2020). Loss of dominant caterpillar genera in a protected tropical forest. *Sci. Rep.*, 10, 1–10.

Sanders, K.L., Malhotra, A. & Thorpe, R.S. (2006). Evidence for a Müllerian mimetic radiation in Asian pitvipers. *Proc. R. Soc. B Biol. Sci.*, 273, 1135–1141.

Sanger, F., Nicklen, S. & Coulson, A.R. (1977). DNA sequencing with chain-terminating inhibitors. *Proc. Natl. Acad. Sci. U. S. A.*, 74, 5463–5467.

Särkinen, T., Bohs, L., Olmstead, R.G. & Knapp, S. (2013). A phylogenetic framework for evolutionary study of the nightshades (Solanaceae): a dated 1000-tip tree. *BMC Evol. Biol.*, 13, 214.

Särkinen, T., Pennington, R.T., Lavin, M., Simon, M.F. & Hughes, C.E. (2012). Evolutionary islands in the Andes: Persistence and isolation explain high endemism in Andean dry tropical forests. *J. Biogeogr.*, 39, 884–900.

Saupe, E.E., Myers, C.E., Peterson, A.T., Soberón, J., Singarayer, J., Valdes, P., *et al.* (2019). Non-random latitudinal gradients in range size and niche breadth predicted by spatial patterns of climate. *Glob. Ecol. Biogeogr.*, 28, 928–942.

Sauquet, H., Von Balthazar, M., Magallón, S., Doyle, J.A., Endress, P.K., Bailes, E.J., *et al.* (2017). The ancestral flower of angiosperms and its early diversification. *Nat. Commun.*, 8.

Sayyari, E. & Mirarab, S. (2016). Fast Coalescent-Based Computation of Local Branch Support from Quartet Frequencies. *Mol. Biol. Evol.*, 33, 1654–1668.

Schneider, F.D., Brose, U., Rall, B.C. & Guill, C. (2016). Animal diversity and ecosystem functioning in dynamic food webs. *Nat. Commun.*, 7, 12718.

Schoener, T.W. (1970). Nonsynchronous Spatial Overlap of Lizards in Patchy Habitats. *Ecology*, 51, 408–418.

Schrodt, F., Santos, M.J., Bailey, J.J. & Field, R. (2019). Challenges and opportunities for biogeography—What can we still learn from von Humboldt? *J. Biogeogr.*, 46, 1631–1642.

Schuettpelz, E., Frandsen, P.B., Dikow, R.B., Brown, A., Orli, S., Peters, M., *et al.* (2017). Applications of deep convolutional neural networks to digitized natural history collections. *Biodivers. Data J.*, 5.

Schulz, S., Beccaloni, G., Brown, K.S., Boppré, M., Freitas, A.V.L., Ockenfels, P., *et al.* (2004). Semiochemicals derived from pyrrolizidine alkaloids in male ithomiine butterflies (Lepidoptera: Nymphalidae: Ithomiinae). *Biochem. Syst. Ecol.*, 32, 699–713.

Sedano, R.E. & Burns, K.J. (2010). Are the Northern Andes a species pump for Neotropical birds? Phylogenetics and biogeography of a clade of Neotropical tanagers (Aves: Thraupini). *J. Biogeogr.*, 37, 325–343.

Segan, D.B., Murray, K.A. & Watson, J.E.M. (2016). A global assessment of current and future biodiversity vulnerability to habitat loss-climate change interactions. *Glob. Ecol. Conserv.*, 5, 12–21.

Sexton, J.O., Song, X.P., Feng, M., Noojipady, P., Anand, A., Huang, C., *et al.* (2013). Global, 30-m resolution continuous fields of tree cover: Landsat-based rescaling of MODIS vegetation continuous fields with lidar-based estimates of error. *Int. J. Digit. Earth*, 6, 427–448.

Shannon, C.E. (1948). A mathematical theory of communication. *Bell Syst. Tech. J.*, 27, 379–423.

Sheldon, K.S., Yang, S. & Tewksbury, J.J. (2011). Climate change and community disassembly: Impacts of warming on tropical and temperate montane community structure. *Ecol. Lett.*, 14, 1191–1200.

Shen, X.X., Steenwyk, J.L. & Rokas, A. (2021). Dissecting Incongruence between Concatenation- and Quartet-Based Approaches in Phylogenomic Data. *Syst. Biol.*, 70, 997–1014.

Sherratt, T.N. (2002). The evolution of imperfect mimicry. *Behav. Ecol.*, 13, 821–826.

Sherratt, T.N. (2006). Spatial mosaic formation through frequency-dependent selection in Müllerian mimicry complexes. *J. Theor. Biol.*, 240, 165–174.

Sherratt, T.N. (2008). The evolution of Müllerian mimicry. *Naturwissenschaften*, 95, 681–695.

Sherratt, T.N., Whissell, E., Webster, R. & Kikuchi, D.W. (2015). Hierarchical overshadowing of stimuli and its role in mimicry evolution. *Anim. Behav.*, 108, 73–79.

Shine, R. (1990). Function and evolution of the frill of the frillneck lizard, Chlamydosaurus kingii (Sauria: Agamidae). *Biol. J. Linn. Soc.*, 40, 11–20.

Shirey, V., Larsen, E., Doherty, A., Kim, C.A., Al-Sulaiman, F.T., Hinolan, J.D., *et al.* (2022). LepTraits 1.0 A globally comprehensive dataset of butterfly traits. *Sci. Data*, 9, 1–7.

Short, A.E.Z., Dikow, T. & Moreau, C.S. (2018). Entomological Collections in the Age of Big Data. *Annu. Rev. Entomol.*, 63, 513–530.

Siddique, R.H., Gomard, G. & Hölscher, H. (2015). The role of random nanostructures for the omnidirectional anti-reflection properties of the glasswing butterfly. *Nat. Commun.*, 6, 1–8.

Simion, P., Belkhir, K., François, C., Veyssier, J., Rink, J.C., Manuel, M., *et al.* (2018). A software tool "CroCo" detects pervasive cross-species contamination in next generation sequencing data. *BMC Biol.*, 16, 1–9.

Simpson, G.G. (1944). *Tempo and mode in evolution*. Columbia University Press.

Slatko, B.E., Gardner, A.F. & Ausubel, F.M. (2018). Overview of Next-Generation Sequencing Technologies. *Curr. Protoc. Mol. Biol.*, 122, 1–15.

Smith, E.P. & van Belle, G. (1984). Nonparametric Estimation of Species Richness. *Biometrics*, 40, 119.

Smith, J.M., Burian, R., Kauffman, S., Alberch, P., Campbell, J., Goodwin, B., *et al.* (1985). Developmental Constraints and Evolution: A Perspective from the Mountain Lake Conference on Development and Evolution. *Q. Rev. Biol.*, 60, 265–287.

Soberón, J. & Nakamura, M. (2009). Niches and distributional areas: Concepts, methods, and assumptions. *Proc. Natl. Acad. Sci. U. S. A.*, 106, 19644–19650.

Soberon, J. & Peterson, A.T. (2005). Interpretation of Models of Fundamental Ecological Niches and Species' Distributional Areas. *Biodivers. Informatics*, 2, 3392–3396.

Sohn, J. & Nam, J. (2016). The present and future of de novo whole-genome assembly. *Brief. Bioinform.*, 19, bbw096.

Sombroek, W. (2000). Amazon landforms and soils in relation to biological diversity. *Acta Amaz.*, 30, 81–81.

Sonter, L.J., Herrera, D., Barrett, D.J., Galford, G.L., Moran, C.J. & Soares-Filho, B.S. (2017). Mining drives extensive deforestation in the Brazilian Amazon. *Nat. Commun.*, 8, 1–7.

La Sorte, F.A. & Jetz, W. (2010). Projected range contractions of montane biodiversity under global warming. *Proc. R. Soc. B Biol. Sci.*, 277, 3401–3410.

Soubrier, J., Steel, M., Lee, M.S.Y., Der Sarkissian, C., Guindon, S., Ho, S.Y.W., *et al.* (2012). The influence of rate heterogeneity among sites on the time dependence of molecular rates. *Mol. Biol. Evol.*, 29, 3345–3358.

Staniczenko, P.P.A., Sivasubramaniam, P., Suttle, K.B. & Pearson, R.G. (2017). Linking macroecology and community ecology: refining predictions of species distributions using biotic interaction networks. *Ecol. Lett.*, 20, 693–707.

Stebbins, R.C. (1949). Speciation in salamanders of the plethodontid genus Ensatina. *Univ. Calif. Publ. Zool.*, 377–526.

Ter Steege, H., Pitman, N., Sabatier, D., Castellanos, H., Van Der Hout, P., Daly, D.C., *et al.* (2003). A spatial model of tree alpha-diversity and tree density for the Amazon. *Biodivers. Conserv.*, 12, 2255–2277.

Ter Steege, H., Pitman, N.C.A., Phillips, O.L., Chave, J., Sabatier, D., Duque, A., *et al.* (2006). Continental-scale patterns of canopy tree composition and function across Amazonia. *Nature*, 443, 444–447.

Ter Steege, H., Pitman, N.C.A., Sabatier, D., Baraloto, C., Salomão, R.P., Guevara, J.E., *et al.* (2013). Hyperdominance in the Amazonian tree flora. *Science (80-.).*, 342.

Stelbrink, P., Pinkert, S., Brunzel, S., Kerr, J., Wheat, C.W., Brandl, R., *et al.* (2019). Colour lightness of butterfly assemblages across North America and Europe. *Sci. Rep.*, 9, 1–10.

Stensland, E., Angerbjörn, A. & Berggren, P. (2003). Mixed species groups in mammals. *Mamm. Rev.*, 33, 205–223.

Stork, N.E. (2018). How Many Species of Insects and Other Terrestrial Arthropods Are There on Earth? *Annu. Rev. Entomol.*, 63, 31–45.

Stork, N.E. & Habel, J.C. (2014). Can biodiversity hotspots protect more than tropical forest plants and vertebrates? *J. Biogeogr.*, 41, 421–428.

Suh, A., Smeds, L. & Ellegren, H. (2015). The dynamics of incomplete lineage sorting across the ancient adaptive radiation of neoavian birds. *PLoS Biol.*, 13, 1–18.

Sumner, S., Law, G. & Cini, A. (2018). Why we love bees and hate wasps. *Ecol. Entomol.*, 43, 836–845.

Suzuki, T.N. & Sakurai, R. (2015). Bent posture improves the protective value of bird dropping masquerading by caterpillars. *Anim. Behav.*, 105, 79–84.

Svenning, J.C., Eiserhardt, W.L., Normand, S., Ordonez, A. & Sandel, B. (2015). The

Influence of Paleoclimate on Present-Day Patterns in Biodiversity and Ecosystems. *Annu. Rev. Ecol. Evol. Syst.*, 46, 551–572.

Svenning, J.C., Gravel, D., Holt, R.D., Schurr, F.M., Thuiller, W., Münkemüller, T., *et al.* (2014). The influence of interspecific interactions on species range expansion rates. *Ecography (Cop.).*, 37, 1198–1209.

Symula, R., Schulte, R. & Summers, K. (2001). Molecular phylogenetic evidence for a mimetic radiation in Peruvian poison frogs supports a Müllerian mimicry hypothesis. *Proc. R. Soc. B Biol. Sci.*, 268, 2415–2421.

Tavaré, S. (1986). Some probabilistic and statistical problems in the analysis of DNA sequences. In: *Lectures on Mathematics in the Life Science*. American Mathematical Society, pp. 57–86.

Thébault, E. & Fontaine, C. (2010). Stability of ecological communities and the architecture of mutualistic and trophic networks. *Science (80-.).*, 329, 853–856.

Thomas, C.D., Cameron, A., Green, R.E., Bakkenes, M., Beaumont, L.J., Collingham, Y.C., *et al.* (2004). Extinction risk from climate change. *Nature*, 427, 145–8.

Thompson, J.N. (1989). Concepts of coevolution. *Trends Ecol. Evol.*, 4, 179–183.

Thompson, J.N. (2005). *The geographic mosaic of coevolution*. Univ. of Chicago Press, Chicago, IL.

Thomson, J.D. & Wilson, P. (2008). Explaining evolutionary shifts between bee and hummingbird pollination: Convergence, divergence, and directionality. *Int. J. Plant Sci.*, 169, 23–38.

Thuiller, W., Georges, D., Engler, R. & Breiner, F. (2020). biomod2: Ensemble Platform for Species Distribution Modeling. R package version 3.4.6.

Thuiller, W., Guéguen, M., Renaud, J., Karger, D.N. & Zimmermann, N.E. (2019). Uncertainty in ensembles of global biodiversity scenarios. *Nat. Commun.*, 10, 1–9.

Tilman, D., Isbell, F. & Cowles, J.M. (2014). Biodiversity and ecosystem functioning. *Annu. Rev. Ecol. Evol. Syst.*, 45, 471–493.

Toby Kiers, E., Palmer, T.M., Ives, A.R., Bruno, J.F. & Bronstein, J.L. (2010). Mutualisms in a changing world: An evolutionary perspective. *Ecol. Lett.*, 13, 1459–1474.

Trew, B.T. & Maclean, I.M.D. (2021). Vulnerability of global biodiversity hotspots to climate change. *Glob. Ecol. Biogeogr.*, 30, 768–783.

Trigo, J.R. & Brown Jr, K.S. (1990). Variation of pyrrolizidine alkaloids in Ithomiinae: A comparative study between species feeding on Apocynaceae and Solanaceae. *Chemoecology*, 1, 22–29.

Trigo, J.R., Brown, K.S., Witte, L., Hartmann, T., Ernst, L. & Barata, L.E.S. (1996). Pyrrolizidine alkaloids: Different acquisition and use patterns in Apocynaceae and Solanaceae feeding ithomiine butterflies (Lepidoptera: Nymphalidae). *Biol. J. Linn. Soc.*, 58, 99–123.

Tuanmu, M. & Jetz, W. (2015). A global, remote sensing-based characterization of terrestrial habitat heterogeneity for biodiversity and ecosystem modelling. *Glob. Ecol. Biogeogr.*,

24, 1329–1339.

Tucker, M.A., Böhning-Gaese, K., Fagan, W.F., Fryxell, J.M., Van Moorter, B., Alberts, S.C., *et al.* (2018). Moving in the Anthropocene: Global reductions in terrestrial mammalian movements. *Science (80-.).*, 359, 466–469.

Turner, J.R.G. (1984). Mimicry: the palatability spectrum and its consequences. In: *The Biology of Butterflies* (eds. Vane-Wright, R.I. & Ackery, P.R.). Academic Press, New York, pp. 141–161.

Tylianakis, J.M., Didham, R.K., Bascompte, J. & Wardle, D.A. (2008). Global change and species interactions in terrestrial ecosystems. *Ecol. Lett.*

Tylianakis, J.M., Laliberté, E., Nielsen, A. & Bascompte, J. (2010). Conservation of species interaction networks. *Biol. Conserv.*, 143, 2270–2279.

Uehara-Prado, M. & Freitas, A.V.L. (2009). The effect of rainforest fragmentation on species diversity and mimicry ring composition of ithomiine butterflies. *Insect Conserv. Divers.*, 2, 23–28.

Ulloa Ulloa, C., Acevedo-Rodríguez, P., Beck, S., Belgrano, M.J., Bernal, R., Berry, P.E., *et al.* (2017). An integrated assessment of the vascular plant species of the Americas. *Science (80-.).*, 358, 1614–1617.

Upham, N.S., Esselstyn, J.A. & Jetz, W. (2019). *Inferring the mammal tree: Species-level sets of phylogenies for questions in ecology, evolution, and conservation*. *PLoS Biol.*

Valavi, R., Elith, J., Lahoz-Monfort, J.J. & Guillera-Arroita, G. (2019). blockCV: An r package for generating spatially or environmentally separated folds for k-fold cross-validation of species distribution models. *Methods Ecol. Evol.*, 10, 225–232.

Valiente-Banuet, A. & Verdú, M. (2007). Facilitation can increase the phylogenetic diversity of plant communities. *Ecol. Lett.*, 10, 1029–1036.

VanDerWal, J., Shoo, L.P., Johnson, C.N. & Williams, S.E. (2009). Abundance and the environmental niche: Environmental suitability estimated from niche models predicts the upper limit of local abundance. *Am. Nat.*, 174, 282–291.

Vega, G.C., Pertierra, L.R. & Olalla-Tárraga, M.Á. (2017). Data Descriptor: MERRAclim, a high-resolution global dataset of remotely sensed bioclimatic variables for ecological modelling Background & Summary. *Sci. Data*, 4, 1–11.

Vences, M., Kosuch, J., Boistel, R., Haddad, C.F.B., La Marca, E., Lötters, S., *et al.* (2003). Convergent evolution of aposematic coloration in Neotropical poison frogs: a molecular phylogenetic perspective. *Org. Divers. Evol.*, 3, 215–226.

Venter, O., Sanderson, E.W., Magrach, A., Allan, J.R., Beher, J., Jones, K.R., *et al.* (2016a). Global terrestrial Human Footprint maps for 1993 and 2009. *Sci. Data*, 3, 1–10.

Venter, O., Sanderson, E.W., Magrach, A., Allan, J.R., Beher, J., Jones, K.R., *et al.* (2016b). Sixteen years of change in the global terrestrial human footprint and implications for biodiversity conservation. *Nat. Commun.*, 7, 1–11.

Vidal, M.M., Banks-Leite, C., Tambosi, L.R., Hasui, É., Develey, P.F., Silva, W.R., *et al.* (2019). Predicting the non-linear collapse of plant–frugivore networks due to habitat loss. *Ecography (Cop.).*, 42, 1765–1776.

de Vienne, D.M., Dray, S., Tricou, T. & Siberchicot, A. (2023). phylter: Detect and Remove Outliers in Phylogenomics Datasets. R package version 0.9.7.

Wallace, A.R. (1855). XVIII. On the law which has regulated the introduction of new species. *Ann. Mag. Nat. Hist.*, 16, 184–196.

Wallace, A.R. (1876). *The geographical distribution of animals*. Harper & Brothers, New York.

Wang, S., Fan, Y., Zhang, C., Xu, H.X., Hao, X. & Hu, Y. (2008). Subspace clustering of high dimensional data streams. *Proc. - 7th IEEE/ACIS Int. Conf. Comput. Inf. Sci. IEEE/ACIS ICIS 2008, conjunction with 2nd IEEE/ACIS Int. Work. e-Activity, IEEE/ACIS IWEA 2008*, 165–170.

Watson, J. & Crick, F. (1953). Molecular Structure of Nucleic Acids: A Structure for Deoxyribose Nucleic Acid. *Nature*, 171, 737–738.

Watt, W.B. (1968). Adaptive Significance of Pigment Polymorphisms in Colias Butterflies. I. Variation of Melanin Pigment in Relation to Thermoregulation. *Evolution (N. Y).*, 22, 437.

Webb, C.O., Ackerly, D.D., McPeek, M.A. & Donoghue, M.J. (2002). Phylogenies and Community Ecology. *Annu. Rev. Ecol. Syst.*, 33, 475–505.

Weinstein, B.G. (2018). Scene-specific convolutional neural networks for video-based biodiversity detection. *Methods Ecol. Evol.*, 9, 1435–1441.

Weir, J.T. (2006). Divergent Timing and Patterns of Species Accumulation in Lowland and Highland Neotropical Birds. *Evolution (N. Y).*, 60, 842.

Weismann, A. (1904). True mimicry. In: *The evolution theory, Vol 1*. (eds. Weismann, A., Thomson, J.A. & Thomson, M.R.). Edward Arnold, London, pp. 91–118.

Wesselingh, F.P., Hoorn, C., Kroonenberg, S.B., Antonelli, A., Lundberg, J.G., Vonhof, H.B., *et al.* (2010). On the Origin of Amazonian Landscapes and Biodiversity: A Synthesis. In: *Amazonia, Landscape and Species Evolution: A Look into the Past*. pp. 421–431.

Whinnett, A., Zimmermann, M., Willmott, K.R., Herrera, N., Mallarino, R., Simpson, F., *et al.* (2005). Strikingly variable divergence times inferred across an Amazonian butterfly ' suture zone ,' 2525–2533.

Wickett, N.J., Mirarab, S., Nguyen, N., Warnow, T., Carpenter, E., Matasci, N., *et al.* (2014). Phylotranscriptomic analysis of the origin and early diversification of land plants. *Proc. Natl. Acad. Sci. U. S. A.*, 111, E4859–E4868.

Wiley, E.O. (1988). Parsimony Analysis and Vicariance Biogeography. *Syst. Zool.*, 37, 271.

Wiley, R.H. (1971). Cooperative Roles in Mixed Flocks of Antwrens (Formicariidae). *Auk*, 88, 881–892.

Williams, P. (2007). The distribution of bumblebee colour patterns worldwide: Possible significance for thermoregulation, crypsis, and warning mimicry. *Biol. J. Linn. Soc.*, 92, 97–118.

Williams, P., Gibbons, D., Margules, C., Rebelo, A., Humphries, C. & Pressey, R. (1996). A comparison of richness hotspots, rarity hotspots, and complementary areas for

conserving diversity of British birds. *Conserv. Biol.*, 10, 155–174.

Williams, P.H. & Humphries, C.J. (1994). Biodiversity, taxonomic relatedness, and endemism in conservation. In: *Systematics and conservation evaluation* (eds. Forey, P.L., Humphries, C.J. & Vane-Wright, R.I.). Clarendon Press, Oxford, pp. 269–287.

Willmott, K.R. & Freitas, A.V.L. (2006). Higher-level phylogeny of the Ithomiinae (Lepidoptera: Nymphalidae): classification, patterns of larval hostplant colonization and diversification. *Cladistics*, 22, 297.

Willmott, K.R. & Lamas, G. (2006). A phylogenetic reassessment of Hyalenna Forbes and Dircenna Doubleday, with a revision of Hyalenna (Lepidoptera: Nymphalidae: Ithomiinae). *Syst. Entomol.*, 31, 419–468.

Willmott, K.R. & Lamas, G. (2007). A revision of Pachacutia, a new genus of rare andean ithomiine butterflies (Nymphalidae: Ithomiinae), with the description of two new species. *Ann. Entomol. Soc. Am.*, 100, 449–469.

Willmott, K.R. & Mallet, J. (2004). Correlations between adult mimicry and larval host plants in ithomiine butterflies. *Proc. R. Soc. B Biol. Sci.*, 271, S266–S269.

Willmott, K.R., Robinson Willmott, J.C., Elias, M. & Jiggins, C.D. (2017). Maintaining mimicry diversity: optimal warning colour patterns differ among microhabitats in Amazonian clearwing butterflies. *Proc. R. Soc. B Biol. Sci.*, 284, 20170744.

Wilson, E. (2010). The Major Historical Trends of Biodiversity Studies. In: *Systema Naturae 250 - The Linnaean Ark*. pp. 1–4.

Wilson, J.S., Jahner, J.P., Forister, M.L., Sheehan, E.S., Williams, K.A. & Pitts, J.P. (2015). North American velvet ants form one of the world's largest known Müllerian mimicry complexes. *Curr. Biol.*, 25, R704–R706.

Wilson, J.S., Pan, A.D., Alvarez, S.I. & Carril, O.M. (2022). Assessing Müllerian mimicry in North American bumble bees using human perception. *Sci. Rep.*, 12, 1–9.

Wilson, J.S., Pan, A.D., Limb, E.S. & Williams, K.A. (2018). Comparison of African and North American velvet ant mimicry complexes: Another example of Africa as the 'odd man out.' *PLoS One*, 13, 1–15.

Windsor, F.M., van den Hoogen, J., Crowther, T.W. & Evans, D.M. (2023). Using ecological networks to answer questions in global biogeography and ecology. *J. Biogeogr.*, 50, 57–69.

Winkler, I.S. & Mitter, C. (2008). The phylogenetic dimension of insect-plant interactions: A review of recent evidence. *Spec. Speciation, Radiat. Evol. Biol. Herbiv. Insects*, 240–263.

Wüest, R.O., Zimmermann, N.E., Zurell, D., Alexander, J.M., Fritz, S.A., Hof, C., *et al.* (2020). Macroecology in the age of Big Data – Where to go from here? *J. Biogeogr.*, 47, 1–12.

Yang, Z. & Rannala, B. (1997). Bayesian phylogenetic inference using DNA sequences: a Markov Chain Monte Carlo Method. *Mol. Biol. Evol.*, 14, 717–724.

Young, A.D. & Gillung, J.P. (2020). Phylogenomics — principles, opportunities and pitfalls of big-data phylogenetics. *Syst. Entomol.*, 45, 225–247.

Zahavi, A. (1975). Mate selection-A selection for a handicap. *J. Theor. Biol.*, 53, 205–214.

Zeuss, D., Brunzel, S. & Brandl, R. (2017). Environmental drivers of voltinism and body size in insect assemblages across Europe. *Glob. Ecol. Biogeogr.*, 26, 154–165.

Zhang, C., Rabiee, M., Sayyari, E. & Mirarab, S. (2018). ASTRAL-III: Polynomial time species tree reconstruction from partially resolved gene trees. *BMC Bioinformatics*, 19, 15–30.

Zuloaga, J., Currie, D.J. & Kerr, J.T. (2019). The origins and maintenance of global species endemism. *Glob. Ecol. Biogeogr.*, 28, 170–183.

Zupan, L., Cabeza, M., Maiorano, L., Roquet, C., Devictor, V., Lavergne, S., *et al.* (2014). Spatial mismatch of phylogenetic diversity across three vertebrate groups and protected areas in Europe. *Divers. Distrib.*, 20, 674–685.

Zurell, D., Franklin, J., König, C., Bouchet, P.J., Dormann, C.F., Elith, J., *et al.* (2020). A standard protocol for reporting species distribution models. *Ecography (Cop.).*, 1–17.

Biodiversity and evolution in Neotropical mimetic butterflies

In the face of global change, understanding the mechanisms underlying species distributions and coexistence is both a priority and a challenge, especially for biodiversity hotspots such as the Neotropics. This research work aims to unravel effects of Müllerian mimicry on large-scale spatial and evolutionary patterns of biodiversity in two tribes of Neotropical butterflies, the Ithomiini (Nymphalidae: Danainae) and Heliconiini (Nymphalidae: Heliconiinae), employing an integrative approach across biogeography, phylogenomics, and community ecology.

I map the taxonomic, phylogenetic and mimetic facets of Ithomiini biodiversity and identify areas of evolutionary and ecological importance for conservation. I show that tropical montane forests that host high species and mimetic diversity as well as rare species and mimicry patterns appear particularly under threat. I present a new phylogeny that resolves deep evolutionary relationships, providing a stable tool to study evolution in ithomiine butterflies. I describe a new method to generate 3D perceptual maps of the variation of heliconiine butterfly wing patterns. I map the local phenotypic diversity as the degree of clustering in the perceptual space and define local mimicry groups. Finally, I show that mimicry drives large scale spatial association and evolutionary convergence of the climatic niche of co-mimetic species, highlighting the importance of mutualistic interactions in shaping both niche evolution and species assemblages at large spatial scales.

Keywords: biodiversity indices, Citizen Science, climatic niche, ecological signals, evolutionary convergence, machine learning, macroevolution, Müllerian mimicry, Neotropical butterflies, perceptual maps, phylogenomics, species assemblages, species distribution models.